

# METHANOL CARBONYLATION VIA PLATINUM GROUP METAL COMPLEXES

By

PHILIPPUS DANIEL RIEKERT KOTZÉ

THESIS

submitted in the fulfillment of the requirements for the degree

PHILOSOPHIAE DOCTOR

in

CHEMISTRY

in the

FACULTY OF SCIENCE

at the

UNIVERSITY OF THE FREE STATE

SUPERVISOR: PROFESSOR ANDREAS ROODT

NOVEMBER 2010

## **PREFACE**

I would like to express my gratitude to the following people:

Firstly, Professor Andreas Roodt, thank you for all your input, suggestions, enthusiasm, encouragement and care. You are truly one of the greatest lecturers and supervisors that I have come across and it was an absolute honor to have the privilege of studying under you. You have supported me from the start as you have promised to do so and I am truly grateful for that. I pray God's blessing over you and your family.

I would also like to thank Professor Ola Wendt at the University of Lund for having me and supporting me during my visit in Sweden. It was a great experience and enjoyed working with you and your colleagues.

Dr. Johan Venter at the University of the Free State for your moral support, friendliness and contributions to the project.

Also Dr. Stefanus Otto at SASOL technology for being my mentor. Your insight and suggestions to this project was of great help.

I want give special thanks to the Inorganic research group at the University of the Free State, especially Carla Pretorius, Kina van der Merwe and Tania Hill for such great friendship and support during my time in Bloemfontein.

I would also like to thank SASOL for the financial support and giving me the opportunity to do my postgraduate studies.

Last, but not least, I thank God Almighty for His everlasting love and support. Without Him I am nothing and without hope.

**Psalm 14:1 The fool hath said in his heart, *There is no God*. They are corrupt, they have done abominable works, *there is none that doeth good*.**

For my parents: Philippus D. R. & Delaine J. S. Kotze

For my grandparents: Jannie A & Delaine Redelinghuys

# **TABLE OF CONTENTS**

TABLE OF CONTENTS.....	I
ABBREVIATIONS AND SYMBOLS.....	V
SUMMARY.....	VII

CHAPTER 1 BASIC CONCEPTS OF RHODIUM CHEMISTRY, LIGAND PROPERTIES AND THE AIM OF THE STUDY.....	1
1.1 Introduction to catalysis.....	1
1.2 Rhodium systems.....	2
1.3 Ligand effects in transition metal chemistry.....	2
1.4 Aim of the study.....	6

CHAPTER 2 THEORETICAL STUDY ON CARBONYLATION/ HOMOLOGATION PROCESSES AND IMPORTANT CHEMISTRY IN CATALYSIS.....	9
2.1 Introduction.....	9
2.2 Syngas (H <sub>2</sub> /CO) as a building block in catalysis.....	9
2.3 Hydrocarbonylation reactions of MeOH and derivatives.....	13
2.4 Chemical reactions related to metal complexes.....	23
2.5 Iodomethane oxidative addition to rhodium(I) complexes.....	29
2.6 Coordination of <i>S,O</i> -thiourea ligands to metal centres.....	33
2.7 Ligand effects.....	35
2.8 Conclusion.....	39



CHAPTER 3 THE SYNTHESIS AND CHARACTERIZATION OF FUNCTIONALISED- <i>S,O</i> -THIOUREA LIGANDS.....	40
3.1 Introduction.....	40
3.2 Reagents and equipment.....	41
3.3 Synthetic procedure for <i>S,O</i> -donor thiourea ligands.....	42
3.4 Conclusion.....	55

CHAPTER 4 X-RAY CRYSTALLOGRAPHIC STUDY OF FUNCTIONALISED- <i>S,O</i> -THIOUREA LIGANDS.....	56
4.1 Introduction.....	56
4.2 Experimental.....	57
4.3 Crystal structure of <i>N</i> -benzoyl- <i>N'</i> -(2,4,6-trimethylphenyl)thiourea ( <i>N</i> -tmPTH).....	60
4.4 Crystal structure of <i>N</i> -benzoyl- <i>N'</i> -(2,6-di-bromo-4-fluorophenyl)thiourea ( <i>N</i> -BFPTH).....	67
4.5 Crystal structure of <i>N</i> -benzoyl- <i>N'</i> -(pentafluorophenyl)thiourea ( <i>N</i> -FPTH).....	73
4.6 Crystal structure of <i>N</i> -benzoyl- <i>N'</i> -(phenethyl)thiourea ( <i>N</i> -PeTH).....	79
4.7 Crystal structure of <i>N</i> -benzoyl- <i>N'</i> -(naphthalene-1-ylmethyl)thiourea ( <i>N</i> -NmTH).....	84
4.8 Crystal structure of <i>N</i> -benzoyl- <i>N'</i> -(cyclohexyl)thiourea ( <i>N</i> -CyTH).....	89
4.9 Crystal structure of <i>N</i> -benzoyl- <i>N'</i> -(isopentyl)thiourea ( <i>N</i> -ipTH).....	94
4.10 Interpretation and correlation of structural properties of thiourea compounds.....	99
4.11 Conclusion.....	108

CHAPTER 5 THE SYNTHESIS AND CHARACTERIZATION OF RHODIUM DIPHOSPHINE COMPLEXES.....	110
5.1 Introduction.....	110
5.2 Attempted synthesis of $[\text{Rh}(\text{diphosphine})(\text{CO})_2]^+$ complexes.....	111
5.3 Results and discussion.....	119
5.4 Crystal structure of dicarbonylchloridodi(bis(diphenylphosphino)methane) dirhodium(I) tetrafluoroborate, $[\text{Rh}_2(\mu\text{-Cl})(\text{dppm})_2(\text{CO})_2]\text{BF}_4$ .....	122
5.5 Conclusion.....	129

## CHAPTER 6 SYNTHETIC ROUTES TO NOVEL Rh(I) and Rh(III)

COMPLEXES WITH <i>S,O</i> -THIOUREA LIGANDS.....	132
6.1 Introduction.....	132
6.2 Reagents and equipment.....	133
6.3 Attempted synthesis of [Rh( <i>S,O</i> -thioureato)(CO) <sub>2</sub> ] <i>via</i> the precursor [Rh( $\mu$ -Cl)(CO) <sub>2</sub> ] <sub>2</sub> .....	134
6.4 Attempted synthesis of [Rh( <i>S,O</i> -thioureato)(CO)(PPh <sub>3</sub> )] complexes.....	145
6.5 Attempted synthesis of [Rh( <i>S,O</i> -thioureato)(CO) <sub>2</sub> ] <i>via</i> the precursor [Rh(COD)(Cl)] <sub>2</sub> .....	154
6.6 Structural characterization of a range of <i>S,O</i> -, <i>N,S</i> - and <i>S</i> - coordinated thiourea complexes of rhodium.....	157
6.7 Results and discussion.....	178
6.8 Conclusion.....	187

## CHAPTER 7 THE SYNTHESIS AND CHARACTERIZATION OF

[Rh( <i>S,O</i> -THIOUREATO)(CO)(PR <sub>1</sub> R <sub>2</sub> R <sub>3</sub> )] COMPLEXES.....	189
7.1 Introduction.....	189
7.2 Reagents and equipment.....	189
7.3 Synthetic procedure for [Rh( <i>S,O</i> -( <i>N</i> -diPT))(CO)(PR <sub>1</sub> R <sub>2</sub> R <sub>3</sub> )] complexes.....	190
7.4 X-ray crystallographic study of [Rh( <i>S,O</i> -( <i>N</i> -diPT))(CO)(PR <sub>1</sub> R <sub>2</sub> R <sub>3</sub> )] complexes.....	198
7.5 Conclusion.....	221

## CHAPTER 8 KINETIC STUDY ON THE OXIDATIVE ADDITION OF IODOMETHANE TO [Rh(*S,O*-THIOUREATO)(CO)<sub>2</sub>] and

[Rh( <i>S,O</i> -THIOUREATO)(CO)(PR <sub>1</sub> R <sub>2</sub> R <sub>3</sub> )] COMPLEXES.....	223
8.1 Introduction.....	223
8.2 Theoretical background.....	225
8.3 Experimental.....	230
8.4 Results and discussion.....	231
8.5 Correlation of electro-steric effects of the [Rh( <i>N</i> -diPT)(CO)(PR <sub>1</sub> R <sub>2</sub> R <sub>3</sub> )]	

complexes.....	259
8.6 Conclusion.....	262
 CHAPTER 9 KINETIC STUDY OF PHOSPHINE EXCHANGE REACTIONS OF VASKA-TYPE Rh COMPLEXES.....	
264	
9.1 Introduction.....	264
9.2 Synthesis of Vaska-type rhodium complexes $[\text{Rh}(\text{Cl})(\text{CO})(\text{PR}_1\text{R}_2\text{R}_3)_2]$ .....	265
9.3 Line broadening study on the exchange reaction of $[\text{Rh}(\text{Cl})(\text{CO})(\text{PPh}_3)_2]$ with $\text{PPh}_3$ .....	269
9.4 Magnetization transfer study on the exchange reaction of $[\text{Rh}(\text{Cl})(\text{CO})(\text{PPh}_2\text{Cy})_2]$ with $\text{PPh}_2\text{Cy}$ .....	279
9.5 Conclusion.....	290
 CHAPTER 10 EVALUATION OF THE Ph.D. STUDY.....	
292	
10.1 Introduction.....	292
10.2 <i>S,O</i> -functionalized thiourea compounds.....	292
10.3 Rhodium(I) diphosphine complexes.....	293
10.4 Rhodium complexes of <i>S,O</i> -functionalized thiourea ligands.....	294
10.5 Iodomethane oxidative addition to rhodium(I) thioureato complexes.....	297
10.6 Phosphine exchange of Vaska-type rhodium(I) complexes.....	297
10.7 Future work.....	298
 APPENDIX A.....	
300	
 APPENDIX B.....	
336	
 APPENDIX C.....	
345	
 APPENDIX D.....	
378	
 APPENDIX E.....	
406	

# ABBREVIATIONS AND SYMBOLS

LABEL	DEFINITIONS
$\delta$	Chemical shift
$\Delta$	Heating
$\nu$	Stretching frequency on IR
$\Theta$	Effective cone angle
$\Delta H^\ddagger$	Enthalpy of activation
$\Delta S^\ddagger$	Entropy of activation
$\Delta G^\ddagger$	Gibbs free energy of activation
d	Doublet
$E_a$	Activation energy
$J$	Coupling constant
dd	Doublet of doublets
dt	Doublet of triplets
q	Quartet
s	Singlet
t	Triplet
<i>m</i>	Meta
<i>o</i>	Ortho
<i>p</i>	Para
ppm	Part per million
CO	Carbon monoxide
COD	1,5-cyclooctadiene
DCM	Dichloromethane
DMF	Dimethylformamide
DMSO	Dimethylsulfoxide
HP	High pressure
IR	Infrared
<i>L,L'</i> -BID	Bidentate ligand
NMR	Nuclear magnetic resonance
<i>N</i> -PTH	<i>N</i> -benzoyl- <i>N'</i> -(phenyl)thiourea (IUPAC: <i>N</i> -(anilinocarbonothioyl)benzamide)
<i>N</i> -tmPTH	<i>N</i> -benzoyl- <i>N'</i> -(2,4,6-trimethylphenyl)thiourea (IUPAC: <i>N</i> -[(mesitylamino)carbonothioyl]benzamide)
<i>N</i> -BFPTH	<i>N</i> -benzoyl- <i>N'</i> -(2,6-dibromo-4-fluorophenyl)thiourea (IUPAC: <i>N</i> -{[(2,6-dibromo-4-fluorophenyl)amino]carbonothioyl}benzamide)
<i>N</i> -FPTH	<i>N</i> -benzoyl- <i>N'</i> -(2,3,4,5,6-pentafluorophenyl)thiourea (IUPAC: <i>N</i> -{[(pentafluorophenyl)amino]carbonothioyl}benzamide)
<i>N</i> -PeTH	<i>N</i> -benzoyl- <i>N'</i> -phenethylthiourea (IUPAC: <i>N</i> -{[(2-phenylethyl)amino]carbonothioyl}benzamide)

<i>N</i> -NmTH	<i>N</i> -benzoyl- <i>N'</i> -(naphthalene-1-ylmethyl)thiourea (IUPAC: <i>N</i> -{[(1-naphthylmethyl)amino]carbonothioyl}benzamide)
<i>N</i> -CyTH	<i>N</i> -benzoyl- <i>N'</i> -(cyclohexyl)thiourea (IUPAC: <i>N</i> -[(cyclohexylamino)carbonothioyl]benzamide)
<i>N</i> -ipTH	<i>N</i> -benzoyl- <i>N'</i> -(isopentyl)thiourea (IUPAC: <i>N</i> -{[(3-methylbutyl)amino]carbonothioyl}benzamide)
<i>N</i> -4h2mPT	<i>N</i> -benzoyl- <i>N'</i> -(4-hydroxy-2-methylphenyl)thiourea (IUPAC: <i>N</i> -{[(4-hydroxy-2-methylphenyl)amino]carbonothioyl}benzamide)
<i>N</i> -NPTH	<i>N</i> -benzoyl- <i>N'</i> -naphthalen-1-yl- <i>N'</i> -phenylthiourea (IUPAC: <i>N</i> -{[1-naphthyl(phenyl)amino]carbonothioyl}benzamide)
<i>N</i> -diBnTH	<i>N</i> -benzoyl- <i>N'</i> , <i>N'</i> -(dibenzyl)thiourea (IUPAC: <i>N</i> -[(dibenzylamino)carbonothioyl]benzamide)
<i>N</i> -diPTH	<i>N</i> -benzoyl- <i>N'</i> , <i>N'</i> -(diphenyl)thiourea (IUPAC: <i>N</i> -[(diphenylamino)carbonothioyl]benzamide)
PR <sub>1</sub> R <sub>2</sub> R <sub>3</sub>	Tertiary phosphine
PPh <sub>3</sub>	Triphenylphosphine
PPh <sub>2</sub> Cy	Cyclohexyldiphenylphosphine
PPhCy <sub>2</sub>	Dicyclohexylphenylphosphine
PCy <sub>3</sub>	Tricyclohexylphosphine
THF	Tetrahydrofuran
UV	Ultraviolet
Vis	Visible
X-X	Single bonded atoms
X=X	Double bonded atoms
X...X	Non-bonded atomic interaction

## SUMMARY

The aim of this study, firstly, involved the synthesis of a range of *S,O*-functionalized thiourea ligands with systematically changing electro-steric properties and investigate these ligands coordination modes to rhodium complexes in an attempt to primarily synthesize a range of  $[\text{Rh}(\text{S},\text{O}\text{-thioureato})(\text{CO})_2]$  and  $[\text{Rh}(\text{S},\text{O}\text{-thioureato})(\text{CO})(\text{PR}_1\text{R}_2\text{R}_3)]$  complexes. Moreover, the aim also included the synthesis of  $[\text{Rh}(\text{diphosphine})(\text{CO})_2]^+$  complexes using a range of diphosphine ligands. These complexes were then to be used to synthesize the corresponding Rh(III)-acyl complexes *via* iodomethane oxidative addition and study the carbonylation/hydrogenation of methanol to ethanol by investigating the kinetic and activation parameters of the iodomethane oxidative addition as well as reductive elimination/hydrogenation of acyl iodide/acyl species.

Several *S,O*-functionalized thiourea ligands were successfully synthesized and characterized from which the X-ray crystallographic structures for several of the ligand systems are reported: *N*-benzoyl-*N'*-(2,4,6-trimethylphenyl)thiourea (Triclinic  $P\bar{1}$ ,  $R_1 = 5.60\%$ ), *N*-benzoyl-*N'*-(2,6-dibromo-4-fluorophenyl)thiourea (Triclinic  $P\bar{1}$ ,  $R_1 = 3.76\%$ ), *N*-benzoyl-*N'*-(pentafluorophenyl)thiourea (Monoclinic  $C2/c$ ,  $R_1 = 3.69\%$ ), *N*-benzoyl-*N'*-(phenethyl)thiourea (Monoclinic  $P2_1/n$ ,  $R_1 = 3.91\%$ ), *N*-benzoyl-*N'*-(naphthalene-1-ylmethyl)thiourea (Monoclinic  $C2/c$ ,  $R_1 = 5.37\%$ ), *N*-benzoyl-*N'*-(cyclohexyl)thiourea (Triclinic  $P\bar{1}$ ,  $R_1 = 2.10\%$ ) and *N*-benzoyl-*N'*-(isopentyl)thiourea (Triclinic  $P\bar{1}$ ,  $R_1 = 5.06\%$ ). It was established that these ligands exhibit a *keto* conformation in the solid state, where the carbonyl oxygen is *trans* to the sulphur atom and is stabilized by a hydrogen bond interaction with the terminal nitrogen atom of the thiourea moiety. The *keto* conformation was also confirmed in solution by NMR spectroscopy. Furthermore, hydrogen bond interactions exist between neighbouring molecules in the solid state, which leads to either dimer or polymer formation in the crystal packing of these thiourea compounds.

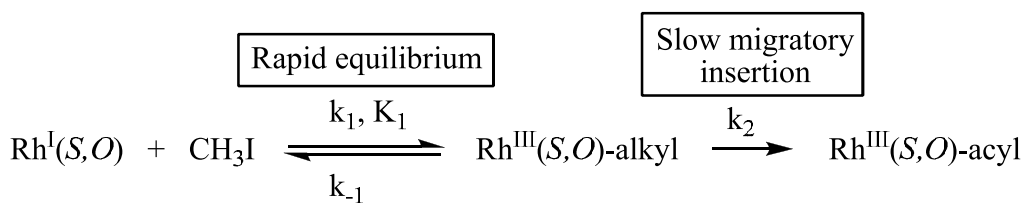
The  $[\text{Rh}(\text{diphosphine})(\text{CO})_2]^+$  complexes could not be successfully synthesized, however, during several attempts one synthetic route led to the formation of a cationic A-frame complex of the type  $[\text{Rh}_2(\mu\text{-Cl})(\text{diphosphine})_2(\text{CO})_2]\text{BF}_4$ . The X-ray crystallographic structure of  $[\text{Rh}_2(\mu\text{-Cl})(\text{dppm})_2(\text{CO})_2]\text{BF}_4$  (Monoclinic  $P2_1/n$ ,  $R_1 = 8.84\%$ ) is reported.

Several  $[\text{Rh}(S,O\text{-thioureato})(\text{CO})_2]$  complexes were synthesized and characterized, however, these complexes were unstable outside of solution. Several attempts were made to synthesize  $[\text{Rh}(S,O\text{-thioureato})(\text{CO})(\text{PPh}_3)]$  complexes, which led to the isolation of rhodium thiourea complexes where the thiourea ligands exhibit *S,O*-, *S*- and *N,S*-coordination modes. The X-ray crystallographic structures of the following complexes are reported:  $[\text{Rh}(N,S\text{-}(N\text{-}4\text{h}2\text{mPT}))(\text{CO})(\text{PPh}_3)_2]$  (Triclinic  $P\bar{1}$ ,  $R_1 = 2.75\%$ ),  $[\text{Rh}(N,S\text{-}(N\text{-PT}))(S,O\text{-}(N\text{-PT}))(\text{PPh}_3)_2]$  (Triclinic  $P\bar{1}$ ,  $R_1 = 4.44\%$ ),  $[\text{Rh}(\text{COD})(\text{Cl})(S\text{-}(N\text{-PTH}))]$  (Triclinic  $P\bar{1}$ ,  $R_1 = 3.18\%$ ),  $[\text{Rh}(\text{COD})(\text{Cl})(S\text{-}(N\text{-tmPTH}))]$  (Monoclinic  $C2/c$ ,  $R_1 = 6.74\%$ ).  $[\text{Rh}(N,S\text{-}(N\text{-}4\text{h}2\text{mPT}))(\text{CO})(\text{PPh}_3)_2]$  is analogous to typical Vaska-type complexes, where the coordinated thiourea ligand is *trans* to the carbonyl ligand and the two  $\text{PPh}_3$  are *trans* to each other on the rhodium centre.  $[\text{Rh}(N,S\text{-}(N\text{-PT}))(S,O\text{-}(N\text{-PT}))(\text{PPh}_3)_2]$  is a Rh(III) species with an octahedral arrangement around the rhodium centre, where one of thiourea ligands coordinated in its *enol* conformation. In both  $[\text{Rh}(\text{COD})(\text{Cl})(S\text{-}(N\text{-PTH}))]$  and  $[\text{Rh}(\text{COD})(\text{Cl})(S\text{-}(N\text{-tmPTH}))]$  the preferred orientation of the free ligands translated to the orientation of the coordinated ligands. These complexes were also stabilized by hydrogen bond interactions between the chlorido ligand and the internal nitrogen atom of the thiourea moiety.

A range of  $[\text{Rh}(S,O\text{-}(N\text{-diPT}))(\text{CO})(\text{PR}_1\text{R}_2\text{R}_3)]$  complexes were successfully synthesized using *N*-benzoyl-*N',N'*-(diphenyl)thiourea and a range of phosphine ligands with systematically changing electro-steric properties ( $\text{PPh}_3$ ,  $\text{PPh}_2\text{Cy}$ ,  $\text{PPhCy}_2$ ,  $\text{PCy}_3$ ). The X-ray crystallographic structures of the following complexes are reported:  $[\text{Rh}(S,O\text{-}(N\text{-diPT}))(\text{CO})(\text{PPh}_3)]$  (Monoclinic  $P2_1/c$ ,  $R_1 = 6.86\%$ ),  $[\text{Rh}(S,O\text{-}(N\text{-diPT}))(\text{CO})(\text{PPh}_2\text{Cy})]$  (Monoclinic  $P2_1/c$ ,  $R_1 = 6.32\%$ ),  $[\text{Rh}(S,O\text{-}(N\text{-diPT}))(\text{CO})(\text{PCy}_3)]$  (Monoclinic  $P2_1/c$ ,  $R_1 = 6.86\%$ ). The respective first order coupling constants ( $^1J_{\text{Rh-P}}$ ) and the carbonyl stretching frequencies ( $\nu_{\text{CO}}$ ) were obtained, from which the expected order of electronic effects of the phosphine ligands was established. The

effective cone angles ( $\theta_E$ ) for the different phosphine ligands were also calculated, which correlated well with the expected steric congestion of the ligands on the rhodium centre.

The reactivity of the  $[\text{Rh}(\text{S},\text{O}-(N\text{-diPT}))(\text{CO})(\text{PR}_1\text{R}_2\text{R}_3)]$  complexes towards the iodomethane oxidative addition was investigated. In general the reaction rate of the individual reactions increased in the order of  $[\text{Rh}(N\text{-diPT})(\text{CO})(\text{PPhCy}_2)] < [\text{Rh}(N\text{-diPT})(\text{CO})(\text{PCy}_3)] < [\text{Rh}(N\text{-diPT})(\text{CO})(\text{PPh}_3)] < [\text{Rh}(N\text{-diPT})(\text{CO})(\text{PPh}_2\text{Cy})]$ . This order of reactivity was ascribed to a combinative effect of both the steric and electronic properties of the phosphine ligands. The activation parameters calculated for the individual reactions were found to be similar. The proposed mechanism for the iodomethane oxidative addition to complexes of the type  $[\text{Rh}(\text{S},\text{O}\text{-thioureato})(\text{CO})(\text{L})]$ , where  $\text{L} = \text{CO}/\text{PR}_1\text{R}_2\text{R}_3$ , is depicted in Scheme I.



where  $\text{Rh}^{\text{I}}(\text{S},\text{O}) = [\text{Rh}(\text{S},\text{O}\text{-thioureato})(\text{CO})(\text{L})]$

$\text{Rh}^{\text{III}}(\text{S},\text{O})\text{-alkyl} = [\text{Rh}(\text{S},\text{O}\text{-thioureato})(\text{Me})(\text{CO})(\text{I})(\text{L})]$

$\text{Rh}^{\text{III}}(\text{S},\text{O})\text{-acyl} = [\text{Rh}(\text{S},\text{O}\text{-thioureato})(\text{COMe})(\text{I})(\text{L})]$

$\text{L} = \text{CO}$  or  $\text{PR}_1\text{R}_2\text{R}_3$ ,  $\text{S} = \text{solvent}$

**Scheme I The reaction scheme for the iodomethane oxidative addition to  $[\text{Rh}(\text{S},\text{O}\text{-thioureato})(\text{CO})(\text{L})]$ , where  $\text{L} = \text{CO}/\text{PR}_1\text{R}_2\text{R}_3$  and  $\text{S} = \text{solvent}$ .**

The electro-steric effects of phosphine ligands in catalytic processes were further investigated by studying these effects in the phosphine exchange reactions of Vaska-type complexes  $[\text{Rh}(\text{Cl})(\text{CO})(\text{PR}_1\text{R}_2\text{R}_3)_2]$  with the corresponding  $\text{PR}_1\text{R}_2\text{R}_3$  ligand *via* NMR techniques. The reaction rate for the exchange reaction was almost two orders of magnitude faster for  $\text{PPh}_3$  than for  $\text{PPh}_2\text{Cy}$ . Both exchange processes exhibited a large negative  $\Delta S^\ddagger$  and a small  $\Delta H^\ddagger$ , which suggested an associative activation, where a stable 5-coordinated transition state is formed.



Keywords: Rhodium

*S,O*-thiourea

Phosphine

Oxidative addition

Exchange reaction

Homologation

Carbonylation

# **CHAPTER 1**

## **BASIC CONCEPTS OF RHODIUM CHEMISTRY, LIGAND PROPERTIES AND THE AIM OF THE STUDY**

### **1.1 Introduction to catalysis**

Catalysis is one of the most important and most widely studied fields in chemistry. It is considered to be the key for the successful initiation and facilitation of a wide range of chemical reactions and in the selective production of valuable compounds. It plays a vital role in biological systems to ensure that an organism functions appropriately in response to demands and its environment, therefore ensuring its survival. In the industry today catalysis has a wide range of applications including the production of liquid fuels and bulk chemicals and is used in the production of many fine chemicals.

About 150 years ago Berzelius<sup>1</sup> discovered that certain species, which were referred to as “ferments”, caused noticeable changes in substances when brought in contact with them and therefrom created the concept of catalysis. In 1895 Oswald designed a definition for the term catalysis, which is as follows: *A catalyst is a substance that changes the rate of a chemical reaction without itself appearing into the products.*<sup>2</sup> This definition was later modified to state that a catalyst increases the rate of a chemical reaction by lowering its activation energy, but does not become involved in the reaction itself.<sup>2</sup>

Catalysis is divided into two major classes namely homogeneous and heterogeneous catalysis. Homogeneous catalysis involves a system where all of the components of a reaction, including the catalyst, exist in one phase, which in most cases is a liquid phase. Good examples include the hydroformylation reaction, Diels-Alder reactions catalysed by Lewis acids, the methanol carbonylation (Monsanto and Cativa processes) and the hydrogenation

---

<sup>1</sup> Roberts, M.W. (2000) *Zeit. Catal. Lett.*, **67**, 1.

<sup>2</sup> van Leeuwen, P.W.N.M. (2004) *Homogeneous Catalysis, Understanding the art*, Kluwer Academic Publishers, Dordrecht.

reaction.<sup>2</sup> In heterogeneous catalysis, on the other hand, multiple phases are present, as in the case, for example, of the Fischer-Tropsch process which uses iron carbides as the catalyst.<sup>3</sup>

## 1.2 Rhodium systems

Rhodium is one of the most studied transition metals to date due to its importance in various applications including catalysis and biological activity.<sup>4</sup> Rhodium is a well-known good catalyst for several industrial processes including the Monsanto process,<sup>5a,b</sup> hydroformylation,<sup>6</sup> and alkene hydrogenation<sup>7</sup>. A large number of rhodium complexes have been synthesised and reported to date, having different kinds of mono-, bi- and tridentate ligands. Amongst them phosphine ligands have been extensively used, since it has been shown to have a significant importance in catalytic processes as was illustrated by Roth *et al.*<sup>5b</sup>

## 1.3 Ligand effects in transition metal chemistry

There are many types of catalysts but amongst them one of the most important classes includes organometallic catalysts. These catalysts involve a metal centre onto which organic ligands are co-ordinated, which in turn is allowed by the metal d-orbitals. Due to the fact that transition metals can alter between several oxidation states and have the ability to exhibit a range of co-ordination numbers, the ligands can co-ordinate in many different ways. Research has shown not only that the type of metal centre determines the activity of a catalyst,<sup>8</sup> but also that the ligands play a vital role in determining the properties of the catalyst. In general, the ligands govern the efficiency and selectivity of the catalyst, which in turn is dependent on the type of ligand, its basicity (or electron density) and its size (steric properties). Some influences of ligands relevant to this study are further discussed below.

---

<sup>3</sup> Parshall, G.W.; Putscher R.E. (1986) *J. Chem. Educ.*, **63**, 189.

<sup>4</sup> Dutta, D.K; Singh, M. M. (1994) *Trans. Met. Chem.*, **19**, 290.

<sup>5</sup> a) Paulik, F. E.; Roth, J. F. (1968) *J. Chem. Soc., Chem. Commun.*, 1578. b) Roth, J. F.; Craddock, J. H.; Hershman, A.; Paulik, F. E. (1971) *Chem. Tech.*, 600.

<sup>6</sup> Evans, D.; Osborn, J.A.; Wilkinson, G. (1968) *J. Chem. Soc. (A)*, 3133.

<sup>7</sup> Halpern, J. (1981) *Inorg. Chim. Acta*, **50**, 11.

<sup>8</sup> Henke, C.O.; Brown, O.W. (1924) *J. Phys. Chem.*, **28**, 71.

### 1.3.1 Phosphine ligands

Phosphine ligands have a wide application in organometallic chemistry as well as in the industry.<sup>2</sup> The basicity of a phosphine ligand is determined by the types of groups that are bonded to the phosphorus atom. If alkyl groups are present on a phosphorus atom, the result will be the formation of strong bases, since the alkyl groups are found to be fairly electron donating.<sup>9</sup> These ligands therefore become good  $\sigma$ -donors and will donate electron density onto a metal centre. On the other hand, organophosphites are considered to be  $\pi$ -acceptors as they form stable complexes with electron-rich transition metals.<sup>10</sup>

This  $\pi$ -acidity and  $\sigma$ -basicity of phosphine ligands can be established on the basis of CO vibrational frequency changes using complexes such as  $\text{NiL}(\text{CO})_3$  or  $\text{CrL}(\text{CO})_5$  (where L = phosphine ligand).<sup>11,12</sup> The steric properties of phosphine ligands also play a large role in the activity of a catalyst. It is quite difficult to separate this parameter from the electronic parameter, as they are often closely related, but a few methods have been developed to describe the relative steric properties of phosphine ligands. These methods are also different for monodentate ligands compared to bidentate ligands, which are discussed in more detail in Chapter 2.

### 1.3.2 Benzoylthiourea ligands

Many bidentate ligands have been studied extensively including acetylacetone, tropolone, etc. and the derivatives thereof,<sup>13</sup> which in many cases only have two  $\sigma$ -donor atoms that can co-ordinate. Moreover, many of these bidentate ligands are found in a *cis* or close to *cis* orientation, which allow them to co-ordination easily in a bidentate fashion. *N*-benzoylthiourea ligands on the other hand have at least four atoms with high amounts of  $\sigma$ -electron density as shown in Figure 1.1, which can all potentially co-ordinate onto a metal centre. Also note that generally these ligands are found in a conformation where the oxygen

---

<sup>9</sup> Ohgomori, Y.; Yoshida S.I.; Watanabe, Y. (1987) *J. Mol. Catal.*, **43**, 249.

<sup>10</sup> Mooney, E.F.; Thornhill, B.S. (1966) *J. Inorg. Nucl. Chem.*, **28**, 2225.

<sup>11</sup> Tolman, C.A. (1970) *J. Am. Chem. Soc.*, **92**, 2953.

<sup>12</sup> Strohmeier, W.; Müller, F.J. (1967) *Chem Ber.*, **100**, 2812.

<sup>13</sup> Typical examples are: a) Boese, R; Antipin, M. Y.; Bläser, D.; Lyssenko, K. A. (1998) *J. Phys. Chem. B*, **102**, 44, 8654. b) Jing, Z.-L.; Zhang, S.-J.; Yang, N.; Feng, S.-C. (2007) *Acta Cryst.*, **E63**, o3203. c) Steyl, G.; Kruger, G. J.; Roodt, A. (2004). *Acta Cryst.* **C60**, m473.

atom lies *trans* with respect to the sulphur atom, as shown and discussed in the Chapters 3 and 4 later on.

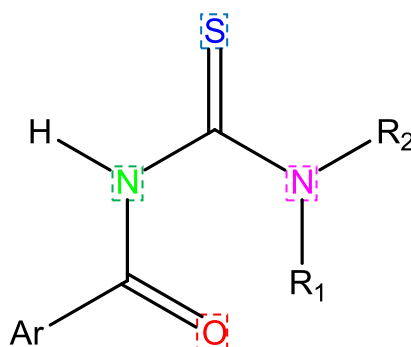


**Figure 1.1 Diagram of a basic *N*-benzoylthiourea compound having four  $\sigma$ -donors**

The way these ligands will co-ordinate to a metal centre is determined by several factors including the type of metal centre used, the reaction conditions (especially pH) and the basicity and nucleophilicity as well as steric properties of the ligand. Generally, metal ions are classified in two groups, which define them as either hard or soft acids.<sup>14</sup> It was discovered that hard metals interact with hard bases and soft metals with soft bases. Therefore in a case where a soft metal such as  $\text{Rh}^+$ ,  $\text{Pd}^{2+}$  and  $\text{Pt}^{2+}$  is used in a reaction with a *N*-benzoylthiourea ligand, the order of tendency for the different  $\sigma$ -donors to complex with the metal centre is normally found to be  $\text{S} \gg \text{O} \gg \text{N}$ . Therefore, it is expected that these ligands would preferably co-ordinate in a *S,O*-fashion with these type of metals, of which some examples can be found in literature.<sup>15</sup>

Furthermore co-ordination of these ligands in this fashion leads to the formation of a six-membered chelate ring, which generally is considered to be energetically favourable. It is also known that the  $\alpha$ -proton found between electron-withdrawing groups, as in the case of  $\beta$ -diketone compounds, is quite acidic and in the presence of a base this proton can easily be withdrawn.<sup>16</sup> This allows electron delocalisation in the ligand that in turn enhances the

<sup>14</sup> Huheey, J. E.; Keiter, E. A.; Keiter, R. L. (1993) *Inorganic Chemistry: Principles of structure and reactivity 4<sup>th</sup> Ed*, New York, HarperCollins College Publishers, 344.

<sup>15</sup> a) Koch, K. R.; du Toit, J.; Caira, M. R.; Sacht, C (1994) *J. Chem. Soc., Dalton Trans.*, 785. b) Koch, K. R.; Hallale, O.; Bourne, S. A.; Miller, J.; Bacsá, J. (2001) *J. Mol. Struct.*, **561**, 185. c) Westra, A. N.; Esterhuysen, C.; Koch, K. R. (2004) *Acta Cryst.*, **C60**, m395. d) Westra, A. N.; Bourne, S. A.; Esterhuysen, C.; Koch, K. R. (2005) *Dalton Trans.*, 2162 and references within.

<sup>16</sup> Solomons, T. W. G.; Fryhle, C. B. (2000) *Organic Chemistry 7<sup>th</sup> Ed.*, New York, John Wiley & Sons, Inc., 878.

ligand's nucleophilicity. Thus reactions of these thiourea ligands with a metal centre in a basic medium will enhance the ability of these ligands to co-ordinate in a bidentate fashion *via* the S and O atoms.

Further co-ordination of a secondary mono-ligand could lead to the formation of possible isomers due to the decrease of the symmetry on the metal centre. However, since sulphur atoms are regarded to be better  $\sigma$ -donors than oxygen atoms, a major isomer is expected in many cases. This is the result of inherent properties of ligands co-ordinated on a metal centre defined by the thermodynamic *trans*-influence.<sup>14</sup> *Trans*-effect on the other hand is the labilization of ligands that are *trans* to specific ligands, which is otherwise defined as *trans*-directing ligands.<sup>17</sup>

Thiourea ligands have been found to have several potential applications. One of many includes liquid-liquid extraction, preconcentration and separation as well as trace determination of platinum group complexes,<sup>18a,b</sup> since these ligands have been found to possess a significant affinity to co-ordinate to these metal centres.<sup>19a,b</sup> Also since these ligands are extremely versatile, where the aryl and R groups (Figure 1.6) can easily be altered, a range of ligands can be obtained having various chemical and physical properties. Thus these ligands can be used to tune the biological activity of platinum complexes for their purpose as chemotherapeutic drugs.<sup>20a,b</sup> Another great application with these ligands is the design of insoluble thiourea-functionalised silica-xerogels, which act as a support to anchor rhodium catalysts.<sup>21</sup> In this manner the catalyst can easily be recovered after undergoing some catalytic process in a soluble medium such as hydroformylation. It has also been shown that chiral thiourea ligands can induce better enantioselectivity in the hydroformylation of styrene without the presence of phosphorus ligands.<sup>22</sup>

---

<sup>17</sup> Basolo, F.; Pearson, R. G. (1962) *Prog. Inorg. Chem.*, **4**, 381.

<sup>18</sup> a) Schuster, M.; Schwarzer, M. (1996) *Anal. Chim. Acta*, **328**, 1. b) Merdivan, M.; Gungor, A.; Savasci, S.; Aygun, R. S. (2000) *Talanta*, **53**, 141.

<sup>19</sup> a) König, K. H.; Schuster, M.; Steinbrech, B.; Schneeweis, G.; Schlodder, R. (1985) *Fresenius' Z. Anal. Chem.*, **321**, 457. b) Vest, P.; Schuster, M.; König, K. H. (1989) *Fresenius' Z. Anal. Chem.*, **335**, 759.

<sup>20</sup> a) Sacht, C.; Datt, M. S.; Otto, S.; Roodt, A. (2000) *J. Chem. Soc., Dalton Trans.*, 727. b) Sacht, C.; Datt, M. S.; Otto, S.; Roodt, A. (2000) *J. Chem. Soc., Dalton Trans.*, 4579.

<sup>21</sup> Cauzzi, D.; Lanfranchi, M.; Marzolini, G.; Predieri, G.; Tiripicchio, A.; Costa, M.; Zanoni, R. (1995) *J. Organomet. Chem.*, **488**, 115.

<sup>22</sup> Breuzard, J. A. J.; Tommasino, M. L.; Bonnet, M. C.; Lemaire, M. (2000) *C. R. Acad. Sci. Paris, Série IIc, Chimie : Chemistry*, **3**, 557.

## 1.4 Aim of the study

As was pointed out in the introduction, rhodium complexes having phosphine or thiourea ligands show potential in many catalytic processes where syngas is utilized. An important technology identified for this study is the homologation of methanol to ethanol using syngas and a range of rhodium complexes and an investigation of factors of some importance thereto. This process is derived from the Monsanto process, where the final step is modified by adding hydrogen gas to allow the hydrogenation of the acyl and reductive elimination to ethanol instead of the reductive elimination of acyl-iodide and hydrolysis to acetic acid. This investigation mainly focuses on the synthesis of rhodium square-planar complexes containing *P,P*- and *S,O*- bidentate ligands (Figure 1.2) and their potential application in the catalytic carbonylation and homologation reaction of methanol.

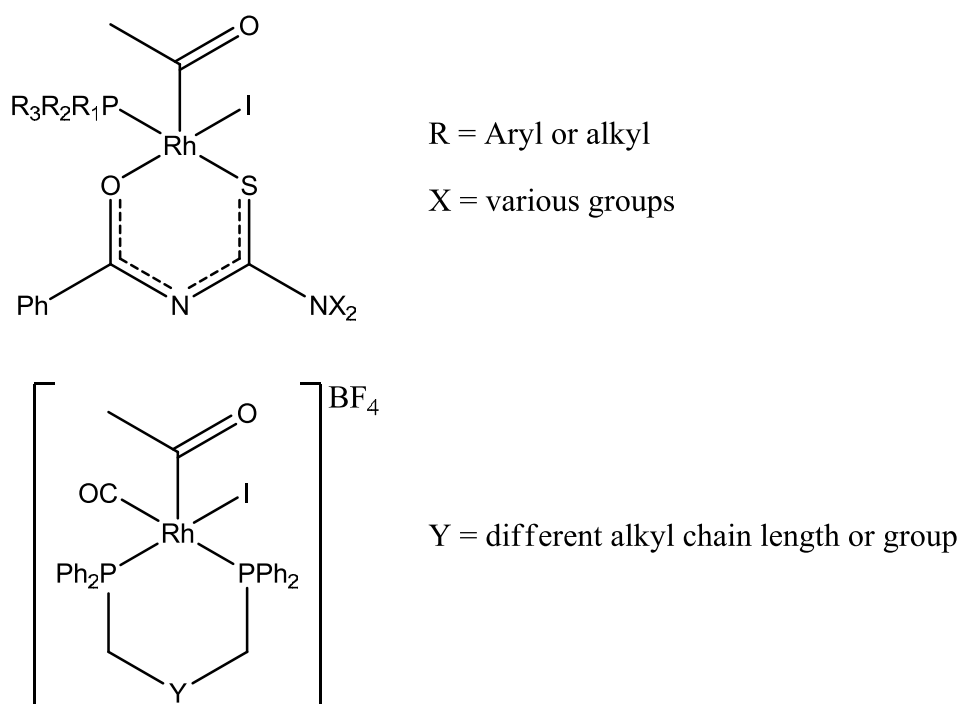


**Figure 1.2 Schematic presentation of typical rhodium acyl complexes having either *S,O*-thiourea or diphosphine ligands.**

Therefore the aims set for this investigation primarily include some key steps involved in the Monsanto process, which consist of the following:

1. Synthesis and characterization of functionalised *S,O*-thiourea ligands.
2. Solid state characterization of the functionalised *S,O*-thiourea ligands to determine molecular geometrical parameters.
3. Synthesis and characterization of rhodium complexes containing diphosphine ligands to obtain the square planar rhodium diphosphine dicarbonyl complexes.
4. Co-ordination of *S,O*-thiourea ligands to rhodium to obtain the square planar rhodium *S,O*-thiourea complexes.
5. Solid state characterization of the rhodium complexes having either diphosphine or *S,O*-thiourea ligands to determine the solid state packing modes as well as the molecular geometrical parameters.
6. Investigation of the influences of functionalised thiourea and various tertiary phosphine ligands on the reactivity of the rhodium centre to the oxidative addition of iodomethane by evaluating the kinetic and thermodynamic parameters.
7. Study the reductive elimination of iodomethane/acetyl iodide from these Rh(III)acyl complexes
8. Investigation of possible phosphine exchange reactions in phosphine modified rhodium complexes by evaluating the kinetic and thermodynamic parameters.
9. Investigation of the viability of  $[\text{Rh}(\text{S},\text{O}\text{-thiourea})(\text{CO})(\text{PR}_1\text{R}_2\text{R}_3)]$  as a catalytic precursor for the homologation of methanol by studying the effect of addition of hydrogen to the isolated  $[\text{Rh}(\text{S},\text{O}\text{-thiourea})(\text{acetyl})(\text{PR}_1\text{R}_2\text{R}_3)(\text{I})]$  complexes.

With this in mind a theoretical overview of related literature is given in Chapter 2. The synthesis and characterization of *S,O*-thiourea ligands will be discussed in Chapters 3 and 4, with their successive use in synthesizing Rh(I) complexes of the type  $[\text{Rh}(\text{S},\text{O}\text{-thiourea})(\text{CO})_2]$  and  $[\text{Rh}(\text{S},\text{O}\text{-thiourea})(\text{CO})(\text{PR}_3)]$ , which will be discussed in Chapter 6 and 7. Some other variations of Rh(I) complexes with the thiourea ligands that were discovered during the study will also be presented in Chapter 6. The synthesis and characterization of possible  $[\text{Rh}(\text{biphosphine})(\text{CO})_2]^+$  complexes will be provided and discussed in Chapter 5. A study on the kinetic and thermodynamic parameters of the iodomethane oxidative addition to  $[\text{Rh}(\text{S},\text{O}\text{-thiourea})(\text{CO})(\text{PR}_3)]$  to obtain the corresponding Rh(III)-acyl species will be shown and discussed in Chapter 8. Lastly due to the importance of chemical exchange processes in



transition metal chemistry and the small contribution in the literature on phosphine exchange reactions on Rh(I) complexes, a study on the kinetic and thermodynamic parameters of phosphine exchange of Vaska-type  $[\text{Rh}(\text{CO})(\text{Cl})(\text{PR}_1\text{R}_2\text{R}_3)_2]$  complexes was also performed, which is presented and discussed in Chapter 9.

# **CHAPTER 2**

## **THEORETICAL STUDY ON**

### **CARBONYLATION/HOMOLOGATION PROCESSES AND**

### **IMPORTANT CHEMISTRY IN CATALYSIS**

#### **2.1 Introduction**

The main aim in the study involved the investigation of possible homologation of methanol to ethanol by determining the outcome of the reaction between syngas and rhodium(III)-acyl complexes consisting of specific bidentate ligands. A literature overview will therefore be given on carbonylation/homologation reactions and related aspects within this chapter. The aspects to be discussed will include direct and indirect routes for the synthesis of commodities using syngas, chemical exchange reactions, oxidative addition and reductive elimination reactions as well as advances in hydrocarbonylation reactions of methanol and derivatives by platinum-group metals.

#### **2.2 Syngas (H<sub>2</sub>/CO) as a building block in catalysis**

A large variety of commodities are produced on a daily basis in industry from the simple combination of hydrogen gas (H<sub>2</sub>) and carbon monoxide (CO), which is commonly referred to as syngas or synthesis gas.<sup>1,2</sup> Syngas is normally produced by the gasification of coal, natural gas or biomass<sup>3,4</sup> and is regarded as one of the most important building blocks as it is used in many well-known catalytic processes for the production of liquid products. Processes that involve syngas are subdivided into direct and indirect processes/routes depending on how the syngas mixture is utilized. These two routes will be discussed in Sections 2.2.1 and 2.2.2, respectively.

---

<sup>1</sup> van Leeuwen, P.W.N.M. (2004) *Homogeneous Catalysis, Understanding the art*, Kluwer Academic Publishers, Dordrecht.

<sup>2</sup> Knifton, J. F.; Lin, J. J. (1989) *App. Organomet. Chem.*, **3**, 557.

<sup>3</sup> Höök, M.; Aleklett, K. (2010) *J. Energy Res.*, **34**, 10, 848.

<sup>4</sup> Rostrup-Nielsen (2004) *Catal. Rev.-Sci. Eng.*, **46**, 247.

### 2.2.1 Direct synthetic routes involving syngas

The direct routes for the synthesis of commodities from syngas involve as defined by the term the direct conversion of a combination of H<sub>2</sub> and CO to a range of products or as otherwise stated the hydrogenation of CO. Depending on the amounts used in the ratio of H<sub>2</sub>/CO a whole series of products are possible as shown in Figure 2.1.

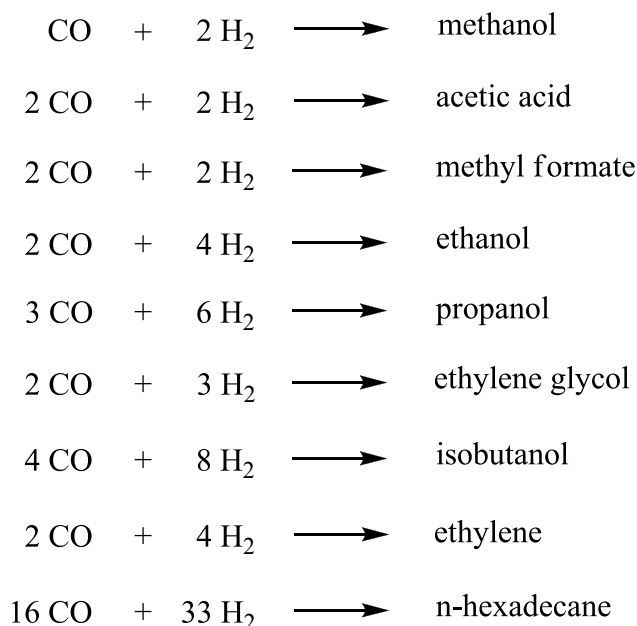


**Figure 2.1 The range of products that can be obtained from the direct utilizing of syngas.**

Extensive research has been done on CO hydrogenation especially in the 1980's, which showed that apart from the syngas amounts, the type of catalyst and reaction conditions determine the outcome of these reactions. A first example includes the use of Ru catalysts in the presence of ionic halide promoters such as KI and PPNCl in donor solvents such as sulfolane, which led to successful transformation of syngas to methanol.<sup>5a,b</sup> This reaction was also accompanied by the synthesis of ethylene glycol. Selectivities towards ethylene glycol could be achieved by performing the reaction in different solvent systems including basic solvents such as N-methylpyrrolidinone or acidic solvents such as carboxylic acids.<sup>2a;6a,b</sup>

<sup>5</sup> a) Dombek, B.D. (1981) *J. Am. Chem. Soc.*, **103**, 6508. b) Ono, H.; Fujiwara, K.; Hashimoto, M.; Watanabe, H.; Yoshida, K. (1990) *J. Mol. Catal.*, **58**, 289.

<sup>6</sup> a) Knifton, J.F. (1982) *J. Catal.*, **76**, 101. b) Dombek, B.D. (1983) *J. Organomet. Chem.*, **250**, 467.

However, by altering the solvent system to phosphine oxides and using a 1:1 ratio of HI and Ru instead, the reaction is directed primarily towards the formation of ethanol.<sup>7</sup> It was shown that as the Ru catalyst is responsible for the hydrogenation of CO to form methanol, the presence of the acidic species  $[R_3POH]^+$  causes the activation of methanol to undergo homologation forming the subsequent ethanol.

The use of an Ir-carbonyl complex at high temperatures and 2000 bar of 1:1 syngas resulted primarily in the formation of methanol and methyl formate, although small amounts of ethanol, propanol and ethylene glycol were also obtained.<sup>8</sup> The first conversion of syngas into ethylene glycol was reported by DuPont where Co complexes were applied as catalysts, but selectivities were low.<sup>9</sup> Later it was shown that Rh catalysts in the presence of nitrogen bases and alkali cations provided much higher yields of ethylene glycol at high temperatures and pressures.<sup>10</sup> A few other catalysts including rhenium,<sup>11</sup> iridium<sup>12</sup> and platinum<sup>13</sup> were also applied for glycol synthesis but did not show to have any advantage above the Ru and Rh systems.

These are but a few examples found in literature, however, it is clear that CO hydrogenation can lead to the formation of different types of liquid products depending on the catalytic system involved. These discoveries led to important applications that are still used in industry today, which include for example the conversion of syngas to gasoline and waxes *via* Fischer-Tropsch synthesis using Co- and Fe-type catalysts.<sup>5,14</sup> The industrial production of methanol and ethanol are also important examples, which will be discussed in more depth later in this chapter.

---

<sup>7</sup> Warren, B. K.; Dombek, B. D. (1983) *J. Catal.*, **79**, 334.

<sup>8</sup> Keim, W.; Anstock, M.; Roper, M.; Schlupp, (1984) *J. C<sub>1</sub> Mol. Chem.*, **1**, 21.

<sup>9</sup> Dombek, B.D. (1983) *Adv. Catal.*, **32**, 325.

<sup>10</sup> Pruett, R.I. (1977) *Annu. N.Y. Acad. Sci.*, **295**, 239.

<sup>11</sup> Ishino, M.; Deguchi, T.; Takano, T.; Nakamura, S. (1989) *J. Mol. Catal.*, **49**, 315.

<sup>12</sup> Takano, T.; Deguchi, T.; Ishino, M.; Nakamura, S. (1986) *J. Organomet. Chem.*, **309**, 209.

<sup>13</sup> Roeper, M.; Schieren, M.; Fumagalli, A. (1986) *J. Mol. Catal.*, **34**, 173.

<sup>14</sup> Huber, G. W.; Iborra, S.; Corma, A. (2006) *Chem. Rev.*, **106**, 4044.

### 2.2.2 Indirect synthetic routes involving syngas

Indirect synthetic routes for different commodities include the use of an extra intermediate or reagent such as methanol, methyl formate and formaldehyde in combination with the syngas.<sup>15</sup> It is known for example that formaldehyde can undergo hydrocarbonylation with Co-catalysts to provide glycolaldehyde, as discovered in 1975 by Yukawa *et al.*<sup>16</sup> By modifying the system with the addition of phosphines and using high temperatures (180 °C), a direct conversion to ethylene glycol was observed due to higher hydrogenation activity of the catalyst.<sup>17</sup> Carbonyl rhodium hydride complexes have also been shown to be effective for the “one-pot” synthesis of ethylene glycol from formaldehyde.<sup>18</sup>

Another important indirect use of syngas includes the hydroformylation of olefins, which have been extensively studied in literature. This reaction was discovered by accident when Roelen was studying the Fischer-Tropsch process with a heterogeneous cobalt catalyst.<sup>19</sup> He showed that the reaction involved the conversion of alkenes to aldehydes and alcohols and that the reaction was not catalysed by the supported cobalt, but in truth by the complex  $[\text{HCo}(\text{CO})_4]$ , which had formed in the liquid state. Later on it was discovered that rhodium could also be used as a catalyst, which in many cases has shown to be more efficient and that milder conditions could be used.<sup>20</sup>

The hydrocarbonylation reactions of methanol and derivatives with syngas are also examples of indirect synthetic routes, which will be discussed in more detail in Section 2.3. The effectiveness of catalysts to transform syngas and other building blocks to certain products is related to their ability to undergo a wide variety of reactions including exchange/substitution, insertion/migration, oxidative addition and reductive elimination reactions. Therefore, brief definitions and descriptions of these chemical reactions of complexes will be provided in Section 2.4.

---

<sup>15</sup> Keim, W. (1989) *J. Organomet. Chem.*, **372**, 15.

<sup>16</sup> Yukawa, T.; Kawasaki, K.; Wakamatsu, H. (1975) *Ger. Patent*, 2427954; (1975) *C. A.*, **82**, 124761.

<sup>17</sup> Murata, K.; Matsuda, A.; Masuda, T. (1988) *Bull. Chem. Soc. Jpn.*, **61**, 325.

<sup>18</sup> Kotowski, W.; Freiberg, J.; Spisak, W.; Zamorowska-Biernacik, S. (1989) *Chem. Biochem. Eng. Q.*, **3**, 47.

<sup>19</sup> Cornils, B.; Hermann, W. A.; Rasch, M. (1994) *Angew. Chem. Int. Ed.*, **33**, 2144.

<sup>20</sup> Evans, D.; Osborn, J.A.; Wilkinson, G. (1968) *J. Chem. Soc. (A)*, 3133.

## 2.3 Hydrocarbonylation reactions of MeOH and derivatives

### 2.3.1. Methanol

Methanol is another important building block for the production of many chemicals and fuels, which include acetic acid, formaldehyde, olefins, gasoline and dimethyl ether.<sup>21a,b,c</sup> As was already shown in section 2.2.1, methanol can be produced directly from syngas using different catalysts. It has also been shown that the addition of a proper amount of CO<sub>2</sub> led to high yields of methanol and therefore much attention has also been given to the hydrogenation of CO<sub>2</sub>.<sup>22a,b</sup> Although there are several catalysts that can perform the syngas conversion to methanol, the best catalytic system found thus far involves a combination of Cu and Zn complexes as discussed in a recent review.<sup>23</sup> It is shown here that many researchers found that the Cu/Zn catalytic system show high activity for both the hydrogenation of CO and CO<sub>2</sub>, where its generally accepted that the Cu activates the CO<sub>x</sub> species, while the Zn allows the splitting of the H<sub>2</sub> molecule.

Several reviews have already been written on the hydrocarbonylation and related reactions of methanol and the range of products that can be obtained as a result.<sup>24</sup> Figure 2.2 gives a schematic diagram of some of the most important synthetic routes that methanol can follow with the addition of CO and/or H<sub>2</sub> under different conditions. The main processes presented in the scheme include homologation (hydrocarbonylation) (**a**), carbonylation (**b**), etherification (**c**), hydrogenation (**d**) and esterification (**e**).

---

<sup>21</sup> a) Ortelli, E. E.; Wambach, J.; Wokaun, A. (2001) *Appl. Catal. A*, **216**, 227. b) Lee, S.; Sardesai, A. (2005) *Top. Catal.*, **32**, 197. c) Cheung, P.; Bhan, A.; Sunley, G.; Iglesia, E. (2006) *Angew. Chem., Int. Ed.*, **45**, 1617.

<sup>22</sup> a) Melian-Cabrera, I.; Granados, M. L.; Fierro, J. L. G. (2002) *J. Catal.*, **210**, 285. b) Jessop, P. G.; Ikariya, T.; Noyori, R. (1995) *Chem. Rev.*, **95**, 2, 259 and references within.

<sup>23</sup> Liu, X.-M.; Lu, G. Q.; Yan, Z.-F.; Beltramini, J. (2003) *Ind. Eng. Chem. Res.*, **42**, 6518.

<sup>24</sup> Braca, G.; Raspolli Galletti, A. M.; Sbrana, G. (1994) *Oxygenates by Homologation or CO Hydrogenation with Metal Complexes*. In *Heterogeneous Enantioselective Hydrogenation: Theory and Practise*, edited by Klabunovskii, E. I.; Smith, G. V.; Zsigmond, A. (2006), Kluwer Academic Publishers, Dordrecht, Ch. 16, 90 and references within.

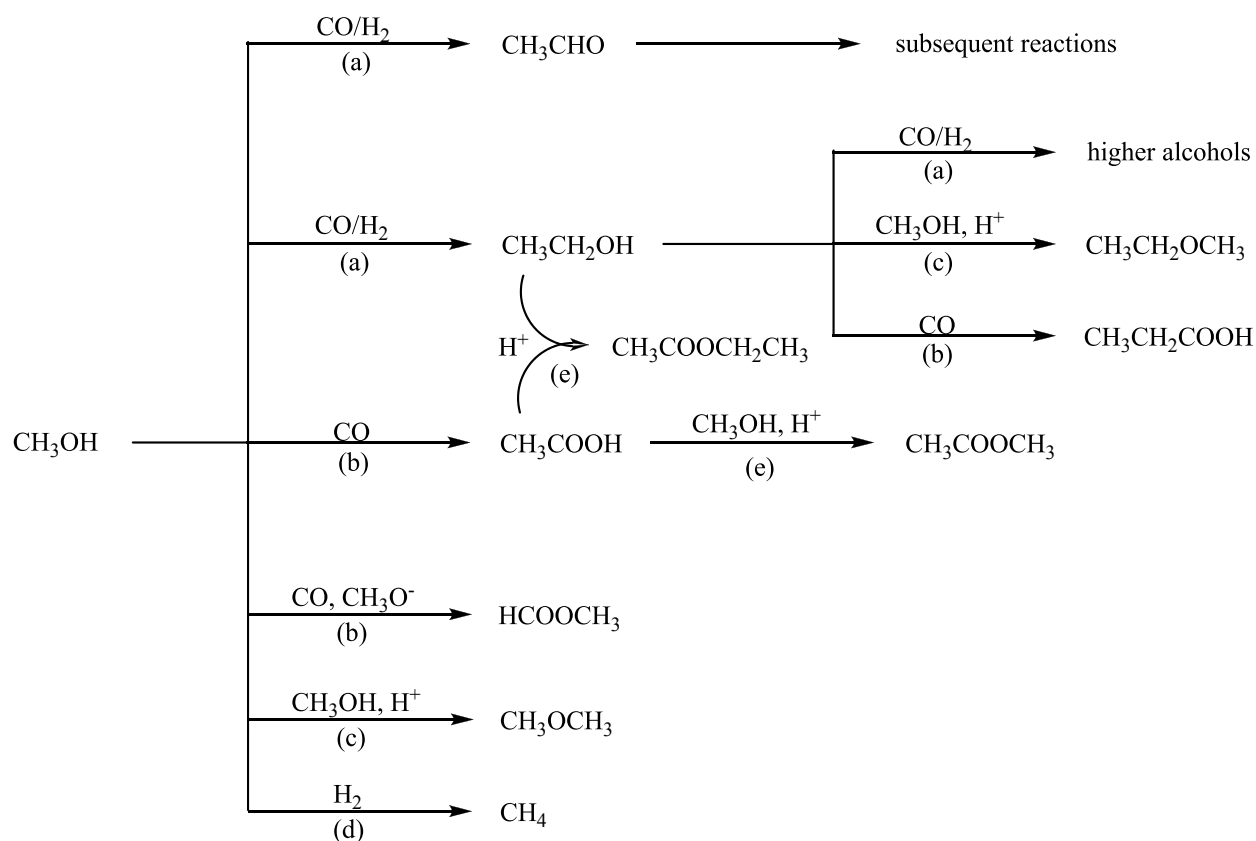


**Figure 2.2 Representation of the range of products that can be obtained from methanol with CO and/or  $\text{H}_2$  under different conditions.**

Most of these processes are utilized in industry for the large-scale production of the defined commodities. Amongst the variations two of the most important processes that have been studied extensively include the carbonylation and homologation of methanol to acetic acid and ethanol, respectively, which will be discussed in more detail in Sections 2.4.2 and 2.4.3.

### 2.3.2. Carbonylation of methanol to acetic acid

The catalytic carbonylation of methanol for the production of acetic acid has become one of the most important industrial applications since its discovery over 80 years ago by Henry Dreyfus.<sup>25</sup> He built the first pilot plant for the process, but due to certain drawbacks this process was not considered to be fit for commercialization. However, in 1965 BASF reported the use of an iodide-promoted cobalt catalyst that could successfully allow the carbonylation of methanol to acetic acid under high pressures, which provided the first commercial use of this process.<sup>26a,b</sup> Not long after this discovery the Monsanto company reported the use of an iodide-promoted rhodium complex  $cis-[Rh(CO)_2(I)_2]^-$  for the carbonylation process, which allowed the use of much milder reaction conditions (30-60 atm, 150-200 °C) and provided 99 % selectivities towards acetic acid.<sup>27a,b</sup> Since then the Monsanto process was responsible for most of the acetic acid production in the world for almost 25 years.

Upon its discovery many researchers investigated the mechanistic pathways of the Monsanto process from which a generally accepted catalytic cycle was formulated as given in Figure 2.3.<sup>28a,b,c;29a,b</sup> The first step involves the oxidative addition of MeI to the rhodium centre of  $cis-[Rh(CO)_2(I)_2]^-$  (A) after the MeI is generated from a reaction between methanol and hydrogen iodide (E). This step is generally considered to be the rate-determining step due to the first-order dependence of the overall rate to the concentrations of both the rhodium and iodide promoter. The oxidative addition reaction involves a nucleophilic attack of the electron-rich rhodium centre onto the electrophilic carbon of the MeI, which results in the formation of an octahedral Rh(III)-alkyl species (B). Although this intermediate was not observed in original studies, work done by Haynes *et al.*<sup>29b</sup> showed that it can be observed by IR and NMR techniques. Successive migratory insertion of a carbonyl ligand into the  $cis$ -Rh-CH<sub>3</sub> bond forms the square pyramidal Rh(III)-acyl species (C), which is also easily observed

---

<sup>25</sup> Wagner, F. S. (1978) *Acetic Acid*. In *Kirk-Othmer Encyclopedia of Chemical Technology 3<sup>rd</sup> ed.* edited by Grayson, M., John Wiley & Sons, New York.

<sup>26</sup> a) von Kutepow, N.; Himmele, W.; Hohenschutz, H. (1965) *Chem.-Ing.-Tech.*, **37**, 383. b) Hohenschutz, H.; von Kutepow, N.; Himmele, W. (1966) *Hydrocarbon Process*, **45**, 11, 141.

<sup>27</sup> a) Paulik, F. E.; Roth, J. F. (1968) *J. Chem. Soc., Chem. Commun.*, 1578. b) Eby, R. T.; Singleton, T. C. (1983) *Applied Industrial Catalysis* edited by Leach, B. E., Academic Press, New York, **1**, Ch. 10.

<sup>28</sup> a) Forster, D. (1979) *Adv. Organomet. Chem.*, **17**, 255. b) Forster, D.; Singleton, T. C. (1982) *J. Mol. Catal.*, **17**, 299. c) Dekleva, T. W.; Forster, D. (1986) *Adv. Catal.*, **34**, 81.

<sup>29</sup> a) Murphy, M.; Smith, B.; Torrence, G.; Aguilo, A. (1987) *J. Mol. Catal.*, **39**, 115 and references within. b) Haynes, A.; Mann, B. E.; Morris, G. E.; Maitlis, P. M. (1993) *J. Am. Chem. Soc.*, **115**, 4093 and references within.



on IR and NMR spectra. A CO molecule coordinates onto the rhodium centre to form the octahedral complex **D**, which upon reductive elimination regenerates the original catalyst **A** and forms an acetyl iodide molecule. The acetyl iodide gets hydrolyzed to form the acetic acid (**E**) and regenerates the hydrogen iodide.

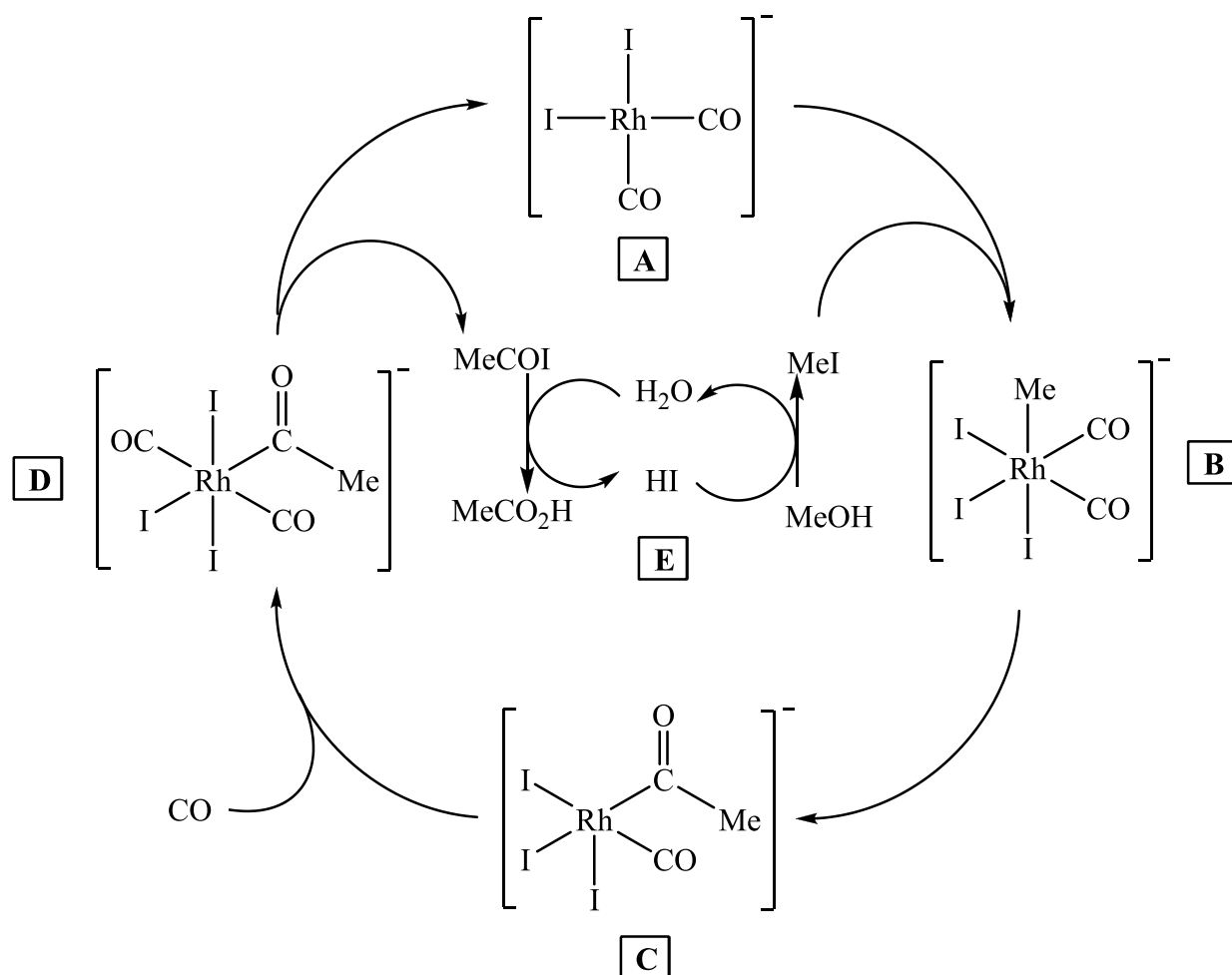


**Figure 2.3 A representation of the general catalytic cycle of carbonylation of methanol in the Monsanto process.**

It has been shown in later research that this process can be utilized not just for the carbonylation of methanol, but also for the carbonylation of other linear alcohols producing the corresponding carboxylic acids.<sup>30</sup> It was shown that the general mechanism and rate expression were similar for each alcohol under study.

<sup>30</sup> Dekleva, T. W.; Forster, D. (1985) *J. Am. Chem. Soc.*, **107**, 3565 and references within.

In 1996 BP Chemicals reported an alternative catalytic system for the carbonylation of methanol, which involved the use of an iodide-promoted iridium complex similar to the rhodium complex of the Monsanto process.<sup>31</sup> This process was found to have significant advantages above the Monsanto process, including the fact that the iridium catalyst is much cheaper, extremely more robust, more soluble in the reaction mixture and have higher stability than the rhodium catalyst. Furthermore, the Cativa process operates at reduced water levels, which provides the advantage of less by-product formation and improved carbon monoxide efficiency. These discoveries led to the immediate commercialization of the Cativa process in the U.S.A. and later in other countries.

The catalytic cycle for the Cativa process is shown in Figure 2.4. As can be observed from the figure the mechanistic pathways of the process are similar to that of the Monsanto process. There are, however, a few key differences found between these catalytic cycles. The first difference to note is that the oxidative addition of MeI to the starting iridium complex **F** was found to be significantly faster than the analogous reaction for the rhodium complex in the Monsanto process with a factor of about 150 times. This alters the rate dependence as the oxidative addition reaction of the Cativa process is not the rate-determining step as in the Monsanto process. Instead the slowest reaction is found to be the substitution of an iodo ligand with a carbonyl molecule forming the octahedral Ir(III)-alkyl species **H**. As a result this process is more favourable under low MeI concentrations in contrast to the increase in rate of the Monsanto process with higher MeI concentrations. The rate of the reaction can therefore be enhanced by the addition of iodide scavengers of which several examples is available in literature including carbonyl-iodide complexes of Pt, W, Os, Re and Ru.<sup>32a,b,c</sup>

---

<sup>31</sup> Maitlis, P. M.; Haynes, A.; Sunley, G. J.; Howard, M.J. (1996). *J. Chem. Soc. Dalton Trans.*, 2187.

<sup>32</sup> a) Gautron, S.; Lassauque, N.; Le Berre, C.; Azam, L.; Giordano, R.; Serp, P.; Laurenczy, G.; Thiébaud, D.; Kalck, P. (2006) *Topics in Catalysis*, **40**, 1-4, 83. b) Sunley, J. G.; Giles, M. F.; Garland, C. S. (1994) *European Patent*, 643034. c) Garland, C. S.; Giles, M. F.; Poole, A. D.; Sunley, J. G. (1994) *European Patent* 728726.

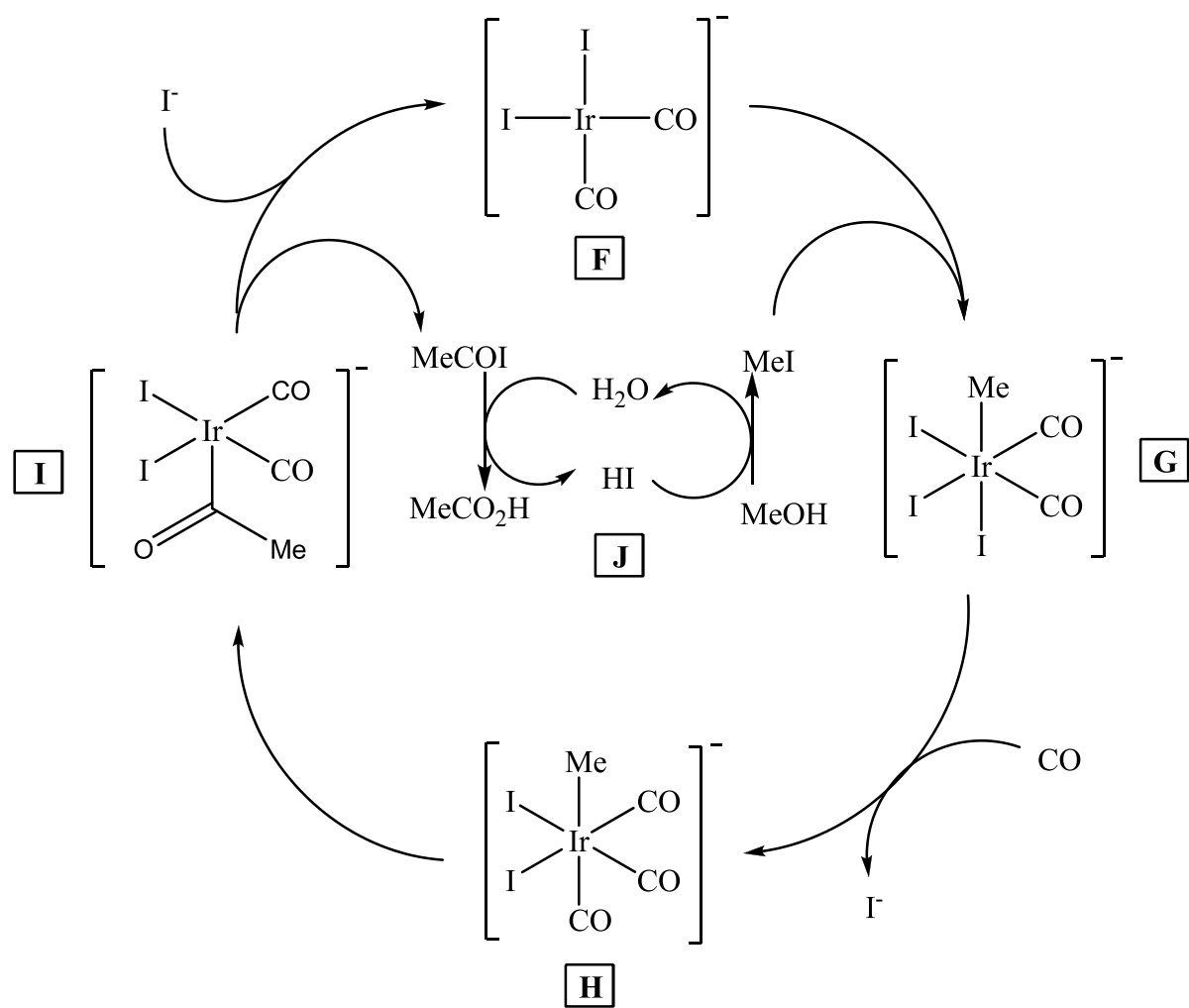


**Figure 2.4** An illustration of the general catalytic cycle of the Cativa process.

### 2.3.3. Homologation of methanol to ethanol

Ethanol is one of the largest commodities produced in mass amounts in industry with over 12 billion gallons been produced in 2005.<sup>33</sup> It is also shown by the corresponding authors that ethanol can be a suitable transportation fuel, since it provides the same chemical energy as that of gasoline with less emission of greenhouse gases and other pollutants. Many countries already use ethanol as a gasoline additive as a result of these discoveries. Ethanol is also known to be a suitable building block for a range of chemicals and polymers.<sup>34a,b</sup> More recently it has been shown that ethanol obtained from the liquefaction of biomass can be utilised as a potential source of renewable hydrogen in fuel cell applications.<sup>35</sup>

With the important use of ethanol in these applications the research on affordable and effective synthesis of ethanol increased over the years. There are currently two major processes from which ethanol is produced. The first involves the hydration of ethylene over a solid acid catalyst, which leads to the production of highly pure ethanol for industrial use.<sup>36</sup> The second process is the biological fermentation of sugars where the ethanol produced from it is mostly utilized in alcoholic beverages. Although the former process is fairly efficient, the large-scale production of ethanol for fuel applications from this process is found to be too expensive and energy-ineffective, since energy-demanding distillation steps are required to purify the ethanol.<sup>37</sup>

Alternative synthetic routes for the mass-production of ethanol have been under investigation for the last couple of decades, which involves mostly the use of syngas derived from either coal or biomass. There are three major methods that have been developed thus far for the catalytic production of ethanol from syngas, as summarized in Figure 2.5.

---

<sup>33</sup> Farrell, A. E.; Plevin, R. J.; Turner, B. T.; Jones, A. D.; O'Hare, M.; Kammen, D. M. (2006) *Science*, **311**, 506.

<sup>34</sup> a) Palsson, B. O.; Faith-Afshar, S.; Rudd, D. F.; Lightfoot, E. N. (1981) *Science*, **213**, 513. b) Ng, T. K.; Busche, R. M.; McDonald, C. C.; Hardy, R. W. F. (1983) *Science*, **219**, 4585.

<sup>35</sup> Velu, S.; Song, C. (2007) *Advances in Catalysis and Processes for Hydrogen Production from Ethanol*. In *Catalysis* edited by Spivey, J. J., Royal Society of Chemistry, London, **20**, 65.

<sup>36</sup> Fougret, C. M.; Holderich, W. F. (2001) *Appl. Catal. A: General*, **207**, 295.

<sup>37</sup> Rostrup-Nielsen, J. R. (2005) *Science*, **308**, 1421.

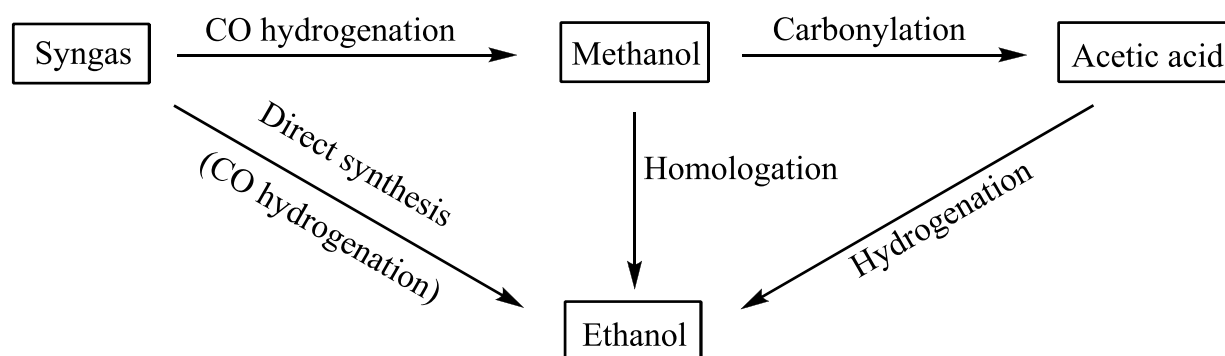


**Figure 2.5** An illustration of possible routes for the synthesis of ethanol from syngas.

The first method involves the direct synthesis of ethanol from syngas by CO hydrogenation as was slightly touched on in Section 2.2.1. This route has been shown to be feasible by several homogeneous catalysts including Co, Ru and Rh-based complexes.<sup>6b,38a,b</sup> These complexes have also been shown to have enhanced activity on supports such as Al<sub>2</sub>O<sub>3</sub>, SiO<sub>2</sub>, etc. for the conversion of syngas to ethanol and even higher alcohols. Amongst the various catalysts attention has been given mostly to the Rh-based catalysts as these catalysts proved to have high selectivities towards ethanol with various types of promoters and supports.<sup>39a,b,c</sup> The only commercial production of ethanol directly from syngas occurs in SASOL's FT refinery process, where ethanol is separated from the main stream as a side-product.

The other methods are indirect synthetic routes of syngas, which first involves the conversion of syngas to methanol and subsequent carbonylation of the methanol to acetic acid as was discussed in Sections 2.4.1 and 2.4.2. The ethanol is then produced either by the homologation of methanol or by the hydrogenation of acetic acid.<sup>40</sup> Although both processes have been well-studied and developed, neither is utilized for commercial use yet due to unacceptable yields and selectivities.

Methanol homologation is basically defined as the carbonylation and subsequent reduction of methanol in the presence of a catalyst where C-C bond formation occurs forming the resulting ethanol. Thus, homologation leads to the insertion of a carbon atom to the carbon

<sup>38</sup> a) Maitlis, P. M. (2003) *J. Mol. Catal. A: Chemical*, **204-205**, 55. b) Bradley, J. S. (1983) *Adv. Organomet. Chem.*, **22**, 1.

<sup>39</sup> a) Hu, J.; Wang, Y.; Cao, C.; Elliott, D. C.; Stevens, D. J.; White, J. F. (2007) *Catal. Today*, **120**, 90. b) Luo, H. Y.; Zhang, W.; Zhou, H. W.; Huang, S. Y.; Lin, P. Z.; Lin, L. W. (2001) *Appl. Catal. A: General*, **214**, 161. c) Yu-Hua, D.; De-An, C.; Khi-Rui, T. (1987) *Appl. Catal.*, **35**, 77.

<sup>40</sup> Winter, C. L. (1986) *Hydrocarbon Process*, **65**, 71.

chain of a compound. As early as 1951 it was already shown that methanol can undergo homologation to form ethanol from syngas using cobalt carbonyls.<sup>41</sup> It was illustrated, however, that when monodentate phosphines were added to modify the catalyst, selectivities towards acetaldehyde were obtained.<sup>42a,b</sup> The same observation was made when (Ph<sub>3</sub>P)<sub>2</sub>N was used as modifier in a polar solvent such as dioxane or sulfolane, where 80% acetaldehyde selectivities were obtained.<sup>15</sup> With the use of biphosphine ligands either products could be obtained with selectivities above 80% depending on the temperature at which the reaction was performed.<sup>43a,b</sup>

Combining the cobalt system with Ruthenium either in the presence of phosphines or not, resulted in selectivities towards ethanol and ether due to the ability of Ru to hydrogenate acetaldehyde.<sup>44a,b</sup> A bimetallic system containing Co and Rh was also reported to provide selectivities as high as 70 % towards ethanol under high temperatures and pressures, however the process was low yielding.<sup>45</sup> High ethanol selectivities were also obtained with catalyst systems containing both Rh and Ru in the presence of MeI and diphosphines under mild conditions.<sup>46a,b</sup> The use of an alkali-promoted Rh-Fe bimetallic catalyst supported on Al<sub>2</sub>O<sub>3</sub> resulted in the production of a mixture of ethanol and methyl acetate.<sup>47a,b</sup> About 46% selectivity towards ethanol could be obtained under mild conditions, while yields could be significantly improved by the addition of heterocyclic amine promoters.

In more recent work Rathke *et al.*<sup>48</sup> reported a very effective synthetic route for ethanol production. The method involved the syngas production from switch grass *via* steam reforming followed by the conventional synthesis of methanol using the commercial Cu/ZnO catalyst and successive hydrocarbonylation of methanol using a homogeneous [HFe(CO)<sub>4</sub>] catalyst. The reaction conditions for the whole process were set at temperatures of 180-220

<sup>41</sup> Wender I.; Friedel, R.A.; Orchin, M. (1951) *Science.*, **113**, 206.

<sup>42</sup> a) Roeper, M.; Loevenich, H.; Korff, J. (1982) *J. Mol. Catal.*, **17**, 315. b) Lindner, E.; Sickinger, A.; Wegner, P. (1988) *J. Organomet. Chem.*, **349**, 75.

<sup>43</sup> a) Sugi, Y.; Bando, K.; Takami, Y. (1981) *Chem. Lett.*, 63. b) Lindner, E.; Bader, A.; Braunling, H.; Jira, R. (1990) *J. Mol. Catal.*, **57**, 291.

<sup>44</sup> a) Watanabe, K.; Kudo, K.; Sugita, N. (1985) *Bull. Chem Soc. Jpn.*, **58**, 2029. b) Lindner, E.; Scheytt, G.; Wegner, P. (1986) *J. Organomet. Chem.*, **308**, 311.

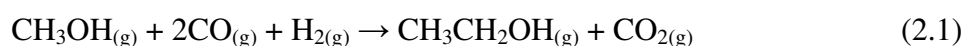
<sup>45</sup> Bartish, C. M. (1979) *U.S. Patent*, 4171461.

<sup>46</sup> a) Moloy, K.G.; Wegman, R.W. (1988) *J. Chem. Soc. Chem. Commun.*, 820. b) Moloy, K.G.; Wegman, R.W. (1989) *Organometallics*, **8**, 2883.

<sup>47</sup> a) Hargis, D. C.; Dubeck, M. (1983) *U.S Patent*, 4370507. b) Hargis, D. C.; Dubeck, M. (1982) *U.S Patent*, 4309314.

<sup>48</sup> Rathke, J. W.; Chen, M. J.; Klinger, R. J.; Gerald, R. E.; Marshall, C. L.; Rodgers, J. L. (2006) *Proceedings of the 2006 Meetings of the DOE/BES Catalysis and Chemical Transformations Program*, Cambridge, MD, May 21-24.

°C and pressures up to 300 bar. The major advantage of this method as shown in equation 2.1 was that it resulted in the production of “dry” ethanol, since no water is formed in the net reaction of the process unlike other conventional homologation processes. The drawback, on the other hand, is that the carbon efficiency is low, since part of the carbon monoxide molecules are converted to carbon dioxide.



The mechanistic pathways for the homologation of methanol haven't been studied in much detail yet, however, there are some proposals that seem plausible for both homogeneous and heterogeneous processes. Two major pathways were elucidated by using isotopic tracer techniques, where the reaction of  $^{13}\text{CO}/\text{H}_2$  and methanol was investigated over K-promoted Cu/MgO/CeO<sub>2</sub> and Cs-promoted Cu/ZnO/Al<sub>2</sub>O<sub>3</sub> catalysts.<sup>49a,b,c</sup> The first pathway included the insertion of CO into methanol followed by hydrogenation, whilst the other involved coupling of two methanol molecules or otherwise known as methanol bimolecular reaction.

Since there are several catalytic systems that can allow the homologation of methanol, it is difficult to assign a general mechanism. However, since the main aim of this study involve rhodium catalysts as the precursors for the homologation of methanol, it can be accepted that the main mechanism important for the homologation reaction most probably follow a similar route as that proposed for the Monsanto process discussed before. Based on the discovery of the reductive carbonylation mechanism it is expected that the addition of hydrogen gas to this carbonylation process should lead to the hydrogenation of either the acyl iodide or acetic acid to form ethanol. With this in mind the oxidative addition as well as reductive elimination reactions involved in the Monsanto process were considered to be of importance in this study. This next section will therefore cover some important aspects and discoveries on the iodomethane oxidative addition reactions to rhodium complexes and ligand effects on the Monsanto process.

---

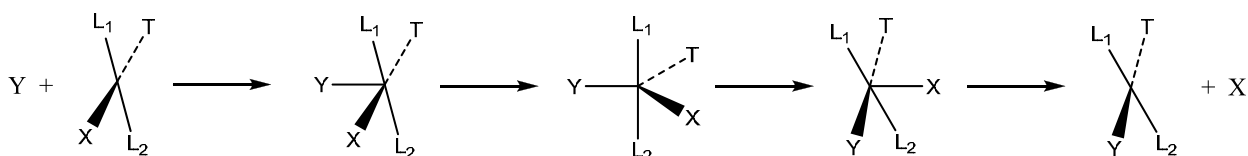
<sup>49</sup> a) Xu, M.; Iglesia, E. (1999) *J. Catal.*, **67**, 149. b) Calverley, E. M.; Smith, K. J. (1992) *Stud. Surf. Sci. Catal.*, **73**, 111. c) Mazanec, T. J. (1986) *J. Catal.*, **98**, 115.

## 2.4 Chemical reactions related to metal complexes

### 2.4.1. Exchange/Substitution reactions

Transition metals are known to exhibit different coordination modes due to their variable coordination number. As a result ligands can either occupy vacant sites on a metal centre, undergo exchange with other ligands in the coordination sphere or be released from the metal centre.<sup>50</sup> These reactions provide a versatile means of synthesizing various types of metal complexes with certain coordinated ligands and ligand orientations. These reactions can be categorized under two major divisions depending on the mechanistic proceedings of the reactions, namely dissociative and associative processes. The differences in the mechanisms of these processes are depicted in Figure 2.6.<sup>51</sup>

**Associative :**



**Dissociative :**

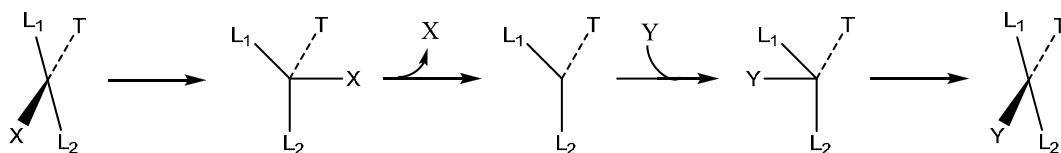


**Figure 2.6 An illustration of mechanistic differences between associative and dissociative substitution reactions.**

In an associative reaction the incoming ligand Y will first occupy the vacant site on a metal complex having some leaving group X and some *trans*-directing ligand T. This is followed by re-orientation of the ligands around the metal centre after which the leaving ligand X labilizes. In a dissociative route the leaving ligand X is first released from the metal centre, forming a vacant site on the metal centre. This vacant site can then be occupied by some

<sup>50</sup> Taube, R. (1975) *Z. Chem.*, **15**, 11, 426.

<sup>51</sup> Huheey, J. E.; Keiter, E. A.; Keiter, R. L. (1993) *Inorganic Chemistry 4<sup>th</sup> Ed., Principles of Structure and Reactivity*, HarperCollins College Publishers, New York, 540.



ligand Y or even by a solvent molecule. In some reactions interchange associative/dissociative mechanisms are also observed where simultaneous bond formation and breaking occurs.

These processes follow a so-called 16/18 electron rule as was introduced by Tolman,<sup>52</sup> where it is stated that diamagnetic transition metal complexes exist mainly as 16- or 18-electron species in measurable concentrations under normal conditions. Furthermore reactions of organometallic complexes proceed with elemental steps where intermediates having 16 or 18 valence electrons are involved.

Exchange and substitution processes are important aspects in coordination chemistry, where ligands on a metal can be replaced by other ligands or where ligands can be exchanged between different metal centres. Several examples are found in literature including olefin exchange in square-planar complexes such as Zeise's anion  $[\text{PtCl}_3(\text{C}_2\text{H}_4)]^-$  and  $[\text{PtCl}_2\text{S}(\text{C}_2\text{H}_4)]^-$  (where S is a solvent molecule).<sup>53,54</sup> These reactions were found to be fairly fast and followed an associative mechanistic pathway, where the entering ethane molecule occupied the vacant site *trans* to the coordinated ethene. However, it was shown that complexes of the type *cis*- $[\text{PtR}_2\text{L}_2]$ , where R = Ph or Me and L = DMSO or Me<sub>2</sub>S ligands that are coordinated *via* the sulphur atom, undergo a dissociative exchange process with the corresponding free ligands L.<sup>55</sup> In this case the weakly coordinated ligands L labilizes forming an unsaturated 14-electron  $[\text{PtR}_2\text{L}]$  intermediate, which is followed by the coordination of an incoming ligand. This observed dissociative exchange was ascribed to the strong  $\sigma$ -donor ability of the R ligands being *trans* to the ligands L.

Another example involves Ni(II) compounds, which have been shown to be effective pre-catalysts for the polymerization of many  $\alpha$ -olefins. It was shown by Fontaine *et al.*<sup>56</sup> that phosphine exchange in complexes such as  $[(1\text{-Me-Indenyl})(\text{PR}_3)\text{Ni-Cl}]$  played a role in the polymerisation reactions catalysed by these complexes. Younkin *et al.*<sup>57</sup> revealed that the catalyst  $[(\eta^2\text{-(N,O)-salicylaldimine})\text{Ni}(\text{PPh}_3)(\text{Ar})]$  followed a non-cationic pathway involving

---

<sup>52</sup> Tolman, C.A. (1970) *J. Am. Chem. Soc.*, **92**, 2953.

<sup>53</sup> Olsson, A.; Kofod, P. (1992) *Inorg. Chem.*, **31**, 183.

<sup>54</sup> Plutino, M. R.; Otto, S.; Roodt, A.; Elding, L. I. (1999) *Inorg. Chem.*, **38**, 1233.

<sup>55</sup> Frey, U.; Helm, L.; Merbach, A. E.; Romeo, R. (1989) *J. Am. Chem. Soc.*, **111**, 8161.

<sup>56</sup> Fontaine, F.-G.; Dubois, M.-A.; Zargarian, D. (2001) *Organomet.*, **20**, 5156.

<sup>57</sup> Younkin, T. R.; Connor, E. F.; Henderson, J. I.; Friedrich, S. K.; Grubbs, R. H.; Bansleben, D.A. (2000) *Science*, **287**, 460.

the predissociation of  $\text{PPh}_3$ . Exchange reactions of *trans* and *cis* isomers of  $[\text{L}(\text{H}_2\text{O})\text{RhH}]^{2+}$ , where  $\text{L} = 1,4,8,11\text{-tetraazacyclotetradecane} = [14]\text{aneN}_4$ , with ligand species  $\text{X} = \text{SCN}^-$ ,  $\text{Cl}^-$ ,  $\text{Br}^-$  and  $\text{I}^-$  were also investigated by  $^1\text{H}$  NMR spectroscopy.<sup>58</sup> Rapid exchange was observed for the *trans* isomer between the coordinated water molecule and the separate ligands  $\text{X}$  in  $\text{D}_2\text{O}$ . The exchange in the *cis* isomer was found to be very slow under similar conditions.

### 2.4.2. Insertion/Migration reactions

Ligands on a transition metal centre can be combined and converted to other type of ligands by processes known as insertion and migration reactions. These processes basically involves the insertion of a  $\pi$ -bonded unsaturated molecule into a metal-anion bond in conjunction with the migration of the corresponding anion onto the unsaturated molecule.<sup>1,59</sup> This process is often referred to as migratory insertion, which is illustrated in Figure 2.7.

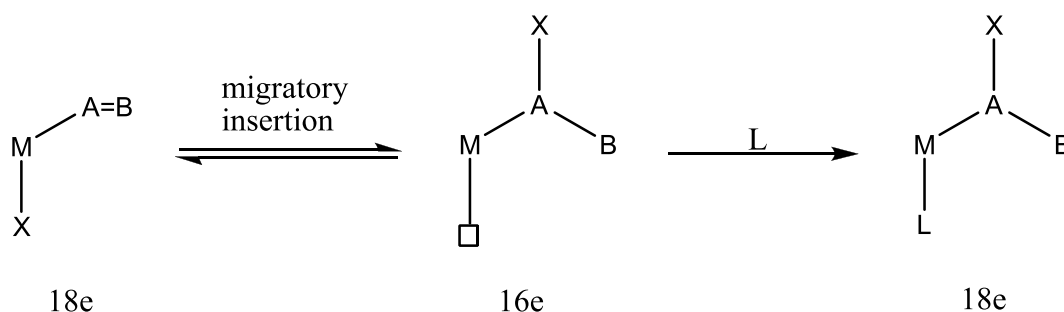


**Figure 2.7 Representation of a general migratory insertion on a transition metal complex.**

The ligand  $\text{A}=\text{B}$  represents a two-electron ligand, which inserts into the  $1\text{e}^-$  ligand  $\text{X}$  to form a one-electron product  $\text{ABX}$  that is coordinated on the metal centre  $\text{M}$ . Thus a two-electron vacant site is generated, which can be occupied by another two-electron ligand  $\text{L}$ . An important requirement for this process to occur is that the corresponding ligands have to be *cis* with respect to each other. There are generally two types of migratory insertion reactions that can occur, namely, a 1,1-insertion, which occurs normally with  $\eta^1$ -molecules such as  $\text{CO}$ , and a 1,2-insertion, which generally occurs with  $\eta^2$ -molecules such as ethane.

<sup>58</sup> Lemma, K.; Ellern, A.; Bakac, A. (2003) *Inorg. Chem.*, **42**, 3662.

<sup>59</sup> Crabtree, R. H. (2009) *The Organometallic Chemistry of the Transition Metals*, John Wiley & Sons, New York, p. 153, p. 177

Carbon monoxide proves to be an effective ligand for migratory insertion, since the carbon atom of a coordinated carbon monoxide exhibits a positive character. This is due to  $\sigma$ -donation of the carbonyl ligand to the metal centre and  $\pi$ -back donation into the antibonding  $\pi^*$  orbitals of the ligand. The most common case known in literature is the insertion of the carbonyl ligand into metal-alkyl bonds forming the consequent metal-acyl species. This reaction plays an important role in carbonylation reactions for the lengthening of the carbon chain of corresponding alkyl reagents by C-C bond formation. The mechanism for this reaction is generally indicative of a dissociative substitution reaction as can be elucidated from Figure 2.7.

### 2.4.3. Oxidative addition and reductive elimination reactions

A common feature of transition metals is their ability to access different oxidation states, which together with the corresponding coordination number allow the coordination of several different neutral and anionic ligands. The different oxidation states for a specified transition metal can be accessed by performing electron-transfer or redox reactions. The most common and well-studied redox reactions in coordination chemistry are oxidative addition and reductive elimination reactions, which is illustrated in Figure 2.8.

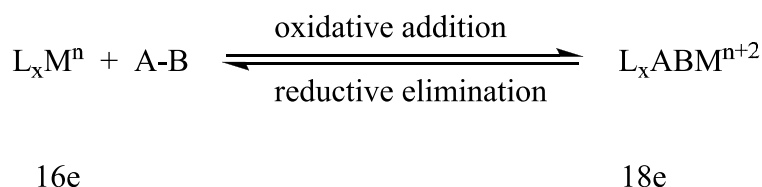


**Figure 2.8 A representation of general oxidative addition and reductive elimination reactions on transition metal complexes.**

Oxidative addition involves the addition of some molecule A-B to the metal centre, which leads to the breaking of the A-B bond and formation of M-A and M-B bonds in most cases.<sup>59</sup> In the process the metal centre gets oxidized leading to a net two electron transfer from the metal to the  $\sigma^*$ -orbital of the A-B bond, which in turn gets reduced to form strong  $\sigma$ -donating species  $\text{A}^-$  and  $\text{B}^-$  that transfer  $\sigma$  electrons to the metal centre upon coordination. As a final result the metal's oxidation state, electron count and coordination number all increase by two units. Therefore, a requirement for oxidative addition to occur on a metal centre includes the

fact that the transition metal should be in a low oxidation state and must have a stable oxidation state of two units higher than the first.

Several metal species meet the requirements for oxidative addition of which a summary of the variants in order of  $d^n$ -configuration change is represented in Table 2.1.

**Table 2.1 A range of well-known oxidative addition reactions.<sup>59</sup>**

$d^n$ - configuration change	Coordination geometry change	Example of reaction	Group
$d^{10} \rightarrow d^8$	Linear $\rightarrow$ square pyramidal	Au(I) $\rightarrow$ Au(III)	11
	Tetrahedral $\rightarrow$ square pyramidal	Pt,Pd(0) $\rightarrow$ Pt,Pd(II)	10
$d^8 \rightarrow d^6$	Square pyramidal $\rightarrow$ octahedral	M(II) $\rightarrow$ M(IV)	10
		Rh,Ir(I) $\rightarrow$ Rh,Ir(III)	9
		M(0) $\rightarrow$ M(II)	8
	Trigonal bipyramidal $\rightarrow$ octahedral	M(I) $\rightarrow$ M(III)	9
		M(0) $\rightarrow$ M(II)	8
$d^7 \rightarrow d^6$	Square pyramidal $\rightarrow$ octahedral	2Co(II) $\rightarrow$ 2Co(III)	8
	octahedral $\rightarrow$ octahedral	2Co(II) $\rightarrow$ 2Co(III)	8
$d^6 \rightarrow d^4$	Octahedral $\rightarrow$ 7-coordination	Re(I) $\rightarrow$ Re(III)	7
		M(0) $\rightarrow$ M(II)	6
		V(-I) $\rightarrow$ V(I)	5
$d^4 \rightarrow d^3$	Square pyramidal $\rightarrow$ octahedral	2Cr(II) $\rightarrow$ 2Cr(III)	6
	octahedral $\rightarrow$ octahedral	2Cr(II) $\rightarrow$ 2Cr(III)	6
$d^4 \rightarrow d^2$	Octahedral $\rightarrow$ 8-coordination	Mo,W(II) $\rightarrow$ Mo,W(IV)	6
$d^2 \rightarrow d^0$	various	M(III) $\rightarrow$ M(V)	5
		M(II) $\rightarrow$ M(IV)	4

A whole range of compounds having covalent bonds (represented by A-B in Figure 2.8) can be oxidatively added to transition metals including dihalogens, alkyl halides, aryl halides, dioxygen, dihydrogen, etc.. Oxidative addition can take place through several mechanistic

pathways depending on the type and nature of the metal and covalent molecules being used.<sup>60</sup> A summary of the various mechanisms for oxidative additions reactions are presented in Figure 2.9.

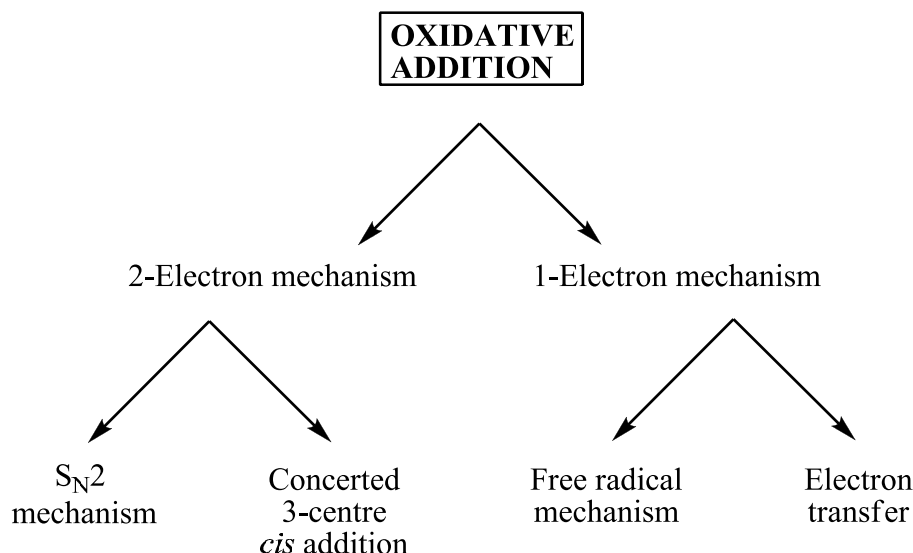


**Figure 2.9 Schematic presentation defining various mechanistic pathways for oxidative addition reactions on metal complexes.**

As can be observed, oxidative addition can occur either by an one-electron or a two-electron mechanism. The one-electron mechanism involves either a free radical or electron transfer mechanism. Examples of one-electron oxidative addition reactions include the complexes  $[\text{Co}(\text{CN})_5]^{3-}$  and  $[\text{Cr}(\text{H}_2\text{O})_6]^{2+}$ , which has been shown to undergo a free radical mechanism. The two-electron mechanism includes either a  $\text{S}_{\text{N}}2$  or a concerted *cis* addition mechanism. Two-electron addition of covalent molecules to metal complexes is amongst the variations the most studied due to the vast applications of these oxidative addition reactions. Some examples include the typical addition of alkyl- or aryl halides to  $\text{Pd}^{61}$ ,  $\text{Rh}$  or  $\text{Ir}^{62}$  metal complexes, which are extremely important in cross-coupling as well as carbonylation reactions.

<sup>60</sup> Ašperger, S. (2003) *Chemical Kinetics and Inorganic Reaction Mechanisms*, Kluwer Academic Publishers, New York, 161.

<sup>61</sup> Diederich, F.; Stang, P. J. (1998) *Metal-Catalyzed Cross-Coupling Reactions*, Wiley-VCH, Weinheim.

<sup>62</sup> Katritzky, A. R.; Ley, S. V.; Meth-Cohn, O; Rees, C. W. (1995) *Comprehensive Organic Functional Group Transformations: Synthesis: Carbon with One Heteroatom Attached by a Single Bond*, Elsevier Science, Oxford.

The reverse of oxidative addition is reductive elimination, which is also indicated in Figure 2.8. This reaction allows metal complexes to return back to the lower oxidation states, where the opposite requirements to that of oxidative addition are needed for reductive elimination to occur. One important requirement for reductive elimination to occur includes the fact that the ligands involved have to be *cis* to each other on the metal centre, whereas oxidative addition of molecules can occur by a *cis* or *trans* mode onto the metal centre. Reductive elimination is usually important in catalytic cycles involving oxidative addition, since it normally releases the products formed by the catalyzed process and is responsible for the regeneration of the original catalyst in order to allow another catalytic cycle to occur. In some catalytic cycles such as the hydrocyanation of olefins,<sup>1</sup> this reaction is considered to be the rate-determining step, whereas in other processes such as the Monsanto process oxidative addition is the slowest step rather.

## 2.5 Iodomethane oxidative addition to rhodium(I) complexes

As was shown in Section 2.4.3 the iodomethane oxidative addition to square planar rhodium(I) complexes and that subsequent insertion of CO are of great importance in the Monsanto production of acetic acid. After the discovery of the Monsanto catalyst,  $[cis-Rh(CO)_2(I)_2]^-$ , extended research has been done on designing more stable and effective rhodium catalysts, since the original catalyst has some drawbacks. These drawbacks included that the catalyst was stable in only a small range of reaction conditions and furthermore side product formation was inevitable leading to loss of rhodium *via* insoluble  $RhI_3$  species.<sup>27a,b</sup> Two of the most studied complex types for this purpose include the well-known Vaska-type complexes  $[Rh(CO)(Cl)(YR_1R_2R_3)_2]$  containing monodentate ligands  $YR_1R_2R_3$  (where Y = P, As or Sb), as well as  $[Rh(L,L'-BID)(CO)(L'')]$  containing bidentate ligands (L,L'-BID). The oxidative addition of methyl iodide to  $[Rh(CO)(Cl)(YR_1R_2R_3)_2]$  complexes have been shown to generally lead to the formation of the Rh(III)-alkyl species  $[Rh(CO)(Cl)(CH_3)(I)(YR_1R_2R_3)_2]$  followed by CO insertion into the Rh-CH<sub>3</sub> bond to form the Rh(III)-acyl species  $[Rh(C(O)CH_3)(Cl)(I)(YR_1R_2R_3)_2]$ .<sup>63</sup> The same hold true for the  $[Rh(L,L'-BID)(CO)(L'')]$  complexes.<sup>64</sup>

<sup>63</sup> Roodt, A.; Otto, S.; Steyl, G. (2003) *Coord. Chem. Rev.*, **245**, 121.

<sup>64</sup> Roodt, A.; Steyn, G. J. J.; Pandalai, S. G. (2000) *Res. Research Dev. Inorg. Chem.*, vol. 2, Transworld Research Network, Trivandrum, 2000, 1.

The mechanism for the oxidative addition of MeI to rhodium complexes is generally accepted to include a S<sub>N</sub>2 mechanism, where the nucleophilic rhodium centre (due to the presence of electron-rich ligands) attacks the electrophilic carbon of MeI substituting the iodide anion.<sup>65</sup> In some cases the concerted three-centred mechanism seems to be the preferable route.<sup>66</sup> The general mechanism from there onwards can take several routes depending on the type of ligands present on the rhodium centre and the solvent system in which the reaction is performed. The full set of routes that this oxidative addition reaction can undertake is summarized in Figure 2.10.

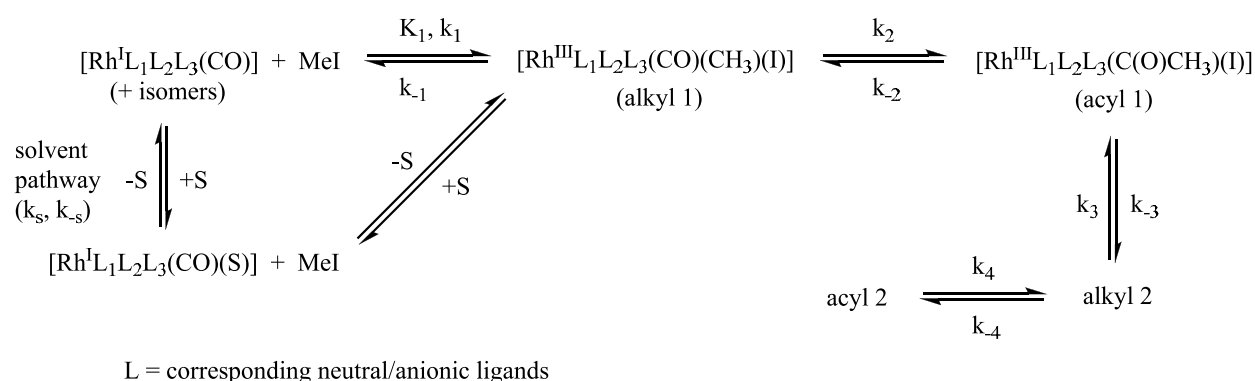


**Figure 2.10 A summary of the general mechanistic pathways that the oxidative addition of MeI to rhodium(I) complexes can follow.**

Several examples can be found in literature where the different species acyl 1, alkyl 2 and acyl 2 did form during the iodomethane oxidative addition to [Rh(L,L'-BID)(CO)(L'')] complexes. Rhodium systems where L,L'-BID = either (O,O), (O,N), (S,O), (S,N), (P,S), (P,P) or (P,O) and L'' = tertiary phosphine or iodide have been reported to undergo oxidative addition with methyl iodide. First the well-known [Rh(acac)(CO)(PPh<sub>3</sub>)] (acac = acetylacetonate, (O,O)-ligand) complex was shown to lead the formation of the acyl 1 intermediate, which was followed by the rearrangement of the intermediate to the alkyl 2 species as the final product.<sup>67</sup> In more recent work done by Conradie *et al.*<sup>68</sup> revealed a similar trend for the acac derivative 2-thenoyltrifluoroacetone during the iodomethane oxidative addition to the resulting [Rh(L,L'-BID)(CO)(PPh<sub>3</sub>)] complex. This complex is

<sup>65</sup> Tolman, W. B. (2006) *Activation of Small Molecules: Organometallic and Bioinorganic Perspective*, Wiley-VCH, Weinheim, 342.

<sup>66</sup> Venter, J. A.; Leipoldt, J. G.; van Eldik, R. (1991) *Inorg. Chem.*, **30**, 2207.

<sup>67</sup> Basson, S. S.; Leipoldt, J. G.; Roodt, A.; Venter, J. A.; van der Walt, T. J. (1986) *Inorg. Chim. Acta.*, **119**, 35.

<sup>68</sup> Conradie, M. M.; Conradie, J. (2008) *Inorg. Chim. Acta*, **361**, 208.

obtained in two different isomeric forms, of which the oxidative addition reaction leads to the conversion to alkyl 2 products for both cases. Previously Conradie *et al.*<sup>69</sup> also showed that  $[\text{Rh}(\text{fctfa})(\text{CO})(\text{PPh}_3)]$ , where (fctfa = ferrocenyltrifluoroacetate), which is another acac derivative, led to the formation of the acyl 2 species upon iodomethane oxidative addition. On the other hand the  $[\text{Rh}(\text{cupf})(\text{CO})(\text{PR}_3)]$  (cupf = cupferrate, (*O,O*)-ligand) led mainly to the formation of the alkyl 1 species as the products for a range of tertiary phosphine ligands  $\text{PR}_3$ .<sup>70a,b</sup> By further investigation of the alkyl 1 species in acetone and acetonitrile in the presence of MeI, a very slow conversion to acyl 1 species could be confirmed.

Replacing one of the oxygens in acac by a sulphur atom to form an *S,O*-ligand (Sacac) also provided a different outcome to the oxidative addition of MeI to  $[\text{Rh}(\text{Sacac})(\text{CO})(\text{PPh}_3)]$ , where the acyl 1 species was found to be the main product in a range of solvents.<sup>66</sup>  $[\text{Rh}(\text{L,L'-BID})(\text{CO})(\text{PPh}_3)]$  complexes where the L,L'-BID ligand is either a range of aminocyclopentane-dithiocarboxylate ligands (*S,N*-donor) or a range of  $\beta$ -aminovinylketonato ligands (AVK, *O,N*-donor) were shown to primarily form acyl 1 complexes as the final products.<sup>71a,b,c</sup>

Some  $[\text{Rh}(\text{L,L'-BID})(\text{CO})(\text{I})]$  complexes have been reported by Gonsalvi *et al.*<sup>72a,b</sup> having several L,L'-BID ligands of the type  $\text{Ph}_2\text{PCH}_2\text{P}(\text{S})\text{Ph}_2$  (dppms, (*P,S*)-donor),  $\text{Ph}_2\text{PCH}_2\text{P}(\text{O})\text{Ph}_2$  (dppmo, (*P,O*)-donor) and  $\text{Ph}_2\text{PCH}_2\text{CH}_2\text{PPh}_2$  (dppe, (*P,P*)-donor). Oxidative addition to these complexes was studied from which the rate was found to be very similar, despite the difference in nucleophilicity of the donor atoms. However, IR spectra of the oxidative addition reaction revealed different quantities of the forming alkyl 1 and acyl 1 species. The (*P,S*)-donor ligand primarily led to the formation of the acyl 1 species, with only a very small detection of the alkyl 1 species. The (*P,P*)-donor ligand on the other hand showed a clear formation of the alkyl 1 complex whereas only a small amount of the acyl 1 complex was detected. Although this difference was observed, both acyl complexes have been isolated, characterized by X-ray analysis and reported within the articles, providing

<sup>69</sup> Conradie, M. M.; Conradie, J. (2007) *Inorg. Chim. Acta*, **361**, 2285.

<sup>70</sup> a) Basson, S. S.; Leipoldt, J. G.; Roodt, A.; Venter, J. A. (1987) *Inorg. Chim. Acta*, **128**, 31. b) Basson, S. S.; Leipoldt, J. G.; Roodt, A.; Venter, J. A. (1986) *Inorg. Chim. Acta*, **118**, L45.

<sup>71</sup> a) Steyn, G. J. J.; Roodt, A.; Leipoldt, J. G. (1993) *Rhodium Express*, **1**, 25. b) Galding, M. R.; Cherkasova, T. G.; Varshavsky, Yu. S.; Osetrova, L. V.; Roodt, A. (1995) *Rhodium Express*, **9**, 36. c) ) Galding, M. R.; Cherkasova, T. G.; Osetrova, L. V.; Varshavsky, Yu. S.; Roodt, A. (1996) *Rhodium Express*, **16**, 23.

<sup>72</sup> a) Gonsalvi, L.; Adams, H.; Sunley, G. J.; Ditzel, E.; Haynes, A. (2002) *J. Am. Chem. Soc.*, **124**, 13597. b) Gonsalvi, L.; Adams, H.; Sunley, G. J.; Ditzel, E.; Haynes, A. (1999) *J. Am. Chem. Soc.*, **121**, 11233.



further proof of definite CO insertion after the formation of the alkyl 1 species. The (*P,O*)-donor ligand provided fairly equal amounts of both alkyl 1 and acyl 1 complexes.

These are but a few examples of studies done on oxidative addition of methyl iodide to Rh(I) complexes, from which it is clear that different ligands can have substantial influences on the outcome of the reaction. This in turn is expected to influence the outcome and reactivity of the carbonylation process or Monsanto process.

A principle aim in this study involved the use of Rh(III)-acyl complexes containing bidentate ligands to study the reductive carbonylation/hydrogenation of methanol to ethanol and as such one set of ligands of choice included the *S,O*-functionalized thiourea ligands. Since it was shown in the examples given before that bidentate ligands containing at least one sulphur donor atom lead primarily to the formation of Rh(III)-acyl species upon iodomethane oxidative addition, it was expected that *S,O*-bidentate ligands should lead to similar results. As these ligands are therefore of importance in this study, this chapter will be concluded with some aspects on the coordination of *S,O*-functionalized thiourea ligands to several metal centres.

## 2.6 Coordination of *S,O*-thiourea ligands to metal centres

It was clear from Chapter 1 that *S,O*-functionalized thiourea ligands have four potential donor sites and although an *S,O*-coordination of these ligands to the rhodium centre is expected, several examples are found in literature where these ligands can exhibit other coordination modes to different metal centres.

Koch *et al.*<sup>73a,b,c,d</sup> reported several Pt, Pd as well as Ni complexes where different *S,O*-functionalized thiourea ligands coordinated in a *S,O*-fashion on the metal centre. In each case two molecules of the same thiourea ligand were found around the equatorial plane of the metal centre in a *cis* conformation. In some cases the authors also illustrated that certain *S,O*-thiourea ligands such as *N*-benzoyl-*N'*-propylthiourea, of which the structure is normally stabilized by the hydrogen bond between the oxygen atom and the terminal nitrogen of the ligand, only *S*-coordination was observed on platinum centres under mild acidic conditions.<sup>74</sup> Pt(II) complexes were also reported where only one molecule of some *S,O*-thiourea ligands were allowed to coordinate onto the metal centre *via* a *S,O*-fashion by using Pt precursors having *S*-coordinated DMSO ligands and other derivatives.<sup>75a,b</sup>

Roodt *et al.*<sup>76a,b</sup> reported the first Rh(I) complexes with a *S,O*-functionalized thiourea ligand, i.e. the carbonyltriphenylphosphine- and carbonyltriphenylarsine rhodium(I) complexes of *N*-benzoyl-*N'*,*N'*-dibenzylthiourea, where the ligand coordinated in a *S,O*-fashion. The high *trans*-directing ability of the sulphur atom led to the formation of one isomer in each case, with the triphenylphosphine and triphenylarsine found *trans* to the sulphur atom at the metal centre. The same authors, in collaboration with Koch, also reported a rhodium complex with *N*-benzoyl-*N'*-phenylthiourea, where the ligand did not only coordinate in a *S,O*-mode on one rhodium centre, but also simultaneously bridged to another rhodium centre *via* one of the nitrogen atoms. One example of a rhodium COD (cyclooctadiene) complex with a *S,O*-functionalized thiourea ligand, namely *N*-benzoyl-*N'*-propylthiourea, was also reported

---

<sup>73</sup> a) Koch, K. R.; du Toit, J.; Cairns, M. R.; Sacht, C (1994) *J. Chem. Soc., Dalton Trans.*, 785. b) Koch, K. R.; Hallale, O.; Bourne, S. A.; Miller, J.; Bacsá, J. (2001) *J. Mol. Struct.*, **561**, 185. c) Westra, A. N.; Esterhuysen, C.; Koch, K. R. (2004) *Acta Cryst.*, **C60**, m395. d) Westra, A. N.; Bourne, S. A.; Esterhuysen, C.; Koch, K. R. (2005) *Dalton Trans.*, 2162 and references within.

<sup>74</sup> Bourne, S. A.; Koch, K. R. (1993) *J. Chem. Soc., Dalton Trans.*, 2071.

<sup>75</sup> a) Sacht, C.; Datt, M. S.; Otto, S.; Roodt, A. (2000) *J. Chem. Soc., Dalton Trans.*, 727. b) Sacht, C.; Datt, M. S.; Otto, S.; Roodt, A. (2000) *J. Chem. Soc., Dalton Trans.*, 4579.

<sup>76</sup> a) Roodt, A.; Leipoldt, J. G. (1994) *Rhodium Express*, **7-8**, 39. b) Kemp, G.; Roodt, A.; Purcell, W. (1996) *Rhodium Express*, **16**, 17.

by Cauzzi *et al.*<sup>77</sup>, where the ligand only coordinated in a *S*-fashion. Apart from these examples, no other rhodium complexes have been reported with *S,O*-functionalized thiourea ligands thus far, as suggested by a search done on the Cambridge Structure Database (CSD).<sup>78</sup>

Other types of *S,O*-functionalized thiourea ligands containing a phosphoryl moiety instead of a benzoyl moiety have also been reported to show unique coordination modes with different metal centres. Sokolov *et al.*<sup>79</sup> showed that *N*-phosphoryl-*N'*-phenylthiourea ligands can coordinate in a *S,O*-fashion with Co(II) centres, while it shows a preferable *N,S*-coordination with metal centres such as Ni(II) and Pd(II) under the same conditions. Safin *et al.*<sup>80</sup> showed that *N*-phosphoryl-*N'*-R-thiourea ligands (where R = tBu, Ph or 4'-benzo-15-crown-5) can lead to the formation of [Pd(L)<sub>2</sub>(Cl)<sub>2</sub>] complexes where two of the ligand molecules coordinate in a *S*-fashion *trans* to each other. These complexes were found to be stabilized by hydrogen bonding between a chloride atom and the nitrogen next to the phosphoryl moiety. In the case where a *N*-phosphoryl-L-thiourea ligand was used with L = Et<sub>2</sub>N or morpholine-*N*-yl, a *S,O*-coordination of two of the ligand molecules around the Pd metal centre was observed in a *cis* conformation.

Several other examples of coordination to metal centres exist in the literature from which, together with those reported above, it is clear that *S,O*-functionalized ligands can exhibit several coordination modes under different conditions with different metals.

---

<sup>77</sup> Cauzzi, D.; Lanfranchi, M.; Marzolini, G.; Predieri, G.; Tiripicchio, A.; Costa, M.; Zanoni, R. (1995) *J. Organomet. Chem.*, **488**, 115.

<sup>78</sup> CSD version 5.31, updated May 2010. Allen, F. H. (2002). *Acta Cryst.*, **B58**, 380

<sup>79</sup> Sokolov, F. D.; Zabirov, N. G.; Yamalieva, L. N.; Shtyrin, V. G.; Garipov, R. R.; Brusko, V. V.; Verat, A. Yu.; Baranov, S. V.; Mlynarz, P.; Glowiak, T.; Kozłowski, H. (2006) *Inorg. Chim. Acta*, **359**, 2087.

<sup>80</sup> Safin, D. A.; Sokolov, F. D.; Szyrwił, L.; Baranov, S. V.; Babashkina, M. G.; Gimadiev, T. R.; Kozłowski, H. (2008) *Polyhedron*, **27**, 1995.

## 2.7 Ligand effects

It was already mentioned in Chapter 1 that the electro-steric properties of ligands can have a substantial influence on the catalytic activity of metal catalysts. The effect and measurement of the electro-steric properties are discussed below in terms of phosphine ligands.

It was mentioned in Chapter 1 that the  $\pi$ -acidity and  $\sigma$ -basicity of phosphine ligands can be established on the basis of CO vibrational frequency changes of corresponding metal carbonyl complexes. As illustrated in Figure 2.11, an electron-rich ligand (Figure 2.11a) donates electron density onto the metal centre, increasing its electron density. This in turn causes a substantial amount of  $\pi$ -back donation to the CO ligands and as a result the IR vibrational frequency lowers in value. Strong  $\pi$ -acceptor ligands on the other hand (Figure 2.11b) remove electron density from the metal centre through back-donation, resulting in a much lower  $\pi$ -back donation onto the CO ligands. The consequence is that the vibrational frequency of CO increases in value.<sup>81</sup>

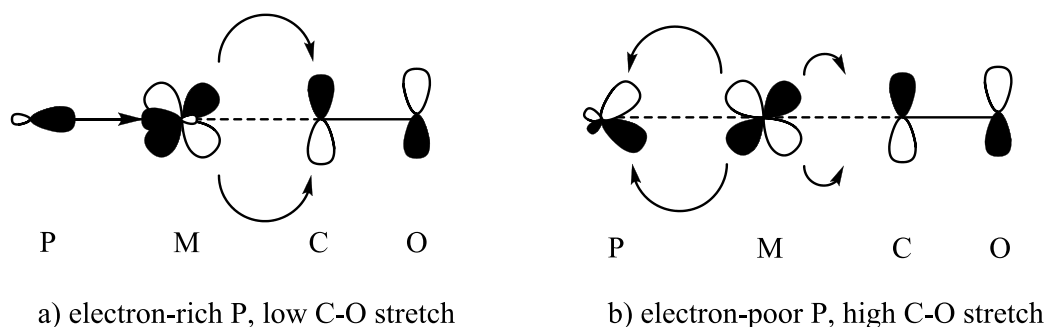


**Figure 2.11 A representation of the effect of basicity of phosphine ligands on metal centres and other co-ordinated ligands.**

Tolman<sup>52</sup> used vibrational spectra of  $\text{NiL}(\text{CO})_3$  with different ligands to define the electronic properties of phosphine ligands in terms of an electronic parameter  $\chi$ . With  $\text{L} = \text{P}(\text{t-Bu})_3$  as a reference ( $2056.1 \text{ cm}^{-1}$ ) this parameter is defined as the difference between the vibrational frequencies of the reference complex and another complex as indicated by equation 2.2.

$$\nu_{\text{CO}} (\text{A}_1) = 2056.1 + \sum_{i=1}^3 \chi_i \text{ cm}^{-1} \quad (2.2)$$

<sup>81</sup> Spessard, G.O.; Miessler, G.L. (1997) *Organometallic Chemistry*, Prentice-Hall, Englewood Cliffs, NJ.

A few examples of the values of the electronic parameter that he obtained for a range of phosphine ligands are given in Table 2.2. From here it can be seen that there is a good correlation between the CO vibrational frequencies and the electronic character of the phosphine ligands, where a decrease in the basicity of the phosphine ligands causes an increase in the electronic parameter  $\chi$ . When attempting to ascertain the contribution of only one substituent ( $\chi_i$ -value) it is sufficiently accurate to simply use 1/3 of the  $\chi$ -value for the 'homo' compound ( $\text{PR}_3$ ) and extrapolate an 'additive' figure/value into an 'hetero' compound (eg.  $\text{R}'_2\text{PR}$ ).

**Table 2.2 Phosphine ligands and their  $\chi$ -values.<sup>52</sup>**

Ligand $\text{PR}_3$ : R =	$\chi$ -value	IR frequency of $\text{NiL}(\text{CO})_3$ ( $\text{cm}^{-1}$ )
t-Bu	0	2056
n-Bu	4	2060
Ph	13	2069
$\text{CH}_3\text{O}$	20	2076
PhO	29	2085
Cl	41	2097
F	55	2111
$\text{CF}_3$	59	2115

The steric properties of ligands can be calculated by different methods. For monodentate ligands the most common method involves the use of Tolman's parameter  $\theta$ , defined as the cone angle of a phosphine ligand.<sup>82</sup> As depicted in Figure 2.12 it involves a cone constructed from the metal centre, set at a distance of 2.28 Å from the phosphorus atom, which then covers all the peripheral atoms of the substituents on the phosphorus atom. From this the effective cone angle  $\theta$  can then be determined using equation 2.3.

$$\theta = 2/3 \sum_{i=1}^3 \theta_i / 2 \quad (2.3)$$

<sup>82</sup> Tolman, C.A. (1977) *Chem Rev.*, **77**, 313.

Crystal structure analysis gives better insight on the actual size of the cone angle, as it usually differs from the cone angles obtained from calculations, and therefore the calculated value is only an approximate value and does not always accurately describe the steric properties. Some of the typical cone angle values calculated by Tolman are given in Table 2.3.

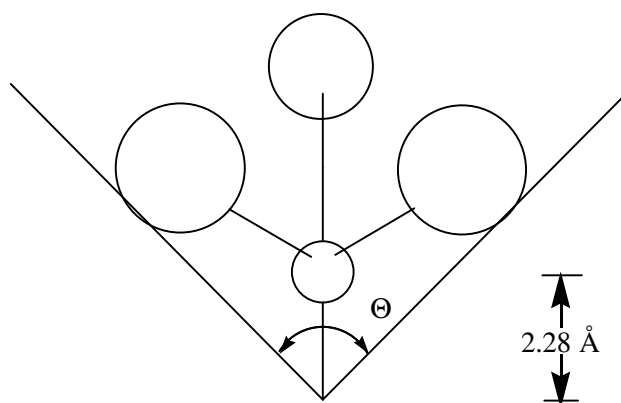


**Figure 2.12 A diagram defining the Tolman cone angle.<sup>82</sup>**

**Table 2.3 Tolman cone angles for some phosphine ligands.<sup>82</sup>**

Ligand $\text{PR}_3$ : R =	$\Theta$ -value ( $^\circ$ )
H	87
F	104
Br	131
$\text{CH}_3$	118
$\text{OCH}_3$	107
Ph	145
OPh	128
$\text{CF}_3$	137
$\text{C}_6\text{F}_5$	184
<i>o</i> - $\text{C}_6\text{H}_4\text{CH}_3$	194

Alternative methods include the measurement of complex dissociation constants for ligands, where the amount of dissociation correlates well with the steric parameter. Examples include the use of cobaloxime complexes<sup>83</sup> as well as molybdenum complexes of the type *cis*- $\text{Mo}(\text{CO})_4\text{L}_2$ .<sup>84</sup> Tolman also determined that the degree of substitution of  $\text{Ni}(\text{CO})_4$  with

<sup>83</sup> Trogler, W.C.; Marzilli, L.G. *Inorg. Chem.* **1975**, *14*, 2942.

<sup>84</sup> Darensbourg, D.J.; Kump, R.L. *Inorg. Chem.* **1978**, *17*, 2680.

phosphine ligands correlates well with the steric parameter.<sup>85</sup> Other methods involve the use of thermochemistry where the heats of formation of metal-phosphine complexes can be determined, which, if the electronic effects are small, is a measurement of the steric hindrance in these complexes.<sup>86</sup> It is found that an increase in the steric bulk of a ligand causes a decrease in the heats of formation.

For bidentate ligands the use of Tolman's parameter is quite complicated, and therefore another method has been developed which includes the concept of a bite angle. Rigid bidentate ligands contain what is known as a ligand backbone which keeps the two  $\sigma$ -donor atoms at a constrained distance from each other. This distance is found to be very specific for each bidentate ligand and together with the flexibility of the backbone determines the bite angle that will result after complexing with a metal centre. This definition of a bite angle is depicted in Figure 2.13 in the case of biphosphine ligands.<sup>87</sup>

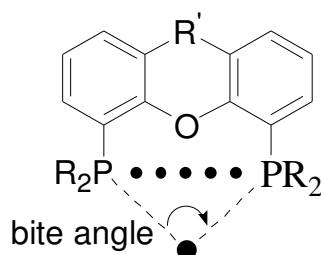


**Figure 2.13 A representation defining the bite angle of bidentate ligands co-ordinated to a metal centre.**

Although a wide variety of bidentate phosphines may be synthesised, not all of them have the correct conformations to co-ordinate onto a metal centre. The lone pairs of electrons on the phosphorus atoms need to point in the direction of the metal centre.<sup>1</sup> A few examples of common bidentate phosphines and their bite angles are given in Figure 2.14.

<sup>85</sup> Tolman, C.A. *J. Am. Chem. Soc.* **1970**, 92, 2956.

<sup>86</sup> Serron, S.; Nolan, S.P.; Moloy, K.G. *Organometallics* **1996**, 15, 4301.

<sup>87</sup> Dierkes, P.; van Leeuwen, P.W.N.M. *J. Chem. Soc. Dalton. Trans.* **1999**, 1519.

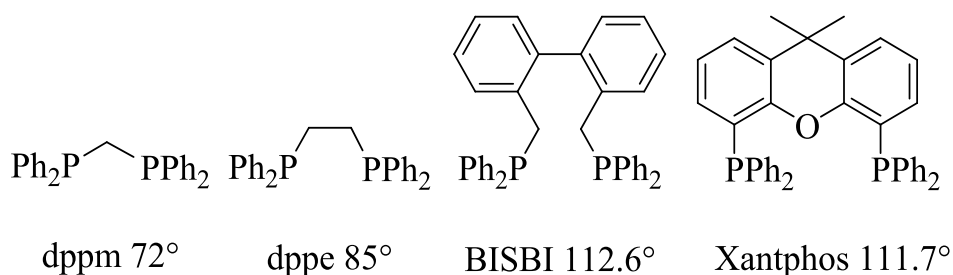


**Figure 2.14** The bite angle of a few examples of biphosphine ligands

## 2.8 Conclusion

With the theoretical background provided in Chapters 1 and 2, it is clear that the design and use of different transition metal complexes with different ligands can have substantial influences on the outcome and reactivity of many catalytic processes known today. Apart from the examples provided above, there is little work done on the effect of *S,O*-donor ligands on the iodomethane oxidative addition to the corresponding Rh(I) complexes as well as on the outcome of carbonylation reactions. This provided the opportunity in studying such systems to obtain more informative data in this regard and also to study the mechanisms and reactivity of the possible homologation of methanol to ethanol. Rhodium systems with *P,P*-donor ligands were also considered for investigation, since these types of ligands generally provide good catalytic activity for many transition metal complexes.



# **CHAPTER 3**

## **THE SYNTHESIS AND CHARACTERIZATION OF FUNCTIONALISED-*S,O*-THIOUREA LIGANDS**

### **3.1 Introduction**

Different aspects of bidentate ligands containing oxygen, nitrogen, phosphorus and sulphur atoms in transition metal co-ordination chemistry has been described in Chapter 2. It was clearly shown in 2.5 that bidentate ligands containing at least one sulphur donor atom allow the formation of Rh(III)-acyl species upon iodomethane oxidative addition to the corresponding complexes. It was further indicated that little work has been done on rhodium complexes containing *S,O*-functionalized bidentate ligands and a search of rhodium systems built from *S,O* donor bidentate ligands on the Cambridge Structure Database (CSD)<sup>1</sup> revealed that little structural data is available on these systems. An advantage in using *S,O*-donor ligands includes the fact that both S and O atoms are relatively strong  $\sigma$ -donors, which would result in fairly electron-rich rhodium centres. It has been shown that in carbonylation processes such as the Monsanto process that electron-rich catalysts favour the reaction rate of the process, since the oxidative addition step is considered to be the rate-determining step.<sup>2</sup> Since a principle aim of this Ph.D study was to investigate basic aspects of the reductive carbonylation/hydrogenation of methanol to ethanol, it was decided to synthesize and characterize a range of Rh(I) complexes with *S,O*-bidentate ligands and investigate their conversion to the corresponding Rh(III)-acyl species by iodomethane oxidative addition as a first step in the catalytic process.

The type of *S,O*-donor bidentate ligands of choice was the thiourea species: reasons being that they can be obtained with ease and high yields and also they are known to be fairly stable. Hundreds of examples of these *S,O*-functionalized thiourea ligands can be found in the CSD.<sup>1</sup> In this chapter the synthesis and general characterization of several *S,O*-functionalized

---

<sup>1</sup> CSD version 5.31, updated May 2010. Allen, F. H. (2002). *Acta Cryst.*, **B58**, 380

<sup>2</sup> van Leeuwen, P.W.N.M. (2004) *Homogeneous Catalysis, Understanding the art*, Kluwer Academic Publishers, Dordrecht.

thiourea ligands will be described in detail. The single crystal X-ray analysis on some of these ligands will be shown and discussed in Chapter 4.

### 3.2 Reagents and equipment

Unless otherwise stated all experiments were carried out in air, using analytical grade reagents. Ammonium thiocyanate was purchased from Fluka, South Africa. Benzoyl chloride as well as the various types of amines that were utilised in this study were obtained from Sigma Aldrich. These reagents were used as received.

NMR spectroscopic data was acquired on a Bruker Advance II 600 MHz spectrometer.  $^1\text{H}$  NMR data are listed in the order: chemical shift ( $\delta$ , reported in ppm and referenced to the residual solvent peak of  $(\text{CD}_3)_2\text{SO}$  [ $\delta = 2.50$  ppm] or  $\text{CDCl}_3$  [ $\delta = 7.26$  ppm]), multiplicity, number of protons, assignment, coupling constant ( $J$ , in Hz). Proton decoupling experiments were used to assist in the assignment of proton signals. Proton-decoupled  $^{13}\text{C}$  NMR data are listed in the order: chemical shift ( $\delta$ , reported in ppm and referenced to the residual solvent peak of  $(\text{CD}_3)_2\text{SO}$  [ $\delta = 39.5$  ppm] or  $\text{CDCl}_3$  [ $\delta = 77.0$  ppm]), multiplicity, number of carbons, assignment, coupling constant ( $J$ , in Hz) where appropriate. HMQC and HMBC experiments were performed to assist in the allocation of signals.  $^{19}\text{F}$  NMR data are listed in the order: chemical shift ( $\delta$ , reported in ppm and referenced to aqueous potassium fluoride [ $\delta = -125.3$  ppm]), multiplicity, number of fluoride atoms, coupling constant ( $J$ , in Hz) where appropriate.

FT-IR spectra were recorded on a Bruker Tensor 27 spectrophotometer in the range of 3000-600  $\text{cm}^{-1}$  via the ATR.

### 3.3 Synthetic procedure for *S,O*-donor thiourea ligands

The general structure as well as the general procedure for the *S,O*-functionalized thiourea ligands are shown in Figure 3.1. As can be observed by varying the type of amine used in this synthesis a range of thiourea ligands can be synthesised with alternate electro-steric properties. This is important in order to elucidate whether a change in the electro-steric properties of thiourea ligands would also have an effect on the properties of the rhodium complexes that can be formed from these ligands.

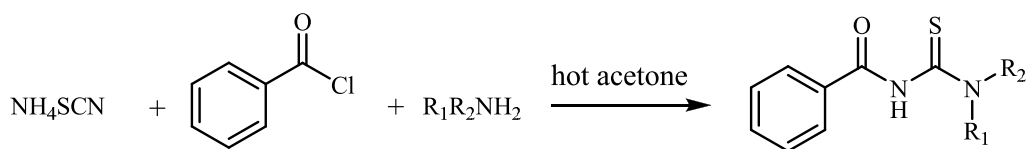
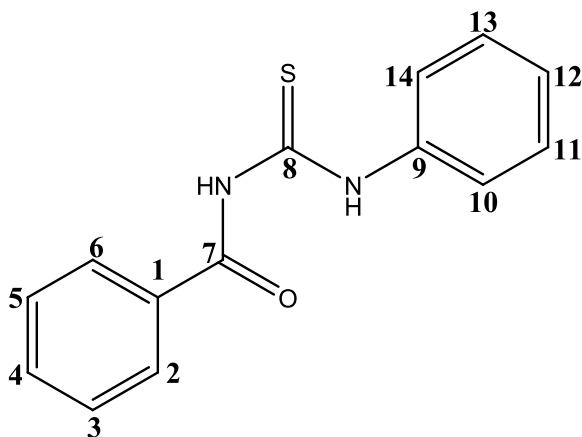


**Figure 3.1: General synthesis of *S,O*-donor bidentate thiourea ligands**

These thiourea ligands were synthesised with a slight variation of the procedure previously described by Douglass *et al.*<sup>3</sup> Ammonium thiocyanate (1.31 g, 0.017 mol) was weighed accurately and dissolved in acetone (10 ml). The solution was heated and stirred until all of the ammonium thiocyanate dissolved. As the solution was still being stirred benzoyl chloride (2 ml, 0.017 mol) was added drop-wise upon which the reaction led to a milky light yellow solution. The byproduct ammonium chloride precipitated out as the reaction proceeded. After about 20 min the reaction mixture was filtered and the filtrate was collected and heated again. As this filtrate was being stirred the desired amine (0.017 mol) was added slowly to the solution, after which the reaction mixture was allowed to stir for another half an hour. The corresponding thiourea ligand was then precipitated out using distilled water, after which it was filtered and washed with a few portions of water. The product was then dissolved in either methanol or ethanol in which most cases the product either crystallised out or formed a white solid. Any alternative treatment that had to be undertaken will be indicated with each individual ligand.

<sup>3</sup> Douglass, I. B.; Dains, F. B. (1934) *J. Am. Chem. Soc.*, **56**, 719

### 3.3.1 *N*-benzoyl-*N'*-(phenyl)thiourea



The ligand *N*-benzoyl-*N'*-phenylthiourea was synthesised using the methodology as described above. Colourless crystalline solid (Yield: g, 95 %).

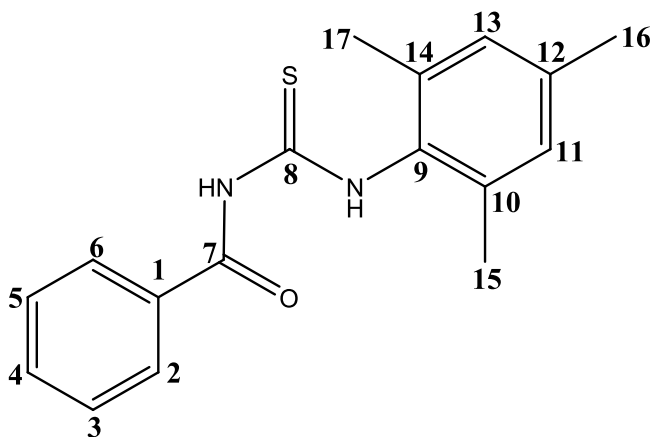
$^1\text{H}$  NMR (600 MHz,  $\text{CDCl}_3$ , 25 °C):  $\delta$  12.61 (s, 1H,  $\text{CONHCS}$ ), 9.14 (s, 1H,  $\text{CSNHCH}$ ), 7.92 (dd, 2H, H2 and H6,  $J_{\text{H-H}} = 8.4$  Hz,  $J_{\text{H-H}} = 1.2$  Hz), 7.74 (d, 2H, H10 and H14,  $J_{\text{H-H}} = 7.2$  Hz), 7.67 (tt, 1H, H4,  $J_{\text{H-H}} = 7.5$  Hz,  $J_{\text{H-H}} = 1.2$  Hz), 7.57 (t, 2H, H3 and H5,  $J_{\text{H-H}} = 7.8$  Hz), 7.45 (t, 2H, H11 and H13,  $J_{\text{H-H}} = 7.8$  Hz), 7.31 (tt, 1H, H12,  $J_{\text{H-H}} = 7.2$  Hz,  $J_{\text{H-H}} = 1.2$  Hz).

$^{13}\text{C}$  NMR (151 MHz,  $\text{CDCl}_3$ , 25 °C):  $\delta$  178.7 (s, 1C, C8), 167.3 (s, 1C, C7), 137.9 (s, 1C, C9), 134.1 (s, 1C, C4), 132.0 (s, 1C, C1), 129.6 (s, 2C, C2 and C6), 129.3 (s, 2C, C11 and C13), 127.8 (s, 2C, C3 and C5), 127.2 (s, 1C, C12), 124.5 (s, 2C, C10 and C14).

IR  $\nu_{\text{max}}$  ATR/ $\text{cm}^{-1}$ : 3260 (free N-H); 2984 (associated N-H); 1671 (C=O); 1600-1447 (phenyl rings); 1357 (aromatic 2° amine C-N); 1255 (C=S); 1142 and 1073 (C-N).

Element analysis (%): Found C, 64.2; H, 4.6; N, 10.7. Calculated for  $\text{C}_{14}\text{H}_{12}\text{N}_2\text{SO}$ : C, 65.6; H, 4.7; N, 10.9.

### 3.3.2 *N*-benzoyl-*N'*-(2,4,6-trimethylphenyl)thiourea



The ligand *N*-benzoyl-*N'*-(2,4,6-trimethylphenyl)thiourea was synthesised using the methodology as described above. Colourless crystalline solid (Yield: g, 97 %).

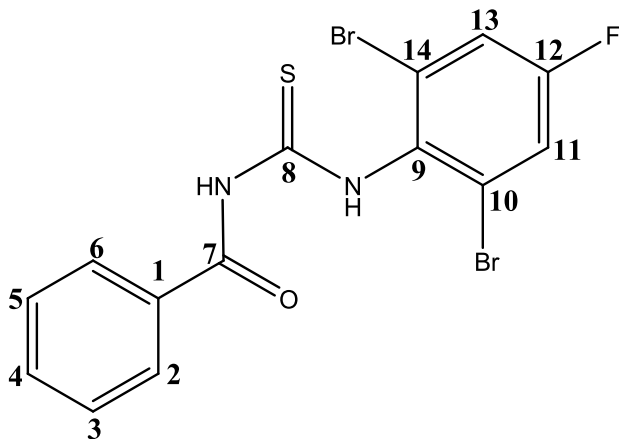
$^1\text{H}$  NMR (600 MHz,  $(\text{CD}_3)_2\text{SO}$ , 25 °C):  $\delta$  11.85 (s, 1H, CONHCS), 11.57 (s, 1H, CSNHCH), 8.02 (dd, 2H, H2 and H6,  $J_{\text{H-H}} = 8.3$  Hz,  $J_{\text{H-H}} = 1.2$  Hz), 7.66 (tt, 1H, H4,  $J_{\text{H-H}} = 7.4$  Hz,  $J_{\text{H-H}} = 1.2$  Hz), 7.53 (t, 2H, H3 and H5,  $J_{\text{H-H}} = 8.2$  Hz), 6.92 (s, 2H, H11 and H13), 2.26 (s, 3H, *p*-CH<sub>3</sub>), 2.17 (s, 6H, *o*-CH<sub>3</sub>).

$^{13}\text{C}$  NMR (151 MHz,  $(\text{CD}_3)_2\text{SO}$ , 25 °C):  $\delta$  180.4 (s, 1C, C8), 168.0 (s, 1C, C7), 136.5 (s, 1C, C9), 134.6 (s, 2C, C10 and C14), 133.7 (s, 1C, C12), 133.0 (s, 1C, C4), 132.0 (s, 1C, C1), 128.7 (s, 2C, C2 and C6), 128.5 (s, 2C, C3 and C5), 128.4 (s, 2C, C11 and C13), 20.5 (s, 1C, *p*-CH<sub>3</sub>), 17.8 (s, 2C, *o*-CH<sub>3</sub>).

IR  $\nu_{\text{max}}$  ATR/ $\text{cm}^{-1}$ : 3392 (free N-H); 3211-3132 (associated N-H); 1659 (C=O); 1500 (broad, aromatic rings); 1324 (aromatic 2° amine C-N); 1266 (C=S); 1164, 1140 and 1089 (C-N).

Element analysis (%): Found C, 68.8; H, 6.0; N, 10.2. Calculated for C<sub>17</sub>H<sub>18</sub>N<sub>2</sub>SO: C, 68.4; H, 6.1; N, 9.4.

### 3.3.3 *N*-benzoyl-*N'*-(2,6-dibromo-4-fluorophenyl)thiourea



The ligand *N*-benzoyl-*N'*-(2,6-dibromo-4-fluorophenyl)thiourea was synthesised using the methodology as described above. Light pink crystalline solid (Yield: g, 90 %).

$^1\text{H}$  NMR (600 MHz,  $(\text{CD}_3)_2\text{SO}$ , 25 °C):  $\delta$  12.08 (s, 1H, CONHCS), 11.91 (s, 1H, CSNHCH), 8.01 (d, 2H, H2 and H6,  $J_{\text{H-H}} = 7.5$  Hz), 7.77 Hz (d, 2H, H11 and H13,  $J_{\text{H-F}} = 8.0$  Hz), 7.67 (t, 1H, H4,  $J_{\text{H-H}} = 7.4$  Hz), 7.54 (t, 2H, H3 and H5,  $J_{\text{H-H}} = 7.8$  Hz).

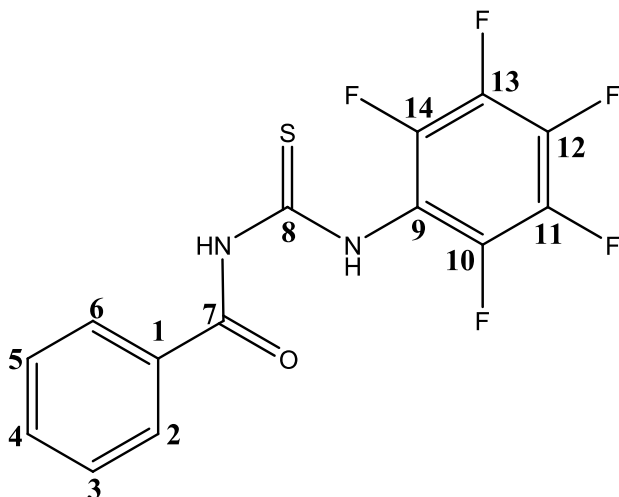
$^{13}\text{C}$  NMR (151 MHz,  $(\text{CD}_3)_2\text{SO}$ , 25 °C):  $\delta$  181.6 (s, 1C, C8), 168.6 (s, 1C, C7), 160.7 (d, 1C, C12,  $J_{\text{C-F}} = 252.5$  Hz), 134.6 (s, 1C, C9,  $J_{\text{C-Br}} = 3.8$  Hz), 133.8 (s, 1C, C4), 132.2 (s, 1C, C1), 129.2 (s, 2C, C2 and C6), 129.0 (s, 2C, C3 and C5), 124.9 (d, 2C, C10 and C14,  $J_{\text{C-Br}} = 11.2$  Hz), 120.0 (d, 2C, C11 and C13,  $J_{\text{C-F}} = 25.2$  Hz).

$^{19}\text{F}$  NMR (564 MHz,  $(\text{CD}_3)_2\text{SO}$ , 25 °C):  $\delta$  -111.08 (t, 1F, F12,  $J_{\text{F-H}} = 7.9$  Hz).

IR  $\nu_{\text{max}}$  ATR/ $\text{cm}^{-1}$ : 3213 (free N-H); 3100 (associated N-H); 1668 (C=O); 1585-1450 (broad, aromatic rings); 1389 (aromatic 2° amine C-N); 1281 (C=S); 1206 and 1160 (C-N).

Element analysis (%): Found C, 38.5; H, 2.0; N, 6.5. Calculated for  $\text{C}_{14}\text{H}_9\text{N}_2\text{SOBr}_2\text{F}$ : C, 38.9; H, 2.1; N, 6.5.

### 3.3.4 *N*-benzoyl-*N'*-(2,3,4,5,6-pentafluorophenyl)thiourea



The ligand *N*-benzoyl-*N'*-(2,3,4,5,6-pentafluorophenyl)thiourea was synthesised using the methodology as described above. Colourless crystalline solid (Yield: g, 85 %).

$^1\text{H}$  NMR (600 MHz,  $(\text{CD}_3)_2\text{SO}$ , 25 °C):  $\delta$  12.14 (s, 1H, CONHCS), 11.87 (s, 1H, CSNHCH), 8.02 (dd, 2H, H2 and H6,  $J_{\text{H-H}} = 8.3$  Hz,  $J_{\text{H-H}} = 1.1$  Hz), 7.68 (tt, 1H, H4,  $J_{\text{H-H}} = 7.4$  Hz,  $J_{\text{H-H}} = 1.2$  Hz), 7.55 (t, 2H, H3 and H5,  $J_{\text{H-H}} = 8.2$  Hz).

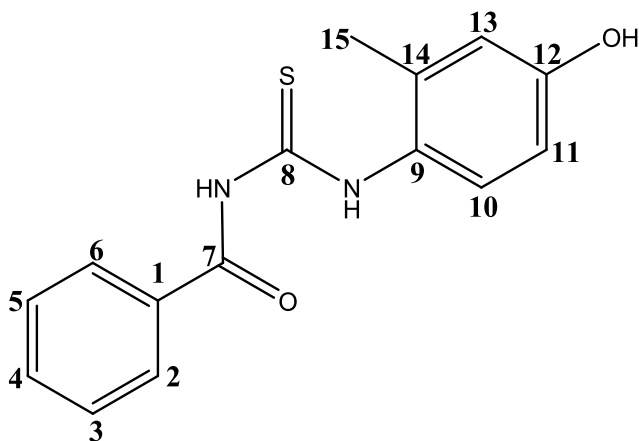
$^{13}\text{C}$  NMR (151 MHz,  $(\text{CD}_3)_2\text{SO}$ , 25 °C):  $\delta$  183.0 (s, 1C, C8), 168.6 (s, 1C, C7), 143.8 (d, 2C, C10 and C14,  $J_{\text{C-F}} = 243.3$  Hz), 140.5 (dt, 1C, C12,  $J_{\text{C-F}} = 251.9$  Hz,  $J_{\text{C-F}} = 13.1$  Hz), 137.6 (dt, 2C, C11 and C13,  $J_{\text{C-F}} = 248.5$  Hz,  $J_{\text{C-F}} = 13.1$  Hz), 133.8 (s, 1C, C4), 132.2 (s, 1C, C1), 129.3 (s, 2C, C2 and C6), 128.9 (s, 2C, C3 and C5), 115.5 (td, 1C, C9,  $J_{\text{C-F}} = 15.1$  Hz,  $J_{\text{C-F}} = 2.4$  Hz).

$^{19}\text{F}$  NMR (564 MHz,  $(\text{CD}_3)_2\text{SO}$ , 25 °C):  $\delta$  -144.6 (d, 2F, F10 and F14,  $J_{\text{F-F}} = 19.2$  Hz), -155.6 (t, 1F, F12,  $J_{\text{F-F}} = 22.9$  Hz), -163.8 (t, 2F, F11 and F13,  $J_{\text{F-F}} = 22.3$  Hz).

IR  $\nu_{\text{max}}$  ATR/ $\text{cm}^{-1}$ : 3345 (free N-H); 3135 (associated N-H); 1669 (C=O); 1505-1453 (phenyl rings); 1333 (aromatic 2° amine C-N); 1252 (C=S); 1179 and 1145 (C-N).

Element analysis (%): Found C, 47.9; H, 1.9; N, 8.0. Calculated for  $\text{C}_{14}\text{H}_7\text{N}_2\text{SOF}_5$ : C, 48.6; H, 2.0; N, 8.1.

### 3.3.5 *N*-benzoyl-*N'*-(4-hydroxy-2-methylphenyl)thiourea



The ligand *N*-benzoyl-*N'*-(4-hydroxy-2-methylphenyl)thiourea was synthesised using the methodology as described above. Light brown crystalline solid (Yield: 97 %).

$^1\text{H}$  NMR (600 MHz,  $(\text{CD}_3)_2\text{SO}$ , 25 °C):  $\delta$  12.08 (s, 1H, CONHCS), 11.51 (s, 1H, CSNHCH), 9.44 (s, 1H, OH), 7.99 (d, 2H, H2 and H6,  $J_{\text{H-H}} = 7.8$  Hz), 7.65 (tt, 1H, H4,  $J_{\text{H-H}} = 7.3$  Hz,  $J_{\text{H-H}} = 0.6$  Hz), 7.53 (t, 2H, H3 and H5,  $J_{\text{H-H}} = 7.8$  Hz), 7.28 (d, 1H, H10,  $J_{\text{H-H}} = 8.4$  Hz), 6.69 (d, 1H, H13,  $J_{\text{H-H}} = 2.4$  Hz), 6.64 (dd, 1H, H11,  $J_{\text{H-H}} = 8.4$  Hz,  $J_{\text{H-H}} = 3.0$  Hz), 2.17 (s, 3H,  $\text{CH}_3$ ).

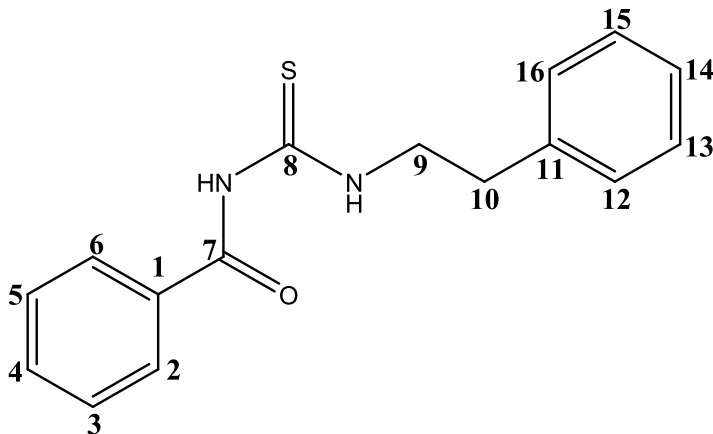
$^{13}\text{C}$  NMR (151 MHz,  $(\text{CD}_3)_2\text{SO}$ , 25 °C):  $\delta$  180.8 (s, 1C, C8), 168.7 (s, 1C, C7), 156.7 (s, 1C, C12), 135.3 (s, 1C, C9), 133.5 (s, 1C, C4), 132.6 (s, 1C, C1), 129.1 (s, 2C, C2 and C6), 128.9 (s, 2C, C3 and C5), 128.8 (s, 1C, C14), 128.3 (s, 1C, C10), 117.2 (s, 1C, C13), 113.3 (s, 1C, C11), 18.3 (s, 1C, *o*- $\text{CH}_3$ ).

IR  $\nu_{\text{max}}$  ATR/ $\text{cm}^{-1}$ : 3358 (free N-H); 3045 (associated N-H); 1673 (C=O); 1615-1434 (phenyl rings); 1354 (aromatic 2° amine C-N); 1282 (C=S); 1224, 1172 and 1150 (C-N).

Element analysis (%): Found C, 61.7; H, 4.5; N, 9.7. Calculated for  $\text{C}_{15}\text{H}_{14}\text{N}_2\text{SO}_2$ : C, 62.9; H, 4.9; N, 9.8.



### 3.3.6 *N*-benzoyl-*N'*-(phenethyl)thiourea



The ligand *N*-benzoyl-*N'*-phenethylthiourea was synthesised using the methodology as described above. Colourless crystalline solid (Yield: 92 %).

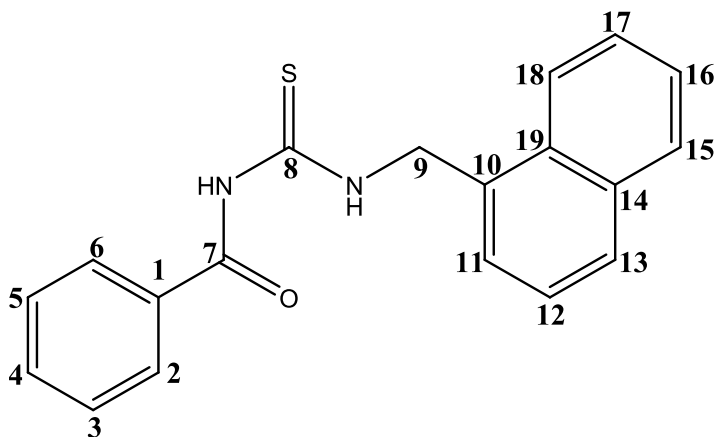
$^1\text{H}$  NMR (600 MHz,  $(\text{CD}_3)_2\text{SO}$ , 25 °C):  $\delta$  11.31 (s, 1H, CONHCS), 10.93 (s, 1H, CSNHCH), 7.90 (d, 2H, H2 and H6,  $J_{\text{H-H}} = 7.8$  Hz), 7.62 (t, 1H, H4,  $J_{\text{H-H}} = 7.2$  Hz), 7.50 (t, 2H, H3 and H5,  $J_{\text{H-H}} = 7.5$  Hz), 7.33-7.28 (m, 4H, H12, H13, H15 and H16), 7.22 (t, 1H, H14,  $J_{\text{H-H}} = 6.6$  Hz), 3.85 (q, 2H, H9,  $J_{\text{H-H}} = 6.6$  Hz), 2.96 (t, 2H, H10,  $J_{\text{H-H}} = 7.2$  Hz).

$^{13}\text{C}$  NMR (151 MHz,  $(\text{CD}_3)_2\text{SO}$ , 25 °C):  $\delta$  181.1 (s, 1C, C8), 169.0 (s, 1C, C7), 139.7 (s, 1C, C11), 133.9 (s, 1C, C4), 133.1 (s, 1C, C1), 129.6 (s, 2C, C2 and C6), 129.4 (s, 4C, C3, C5, C12 and C16), 129.3 (s, 2C, C13 and C15), 127.3 (s, 1C, C14), 47.2 (s, 1C, C9), 34.4 (s, 1C, C10).

IR  $\nu_{\text{max}}$  ATR/ $\text{cm}^{-1}$ : 3402-3341 (free N-H), 3196-3177 (associated N-H); 3064, 3033, 2930 and 2869 (C-H, alkyl); 1672 (C=O); 1555-1451 (phenyl rings); 1319 (aromatic 2° amine C-N); 1289 (C=S); 1154, 1100 and 1071 (C-N).

Element analysis (%): Found C, 68.0; H, 5.6; N, 9.3. Calculated for  $\text{C}_{16}\text{H}_{16}\text{N}_2\text{SO}$ : C, 67.6; H, 5.7; N, 9.85.

### 3.3.7 N-benzoyl-N'-(naphthalen-1-ylmethyl)thiourea



The ligand *N*-benzoyl-*N'*-(naphthalen-1-ylmethyl)thiourea was synthesised using the methodology as described above. Colourless crystalline solid (Yield: 93 %).

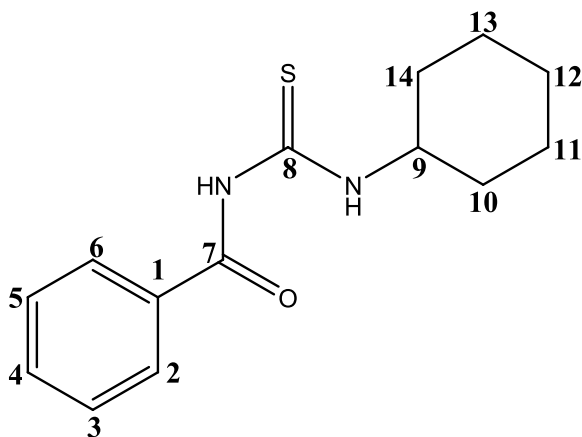
$^1\text{H}$  NMR (600 MHz,  $(\text{CD}_3)_2\text{SO}$ , 25 °C):  $\delta$  11.51 (s, 1H, CONHCS), 11.30 (t, 1H, CSNHCH,  $J_{\text{H-H}} = 4.8$  Hz), 8.12 (d, 1H, H18,  $J_{\text{H-H}} = 8.4$  Hz), 7.99 (d, 1H, H15,  $J_{\text{H-H}} = 7.8$  Hz), 7.92 (m, 3H, H2, H6 and H13), 7.62-7.48 (m, 7H, H3, H4, H5, H11, H12, H16 and H17), 5.36 (d, 2H, H9,  $J_{\text{H-H}} = 4.8$  Hz).

$^{13}\text{C}$  NMR (151 MHz,  $(\text{CD}_3)_2\text{SO}$ , 25 °C):  $\delta$  180.9 (s, 1C, C8), 168.7 (s, 1C, C7), 133.9 (s, 1C, C10), 133.5 (s, 1C, C4), 133.0 (s, 1C, C14), 132.6 (s, 1C, C19), 131.3 (s, 1C, C1), 129.2 (s, 1C, C11), 129.1 (s, 2C, C2 and C6), 128.8 (s, 2C, C3 and C5), 128.6 (s, 1C, C15), 127.1 (s, 1C, C13), 126.5 (s, 2C, C16 and C17), 126.0 (s, 1C, C12), 123.7 (s, 1C, C18), 46.9 (s, 1C, C9).

IR  $\nu_{\text{max}}$  ATR/ $\text{cm}^{-1}$ : 3400 (free N-H); 3212 (associated N-H); 1667 (C=O); 1600-1510 (aromatic rings); 1310 (aromatic 2° amine C-N); 1284 or 1251 (C=S); 1172, 1156 and 1102 (C-N).

Element analysis (%): Found C, 69.9; H, 4.85; N, 8.7. Calculated for  $\text{C}_{19}\text{H}_{16}\text{N}_2\text{SO}$ : C, 71.2; H, 5.0; N, 8.7.

### 3.3.8 *N*-benzoyl-*N'*-(cyclohexyl)thiourea



The ligand *N*-benzoyl-*N'*-cyclohexylthiourea was synthesised using the methodology as described above. Colourless crystalline solid (Yield: 65 %).

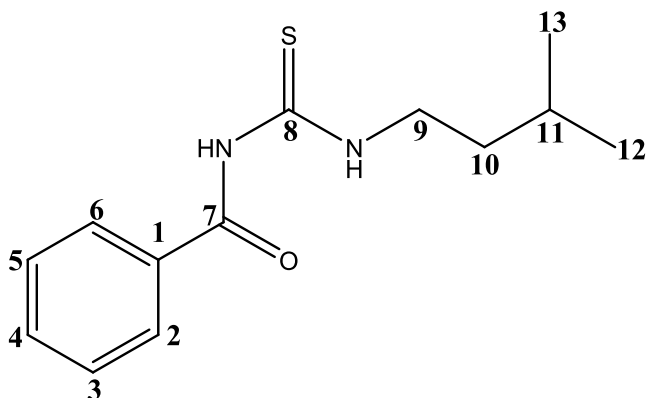
$^1\text{H}$  NMR (600 MHz,  $(\text{CD}_3)_2\text{SO}$ , 25 °C):  $\delta$  11.27 (s, 1H, CONHCS), 10.95 (s, 1H, CSNHCH), 7.92 (dd, 2H, H2 and H6,  $J_{\text{H-H}} = 8.4$  Hz), 7.64 (t, 1H, H4,  $J_{\text{H-H}} = 7.5$  Hz), 7.50 (t, 2H, H3 and H5,  $J_{\text{H-H}} = 7.8$  Hz), 4.21 (m, 1H, H9), 1.96 and 1.67 (m, 4H, H10 and H14), 1.55 (m, 1H, H12), 1.38 (m, 4H, H11 and H13), 1.27 (m, 1H, H12). ).

$^{13}\text{C}$  NMR (151 MHz,  $(\text{CD}_3)_2\text{SO}$ , 25 °C):  $\delta$  179.3 (s, 1C, C8), 168.9 (s, 1C, C7), 133.4 (s, 1C, C4), 132.7 (s, 1C, C1), 129.0 (s, 2C, C2 and C6), 128.8 (s, 2C, C3 and C5), 53.4 (s, 1C, C9), 31.3 (s, 2C, C10 and C14), 25.5 (s, 1C, C12), 24.5 (s, 2C, C11 and C13).

IR  $\nu_{\text{max}}$  ATR/ $\text{cm}^{-1}$ : 3170 (broad, N-H); 1669 (C=O); 1525 and 1445 (broad, phenyl ring); 1341 (aromatic 2° amine C-N); 1260 (C=S); 1196, 1169 and 1100 (C-N).

Element analysis (%): Found C, 62.2; H, 7.1; N, 11.45. Calculated for  $\text{C}_{14}\text{H}_{18}\text{N}_2\text{SO}$ : C, 64.1; H, 6.9; N, 10.7.

### 3.3.9 *N*-benzoyl-*N'*-(isopentyl)thiourea



The ligand *N*-benzoyl-*N'*-isopentylthiourea was synthesised using the methodology as described above. Colourless crystalline solid (Yield: 60 %).

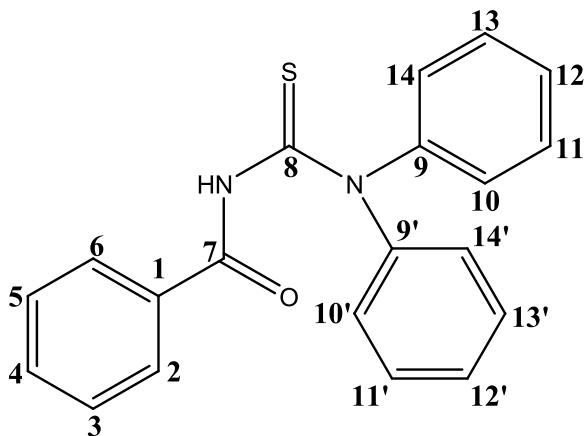
$^1\text{H}$  NMR (600 MHz,  $(\text{CD}_3)_2\text{SO}$ , 25 °C):  $\delta$  11.24 (s, 1H,  $\text{CONHCS}$ ), 10.88 (s, 1H,  $\text{CSNHCH}_2$ ), 7.93 (d, 2H, H2 and H6,  $J_{\text{H-H}} = 8.4$  Hz), 7.61 (t, 1H, H4,  $J_{\text{H-H}} = 7.2$  Hz), 7.50 (t, 2H, H3 and H5,  $J_{\text{H-H}} = 7.8$  Hz), 3.64 (m, 2H, H9), 1.60 (m, 1H, H11), 1.53 (m, 2H, H10), 0.91 (s, 6H,  $\text{CH}_3$ ).

$^{13}\text{C}$  NMR (151 MHz,  $(\text{CD}_3)_2\text{SO}$ , 25 °C):  $\delta$  180.44 (s, 1C, C8), 168.50 (s, 1C, C7), 133.33 (s, 1C, C4), 132.70 (s, 1C, C1), 128.96 (s, 2C, C2 and C6), 128.80 (s, 2C, C3 and C5), 43.52 (s, 1C, C9), 36.95 (s, 1C, C10), 25.93 (s, 1C, C11), 22.76 (s, 2C, C12 and C13).

IR  $\nu_{\text{max}}$  ATR/ $\text{cm}^{-1}$ : 3228 (broad, N-H); 1672 (C=O); 1555-1446 (phenyl ring); 1341 (aromatic 2° amine C-N); 1270 or 1243 (C=S); 1178, 1147, 1123 and 1073 (C-N).

Element analysis (%): Found C, 62.0; H, 7.1; N, 11.3. Calculated for  $\text{C}_{13}\text{H}_{18}\text{N}_2\text{SO}$ : C, 62.4; H, 7.3; N, 11.2.

### 3.3.10 *N*-benzoyl-*N',N'*-(diphenyl)thiourea



The ligand *N*-benzoyl-*N',N'*-diphenylthiourea was synthesised using the methodology as described above. White powder (Yield: 98 %).

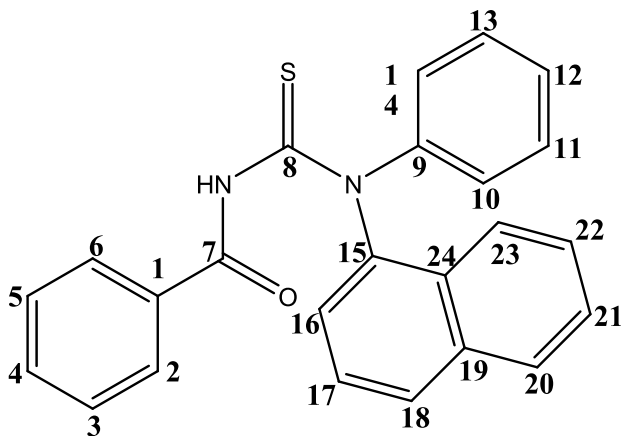
<sup>1</sup>H NMR (600 MHz, (CD<sub>3</sub>)<sub>2</sub>SO, 25 °C): δ 11.19 (s, 1H, CONHCS), 7.63 (d, 2H, H2 and H6, *J*<sub>H-H</sub> = 8.4 Hz), 7.51 (t, 1H, H4, *J*<sub>H-H</sub> = 7.3 Hz), 7.39 (t, 2H, H3 and H5, *J*<sub>H-H</sub> = 7.8 Hz), 7.36-7.35 (m, 4H, H10, H10', H14 and H14'), 7.30-7.28 (m, 4H, H11, H11', H13 and H13'), 7.23-7.21 (m, 2H, H12 and H12').

<sup>13</sup>C NMR (151 MHz, (CD<sub>3</sub>)<sub>2</sub>SO, 25 °C): δ 184.5 (s, 1C, C8), 167.3 (s, 1C, C7), 145.6 (s, 2C, C9 and C9'), 132.7 (s, 1C, C1), 132.3 (s, 1C, C4), 129.1 (s, 4C, C10, C10', C14 and C14'), 128.2 (s, 2C, C2 and C6), 128.1 (s, 2C, C3 and C5), 127.0 (s, 2C, C12 and C12'), 126.8 (s, 4C, C11, C11', C13 and C13').

IR ν<sub>max</sub> ATR/cm<sup>-1</sup>: 3215-3125 (broad, N-H); 1691 (C=O); 1504-1447 (broad, phenyl rings); 1354 (aromatic 2° amine C-N); 1255 (C=S); 1183, 1160 and 1072 (C-N).

Element analysis (%): Found C, 67.2; H, 5.0; N, 8.35. Calculated for C<sub>20</sub>H<sub>16</sub>N<sub>2</sub>SO: C, 72.3; H, 4.85; N, 8.4.

### 3.3.11 *N*-benzoyl-*N'*-(naphthalen-1-yl-*N'*-phenyl)thiourea



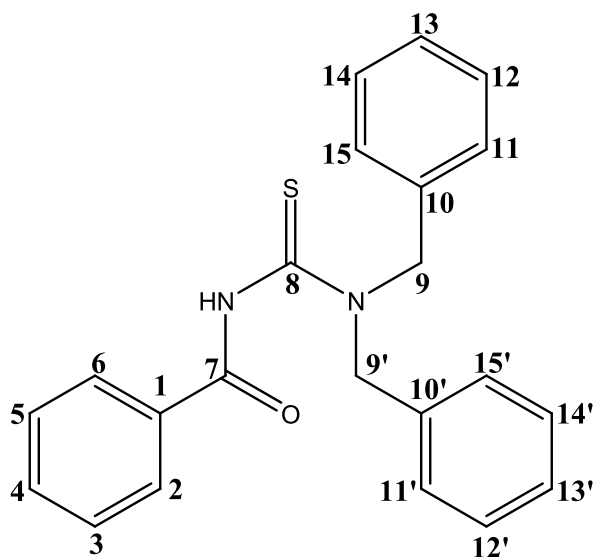
The ligand *N*-benzoyl-*N'*-naphthalen-1-yl-*N'*-phenylthiourea was synthesised using the methodology as described above. White solid (Yield: 80 %).

$^1\text{H}$  NMR (600 MHz,  $(\text{CD}_3)_2\text{SO}$ , 25 °C):  $\delta$  11.35 (s, 1H, CONHCS), 8.01 (d, 1H, H23,  $J_{\text{H-H}} = 8.1$  Hz), 7.92 (d, 1H, H20,  $J_{\text{H-H}} = 8.1$  Hz), 7.71-7.34 (m, 13H, H2, H3, H4, H5, H6, H10, H14, H16, H17, H18, H21, H22), 7.25 (t, 2H, H11 and H13,  $J_{\text{H-H}} = 7.5$  Hz), 7.09 (t, 1H, H12,  $J_{\text{H-H}} = 6.6$  Hz).

IR  $\nu_{\text{max}}$  ATR/ $\text{cm}^{-1}$ : 3150 (broad N-H); 1690 (C=O); 1593 and 1493-1481 (phenyl rings); 1367 (aromatic 2° amine C-N); 1251 (C=S); 1170 (C-N).

Element analysis (%): Found C, 74.3; H, 4.55; N, 7.3. Calculated for  $\text{C}_{24}\text{H}_{18}\text{N}_2\text{SO}$ : C, 75.4; H, 4.7; N, 7.3.

### 3.3.12 *N*-benzoyl-*N*',*N*'-(dibenzyl)thiourea



The ligand *N*-benzoyl-*N*',*N*'-dibenzylthiourea was synthesised using the methodology as described above. Colourless crystalline solid (Yield: 97 %).

$^1\text{H}$  NMR (600 MHz,  $(\text{CD}_3)_2\text{SO}$ , 25 °C):  $\delta$  11.01 (s, 1H, CONHCS), 7.93 (d, 2H, H2 and H6,  $J_{\text{H-H}} = 8.4$  Hz), 7.59 (t, 1H, H4,  $J_{\text{H-H}} = 7.4$  Hz), 7.53-7.28 (m, 10H, H3, H5, H11, H11', H12, H13, H13', H14, H15 and H15',  $J_{\text{H-H}} = 7.8$  Hz), 7.21 (m, 2H, H12' and H14'), 5.26 (s, 2H, H9) 4.70 (s, 2H, H9').

$^{13}\text{C}$  NMR (151 MHz,  $(\text{CD}_3)_2\text{SO}$ , 25 °C  $\delta$  183.5 (s, 1C, C8), 164.6 (s, 1C, C7), 135.8 (s, 1C, C10), 135.1 (s, 1C, C10'), 132.7 (s, 1C, C4), 132.5 (s, 1C, C1), 128.8 (s, 2C, C11 and C15), 128.5-128.3 (m, 6C, C2, C3, C5, C6, C11' and C15'), 127.9 (s, 1C, C13), 127.5-127.3 (m, 5C, C12, C12', C13', C14 and C14'), 55.6 (s, 1C, C9), 54.7 (s, 1C, C9').

IR  $\nu_{\text{max}}$  ATR/ $\text{cm}^{-1}$ : 3326 (broad N-H); 1687 (C=O); 1511-1417 (phenyl rings); 1354 (aromatic 2° amine C-N); 1266 (C=S); 1209-1191 (C-N).

Element analysis (%): Found C, 73.0; H, 5.45; N, 7.9. Calculated for  $\text{C}_{22}\text{H}_{20}\text{N}_2\text{SO}$ : C, 73.3; H, 5.6; N, 7.8.

### 3.4 Conclusion

A range of *S,O*-functionalized thiourea compounds were successfully synthesized with ease and with high yields using the method described in Figure 3.1. These compounds were characterized by NMR and IR spectroscopy as well as element analysis, which confirmed the identity and purity of each ligand.  $^1\text{H}$  NMR spectroscopy provided characteristic peaks at  $\pm 10$ - $12$  ppm for the NH protons of the thiourea moieties.  $^{13}\text{C}$  NMR spectroscopy also provided some characteristic chemical shifts of  $\pm 180$  and  $\pm 170$  ppm for the carbons of the C=S and C=O groups, respectively. These peaks generally indicate that both the C-S and C-O bonds have a double bond character about them. This suggested, together with the presence of the NH protons found on the  $^1\text{H}$  NMR spectrum, that these thiourea compounds are mainly found in their *keto* conformation in solution. This conformation is also found in the solid state of these compounds as will be shown and discussed in Chapter 4. IR analysis on these ligands revealed characteristic stretching frequencies at  $\pm 3100$ - $3400\text{ cm}^{-1}$  for the NH groups,  $\pm 1660$ - $1690\text{ cm}^{-1}$  for the C=O groups as well as  $\pm 1250$ - $1290\text{ cm}^{-1}$  for the C=S groups.

Some of these thiourea ligands provided suitable crystalline solids for single crystal X-ray diffraction. Therefore some of the structures were characterized by X-ray analysis, which are shown and discussed in detail in Chapter 4.



# **CHAPTER 4**

## **X-RAY CRYSTALLOGRAPHIC STUDY OF**

## **FUNCTIONALISED-S,O-THIOUREA LIGANDS**

### **4.1 Introduction**

In previous chapters the importance of bidentate ligands in transition metal co-ordination chemistry was discussed. Amongst the various aspects the electro-steric effects of the ligand on the catalytic properties of a metal such as rhodium is a popular study in chemistry, since this is important in industrial applications. Understanding these properties and functionalities of ligands may assist to explain the consequent effects on metal catalysts and also provide necessary information on how to alter or tune these ligands in order to direct catalytic processes to specific outcomes. Obtaining data from the physical structure of a ligand *via* X-ray techniques may provide more insight into the possible interactions, steric demands as well as preferable conformations of the ligand, which in turn can have significant influences on co-ordination chemistry and catalysis. In this chapter the structural data for some of the thiourea ligands that were obtained as discussed in Chapter 3, will be provided together with the different molecular interactions and various crystal packing modes. *S,O* donor thiourea ligands, unlike some of the other bidentate analogues, have shown throughout this study to have some interesting properties and co-ordination modes as will be seen later.

The X-ray determined single crystal structures of the following molecules are reported:

1. *N*-benzoyl-*N'*-(2,4,6-trimethylphenyl)thiourea (*N*-tmPTH)
2. *N*-benzoyl-*N'*-(2,6-dibromo-4-fluorophenyl)thiourea (*N*-BFPTH)
3. *N*-benzoyl-*N'*-(2,3,4,5,6-pentafluorophenyl)thiourea (*N*-FPTH)
4. *N*-benzoyl-*N'*-(phenethyl)thiourea (*N*-PeTH)
5. *N*-benzoyl-*N'*-(naphthalene-1-ylmethyl)thiourea (*N*-NmTH)
6. *N*-benzoyl-*N'*-(cyclohexyl)thiourea (*N*-CyTH)
7. *N*-benzoyl-*N'*-(isopentyl)thiourea (*N*-ipTH)

## 4.2 Experimental

The above mentioned compounds were analysed by single crystal X-ray diffraction. The initial unit cell and data collections were performed on a Bruker X8 Apex II 4K Kappa CCD diffractometer using graphite monochromated Mo  $K\alpha$  radiation ( $\lambda = 0.70926 \text{ \AA}$ ) with  $\omega$ - and  $\phi$ -scans at 100(2) K as well as the Apex2 software package.<sup>1</sup> The optimum measurement method to collect more than a hemisphere of reciprocal space was predicted by COSMO.<sup>2</sup> Frame integration and data reductions were performed using the SAINT-Plus and XPREP<sup>3</sup> software packages, and a multi-scan absorption correction was performed on the data using SADABS.<sup>4</sup> The structures were solved by the direct methods package SIR97,<sup>5</sup> and refinement using the WinGX software package<sup>6</sup> incorporating SHELXL.<sup>7</sup> All non H-atoms were refined anisotropically. All H-atoms were positioned geometrically and refined using a riding model with fixed C-H distances of 0.95  $\text{\AA}$  (CH) [ $U_{\text{iso}}(\text{H}) = 1.2U_{\text{eq}}$ ] for aromatic H-atoms and 0.98  $\text{\AA}$  (CH) [ $U_{\text{iso}}(\text{H}) = 1.2U_{\text{eq}}$ ] for methyl H-atoms as well as fixed N-H distances of 0.88  $\text{\AA}$  (NH) [ $U_{\text{iso}}(\text{H}) = 1.2U_{\text{eq}}$ ]. Molecular diagrams were drawn using the Mercury<sup>8</sup> package with a 50% thermal envelope probability for non-hydrogen atoms. General crystal data and refinement parameters are presented in Tables 4.1 and 4.2. A complete list of atomic coordinates, equivalent isotropic parameters, bond distances and angles, anisotropic displacement parameters and hydrogen coordinates for each individual dataset is given in Appendix A.

---

<sup>1</sup> Bruker (2005). Apex2 (Version 1.0-27). Bruker AXS Inc., Madison, Wisconsin, USA.

<sup>2</sup> Bruker (2003). COSMO (Version 1.48). Bruker AXS Inc., Madison, Wisconsin, USA.

<sup>3</sup> Bruker (2004a). SAINT-Plus. Version 7.12 (including XPREP). Bruker AXS Inc., Madison, Wisconsin, USA.

<sup>4</sup> Bruker (2004b). SAINT-Plus. Version 7.12 (including XPREP). Bruker AXS Inc., Madison, Wisconsin, USA.

<sup>5</sup> Altomare, A., Burla, M. C., Camalli, M., Cascarano, G. L., Giacovazzo, C., Guagliardi, A., Moliterni, A. G. G., Polidori, G. & Spagna, R. (1999). *J. Appl. Cryst.*, **32**, 115.

<sup>6</sup> Farrugia, L. J. (1999). WinGX, *J. Appl. Cryst.*, **32**, 837.

<sup>7</sup> Sheldrick, G.M. (1997). SHELXL97. *Program for crystal structure refinement*. University of Göttingen, Germany.

<sup>8</sup> Macrae, C. F., Edgington, P. R., McCabe, P., Pidcock, E., Shields, G. P., Taylor, R., Towler, M. & van de Streek, J. (2006). *J. Appl. Cryst.* **39**, 453.

**Table 4.1 General crystal data for the following thiourea compounds,  
N-tmPTH, N-BFPTH, N-FPTH and N-PeTH.**

Identification code	N-tmPTH	N-BFPTH	N-FPTH	N-PeTH
Empirical formula	C17 H18 O1 S1 N2	C14 H9 O1 S1 N2 Br2 F1	C14 H7 O1 S1 N2 F5	C16 H16 O1 S1 N2
Formula weight	298.4	432.1	692.6	284.4
Crystal system, space group	Triclinic, $P\bar{1}$	Triclinic, $P\bar{1}$	Monoclinic, $C2/c$	Monoclinic, $P2_1/n$
Unit cell dimensions				
a (Å)	10.7147(7)	7.7703(5)	29.6111(13)	11.9389(3)
b (Å)	10.8758(9)	10.1074(7)	9.5272(4)	6.0845(2)
c (Å)	15.6502(13)	10.1542(7)	10.1637(4)	19.5220(5)
$\alpha$ (°)	71.071(3)	99.707(3)	90	90
$\beta$ (°)	84.066(3)	106.339(3)	107.863(3)	98.166(2)
$\gamma$ (°)	65.702(3)	93.665(3)	90	90
Volume (Å <sup>3</sup> )	1571.3(2)	749.0(7)	2729.(2)	1403.7(1)
Z	4	2	8	4
Density (calculated) (g/mL)	1.261	1.916	1.686	1.346
Absorption coefficient (mm <sup>-1</sup> )	0.206	5.56	0.301	0.227
F(000)	632	420	1392	600
Crystal size (mm <sup>3</sup> )	0.46 x 0.13 x 0.06	0.38 x 0.20 x 0.11	0.28 x 0.13 x 0.05	0.32 x 0.23 x 0.23
$\Theta$ range (°)	1.38 to 25.00	2.06 to 28.41	1.45 to 28.31	3.51 to 28.24
Completeness (%)	99.0	99.2	99.9	98.8
Index ranges	-12 $\leq h \leq$ 9, -12 $\leq k \leq$ 11, -18 $\leq l \leq$ 17	-10 $\leq h \leq$ 9, -13 $\leq k \leq$ 13, -13 $\leq l \leq$ 12	-39 $\leq h \leq$ 39, -12 $\leq k \leq$ 12, -10 $\leq l \leq$ 13	-11 $\leq h \leq$ 15 -7 $\leq k \leq$ 8 -26 $\leq l \leq$ 26
Reflections collected	16098	19391	19145	18199
Independent reflections	5463 [R <sub>int</sub> = 0.0560]	3750 [R <sub>int</sub> = 0.0376]	3397 [R <sub>int</sub> = 0.0369]	3441 [R <sub>int</sub> = 0.0391]
Observed reflections	3717	3438	2775	2909
Max/min transmission	0.988 and 0.911	0.580 and 0.227	0.985 and 0.921	0.950 and 0.931
Data/ restraints/ parameters	5463/ 0/ 383	3750/ 0/ 190	3397/ 0/ 208	3441/0/181
Goodness-of-fit on F <sup>2</sup>	1.051	1.249	1.046	1.065
Final R indices [I>2 $\sigma$ (I)]	R1 = 0.0481 wR2 = 0.0959	R1 = 0.0198 wR2 = 0.0554	R1 = 0.0330 wR2 = 0.0809	R1 = 0.0390 wR2 = 0.0985
R indices (all data)	R1 = 0.0811 wR2 = 0.1090	R1 = 0.0242 wR2 = 0.0803	R1 = 0.0439 wR2 = 0.0878	R1 = 0.0474 wR2 = 0.1041
Largest diff. Peak/hole (e.Å <sup>-3</sup> )	0.264 and -0.307	0.691 and -0.586	0.354 and -0.214	0.331 and -0.363

**Table 4.2 General crystal data for the following thiourea compounds, *N*-NmTH, *N*-CyTH, *N*-ipTH.**

Identification code	<i>N</i> -NmTH	<i>N</i> -CyTH	<i>N</i> -ipTH
<b>Empirical formula</b>	C19 H16 O1 S1 N2	C14 H18 O1 S1 N2	C13 H18 O1 S1 N2
<b>Formula weight</b>	320.4	262.4	250.4
<b>Crystal system, space group</b>	Monoclinic, <i>C2/c</i>	Triclinic, <i>P</i> $\bar{1}$	Triclinic, <i>P</i> $\bar{1}$
<b>Unit cell dimensions</b>			
<b>a = (Å)</b>	22.2245(18)	5.5043(2)	9.6169(3)
<b>b = (Å)</b>	10.9999(9)	15.1084(5)	10.8180(3)
<b>c = (Å)</b>	16.5075(11)	17.4695(7)	14.1216(5)
<b><math>\alpha</math> = (°)</b>	90	74.275(1)	106.951(1)
<b><math>\beta</math> = (°)</b>	130.104(2)	81.245(1)	104.394(1)
<b><math>\gamma</math> = (°)</b>	90	81.702(1)	98.969(1)
<b>Volume (Å<sup>3</sup>)</b>	3086.7(4)	1373.9(14)	1319.2(1)
<b>Z</b>	8	4	4
<b>Density (calculated) (g/mL)</b>	1.379	1.268	1.261
<b>Absorption coefficient (mm<sup>-1</sup>)</b>	0.216	0.226	0.232
<b><i>F</i>(000)</b>	1344	560	536
<b>Crystal size (mm<sup>3</sup>)</b>	0.32 x 0.15 x 0.14	0.28 x 0.23 x 0.12	0.25 x 0.21 x 0.10
<b><math>\Theta</math> range for data collection (°)</b>	4.13 to 28.28	4.09 to 27.00	4.13 to 28.28
<b>Completeness for collection (%)</b>	99.0	98.8	98.9
<b>Index ranges</b>	-28 ≤ <i>h</i> ≤ 29 -14 ≤ <i>k</i> ≤ 14 -21 ≤ <i>l</i> ≤ 21	-7 ≤ <i>h</i> ≤ 7 -19 ≤ <i>k</i> ≤ 18 -23 ≤ <i>l</i> ≤ 23	-12 ≤ <i>h</i> ≤ 12 -13 ≤ <i>k</i> ≤ 14 -18 ≤ <i>l</i> ≤ 18
<b>Reflections collected</b>	23131	24222	24091
<b>Independent reflections</b>	3800 [ <i>R</i> <sub>int</sub> = 0.0537]	5921 [ <i>R</i> <sub>int</sub> = 0.0210]	6488 [ <i>R</i> <sub>int</sub> = 0.0506]
<b>Observed reflections</b>	2920	5328	4774
<b>Max and min transmission</b>	0.970 and 0.934	0.973 and 0.939	0.977 and 0.944
<b>Data/ restraints/ parameters</b>	3800/0/208	6582/0/352	6488/0/307
<b>Goodness-of-fit on <i>F</i><sup>2</sup></b>	1.067	1.034	1.076
<b>Final <i>R</i> indices [<i>I</i> &gt; 2σ(<i>I</i>)]</b>	<i>R</i> 1 = 0.0474 w <i>R</i> 2 = 0.1078	<i>R</i> 1 = 0.0477 w <i>R</i> 2 = 0.1193	<i>R</i> 1 = 0.0476 w <i>R</i> 2 = 0.0972
<b><i>R</i> indices (all data)</b>	<i>R</i> 1 = 0.0651 w <i>R</i> 2 = 0.1200	<i>R</i> 1 = 0.0524 w <i>R</i> 2 = 0.1234	<i>R</i> 1 = 0.0692 w <i>R</i> 2 = 0.1105
<b>Largest diff. Peak and hole (e.Å<sup>-3</sup>)</b>	0.383 and -0.368	1.161 and -0.409	0.398 and -0.321

### 4.3. Crystal structure of N-benzoyl-N'-(2,4,6-trimethylphenyl)thiourea (*N*-tmPTH)

#### 4.3.1 Results and discussion

(Synthesis described in Section 3.3.2; Supplementary data A1)

The compound N-benzoyl-N'-(2,4,6-trimethylphenyl)thiourea, *N*-tmPTH, crystallised in the triclinic space group  $P\bar{1}$  with two crystallographic independent molecules in the asymmetric unit. The atom labelling of the compound is presented in Figure 4.1 and some of the important bond distances as well as bond angles are given in Table 4.3.

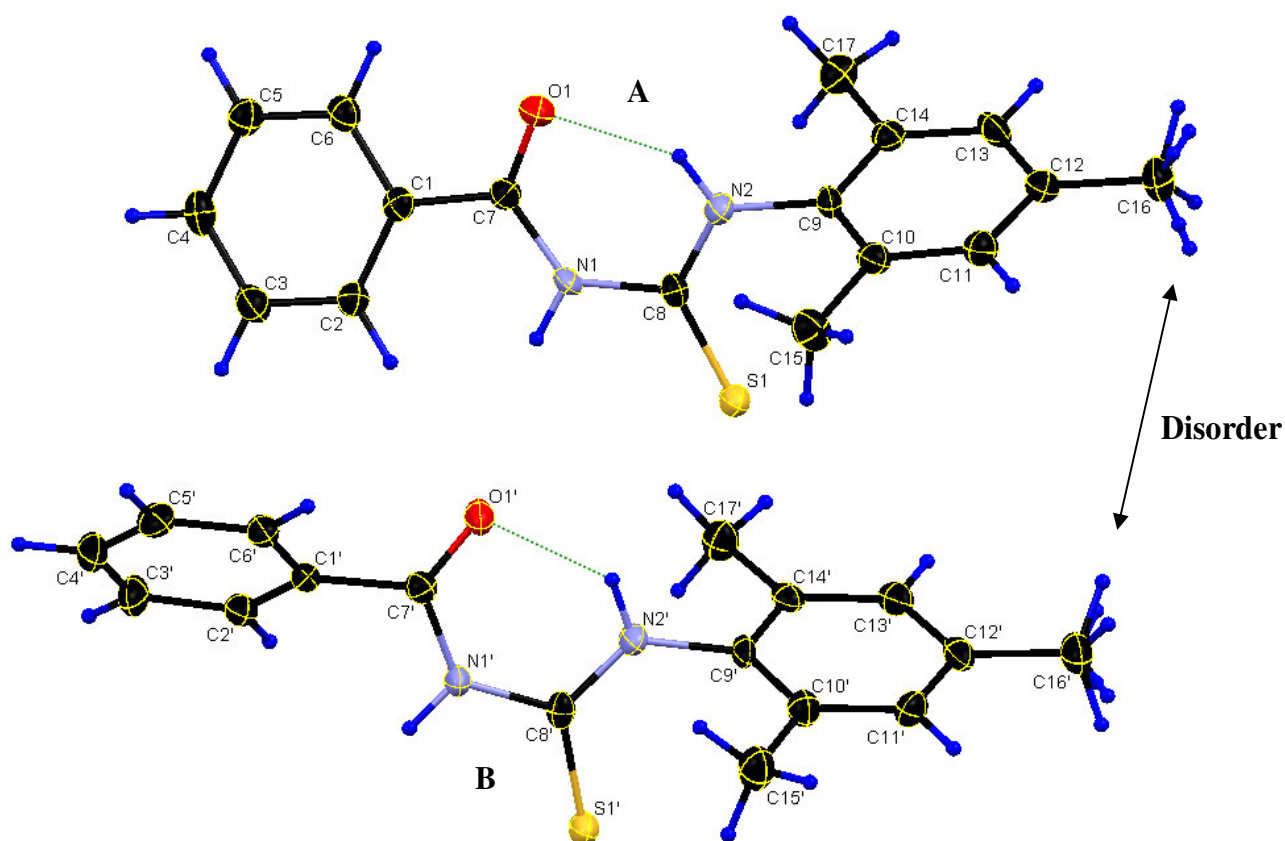


**Figure 4.1:** A structural representation of the compound *N*-tmPTH, showing the two molecules A and B, where the atom numbering scheme is also shown (ellipsoid probability = 50%). Hydrogen atoms labels have been omitted for clarity. The disorders at C16 and C16' are clearly shown.

**Table 4.3: List of selected bond distances and angles for the compound *N*-tmPTH.**

Molecule A		Molecule B	
Atoms	Distance (Å)	Atoms	Distance (Å)
C7-O1	1.235(4)	C7'-O1'	1.228(5)
C8-S1	1.662(4)	C8'-S1'	1.670(4)
C9-N2	1.441(5)	C9'-N2'	1.439(5)
C8-N2	1.328(5)	C8'-N2'	1.328(5)
C8-N1	1.406(5)	C8'-N1'	1.406(5)
C7-N1	1.372(5)	C7'-N1'	1.378(4)
Molecule A		Molecule B	
Atoms	Angle (°)	Atoms	Angle (°)
N1-C7-O1	121.9(3)	N1'-C7'-O1'	122.8(3)
N1-C8-S1	118.0(3)	N1'-C8'-S1'	118.4(3)
C8-N2-C9	123.2(3)	C8'-N2'-C9'	125.7(3)
C1-C2-C3-C4	1.6(4)	C1'-C2'-C3'-C4'	-1.5(4)
C2-C1-C7-O1	-167.4(2)	C2'-C1'-C7'-O1'	136.7(3)
C9-C10-C11-C12	-0.4(4)	C9'-C10'-C11'-C12'	1.4(4)
O1-C7-C8-S1	-169.1	O1'-C7'-C8'-S1'	177.2
C8-N2-C9-C10	-75.7(3)	C8'-N2'-C9'-C10'	-78.7(3)

Note that the nitrogen atoms N1, N1', N2 and N2' are found to be protonated due to the presence of electron density at a suitable distance from these atoms. In order to position the proton accurately from the nitrogen atoms, they were geometrically positioned and refined using a riding model with a fixed N-H distance of 0.88 Å (NH) [ $U_{\text{iso}}(\text{H}) = 1.2U_{\text{eq}}$ ]. The respective distances for the C8-S1, C8'-S1', C7-O1 and C7'-O1' bonds were found to be 1.662(4) and 1.235(4) Å in molecule **A** and 1.670(4) and 1.228(5) Å in molecule **B**. The short distances clearly indicated the double bond character of these bonds, which correlates well with literature values.<sup>9</sup> Small deviations exist due to the electronic influence of the aromatic substituents, since C=S and C=O groups can participate in  $\pi$ -conjugation. This is also further supported by the angles N-C-O and N-C-S, which as given in Table 4.3 are approximately 120 ° and therefore indicate that carbon atoms C7 and C8 have  $sp^2$ -hybridization. From these observations it is clearly established that the thiourea compound mainly exists in its *keto* conformation in the solid state.

The trimethylphenyl group is found to be *cis* to the sulphur atom with respect to the C8-N2 and C8'-N2' bond, respectively in each molecule of the asymmetric unit. With dihedral angles C8-N2-C9-C14 and C8'-N2'-C9'-C14' of 105.65 and 106.78 ° found in each molecule,

<sup>9</sup> Allen, F. H.; Kennard, O.; Watson, D. G.; Brammer, L.; Orpen, A. G.; Taylor, R. (1992) *International Tables for Crystallography, Vol. C*, Dordrecht: Kluwer Academic Publishers, edited by Wilson, A. J. C., 685.

respectively, it is clear that the face of the trimethylphenyl group is out of plane with respect to the plane across the thiourea bridge (for reference across this chapter the thiourea bridge is defined as C7-N1-C8(S1)-N2). Both phenyl rings in the molecule are found to be essentially planar. The methyl groups labelled as C16 and C16' display a typical positional disorder, where the hydrogen atoms of the methyl groups occupy two different positions with a site occupancy factor (s.o.f) of 50%. Several examples of this disorder are found in literature.<sup>10</sup>

Due to the close proximity of the molecules in the asymmetric unit the one molecule unit has slight distortions in its structure compared to the other. The torsion angle for the atom series C2-C1-C7-O1 of  $-167.7^\circ$  shows that the phenyl ring of the benzoyl group is almost in plane with the carbonyl group in molecule **A**. However, with a torsion angle of  $136.7^\circ$  for the atom series C2'-C1'-C7'-O1' the phenyl ring of the benzoyl group in molecule **B** is slightly distorted out of plane with respect to the carbonyl group (C7'-O1'). This could be attributed to the presence of intermolecular soft contacts (Van der Waals interactions) between several molecules (**A**, **B** and **C**) as shown in Figure 4.2 by means of green dotted lines. The oxygen O1' in the benzoyl group of molecule **B** is stabilised by soft contacts with H1 and H2A in the phenyl group of molecule **A** with respective distances of 2.403 Å and 2.356 Å. The angles of these contacts given by C7'-O1'...H1 and C7'-O1'...H2A are  $150.39^\circ$  and  $104.87^\circ$ .

Molecules **B** and **C** are packed in a centrosymmetric fashion and one of the carbons C2' in the benzoyl group in both molecules show an intermolecular short contact with the sulphur atom S1' on the other molecule with a distance of 3.219 Å and an angle of C8'-S1'...C2' =  $148.35^\circ$ . This contact could be the cause of the slight distortion found in the phenyl ring of this benzoyl group with respect to the carbonyl group (C7'-O1'). The sulphur atom S1' also has an intermolecular hydrogen bond with N1' found between molecules **B** and **C**, with a distance of 2.632 Å and an angle N1'-H1'...S1' of  $162.97^\circ$ .

The two molecules in the asymmetric unit **A** and **B** is also stabilised by the presence of soft contacts between the atom S1 on molecule **A** and the atoms H17E, H2', C9' and C14' on molecule **B**. The distances of these contacts are 2.997, 2.825, 3.394 and 3.370 Å and the

<sup>10</sup> For a few examples see: a) Logothetis, T. A.; Meyer, F.; Metrangolo, P.; Pilati, T.; Resnati, G. (2004) *New J. Chem.*, **28**, 760. b) Britton, D (2002) *Acta Cryst.*, **B58**, 553. c) Dobson, A. J.; Gerkin, R. E. (1999) *Acta Cryst.*, **C55**, 1496.

angles given by C8-S1...H17E, C8-S1...H2', C8-S1...C9' and C8-S1...C14' are 116.07, 118.67, 154.44 and 153.16 °, respectively.

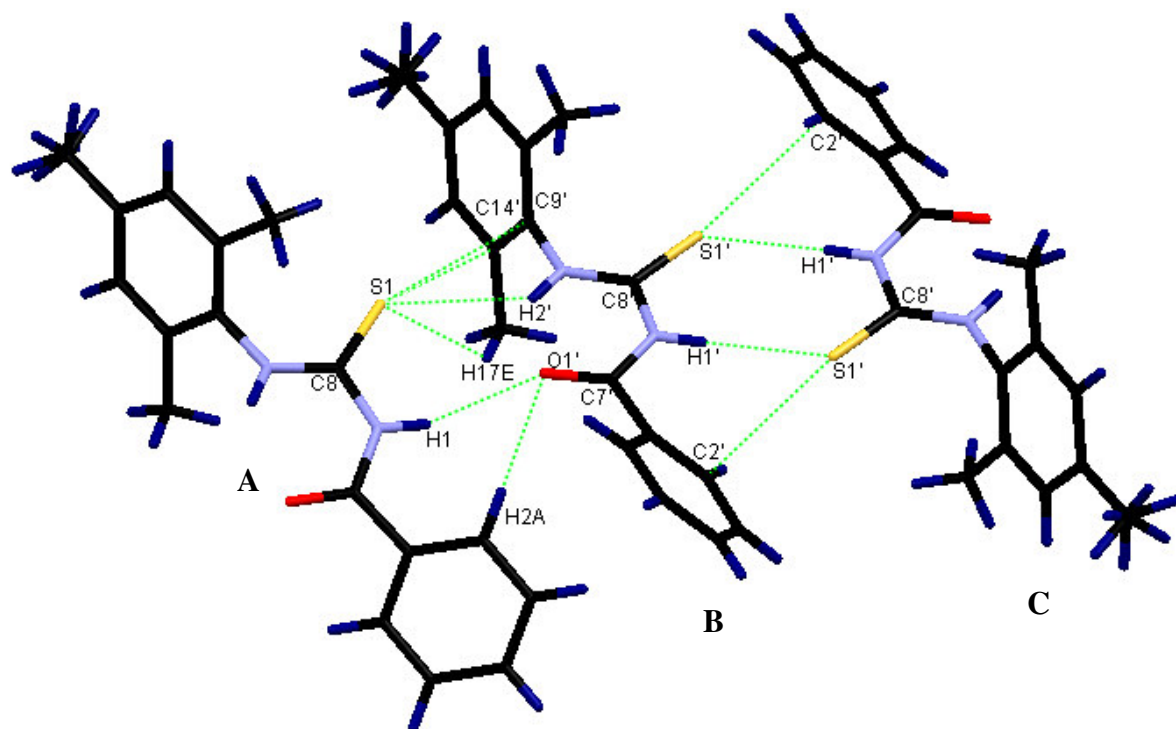


**Figure 4.2:** An illustration of soft contacts between several molecules of the compound *N*-tmPTH. (Distances given in Table 4.4)

**Table 4.4:** List of bond distances of selected soft contacts between molecules of the compound *N*-tmPTH represented in Figure 4.2.

Molecules A and B	
Atoms	Distances (Å)
S1...H17E	2.997
S1...H2'	2.825
S1...C9'	3.394
S1...C14'	3.370
O1'...H1	2.403
O1'...H2A	2.356
Molecules B and C	
Atoms	Distances (Å)
S1'...H1'	2.632
S1'...C2'	3.219



The molecular packing is also stabilised by a few other intermolecular soft contacts as shown in Figure 4.3. Firstly, contacts found in molecules **D** and **F** between H3' and C16 as well as H4' and H16C are present with distances of 2.803 and 2.330 Å, respectively. The angles of contact are given as C3'-H3'...C16 and C4'-H4'...H16C, which have values of 132.48 and 127.43 °, respectively. These contacts could also be responsible for the distortion found in the benzoyl group of molecule **F**. Secondly, soft contacts are found between molecules **D** and **E** between atoms S1 and H13 as well as H16F and H17C with distances of 2.943 Å and 2.392 Å and angles C8-S1...H13 and C17-H17C...H16F of 103.7 and 168.89 °, respectively.

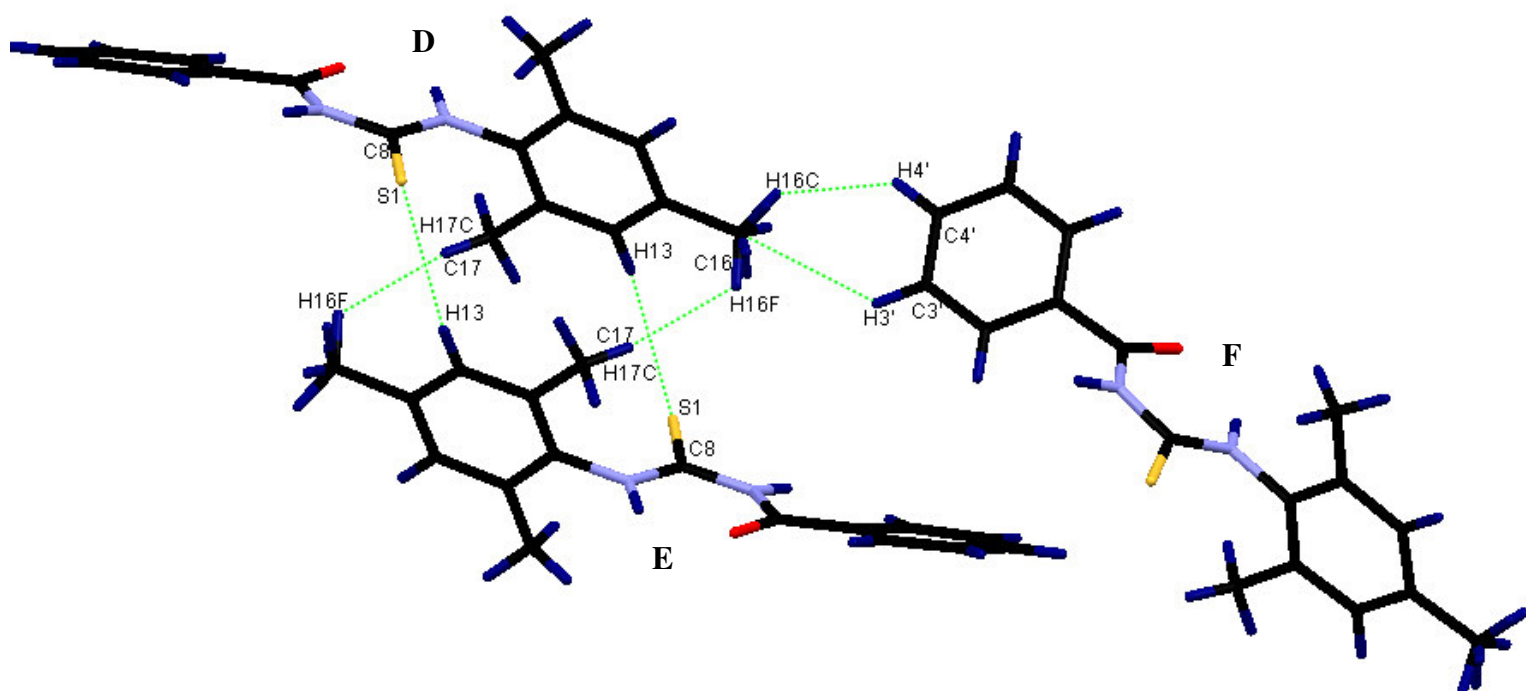


**Figure 4.3:** An illustration of soft contacts between molecules of the compound *N*-tmPTH. Distances: S1...H13 = 2.943 Å, H17C...H16F = 2.392 Å, C16...H3' = 2.803 Å, H16C...H4' = 2.330 Å; Angles: C8-S1...H13 = 103.7 °, C17-H17C...H16F = 168.89 °, C3'-H3'...C16 = 132.48 °, C4'-H4'...H16C = 127.43 °.

The last set of soft contacts that were observed is illustrated in Figure 4.4, once again by green dotted lines. The molecules **G** and **H** are packed in a centrosymmetric manner such that the oxygen atom O1 of the one molecule came in close proximity to the nitrogen atom N2 of the other. This then resulted in the formation of a soft contact between the oxygen atom and the hydrogen atom H2 on N2 with a distance of 2.432 Å and a contact angle N2-H2...O1 of 135.39 °. The packing is further stabilised by the presence of soft contacts between H6 and C10 and C9, respectively, which have distances of 2.881 and 2.885 Å, respectively. The

angles defining these contacts are given by C6-H6...C10 and C6-H6...C9 and have respective values of 154.93 and 147.58 °.

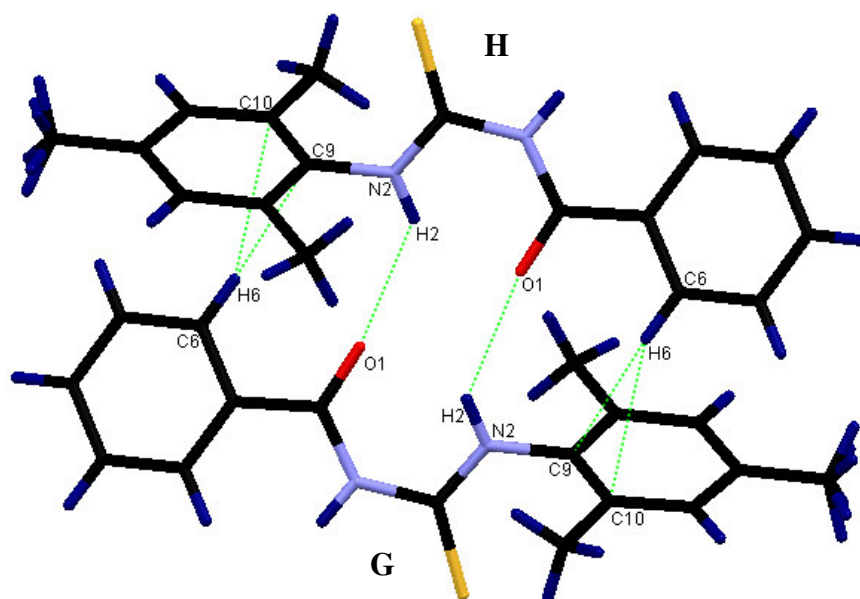


**Figure 4.4: An illustration of some soft contacts present in the compound *N*-tmPTH amongst several molecules. Distances: O1...H2 = 2.432 Å, H6...C9 = 2.885 Å, H6...C10 = 2.881 Å; Angles: N2-H2...O1 = 135.39 °, C6-H6...C9 = 147.58 °, C6-H6...C10 = 154.93 °.**

A unique feature found in these thiourea ligands having an *S,O*-moiety in a 1,5 position is the intramolecular hydrogen bond that is present in each case between the oxygen atom and the second nitrogen along the thiourea bridge. Some examples of this are found in literature<sup>11a,b,c</sup> and this soft contact is present in every thiourea structure presented in this chapter. As a result of this hydrogen bonding the structure is orientated in such a way that the oxygen atom is found *trans* to the sulphur atom with respect to the C-N-C chain across the thiourea bridge. This is an interesting case compared to other analogues such as acetylacetone and derivatives<sup>12a,b,c</sup> and 4-iminopentan-2-one and derivatives<sup>13a,b</sup> where the *O,O* and *O,N* moieties in these molecules are found to be either in the *cis* conformation or having twisted

<sup>11</sup> Typical examples are: a) Saeed, S.; Bhatti, M. H.; Yunus, U.; Jones, P. G. (2008) *Acta Cryst.*, **E64**, o1485 b) Dago, A.; Shepelev, Yu. (1989) *Acta Cryst.*, **C45**, 1192 c) Raj, S. S. S.; Puviarasan, Velmurugan, D.; Jayanthi, G.; Fun, H. (1999) *Acta Cryst.* **C55**, 1318.

<sup>12</sup> Typical examples are: a) Boese, R.; Antipin, M. Y.; Bläser, D.; Lyssenko, K. A. (1998) *J. Phys. Chem. B*, **102**, 44, 8654 b) Williams, D. E.; Dumke, W. L.; Rundle, R. E. (1962) *Acta Cryst.*, **15**, 627 c) Pandolfo, L.; Bertani, R.; Facchin, G.; Zanutto, L.; Ganis, P.; Valle, G.; Seraglia, R. (1995) *Inorg. Chim. Acta.*, **237**, 27.

<sup>13</sup> a) Jing, Z.-L.; Zhang, S.-J.; Yang, N.; Feng, S.-C. (2007) *Acta Cryst.*, **E63**, o3203. b) Xin, W.; Ru-wen, D.; Jigui, W.; Zhong-ning, C (1992) *Acta Cryst.*, **C48**, 1295.

orientations slightly away from *cis* conformation. Generally these moieties are stabilised by hydrogen bonding amongst themselves which then ensures the *cis* orientation in some cases.

In the present compound N-benzoyl-N'-(2,4,6-trimethylphenyl)thiourea, *N*-tmPTH, this hydrogen bonding is shown in Figure 4.5 by means of a green dotted line. This forms a six-membered ring, which with dihedral angles C7-O1-N2-C8 and C7'-O1'-N2'-C8' of 3.71 ° and 3.23 ° in the respective molecules of the asymmetric unit was found to be nearly planar in both cases. This contact is found between O1 and N2 and between O1' and N2' having respective distances of 2.682(2) Å and 2.664(2) Å and the angles of bonding are given by N2-H2...O1 = 131.65 ° and N2'-H2'...O1' = 136.57 °. The dihedral angles O1-C7-C8-S1 and O1'-C7'-C8'-S1' were calculated and found to be -169.14 ° and 177.19 °, which indicated that the oxygen atoms on the separate molecules were found to be approximately in plane with respect to the sulphur atoms, respectively, in each case.

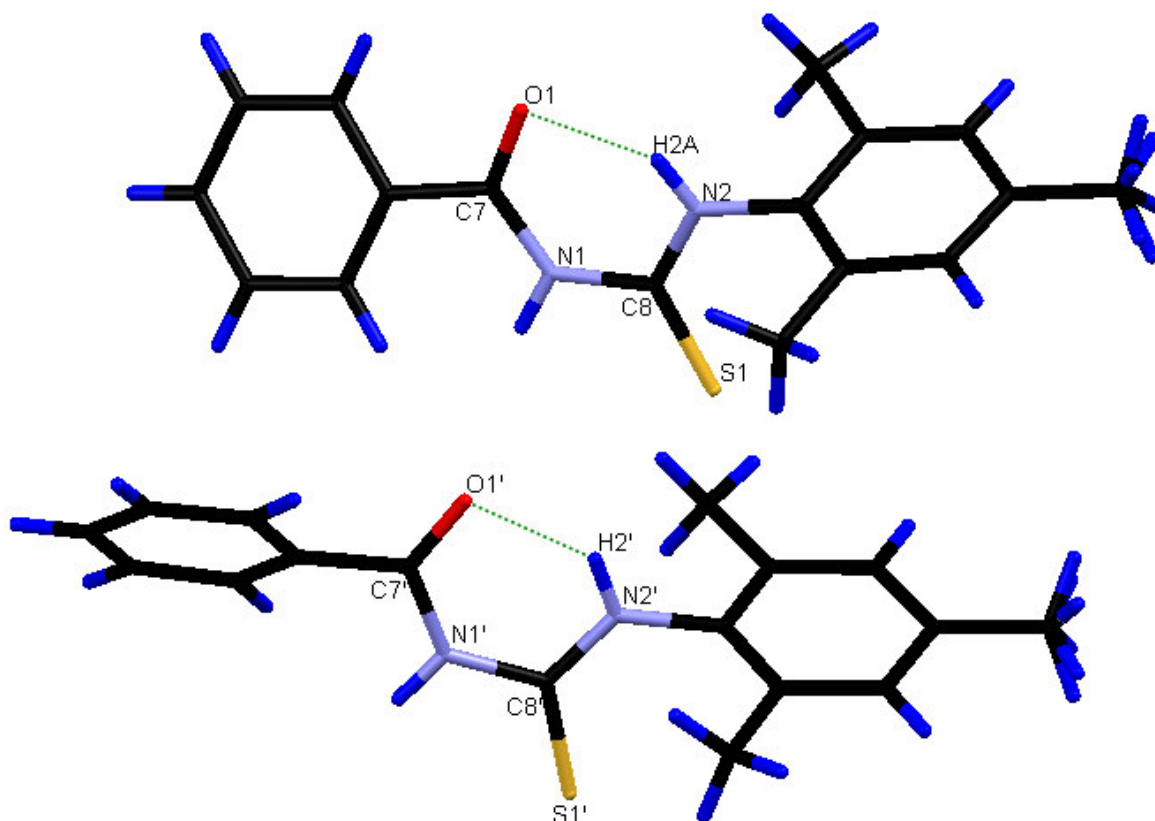


**Figure 4.5: An illustration of the hydrogen bonding found in compound *N*-tmPTH. Distances: N2-H2...O1 = 2.682(2) Å, N2'-H2'...O1' = 2.664(2) Å; Angles: N2-H2...O1 = 131.65 °, N2'-H2'...O1' = 136.57 °.**

## 4.4. Crystal structure of N-benzoyl-N'-(2,6-di-bromo-4-fluorophenyl)thiourea (*N*-BFPTH)

### 4.4.1 Results and discussion

(Synthesis described in Section 3.3.3; Supplementary data A2)

The compound N-benzoyl-N'-(2,6-di-bromo-4-fluorophenyl)thiourea, *N*-BFPTH, crystallised in the triclinic space group  $P\bar{1}$  with one molecules in the asymmetric unit. The atom labelling of the compound is presented in Figure 4.6 and the main bond distances as well as bond angles are presented in Table 4.5.

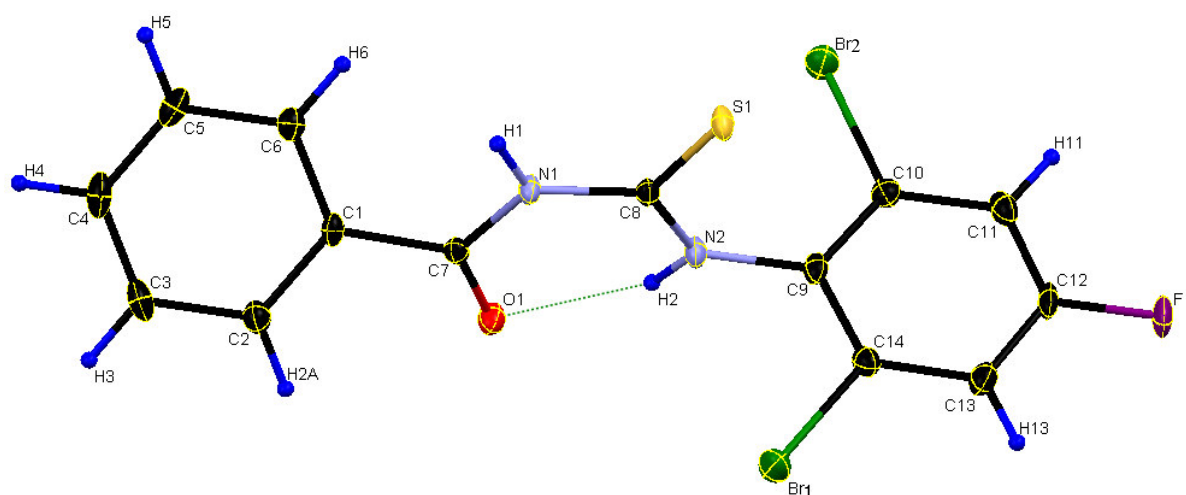


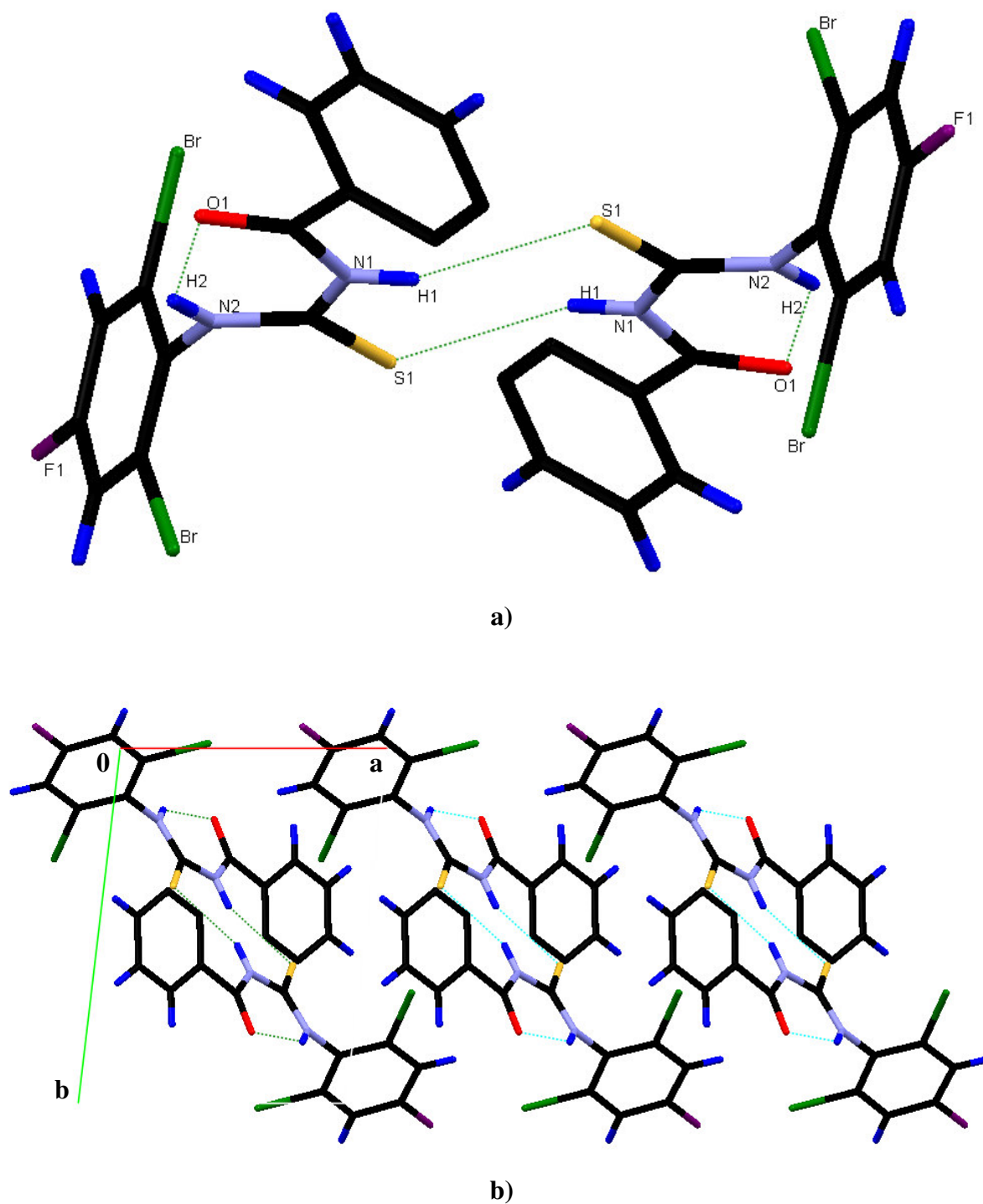
Figure 4.6: A structural representation of the compound *N*-BFPTH, where the atom numbering scheme is shown (ellipsoid probability = 50 %).

Table 4.5: List of selected bond distances and angles for *N*-BFPTH.

Atoms	Distance (Å)	Atoms	Angle (°)
C7-O1	1.226(2)	N1-C7-O1	122.3(1)
C8-S1	1.669(2)	N1-C8-S1	120.4(1)
C9-N2	1.420(2)	C8-N2-C9	121.5(1)
C8-N2	1.336(2)	C1-C2-C3-C4	1.2(2)
C8-N1	1.380(2)	C2-C1-C7-O1	26.8(2)
C7-N1	1.382(2)	C9-C10-C11-C12	-0.6(2)
		O1-C7-C8-S1	-168.54
		C8-N2-C9-C14	88.9(2)

As described before in Section 4.3, the carbonyl oxygen atom O1 is found *trans* to the sulphur atom S1 having a dihedral angle O1-C7...C8-S1 of  $-168.54^\circ$ . This angle suggests that the oxygen and sulphur atoms are fairly on the same plane across the C-N-C chain of the thiourea bridge, whilst the phenyl groups are twisted out of this plane with torsion angles C2-C1-C7-O1 and C8-N2-C9-C14 of  $26.8(2)^\circ$  and  $88.9(2)^\circ$ , respectively. The N-H protons were also placed as riding with the same argument as was discussed in Section 4.3. The respective distances for the carbonyl group C7-O1 and the carbonsulfide group C8-S1 are  $1.226(2)$  and  $1.669(2)$  Å, which as before are indicative of the double-bond character of these groups.

Two sets of hydrogen bonding occur between adjacent molecules of this compound that play a role in the orientation and packing of this compound in the crystal lattice (Figure 4.7). First is the intramolecular hydrogen bonding that is typically found between the nitrogen atom N2 and the carbonyl oxygen atom O1 having a distance of  $2.595(2)$  Å and an angle N2-H2...O1 of  $131.8^\circ$ . The second set of intermolecular hydrogen bonding occurs between the nitrogen atom N1 of one molecule and the sulphur atom S1 of another molecule that is located around a centre of symmetry to the first molecule. This hydrogen bond has a distance of  $3.424(2)$  Å and the interaction N2-H2...O1 has an angle of  $158.8^\circ$ . In the process this hydrogen bonding creates a closed 8-membered ring as shown in Figure 4.7, which is found to be in a “chair-conformation”. Furthermore this hydrogen bonding leads to dimer formation between the molecules in the packing, which stacks up along the a-axis.



**Figure 4.7** An illustration of a) the hydrogen bonding found between molecules in the crystal packing of the compound *N*-BFPTH and b) the resulting dimer formation along the *a*-axis. Distances and angles: N2-H2...O1 = 2.595(2) Å, 131.8 °; N1-H1...S1 = 3.424(2) Å, 158.8 °. Some of the hydrogen atoms were omitted for clarity.

Some  $\pi$ - $\pi$  interactions exist between molecules in the crystal packing as indicated by green dotted lines in Figure 4.8, which form chains of stacks between interchanging phenyl rings

along the a-axis. The  $\pi$ -stacking takes place in a “head-to-tail” fashion and the corresponding interplanar distances of the different stacks are 3.579 and 3.324 Å, respectively.

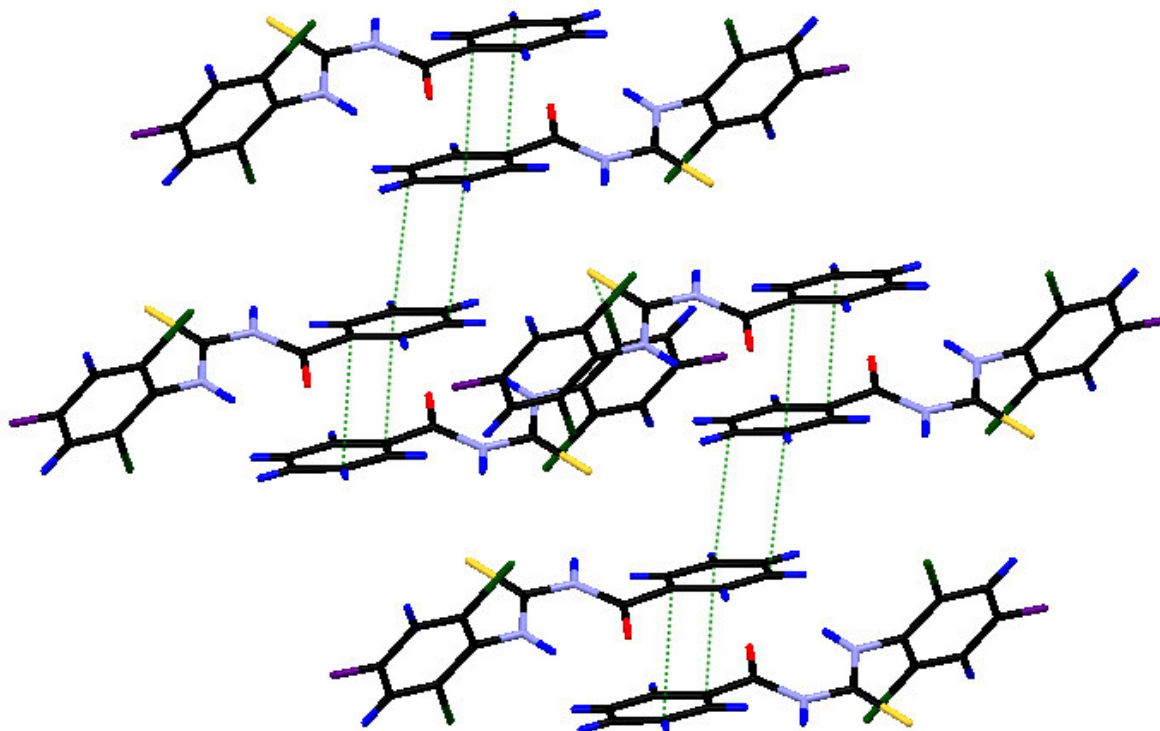


**Figure 4.8** An illustration of  $\pi$ -stacking between adjacent molecules in the crystal packing of the compound *N*-BFPTH with an interplanar distances of 3.579 and 3.324 Å.

A few other soft contacts through Van der Waals interactions are also present. One set involves intermolecular interactions of the bromine atoms Br1/Br2 with each other and with the oxygen and sulphur atoms between different molecules as illustrated in Figure 4.9. These interactions hold the molecules in the packing together in a chain-like fashion parallel to the (11-1) plane as shown in Figure 4.10. The corresponding distances of these contacts, namely, Br1...Br1, Br1...O1 and Br2...S1 are 3.656, 3.230 and 3.394 Å and the subsequent angles given by C14-Br1...Br1, C14-Br1...O1 and C10-Br2...S1 are 131.6, 148.6 and 167.6 °, respectively.



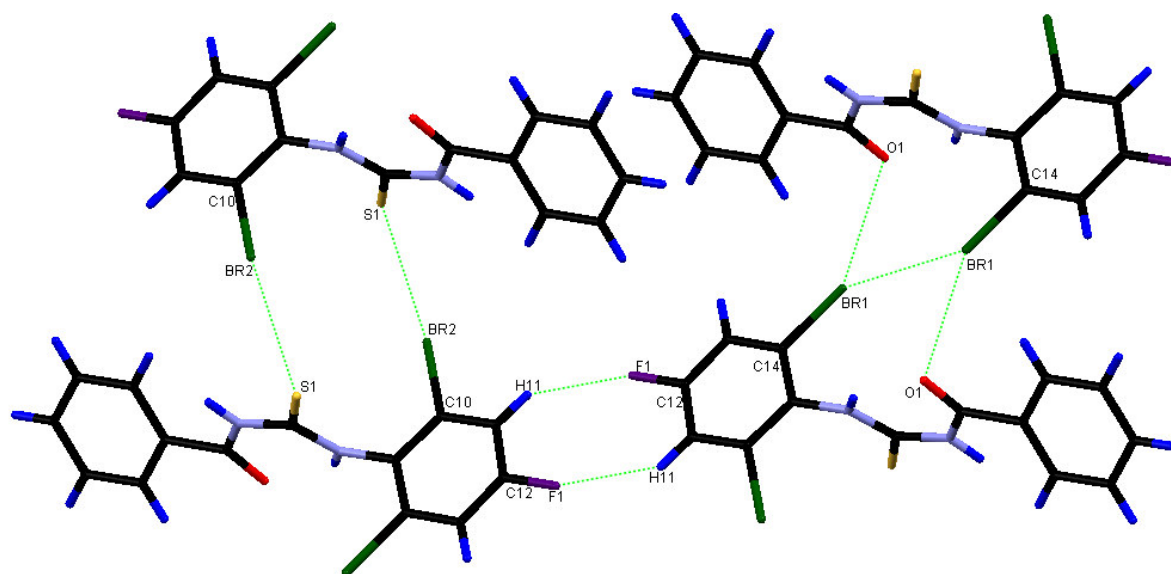


**Figure 4.9** A representation of soft contacts found between the halogen atoms of the compound *N*-BFPTH and several other atoms of neighbouring molecules. Distances: Br1-Br1 = 3.656 Å, Br1...O1 = 3.230 Å, Br2...S1 = 3.394 Å, F1...H11 = 2.570 Å. Angles: C14-Br1...Br1 = 131.6 °, C14-Br1...O1 = 148.6 °, C10-Br2...S1 = 167.6 °, C12-F1...H11 = 161.1 °.

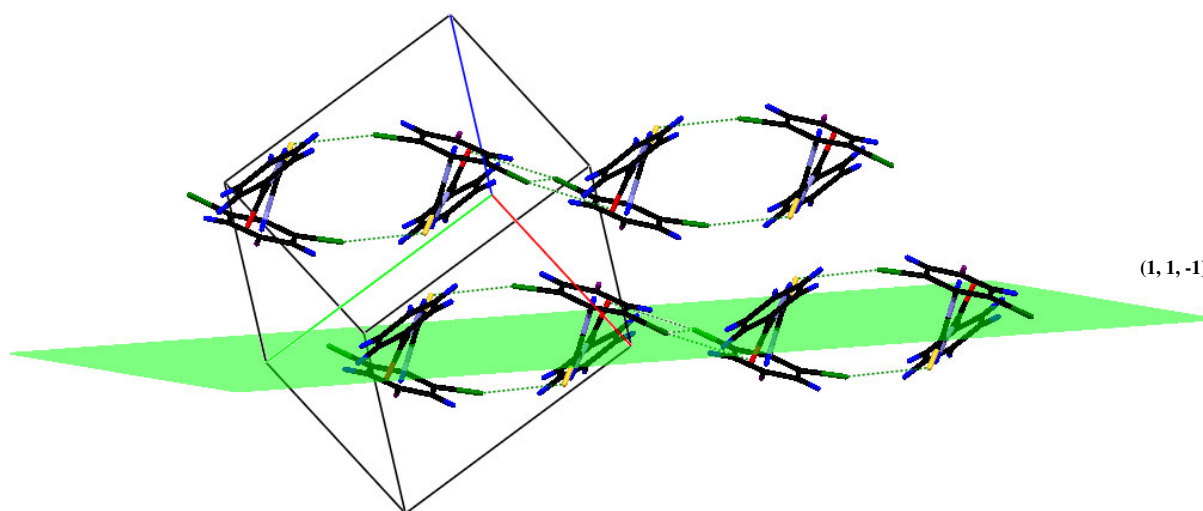


**Figure 4.10** A representation of the polymeric chain formation attributed to Br...Br interactions between molecules of the compound *N*-BFPTH parallel to the (11-1) plane.



G. Steyl and A. Roodt<sup>14</sup> discussed the significance of Br-Br interactions in the crystal packing of molecules. Some of the important observations that they mention includes a study of Br...Br interactions across a range of compounds in the CSD,<sup>15</sup> which reveals that a significant number of these interactions fall in the distance range of 3.6-4.6 Å. Moreover, the angles defined by C-Br...Br for this range of compounds are mostly related to the distance of this interaction. Long distance interactions (> 4.0 Å) indicate C-Br...Br angles of 70-120 °, thus leading to weaker perpendicular interactions. However, shorter distance interactions (3.6-4.0 Å) lead to more linear angles of 130-170 °. This relationship is attributed to the inherent properties of the bromine atom, where the bromine atom can polarise a covalently formed bond (C-Br) as well as donate electron density to the carbon atom. In the solid state it is expected that these Br...Br interactions lessen this decrease in electron density, and therefore the nature of the compound involved could determine the extent of these interactions.

The Br...Br interactions found in the solid state for the ligand *N*-BFPTH mentioned above correlated with these findings, where the short Br...Br interaction of 3.656 Å and C-Br...Br angle of 131.6 ° indicate the significance of this interaction in stabilising the packing of the compound in solid state.

Only one interaction was found for the fluorine atom F1 and that with the hydrogen atom H11 of an adjacent molecule that is orientated around a centre of symmetry to the first molecule (Figure 4.9). This interaction has a distance of 2.570 Å and an angle C12-F1...H11 of 161.1 °. These interactions are generally considered to be weak and are therefore classified as ordinary Van der Waals contacts rather than hydrogen bonding.<sup>16a,b</sup> However, these interactions were found to play a vital role in crystal packing as the resulting connected molecules are more energetically stable<sup>17</sup> and it has been reported that the properties of these interactions could be utilised in crystal engineering.<sup>18</sup>

<sup>14</sup> Steyl, G.; Roodt, A. (2008) *Models, Mysteries and Magic of Molecules*, Dordrecht: Springer Publishers, edited by Boeyens, J. C. A., Ch.15, 330.

<sup>15</sup> CSD version 5.31, updated May 2010. Allen, F. H. (2002). *Acta Cryst.*, **B58**, 380

<sup>16</sup> a) Howard, J. A. K.; Hoy, V. J.; O'Hagan, D.; Smith, G. T. (1996) *Tetrahedron*, **38**, 12613. b) Dunitz, J. D.; Schweizer, W.B. (2006) *Chem. Eur. J.*, **12**, 6804.

<sup>17</sup> D'Oria, E.; Novoa, J. J. (2008) *Cryst. Eng. Commun.*, **10**, 423.

<sup>18</sup> Desiraju, G. R. (2002) *Acc. Chem. Res.*, **35**, 565.

## 4.5. Crystal structure of N-benzoyl-N'-(pentafluorophenyl)thiourea (N-FPTH)

### 4.5.1 Results and discussion

(Synthesis described in Section 3.3.4; Supplementary data A3)

The compound N-benzoyl-N'-(pentafluorophenyl)thiourea, N-FPTH, crystallised with eight molecules in the unit cell of the monoclinic space group  $C2/c$ . Figure 4.11 represents the structure and subsequent atom labelling of the compound whilst the main bond distances as well as bond angles are presented in Table 4.6.

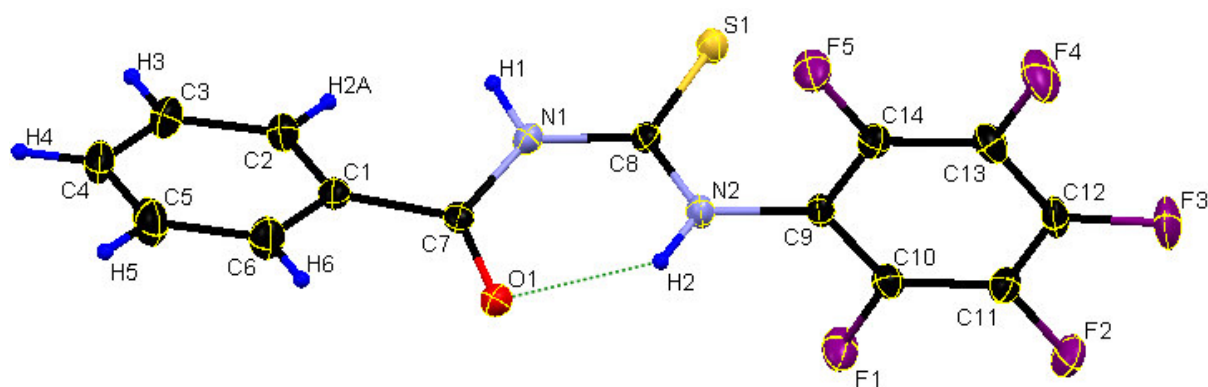


**Figure 4.11:** A structural representation of the compound *N*-FPTH, where the atom numbering scheme is shown (ellipsoid probability = 50 %).

**Table 4.6:** List of selected bond distances and angles for *N*-FPTH.

Atoms	Distance (Å)	Atoms	Angle (°)
C7-O1	1.226(2)	N1-C7-O1	122.4(1)
C8-S1	1.664(2)	N1-C8-S1	120.0(1)
C9-N2	1.419(2)	C8-N2-C9	121.3(1)
C8-N2	1.338(2)	C1-C2-C3-C4	0.4(2)
C8-N1	1.387(2)	C2-C1-C7-O1	-153.3(1)
C7-N1	1.382(2)	C9-C10-C11-C12	0.0(2)
		O1-C7-C8-S1	164.6
		C8-N2-C9-C14	88.2(2)

Again, as was discussed before in Section 4.3, the carbonyl oxygen atom is found *trans* to the sulphur atom with a dihedral angle of 164.6 °. The penta-fluorophenyl group is found to be almost perpendicular to the plane across the thiourea bridge as defined by the torsion angle C8-N2-C9-C14 of 88.2(2) °. However, the phenyl group of the benzoyl moiety is only slightly out of this plane across the thiourea bridge with a dihedral angle C2-C1-C7-O1 of -153.3(1) °. These phenyl rings are virtually planar as indicated by the torsion angles C1-C2-C3-C4 and C9-C10-C11-C12 of 0.4(2) and 0.0(2) °, respectively. This compound is also found in the *keto* formation as defined by the bond lengths C7-O1 and C8-S1, which equal 1.226(2) and 1.664(2) Å, respectively.

Several hydrogen bond interactions are found between adjacent molecules in the crystal packing as shown in Figure 4.12a. The first interaction is the expected intramolecular hydrogen bond between the oxygen atom O1 and the nitrogen atom N2, which has a distance of 2.661(2) Å and an angle N2-H2...O1 of 132.8 °. Two intermolecular hydrogen bond interactions are found between neighbouring molecules orientated across the c-glide plane. These interactions, namely, N1-H1...O1 and N2-H2...S1 have respective distances of 3.126(2) and 3.243(2) Å and respective angles of 164.4 and 129 °. Together with the intramolecular hydrogen bonding mentioned before in Figure 4.12a, these interactions form a 6-membered ring interaction between each molecule across the c-glide plane resulting in the formation of a polymeric chain network on this glide plane along the c-axis (Figure 4.12b).

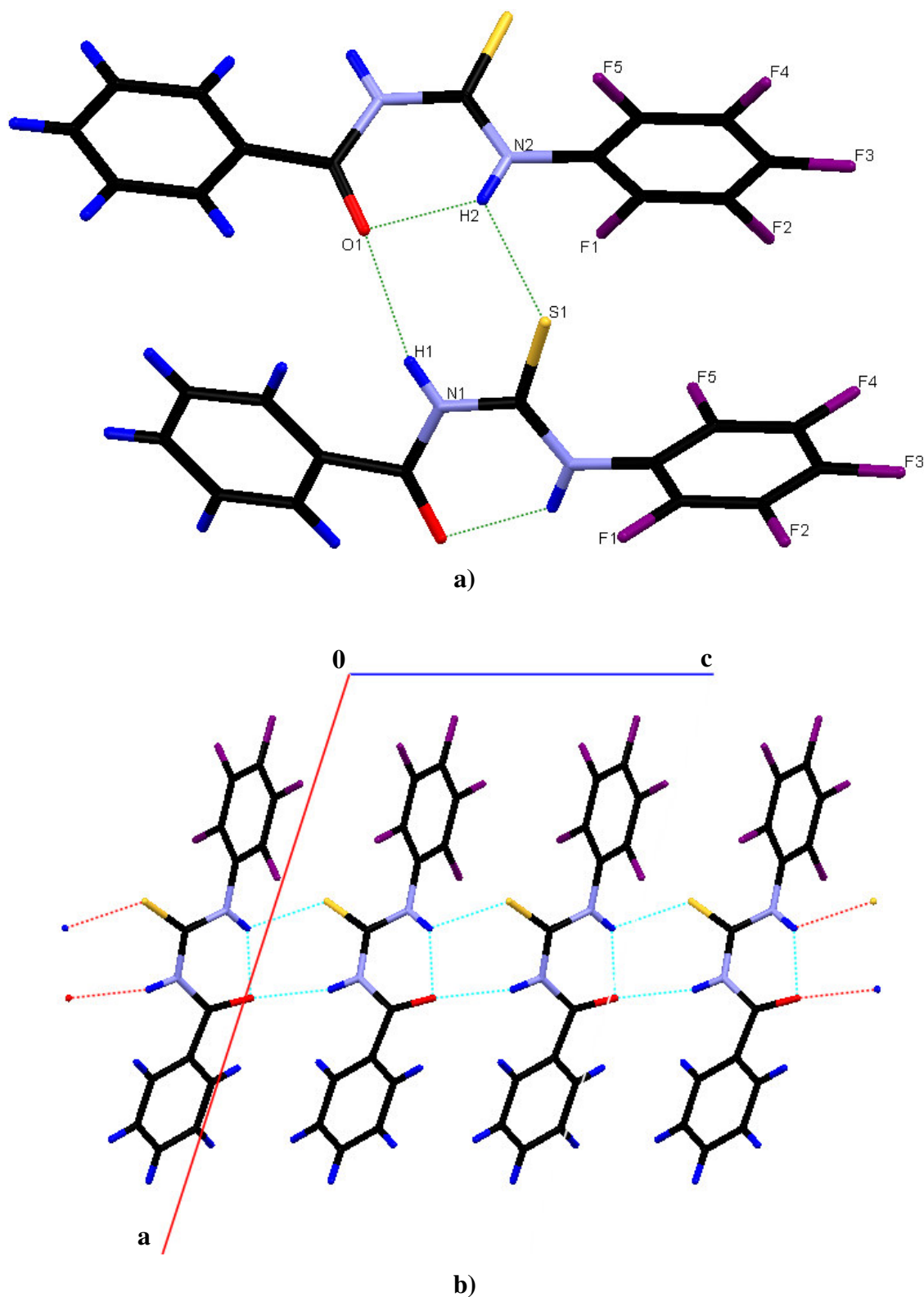


**Figure 4.12** An illustration of a) the hydrogen bonding found in the compound *N*-FPTH and b) the resulting polymeric chain formation along the *c*-axis (partial unit cell). Distances and angles: N1-H1...O1 = 3.126(2) Å, 164.4 °; N2-H2...O1 = 2.661(2) Å, 132.8 °; N2-H2...S1 = 3.243(2) Å, 129.0 °.

A variety of short contacts *via* Van der Waals interactions are observed in the crystal packing. The fluorine atoms of the compound *N*-FPTH show interconnections with each other and with other atoms through seven distinct soft contacts, as presented in Figure 4.13. The different distances and angles defining these interactions are provided in Table 4.7.

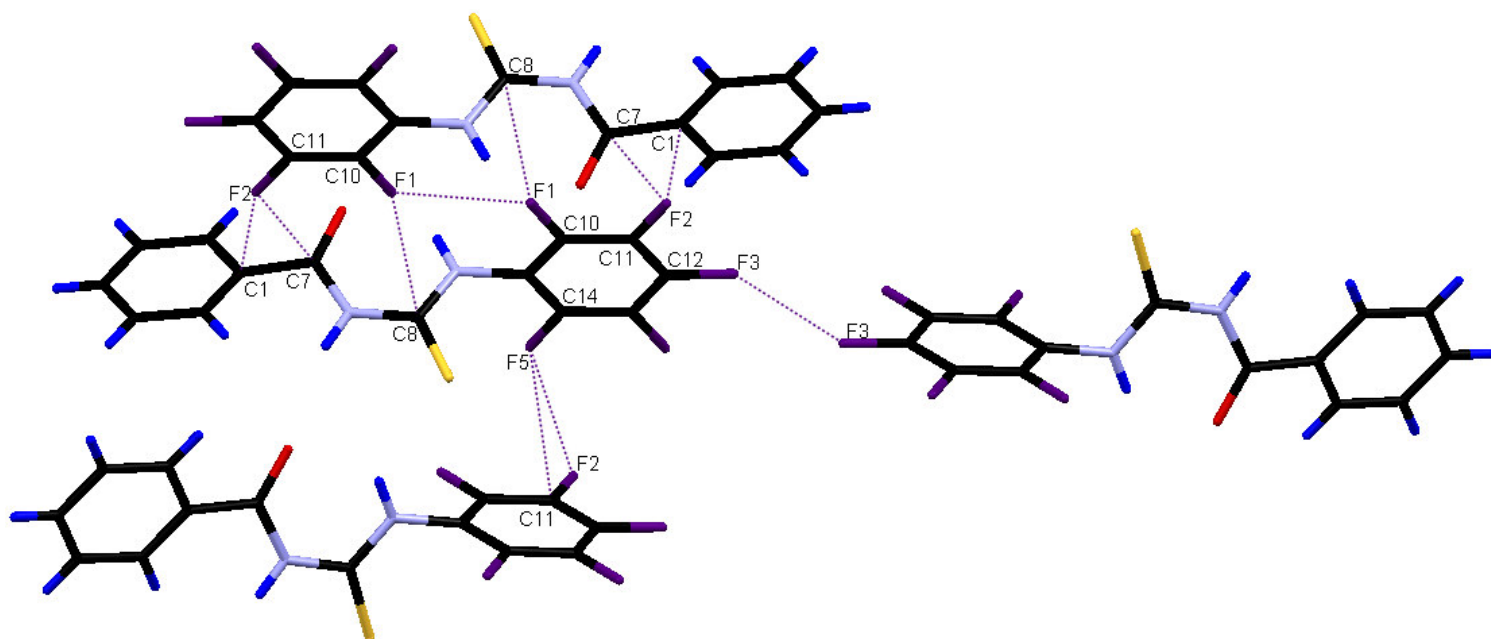


**Figure 4.13** A representation of the soft contacts found between the fluorine atoms and several other atoms of neighbouring molecules in the packing of the compound *N*-FPTH. For distances and angles see Table 4.7.

**Table 4.7** The distances and angles defining the short contacts between the fluorine atoms and several other atoms of neighbouring molecules in the packing of the compound *N*-FPTH.

Soft contact	Distance (Å)	Bond angle	Angle value (°)
F1...F1	2.812	C10-F1...F1	127.5
F1...C8	3.047	C10-F1...C8	154.5
F2...F5	2.860	C11-F2...F5	87.8
F2...C1	3.129	C11-F2...C1	154.3
F2...C7	3.113	C11-F2...C7	126.8
F3...F3	2.601	C12-F3...F3	146.4
F5...C11	3.111	C14-F5...C11	112.9

F...F interactions and their role in crystal packing is difficult to interpret and define.<sup>19</sup> Based on Pauling's principle<sup>20</sup> where it is stated that fluorine atoms have a low polarization ability, it is believed that the attraction forces between fluorine atoms should be small and therefore F...F intramolecular short contacts cannot form. However, recent work done on fluorinated aromatic compounds, where calculations were performed on the electron density distribution between neighbouring fluorine atoms, revealed that critical points of electron density (3, -1) existed in the intermolecular space between some fluorine atoms.<sup>21</sup> This suggested that binding interactions between these atoms were present. Also earlier quantum-chemical calculations done on these systems showed that the major contribution to the total energy found between F...F atoms was from attraction forces, as determined by the Van der Waals component.<sup>22</sup>

By comparing the values found for the F...F interactions in the thiourea compound *N*-FPTH given in Table 4.7, it would seem that a similar trend might exist as was found for the Br...Br interactions discussed in the previous section. Since a fluorine atom has a much smaller Van der Waals radius than a bromine atom (1.47 Å vs 1.95 Å),<sup>23</sup> it is expected that these F...F interactions will be much shorter. It is clear from Table 4.7 that the F...F interactions ranges from 2.6-2.9 Å, while the angle defined by C-F...F for these interactions decreases from 146.4 ° to 87.8 ° as the interaction distance increases. Thus, a strong F...F interaction displays a more linear angle, but as the C-F...F interaction becomes weaker the angle of the interaction becomes more perpendicular. This effect in halogen-halogen interactions have been studied some time ago by Ramasubbu *et al.*<sup>24</sup> who classified these interactions in two groups of "forced" and energy-favourable interactions. Unfortunately F...F interactions could not be clearly defined by this means and was regarded as an exception.

C-F... $\pi$  interactions, also play an important role in the packing of molecules in the unit cell as was elucidated by Prasana and Row Guru<sup>25</sup> who did a study on the CSD across a range of fluoro-organic compounds. They showed that when fluorinated aromatic rings are packed in the crystal lattice the C-F... $\pi$  interaction causes one of the rings to interact in a T form to the

<sup>19</sup> Reichenbacher, K.; Heike, I.; Suss, H. I.; Jurg Hulliger, J. (2005) *Chem. Soc. Rev.*, **34**, 22.

<sup>20</sup> Pauling, L. C. (1960) *The Nature of the Chemical Bond*, Cornell University Press, Ithaca, 449.

<sup>21</sup> Rybalova, T. V.; Bagryanskaya, I. Yu. (2009) *J. Struct. Chem.*, **50**, 4, 741.

<sup>22</sup> Lorenza, S.; Lewis, G. R.; Dance, I. (2000) *New. J. Chem.*, **24**, 295.

<sup>23</sup> Bondi, A. (1964) *J. Phys. Chem.*, **68**, 3, 441.

<sup>24</sup> Ramasubbu, N.; Parthasarathy, R.; Murray-Rust, P. (1986) *J. Am. Chem. Soc.*, **108**, 4308.

<sup>25</sup> Prasana, M. D.; Row Guru, T. N. (2000) *Cryst. Eng.*, **3**, 135.

other ring as illustrated in Figure 4.14a, which in turn leads to a parquet-like packing of these molecules as shown in Figure 4.14b. This seems to hold true for the thiourea compound discussed in this section (*N*-FPTH) as shown in Figure 4.14c. This interaction is not only found between two of the pentafluorophenyl rings, but also between a pentafluorophenyl ring and a normal phenyl ring in this case. A further look into the packing of this thiourea ligand reveals that it might also be true for interaction of C-F moieties with  $sp^2$ -hybridised carbons having delocalised electron density as indicated by the interaction of F2 with C7 as well as F1 with C8. In these interactions the pentafluorophenyl rings are almost perpendicular to the thiourea bridge of the next molecule. The distances of all the C...F interactions in this thiourea compound are found to be similar having a value of  $\pm 3.1$  Å.

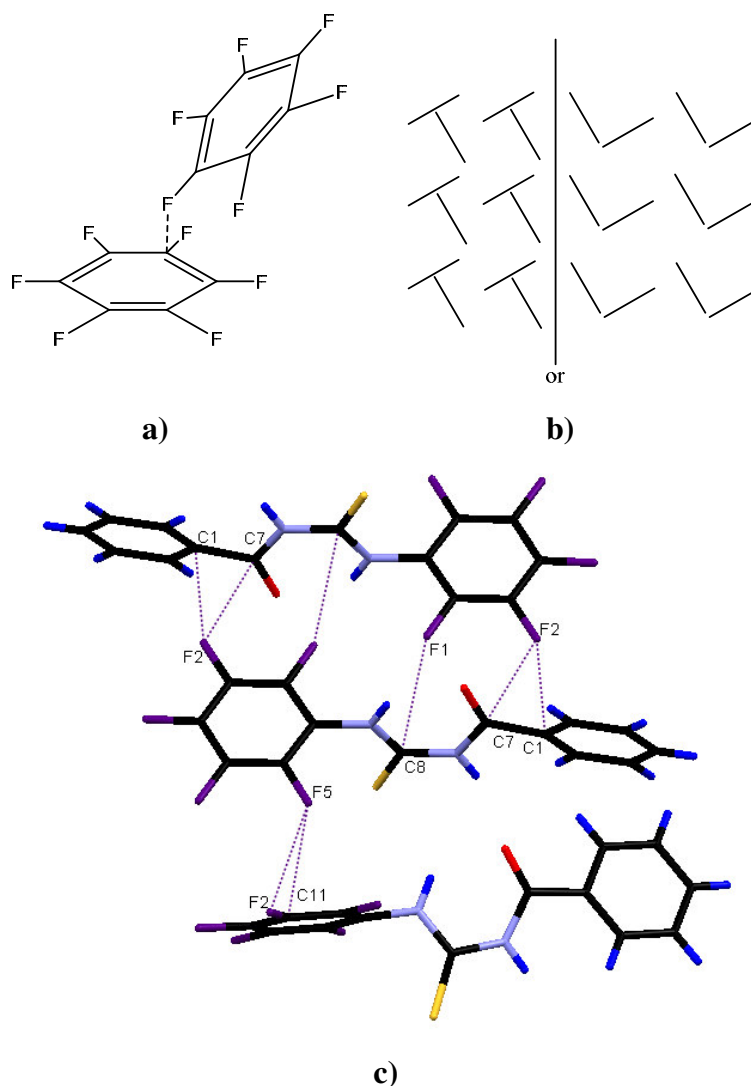


**Figure 4.14 a) An illustration of the T-interaction and b) the typical parquet-like architecture found in the packing of fluorinated aromatic rings. In c) this T-formation found in the compound *N*-FPTH is illustrated.**

## 4.6. Crystal structure of N-benzoyl-N'-(phenethyl)thiourea (*N*-PeTH)

### 4.6.1 Results and discussion

(Synthesis described in Section 3.3.6; Supplementary data A4)

The compound N-benzoyl-N'-(phenethyl)thiourea, *N*-PeTH, crystallised with four molecules in the unit cell of the monoclinic space group  $P2_1/n$ . The structure and subsequent atom labelling of the compound are provided in Figure 4.15, while Table 4.8 gives the main bond distances and angles.

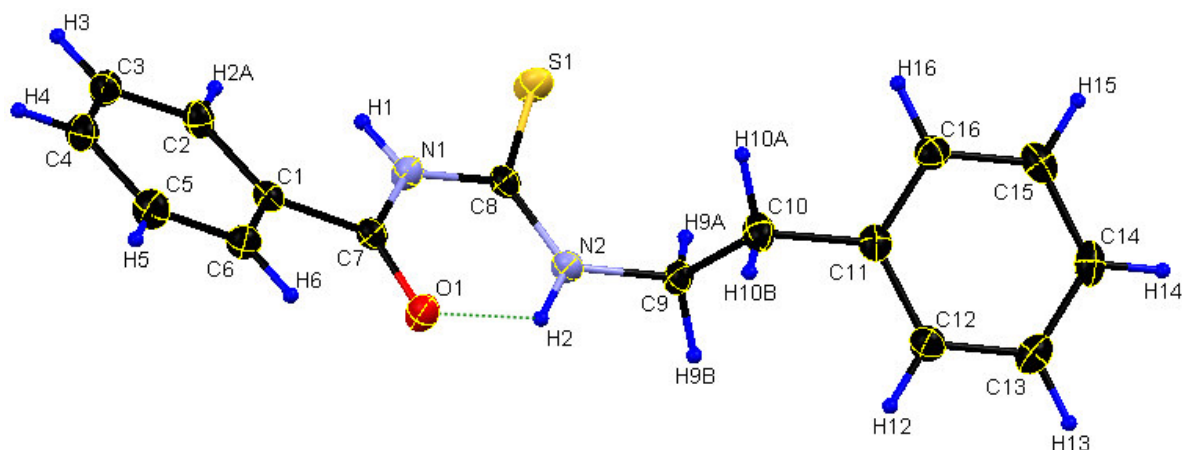


**Figure 4.15:** A structural representation of the compound *N*-PeTH, where the atom numbering scheme is shown (ellipsoid probability = 50%).

**Table 4.8:** List of selected bond distances and angles for *N*-PeTH.

Atoms	Distance (Å)	Atoms	Angle (°)
C7-O1	1.224(2)	N1-C7-O1	122.5(1)
C8-S1	1.672(1)	N1-C8-S1	117.6(1)
C9-N2	1.461(2)	C8-N2-C9	122.7(1)
C8-N2	1.324(2)	C1-C2-C3-C4	1.1(2)
C8-N1	1.396(2)	C2-C1-C7-O1	12.3(2)
C7-N1	1.380(2)	C11-C12-C13-C14	0.7(2)
		O1-C7-C8-S1	-172.6
		C8-N2-C9-C10	93.6(1)



In this compound the expected *keto* formation is also observed as suggested by the C7-O1 and C8-S1 bond lengths of 1.224(2) and 1.672(1) Å as well as by the bond angles N1-C7-O1 and N1-C8-S1 of 122.5(1) and 117.6(1) °, respectively. The protons on the nitrogen atoms also exist and were placed as riding by the same argument discussed in Section 4.3. The *trans* orientation of the carbonyl oxygen with respect to the sulphur atom is also observed and with a dihedral angle of -172.6 ° it is clear that these two atoms lie on the same plane along the C-N-C chain. The phenyl rings present in the molecule are found to have molecular planarity as suggested by the torsion angles C1-C2-C3-C4 and C11-C12-C13-C14 of 1.1(2) and 0.7(2) °. With a torsion angle C2-C1-C7-O1 of 12.3(2) ° the phenyl ring of the benzoyl group is almost parallel to the plane across the thiourea bridge, while the phenethyl group is found to be closely perpendicular to this plane with a torsion angle of 93.6(1).

Intra- and intermolecular hydrogen bond interactions are established in the crystal packing (Figure 4.16a). The typical N2-H2...O1 interaction is observed and has a distance and angle of 2.672(1) Å and 130.2 °, respectively. Only one intermolecular hydrogen bond interaction exists in the packing, namely N2-H2...S1, which is found between neighbouring molecules having the same orientation. This interaction, which has a distance of 3.466(1) Å and an angle of 122.2 °, leads to the formation of a chain network of polymeric units along the b-axis as illustrated in Figure 4.16b.

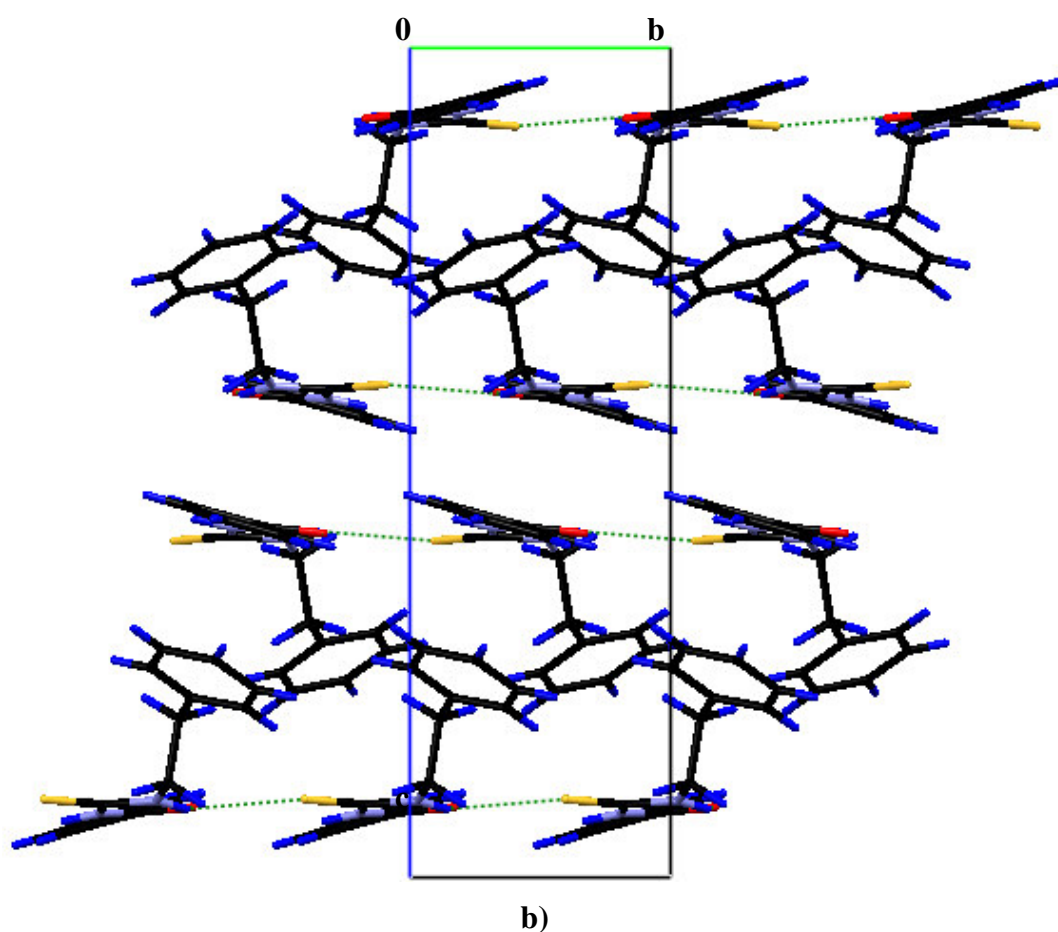
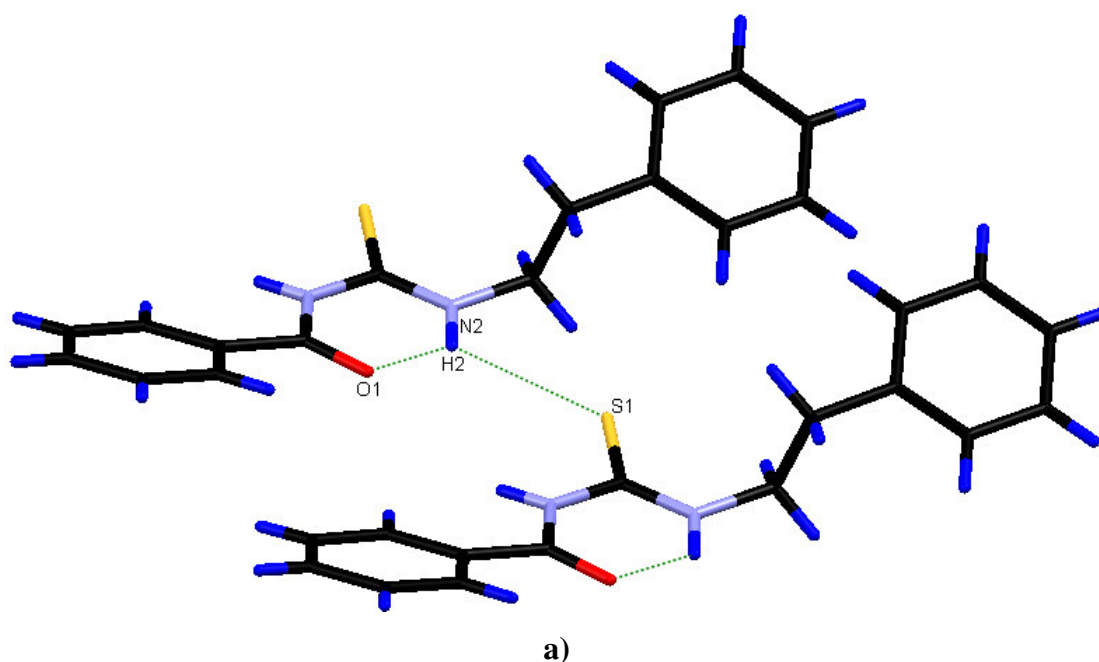
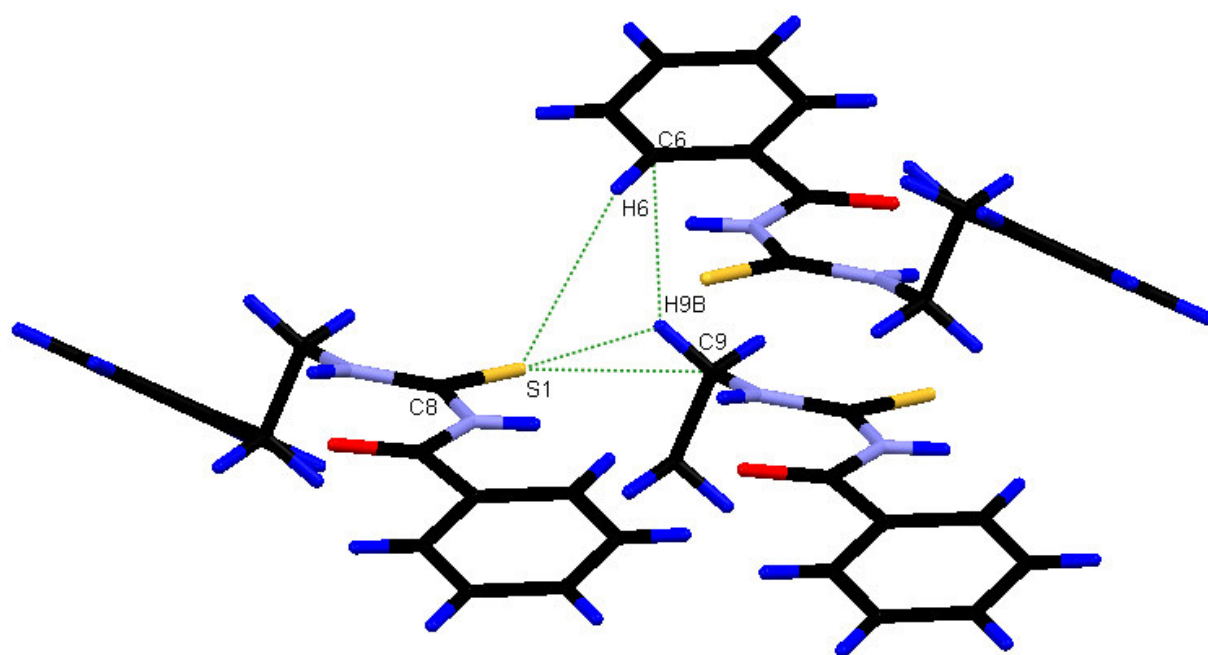


**Figure 4.16** A representation of a) the hydrogen bond interactions found between adjacent molecules of the compound *N*-PeTH and b) the resulting chain network formed along the *b*-axis. Distances and angles: N2-H2..O1 = 2.672(1) Å, 130.2 °; N2-H2...S1 = 3.466(1) Å, 122.2 °.

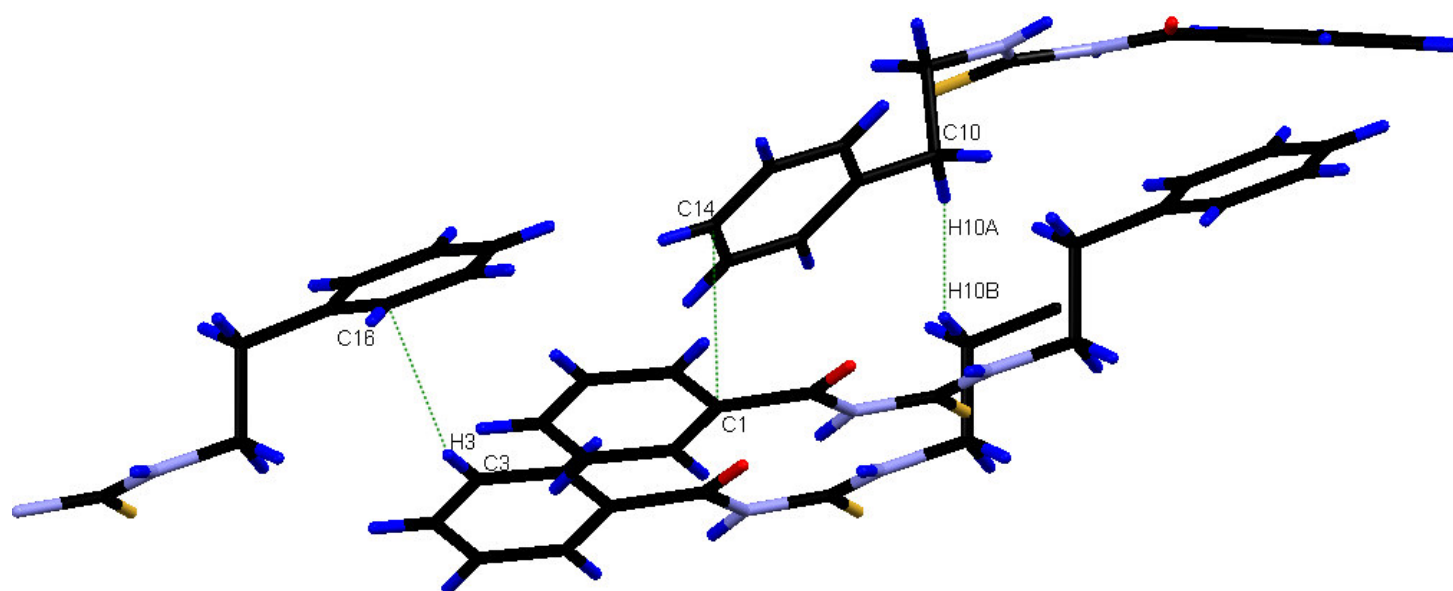
There are only minor short contacts that help to stabilise the packing, as shown in Figure 4.17. All the corresponding distances and angles for these soft contacts are provided in Table 4.9. Firstly the sulphur atom has several interactions apart from the hydrogen bonding discussed before, as shown in Figure 4.16a. These interactions are defined by C8-S1...H6, C8-S1...H9B and C8-S1...C9, which have interaction distances of 2.933, 2.742 and 3.353 Å, respectively and respective angles of 110.8, 173.2 and 165.2 °. Further contacts involve some hydrogen-hydrogen interactions between H10A and H10B having a distance of 2.174 Å as well as carbon-hydrogen interactions between C6 and H9B and C16 and H3, respectively, having respective distances of 2.852 and 2.900 Å. The subsequent angles of these interactions are C10-H10A...H10B = 160.5 °, C3-H3...C16 = 148.9 ° and C9-H9B...C6 = 131.1 °. The last interaction seems to be a  $\pi$ - $\pi$  interaction found between C1 and C14 having a distance of 3.336 Å.

**Table 4.9 A list of the distances and angles defining the short contacts found in the crystal packing of the compound *N*-PeTH.**

Short contact	Distance (Å)	Bond angle	Angle value (°)
S1...H6	2.933	C8- S1...H6	110.8
S1...H9B	2.742	C8- S1...H9B	173.2
S1...C9	3.353	C8- S1...C9	165.2
C6...H9B	2.852	C9-H9B...C6	131.1
C16...H3	2.900	C3-H3...C16	148.9
H10A...H10B	2.174	C10-H10A...H10B	160.5
C1...C14	3.336	-	-



a)



b)

**Figure 4.17** Some short contacts found in the crystal packing of the compound *N*-PeTH represented by different orientations of the molecules in a) and b). Some of the atoms have been omitted for clarity. For distances and angles, see Table 4.9.

## 4.7. Crystal structure of N-benzoyl-N'-(naphthalene-1-ylmethyl)thiourea (N-NmTH)

### 4.7.1 Results and discussion

(Synthesis described in Section 3.3.7; Supplementary data A5)

The compound N-benzoyl-N'-(naphthalen-1-ylmethyl)thiourea, *N*-NmTH, crystallised in the monoclinic space group *C*2/*c* with eight molecules in the unit cell. The structure and subsequent atom labelling of the compound are provided in Figure 4.18 while Table 4.10 gives the main bond distances and angles.

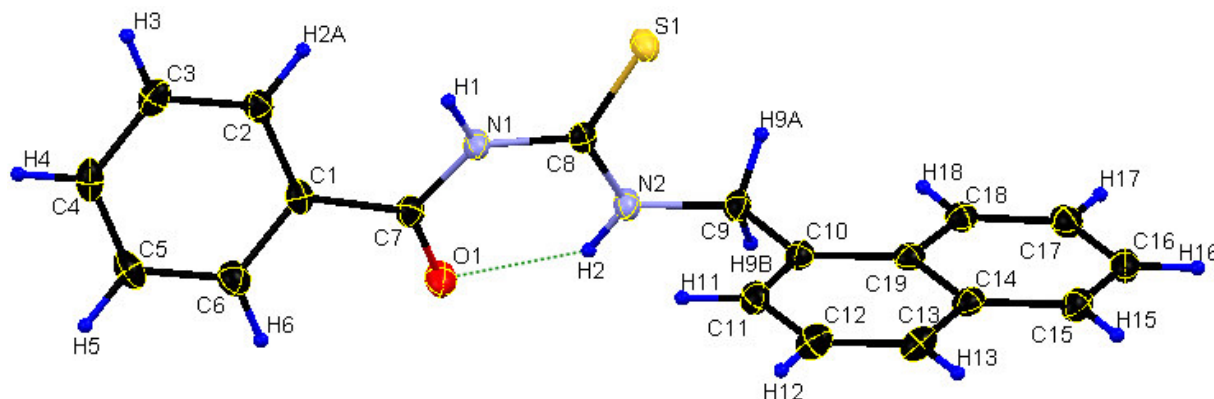


**Figure 4.18:** A structural representation of the compound *N*-NmTH, where the atom numbering scheme is shown (ellipsoid probability = 50%).

**Table 4.10:** List of selected bond distances and angles for the compound *N*-NmTH.

Atoms	Distance (Å)	Atoms	Angle (°)
C7-O1	1.229(2)	N1-C7-O1	122.1(2)
C8-S1	1.676(2)	N1-C8-S1	118.2(1)
C9-N2	1.455(2)	C8-N2-C9	123.0(1)
C8-N2	1.326(2)	C1-C2-C3-C4	-0.1(3)
C8-N1	1.396(2)	C2-C1-C7-O1	-160.8(2)
C7-N1	1.378(2)	C10-C19-C14-C15	179.0(2)
		O1-C7-C8-S1	179.5
		C8-N2-C9-C10	78.5(2)

In this thiourea ligand the *keto* formation is also observed as with the other ligands in Sections 4.3-4.6, which is suggested by the bond distances of C7-O1 and C8-S1 being 1.229(2) and 1.676(2) Å and the bond angles N1-C7-O1 and N1-C8-S1 of 122.1(2) and 118.2(1) °, respectively. Also the nitrogen atoms N1 and N2 are protonated by the same argument as discussed in Section 4.3 and therefore the corresponding hydrogen atoms were also placed as riding. With a dihedral angle O1-C7-C8-S1 of 179.5, the oxygen atom O1 is found *trans* with respect to the sulphur atom S1 across the thiourea bridge. The phenyl ring of the benzoyl group is fairly in plane with the thiourea moiety having a torsion angle C2-C1-C7-O1 of -160.8(2) °. The naphthyl group is twisted out of the plane across the thiourea moiety with a torsion angle of 78.5(2) °. With torsion angles C1-C2-C3-C4 and C10-C19-C14-C15 of -0.1(3) and 179.0(2), respectively, the phenyl and naphthyl groups are found to have molecular planarity.

Two sets of hydrogen bond interactions are found in the crystal packing of the thiourea ligand as given in Figure 4.19a. Firstly is the expected intramolecular hydrogen bonding between N2 and O1 having a distance of 2.655(2) Å and an angle of 134.0 °. The other hydrogen bond is an intermolecular interaction between N1 and S1 with a distance of 3.426(2) Å and an angle of 140.6 °. This interaction leads to the closure of an eight-membered ring, which has a “chair”-conformation, and in turn forms dimers that are packed in the unit cell along the c-axis (Figure 4.19b).

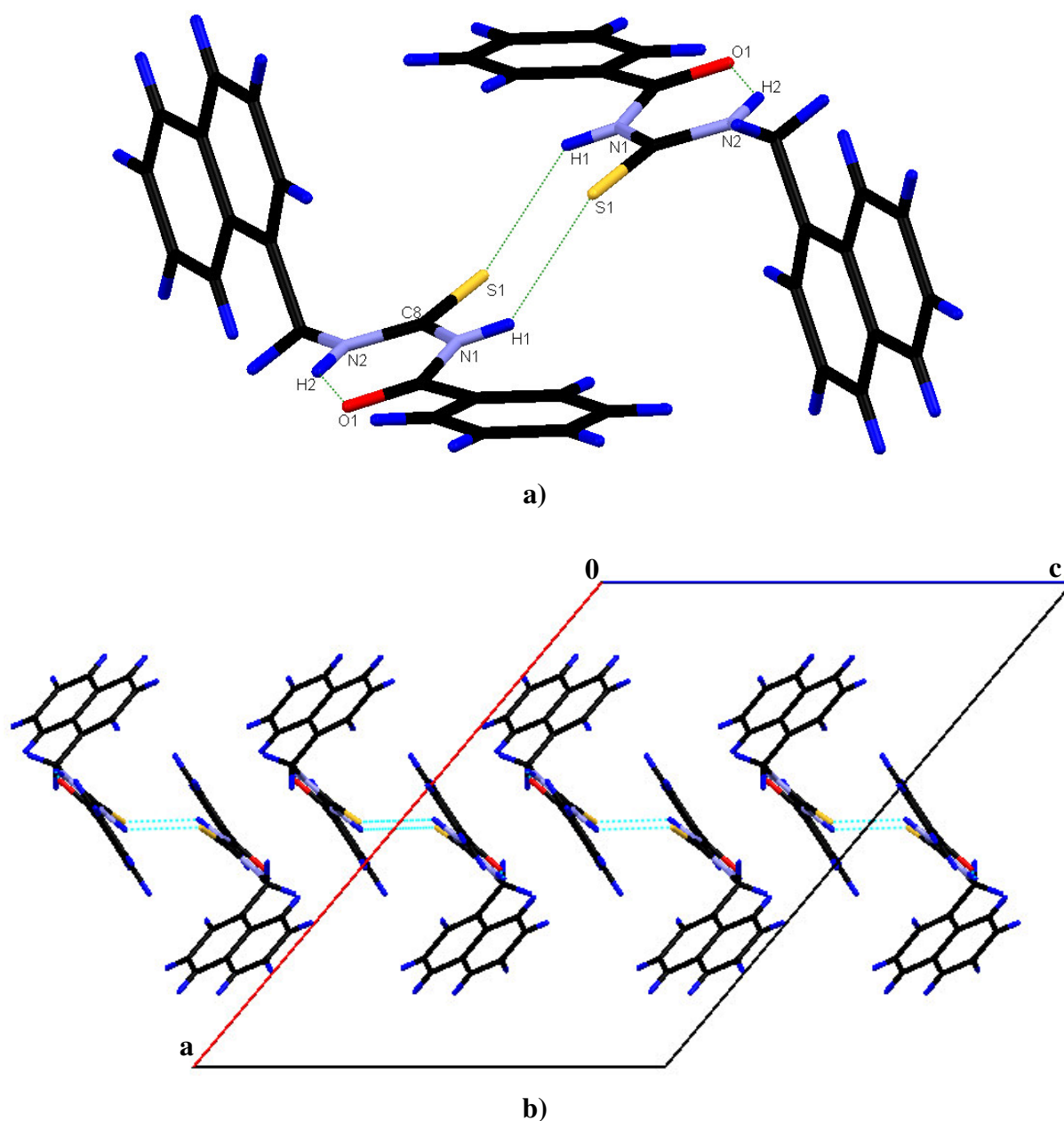


**Figure 4.19** A representation of a) the hydrogen bond interactions found in the packing of the compound *N*-NmTH and b) the resulting dimer formation in the packing along the *c*-axis. Distances and angles: N2-H2...O1 = 2.655(2) Å, 134.0 °; N1-H1...S1 = 3.426(2) Å, 140.6 °.

Some  $\pi$ -stacking interactions are also observed in the crystal packing between the naphthyl groups of two molecules that are orientated around a centre of symmetry. These interactions are found between the carbons C10 and C18 in a “head-to-tail” mode as illustrated in Figure 4.20a and have an interplanar distance of 3.430 Å. The  $\pi$ -stacking takes place in two different directions, namely, along the plane (110) as shown in Figure 4.20b and along the plane (100) as shown in Figure 4.20c.

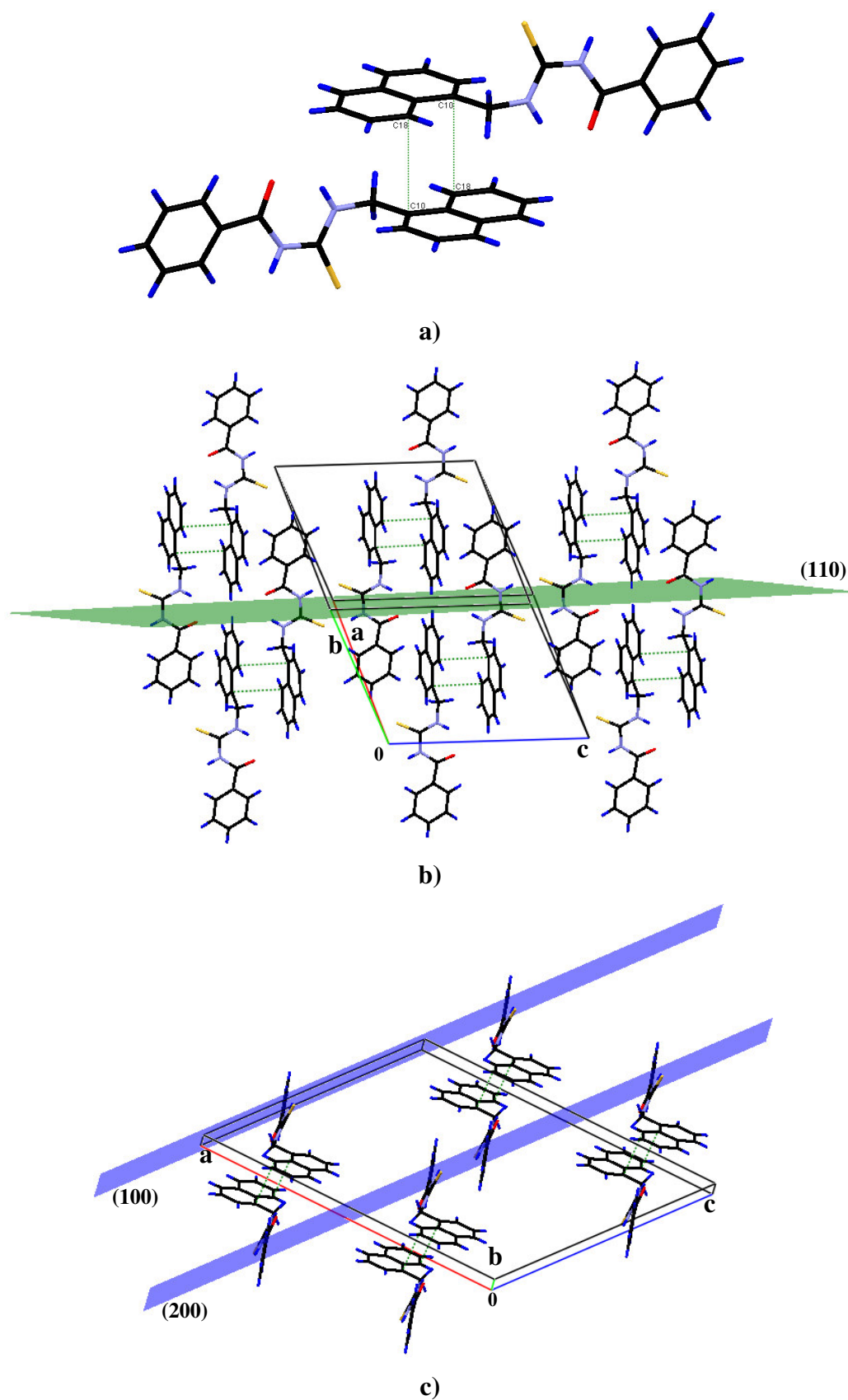


**Figure 4.20 a) An illustration of the  $\pi$ - $\pi$  stacking found between molecules in the packing of the compound *N*-NmTH. Two different sets of stacking are observed along the planes b) (110) and c) (100).**



Several other soft contacts are also present in the crystal packing of the compound *N*-NmTH as given in Figure 4.21. The relevant distances and angles of these contacts are provided in Table 4.11.

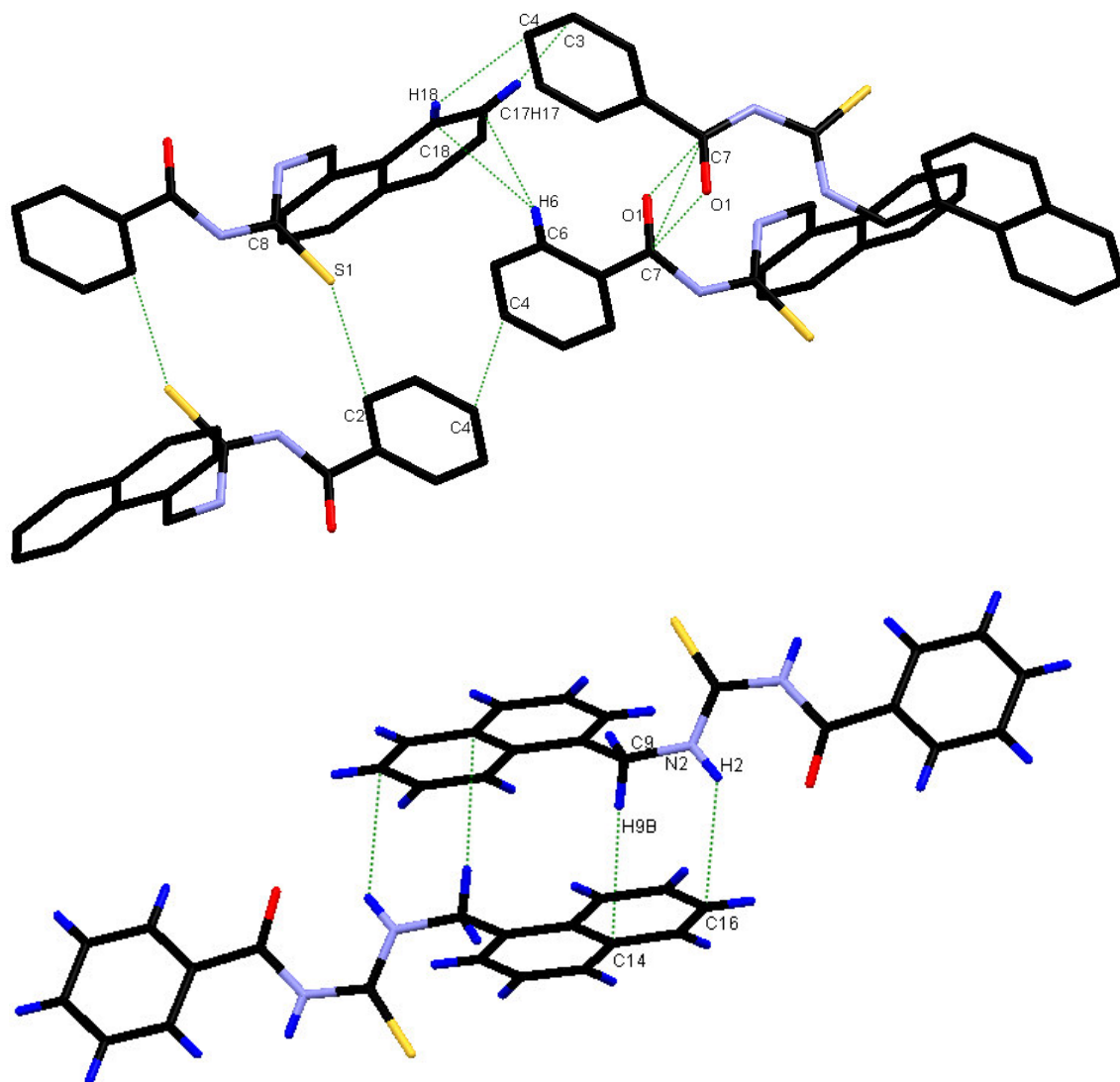


**Figure 4.21** An illustration of several short contacts found between molecules in the crystal packing of the compound *N*-NmTH. Some of the hydrogen atoms have been omitted for clarity. Distances and angles are provided in Table 4.11.

**Table 4.11 The distances and angles defining the short contacts found in the crystal packing of the compound *N*-NmTH.**

Short contact	Distance (Å)	Bond angle	Angle value (°)
S1...C2	3.428	C8-S1...C2	136.3
O1...C7	3.060	C7-O1...C7	91.4
C4...C4	3.370	-	-
C7...C7	3.326	-	-
C3...H17	2.772	C17-H17...C3	147.0
C4...H18	2.870	C18-H18...C4	134.5
C14...H9B	2.880	C9-H9B...C14	169.0
C16...H2	2.797	N2-H2...C16	137.3
C17...H6	2.766	C6-H6...C17	164.5
C18...H6	2.864	C6-H6...C18	136.4

## 4.8. Crystal structure of *N*-benzoyl-*N'*-(cyclohexyl)thiourea (*N*-CyTH)

### 4.8.1 Results and discussion

(Synthesis described in Section 3.3.8; Supplementary data A6)

The compound *N*-benzoyl-*N'*-(cyclohexyl)thiourea, *N*-CyTH, crystallised in the triclinic space group  $P\bar{1}$  with two molecules found in the asymmetric unit. Figure 4.22 represents the structure and subsequent atom labelling of the compound, while Table 4.12 gives the main bond distances and angles.

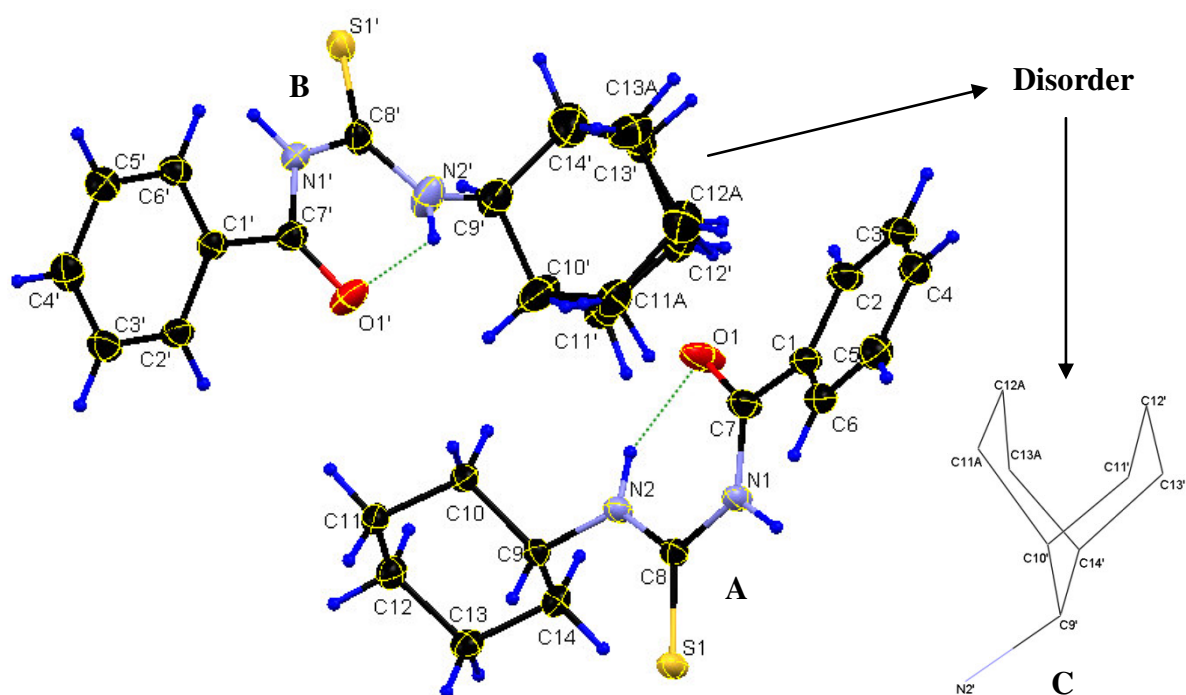


**Figure 4.22:** A structural representation of the compound *N*-CyTH showing both independent molecules A and B, where the atom labelling is shown (ellipsoid probability = 50%). The hydrogen atom labels have been omitted for clarity. The disorder in the cyclohexyl group of molecule B is clearly indicated by a wireframe representation C.

**Table 4.12:** List of selected bond distances and angles for the compound *N*-CyTH.

Molecule A		Molecule B	
Atoms	Distance (Å)	Atoms	Distance (Å)
C7-O1	1.225(2)	C7'-O1'	1.227(2)
C8-S1	1.679(2)	C8'-S1'	1.677(2)
C9-N2	1.465(2)	C9'-N2'	1.475(3)
C8-N2	1.326(2)	C8'-N2'	1.338(2)
C8-N1	1.390(2)	C8'-N1'	1.394(2)
C7-N1	1.380(2)	C7'-N1'	1.384(2)
Atoms	Angle (°)	Atoms	Angle (°)
N1-C7-O1	122.5(2)	N1'-C7'-O1'	123.0(2)
N1-C8-S1	119.1(1)	N1'-C8'-S1'	119.2(1)
C8-N2-C9	124.0(1)	C8'-N2'-C9'	125.8(2)
C1-C2-C3-C4	-0.4(3)	C1'-C2'-C3'-C4'	-1.2(3)
C2-C1-C7-O1	-27.4(3)	C2'-C1'-C7'-O1'	-33.4(2)
C8-N2-Ct(C10, C14)-C10	129.8	C8'-N2'-Ct(C10', C14')-C10'	-144.0
O1-C7-C8-S1	178.6	O1'-C7'-C8'-S1'	167.2

Both molecules **A** and **B** are found in the *keto* form as indicated by the bond lengths of 1.225(2) and 1.227(2) Å for the C7-O1 and C7'-O1' bonds as well as 1.679(2) and 1.677(2) Å for the C8-S1 and C8'-S1' bonds, respectively. This is also supported by the angles N1-C7-O1, N1'-C7'-O1', N1-C8-S1 and N1'-C8'-S1' having respective values of 122.5(2), 123.0(2), 119.1(1) and 119.2(1) °. Furthermore, the protons of the nitrogen atoms N1, N1', N2 and N2' were found to exist and placed as riding by the same argument as in Section 4.3. The phenyl rings of the benzoyl groups have molecular planarity as indicated by the torsion angles C1-C2-C3-C4 and C1'-C2'-C3'-C4' of -0.4(3) and -1.2(3) °, respectively. In both molecules these phenyl rings are twisted slightly out of the plane across the thiourea bridge with torsion angles C2-C1-C7-O1 and C2'-C1'-C7'-O1' of -27.4(3) and -33.4(2) °, respectively. The dihedral angles O1-C7-C8-S1 and O1'-C7'-C8'-S1' having values of 178.6 and 167.2 ° reveal that the carbonyl oxygen atoms are *trans* with respect to the sulphur atoms along the C-N-C chain of the thiourea bridge.

As indicated in Figure 4.22 the cyclohexyl group of molecule **B** displays a positional disorder, where three of the carbon atoms C11', C12' and C13' occupies two different positions with a s.o.f of 50%. This is illustrated by the wireframe representation **C** in Figure 4.22, where both sets of atoms exhibit the chair conformation, but in a different orientation. Some unresolved electron density exists among the cyclohexyl rings, which cannot be allocated and refined. As a result the highest differential peak exhibit a high value of 1.161 e.Å<sup>-3</sup>.

The intramolecular hydrogen bond interactions between N2/N2' and O1/O1' are found as expected having respective distances of 2.625(2) and 2.597(2) Å as well as respective angles of 133.0 and 133.7 ° (Figure 4.23a). There is also intermolecular hydrogen bond interactions found between the sulphur atoms S1/S1' and the nitrogen atoms N1/N1' of neighbouring molecules that are orientated around a centre of symmetry. The respective distances and angles of these interactions are given by N1-H1...S1 = 3.381(2) Å, 161.7 ° and N1'-H1'...S1' = 3.438(2) Å, 153.7 °. These interactions lead to the closure of 8-membered rings, which are found in a “chair”-conformation. Furthermore this also results in the formation of dimers that are packed on top of each other along the a-axis as shown in Figure 4.23b.

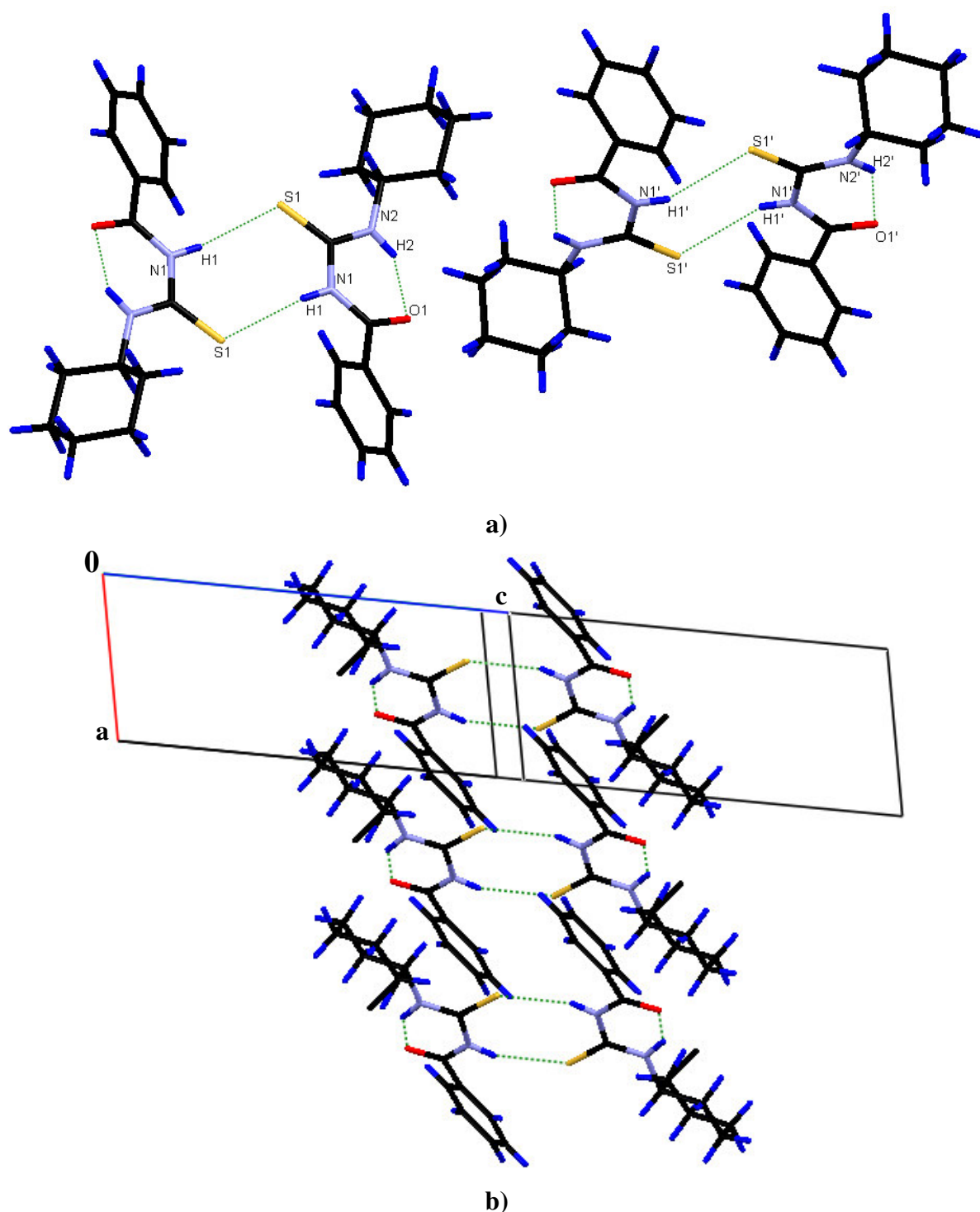


**Figure 4.23** A representation of a ) the intra- and intermolecular hydrogen bond interactions found in the crystal packing of the compound *N*-CyTH and b) the resulting dimer formation packed along the *a*-axis.

Other interactions found in the crystal packing majorly involve H...H Van der Waals interactions, while there is only one of each of C...H, S...C and O...H. The two independent molecules in the asymmetric unit seem to interact differently from each other. In Figures

4.24a and 4.24b the different interactions and packing of the two independent molecules in the asymmetric unit are shown. The molecule **A** defined in Figure 4.22, are packed in such a manner that the cyclohexyl groups of neighbouring molecules of molecule **A** are brought together, and as a result several H...H short contacts are established amongst them. A further consequence of these interactions together with the hydrogen bond interactions is the wave-like packing of molecules of the type **A** in Figure 4.22, where a bent is observed across the thiourea bridge.

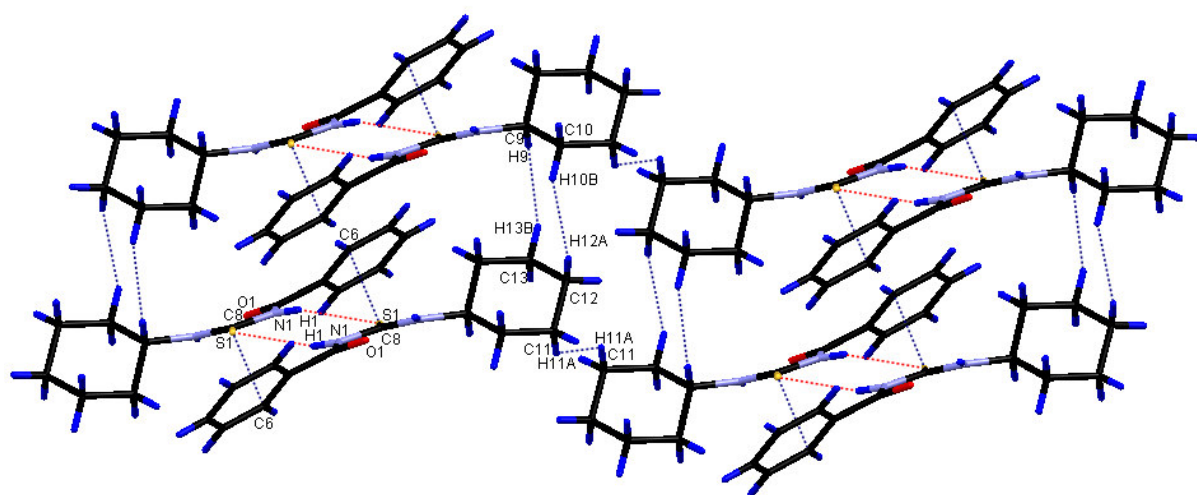


**Figure 4.24** A representation of the general Van der Waals interactions and subsequent packing of the compound *N*-CyTH for molecule **A** in the asymmetric unit defined in **Figure 4.23**.

The molecule **B** defined in Figure 4.22, on the other hand, is also packed in such a manner that the cyclohexyl groups of neighbouring molecules of molecule **B** are in close approximation. However, due to the positional disorder found in these rings a large variety of possible short contacts exist between the different rings at different positions. It is difficult to resolve these contacts and as such the no representation of these contacts will be shown.

## 4.9. Crystal structure of N-benzoyl-N'-(isopentyl)thiourea (*N*-ipTH)

### 4.9.1 Results and discussion

(Synthesis described in Section 3.3.9; Supplementary data A7)

The compound N-benzoyl-N'-(isopentyl)thiourea, *N*-ipTH, crystallised in the triclinic space group  $P\bar{1}$  with two independent molecules in the asymmetric unit. The compound together with the corresponding atom labelling is presented in Figure 4.25, whilst some of the important bond distances and bond angles are presented in Table 4.13.

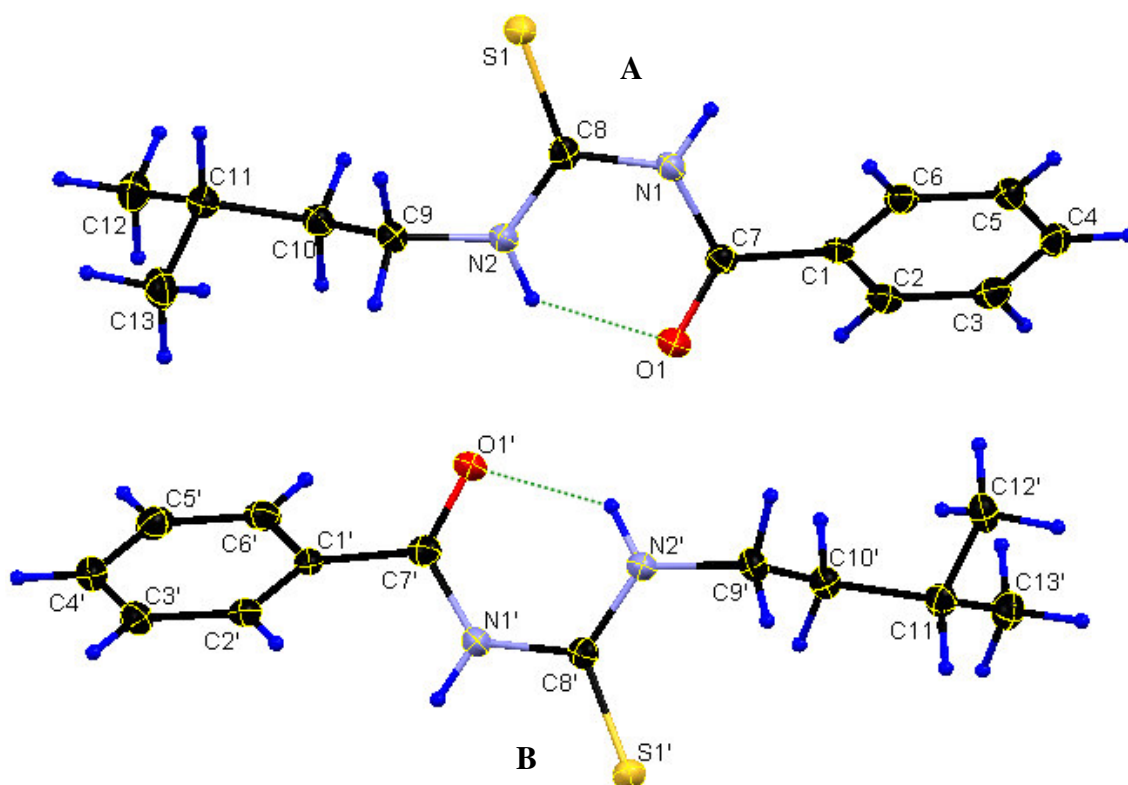


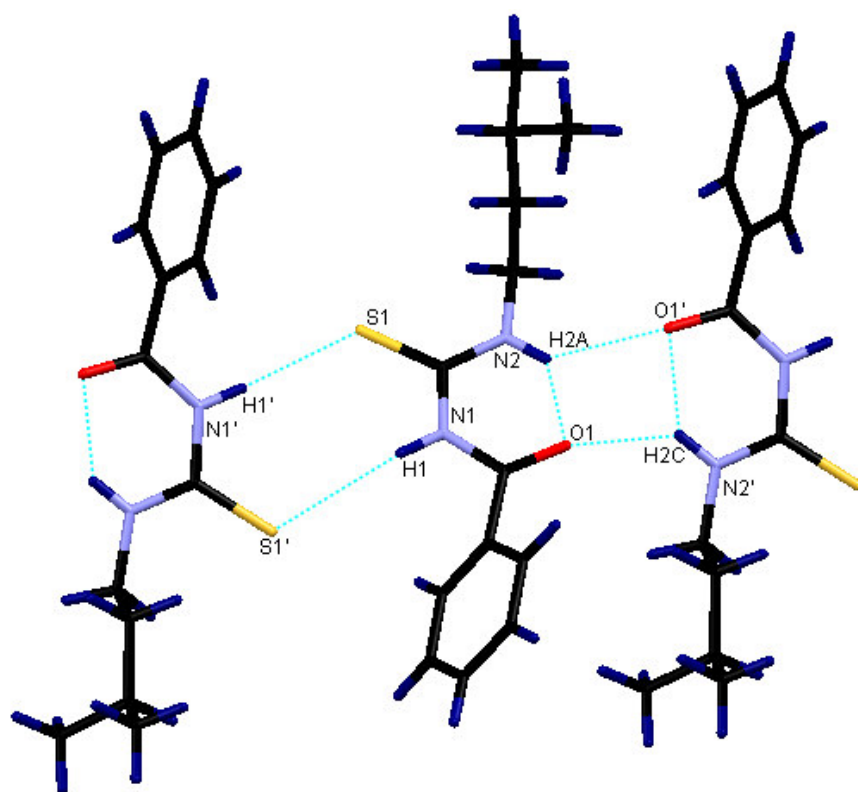
**Figure 4.25:** A structural representation of the compound *N*-ipTH showing the independent molecules A and B, where the atom numbering scheme is shown (ellipsoid probability = 50%). Hydrogen atoms labels have been omitted for clarity.

**Table 4.13: List of selected bond distances and angles for the compound *N*-ipTH.**

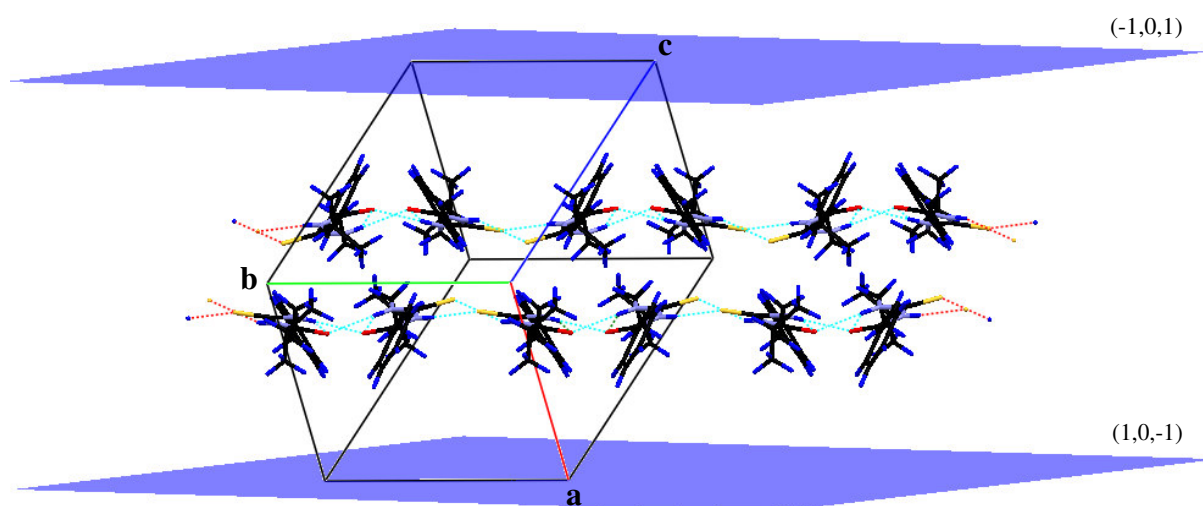
Molecule A		Molecule B	
Atoms	Distance (Å)	Atoms	Distance (Å)
C7-O1	1.226(2)	C7'-O1'	1.229(2)
C8-S1	1.681(2)	C8'-S1'	1.679(2)
C9-N2	1.461(2)	C9'-N2'	1.457(2)
C8-N2	1.323(2)	C8'-N2'	1.324(2)
C8-N1	1.394(2)	C8'-N1'	1.398(2)
C7-N1	1.379(5)	C7'-N1'	1.379(2)
Atoms		Atoms	
	Angle (°)		Angle (°)
N1-C7-O1	122.6(2)	N1'-C7'-O1'	122.9(2)
N1-C8-S1	118.7(1)	N1'-C8'-S1'	118.4(1)
C8-N2-C9	123.6(2)	C8'-N2'-C9'	123.5(1)
C1-C2-C3-C4	0.2(3)	C1'-C2'-C3'-C4'	0.4(3)
C2-C1-C7-O1	43.8(3)	C2'-C1'-C7'-O1'	-133.5(2)
C10-C9-N2-C8	91.5(2)	C10'-C9'-N2'-C8'	89.7(2)
O1-C7-C8-S1	-169.53	O1'-C7'-C8'-S1'	170.57

The two independent molecules **A** and **B** orientated in a back-to-back fashion such that their oxygen atoms O1/O1' and one set of the nitrogen atoms N2/N2' were brought in close approximation to each other. As a result inter- and intramolecular hydrogen bonding exists between these atoms (Figure 4.26a). Also the molecules in the asymmetric unit form more intermolecular hydrogen bonding with neighbouring molecules between the sulphur atoms S1/S1' and the nitrogen atoms N1/N1' leading to the closure of a 8-membered ring. Altogether these hydrogen bonding described above leads to the formation of polymeric chains that are packed parallel to the (10-1) plane (Figure 4.26b). The corresponding distances and angle of these hydrogen bonds are summarised in Table 4.14.





a)



b)

**Figure 4.26:** a) An illustration of the hydrogen bonding found in compound *N*-ipTH and b) the resulting polymeric chain formation packed along (10-1). For distances and angles see Table 4.14.

**Table 4.14 Distances and angles of the separate hydrogen bonding found in the crystal packing of the compound *N*-ipTH.**

Hydrogen bond	Distance (Å)	Angle (°)
N2-H2A...O1	2.671(2)	134.0
N2'-H2C...O1	3.028(2)	134.0
N2-H2A...O1'	3.020(2)	136.0
N2'-H2C...O1'	2.664(2)	135.0
N1-H1...S1	3.619(2)	162.0
N1'-H1'...S1	3.448(1)	175.0

The packing of these polymeric chains are also further stabilised by the presence of intermolecular shorts contacts *via* Van der Waals radii between the sulfur atoms S1/S1' and several other hydrogen and carbon atoms on adjacent molecules (Figure 4.27). Each sulphur atom is in close contact with four other different atoms as indicated in Figure 4.27 of which the respective distances are provided in Table 4.15.

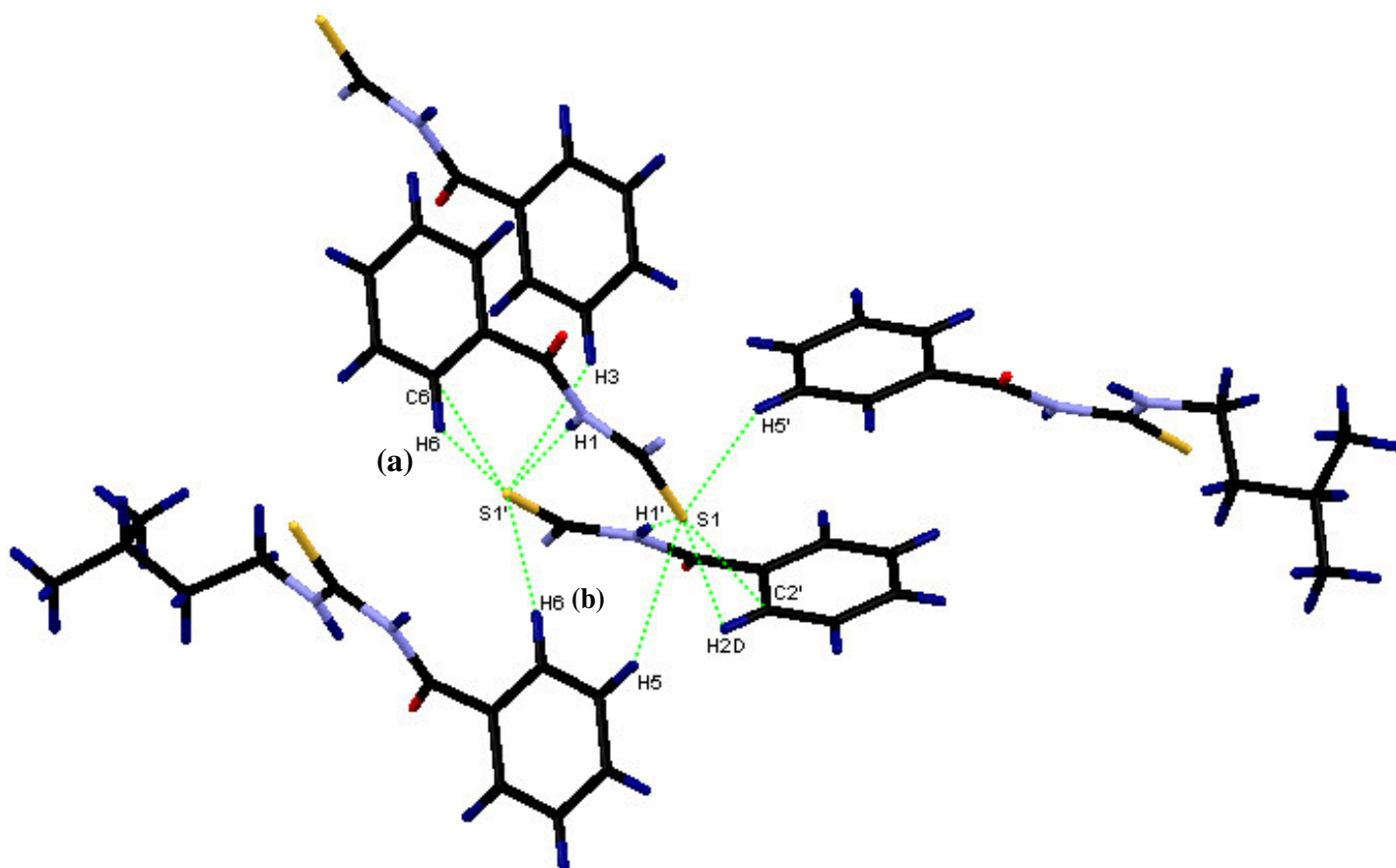


**Figure 4.27: An illustration of soft contacts between the sulphur atoms S1/S1' and several molecules of the compound *N*-ipTH. For distances see Table 4.15.**

**Table 4.15** The distances of the soft contacts found between the sulphur atoms S1/S1' and other atoms on adjacent molecules defined in Figure 4.27.

Soft contact	Distance (Å)
S1-H5	2.944
S1-H5'	2.903
S1-H2D	2.899
S1-C2'	3.248
S1'-H3	2.912
S1'-H6(a)*	2.854
S1'-H6(b)*	2.985
S1'-C6	3.365

\* As indicated in Figure 4.27

Another set of interactions that can be found is a “head-on-tail”  $\pi$ -stacking between phenyl groups of neighbouring molecules along the *ab*-axis. This stacking illustrated in Figure 4.28 by dotted green lines has an interplanar distance of 3.528 Å. This stacking also acts as a stabiliser for the molecular packing.

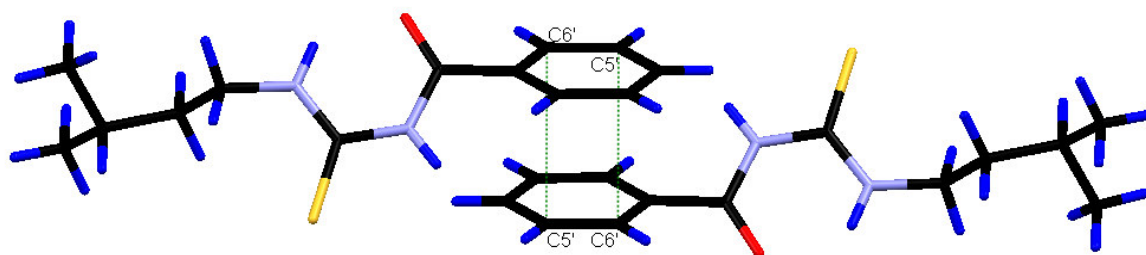


**Figure 4.28** An illustration of  $\pi$ -stacking between adjacent molecules in the crystal packing of the compound *N*-ipTH with an interplanar distance of 3.528 Å.

The respective distances for the C8-S1 and C8'-S1' bonds are 1.681(2) and 1.679(2) Å and for the C7-O1 and C7'-O1' bonds are 1.226(2) and 1.229(2) Å. These distances suggest the double bond character of the corresponding bonds indicating that these molecules are mainly found in their *keto* forms. Once more, the carbonyl oxygen atom is found *trans* to the sulfur atom with respect to the C-N-C chain across the thiourea bridge. The hydrogen bonding that was defined before in Figure 4.27 also stabilises this *trans* orientation. The torsion angles O1-C7...C8-S1 and O1'-C7'...C8'-S1' are -169.53 and 170.57 °, respectively, which suggest that the oxygen and sulfur atoms lie fairly in the plane across the thiourea bridge. The phenyl ring of the benzoyl group is found to be out of this plane with torsion angles C2-C1-C7-O1 and C2'-C1'-C7'-O1' of 43.8(3) and -133.5(2) °, respectively. The isopropyl group is also found

to be out of this plane with torsion angles C10-C9-N2-C8 and C10'-C9'-N2'-C8' of 91.5(2) and 89.7(2) °, respectively. The phenyl rings of the benzoyl groups are found to be planar as indicated by torsion angles C1-C2-C3-C4 and C1'-C2'-C3'-C4' of 0.2(3) ° and 0.4(3) °, respectively.

## 4.10. Interpretation and correlation of structural properties of thiourea compounds

### 4.10.1 Molecular geometry

Table 4.16 provides relevant geometric parameters for comparison between the several thiourea compounds discussed before. The basic thiourea compounds *N*-Bz(tu) and *N*-Ph(tu) given in Figure 4.29 are used as reference compounds of which their data were retrieved from published articles.<sup>26,27</sup>

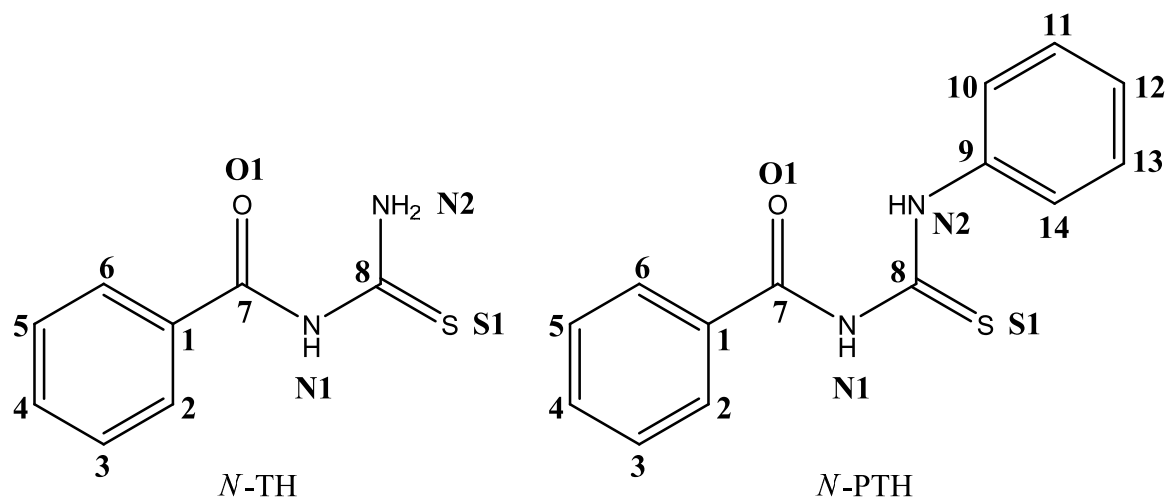


**Figure 4.29 Representation of the two thiourea ligands used as reference compounds in Table 4.16.**

<sup>26</sup> Wagner, P.; Niemczyk-Baltro, S.; Kubicki, M (2003) *Acta Cryst.*, **C59**, o83.

<sup>27</sup> Yamin, B. M.; Yusof, M. S. M. (2003) *Acta Cryst.*, **E59**, o151.

It was described in Figure 3.1 in Chapter 3 that the major difference between these thiourea ligands, having the formula  $\text{PhC(O)NHC(S)NHR}$ , is the distinct substituents (R) bonded to the terminal nitrogen atom on the one side of the thiourea. A feature observed for these thiourea compounds where at least one of the substituents is a hydrogen atom, is the intramolecular hydrogen bonding that takes place between this nitrogen atom and the oxygen atom of the carbonyl group. This leads to the closure of a 6-membered ring, which is fairly planar and considered to be energetically favourable. This was observed and shown in all cases of the structures reported in this chapter. A few examples were also given in reference 12, but a thorough search on the Cambridge Crystallographic Database (CSD)<sup>15</sup> revealed that this holds true for over 300 thiourea compounds of this kind.

By comparing the values in Table 4.16 it is clear that the angles at which these interactions take place and the distances of these interactions for the different thiourea compounds display significant differences. It was therefore suggested that this interaction might directly be influenced by the nature of the different substituents on the nitrogen (N2) involved here. In order to try and define the order of influence a histogram is presented in Figure 4.30 relating the angles and distances that were observed for the hydrogen bond interaction to the different substituents present on the nitrogen of the thiourea moiety. Note that since some of the compounds had different independent molecules in the unit cell, the mean values of the different hydrogen bond distances and angles are plotted for the ease of comparison, since most of the values are similar.

**Table 4.16 Selected geometric parameters of the thiourea compounds *N*-TH, *N*-PTH, *N*-tmPTH, *N*-BFPTH, *N*-FPTH, *N*-PeTH, *N*-NmTH, *N*-CyTH and *N*-ipTH.**

Geometric parameters	<i>N</i> -TH <sup>a</sup>	<i>N</i> -PTH <sup>a</sup>	<i>N</i> -tmPTH	<i>N</i> -BFPTH	<i>N</i> -FPTH
<b>Bond (Å)</b>					
<b>N2-H2...O1</b>	2.669(3)/2.618(3) <sup>b</sup>	2.599(2)	2.682(2)/2.664(2) <sup>b</sup>	2.595(2)	2.661(2)
<b>C7-O1</b>	1.220(2)/1.220(3)	1.222(2)	1.235(4)/1.228(5)	1.226(2)	1.226(2)
<b>C8-S1</b>	1.678(2)/1.679(2)	1.657(2)	1.662(4)/1.670(4)	1.669(2)	1.664(2)
<b>C9-N2</b>	-	1.408(2)	1.441(5)/1.439(5)	1.420(2)	1.419(2)
<b>C8-N2</b>	1.303(3)/1.295(3)	1.326(2)	1.3328(5)/1.328(5)	1.336(2)	1.338(2)
<b>Angle (°)</b>					
<b>N2-H2...O1</b>	136(2)/140(3)	143	131.7/136.6	131.8	132.8
<b>N1-C7-O1</b>	-	121.8(2)	121.9(3)/122.8(3)	122.3(1)	122.4(1)
<b>N1-C8-S1</b>	118.7(2)/120.5(2)	117.9(1)	118.0(3)/118.4(3)	120.4(1)	120.0(1)
<b>Torsion angle (°)</b>					
<b>O1-C7-C8-S1</b>	-	-	-169.1/177.2	-168.5	164.6
<b>C2-C1-C7-O1</b>	135.1(2)/145.3(2)	28.8(9)	-167.4(2)/136.7(3)	26.8(2)	-153.3(1)
<b>C8-N2-C9-C10</b>	-	7.52(9)	-75.7(3)/-78.7(3)	88.9(2)	88.2(2)

Geometric parameters	<i>N</i> -PeTH	<i>N</i> -NmTH	<i>N</i> -CyTH	<i>N</i> -ipTH
<b>Bond (Å)</b>				
<b>N2-H2...O1</b>	2.672(1)	2.655(2)	2.625(2)/2.597(2) <sup>b</sup>	2.671(2)/2.664(2) <sup>b</sup>
<b>C7-O1</b>	1.224(2)	1.229(2)	1.225(2)/1.227(2)	1.226(2)/1.229(2)
<b>C8-S1</b>	1.672(1)	1.676(2)	1.679(2)/1.677(2)	1.681(2)/1.679(2)
<b>C9-N2</b>	1.461(2)	1.455(2)	1.465(2)/1.475(3)	1.461(2)/1.457(2)
<b>C8-N2</b>	1.324(2)	1.326(2)	1.326(2)/1.338(2)	1.323(2)/1.324(2)
<b>Angle (°)</b>				
<b>N2-H2...O1</b>	130.2	134.0	133.0/133.7	134.0/135.0
<b>N1-C7-O1</b>	122.5(1)	122.1(2)	122.5(2)/123.0(2)	122.6(2)/122.9(2)
<b>N1-C8-S1</b>	117.6(1)	118.2(1)	119.1(1)/119.2(1)	118.7(1)/118.4(1)
<b>Torsion angle (°)</b>				
<b>O1-C7-C8-S1</b>	-172.6	179.5	178.6/167.2	-169.53/170.57
<b>C2-C1-C7-O1</b>	12.3(2)	-160.8(2)	-27.4(3)/-33.4(2)	43.8(3)/-133.5(2)
<b>C8-N2-C9-C10</b>	93.6(1)	78.5(2)	129.8/-144.0 <sup>c</sup>	91.5(2)/89.7(2)

<sup>a</sup> See references 26 and 27. <sup>b</sup> values for independent molecules in the asymmetric unit. <sup>c</sup> Measured as C8-N2-Centroid(C10,C14)-C10 and C8'-N2'-Centroid(C10',C14')-C10'

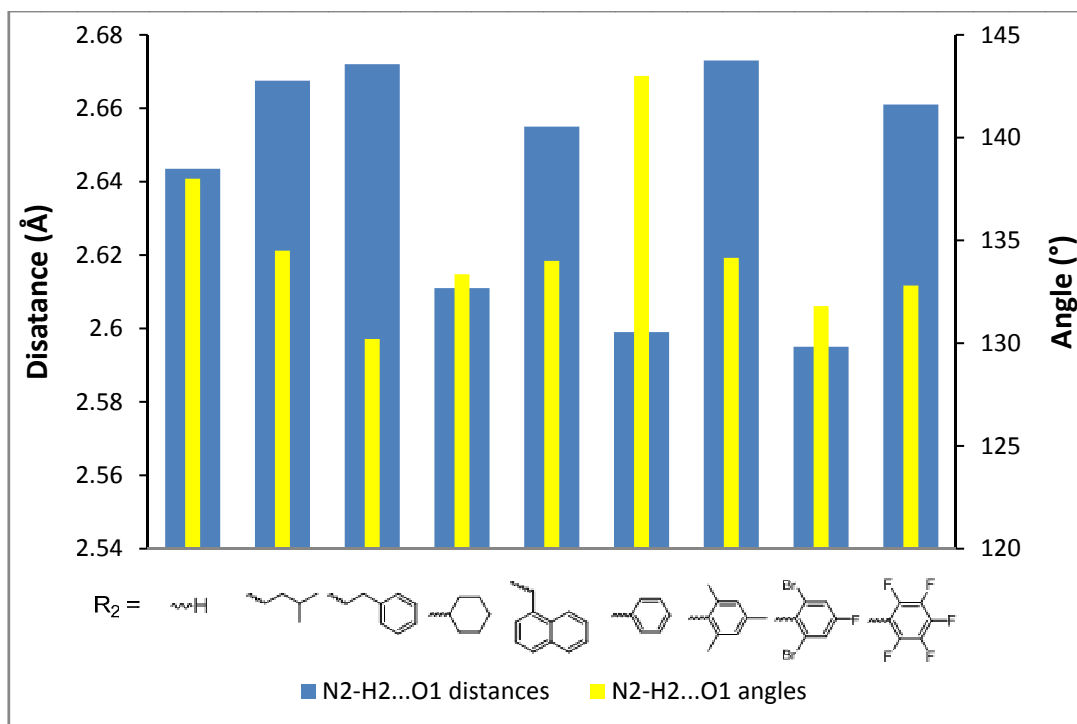


**Figure 4.30** A histogram showing the relationship between the distances and angles of the hydrogen bond N2-H2...O1 and the different substituents ( $R_2$ ) of the thiourea compounds under study (Figure 4.1). (While narrow yellow bar = distance (Å), broad blue bar = angle (°))

- It is observed in Figure 4.30 that there is some correlation between the electro-steric properties of the substituents and the values of the hydrogen bond distances and angles observed. When no substituent is present as on the compound *N*-TH (Figure 4.29) a mean interaction distance of 2.644 Å and angle of 138.0 ° is observed. With the substitution of strongly electron-donation groups isopropyl (*N*-ipTH) and phenethyl (*N*-PeTH) the hydrogen bond distances increased to about 2.668 and 2.672 Å, respectively, while the angles of interaction decreased slightly to 134.5 and 130.2 °. Substitution of a cyclohexyl group (*N*-CyTH), however, showed a decrease in the hydrogen bond distance to a mean value of 2.611 Å despite its large electron-donating nature. It could be assumed that the larger steric properties of the cyclohexyl group in this compound compared to the other electron-donating groups, could have rather dominated the electronic effect here. This substituent also caused a slight decrease in the interaction angle to about 133.4 °. The methylnaphthyl substituent (*N*-NmTH) is more difficult to interpret since the presence of the methyl lowers the electron-withdrawing ability of the naphthyl group. With a hydrogen bond distance

value of 2.655 Å it would seem that the substituent might have a slightly more electron-donating effect. However, as was discussed before the naphthyl groups of neighbouring molecules packed closely together in the unit cell by  $\pi$ -stacking interactions, which could have had a steric influence on the hydrogen bond interaction.

On the other hand the substitution of an electron-withdrawing group such as a phenyl ring (*N*-PTH) led to a decrease in the hydrogen bond interaction distance of 2.599 Å. The angle of the interaction also increased slightly to 143 °. Adding various substituents on this phenyl ring seems to also affect the hydrogen bond interaction. The presence of methyl groups on the substituent 2,4,6-trimethylphenyl group (*N*-tmPTH) added electron-donating properties to the substituent. This effect rather led to the increase of the hydrogen bond interaction distance to a mean value of 2.673 Å, but also led to the decrease in the mean interaction angle of 134.2 °. The presence of bromine atoms as well as a fluorine atom in the substituent 2,6-dibromo-4-fluoro group (*N*-BFPTH) added electron-donating properties of the substituent, which led to an even lower hydrogen bond distance of 2.595 Å and interaction angle of 131.8 °.

The penta-fluorophenyl substituent (*N*-FPTH), on the other hand, revealed a different effect, since an increase in the hydrogen bond interaction distance of 2.661 Å was observed. Though this is not uncommon as these observations are in line with frontier molecular orbital theory,<sup>28</sup> where it is stated that within halidebenzenes (or then aromatic rings with substituted halogens) the halogen shows a mixture of the properties of electron-withdrawing groups and electron-donating groups. The halogen undergoes some overlapping with its lone pairs to gain some covalent bonding, but its high electronegativity causes it to hold tightly onto its electrons at the same time. A lower interaction angle of 132.8 ° is also observed for the penta-fluorophenyl substituent.

- The electro-steric effects of the substituents can also be observed in the bond length value of the bond C9-N2 across the range of the thiourea compounds. The thiourea

---

<sup>28</sup> Fleming, I. (1976) *Frontier Orbitals and Organic Chemical Reactions*, John Wiley and Sons, New York.



compounds having more electron-withdrawing substituents on the nitrogen atom N2, namely *N*-PTH, *N*-tmPTH, *N*-BFPTH and *N*-FPPTH, have C9-N2 bond lengths ranging from 1.408 to 1.441 Å. The other thiourea compounds having more electron-donating substituents on N2, namely *N*-PeTH, *N*-NmTH, *N*-CyTH and *N*-ipTH, have C9-N2 bond lengths in the range of 1.455-1.475 Å.

- Another internal property of these thiourea compounds with an *N*-substituted benzoyl group is that they could undergo *keto/enol* tautomerisation as depicted in Figure 4.31. The proton on the nitrogen between the carbonyl and carbonsulfide is quite acidic, and therefore in the presence of a basic medium the equilibrium can easily be shifted from the *keto* isomer to the different *enol* isomers. This aspect plays an important role in co-ordination chemistry when utilising these ligands in the synthesis of several metal complexes.

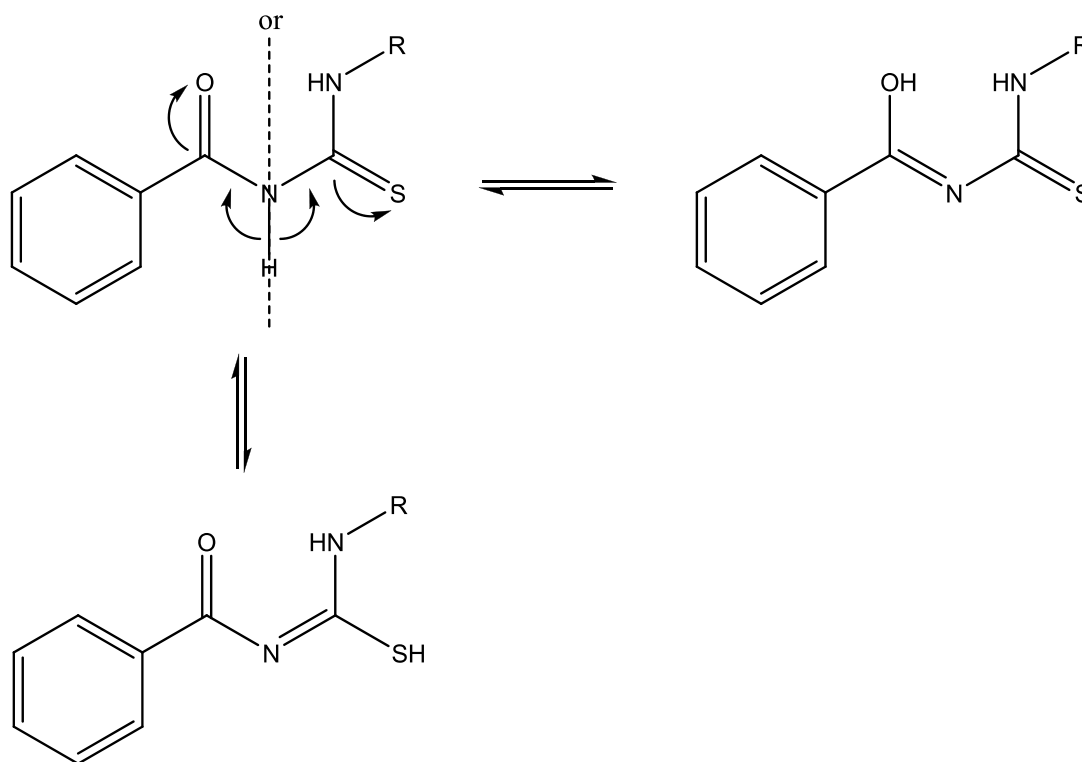


**Figure 4.31** An illustration of the *keto/enol* tautomerisation that can happen in thiourea compounds having a benzoyl moiety on one of the nitrogens.

It is easy to determine the configuration of the thiourea compounds in solid state using the corresponding structural data by looking at the C-O and C-S bond distances as

well as the angles around the thiourea moiety. Moreover, the presence or absence of protons on the nitrogen atoms will also give an indication of the configuration, since the nitrogen atoms are protonated in the *keto* form compared to the *enol* form. It is well known that  $sp^2$ -carbons have bonds in angles of  $120^\circ$ , while  $sp^3$ -carbons have bonds with angles of  $109.5^\circ$ . Typical bond lengths for C-O and C-S single bonds are  $\pm 1.43$  and  $\pm 1.82$  Å, respectively, while C=O and C=S bonds have respective lengths of  $\pm 1.24$  and  $\pm 1.56$  Å.<sup>29</sup> It is observed in Table 4.16 that the general bond lengths for the C-O and C-S bonds across the thiourea compounds are all in the range of 1.22-1.24 and 1.66-1.68 Å, respectively. Moreover, the general values for the bond angles N1-C7-O1 and N1-C8-S1 are in the range of  $122$ - $123^\circ$  and  $118$ - $120^\circ$ , respectively. Lastly, the nitrogen atoms on all of the structures reported in this chapter were found to be protonated. This suggests that these thiourea compounds discussed in this chapter are generally found in the *keto* formation and this holds true in general for thiourea compounds of the type defined in Figure 3.1 in Chapter 3 found on the CSD<sup>15</sup>. It was shown in Chapter 3 that this also holds true for the thiourea ligands in solution, since  $^1\text{H}$  NMR as well as  $^{13}\text{C}$  NMR spectroscopy revealed the presence of NH protons as well as C=O and C=S groups within these ligands. It is therefore concluded that the *keto* configuration of the thiourea compounds is the most stable state in solution and in solid state.

- Another interesting observation that could be made is the large differences found in the torsion angles of the phenyl ring of the benzoyl moiety and the different substituents on N2 with respect to the plane across the thiourea bridge (C7-N1-C8(S1)-N2). The phenyl ring of the benzoyl moiety has an average variation from the plane across the thiourea bridge ranging from  $12.3$  to  $44.9^\circ$ . This could be attributed to possible steric hindrance as a result of different packings in the unit cell. The different substituents on nitrogen N2 is then possibly too far to have a more pronounced effect on the phenyl ring of the benzoyl moiety.

The torsion angles for most of the substituents on nitrogen N2 relative to the thiourea plane are found to be close to a perpendicular angle. A few exceptions exist amongst the variations, which first includes the compound *N*-PTH where the phenyl substituent

---

<sup>29</sup> Weast, R. C. (1984) *CRC Handbook of Chemistry and Physics 65 Ed*, CRC Press.

is found to be almost planar to this plane. With the addition of substituents on this phenyl ring the torsion angle changes suddenly to a perpendicular value, which suggests that a small steric variation twists aryl substituents on nitrogen N2 out of the plane across the thiourea bridge. The other compound showing a large variation is *N*-CyTH, where an average variation of the cyclohexyl group to the plane across the thiourea bridge of 36.0 and 50.2 ° is obtained for each independent molecule in the unit cell. Being that a cyclohexyl ring has a larger steric hindrance than a phenyl ring could explain its slight rotation out of the thiourea bridge plane. However, since no large substituents are found on the cyclohexyl ring there is no significant steric hindrance that would require the ring to rotate to a torsion angle of 90 °.

#### 4.10.2 Molecular packing

Looking at the data provided in Tables 4.1 and 4.2 it can be observed that the thiourea compounds discussed in this chapter generally crystallised in the triclinic space group  $P\bar{1}$  or monoclinic space group  $C2/c$ . A study on the CSD<sup>15</sup> revealed that the most common space groups for these compounds are indeed triclinic space group  $P\bar{1}$  (127 hits) as well as monoclinic space group  $P2_1/n$  (44 hits),  $P2_1/c$  (86 hits) and  $C2/c$  (20 hits). A summary of the compounds and the space group they crystallised in is provided in Table 4.17. The space groups for the compounds defined in Figure 4.29 are also added for reference. Note that none of the compounds having the same space group are isomorphous.

**Table 4.17 Space group comparison between the reported thiourea compounds.**

Compound	Space group	
<i>N</i> -TH	Triclinic	$P\bar{1}$
<i>N</i> -PTH	Monoclinic	$P2_1/c$
<i>N</i> -tmPTH	Triclinic	$P\bar{1}$
<i>N</i> -BFPTH	Triclinic	$P\bar{1}$
<i>N</i> -FPTH	Monoclinic	$C2/c$
<i>N</i> -PeTH	Monoclinic	$P2_1/n$
<i>N</i> -NmTH	Monoclinic	$C2/c$
<i>N</i> -CyTH	Triclinic	$P\bar{1}$
<i>N</i> -ipTH	Triclinic	$P\bar{1}$

A summary of the general molecular packing of the various *S,O*-thiourea ligands are shown in Figure 4.32.

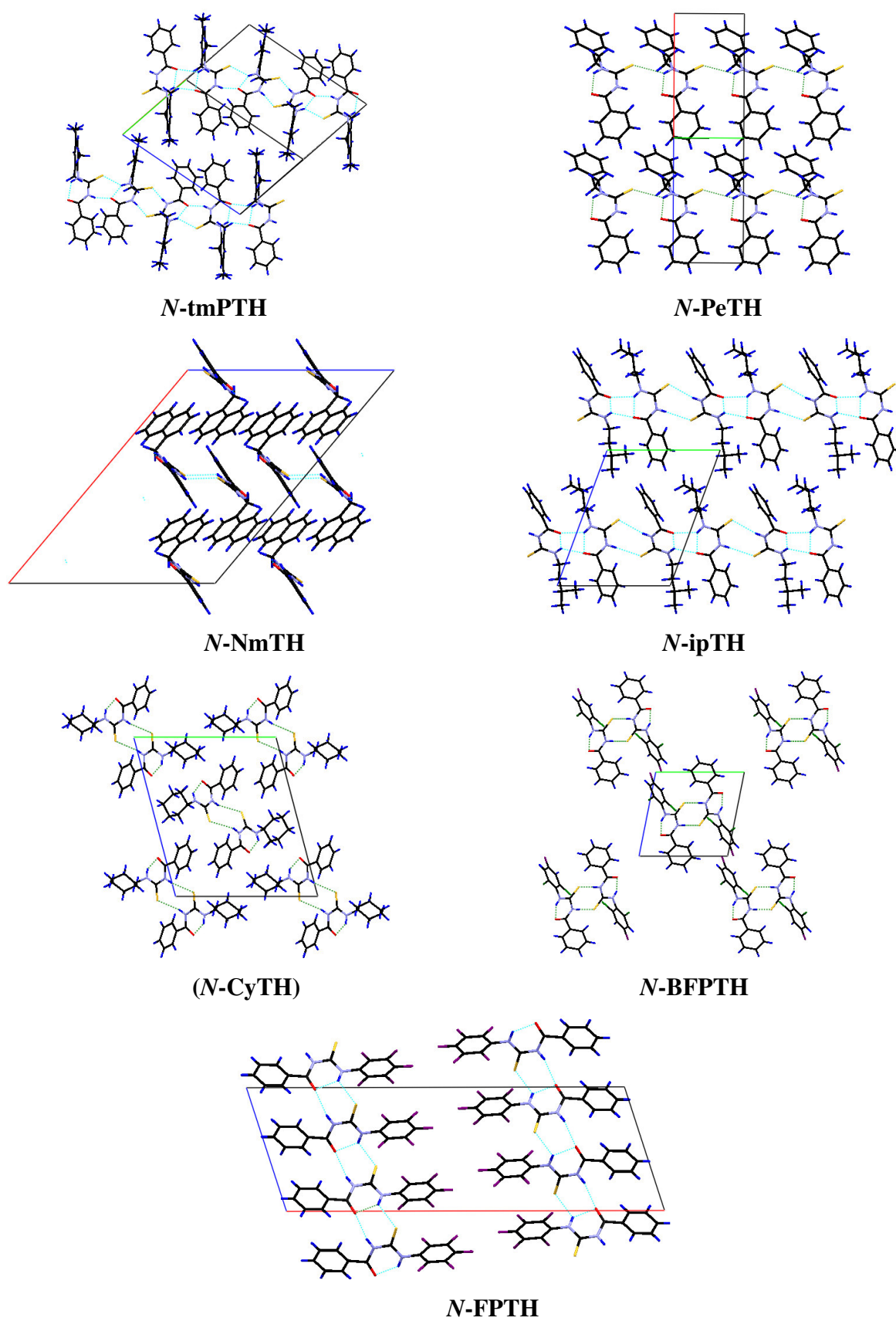


**Figure 4.32** The general molecular packing of the *S,O*-thiourea ligand structures reported in this chapter.

Figure 4.32 clearly shows the dimer or polymer formation in the packing due to hydrogen bond interactions between molecules for each thiourea compound. Four of the molecular compounds, namely *N*-tmPTH, *N*-PeTH, *N*-FPTH and *N*-ipTH show polymeric chain formation, while the other three compounds *N*-NmTH, (*N*-CyTH) and *N*-BFPTH show dimer formation in the packing. By comparing these packing modes with the space groups summarized in Table 4.17 for each ligand, no direct correlation is observed. Thus, dimer or polymer formation can occur regardless of the space group in which the thiourea ligand crystallizes in.

## 4.11. Conclusion

Seven of the *S,O*-thiourea molecular compounds, to be used as ligands, are shown and discussed in Chapter 3 have been successfully characterized by single crystal X-ray diffraction and reported in Chapter 4. Generally, these ligands were found in the *keto* conformation as suggested by the double bond character of the C-O and C-S bonds. Since they were all crystallized from a neutral medium, one of the characteristic features of these thiourea ligands includes the *trans* orientation of the carbonyl oxygen atom with respect to the sulphur atom across the C-N-C chain of the thiourea bridge. Furthermore, the structural orientation is stabilized by a hydrogen bond formed between the carbonyl oxygen atom and the terminal nitrogen atom of the thiourea moiety. The length of this hydrogen bond seems to be affected by the electro-steric properties of the substituents on the terminal nitrogen of the ligand. This effect does not necessarily follow a chronological order in all of the cases reported, but there is a clear change in the hydrogen bond distance with a large modification in the electro-steric properties of the substituents.

The packing of the ligand molecules in all of the reported structures are primarily stabilized by intermolecular hydrogen-bonding formed between the oxygen and/or sulphur atoms and the separate nitrogen atoms of the neighbouring molecules. This resulted either in the formation of dimers or polymeric chains of molecules in the crystal packing. Only three of the ligands namely *N*-BFPTH, *N*-NmTH and *N*-ipTH showed additional  $\pi$ -stacking interactions that further stabilized the corresponding packings. The structures of *N*-BFPTH and *N*-FPTH exhibit typical halogen-halogen interactions with orientations and distances that are similar to that reported in literature.<sup>14,19</sup>

With the success of synthesizing and characterizing the range of thiourea ligands as discussed in Chapters 3 and 4, further investigation into their co-ordination modes on rhodium complexes will be discussed in Chapters 6 and 7.

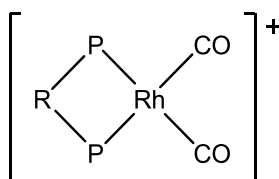
# **CHAPTER 5**

## **THE SYNTHESIS AND CHARACTERIZATION OF**

### **RHODIUM DIPHOSPHINE COMPLEXES**

#### **5.1 Introduction**

Part of the aim of this study involved the synthesis of rhodium acyl complexes containing neutral bidentate diphosphine ligands. The importance and effects of phosphine ligands on the catalytic activity of rhodium complexes have already been discussed in Chapters 1 and 2. Due to the great efficiency of diphosphine ligands in transition metal catalysis, as was discussed in Section 2.5 in Chapter 2, it was decided to synthesize a range of  $[\text{Rh}(\text{diphosphine})(\text{CO})_2]^+$  complexes (Figure 5.1) and evaluate their reactivity by studying the oxidative addition of iodomethane and the subsequent CO-insertion to form the acyl species. The corresponding rhodium acyl complexes would then be used to study the reductive elimination reaction of acyl iodide/iodomethane and elucidate whether this species can be converted to ethanol instead of acetic acid under selected conditions.



P-R-P = dppe, dppe, dppp, dppb, dppPh, dppf

**Figure 5.1 Schematic presentation of the  $[\text{Rh}(\text{diphosphine})(\text{CO})_2]^+$  complex with the different diphosphine ligands planned for this study.**

The different attempts to the synthesize  $[\text{Rh}(\text{diphosphine})(\text{CO})_2]^+$  complexes together with the characterization of the resulting products will be presented and discussed in this chapter.

## 5.2 Attempted synthesis of $[\text{Rh}(\text{diphosphine})(\text{CO})_2]^+$ complexes

A challenge in producing these types of complexes was that all the ligands coordinated to the metal centre are neutral and therefore counter-ions are required to balance the charge. Since the starting material for rhodium complexes often involves rhodium(III) chloride as initial precursor, this means that ionic compounds are required that can replace the chloride ion and remove it from the system. Compounds that have shown to be efficient in this regard usually involve anion metathesis with silver salts of tetrafluoroborate ( $\text{AgBF}_4$ ) and hexafluorophosphate ( $\text{AgPF}_6$ ). Silver chloride has a low solubility in most solvents and the counter-ions  $\text{BF}_4^-$  and  $\text{PF}_6^-$  have been shown to stabilise cationic metal complexes.<sup>1</sup> With this in mind several possible routes to the synthesis of  $[\text{Rh}(\text{diphosphine})(\text{CO})_2]^+$  complexes were found in the literature and explored herein.

### 5.2.1 Use of $[\text{Rh}(\text{COD})_2]\text{X}$ ( $\text{X}^- = \text{BF}_4^-$ or $\text{PF}_6^-$ ) as precursor

The first approach in synthesizing the possible  $[\text{Rh}(\text{diphosphine})(\text{CO})_2]^+$  complexes involved the use of  $[\text{Rh}(\text{COD})_2]^+$  (COD = 1,5-cyclooctadiene) complexes as the precursor, which is found in literature to be the preferred route for synthesizing cationic rhodium complexes.  $[\text{Rh}(\text{COD})_2]\text{BF}_4$ <sup>2</sup> or  $[\text{Rh}(\text{COD})_2]\text{PF}_6$ <sup>3</sup> complexes have been shown by the respective authors to react easily with diphosphine ligands. This leads to the substitution of one of the 1,5-cyclooctadiene rings (COD) forming the respective  $[\text{Rh}(\text{diphosphine})(\text{COD})]\text{BF}_4$  and  $[\text{Rh}(\text{diphosphine})(\text{COD})]\text{PF}_6$  complexes. Furthermore, it has been shown that COD can easily be substituted by CO ligands when carbon monoxide gas is bubbled through a solution containing the rhodium COD complex.<sup>4</sup> Therefore, synthesizing the different  $[\text{Rh}(\text{diphosphine})(\text{COD})]\text{X}$  complexes and substituting COD with CO ligands should result in the formation of the desired  $[\text{Rh}(\text{diphosphine})(\text{CO})_2]\text{X}$  complexes (where,  $\text{X} = \text{BF}_4^-$  or  $\text{PF}_6^-$ ). However, it was also noted by Marinetti *et al.*<sup>3</sup> that diphosphine ligands have the ability to coordinate not only in a bidentate fashion to one metal centre, but can also form binuclear complexes where it is coordinated in a monodentate fashion to two metal centres, depending on the conditions.

<sup>1</sup> Jung, O.-S.; Kim, Y. J.; Lee, Y.-A.; Park, K.-M.; Lee, S. S. (2003) *Inorg. Chem.*, **42**, 3, 844 and references within.

<sup>2</sup> Hoge, G.; Wu, H.-P.; Kissel, W. S.; Pflum, D. A.; Greene, D. J.; Bao, J. (2004) *J. Am. Chem. Soc.*, **126**, 5966.

<sup>3</sup> Marinetti, A.; Le Menn, C.; Ricard, L. (1995) *Organometallics*, **14**, 4983.

<sup>4</sup> Neveling, A.; Julius, G. R.; Cronje, S.; Esterhuysen, C.; Raubenheimer, H. G. (2005) *Dalton Trans.*, 181.



Using this information and the necessary conditions it was decided to attempt the synthesis of  $[\text{Rh}(\text{diphosphine})(\text{CO})_2]\text{X}$  complexes (where,  $\text{X}^- = \text{BF}_4^-$  or  $\text{PF}_6^-$ ) by following the synthetic procedure as shown in Figure 5.2.

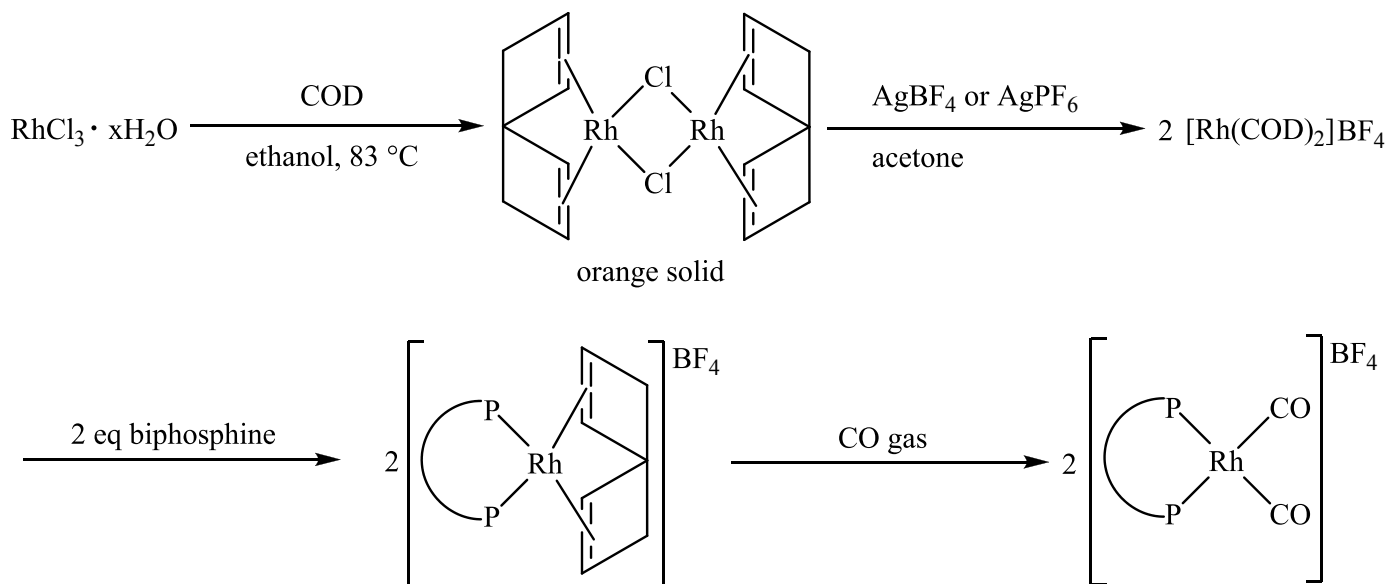


**Figure 5.2 Schematic representation of the route followed for the synthesis of  $[\text{Rh}(\text{diphosphine})(\text{CO})_2]^+$  complexes through the precursor  $[\text{Rh}(\text{COD})_2]\text{BF}_4$ .**

### 5.2.1.1 Dichlorido-di(1,5-cyclooctadiene)dirhodium(I), $[\text{Rh}(\text{COD})(\mu\text{-Cl})]_2$

Dichlorido-di(1,5-cyclooctadiene)dirhodium(I),  $[\text{Rh}(\text{COD})(\mu\text{-Cl})]_2$ , was synthesized from rhodium tri-chloride as described by Chatt *et al.*<sup>5</sup>.  $\text{RhCl}_3 \cdot x\text{H}_2\text{O}$  (1g, 4.78 mmol) was dissolved in pre-boiled ethanol after which an excess (1.17 mL, 9.56 mmol) of 1,5-cyclooctadiene was added to the solution. The solution was heated under reflux for 3 hrs at about 83 °C, which resulted in the formation of an orange powder that precipitated from the ethanol solution. This precipitate was filtered and washed with cold methanol. (Yield = 1.86 g, 79 %).

IR  $\nu_{\text{max}}$  ATR/ $\text{cm}^{-1}$ : 2986-2825 (C-H), 1466-773 (C-C, C-Cl).

<sup>5</sup> Chatt, J.; Venanzi, L. M. (1956) *Nature*, **177**, 852.

#### **5.2.1.2 Dicarbonyl-*P,P*-bis(diphenylphosphino)methanerrhodium(I) tetrafluoroborate, [Rh(dppm)(CO)<sub>2</sub>]BF<sub>4</sub>**

The synthesis of Dicarbonyl-*P,P*-bis(diphenylphosphino)methanerrhodium(I) tetrafluoroborate, [Rh(dppm)(CO)<sub>2</sub>]BF<sub>4</sub>, was attempted by reacting [Rh(COD)(μ-Cl)]<sub>2</sub> (20.0 mg, 0.0405 mmol) with silver tetrafluoroborate (16.0 mg, 0.0810 mmol) in acetone/ether (± 5 mL) to obtain the cationic species di(1,5-cyclooctadiene)rhodium(I) tetrafluoroborate [Rh(COD)<sub>2</sub>]BF<sub>4</sub>. This was reacted with the desired bis(diphenylphosphino)methane ligand (31.1 mg, 0.0810 mmol) and left to stir for a short while. CO gas was then bubbled through the solution for about 5 min, which resulted in the formation of the dicarbonyl-diphosphine rhodium(I) tetrafluoroborate complex. The solvent was allowed to evaporate, resulting in the formation of an orange-red solid. (Yield = *ca.* 15 mg, 80 %).

NMR and IR analysis were performed on the resulting solid product, from which the expected product could not be identified. Large C-C and C-H bands were mainly observed in the IR spectrum, whereas in some attempts only a small single carbonyl band was observed. <sup>1</sup>H NMR spectroscopy provided a range of overlapping peaks in the aromatic region of the spectrum (7.0-7.9 ppm) as well as some random peaks in the region of 0.8-2.0 ppm. A peak at 4.1 ppm was observed that might be related to the dppm ligand. No carbonyl peaks were observed in the <sup>13</sup>C NMR spectrum, whereas several peaks were also observed in the region of 129-135 ppm as well as 14-32 ppm, which could not be resolved. <sup>31</sup>P NMR spectroscopy revealed several peaks that could not be resolved.

#### **5.2.1.3 Dicarbonyl-*P,P*-bis(diphenylphosphino)ethanerrhodium(I) tetrafluoroborate, [Rh(dppe)(CO)<sub>2</sub>]BF<sub>4</sub>**

The synthesis of dicarbonyl-*P,P*-bis(diphenylphosphino)ethanerrhodium(I) tetrafluoroborate, [Rh(dppe)(CO)<sub>2</sub>]BF<sub>4</sub>, was attempted using the methodology as described in Section 5.2.1.2, where bis(diphenylphosphino)ethane (dppe, 32.3 mg, 0.0810 mmol) was used as the ligand. (Yield = *ca.* 15 mg, 60 %). IR and NMR spectroscopy were also performed on the resulting solid product, which provided similar results to that obtained in Section 5.2.1.2. It was concluded from this that the expected product was not obtained.

#### 5.2.1.4 Dicarbonyl-*P,P*-bis(diphenylphosphino)methanerhodium(I) hexafluorophosphate, $[\text{Rh}(\text{dppm})(\text{CO})_2]\text{PF}_6$

The synthesis of dicarbonyl-*P,P*-bis(diphenylphosphino)methanerhodium(I) hexafluorophosphate,  $[\text{Rh}(\text{dppm})(\text{CO})_2]\text{PF}_6$ , was attempted using the methodology as described in Section 5.2.1.2, where  $\text{AgPF}_6$  (20.5 mg, 0.0810 mmol) was utilized as the Lewis acid. (Yield = *ca.* 15 mg, 54 %). IR and NMR spectroscopy were also performed on the resulting solid product, which provided similar results to that obtained in Section 5.2.1.2. It was concluded from this that the expected product was not obtained.

#### 5.2.1.5 Dicarbonyl-*P,P*-bis(diphenylphosphino)ethanerhodium(I) hexafluorophosphate, $[\text{Rh}(\text{dppe})(\text{CO})_2]\text{PF}_6$

The synthesis of dicarbonyl-*P,P*-bis(diphenylphosphino)ethanerhodium(I) hexafluorophosphate,  $[\text{Rh}(\text{dppe})(\text{CO})_2]\text{PF}_6$ , was attempted using the methodology as described in Section 5.2.1.2, where  $\text{AgPF}_6$  (20.5 mg, 0.0810 mmol) was utilized as the Lewis acid and bis(diphenylphosphino)ethane (32.3 mg, 0.0810 mmol) was used as the ligand. (Yield = *ca.* 15 mg, 52 %). IR and NMR spectroscopy were also performed on the resulting solid product, which provided similar results to that obtained in Section 5.2.1.2. It was concluded from this that the expected product was not obtained.

### 5.2.2 Use of $[\text{Rh}(\text{coe})_2]\text{BF}_4$ as precursor

An alternative route was reported in literature, which was found to be useful in the synthesis of  $[\text{Rh}(\text{phosphine})_2(\text{CO})_2]^+$  complexes using monodentate phosphine ligands.<sup>6</sup> A modification of the procedure led to the formation of  $[\text{Rh}(\text{acetone})_2(\text{coe})_2]^+$  complexes (coe = cyclo-octene) as described by Windmüller *et al.*<sup>7</sup> It was found that the coe ligands coordinate *cis* to each other and that these ligands have weaker  $\pi$ -bonds to the metal centre. The addition of phosphine would thus preferably substitute the coe ligands, above acetone. Montag *et al.*<sup>6</sup> reported that by bubbling CO gas through a solution containing  $[\text{Rh}(\text{acetone})_2(\text{coe})_2]^+$  leads to

<sup>6</sup> Montag, M.; Efremenko, I.; Cohen, R.; Leitus, G.; Shimon, L. J. W.; Diskin-Posner, Y.; Ben-David, Y.; Martin, J. M. L.; Milstein, D. (2008) *Chem. Eur. J.*, **14**, 8183.

<sup>7</sup> Windmüller, B.; Nürnberg, O.; Wolf, J.; Werner, H. (1999) *Eur. J. Inorg. Chem.*, 613.

the substitution of the acetone ligands to form the subsequent  $[\text{Rh}(\text{phosphine})_2(\text{CO})_2]^+$  complex. It was therefore decided to attempt this route for the synthesis of  $[\text{Rh}(\text{diphosphine})(\text{CO})_2]^+$  complexes as summarized in Figure 5.3.

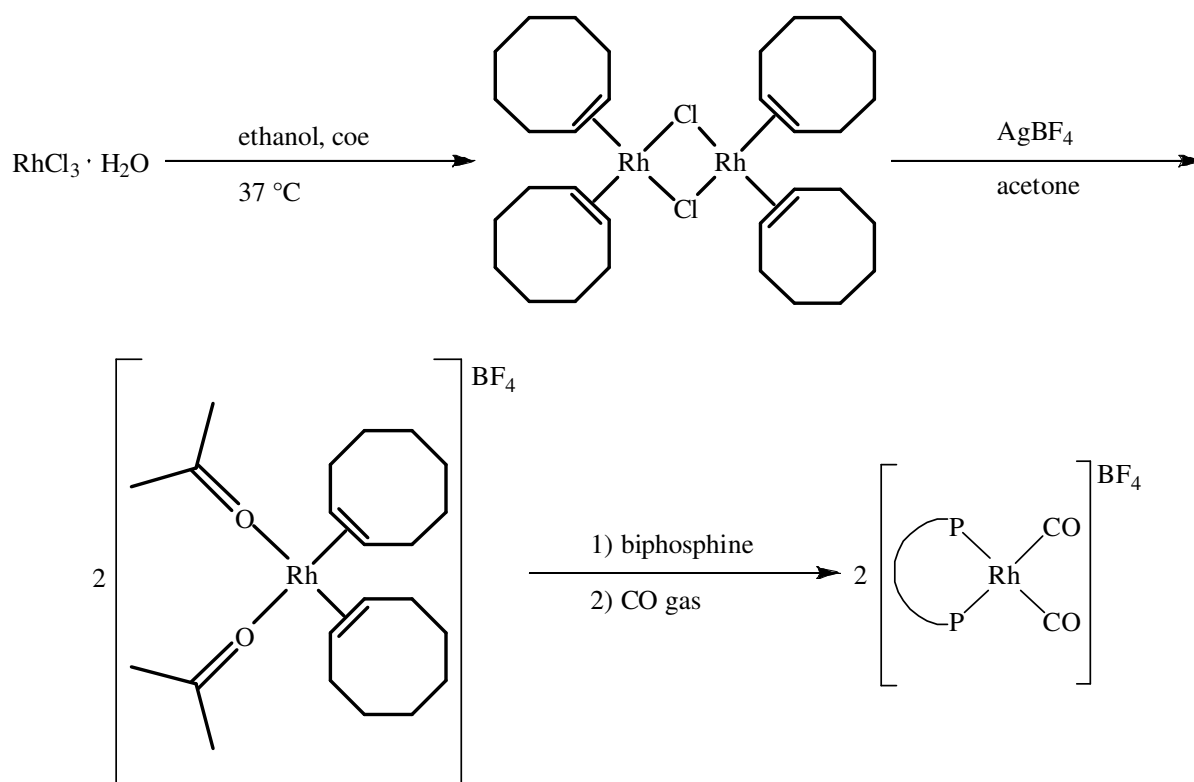


**Figure 5.3** Schematic representation of the route followed for the synthesis of  $[\text{Rh}(\text{diphosphine})(\text{CO})_2]^+$  complexes through the precursor  $[\text{Rh}(\text{acetone})_2(\text{coe})_2]\text{BF}_4$ .

### 5.2.2.1 dichlorido-tetracyclooctenedirrhodium(I), $[\text{Rh}(\text{coe})_2(\mu\text{-Cl})_2]$

Dichlorido-tetracyclooctenedirrhodium(I),  $[\text{Rh}(\text{coe})_2(\mu\text{-Cl})_2]$ , was synthesized using a modification of the methodology described by van der Ent *et al.*<sup>8</sup>.  $\text{RhCl}_3 \cdot x\text{H}_2\text{O}$  (200 mg, 0.956 mmol) was dissolved in ethanol (5 mL) after which the cyclooctene (0.6 mL, 1.91 mmol) was added and the reaction mixture heated to  $37^\circ\text{C}$  in an inert atmosphere. As the reaction proceeded the  $[\text{Rh}(\text{coe})_2(\mu\text{-Cl})_2]$  complex precipitated from the ethanol solution as a

<sup>8</sup> Van der Ent, A.; Onderdelinden, A. L. (1973) *Inorg. Synth.*, **14**, 92.

yellow powder. The product was then filtered and washed with several portions of ethanol. (Yield = 212 mg, 31 %).

IR  $\nu_{\max}$  ATR/ $\text{cm}^{-1}$ : 2995-2843 (C-H), 1463-617 (C-C, C-Cl).

#### 5.2.2.2 Dicarbonyl-*P,P*-bis(diphenylphosphino)methanerrhodium(I) tetrafluoroborate, $[\text{Rh}(\text{dppm})(\text{CO})_2]\text{BF}_4$

The synthesis of Dicarbonyl-*P,P*-bis(diphenylphosphino)methanerrhodium(I) tetrafluoroborate,  $[\text{Rh}(\text{dppm})(\text{CO})_2]\text{BF}_4$ , was attempted by reacting  $[\text{Rh}(\text{coe})_2(\mu\text{-Cl})]_2$  (20 mg, 0.0403 mmol) with  $\text{AgBF}_4$  (13 mg, 0.0806 mmol) in acetone (2 mL). The desired diphosphine ligand (2 eq) was added afterwards followed by the bubbling of CO gas through the resulting solution for about 5 min, which was expected to form the  $[\text{Rh}(\text{diphosphine})(\text{CO})_2]\text{BF}_4$ . The synthesis of  $[\text{Rh}(\text{dppm})(\text{CO})_2]\text{BF}_4$  was attempted using the methodology as described above. (Yield = *ca.* 15 mg, 86 %).

IR analysis was performed on the resulting solid product, from which the expected product could not be identified. Large C-C and C-H bands were mainly observed in the IR spectrum, whereas several small carbonyl bands were observed around 1970-1800  $\text{cm}^{-1}$ . This suggested that several species were present in the isolated product and as such it was deemed unnecessary to perform NMR spectroscopy on the sample.

#### 5.2.3 Use of $[\text{Rh}(\text{CO})_4]\text{BF}_4$ as precursor

In more recent work it has been shown that, although fairly difficult, it is possible to obtain the cationic complex  $[\text{Rh}(\text{CO})_4]^+$ .<sup>9</sup> It was stated that it was possible to obtain these species as long as non-oxidizing Lewis acids are used. Although  $\text{AgBF}_4$  hasn't been used before in the synthesis of these  $[\text{Rh}(\text{CO})_4]^+$  complexes, its properties correspond with the required conditions. It was therefore decided to attempt the synthesis of  $[\text{Rh}(\text{CO})_4]\text{BF}_4$  followed by the addition of a diphosphine ligand to form the desired  $[\text{Rh}(\text{diphosphine})(\text{CO})_2]\text{BF}_4$  complexes using the procedure shown in Figure 5.4.

<sup>9</sup> Von Ahsen, B.; Bach, C.; Berkei, M.; Köckerling, M.; Willner, H.; Hägele, G.; Aubke, F. (2003) *Inorg. Chem.*, **42**, 3801 and references within.

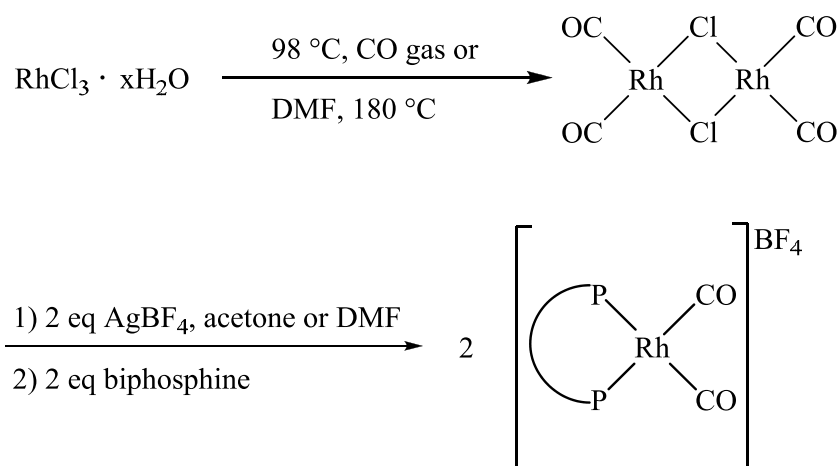


**Figure 5.4 Schematic representation of the route followed for the synthesis of  $[\text{Rh}(\text{diphosphine})(\text{CO})_2]^+$  complexes through the precursor  $[\text{Rh}(\text{CO})_4]\text{BF}_4$ .**

### 5.2.3.1 Tetracarbonyldichloridodirhodium(I) $[\text{Rh}(\mu\text{-Cl})(\text{CO})_2]_2$

The synthesis of the dinuclear rhodium complex  $[\text{Rh}(\mu\text{-Cl})(\text{CO})_2]_2$  may proceed *via* two synthetic routes as found in literature.<sup>10a,b</sup> The first route involves the heating of  $\text{RhCl}_3 \cdot x\text{H}_2\text{O}$  (20 mg, 0.0956 mmol) in DMF under reflux at 180 °C. A color change from red to a yellow solution was observed after about an hour, indicating the formation of the desired complex.

The other method involves a sublimation process where the  $\text{RhCl}_3 \cdot x\text{H}_2\text{O}$  (2 g, 9.56 mmol) was pulverised and heated in a sublimation tube at about 98 °C, while CO gas was flushed through the sample for 6 hours. Red crystals of  $[\text{Rh}(\mu\text{-Cl})(\text{CO})_2]_2$  formed during the process, which was collected and washed with hexane. (Yield = 1.058 g, 53%).

IR  $\nu_{\text{max}}$  ATR/ $\text{cm}^{-1}$ : 1991 and 1967 (CO stretching).

<sup>10</sup> a) McCleverty, J. A.; Wilkinson, G. (1990) *Inorganic Synth.*, **28**, 84. b) Szafran, Z.; Pike, R. M.; Singh, M. M. (1990) *Microscale Inorganic Laboratory*, Wiley, New York.

### 5.2.3.2 Dicarbonylchloridodi(bis(diphenylphosphino)methane)dirhodium(I) tetrafluoroborate, $[\text{Rh}_2(\mu\text{-Cl})(\text{dppm})_2(\text{CO})_2]\text{BF}_4$

The synthesis of Dicarbonyl-*P,P*-bis(diphenylphosphino)methanerhodium(I) tetrafluoroborate,  $[\text{Rh}(\text{dppm})(\text{CO})_2]\text{BF}_4$  was attempted by reacting  $[\text{Rh}(\mu\text{-Cl})(\text{CO})_2]_2$  (20 mg, 0.0697 mmol) with  $\text{AgBF}_4$  (27 mg, 0.1394 mmol) in either acetone or DMF, depending on the method applied for the synthesis of the starting material. This was expected to produce  $[\text{Rh}(\text{CO})_4]\text{BF}_4$ , which upon addition of the ligand dppm resulted in the formation of a red-orange solid that crystallized from the solution. These crystals were analysed by single crystal X-ray diffraction and presented in Section 5.4. The resulting product was identified to be  $[\text{Rh}_2(\mu\text{-Cl})(\text{dppm})_2(\text{CO})_2]\text{BF}_4$  instead. (Yield = 32.0 mg, 40 %).

$^{13}\text{C}$  NMR (151 MHz,  $\text{CDCl}_3$ , 25 °C):  $\delta$  133.0 (dt, *ortho*-C, phenyl,  $J = 77.0$  Hz,  $J = 3.4$  Hz), 131.7 (s, *ipso*-C, phenyl), 131.3 (s, *para*-C, phenyl), 129.2 (dt, *meta*-C, phenyl,  $J = 29.4$  Hz,  $J = 2.3$  Hz), 26.4 ppm (t,  $\text{P}-\underline{\text{C}}\text{H}_2-\text{P}$ ,  $J = 5.3$  Hz).

IR  $\nu_{\text{max}}$  ATR/ $\text{cm}^{-1}$ : 1982 and 1965  $\text{cm}^{-1}$  (CO stretching).

### 5.2.3.3 Dicarbonyl-*P,P*-bis(diphenylphosphino)ethanerhodium(I) tetrafluoroborate, $[\text{Rh}(\text{dppe})(\text{CO})_2]\text{BF}_4$

The synthesis of  $[\text{Rh}(\text{dppe})(\text{CO})_2]\text{BF}_4$  was attempted using the methodology as described in Section 5.2.3.2 using the ligand bis(diphenylphosphino)ethane in this case. NMR and IR analysis on the resulting product did not identify any of the expected products. (Yield = *ca.* 15 mg, 46 %). No carbonyl peaks were observed in either the IR or  $^{13}\text{C}$  NMR spectrum.  $^1\text{H}$  and  $^{13}\text{C}$  NMR spectroscopy mostly revealed the peaks for the free ligand as well as some other random peaks that could not be resolved. Large C-C and C-H bands were mostly observed in the IR spectrum.

#### 5.2.3.4 Dicarboxylchloridodi(bis(diphenylphosphino)propane)dirhodium(I) tetrafluoroborate, $[\text{Rh}_2(\mu\text{-Cl})(\text{dppp})_2(\text{CO})_2]\text{BF}_4$

The synthesis of  $[\text{Rh}(\text{dppp})(\text{CO})_2]\text{BF}_4$  was attempted using the methodology as described in Section 5.2.3.2 using the ligand bis(diphenylphosphino)propane in this case. A red crystalline solid was obtained, which in conjunction with 5.2.3.2 was identified to be  $[\text{Rh}_2\text{Cl}(\text{dppp})_2(\text{CO})_2]\text{BF}_4$  instead. (Yield = 26.8 mg, 32 %)

IR  $\nu_{\text{max}}$  ATR/ $\text{cm}^{-1}$ : 1960 and 1947  $\text{cm}^{-1}$  (C=O).

#### 5.2.3.5 Dicarboxyl-*P,P*-bis(diphenylphosphino)butanerhodium(I) tetrafluoroborate, $[\text{Rh}(\text{dppb})(\text{CO})_2]\text{BF}_4$

The synthesis of  $[\text{Rh}(\text{dppb})(\text{CO})_2]\text{BF}_4$  was attempted using the methodology as described in Section 5.2.3.2 using the ligand bis(diphenylphosphino)butane in this case. (Yield = *ca.* 15 mg, 44 %). IR spectroscopy was performed on the product, which provided similar results to that obtained in Section 5.2.3.3. None of the expected products could therefore be identified.

### 5.3 Results and discussion

Dppm, bis(diphenylphosphino)methane, and dppe, bis(diphenylphosphino)ethane, were first utilized as ligands in order to establish the possibility of obtaining the  $[\text{Rh}(\text{diphosphine})(\text{CO})_2]^+$  complexes *via* the first route defined in Section 5.2.1. After several attempts the desired product could not be isolated, as observed on either IR or NMR spectroscopy. A small carbonyl band was observed in the IR spectrum, along with several large C-C and C-H bands in both cases of the  $[\text{Rh}(\text{diphosphine})(\text{CO})_2]^+$  complexes mentioned. This suggested in the first place that several possible species might be present in the sample and secondly that it was unlikely that the carbonyl stretching peak represented a dicarbonyl complex. It is predicted by group theory and confirmed in literature<sup>11</sup> that

---

<sup>11</sup> Zhou, M.; Andrews, L. (1999) *J. Am. Chem. Soc.*, **121**, 9171.



dicarbonyl rhodium complexes reveal two carbonyl bands next to each other, where one represents the symmetric and the other the asymmetric stretching.

NMR spectroscopy did not provide more insight as to what species were forming during the reactions. Several random peaks were observed in the aromatic and aliphatic region of the  $^1\text{H}$  and  $^{13}\text{C}$  NMR spectra, which could not be identified. The observed carbonyl species could also not be identified on  $^{13}\text{C}$  NMR, since no carbonyl chemical shift was observed on the spectrum. This suggested that the amount of these species were too low to be determined by NMR techniques. Some crystals were obtained from one of the resulting complexes where dppm was used, however these crystals were not found to be useful for single crystal X-ray diffraction.

Attempts to synthesise these complexes using  $\text{AgPF}_6$  instead, as were shown in Sections 5.2.1.4 and 5.2.1.5, gave similar results. As such this synthetic route was therefore discarded and alternative routes were investigated.

Several attempts were made to produce the  $[\text{Rh}(\text{diphosphine})(\text{CO})_2]\text{BF}_4$  complexes with the diphosphine ligand dppm utilizing the synthetic procedure described in Section 5.2.2. This resulted seemingly in the formation of a mixture of products as no significant carbonyl stretching bands were observed in the IR spectrum. Several very small peaks were observed in the area of  $1970\text{--}1800\text{ cm}^{-1}$ , which suggested that small amounts of different rhodium carbonyl species have formed. However, these species were dominated by the presence of other species in the sample as suggested by several large C-C, C-H and other bands. Failing to obtain any positive results from this synthetic procedure, this route was also discarded, which left one possible route described in Section 5.2.3.

The first attempt in utilizing the synthetic procedure described in Section 5.2.3 involved the use of dppm, which resulted in the formation of red-orange crystals from both methods where the different solvents acetone and DMF were utilized. These crystals were analysed by IR and NMR spectroscopy from which completely different spectra were obtained compared to those obtained from the other synthetic routes discussed in Sections 5.2.1 and 5.2.2. Two carbonyl stretching bands were observed in the IR spectrum at  $1982$  and  $1965\text{ cm}^{-1}$ , which suggested the formation of a possible rhodium dicarbonyl complex.  $^{13}\text{C}$  NMR revealed the presence of phenyl rings with chemical shifts observed at  $\delta\ 133.0\text{ ppm}$  (dt,  $J = 77.0\text{ Hz}$ ,  $J =$

3.4 Hz), 131.7 ppm (s), 131.3 ppm (s) and 129.2 ppm (dt,  $J = 29.4$  Hz,  $J = 2.3$  Hz). Furthermore, a peak was observed at a chemical shift of 26.4 ppm (t,  $J = 5.3$  Hz), which confirmed the presence of the expected CH<sub>2</sub> moiety of the phosphine ligand. The expected carbonyl chemical shifts could not be observed, although a small indication was observed at about 205.5 ppm.

This was positive as the resulting spectra indicated a fraction of the [Rh(dppm)(CO)<sub>2</sub>]BF<sub>4</sub> complex. However, with an analysis performed by single-crystal X-ray diffraction a surprisingly different result was obtained. A structure of a Rh-Rh bridged A-frame complex was obtained, namely [Rh<sub>2</sub>Cl(dppm)<sub>2</sub>(CO)<sub>2</sub>]BF<sub>4</sub> (di-carbonyl-chlorido-di-(bis(diphenylphosphino)methane)-di-rhodium(I) tetrafluoroborate), which is discussed in Section 5.4. Complexes of this type are not unknown as several authors have published some of these variations.<sup>12a,b,c</sup> The [Rh<sub>2</sub>Cl(dppm)<sub>2</sub>(CO)<sub>2</sub>]BF<sub>4</sub> complex has been published before,<sup>13</sup> but it was reported to crystallize in a different space group (Triclinic  $P\bar{1}$ ) than that observed for the present data (Monoclinic  $P2_1/n$ ) that was obtained. Therefore the molecular geometry and packing of the structure are still discussed in Section 5.4 in comparison to the published structure.

After obtaining these results utilizing the dppm ligand, the synthesis of other diphosphine ligand complexes was attempted. The synthesis was repeated using the diphosphine ligands dppe, dppp and dppb, of which only the dppp ligand provided a similar result. Neither dppe nor dppb provided any rhodium carbonyl complexes, as confirmed from IR spectroscopy. The dppp ligand, on the other hand, provided a rhodium dicarbonyl species as indicated by the observation of two  $\nu_{\text{CO}}$  peaks at 1960 and 1947 cm<sup>-1</sup>. The product was also obtained as red crystals that precipitated from DMF, however, these crystals were not found suitable for X-ray analysis and therefore no further proof on the possible structure of the resulting complex could be obtained. Several attempts have been made in order to recrystallize the product, but neither method proved successful.

---

<sup>12</sup> a) Balch, A. L.; Tulyathan, B. (1977) *Inorg. Chem.*, **16**, 2840. b) Cowie, M.; Mague, J. T.; Sanger, A. R. (1978) *J. Am. Chem. Soc.*, 3628 and references within. c) Cowie, M. (1979) *Inorg. Chem.*, **18**, 286 and references within.

<sup>13</sup> Cowie, M.; Dwight, S. K. (1979) *Inorg. Chem.*, **18**, 10, 2700.

## 5.4 Crystal structure of dicarbonylchloridodi(bis(diphenylphosphino) methane)dirhodium(I) tetrafluoroborate, $[\text{Rh}_2(\mu\text{-Cl})(\text{dppm})_2(\text{CO})_2]\text{BF}_4$

### 5.4.1 Results and discussion

(Synthesis described in Section 5.2.3.2, Supplementary data B1)

The compound  $[\text{Rh}_2(\mu\text{-Cl})(\text{dppm})_2(\text{CO})_2]\text{BF}_4$ , crystallised in the monoclinic space group  $P2_1/n$  with one molecule in the asymmetric unit. The structure and subsequent atom numbering scheme are provided in Figure 5.5, while the general crystal data of the structure are summarized in Table 5.1. Table 5.2 lists some of the important bond distances and angles.

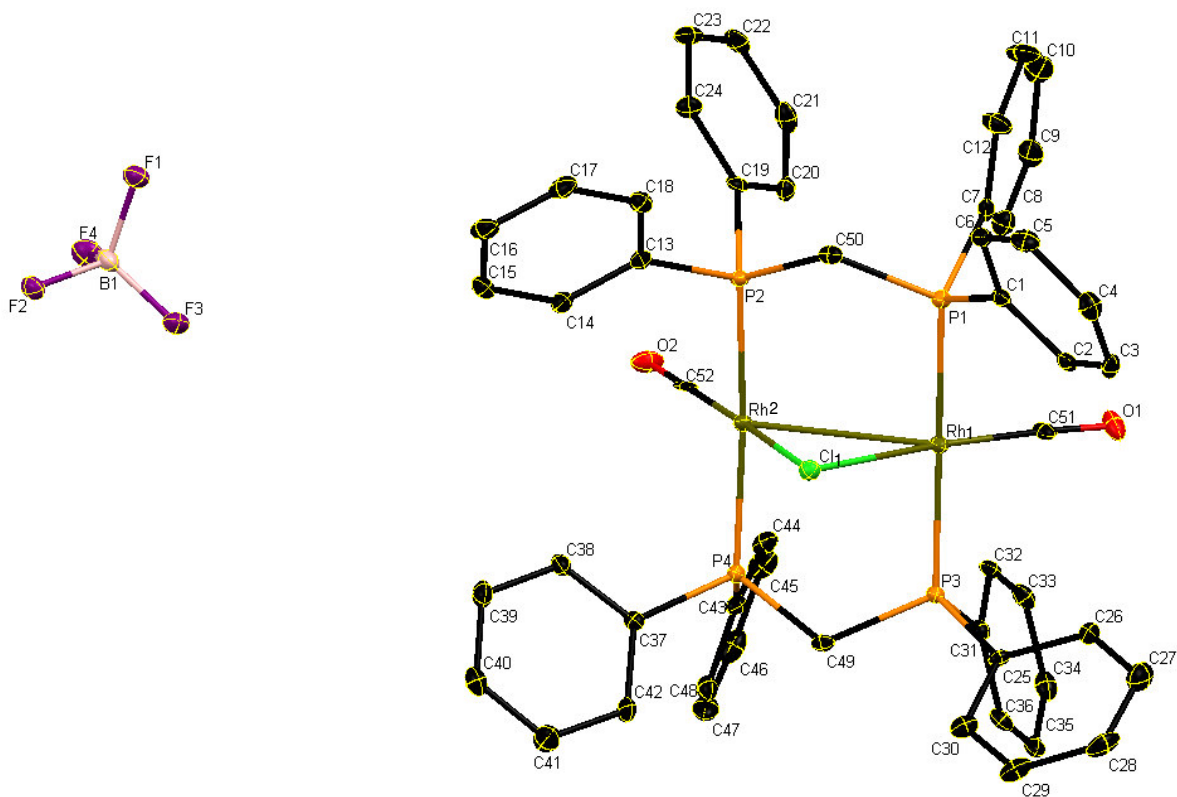


**Figure 5.5** A structural representation of the compound  $[\text{Rh}_2\text{Cl}(\text{dppm})_2(\text{CO})_2]\text{BF}_4$ , with the atom numbering scheme shown (ellipsoid probability = 30%). Hydrogen atoms have been omitted for clarity.

**Table 5.1 General crystal data for [Rh<sub>2</sub>Cl(dppm)<sub>2</sub>(CO)<sub>2</sub>]BF<sub>4</sub>.**

<b>Identification code</b>	<b>[Rh<sub>2</sub>Cl(dppm)<sub>2</sub>(CO)<sub>2</sub>]BF<sub>4</sub></b>
<b>Empirical formula</b>	Rh2 C52 H44 O2 P4 Cl1 B1 F4
<b>Formula weight</b>	1152.83
<b>Crystal system, space group</b>	Monoclinic <i>P</i> 2 <sub>1</sub> / <i>n</i>
<b>Unit cell dimensions</b>	
<b>a (Å)</b>	9.5606(7)
<b>b (Å)</b>	23.8602(19)
<b>c (Å)</b>	21.2709(19)
<b>α (°)</b>	90.000
<b>β (°)</b>	91.676(5)
<b>γ (°)</b>	90.000
<b>Volume (Å<sup>3</sup>)</b>	4850.2(7)
<b>Z</b>	4
<b>Density (calculated) (g/mL)</b>	1.579
<b>Absorption coefficient (mm<sup>-1</sup>)</b>	0.924
<b><i>F</i>(000)</b>	2320
<b>Crystal size (mm<sup>3</sup>)</b>	0.52 x 0.06 x 0.06
<b>Θ range for data collection (°)</b>	1.28 to 25.00
<b>Completeness for collection (%)</b>	99.9
<b>Index ranges</b>	-11 ≤ <i>h</i> ≤ 11 -28 ≤ <i>k</i> ≤ 28 -25 ≤ <i>l</i> ≤ 25
<b>Reflections collected</b>	30416
<b>Independent reflections</b>	8548 [ <i>R</i> <sub>int</sub> = 0.0884]
<b>Observed reflections</b>	5779
<b>Max and min transmission</b>	0.947 and 0.645
<b>Refinement method</b>	Full-matrix least squares on <i>F</i> <sup>2</sup>
<b>Data/ restraints/ parameters</b>	8548/0/612
<b>Goodness-of-fit on <i>F</i><sup>2</sup></b>	1.004
<b>Final <i>R</i> indices [<i>I</i> &gt; 2σ(<i>I</i>)]</b>	<i>R</i> 1 = 0.0466 <i>wR</i> 2 = 0.0913
<b><i>R</i> indices (all data)</b>	<i>R</i> 1 = 0.0815 <i>wR</i> 2 = 0.1099
<b>Largest diff. Peak and hole (e.Å<sup>-3</sup>)</b>	0.736 and -0.631

**Table 5.2: List of selected bond distances and angles for the compound  
[Rh<sub>2</sub>Cl(dppm)<sub>2</sub>(CO)<sub>2</sub>]BF<sub>4</sub>.**

Atoms	Distance (Å)	Atoms	Angle (°)
Rh1-P1	2.323(2)	P1-Rh1-Rh2	89.8(1)
Rh1-P3	2.315(1)	P2-Rh2-Rh1	92.3(1)
Rh2-P2	2.315(1)	P3-Rh1-Rh2	91.4(1)
Rh2-P4	2.329(1)	P4-Rh2-Rh1	89.8(1)
Rh1-Cl1	2.405(1)	Rh1-Cl1-Rh2	78.3(1)
Rh1-C51	1.815(6)	P1-C50-P2	115.4(3)
Rh2-Cl1	2.393(1)	P3-C49-P4	114.5(3)
Rh2-C52	1.805(6)	Rh1-C51-O1	175.9(5)
Rh1-Rh2	3.027(1)	Rh2-C52-O2	178.1(5)
C51-O1	1.148(6)	P1-Rh1-Rh2-Cl1	-87.0(1)
C52-O2	1.154(6)	P1-Rh1-Rh2-P2	-0.8(1)
B1-F1	1.391(7)	P1-Rh1-Rh2-P4	-173.6(1)

The structure involves a monodentate coordination of the separate phosphorus atoms of dppm bridging two rhodium centres as shown in Figure 5.5. Another dppm ligand coordinated *trans* to the first dppm ligand with a similar orientation. The two rhodium centres are also bridged by a chlorido ligand, whereas carbonyl ligands are found *trans* thereof, so that both metal centres form the A-frame coordination mode. Taking these orientations in consideration, it can be described as a double Vaska-type complex where each rhodium centre is coordinated by two phosphine ligands *trans* to each other, as well as a chlorido and carbonyl ligand *trans* to each other. This explains the preferred formation of this complex, since rhodium complexes usually allow coordination of phosphine ligands *trans* to each other rather than *cis* coordination.<sup>14</sup> From this point of view the difficulty of forming [Rh(*cis*-(diphosphine))(CO)<sub>2</sub>]<sup>+</sup> (Figure 5.1) from [Rh(CO)<sub>4</sub>]<sup>+</sup> was more evident, since there is no limiting parameter that would cause the diphosphine ligand to coordinate in a *cis* fashion to the metal centre.

By comparing this structure with that obtained by Cowie *et al.*<sup>13</sup>, several significant differences are observed. A summary of selected parameters are therefore provided in Table 5.3. Note that the two X-ray analyses were performed at different temperatures, which makes exact comparison slightly difficult.

<sup>14</sup> Roodt, A; Otto, S.; Steyl, G. (2003) *Coord. Chem. Rev.*, **245**, 121.

**Table 5.3: Comparison of selected geometric and crystallographic parameters for [Rh<sub>2</sub>Cl(dppm)<sub>2</sub>(CO)<sub>2</sub>]<sup>+</sup>BF<sub>4</sub><sup>-</sup> found in literature<sup>13</sup> and that presented in this chapter.**

Parameter	Present data	Literature data <sup>13</sup>
Space group	<i>P</i> 2 <sub>1</sub> /n	<i>P</i> $\bar{1}$
Collection temperature (K)	100	293.15
<i>Z</i>	4	2
<b>Bond (Å)</b>		
Rh1-Rh2	3.027(1)	3.152(1)
P1...P2 <sub>intraligand distance</sub>	3.110	3.088
P3...P4 <sub>intraligand distance</sub>	3.074	3.097
Rh1-P1	2.323(2)	2.324(2)
Rh1-P3	2.315(1)	2.320(2)
Rh2-P2	2.315(1)	2.319(2)
Rh2-P4	2.329(1)	2.322(2)
Rh1-Cl1	2.405(1)	2.406(2)
Rh1-C51	1.815(6)	1.807(7)
Rh2-Cl1	2.393(1)	2.380(2)
Rh2-C52	1.805(6)	1.799(7)
C51-O1	1.148(6)	1.184(8)
C52-O2	1.154(6)	1.202(9)
<i>v</i> <sub>CO</sub> (cm <sup>-1</sup> )	1982 and 1965	1995 and 1978
<b>Angle (°)</b>		
Rh1-Cl1-Rh2	78.3(1)	82.4(1)
Rh1-C51-O1	175.9(5)	177.4(7)
Rh2-C52-O2	178.1(5)	177.0(8)
P1-Rh1-P3	173.75(5)	176.20(6)
P2-Rh2-P4	172.50(5)	176.12(6)
P1-C50-P2	115.4(3)	114.7(3)
P3-C49-P4	114.5(3)	114.7(3)

It is clear from Table 5.3 that [Rh<sub>2</sub>Cl(dppm)<sub>2</sub>(CO)<sub>2</sub>]BF<sub>4</sub> crystallized in different space groups for the two structures. The literature structure was found to crystallize in the triclinic space group *P* $\bar{1}$  with only two molecules in the unit cell. The rhodium-rhodium interaction in the present structure has a distance of 3.027(1) Å, which is significantly shorter than the reported value of 3.152(1) Å. Cowie *et al.* describe the Rh-Rh interaction as not being a formal Rh-Rh bond for several reasons. In the first place they have shown in previously published work<sup>12b,c</sup> by other rhodium complexes that formal Rh-Rh bonds are of the order of 2.842(1) Å. This was much shorter than the 3.152 Å for the reported complex and therefore suggested rather an Rh-Rh interaction than a bond. Furthermore, the Rh-Rh distance (3.152 Å) was found to be substantially longer than the P-P intraligand distance (3.088 and 3.097 Å), which is in contrast with the values obtained for complexes where the Rh-Rh interaction was found to be a bond in the same published work.<sup>12b,c</sup> Finally, the Rh-Cl-Rh angle has a value of 82.4(1) °,

which was found to be within the range of the typical values (80-95 °) observed in literature<sup>13</sup> where no formal Rh-Rh bonds are considered.

In the present structure the values obtained for the defined geometric parameters suggested otherwise, in that the Rh-Rh interaction was possibly more of a bond. The Rh-Rh interaction is much shorter (3.027(1) Å) than that of the literature value (3.152(1) Å), however, it still does not compare well with the shorter literature values<sup>12b,c</sup> of around 2.842 (1) Å. Moreover, this Rh-Rh interaction is significantly shorter than the P-P intraligand distances of 3.110 and 3.074 Å, respectively. This is the opposite to that found in the literature as discussed before. Finally, the Rh1-Cl1-Rh2 angle is found to have a value of 78.3(1) °, which is slightly smaller than the reported value of 82.4(1) °. Although the respective geometric values suggested that the Rh-Rh interaction in the present structure has more bond character compared to the literature Rh-Rh interaction, it is not significant enough to define the interaction absolutely as a bond.

Large differences between the two reported structures are also found in the geometric values of the carbonyl ligands and Rh-Cl bonds as can be seen in Table 5.3. In both cases the chlorido ligand is found to be asymmetric in the Rh-Cl-Rh bridge, as concluded from the respective Rh-Cl bond lengths of 2.405(1) and 2.393(1) Å for the present structure versus 2.406(2) and 2.380(2) Å in the literature structure. It has been shown in the literature structure that there is a tendency that the differences in the Rh-Cl bonds are also reflected in the Rh-C and C-O bonds of the carbonyl ligands. The respective Rh-C bond lengths were reported to be 1.807(7) and 1.799(7) Å, while the C-O bond lengths had values of 1.184(8) and 1.202(9) Å, respectively. It was stated that the chlorido ligand had a weaker  $\pi$  donation to the Rh1 centre than to the Rh2 centre, which resulted in the one C-O having a weaker  $\pi$ -accepting ability than the other.

In the present structure this asymmetric contribution of the chlorido ligand is not as prominent as in the literature structure. The difference in the Rh-Cl bonds is relatively small, which also bring about small differences in the Rh-C and C-O bonds of the carbonyl ligands. The respective Rh-C bond lengths are found to be 1.815(6) and 1.805(6) Å, while the C-O bond lengths have values of 1.148(8) and 1.154(9) Å, respectively. Therefore no significant differences are found between the separate carbonyl ligands of the present structure, however, it is observed that these C-O bond distances have a tendency to be significantly shorter than

those obtained for the literature structure. This is also evident from the  $\nu_{\text{CO}}$  values of the two structures where the reported literature values were 1995 and 1978  $\text{cm}^{-1}$  in the solid state whilst the present structure provided  $\nu_{\text{CO}}$  values of 1982 and 1965  $\text{cm}^{-1}$  in the solid state. These values can be correlated directly to the C-O bond distances, since longer C-O bonds usually tend to provide higher wavenumber values.

The Rh-P bond distances in the two structures are similar with values between 2.315 and 2.329 Å as indicated in Table 5.3. The phosphorus atoms coordinated in a perpendicular fashion to the rhodium centres as suggested by the P-Rh-Rh angles in Table 5.2. The P-C-P angles of the dppm ligands have an average value of 115 °, which is typical of tetrahedral conformations of these ligands to metal centres. The methylene groups of the dppm ligands have a *cis* conformation facing the same direction as the chlorido ligand. The orientation around the rhodium centres in the present structure exhibit distorted square planar conformation when excluding the Rh-Rh interaction as suggested by P1-Rh1-P3, P2-Rh2-P4, C51-Rh1-Cl1 and C52-Rh2-Cl1 with angles of 173.7(1), 172.5(1), 172.9(2) and 176.1(2) °, respectively. This distortion in the square planar orientations was also observed in the literature structure. By taking a plane across the square planar conformation of the individual rhodium centres, it is observed that the rhodium atoms are slightly out of plane towards each other with an average value of  $\pm 0.2$  Å. This is probably the best proof that the Rh-Rh represents a more formal bond and not just an interaction.



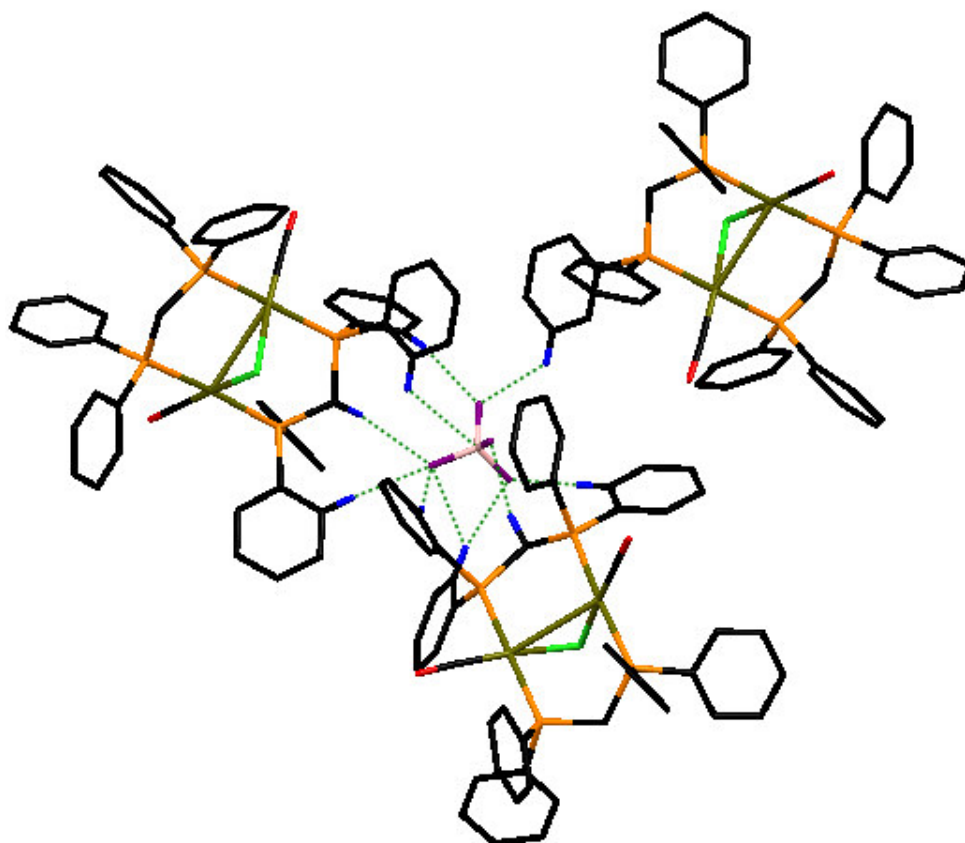


**Figure 5.6** Some soft contacts found between the  $\text{BF}_4^-$  anion and several of the cationic complex molecules in the packing of  $[\text{Rh}_2\text{Cl}(\text{dppm})_2(\text{CO})_2]\text{BF}_4$ .

The crystal packing of  $[\text{Rh}_2\text{Cl}(\text{dppm})_2(\text{CO})_2]\text{BF}_4$  is mainly stabilized by Van der Waals interactions, of which the most important is a set of interactions between the  $\text{BF}_4^-$  anion and four neighbouring cationic complex molecules. These contacts, together with a few other soft contacts are illustrated in Figure 5.6. The general packing of the present structure of  $[\text{Rh}_2\text{Cl}(\text{dppm})_2(\text{CO})_2]\text{BF}_4$  are shown in Figure 5.7. Due to the close interactions established between the  $\text{BF}_4^-$  anion and the cationic complexes, the molecules packed closely together in a wave-formation along the b-axis as illustrated in Figure 5.7.

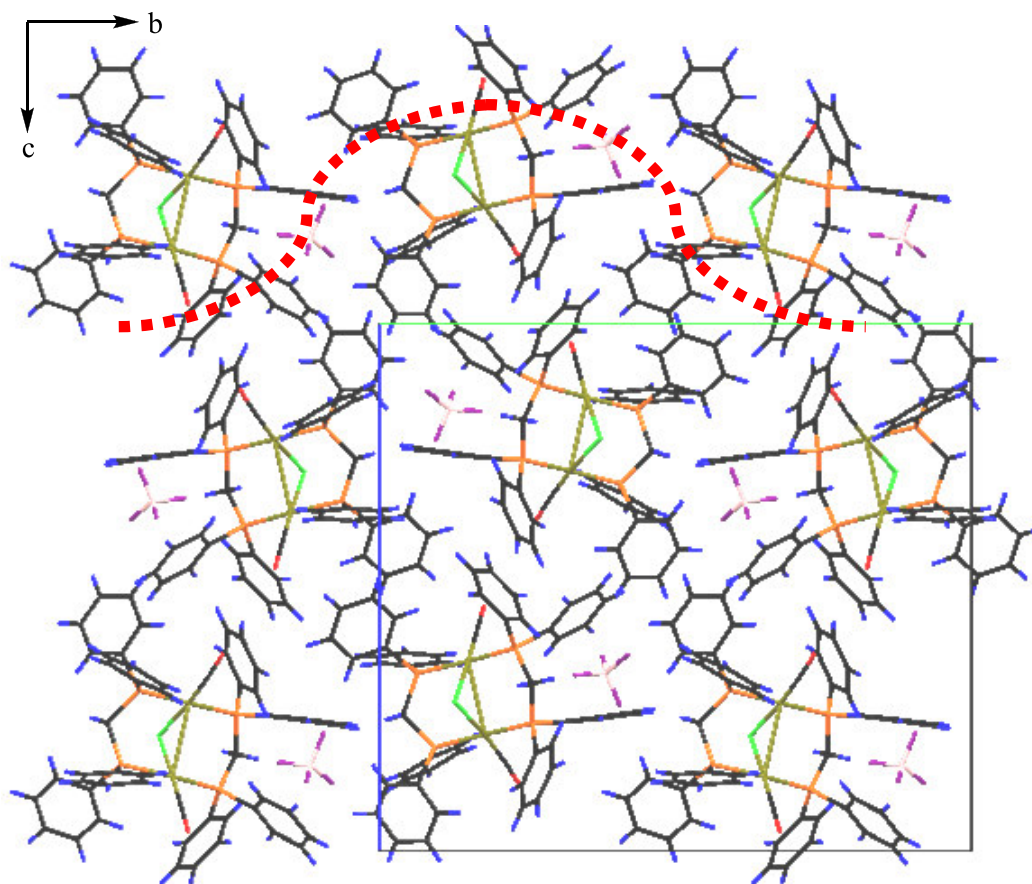


**Figure 5.7** An illustration of the general packing of  $[\text{Rh}_2\text{Cl}(\text{dppm})_2(\text{CO})_2]\text{BF}_4$  in the unit cell along bc.

## 5.5 Conclusion

A series of different synthetic methods was considered and discussed in Chapter 5 to synthesize  $[\text{Rh}(\text{diphosphine})(\text{CO})_2]^+$  complexes. Since these complexes are cationic species, it is necessary to utilize stable cationic starting materials. The most efficient starting material found was the  $[\text{Rh}(\text{COD})_2]^+$  complexes, which are formed by reacting  $[\text{Rh}(\text{COD})(\mu\text{-Cl})]_2$  with silver salts *via* ionic metathesis. These silver salts usually consist of anionic species that stabilizes the complexes in the outer coordination sphere. The most common silver salts used in literature are the  $\text{AgBF}_4$  and  $\text{AgPF}_6$  compounds. A similar, but slightly different starting material found in literature included the  $[\text{Rh}(\text{acetone})_2(\text{coe})_2]^+$  complexes, which is formed by reacting  $[\text{Rh}(\text{coe})_2(\mu\text{-Cl})]_2$  with silver salts in acetone.

Although both of these starting materials proved to be efficient in synthesizing cationic  $[\text{Rh}(\text{phosphine})_x(\text{CO})_x]^+$  complexes with monodentate phosphine ligands, difficulties were encountered in their use in synthesizing  $[\text{Rh}(\text{diphosphine})(\text{CO})_2]^+$  complexes. One major factor that makes it difficult to produce these cationic species is the fact that rhodium complexes would prefer a *trans* rather than a *cis* configuration of phosphine ligands around the metal centre.<sup>14</sup> After several attempts using both starting materials, the reaction with diphosphine ligands led to a mixture of unknown products, which either contained some kind of rhodium carbonyl species or none whatsoever.

An alternative route was also considered from literature that involved the synthesis of  $[\text{Rh}(\text{CO})_4]^+$  species in solution using  $[\text{Rh}(\mu\text{-Cl})(\text{CO})_2]_2$  and a non-oxidizing Lewis acid. Since  $\text{AgBF}_4$  is a good Lewis acid with little oxidizing abilities it was established to be a good candidate for this synthetic route. The products obtained from this synthetic procedure with the ligands dppm and dppp, resulted in rhodium carbonyl species displaying two  $\nu_{\text{CO}}$  peaks in the IR spectrum. Due to the resulting spectra obtained from both IR and NMR techniques it was first deduced that possible  $[\text{Rh}(\text{diphosphine})(\text{CO})_2]^+$  complexes had formed. However, X-ray analysis of the rhodium dppm carbonyl species revealed that the synthetic procedure led to the synthesis of the cationic A-frame complex  $[\text{Rh}_2(\mu\text{-Cl})(\text{dppm})_2(\text{CO})_2]\text{BF}_4$ . Although crystals of the rhodium dppp carbonyl species were not suitable for X-ray analysis, it was suspected that the complex involved was probably a similar cationic A-frame complex. It was interesting to note that the same synthetic route did not provide any rhodium carbonyl products for dppe as well as dppb as was elucidated by IR spectra.

The crystal structure and crystallographic data of  $[\text{Rh}_2(\mu\text{-Cl})(\text{dppm})_2(\text{CO})_2]\text{BF}_4$  were reported and discussed in this chapter. This structure was found to be a possible polymorph from that reported in literature, where the complex crystallised in the monoclinic space group  $P2_1/n$  ( $Z = 4$ ) compared to the reported triclinic space group  $P\bar{1}$  ( $Z = 2$ ). A few large differences were discovered between the two different structures, which is summarised in Table 5.3. Some of the most important differences include the different Rh-Rh interaction distances found between the two reported structures, where the present structure was more indicative of a formal Rh-Rh bond.

Other differences that were significant are found in the Rh-Cl and C-O bond distances of the carbonyl ligands. The literature structure showed asymmetry of the chlorido ligand across the

Rh-Cl-Rh bridge with large differences in the Rh-Cl and C-O bond lengths, while these differences were not that prominent in the structure reported in the current study. The C-O bond distances for the latter structure also tend to be much shorter than those obtained in the literature structure. This is also reflected in the solid state IR spectra where the  $\nu_{\text{CO}}$  values of the different structures differ by about  $13\text{ cm}^{-1}$ . This observation cannot be fully explained, but it is suspected that some steric effects due to different orientations of the phenyl rings on the dppe ligands might play a role. It was also shown that the major interactions involved in stabilizing the packing was the Van der Waals contacts found between the  $\text{BF}_4^-$  anions and several other atoms in the cationic complex, which might be temperature sensitive.

Although the desired  $[\text{Rh}(\text{diphosphine})(\text{CO})_2]^+$  complexes could not be obtained, a new and effective route to the cationic A-frame complexes was discovered. This could lead to the synthesis of other possible cationic rhodium A-frame complexes and might provide better understanding in the formation as well as packing modes in the solid state. Since that was not part of the main focus of this investigation, it was decided to investigate other types of rhodium acyl complexes that could be utilised for the purpose of the study. A possible alternative that was considered included the use of thiourea ligands having functionalised *S,O*-bonding moieties. The formation of these ligands and their characterization have already been described in Chapters 3 and 4. The subsequent use of these ligands in the coordination chemistry of rhodium complexes with the aim to synthesize  $\text{Rh}(\text{S,O-thioureato})$  acyl complexes are provided and discussed in Chapters 6 and 7.

# **CHAPTER 6**

## **SYNTHETIC ROUTES TO NOVEL Rh(I) and Rh(III)**

### **COMPLEXES WITH *S,O*-THIOUREA LIGANDS**

#### **6.1 Introduction**

After successfully synthesizing and characterizing a range of *S,O*-functionalized thiourea ligands having a benzoyl moiety, as was presented and discussed in Chapters 3 and 4, the next step in the study involved the synthesis of  $[\text{Rh}(\text{S},\text{O}\text{-thioureato})(\text{CO})_2]$  and subsequent  $[\text{Rh}(\text{S},\text{O}\text{-thioureato})(\text{CO})(\text{PR}_1\text{R}_2\text{R}_3)]$  complexes. It was already discussed and illustrated in Chapters 2 and 3 that sulphur-containing bidentate ligands seemingly ensured the definite conversion of Rh(I) complexes to Rh(III)-acyl species upon the oxidative addition of MeI *via* a rapid initial equilibrium step. These ligands have strong  $\sigma$ -donor atoms, which allow the formation of a highly electron-rich rhodium centre. It is therefore expected that this would increase the reactivity of a carbonylation reaction performed with the corresponding metal catalysts resulting possibly in a higher production of acetyl iodide, since the reductive elimination step is significantly large compared to the MeI oxidative addition step. The acetyl iodide in turn can either be converted to acetic acid by hydrolysis or as part of the aim of this study, to ethanol by hydrogenation with  $\text{H}_2$  gas.

It was also mentioned in Chapter 1 that *S,O*-thiourea ligands have potentially four donor sites. However, with the order of tendency of the donor atoms in these ligands to coordinate to the rhodium centre ( $\text{S} \gg \text{O} \gg \text{N}$ ), it is expected that the sulphur and oxygen would preferably coordinate above the nitrogen atoms. It is therefore illustrated in this chapter that this expectation does not hold entirely true, as several types of coordination modes of the thiourea ligands were discovered apart from the expected *S,O*-mode. Several examples are also found in literature where these ligands exhibit *S,O*- as well as other coordination modes, which were already shown and discussed in Section 2.6 in Chapter 2.

In this chapter the synthesis of  $[\text{Rh}(\text{S},\text{O}\text{-thioureato})(\text{CO})_2]$  as well as  $[\text{Rh}(\text{S},\text{O}\text{-thioureato})(\text{CO})(\text{PR}_1\text{R}_2\text{R}_3)]$  complexes are presented. Some unexpected rhodium(I) and

rhodium(III) complexes that were obtained during the search for feasible synthetic routes for the former complexes, together with the X-ray characterization of these, are reported and discussed here.

## 6.2 Reagents and equipment

Unless otherwise stated all experiments were carried out in air, using analytical grade reagents.  $\text{RhCl}_3 \cdot x\text{H}_2\text{O}$  as well as triphenylphosphine were purchased from Sigma-Aldrich. The solvents DMF, acetone, DMSO and diethyl ether were obtained from Merck. These reagents were used as received. The range of thiourea ligands that were used as indicated in this chapter were synthesized and characterized as was discussed in Chapter 3. FT-IR spectra were recorded on a Bruker Tensor 27 spectrophotometer in the range of  $3000\text{-}600\text{ cm}^{-1}$  via the ATR.

NMR spectroscopic data was acquired on either a Bruker Advance DPX 300 or Advance II 600 MHz spectrometer.  $^1\text{H}$  NMR data are listed in the order: chemical shift ( $\delta$ , reported in ppm and referenced to the residual solvent peak of  $(\text{CD}_3)_2\text{CO}$  [ $\delta = 2.09$  ppm], multiplicity, number of protons, assignment, coupling constant ( $J$ , in Hertz). Proton-decoupled  $^{13}\text{C}$  NMR data are listed in the order: chemical shift ( $\delta$ , reported in ppm and referenced to the residual solvent peak of  $(\text{CD}_3)_2\text{CO}$  [ $\delta = 29.9, 206.7$  ppm]), multiplicity, number of carbons, assignment, coupling constant ( $J$ , in Hertz) where appropriate. HMQC and HMBC experiments were performed to assist in the allocation of signals.  $^{31}\text{P}$  NMR data are listed in the order: chemical shift ( $\delta$ , reported in ppm and referenced to aqueous 85% phosphoric acid [ $\delta = 0.0$  ppm]), multiplicity, number of phosphorus atoms, coupling constant ( $J$ , in Hertz) where appropriate.

### 6.3 Attempted synthesis of $[\text{Rh}(\text{S},\text{O}\text{-thioureato})(\text{CO})_2]$ via the precursor $[\text{Rh}(\mu\text{-Cl})(\text{CO})_2]_2$

One of the most common methodologies used in synthesizing  $[\text{Rh}(\text{L},\text{L}'\text{-BID})(\text{CO})_2]$  complexes involve the use of the precursor  $[\text{Rh}(\mu\text{-Cl})(\text{CO})_2]_2$ , which can be synthesized by the reduction of hydrated Rh(III)chloride either in a boiling DMF solution or by a sublimation process using CO gas, as was already discussed in Chapter 5. It was therefore logical to first investigate this route for the synthesis of  $[\text{Rh}(\text{S},\text{O}\text{-thioureato})(\text{CO})_2]$  complexes with the different thiourea ligands, as illustrated in Figure 6.1.

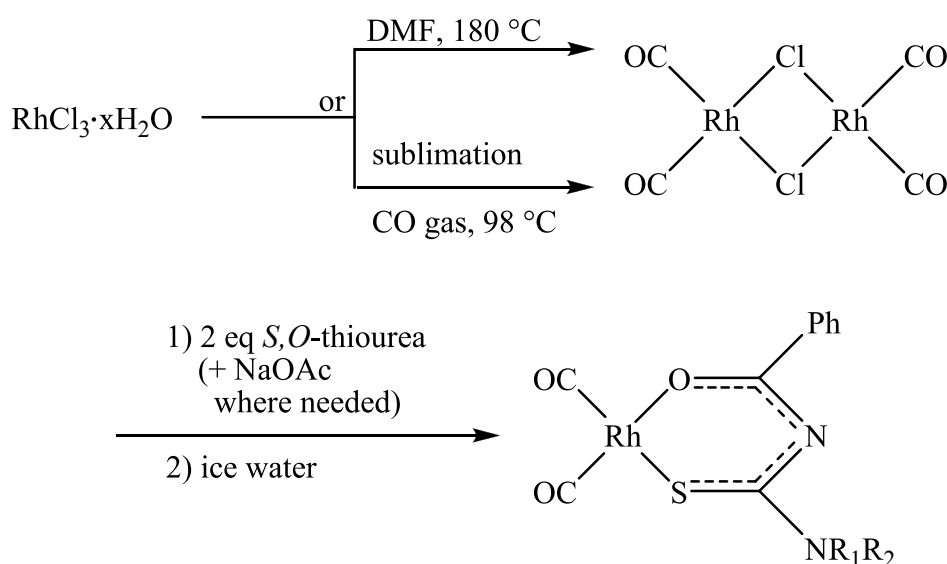


**Figure 6.1** General route for the synthesis of  $[\text{Rh}(\text{S},\text{O}\text{-thioureato})(\text{CO})_2]$  complexes.

#### 6.3.1 Tetracarbonyldichlororhodium(I), $[\text{Rh}(\mu\text{-Cl})(\text{CO})_2]_2$

The complex tetracarbonyldichlororhodium(I),  $[\text{Rh}(\mu\text{-Cl})(\text{CO})_2]_2$ , was synthesized by two different routes: In the first route  $\text{RhCl}_3 \cdot x\text{H}_2\text{O}$  (20.0 mg, 0.0956 mmol) was dissolved in DMF (5 mL) and heated under reflux to ca.  $180^\circ\text{C}$  for about an hour. A color change from a red to yellow solution indicated the formation of the Rh(I) precursor. In the second route  $\text{RhCl}_3 \cdot x\text{H}_2\text{O}$  (2.0 g, 9.56 mmol) was pulverized and added into a sublimation tube upon which the sample was heated at  $98^\circ\text{C}$  while flushing it with CO gas for 6 hours. This resulted in the formation of red crystals of the  $[\text{Rh}(\mu\text{-Cl})(\text{CO})_2]_2$  complex, which was collected and washed with hexane. (Yield = 1.058 g, 53%)

IR  $\nu_{\max}$  ATR/cm<sup>-1</sup>: 1991 and 1967 (carbonyl stretching).

### 6.3.2 Dicarboxyl(*S,O*-(*N*-benzoyl-*N'*-phenylthioureaato)rhodium(I), [Rh(*S,O*-(*N*-PT))(CO)<sub>2</sub>]

First attempt: Dicarboxyl(*S,O*-(*N*-benzoyl-*N'*-phenylthioureaato)rhodium(I), [Rh(*S,O*-(*N*-PT))(CO)<sub>2</sub>] was synthesized by adding *N*-benzoyl-*N'*-phenylthiourea (52.6 mg, 0.2056 mmol) to a cold DMF (5 mL) solution of [Rh( $\mu$ -Cl)(CO)<sub>2</sub>]<sub>2</sub> (30.0 mg, 0.1028 mmol). After stirring the reaction mixture for a couple of minutes ice water was added to the solution, which allowed the precipitation a red-brown solid product. The solid product was separated and isolated from the liquid medium by centrifugation after which IR analysis was performed on the product. Upon drying the product transformed into a dark red-brown oily product, which was also analysed *via* IR spectroscopy. This transformation was also observed while drying the product under vacuum. (Yield = *ca.* 26 mg, 30 %)

<sup>1</sup>H and <sup>13</sup>C NMR were also performed on this product, however, several peaks were observed in the aromatic region (120-140 ppm) of the spectra, which could not be resolved. Several carbonyl peaks were also observed with chemical shifts between 160 and 200 ppm, which could not be allocated. This along with the IR data that was obtained indicated a mixture of products, which could not be separated. Furthermore, <sup>1</sup>H NMR revealed that the sample consisted of more than 70 % of water (2.98 ppm), which suggested that the the yield of the product was less than 30 %.

IR  $\nu_{\max}$  ATR/cm<sup>-1</sup>: solid product: primary product = 2068 and 1998, secondary product = 2039 and 1989 (CO stretching); oily product, 2024 and 1970 (CO stretching).

Second attempt: The synthesis of Dicarboxyl(*S,O*-(*N*-benzoyl-*N'*-phenylthioureaato)rhodium(I), [Rh(*S,O*-(*N*-PT))(CO)<sub>2</sub>] was performed in the same manner as in the first attempt described above with the exception that an excess of sodium acetate was added prior to the addition of the thiourea ligand. A red-brown solid product was obtained, which transformed into a dark red-brown oil upon drying. (Yield = *ca.* 26 mg, 30 %)



$^1\text{H}$  and  $^{13}\text{C}$  NMR spectroscopy also provided several peaks observed in the aromatic region of the spectra, which could not be resolved. Several carbonyl peaks were also observed with chemical shifts between 160 and 200 ppm, which could not be allocated. This along with the IR data that was obtained indicated a mixture of products, which could not be separated.  $^1\text{H}$  NMR also revealed that the product consisted of more than 70 % of water, which suggested a yield of less than 30 % for the product.

IR  $\nu_{\text{max}}$  ATR/ $\text{cm}^{-1}$ : solid product, primary product = 2068 and 1998, secondary product = 2039 and 1989 (CO stretching); oily product, 2024 and 1970 (CO stretching).

### **6.3.3 Dicarbonyl(*S,O*-(*N*-benzoyl-*N'*-(2,3,4,5,6-pentafluorophenyl)thioureato), rhodium(I), [Rh(*S,O*-(*N*-FPT))( $\text{CO}$ ) $_2$ ]**

Dicarbonyl(*S,O*-(*N*-benzoyl-*N'*-(2,3,4,5,6-pentafluorophenyl)thioureato)rhodium(I), [Rh(*S,O*-(*N*-FPT))( $\text{CO}$ ) $_2$ ] was synthesized by the same method described in the first attempt in Section 6.3.2 using the ligand *N*-benzoyl-*N'*-(2,3,4,5,6-pentafluorophenyl)thiourea (71.2 mg, 0.2056 mmol) in this case. An orange solid product was obtained, which transformed into a dark red-brown oily product upon drying. This transformation was also observed while drying the product under vacuum. Both the solid and oily product were analysed *via* IR spectroscopy. (Yield = *ca.* 31 mg, 30 %)

$^1\text{H}$  and  $^{13}\text{C}$  NMR spectroscopy were also performed on the product, which provided similar results as were observed for the products in Section 6.3.2.  $^1\text{H}$  NMR also revealed that the sample consisted of more than 70 % of water, which suggested a yield of less than 30 % for the product.

IR  $\nu_{\text{max}}$  ATR/ $\text{cm}^{-1}$ : solid product, primary product = 2074 and 2010, secondary product = 2040 and 1987 (CO stretching); oily product, 2023 and 1971 (CO stretching).

#### 6.3.4 Dicarbonyl(*S,O*-(*N*-benzoyl-*N'*-(2,6-dibromo-4-fluorophenyl)thioureato) rhodium(I), [Rh(*S,O*-(*N*-BFPT))(CO)<sub>2</sub>]

First attempt: Dicarbonyl(*S,O*-(*N*-benzoyl-*N'*-(2,6-dibromo-4-fluorophenyl)thioureato) rhodium(I), [Rh(*S,O*-(*N*-BFPT))(CO)<sub>2</sub>] was synthesized by the same method described in the first attempt in Section 6.3.2 using the ligand *N*-benzoyl-*N'*-(2,6-dibromo-4-fluorophenyl)thiourea (83.0 mg, 0.2056 mmol) in this case. A bright yellow solid product was obtained, which transformed into a dark red-brown oily product upon drying. This transformation was also observed while drying the product under vacuum. Both the solid and oily product were analysed *via* IR spectroscopy. (Yield = *ca.* 34 mg, 30 %)

<sup>1</sup>H and <sup>13</sup>C NMR spectroscopy provided similar results as were observed for the products in Section 6.3.2 and 6.3.3. <sup>1</sup>H NMR also revealed that the sample consisted of more than 70 % of water, which suggested a yield of less than 30 % for the product.

IR  $\nu_{\max}$  ATR/cm<sup>-1</sup>: solid product, 2070 and 2003 as well as some other peaks obscured behind the first (CO stretching); oily product, 2022 and 1969 (CO stretching).

Second attempt: The synthesis of Dicarbonyl(*S,O*-(*N*-benzoyl-*N'*-(2,6-dibromo-4-fluorophenyl)thioureato)rhodium(I), [Rh(*S,O*-(*N*-BFPT))(CO)<sub>2</sub>] was performed in the same manner as in the first attempt described above with the exception that an excess of sodium acetate was added prior to the addition of the thiourea ligand. A bright yellow solid product was obtained, which transformed into a dark red-brown oil upon drying. (Yield = *ca.* 34 mg, 30 %)

<sup>1</sup>H and <sup>13</sup>C NMR revealed overlapping peaks observed in the aromatic region (120-140 ppm) of the spectra, which could not be resolved. Several carbonyl peaks were also still observed between 160 and 200 ppm, which could not be allocated. The product consisted of more than 70 % of water as revealed by <sup>1</sup>H NMR, which suggested less than 30 % yield of the product.

IR  $\nu_{\max}$  ATR/cm<sup>-1</sup>: solid product, 2070 and 2003 (CO stretching); oily product, 2022 and 1969 (CO stretching).

### 6.3.5 Dicarbonyl(*S,O*-(*N*-benzoyl-*N'*-(2,4,6-trimethylphenyl)thioureato)rhodium(I), [Rh(*S,O*-(*N*-tmPT))](CO)<sub>2</sub>]

First attempt: Dicarbonyl(*S,O*-(*N*-benzoyl-*N'*-(2,4,6-trimethylphenyl)thioureato)rhodium(I), [Rh(*S,O*-(*N*-tmPT))](CO)<sub>2</sub>] was synthesized by the same method described in the first attempt in Section 6.3.2 using the ligand *N*-benzoyl-*N'*-(2,4,6-trimethylphenyl)thiourea (61.4 mg, 0.2056 mmol) in this case. A yellow solid product was obtained, which transformed into a dark red-brown oily product upon drying. This transformation was also observed while drying the product under vacuum. Both the solid and oily product were analysed *via* IR spectroscopy. (Yield = *ca.* 28 mg, 30 %)

<sup>1</sup>H and <sup>13</sup>C NMR spectroscopy were also performed on the product, however, several peaks were observed in the aromatic (120-140 ppm) as well as aliphatic region (20-40 ppm) of the spectra, which could not be resolved. The spectra also revealed several carbonyl peaks with chemical shifts between 160 and 200 ppm. This along with the IR data that was obtained indicated a mixture of products, which could not be separated. The product consisted of more than 70 % of water as revealed by <sup>1</sup>H NMR, which suggested less than 30 % yield of the product.

IR  $\nu_{\text{max}}$  ATR/cm<sup>-1</sup>: solid product, 2069 and 2001 as well as some other peaks obscured behind the first (CO stretching); oily product, 2020 and 1967 (CO stretching).

Second attempt: The synthesis of Dicarbonyl(*S,O*-(*N*-benzoyl-*N'*-(2,4,6-trimethylphenyl)thioureato)rhodium(I), [Rh(*S,O*-(*N*-tmPT))](CO)<sub>2</sub>] was performed in the same manner as in the first attempt described above with the exception that an excess of sodium acetate was added prior to the addition of the thiourea ligand. A yellow solid product was obtained, which transformed into a dark red-brown oil upon drying. (Yield = *ca.* 28 mg, 30 %)

<sup>1</sup>H and <sup>13</sup>C NMR spectroscopy revealed similar results as was observed for the product above in the first attempt.

IR  $\nu_{\text{max}}$  ATR/cm<sup>-1</sup>: solid product, 2069 and 2001 (CO stretching); oily product, 2020 and 1967 (CO stretching).

### 6.3.6 Dicarboxyl(*S,O*-(*N*-benzoyl-*N'*-(4-hydroxy-2-methylphenyl)thioureaato) rhodium(I), [Rh(*S,O*-(*N*-4h2mPT))](CO)<sub>2</sub>]

First attempt: Dicarboxyl(*S,O*-(*N*-benzoyl-*N'*-(4-hydroxy-2-methylphenyl)thioureaato)rhodium(I), [Rh(*S,O*-(*N*-4h2mPT))](CO)<sub>2</sub>] was synthesized by the same method described in the first attempt in Section 6.3.2 using the ligand *N*-benzoyl-*N'*-(4-hydroxy-2-methylphenyl)thiourea (58.8 mg, 0.2056 mmol) in this case. An orange solid product was obtained, which transformed into a dark red-brown oily product upon drying. This transformation was also observed while drying the product under vacuum. Both the solid and oily product were analysed *via* IR spectroscopy. (Yield = *ca.* 27 mg, 30 %)

<sup>1</sup>H and <sup>13</sup>C NMR spectroscopy were not performed, since similar results were expected as were obtained for the products in Sections 6.3.2-6.3.6.

IR  $\nu_{\text{max}}$  ATR/cm<sup>-1</sup>: solid product, 2068 and 2001 as well as some other peaks obscured behind the first (CO stretching); oily product, 2020 and 1967 (CO stretching).

Second attempt: The synthesis of Dicarboxyl(*S,O*-(*N*-benzoyl-*N'*-(4-hydroxy-2-methylphenyl)thioureaato)rhodium(I), [Rh(*S,O*-(*N*-4h2mPT))](CO)<sub>2</sub>] was performed in the same manner as in the first attempt described above with the exception that an excess of sodium acetate was added prior to the addition of the thiourea ligand. An orange solid product was obtained, which transformed into a dark red-brown oil upon drying. (Yield = *ca.* 27 mg, 30 %)

<sup>1</sup>H and <sup>13</sup>C NMR spectroscopy were not performed, since similar results were expected as were obtained for the products in Sections 6.3.2-6.3.6.

IR  $\nu_{\text{max}}$  ATR/cm<sup>-1</sup>: solid product, 2068 and 2001 (CO stretching); oily product, 2020 and 1967 (CO stretching).

### 6.3.7 Dicarboxyl(*S,O*-(*N*-benzoyl-*N'*-cyclohexylthioureaato)rhodium(I), [Rh(*S,O*-(*N*-CyT))(CO)<sub>2</sub>]

Dicarboxyl(*S,O*-(*N*-benzoyl-*N'*-cyclohexylthioureaato)rhodium(I), [Rh(*S,O*-(*N*-CyT))(CO)<sub>2</sub>] was synthesized by the same method described in the first attempt in Section 6.3.2 using the ligand *N*-benzoyl-*N'*-cyclohexylthiourea (53.8 mg, 0.2056 mmol) in this case. A brown solid product was obtained, which transformed into a dark red-brown oily product upon drying. This transformation was also observed while drying the product under vacuum. Both the solid and oily product were analysed *via* IR spectroscopy. (Yield = *ca.* 26 mg, 30 %)

<sup>1</sup>H and <sup>13</sup>C NMR spectroscopy were not performed, since similar results were expected as were obtained for the products in Sections 6.3.2-6.3.6.

IR  $\nu_{\text{max}}$  ATR/cm<sup>-1</sup>: solid product, primary product = 2061 and 1985, secondary product = 2040 as well as some other peaks obscured behind the first (CO stretching); oily product, 2018 and 1966 (CO stretching).

### 6.3.8 Dicarboxyl(*S,O*-(*N*-benzoyl-*N'*-naphthalen-1-ylmethylthioureaato)rhodium(I), [Rh(*S,O*-(*N*-NmT))(CO)<sub>2</sub>]

First attempt: Dicarboxyl(*S,O*-(*N*-benzoyl-*N'*-(naphthalene-1-ylmethyl)thioureaato)rhodium(I), [Rh(*S,O*-(*N*-NmT))(CO)<sub>2</sub>] was synthesized by the same method described in the first attempt in Section 6.3.2 using the ligand *N*-benzoyl-*N'*-(naphthalen-1-ylmethyl)thiourea (63.0 mg, 0.2056 mmol) in this case. A yellow solid product was obtained, which transformed into a dark red-brown oily product upon drying. This transformation was also observed while drying the product under vacuum. Both the solid and oily product were analysed *via* IR spectroscopy. (Yield = *ca.* 28 mg, 30 %)

<sup>1</sup>H and <sup>13</sup>C NMR spectroscopy were not performed, since similar results were expected as were obtained for the products in Sections 6.3.2-6.3.6.

IR  $\nu_{\text{max}}$  ATR/cm<sup>-1</sup>: solid product, primary product = 2065 and 1996, secondary product = 2040 and 1986 (CO stretching); oily product, 2020 and 1967 (CO stretching).

Second attempt: The synthesis of Dicarboxyl(*S,O*-(*N*-benzoyl-*N'*-(naphthalene-1-ylmethylthioureaato)rhodium(I),  $[\text{Rh}(\text{S},\text{O}-(\text{N-NmT}))(\text{CO})_2]$  was performed in the same manner as in the first attempt described above with the exception that an excess of sodium acetate was added prior to the addition of the thiourea ligand. A yellow solid product was obtained, which transformed into a dark red-brown oil upon drying. (Yield = *ca.* 28 mg, 30 %)

$^1\text{H}$  and  $^{13}\text{C}$  NMR spectroscopy were not performed, since similar results were expected as were obtained for the products in Sections 6.3.2-6.3.6.

IR  $\nu_{\text{max}}$  ATR/ $\text{cm}^{-1}$ : solid product, 2065 and 1996 (CO stretching); oily product, 2020 and 1967 (CO stretching).

### **6.3.9 Dicarboxyl(*S,O*-(*N*-benzoyl-*N',N'*-diphenylthioureaato)rhodium(I), $[\text{Rh}(\text{S},\text{O}-(\text{N-diPT}))(\text{CO})_2]$**

Dicarboxyl(*S,O*-(*N*-benzoyl-*N',N'*-diphenylthioureaato)rhodium(I),  $[\text{Rh}(\text{S},\text{O}-(\text{N-diPT}))(\text{CO})_2]$  was synthesized by the same method described in the first attempt in Section 6.3.2 using the ligand *N*-benzoyl-*N',N'*-diphenylthiourea (68.4 mg, 0.2056 mmol) in this case. A bright orange product was obtained, which transformed into a dark red-brown oily product upon drying. This transformation was also observed while drying the product under vacuum. Only the solid product was analysed *via* IR spectroscopy. (Yield = *ca.* 30 mg, 30 %)

$^1\text{H}$  and  $^{13}\text{C}$  NMR spectroscopy were not performed, since similar results were expected as were obtained for the products in Sections 6.3.2-6.3.6.

IR  $\nu_{\text{max}}$  ATR/ $\text{cm}^{-1}$ : 2071 and 2004 (CO stretching).

### 6.3.10 Dicarbonyl(*S,O*-(*N*-benzoyl-*N'*,*N'*-dibenzylthioureato)rhodium(I), [Rh(*S,O*-(*N*-diBnT))(CO)<sub>2</sub>]

Dicarbonyl(*S,O*-(*N*-benzoyl-*N'*,*N'*-dibenzylthioureato)rhodium(I), [Rh(*S,O*-(*N*-diBnT))(CO)<sub>2</sub>] was synthesized by the same method described in the first attempt in Section 6.3.2 using the ligand *N*-benzoyl-*N'*,*N'*-dibenzylthiourea (74 mg, 0.2056 mmol) in this case. A bright orange product was obtained, which transformed into a dark red-brown oily product upon drying. This transformation was also observed while drying the product under vacuum. Only the solid product was analysed *via* IR spectroscopy. (Yield = *ca.* 32 mg, 30 %)

<sup>1</sup>H and <sup>13</sup>C NMR spectroscopy were not performed, since similar results were expected as were obtained for the products in Sections 6.3.2-6.3.6.

IR  $\nu_{\max}$  ATR/cm<sup>-1</sup>: 2069 and 2002 (CO stretching).

### 6.3.11 Dicarbonyl(*S,O*-(*N*-benzoyl-*N'*-naphthalen-1-yl-*N'*-phenylthioureato)rhodium(I), [Rh(*S,O*-(*N*-NPT))(CO)<sub>2</sub>]

Dicarbonyl(*S,O*-(*N*-benzoyl-*N'*-naphthalen-1-yl-*N'*-phenylthioureato)rhodium(I), [Rh(*S,O*-(*N*-NPT))(CO)<sub>2</sub>] was synthesized by the same method described in the first attempt in Section 6.3.2 using the ligand *N*-benzoyl-*N'*-naphthalen-1-yl-*N'*-phenylthiourea (73.6 mg, 0.2056 mmol) in this case. A brown product was obtained, which transformed into a dark red-brown oily product upon drying. This transformation was also observed while drying the product under vacuum. Only the solid product was analysed *via* IR spectroscopy. (Yield = *ca.* 32 mg, 30 %)

<sup>1</sup>H and <sup>13</sup>C NMR spectroscopy were not performed, since similar results were expected as were obtained for the products in Sections 6.3.2-6.3.6.

IR  $\nu_{\max}$  ATR/cm<sup>-1</sup>: 2073 and 2007 (CO stretching).

### 6.3.12 (*O,O*-acetylacetonato)dicarbonylrhodium(I), [Rh(*O,O*-acac)(CO)<sub>2</sub>]

The well-known complex (*O,O*-acetylacetonato)dicarbonylrhodium(I), [Rh(*O,O*-acac)(CO)<sub>2</sub>] was also synthesized as a reference compound by the same method described in the first attempt in Section 6.3.2 using the ligand acetylacetone (20.6 mg, 0.2056 mmol) in this case. A red solid product was obtained, which was recrystallized from acetone to provide dark green crystalline needles. (Yield = 42.0 mg, 80 %)

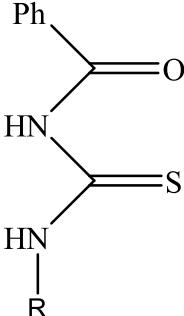
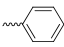
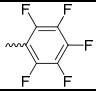
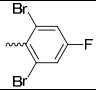
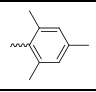
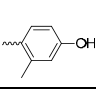
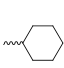
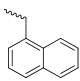
<sup>1</sup>H NMR (600 MHz, CDCl<sub>3</sub>, 25 °C): δ 5.60 (s, 1H, CH), 2.05 (s, 6H, CH<sub>3</sub>).

IR  $\nu_{\text{max}}$  ATR/cm<sup>-1</sup>: 2061 and 1993 (CO stretching).

The range of products that were obtained from Section 6.3 are summarized in Tables 6.1 and 6.2 together with the corresponding  $\nu_{\text{CO}}$  values.

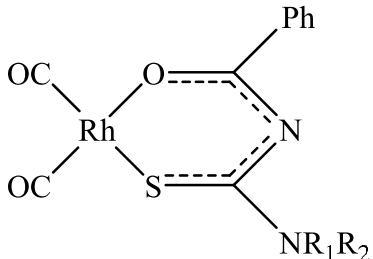
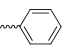
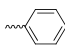
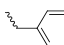
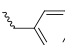
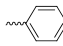
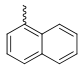


**Table 6.1 Summary of different products obtained from the reaction defined in Figure 6.1 for several *S,O*-thiourea ligands and corresponding  $\nu_{\text{CO}}$  values.**

Ligand	R =	Carbonyl stretching frequencies $\nu_{\text{CO}}$ ( $\text{cm}^{-1}$ )		
		Primary rhodium product (solid)	Secondary rhodium product (solid)	Decomposition product (oil)
acetylacetone	-	2061, 1993	-	-
		2068, 1998	2039, 1989	2024, 1970
		2074, 2010	2040, 1987	2023, 1971
		2070, 2003	*	2022, 1969
		2069, 2001	*	2020, 1967
		2068, 2001	*	2020, 1967
		2061, *	2040, 1985	2018, 1966
		2065, 1996	2040, 1986	2020, 1967

\* Corresponding peaks were obscured behind the other observed peaks and therefore exact values could not be provided

**Table 6.2 Some  $[\text{Rh}(\text{S},\text{O}\text{-thioureato})(\text{CO})_2]$  complexes and the corresponding  $\nu_{\text{CO}}$  values.**

Complex	$\text{R}_1, \text{R}_2 =$	$\nu_{\text{CO}}$ ( $\text{cm}^{-1}$ )
$[\text{Rh}(\text{acac})(\text{CO})_2]$	-	2061, 1993
	 , 	2071, 2004
	 , 	2069, 2002
	 , 	2073, 2007

## 6.4 Attempted synthesis of $[\text{Rh}(\text{S},\text{O}\text{-thioureato})(\text{CO})(\text{PPh}_3)]$ complexes

The  $[\text{Rh}(\text{S},\text{O}\text{-thioureato})(\text{CO})(\text{PPh}_3)]$  complexes were synthesized using the route shown in Figure 6.2 in conjunction with the synthetic route defined in Figure 6.1.

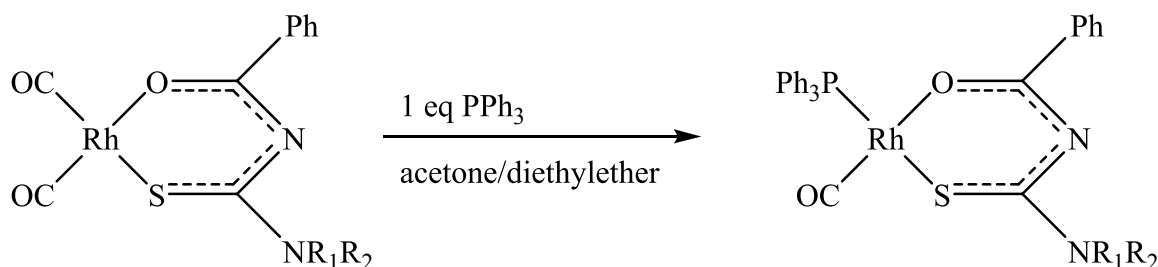


**Figure 6.2 Synthetic route for  $[\text{Rh}(\text{S},\text{O}\text{-thioureato})(\text{CO})(\text{PPh}_3)]$  complexes from  $[\text{Rh}(\text{S},\text{O}\text{-thioureato})(\text{CO})_2]$ .**

### 6.4.1 Carbonyltriphenylphosphine(*S,O*-(*N*-benzoyl-*N'*-phenylthioureato)rhodium(I), $[\text{Rh}(\text{S},\text{O}\text{-(N-PT)})(\text{CO})(\text{PPh}_3)]$

The precursor  $[\text{Rh}(\text{S},\text{O}\text{-(N-PT)})(\text{CO})_2]$  was synthesized by the method described in the first attempt in Section 6.3.2. The complex (26.0 mg, 0.06168 mmol) was re-dissolved in either acetone or diethyl ether, after which triphenylphosphine  $\text{PPh}_3$  (16.2 mg, 0.06168 mmol) was added until no more CO bubbles were observed in the sample. The solvent was allowed to evaporate and the resulting solid product was analysed by NMR and IR spectroscopy. (Yield = ca. 32 mg, 80 %)

Although IR spectroscopy indicated that the sample included a possible monocarbonyl rhodium species, NMR spectroscopy revealed that the major compound in the sample was triphenylphosphine oxide.

$^1\text{H}$  NMR (600 MHz,  $(\text{CD}_3)_2\text{CO}$ , 25 °C):  $\delta_{\text{H}}$  7.75-7.50 (m, phenyl rings).

$^{13}\text{C}$  NMR (151 MHz,  $(\text{CD}_3)_2\text{CO}$ , 25 °C):  $\delta_{\text{C}}$  133.6 (s, 1C, *ipso*-C), 132.1 (s, 1C, *para*-C), 131.8 (d, 2C, *meta*-C,  $J_{\text{C-P}} = 39$  Hz), 128.7 (d, 2C, *ortho*-C,  $J_{\text{C-P}} = 48$  Hz).

$^{31}\text{P}$  NMR (121 MHz,  $(\text{CD}_3)_2\text{CO}$ , 25 °C):  $\delta_{\text{P}}$  29.9 (s, 1P).

IR  $\nu_{\text{max}}$  ATR/cm<sup>-1</sup>: 1972 (CO stretching).

#### **6.4.2 Carbonylbis(triphenylphosphine)(*N,S*-(*N*-benzoyl-*N'*-phenylthioureato) rhodium(I), [Rh(*N,S*-(*N*-PT))(CO)(PPh<sub>3</sub>)<sub>2</sub>]**

An attempt was also made to synthesize [Rh(*S,O*-(*N*-PT))(CO)(PPh<sub>3</sub>)] from the precursor [Rh(*S,O*-(*N*-PT))(CO)<sub>2</sub>] synthesized by the method described in the second attempt in Section 6.3.2. [Rh(*S,O*-(*N*-PT))(CO)<sub>2</sub>] (26.0 mg, 0.06168 mmol) was re-dissolved in diethyl ether, after which triphenylphosphine PPh<sub>3</sub> (16.2 mg, 0.06168 mmol) was added until no more CO bubbles were observed in the sample. The solvent was allowed to evaporate, which resulted in the formation of an orange crystalline solid. The crystals were not suitable for X-ray analysis, but results provided in Section 6.4.8 suggests that the product was the [Rh(*N,S*-(*N*-PT))(CO)(PPh<sub>3</sub>)<sub>2</sub>] complex. (Yield = ca. 10 mg, 17 %).

IR  $\nu_{\text{max}}$  ATR/cm<sup>-1</sup>: 1927 (CO stretching).

Since the main focus in this study was on synthesizing the [Rh(*S,O*-(*N*-PT))(CO)(PPh<sub>3</sub>)] complex and due to limited time full characterization of this compound could not be achieved.

#### **6.4.3 Bis(triphenylphosphine)(*N,S*-(*N*-benzoyl-*N'*-phenylthioureato) (*S,O*-(*N*-benzoyl-*N'*-phenylthioureato)rhodium(III), [Rh(*N,S*-(*N*-PT))(*S,O*-(*N*-PT))(PPh<sub>3</sub>)<sub>2</sub>]**

Another attempt was made to synthesize [Rh(*S,O*-(*N*-PT))(CO)(PPh<sub>3</sub>)] from the precursor [Rh(*S,O*-(*N*-PT))(CO)<sub>2</sub>] synthesized by the method described in the first attempt in Section 6.3.2. [Rh(*S,O*-(*N*-PT))(CO)<sub>2</sub>] (26.0 mg, 0.06168 mmol) was re-dissolved in DMSO, after which triphenylphosphine PPh<sub>3</sub> (16.2 mg, 0.06168 mmol) was added until no more CO bubbles were observed in the sample. The sample was left for two days, after which acetone was added to four times the volume. The solvent was allowed to evaporate during which orange crystals suitable for X-ray analysis was obtained. X-ray analysis revealed that the product was the [Rh(*N,S*-(*N*-PT))(*S,O*-(*N*-PT))(PPh<sub>3</sub>)<sub>2</sub>] complex. (Yield = ca. 10 mg, 14 %)

Since the main focus in this study was on synthesizing the  $[\text{Rh}(\text{S},\text{O}-(\text{N-PT}))(\text{CO})(\text{PPh}_3)]$  complex and due to limited time full characterization of this compound could not be achieved. The structural data obtained for this product is discussed in Section 6.6.3.

#### **6.4.4 Carbonyltriphenylphosphine (*S,O*-(*N*-benzoyl-*N'*-(2,3,4,5,6-pentafluoro phenyl)thioureato)rhodium(I), $[\text{Rh}(\text{S},\text{O}-(\text{N-FPT}))(\text{CO})(\text{PPh}_3)]$**

The precursor  $[\text{Rh}(\text{S},\text{O}-(\text{N-FPT}))(\text{CO})_2]$  was synthesized by the method described in the first attempt in Section 6.3.3. The complex (31.2 mg, 0.06168 mmol) was re-dissolved in either acetone or diethyl ether, after which triphenylphosphine  $\text{PPh}_3$  (16.2 mg, 0.06168 mmol) was added until no more CO bubbles were observed in the sample. The solvent was allowed to evaporate and the resulting solid product was analysed by NMR and IR spectroscopy. (Yield = *ca.* 36 mg, 80 %)

Although IR spectroscopy indicated that the sample included a possible monocarbonyl rhodium species, NMR spectroscopy revealed that the major compound in the sample was triphenylphosphine oxide.

$^1\text{H}$  NMR (600 MHz,  $(\text{CD}_3)_2\text{CO}$ , 25 °C):  $\delta_{\text{H}}$  7.75-7.50 (m, phenyl rings).

$^{13}\text{C}$  NMR (151 MHz,  $(\text{CD}_3)_2\text{CO}$ , 25 °C):  $\delta_{\text{C}}$  133.6 (s, 1C, *ipso*-C), 132.1 (s, 1C, *para*-C), 131.8 (d, 2C, *meta*-C,  $J_{\text{C-P}} = 39$  Hz), 128.7 (d, 2C, *ortho*-C,  $J_{\text{C-P}} = 48$  Hz).

$^{31}\text{P}$  NMR (121 MHz,  $(\text{CD}_3)_2\text{CO}$ , 25 °C):  $\delta_{\text{P}}$  29.9 (s, 1P).

IR  $\nu_{\text{max}}$  ATR/ $\text{cm}^{-1}$ : 1976 (CO stretching).

#### 6.4.5 Carbonyltriphenylphosphine (*S,O*-(*N*-benzoyl-*N'*-(2,6-dibromo-4-fluoro phenyl)thioureato)rhodium(I) [Rh(*S,O*-(*N*-BFPT))(CO)(PPh<sub>3</sub>)]

The precursor [Rh(*S,O*-(*N*-BFPT))(CO)<sub>2</sub>] was synthesized by the method described in the first attempt in Section 6.3.4. The complex (34.8 mg, 0.06168 mmol) was re-dissolved in either acetone or diethyl ether, after which triphenylphosphine PPh<sub>3</sub> (16.2 mg, 0.06168 mmol) was added until no more CO bubbles were observed in the sample. The solvent was allowed to evaporate and the resulting solid product was analysed by NMR and IR spectroscopy. (Yield = *ca.* 39 mg, 80 %)

Although IR spectroscopy indicated that the sample included a possible monocarbonyl rhodium species, NMR spectroscopy revealed that the major compound in the sample was triphenylphosphine oxide.

<sup>1</sup>H NMR (600 MHz, (CD<sub>3</sub>)<sub>2</sub>CO, 25 °C): δ<sub>H</sub> 7.75-7.50 (m, phenyl rings).

<sup>13</sup>C NMR (151 MHz, (CD<sub>3</sub>)<sub>2</sub>CO, 25 °C): δ<sub>C</sub> 133.6 (s, 1C, *ipso*-C), 132.1 (s, 1C, *para*-C), 131.8 (d, 2C, *meta*-C, *J*<sub>C-P</sub> = 39 Hz), 128.7 (d, 2C, *ortho*-C, *J*<sub>C-P</sub> = 48 Hz).

<sup>31</sup>P NMR (121 MHz, (CD<sub>3</sub>)<sub>2</sub>CO, 25 °C): δ<sub>P</sub> 29.9 (s, 1P).

IR ν<sub>max</sub> ATR/cm<sup>-1</sup>: 1974 (CO stretching).

#### 6.4.6 Carbonyltriphenylphosphine (*S,O*-(*N*-benzoyl-*N'*-(2,4,6-trimethyl phenyl)thioureato)rhodium(I), [Rh(*S,O*-(*N*-tmPT))(CO)(PPh<sub>3</sub>)]

The precursor [Rh(*S,O*-(*N*-tmPT))(CO)<sub>2</sub>] was synthesized by the method described in the first attempt in Section 6.3.5. The complex (28.2 mg, 0.06168 mmol) was re-dissolved in either acetone or diethyl ether, after which triphenylphosphine PPh<sub>3</sub> (16.2 mg, 0.06168 mmol) was added until no more CO bubbles were observed in the sample. The solvent was allowed to evaporate and the resulting solid product was analysed by NMR and IR spectroscopy. (Yield = *ca.* 32 mg, 80 %)

Although IR spectroscopy indicated that the sample included a possible monocarbonyl rhodium species, NMR spectroscopy revealed that the major compound in the sample was triphenylphosphine oxide.

$^1\text{H}$  NMR (600 MHz,  $(\text{CD}_3)_2\text{CO}$ , 25 °C):  $\delta_{\text{H}}$  7.75-7.50 (m, phenyl rings).

$^{13}\text{C}$  NMR (151 MHz,  $(\text{CD}_3)_2\text{CO}$ , 25 °C):  $\delta_{\text{C}}$  133.6 (s, 1C, *ipso*-C), 132.1 (s, 1C, *para*-C), 131.8 (d, 2C, *meta*-C,  $J_{\text{C-P}} = 39$  Hz), 128.7 (d, 2C, *ortho*-C,  $J_{\text{C-P}} = 48$  Hz).

$^{31}\text{P}$  NMR (121 MHz,  $(\text{CD}_3)_2\text{CO}$ , 25 °C):  $\delta_{\text{P}}$  29.9 (s, 1P).

IR  $\nu_{\text{max}}$  ATR/ $\text{cm}^{-1}$ : 1975 (CO stretching).

#### **6.4.7 Carbonylbis(triphenylphosphine)(*N,S*-(*N*-benzoyl-*N'*-2,4,6-trimethylphenylthioureato) rhodium(I), $[\text{Rh}(\text{N},\text{S}-(\text{N-tmPT}))(\text{CO})(\text{PPh}_3)_2]$**

An attempt was also made to synthesize  $[\text{Rh}(\text{S},\text{O}-(\text{N-tmPT}))(\text{CO})(\text{PPh}_3)]$  from the precursor  $[\text{Rh}(\text{S},\text{O}-(\text{N-tmPT}))(\text{CO})_2]$  synthesized by the method described in the second attempt in Section 6.3.5.  $[\text{Rh}(\text{S},\text{O}-(\text{N-tmPT}))(\text{CO})_2]$  (28.2 mg, 0.06168 mmol) was re-dissolved in diethyl ether, after which triphenylphosphine  $\text{PPh}_3$  (16.2 mg, 0.06168 mmol) was added until no more CO bubbles were observed in the sample. The solvent was allowed to evaporate, which resulted in the formation of a dark red crystalline solid. The crystals were not suitable for X-ray analysis, but results provided in Section 6.4.8 suggests that the product was the  $[\text{Rh}(\text{N},\text{S}-(\text{N-tmPT}))(\text{CO})(\text{PPh}_3)_2]$  complex. (Yield = *ca.* 10 mg, 17 %)

IR  $\nu_{\text{max}}$  ATR/ $\text{cm}^{-1}$ : 1919 (CO stretching).

Since the main focus in this study was on synthesizing the  $[\text{Rh}(\text{S},\text{O}-(\text{N-tmPT}))(\text{CO})(\text{PPh}_3)]$  complex and due to limited time full characterization of this compound could not be achieved.

#### 6.4.8 Carbonylbis(triphenylphosphine)(*N,S*-(*N*-benzoyl-*N'*-(4-hydroxy-2-methylphenyl)thioureato)rhodium(I), [Rh(*N,S*-(*N*-4h2mPT))(CO)(PPh<sub>3</sub>)<sub>2</sub>]

An attempt was made to synthesize [Rh(*S,O*-(*N*-4h2mPT))(CO)(PPh<sub>3</sub>)] from the precursor [Rh(*S,O*-(*N*-4h2mPT))(CO)<sub>2</sub>] synthesized by the method described in the second attempt in Section 6.3.6. [Rh(*S,O*-(*N*-4h2mPT))(CO)<sub>2</sub>] (27.4 mg, 0.06168 mmol) was re-dissolved in diethyl ether, after which triphenylphosphine PPh<sub>3</sub> (16.2 mg, 0.06168 mmol) was added until no more CO bubbles were observed in the sample. The solvent was allowed to evaporate, which resulted in the formation of a bright orange crystals that were suitable for X-ray analysis. The structural data obtained from the X-ray analysis revealed that the product was the [Rh(*N,S*-(*N*-4h2mPT))(CO)(PPh<sub>3</sub>)<sub>2</sub>] complex. (Yield = *ca.* 10 mg, 17 %)

IR  $\nu_{\text{max}}$  ATR/cm<sup>-1</sup>: 1920 (CO stretching).

Since the main focus in this study was on synthesizing the [Rh(*S,O*-(*N*-4h2mPT))(CO)(PPh<sub>3</sub>)] complex and due to limited time full characterization of this compound could not be achieved. The structural data obtained for this product is discussed in Section 6.6.2.

#### 6.4.9 Carbonyltriphenylphosphine (*S,O*-(*N*-benzoyl-*N'*-naphthalen-1-ylmethyl thioureato)rhodium(I), [Rh(*S,O*-(*N*-NmT))(CO)(PPh<sub>3</sub>)]

The precursor [Rh(*S,O*-(*N*-NmT))(CO)<sub>2</sub>] was synthesized by the method described in the first attempt in Section 6.3.8. The complex (28.6 mg, 0.06168 mmol) was re-dissolved in either acetone or diethyl ether, after which triphenylphosphine PPh<sub>3</sub> (16.2 mg, 0.06168 mmol) was added until no more CO bubbles were observed in the sample. The solvent was allowed to evaporate and the resulting solid product was analysed by NMR and IR spectroscopy. (Yield = *ca.* 34 mg, 80 %)

Although IR spectroscopy indicated that the sample included a possible monocarbonyl rhodium species, NMR spectroscopy revealed that the major compound in the sample was triphenylphosphine oxide.

<sup>1</sup>H NMR (600 MHz, (CD<sub>3</sub>)<sub>2</sub>CO, 25 °C):  $\delta_{\text{H}}$  7.75-7.50 (m, phenyl rings).

$^{13}\text{C}$  NMR (151 MHz,  $(\text{CD}_3)_2\text{CO}$ , 25 °C):  $\delta_{\text{C}}$  133.6 (s, 1C, *ipso*-C), 132.1 (s, 1C, *para*-C), 131.8 (d, 2C, *meta*-C,  $J_{\text{C-P}} = 39$  Hz), 128.7 (d, 2C, *ortho*-C,  $J_{\text{C-P}} = 48$  Hz).

$^{31}\text{P}$  NMR (121 MHz,  $(\text{CD}_3)_2\text{CO}$ , 25 °C):  $\delta_{\text{P}}$  29.9 (s, 1P).

IR  $\nu_{\text{max}}$  ATR/ $\text{cm}^{-1}$ : 1971 (CO stretching).

#### **6.4.10 Carbonylbis(triphenylphosphine)( *N*-benzoyl-*N'*-naphthalen-1-ylmethyl thioureato)rhodium(I), $[\text{Rh}(\text{N},\text{S}-(\text{N-NmT}))(\text{CO})(\text{PPh}_3)_2]$**

Another attempt was made to synthesize  $[\text{Rh}(\text{S},\text{O}-(\text{N-NmT}))(\text{CO})(\text{PPh}_3)]$  from the precursor  $[\text{Rh}(\text{S},\text{O}-(\text{N-NmT}))(\text{CO})_2]$  synthesized by the method described in the second attempt in Section 6.3.8.  $[\text{Rh}(\text{S},\text{O}-(\text{N-NmT}))(\text{CO})_2]$  (28.6 mg, 0.06168 mmol) was re-dissolved in diethyl ether, after which triphenylphosphine  $\text{PPh}_3$  (16.2 mg, 0.06168 mmol) was added until no more CO bubbles were observed in the sample. The solvent was allowed to evaporate, which resulted in the formation of a dark red crystalline solid. The crystals were not suitable for X-ray analysis, but results provided in Section 6.4.8 suggests that the product was the  $[\text{Rh}(\text{N},\text{S}-(\text{N-NmT}))(\text{CO})(\text{PPh}_3)_2]$  complex. (Yield = *ca.* 10 mg, 17 %)

IR  $\nu_{\text{max}}$  ATR/ $\text{cm}^{-1}$ : 1930 (CO stretching).

Since the main focus in this study was on synthesizing the  $[\text{Rh}(\text{S},\text{O}-(\text{N-NmT}))(\text{CO})(\text{PPh}_3)]$  complex and due to limited time full characterization of this compound could not be achieved.



#### 6.4.11 Carbonyltriphenylphosphine (*S,O*-(*N*-benzoyl-*N'*,*N'*-dibenzylthioureato) rhodium(I), [Rh(*S,O*-(*N*-diBnT))(CO)(PPh<sub>3</sub>)]

The precursor [Rh(*S,O*-(*N*-diBnT))(CO)<sub>2</sub>] was synthesized by the method described in the first attempt in Section 6.3.10. The complex (32.0 mg, 0.06168 mmol) was re-dissolved in either acetone or diethyl ether, after which triphenylphosphine PPh<sub>3</sub> (16.2 mg, 0.06168 mmol) was added until no more CO bubbles were observed in the sample. The solvent was allowed to evaporate and the resulting solid product was analysed by NMR and IR spectroscopy. (Yield = *ca.* 37 mg, 80 %)

Although IR spectroscopy indicated that the sample included a possible monocarbonyl rhodium species, NMR spectroscopy revealed that the major compound in the sample was triphenylphosphine oxide.

<sup>1</sup>H NMR (600 MHz, (CD<sub>3</sub>)<sub>2</sub>CO, 25 °C): δ<sub>H</sub> 7.75-7.50 (m, phenyl rings).

<sup>13</sup>C NMR (151 MHz, (CD<sub>3</sub>)<sub>2</sub>CO, 25 °C): δ<sub>C</sub> 133.6 (s, 1C, *ipso*-C), 132.1 (s, 1C, *para*-C), 131.8 (d, 2C, *meta*-C, *J*<sub>C-P</sub> = 39 Hz), 128.7 (d, 2C, *ortho*-C, *J*<sub>C-P</sub> = 48 Hz).

<sup>31</sup>P NMR (121 MHz, (CD<sub>3</sub>)<sub>2</sub>CO, 25 °C): δ<sub>P</sub> 29.9 (s, 1P).

IR ν<sub>max</sub> ATR/cm<sup>-1</sup>: 1973 (CO stretching).

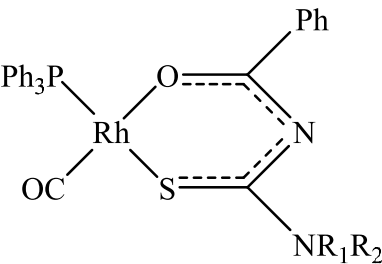
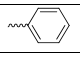
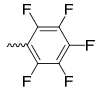
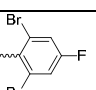
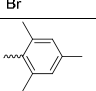
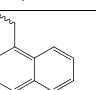
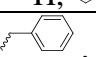
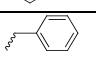
### 6.4.12 (*O,O*-acetylacetonato)carbonyltriphenylphosphinerhodium(I), [Rh(*O,O*-acac)(CO)(PPh<sub>3</sub>)]

The precursor [Rh(*O,O*-acac)(CO)<sub>2</sub>] was synthesized by the method described in the first attempt in Section 6.3.12. The complex (42.0 mg, 0.06168 mmol) was re-dissolved in acetone, after which triphenylphosphine PPh<sub>3</sub> (16.2 mg, 0.06168 mmol) was added until no more CO bubbles were observed in the sample. The solvent was allowed to evaporate, which resulted in the formation of a light yellow crystalline solid. (Yield = *ca.* 24 mg, 80 %)

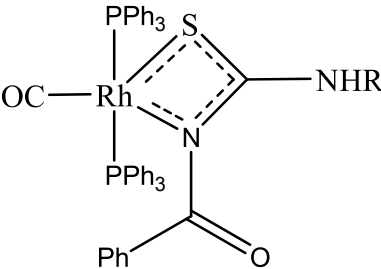
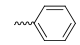
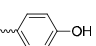
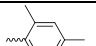
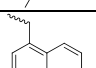
IR  $\nu_{\max}$  ATR/cm<sup>-1</sup>: 1975 (CO stretching).

The range of products that were obtained from Section 6.4 are summarized in Tables 6.3 and 6.4 together with the corresponding  $\nu_{\text{CO}}$  values. The crystal structures obtained from Section 6.4 are presented in Sections 6.7 and 6.8.

**Table 6.3 Expected rhodium thiourea products obtained from the synthetic route in Figure 6.2 and the corresponding  $\nu_{\text{CO}}$  values.**

Expected complex	Structure R <sub>1</sub> , R <sub>2</sub> =	CO stretching frequency $\nu_{\text{CO}}$ (cm <sup>-1</sup> )
	-	1975
	H, 	1972
	H, 	1976
	H, 	1974
	H, 	1975
	H, 	1971
	 , 	1973

**Table 6.4 [Rh(*N,S*-thioureato)(CO)(PPh<sub>3</sub>)<sub>2</sub>] complexes and the corresponding  $\nu_{\text{CO}}$  values.**

Complex	R =	$\nu_{\text{CO}}$ (cm <sup>-1</sup> )
		1927
		1920
		1919
		1930

## 6.5 Attempted synthesis of [Rh(*S,O*-thioureato)(CO)<sub>2</sub>] via the precursor [Rh(COD)(Cl)]<sub>2</sub>

Another alternative route for the synthesis of [Rh(*S,O*-thioureato)(CO)<sub>2</sub>] complexes that was undertaken included the use of [Rh(COD)(Cl)]<sub>2</sub> as the precursor. Reasons for the use of this precursor firstly involves the ease of preparing this complex as was already shown in Section 5.2.1 in Chapter 5 and some examples<sup>1a,b,c</sup> exist that show that rhodium COD derivatives of some ligands can also easily crystallize from out solutions. Furthermore, it was already mentioned in Section 5.2.1 that COD can easily be substituted by incoming CO molecules. The general route that was followed in order to firstly try and synthesize the [Rh(COD)(*S,O*-thioureato)] species is shown in Figure 6.3. Later it was found that the route led to the formation of complex **B** instead of **A**. This will be discussed in more detail in Section 6.6.

<sup>1</sup> Typical examples include: a) Delferro, M.; Cauzzi, D.; Pattacini, R.; Tegoni, M.; Graiff, C.; Tiripicchio, A. (2008) *Eur. J. Inorg. Chem.*, 2302. b) Leipoldt, J. G.; Grobler, E. C. (1983) *Inorg. Chim. Acta*, **72**, 17. c) Leipoldt, J. G.; Basson, S. S.; Lamprecht, G. J.; Bok, L. D. C.; Schlebusch, J. J. J. (1980) *Inorg. Chim. Acta*, **40**, 43.

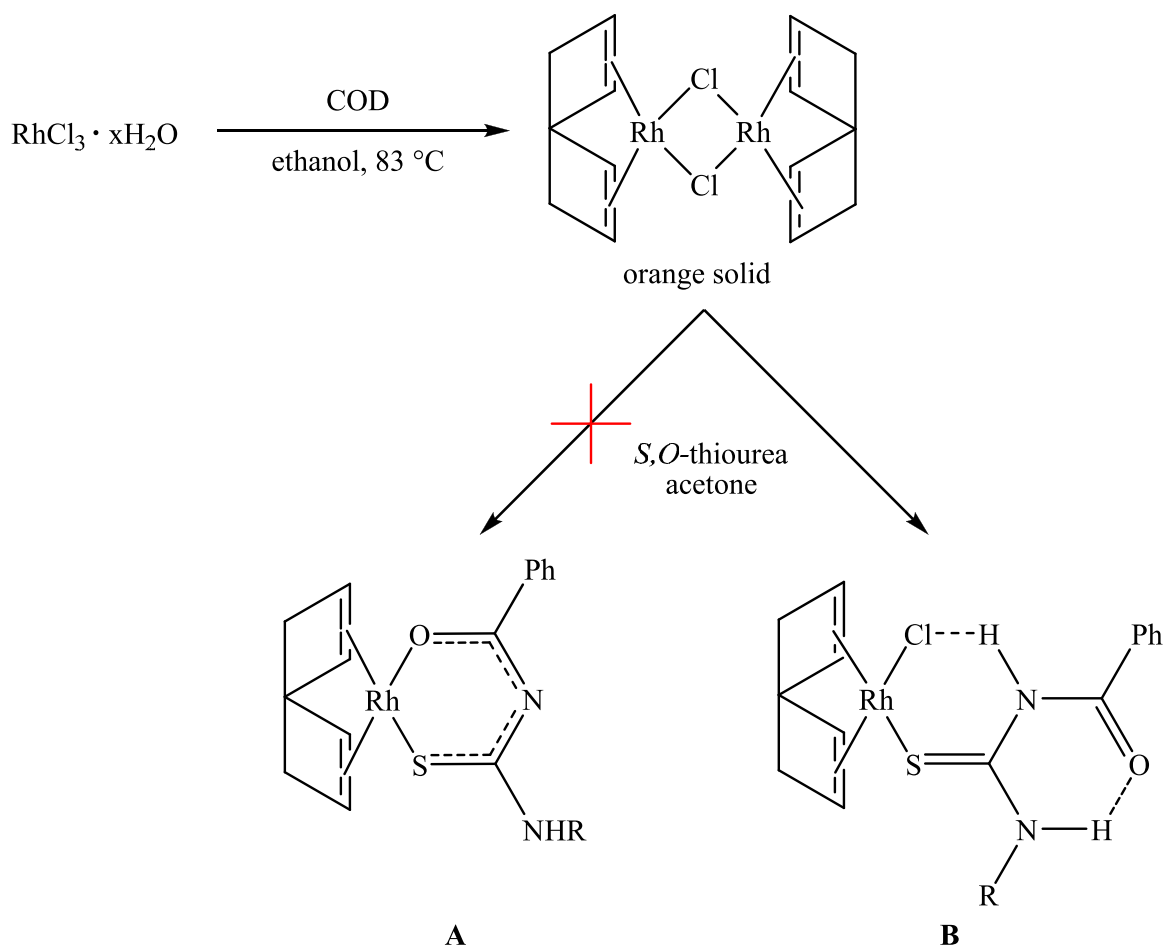


**Figure 6.3 Synthetic route to the rhodium COD derivatives of *S,O*-functionalized thiourea ligands.**

### 6.5.1. Chlorido(1,5-cyclooctadiene)(*S*-(*N*-benzoyl-*N'*-phenylthioureato))rhodium(I), [Rh(COD)(Cl)(*S*-(*N*-PTH))]

An attempt was made to synthesize Cyclo(1,5-octadiene)(*S,O*-(*N*-benzoyl-*N'*-phenylthioureato))rhodium(I), [Rh(COD)(*S,O*-(*N*-PT))] (**A**) by the following method: RhCl<sub>3</sub>·xH<sub>2</sub>O (1.0 g, 4.78 mmol) was dissolved in pre-boiled ethanol after which an excess (1.17 mL, 9.56 mmol) of cyclo-octadiene was added to the solution. The solution was heated under reflux for 3 hrs at about 83 °C, which led to the precipitation of an orange solid from out of the ethanol solution. The orange precipitate was filtered off and washed with cold methanol. As was already discussed in Section 5.2.1 in Chapter 5, IR analysis confirmed the product to be the [Rh(COD)(Cl)]<sub>2</sub> species. The next step included the addition of *N*-benzoyl-*N'*-phenylthiourea (20.8 mg, 0.0811 mmol) to an acetone (2 mL) solution of [Rh(COD)(Cl)]<sub>2</sub> (20 mg, 0.0405 mmol), which was vigorously stirred until all of the reagents fully dissolved.

The acetone was allowed to slowly evaporate upon which bright yellow crystals suitable for X-ray analysis formed in solution. Structural data obtained from the X-ray analysis revealed that the product was in fact the complex  $[\text{Rh}(\text{COD})(\text{Cl})(S-(N\text{-PTH}))]$ . (Yield = *ca.* 10 mg, 49 %).

Since this product was not part of the main objectives of this study and due to limited time full characterization for this product could not be obtained.

#### **6.5.2. Chlorido(1,5-cyclooctadiene)(*S*-(*N*-benzoyl-*N'*-(2,4,6-trimethyl)phenylthioureato))rhodium(I), $[\text{Rh}(\text{COD})(\text{Cl})(S-(N\text{-tmPTH}))]$**

An attempt was made to synthesize Cyclo(1,5-octadiene)(*S,O*-(*N*-benzoyl-*N'*-(2,4,6-trimethyl)phenylthioureato))rhodium(I),  $[\text{Rh}(\text{COD})(S,O-(N\text{-tmPT}))]$  using the same methodology as described in Section 6.5.1. This resulted in the formation of bright orange crystals suitable for X-ray analysis. Structural data obtained from the X-ray analysis revealed that the product was in fact the complex  $[\text{Rh}(\text{COD})(\text{Cl})(S-(N\text{-tmPTH}))]$ . (Yield = *ca.* 10 mg, 45 %).

Since this product was not part of the main objectives of this study and due to limited time full characterization for this product could not be obtained.

The resulting crystal structures obtained in Section 6.5 are presented in Sections 6.6.4 and 6.6.5.

## 6.6 Structural characterization of a range of *S,O*-, *N,S*- and *S*- coordinated thiourea complexes of rhodium

### 6.6.1 Experimental

The X-ray determined single crystal structures of the following compounds are reported:

1. Carbonylbis(triphenylphosphine)(*N,S*-(*N*-benzoyl-*N'*-(4-hydroxy-2-methylphenyl)thioureato)rhodium(I), [Rh(*N,S*-(*N*-4h2mPT))(CO)(PPh<sub>3</sub>)<sub>2</sub>]
2. Bis(triphenylphosphine)(*N,S*-(*N*-benzoyl-*N'*-phenylthioureato)(*S,O*-(*N*-benzoyl-*N'*-phenylthioureato)rhodium(III), [Rh(*N,S*-(*N*-PT))(*S,O*-(*N*-PT))(PPh<sub>3</sub>)<sub>2</sub>]
3. Chloridocyclooctadienyl(*S*-(*N*-benzoyl-*N'*-phenylthioureato))rhodium(I), [Rh(COD)(Cl)(*S*-(*N*-PTH))]
4. Chloridocyclooctadienyl(*S*-(*N*-benzoyl-*N'*-(2,4,6-trimethyl)phenylthioureato))rhodium(I), [Rh(COD)(Cl)(*S*-(*N*-tmPTH))]

The above mentioned compounds were analysed by single crystal X-ray diffraction. The initial unit cell and data collections were performed on a Bruker X8 Apex II 4K Kappa CCD diffractometer using graphite monochromated Mo  $K\alpha$  radiation ( $\lambda = 0.71073 \text{ \AA}$ ) with  $\omega$ - and  $\phi$ -scans at 100(2) K as well as the Apex2 software package.<sup>2</sup> The optimum measurement method to collect more than a hemisphere of reciprocal space was predicted by COSMO.<sup>3</sup> Frame integration and data reductions were performed using the SAINT-Plus and XPREP<sup>4</sup> software packages, and a multi-scan absorption correction was performed on the data using SADABS.<sup>5</sup> The structures were solved by the direct methods package SIR97,<sup>6</sup> and refinement using the WinGX software package<sup>7</sup> incorporating SHELXL.<sup>8</sup> All non H-atoms were refined anisotropically. All H-atoms were positioned geometrically and refined using a riding model with fixed C-H distances of 0.95  $\text{\AA}$  (CH) [ $U_{\text{iso}}(\text{H}) = 1.2U_{\text{eq}}$ ] for aromatic H-atoms and

<sup>2</sup> Bruker (2005). Apex2 (Version 1.0-27). Bruker AXS Inc., Madison, Wisconsin, USA.

<sup>3</sup> Bruker (2003). COSMO (Version 1.48). Bruker AXS Inc., Madison, Wisconsin, USA.

<sup>4</sup> Bruker (2004a). SAINT-Plus. Version 7.12 (including XPREP). Bruker AXS Inc., Madison, Wisconsin, USA.

<sup>5</sup> Bruker (2004b). SAINT-Plus. Version 7.12 (including XPREP). Bruker AXS Inc., Madison, Wisconsin, USA.

<sup>6</sup> Altomare, A., Burla, M. C., Camalli, M., Cascarano, G. L., Giacovazzo, C., Guagliardi, A., Moliterni, A. G. G., Polidori, G. & Spagna, R. (1999). *J. Appl. Cryst.*, **32**, 115.

<sup>7</sup> Farrugia, L. J. (1999). WinGX, *J. Appl. Cryst.*, **32**, 837.

<sup>8</sup> Sheldrick, G.M. (1997). SHELXL97. *Program for crystal structure refinement*. University of Göttingen, Germany.

0.98 Å (CH) [ $U_{\text{iso}}(\text{H}) = 1.2U_{\text{eq}}$ ] for methyl H-atoms as well as fixed N-H distances of 0.88 Å (NH) [ $U_{\text{iso}}(\text{H}) = 1.2U_{\text{eq}}$ ]. Molecular diagrams were drawn using the Mercury<sup>9</sup> package with a 30% thermal envelope probability for non-hydrogen atoms. General crystal data and refinement parameters are presented in Table 6.5. A complete list of atomic coordinates, equivalent isotropic parameters, bond distances and angles, anisotropic displacement parameters and hydrogen coordinates for each individual dataset is given in Appendix C.

---

<sup>9</sup> Macrae, C. F., Edgington, P. R., McCabe, P., Pidcock, E., Shields, G. P., Taylor, R., Towler, M. & van de Streek, J. (2006). *J. Appl. Cryst.* **39**, 453.

**Table 6.5 General crystal data for (i) [Rh(*N,S*-(*N*-4h2mPT))(CO)(PPh<sub>3</sub>)<sub>2</sub>],  
(ii) [Rh(*N,S*-(*N*-PT))(*S,O*-(*N*-PT))(PPh<sub>3</sub>)<sub>2</sub>], (iii) [Rh(COD)(Cl)(*S*-(*N*-PTH)))] and  
(iv) [Rh(COD)(Cl)(*S*-(*N*-tmPTH))].**

Identification code	(i)	(ii)	(iii)	(iv)
Empirical formula	Rh1 C52 H43 O3 P2 S1 N2	Rh1 C69 H64 O4 P2 S3 N4	Rh1 C22 H24 O1 S1 N2 Cl1	Rh1 C25 H30 O1 S1 N2 Cl1
Formula weight	940.8	1274.3	502.9	502.9
Crystal system, space group	Triclinic $P\bar{1}$	Triclinic $P\bar{1}$	Triclinic $P\bar{1}$	Monoclinic $C2/c$
Unit cell dimensions				
a (Å)	10.6260(3)	12.548(1)	6.6703(2)	22.5075(15)
b (Å)	11.7305(3)	13.335(1)	10.1665(4)	8.5005(7)
c (Å)	19.6582(5)	21.352(3)	14.9616(5)	24.8836(17)
$\alpha$ (°)	76.4886(5)	94.966(6)	96.891(2)	90.000
$\beta$ (°)	82.0265(7)	103.157(6)	91.588(2)	93.551(4)
$\gamma$ (°)	64.8478(10)	117.764(4)	90.616(2)	90.000
Volume (Å <sup>3</sup> )	2154.5(1)	3000.6(2)	1006.78(6)	4751.7(6)
Z	2	2	2	8
Density (calculated) (g/mL)	1.450	1.410	1.659	1.523
Absorption coefficient (mm <sup>-1</sup> )	0.567	0.496	1.100	0.939
$F(000)$	968	1322	512	2240
Crystal size (mm <sup>3</sup> )	0.28 x 0.16 x 0.05	0.40 x 0.39 x 0.12	0.18 x 0.17 x 0.08	0.17 x 0.16 x 0.13
$\Theta$ range (°)	3.41 to 27.00	2.59 to 25.00	1.37 to 28.34	3.51 to 28.28
Completeness (%)	99.5	96.5	99.1	99.8
Index ranges	-13 ≤ <i>h</i> ≤ 13 -14 ≤ <i>k</i> ≤ 14 -25 ≤ <i>l</i> ≤ 25	-14 ≤ <i>h</i> ≤ 13 -15 ≤ <i>k</i> ≤ 15 -25 ≤ <i>l</i> ≤ 25	-8 ≤ <i>h</i> ≤ 8 -13 ≤ <i>k</i> ≤ 13 -19 ≤ <i>l</i> ≤ 19	-30 ≤ <i>h</i> ≤ 30 -11 ≤ <i>k</i> ≤ 10 -33 ≤ <i>l</i> ≤ 33
Reflections collected	44786	22388	18721	41268
Independent reflections	9357 [ <i>R</i> <sub>int</sub> = 0.0275]	10190 [ <i>R</i> <sub>int</sub> = 0.0444]	4980 [ <i>R</i> <sub>int</sub> = 0.0318]	5886 [ <i>R</i> <sub>int</sub> = 0.0674]
Observed reflections	8249	8205	4476	4578
Max/min transmission	0.972 and 0.858	0.943 and 0.826	0.917 and 0.827	0.888 and 0.857
Data/ restraints/ parameters	9357/0/552	10190/0/752	4980/0/253	5886/0/281
Goodness-of-fit on $F^2$	1.039	1.071	1.039	1.079
Final <i>R</i> indices [ <i>I</i> > 2σ( <i>I</i> )]	<i>R</i> 1 = 0.0269 w <i>R</i> 2 = 0.0660	<i>R</i> 1 = 0.0524 w <i>R</i> 2 = 0.1280	<i>R</i> 1 = 0.0288 w <i>R</i> 2 = 0.0756	<i>R</i> 1 = 0.0355 w <i>R</i> 2 = 0.0725
<i>R</i> indices (all data)	<i>R</i> 1 = 0.0324 w <i>R</i> 2 = 0.0690	<i>R</i> 1 = 0.0698 w <i>R</i> 2 = 0.1407	<i>R</i> 1 = 0.0353 w <i>R</i> 2 = 0.1025	<i>R</i> 1 = 0.0516 w <i>R</i> 2 = 0.0780
Largest diff. Peak/hole (e.Å <sup>-3</sup> )	0.426 and -0.414	1.726 and -1.297	0.774 and -0.661	0.873 and -0.531



### 6.6.2 Crystal structure of $[\text{Rh}(\text{N},S\text{-(N-4h2mPT)})(\text{CO})(\text{PPh}_3)_2]$

(Synthesis described in Section 6.4.8; Supplementary data C1)

$[\text{Rh}(\text{N},S\text{-(N-4h2mPT)})(\text{CO})(\text{PPh}_3)_2]$  crystallised in the triclinic space group  $P\bar{1}$  having only one independent molecule in the asymmetric unit. The structure together with the atom numbering scheme are shown in Figure 6.4. The general crystallographic data are given in Table 6.5, while the most important bond lengths and angles are provided in Table 6.6.

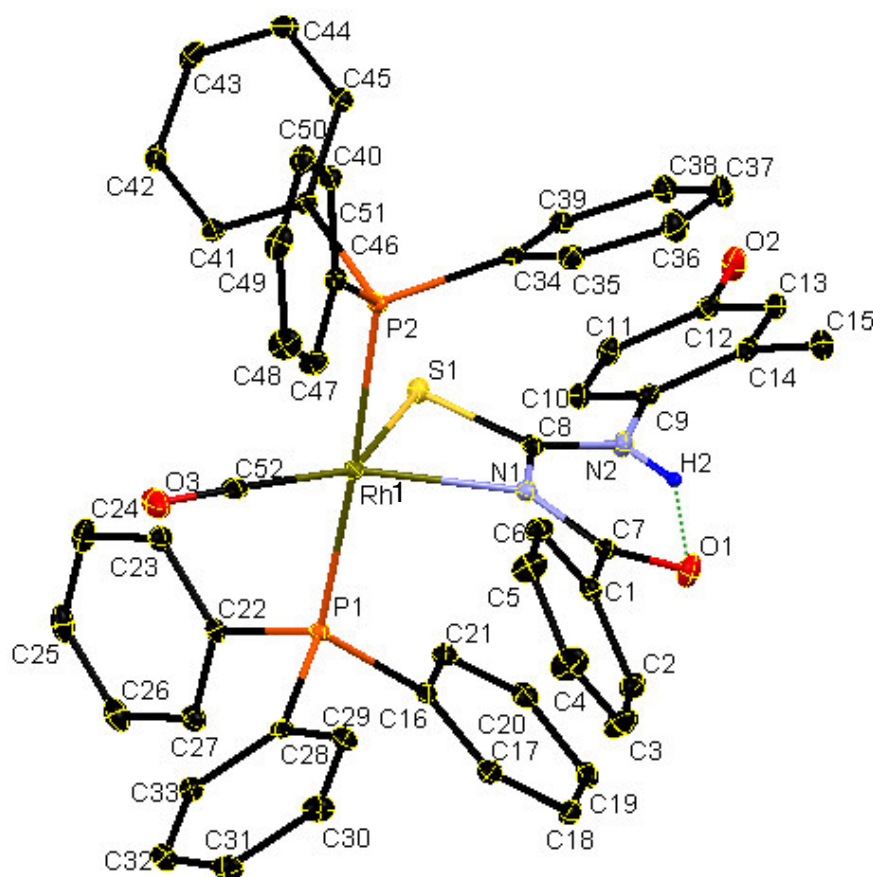


**Figure 6.4** A structural representation of the compound

$[\text{Rh}(\text{N},S\text{-(N-4h2mPT)})(\text{CO})(\text{PPh}_3)_2]$ , where the atom numbering scheme is provided (ellipsoid probability = 30%). Phenyl and methyl hydrogen atoms have been omitted for clarity.

**Table 6.6 List of selected bond distances and angles for the compound  
[Rh(*N,S*-(*N*-4h2mPT))(CO)(PPh<sub>3</sub>)<sub>2</sub>].**

Atoms	Distance (Å)	Atoms	Angle (°)
Rh1-P1	2.310(1)	N1-Rh1-S1 <sub>bite angle</sub>	63.07(4)
Rh1-P2	2.331(1)	C52-Rh1-S1	139.84(7)
Rh1-S1	2.623(1)	C52-Rh1-N1	156.74(8)
Rh1-N1	2.278(2)	P1-Rh1-S1	93.17(4)
Rh1-C52	1.800(2)	P1-Rh1-N1	89.16(4)
C52-O3	1.158(2)	P1-Rh1-C52	85.88(6)
C8-S1	1.704(2)	P2-Rh1-S1	86.60(4)
C8-N1	1.372(2)	P2-Rh1-N1	93.94(4)
C7-O1	1.251(2)	P2-Rh1-C52	91.98(6)
C12-O2	1.372(2)	Rh1-C52-O3	176.86(17)

It is clear from Figure 6.4 that the thiourea ligand (*N*-4h2mPTH) coordinated to the metal centre in a *N,S*-fashion forming a 4-membered ring. The corresponding bite angle given by N1-Rh1-S1 is small having a value of 63.07(4) °, while the bonds Rh1-N1 and Rh1-S1 have respective distances of 2.278(2) and 2.623(1) Å. These long bond distances suggest that S1 and N1 coordinated together as a mono-charged moiety, where electron delocalization occurs along the S-C-N moiety. The nitrogen atom N2 was confirmed to be protonated due to the presence of electron density at a suitable distance from the nitrogen. In order to position the proton accurately from the nitrogen, it was geometrically positioned and refined using a riding model with a fixed N-H distance of 0.88 Å (NH) [*U*<sub>iso</sub>(H) = 1.2U<sub>eq</sub>]. The two triphenylphosphine ligands coordinated *trans* with respect to each other having respective Rh1-P1 and Rh1-P2 bond distances of 2.310(1) and 2.331(1) Å. The corresponding P1-Rh1-P2 angle is found to be 176.39(2) °. The carbonyl ligand is located *trans* to the thiourea ligand having Rh1-C52 and C52-O3 bond lengths of 1.800(2) and 1.158(2) Å, respectively. The Rh1-C52-O3 and slightly bent away from linearity with a value of 176.86(17) °.

These orientations together with the angles P1-Rh1-S1, P1-Rh1-N1, P1-Rh1-C52, P2-Rh1-S1, P2-Rh1-N1 and P2-Rh1-C52 being all close to 90 ° suggest that the 5-coordinated rhodium exhibit a trigonal bipyramidal conformation. However, the large C52-Rh1-S1 and C52-Rh1-N1 angles of 139.84(7) and 156.74(8) ° together with the small bite angle N1-Rh1-S1 defines this conformation to be largely distorted trigonal bipyramidal. This complex structure is also analogous to the square planar Vaska-type complexes [Rh(Cl)(CO)(YR<sub>1</sub>R<sub>2</sub>R<sub>3</sub>)<sub>2</sub>],<sup>10</sup> where the chlorido ligand in the latter complexes are replaced by

<sup>10</sup> Roodt, A.; Otto, S.; Steyl, G. (2003) *Coord. Chem. Rev.*, **245**, 121.

a mono-charged *N,S*-coordinated thiourea ligand. A comparison between the well-known complex  $[\text{Rh}(\text{Cl})(\text{CO})(\text{PPh}_3)_2]$ <sup>11</sup> and the present complex  $[\text{Rh}(\text{N},\text{S}-(\text{N}-4\text{h}2\text{mPT}))(\text{CO})(\text{PPh}_3)_2]$  shows that the carbonyl stretching frequency values shifted with a large value from 1965-1983  $\text{cm}^{-1}$  (found for several solid state forms of the  $[\text{Rh}(\text{Cl})(\text{CO})(\text{PPh}_3)_2]$  complex) to 1920  $\text{cm}^{-1}$  in the solid state. This suggested that the replacement of the chloro ligand with a *N,S*-coordinated substantially increased the electron density on metal centre. This is not reflected in the C52-O3 bond distance of 1.158(2) Å though, as this value is similar to that for the  $[\text{Rh}(\text{Cl})(\text{CO})(\text{PPh}_3)_2]$  complex. The authors also reported that the lower  $\nu_{\text{CO}}$  value in some of the forms of  $[\text{Rh}(\text{Cl})(\text{CO})(\text{PPh}_3)_2]$  is in agreement with the bent in the Rh-C-O angle. However, the Rh1-C52-O3 angle is 176.86(17) ° and only slightly bended compared to the reported values of 164-169 °. Therefore, no structural correlation can be established to explain the very low  $\nu_{\text{CO}}$  value of the  $[\text{Rh}(\text{N},\text{S}\text{-thioureato})(\text{CO})(\text{PPh}_3)_2]$  complexes and it is assumed to be linked to the electron-donating properties of the *N,S*-coordination.

The crystal packing of  $[\text{Rh}(\text{N},\text{S}-(\text{N}-4\text{h}2\text{mPT}))(\text{CO})(\text{PPh}_3)_2]$  is stabilized by several hydrogen bond interactions found between molecules orientated around a centre of symmetry, as shown in Figure 6.5. Firstly, intramolecular hydrogen bonding exists between the oxygen atom O1 and the nitrogen atom N2 of the coordinated thiourea ligand having a N2-H2...O1 distance and angle of 2.584(2) Å and 136.3 °, respectively. This is a typical interaction found in these ligands as was shown in Chapter 4. Furthermore, intermolecular hydrogen bonding is found between the oxygen atoms O1 and O2 with a respective distance and angle O2-H2B...O1 of 2.757(2) Å and 151.1 °. These interactions bring the 4-hydroxy-2-methylphenyl moieties of the different molecules in close approximation to each, which leads to a  $\pi$ -stacking interaction found between the carbon atoms C14 of each molecule. This interaction is also indicated in Figure 6.5 And has an interplanar distance of 3.433 Å. These interactions altogether lead to the formation of dimmers packed in the unit cell along the *ab* plane.

---

<sup>11</sup> Kemp, G.; Roodt, A.; Purcell, W. (1995) *Rhodium Express*, nr 12, 21.

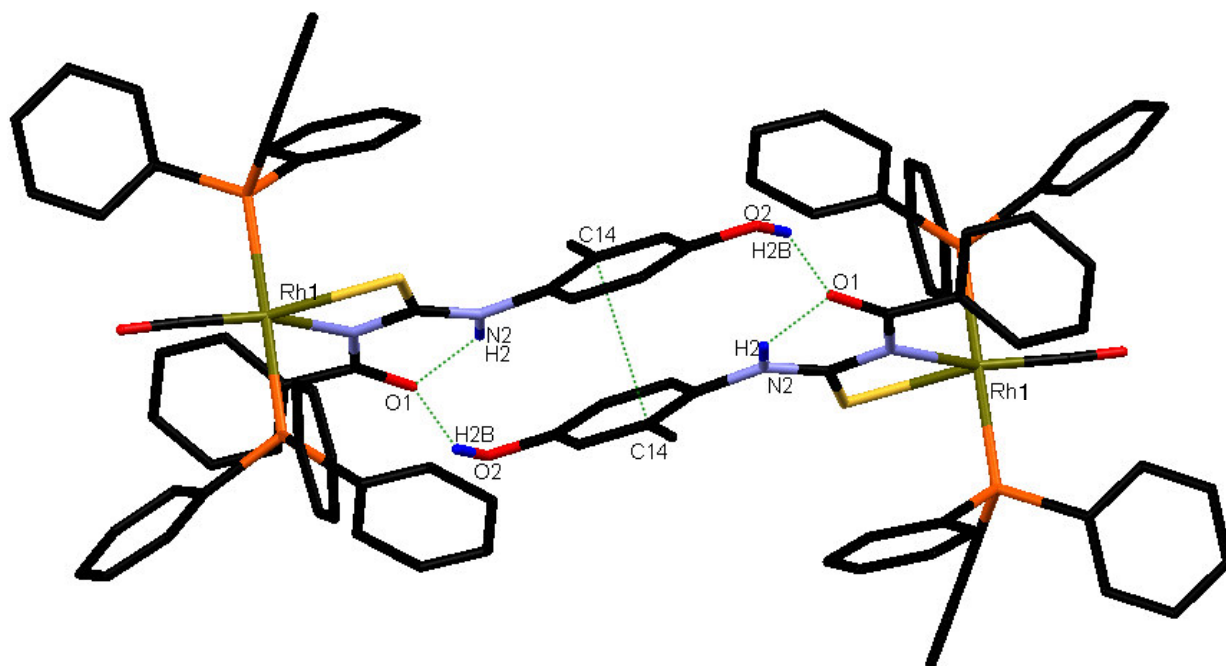


**Figure 6.5** An illustration of hydrogen bond as well as  $\pi$ -stacking interactions found in the crystal packing of  $[\text{Rh}(\text{N},\text{S}-(\text{N}-4\text{h}2\text{mPT}))(\text{CO})(\text{PPh}_3)_2]$  leading to dimer formation. Distances and angles:  $\text{N}2-\text{H}2\cdots\text{O}1 = 2.584(2) \text{ \AA}$ ,  $136.3^\circ$ ;  $\text{O}2-\text{H}2\text{B}\cdots\text{O}1 = 2.757(2) \text{ \AA}$ ,  $151.1^\circ$ ;  $\text{C}14\cdots\text{C}14 = 3.433 \text{ \AA}$ .

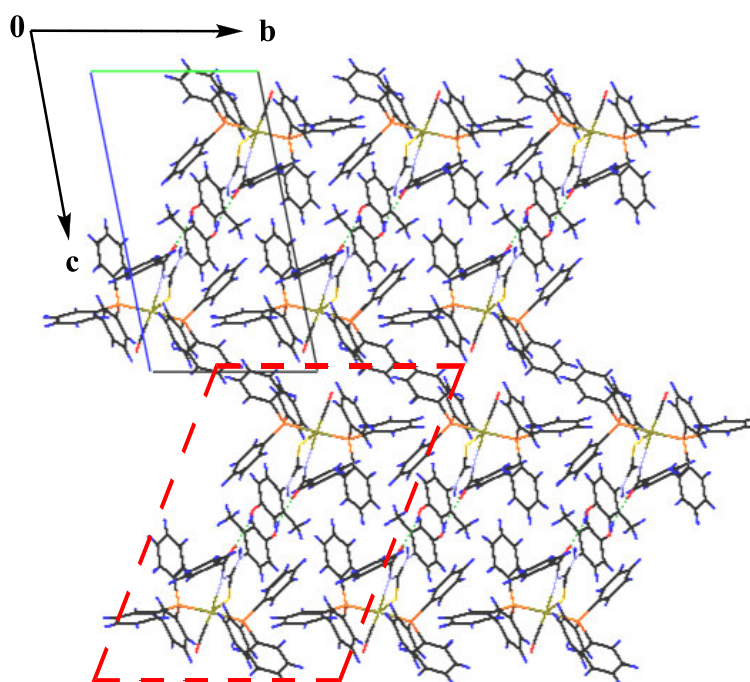


**Figure 6.6** The general packing of the  $[\text{Rh}(\text{N},\text{S}-(\text{N}-4\text{h}2\text{mPT}))(\text{CO})(\text{PPh}_3)_2]$  across the  $bc$ -plane.

Several other Van der Waals interactions are also present in the packing, which primarily involve  $\text{C}\cdots\text{C}$  contacts. A general packing of the  $[\text{Rh}(\text{N},\text{S}-(\text{N}-4\text{h}2\text{mPT}))(\text{CO})(\text{PPh}_3)_2]$  is

presented in Figure 6.6. The dimer units defined in Figure 6.5 are packed along the bc plane, where one of the dimer units is indicated by a red striped block. This packing brings the triphenylphosphine moieties in close approximation to each other, where C...C short contacts amongst them also stabilizes the packing.

### **6.6.3 Crystal structure of [Rh(*N,S*-(*N*-PT))(*S,O*-(*N*-PT))(PPh<sub>3</sub>)<sub>2</sub>].acetone.DMSO**

(Synthesis described in Section 6.4.3; Supplementary data C2)

The [Rh(*N,S*-(*N*-PT))(*S,O*-(*N*-PT))(PPh<sub>3</sub>)<sub>2</sub>].acetone.DMSO complex crystallized in the triclinic space group  $P\bar{1}$  ( $Z = 2$ ). The subsequent structure and the atom labelling is given in Figure 6.7, whereas the general crystallographic data as well as most important distances and angles are provided in Tables 6.5 and 6.7, respectively.

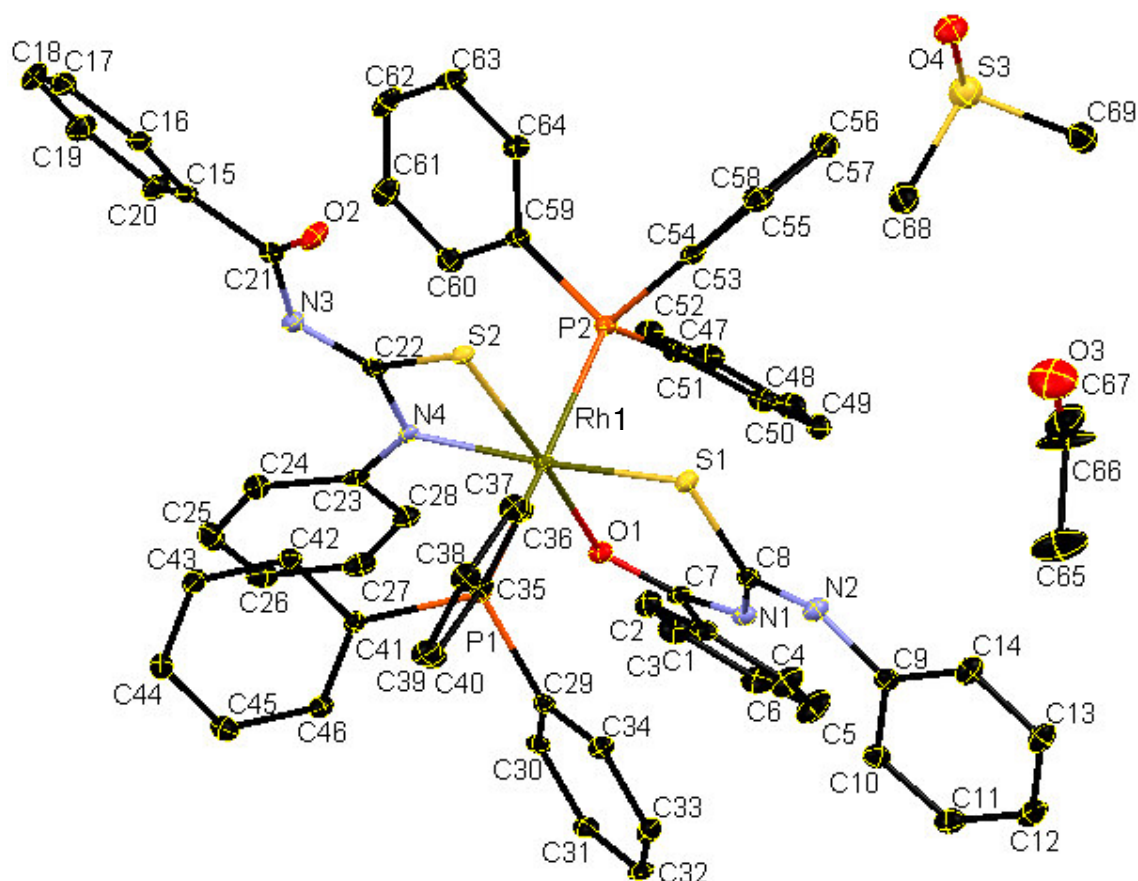


**Figure 6.7 A structural representation of the compound**  
**[Rh(*N,S*-(*N*-PT))(*S,O*-(*N*-PT))(PPh<sub>3</sub>)<sub>2</sub>], where the atom labelling is provided (ellipsoid probability = 30%). The hydrogen atoms have been omitted for clarity.**

**Table 6.7 List of selected bond distances and angles for the compound**  
**[Rh(*N,S*-(*N*-PT))(*S,O*-(*N*-PT))(PPh<sub>3</sub>)<sub>2</sub>].**

Atoms	Distance (Å)	Atoms	Angle (°)
Rh1-P1	2.361(1)	N4-Rh1-S2 <sub>bite angle</sub>	68.52(10)
Rh1-P2	2.369(1)	S1-Rh1-O1 <sub>bite angle</sub>	88.15(9)
Rh1-S1	2.339(1)	S1-Rh1-S2	101.79(4)
Rh1-S2	2.330(1)	O1-Rh1-N4	101.65(13)
Rh1-O1	2.133(3)	P1-Rh1-P2	175.88(4)
Rh1-N4	2.087(4)	P1-Rh1-S1	88.82(5)
C8-S1	1.733(5)	P1-Rh1-S2	92.08(4)
C7-O1	1.260(5)	P2-Rh1-S1	89.89(5)
C22-S2	1.780(5)	P2-Rh1-S2	84.35(4)
C22-N4	1.342(6)		
C21-O2	1.239(6)		

The structure involves an octahedral rhodium centre, where two molecules of the ligand *N*-PT coordinated in a *S,O*- and *N,S*-fashion, respectively, on the equatorial positions of the octahedral arrangement. The bite angles of these ligands on the metal centre are given by N4-

Rh1-S2 = 68.52(10) ° and S1-Rh1-O1 = 88.15(9) °. It is observed that the sulphur atoms of the two ligands are *cis* to each other around the metal centre, which seems to be a typical conformation when comparing it to the coordination modes for these ligands on several metal centres discussed before in Section 2.6 in Chapter 2. The corresponding Rh1-S1, Rh1-S2, Rh1-N4 and Rh1-O1 bond distances are found to be equal to 2.339(1), 2.330(1), 2.087(4) and 2.133(3) Å, respectively. Two triphenylphosphine ligands coordinated *trans* to each other on the axial axis of the octahedral metal centre having respective Rh1-P1 and Rh1-P2 bond lengths of 2.361(1) and 2.369(1) Å. The angles S1-Rh1-S2 and O1-Rh1-N4 have large values of 101.79(4) and 101.65(13) °, which in conjunction with the bite angles reveals that the octahedral conformation is largely distorted around the equatorial position.

The nitrogen atom N2 is protonated as concluded from the presence of electron density at a suitable distance from the nitrogen atom. In order to place the proton accurately it was geometrically positioned and refined using a riding model with a fixed N-H distance of 0.88 Å (NH) [ $U_{\text{iso}}(\text{H}) = 1.2U_{\text{eq}}$ ]. However, the nitrogen atom N3 was not found to be protonated, which together with the long C22-S2 distance of 1.780(5) Å and short C22-N3 distance of 1.314(6) Å suggested that the corresponding ligand coordinated in its *enol* form and is therefore in the dianionic form. Unlike the previous structure of [Rh(*N,S*-(*N*-4h2mPT))(CO)(PPh<sub>3</sub>)<sub>2</sub>] that was discussed in Section 6.6.2, the bonds Rh1-S2 and Rh1-N4 have significantly short distances of 2.330(1) and 2.087(4) Å as was already mentioned above. This provided further confirmation that the ligand is in its *enol* conformation, since the sulphur atom S2 coordinated as a mono-charged ligand forming a strong Rh-S bond. The nitrogen atom N4 being deprotonated is also coordinated as a mono-charged ligand onto the metal centre as suggested by the short Rh-N bond length. These observations therefore suggest that the complex has a rhodium(III) centre instead of the expected rhodium(I) centre. The mechanism leading to the oxidation of the Rh(I) centre to the Rh(III) centre to form this complex is not understood yet and further investigations will be required.

The DMSO and acetone molecules in the structure of the [Rh(*N,S*-(*N*-PT))(*S,O*-(*N*-PT))(PPh<sub>3</sub>)<sub>2</sub>] play an important role in stabilizing the crystal packing. Firstly an intermolecular hydrogen bond interaction is found between O4 of the DMSO molecule and N2 on one of the coordinated thiourea ligands as shown in Figure 6.8. This interaction has a distance of 2.931(5) Å and an angle N2-H2...O4 of 154.3 °.

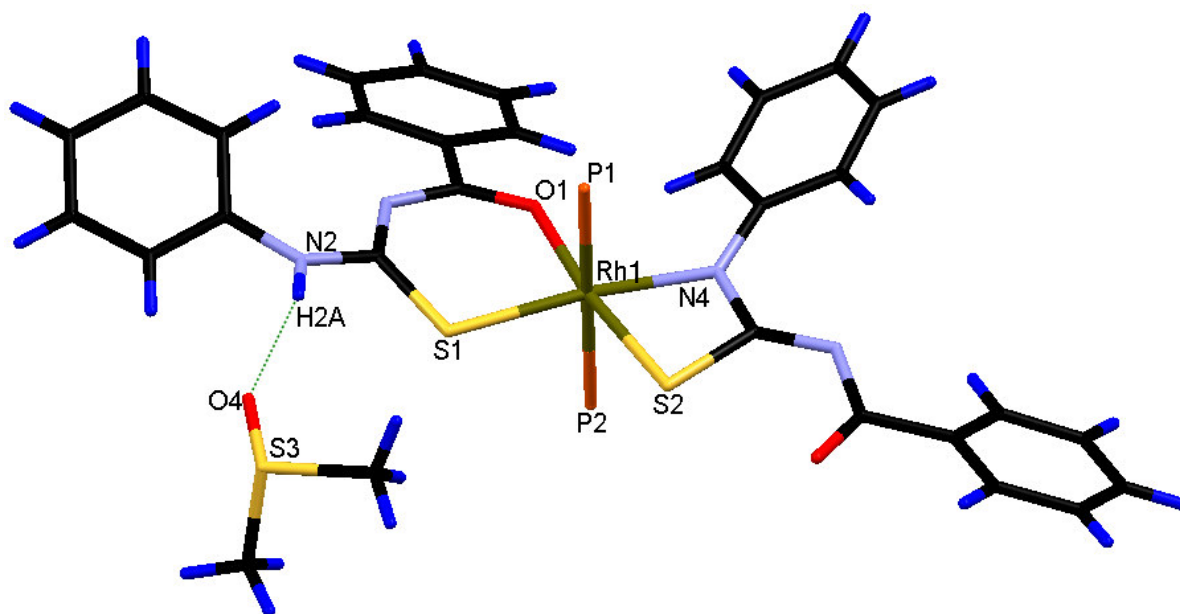


**Figure 6.8** A representation of the hydrogen bond interaction found between a DMSO molecule and a neighbouring  $[\text{Rh}(\text{N},\text{S}-(\text{N-PT}))(\text{S},\text{O}-(\text{N-PT}))(\text{PPh}_3)_2]$  molecule. Some fragments of the compound have been omitted for clarity.  $\text{N2-H2}\cdots\text{O4} = 2.931(5) \text{ \AA}$ ,  $154.3^\circ$ .

There are also several Van der Waals interactions found between the different solvent molecules and the molecules of  $[\text{Rh}(\text{N},\text{S}-(\text{N-PT}))(\text{S},\text{O}-(\text{N-PT}))(\text{PPh}_3)_2]$  as shown in Figure 6.9. This include  $\text{S}\cdots\text{S}$  and  $\text{S}\cdots\text{O}$  interactions between two adjacent DMSO molecules, which are both linked to a couple of complex molecules through several  $\text{C}\cdots\text{C}$  and  $\text{C}\cdots\text{O}$  soft contacts *via* the acetone molecules.



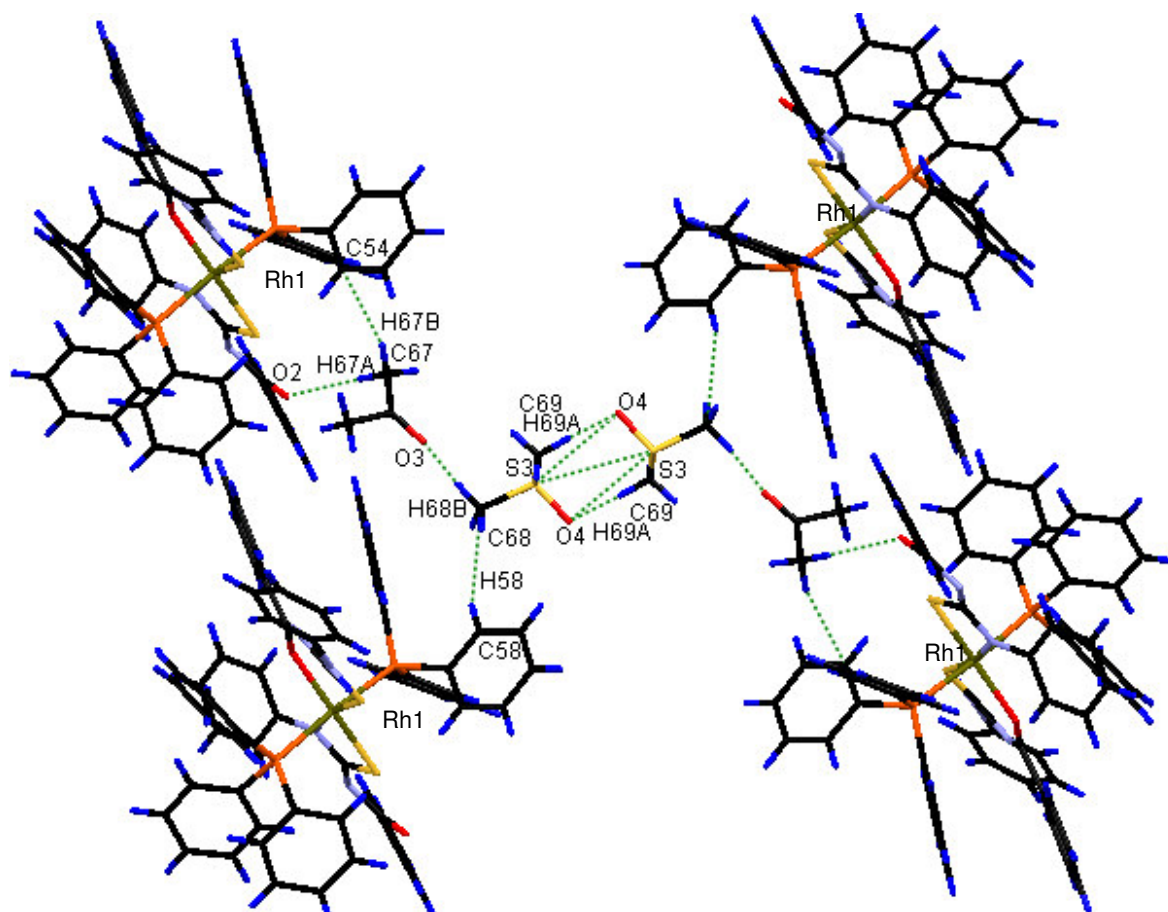


**Figure 6.9** Van der Waals interactions found between the solvent molecules and molecules of the compound  $[\text{Rh}(\text{N},\text{S}-(\text{N-PT}))(\text{S},\text{O}-(\text{N-PT}))(\text{PPh}_3)_2]$ . For distances and angles, see Table 6.8.

**Table 6.8** List of distances and angles for the short contacts defined in Figure 6.9.

Interaction	Distance (Å)	Angle (°)
S3...S3	3.585	-
S3-O4...S3	3.213	91.81
C69-H69A...O4	2.620	125.69
C58-H58...C68	2.866	132.10
C68-H68B...O3	2.608	137.26
C67-H67A...O2	2.536	171.07
C67-H67B...C54	2.779	63.08

#### 6.6.4 Crystal structure of [Rh(COD)(Cl)(*S*-(*N*-PTH))]

(Synthesis described in Section 6.5.1; Supplementary data C3)

[Rh(COD)(Cl)(*S*-(*N*-PTH))] (*N*-PTH = *N*-benzoyl-*N'*-phenylthiourea crystallized in the triclinic space group  $P\bar{1}$  having one independent molecule in the asymmetric unit. The structure is shown in Figure 6.10, where the atom labelling is indicated. Table 6.5 gives the general crystallographic data on the structure, while the most important bond distances and angles are provided in Table 6.10.

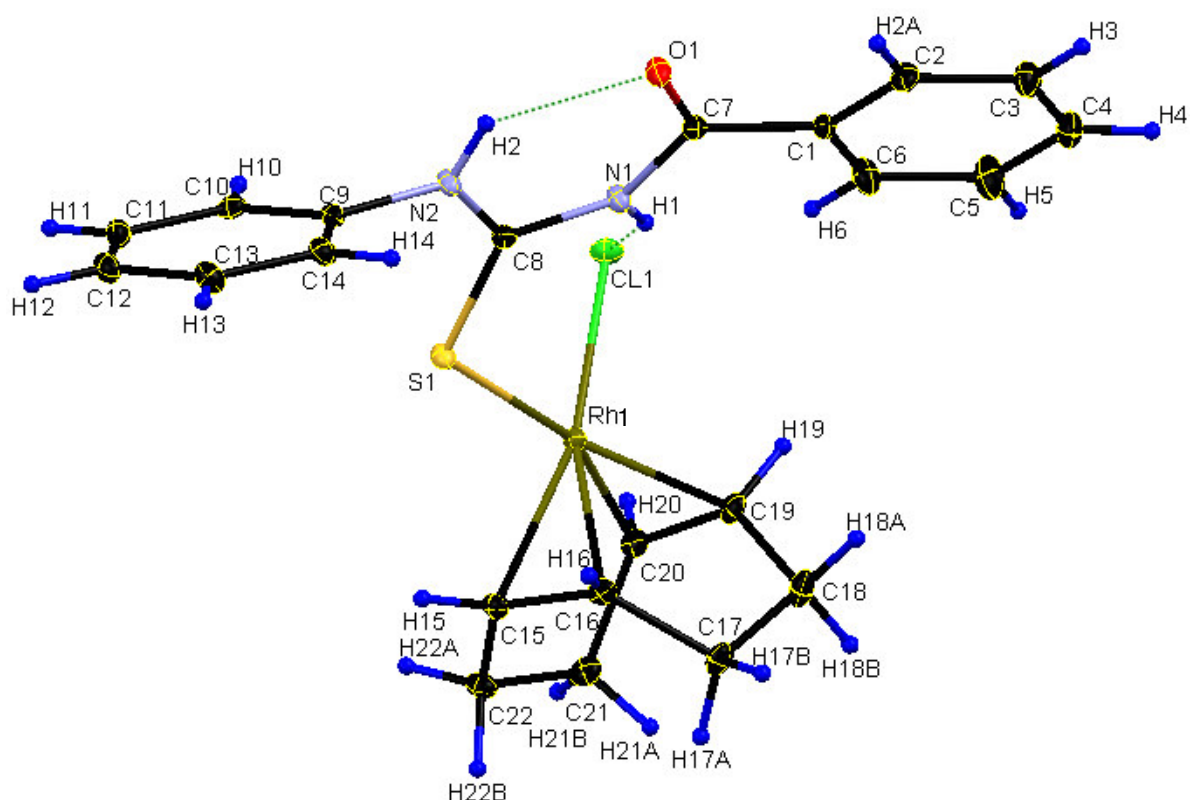


**Figure 6.10** Structural representation of the compound [Rh(COD)(Cl)(*S*-(*N*-PTH))] where the atom numbering scheme is shown (ellipsoid probability = 30%).

**Table 6.10 List of selected bond distances and angles for the compound [Rh(COD)(Cl)(S-(N-PTH))].**

Atoms	Distance (Å)	Atoms	Angle (°)
Rh1-S1	2.380(1)	S1-Rh1-Cl1	94.05(2)
Rh1-Cl1	2.385(1)	Ct(C15,C16)-Rh1-Cl1	178.56
Rh1-C15	2.105(3)	Ct(C15,C16)-Rh1-S1	87.30
Rh1-C16	2.121(3)	Ct(C15,C16)-Rh1-Ct(C19,C20)	87.46
Rh1-C19	2.144(3)	Ct(C19,C20)-Rh1-Cl1	91.19
Rh1-C20	2.170(3)	Ct(C19,C20)-Rh1-S1	174.72
C8-S1	1.696(3)	C8-S1-Rh1	112.68(10)
C7-O1	1.224(3)	S1-C8...C7-O1	162.53
C15-C16	1.410(4)		
C19-C20	1.382(4)		
Ct(C15,C16)-Rh1	1.992		
Ct(C19,C20)-Rh1	2.043		

By calculating centroids for the carbon atoms C15 and C16 as well as C19 and C20 on the COD ring and linking the centroids with the rhodium atom Rh1 as shown in Figure 6.11, it is observed that the structure exhibit a square planar geometry about the rhodium centre. The chlorine atom Cl1 is *cis* to the sulfur atom S1, where the Rh1-Cl1 and Rh1-S1 bond lengths have values of 2.385(1) and 2.380(1) Å, respectively. The Ct(C15,C16)-Rh1 and Ct(C19,C20)-Rh1 distances were calculated to be 1.992 and 2.043 Å, respectively. The angles Ct(C15,C16)-Rh1-S1, Ct(C15,C16)-Rh1-Ct(C19,C20), Ct(C19,C20)-Rh1-Cl1 and S1-Rh1-Cl1 are close to 90 ° having respective values of 87.30, 87.46, 91.19 and 94.05(2) °, whereas the angles Ct(C15,C16)-Rh1-Cl1 and Ct(C19,C20)-Rh1-S1 are slightly bent away from linearity with respective values of 178.56 and 174.72 °. These values all reveal that the square planar conformation of the rhodium complex is only slightly distorted.

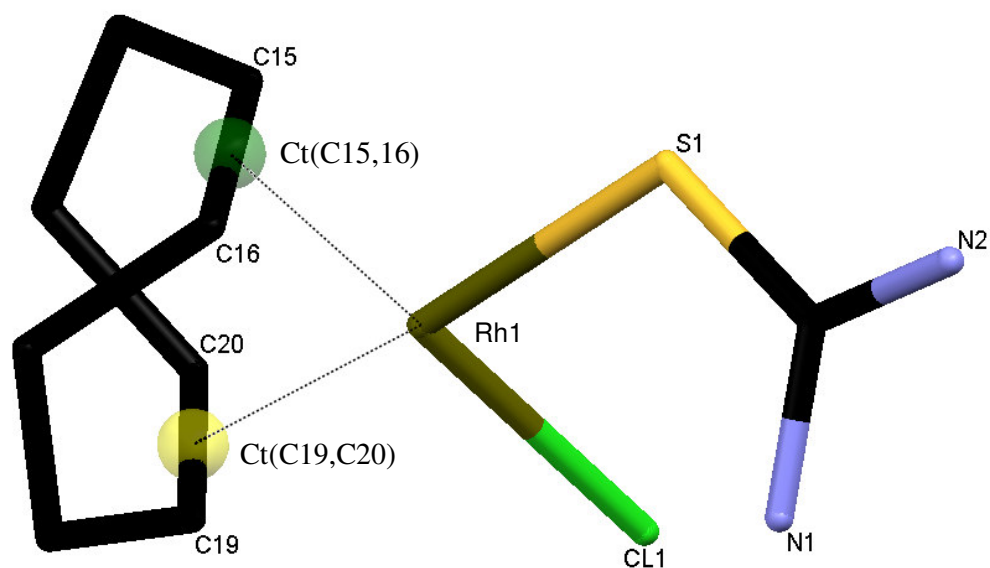


**Figure 6.11** The centroids Ct(C15,C16) and Ct(C19,C20) calculated in order to reveal the square planar conformation of the complex [Rh(COD)(Cl)(S-(N-PTH))]. Some fragments of the structure have been omitted for clarity.

The nitrogen atoms N1 and N2 were both found to be protonated due to the presence of electron density at a suitable distance from these atoms. In order to place these protons accurately they were geometrically positioned and refined using a riding model with a fixed N-H distance of 0.88 Å (NH) [ $U_{\text{iso}}(\text{H}) = 1.2U_{\text{eq}}$ ]. This suggested that the coordinated ligand *N*-PTH is neutral and in the *keto* formation, which is also confirmed by the double bond character of the C8-S1 and C7-O1 bonds having distances of 1.696(3) and 1.224(3) Å, respectively.

Several hydrogen bond interactions are found in the crystal packing of the compound [Rh(COD)(Cl)(S-(N-PTH))] as illustrated in Figure 6.12. The intramolecular hydrogen bonding between O1 and N2 (**a**), which is typical in thiourea ligands as was shown in Chapter 4, has an interaction distance of 2.657(3) Å and an angle N2-H2...O1 of 131.7°. This interaction suggested that the preferred orientation of the free ligand to have its oxygen atom *trans* to the sulfur atom as was discussed in Chapter 4, is translated to the orientation found in the compound [Rh(COD)(Cl)(S-(N-PTH))]. Intramolecular hydrogen bonding was also observed between the nitrogen atom N1 and the chlorine atom Cl1, with a distance of 3.253(3) Å and an angle N1-H1...Cl1 of 147.7°, which added onto the effect of stabilizing the orientation within the rhodium structure. Since two molecules are orientated about an inversion centre, the oxygen atom O1 as well as the nitrogen atom N2 was found in close

approximation to the oxygen atom in the next molecule. As a result intermolecular hydrogen bonding (b) between the atoms N2 and O1 were established with a distance of 3.053(3) Å and an angle of 140.8 °. The intermolecular hydrogen bonding leads to a layered assembly of the molecules, extending approximately parallel to (011).

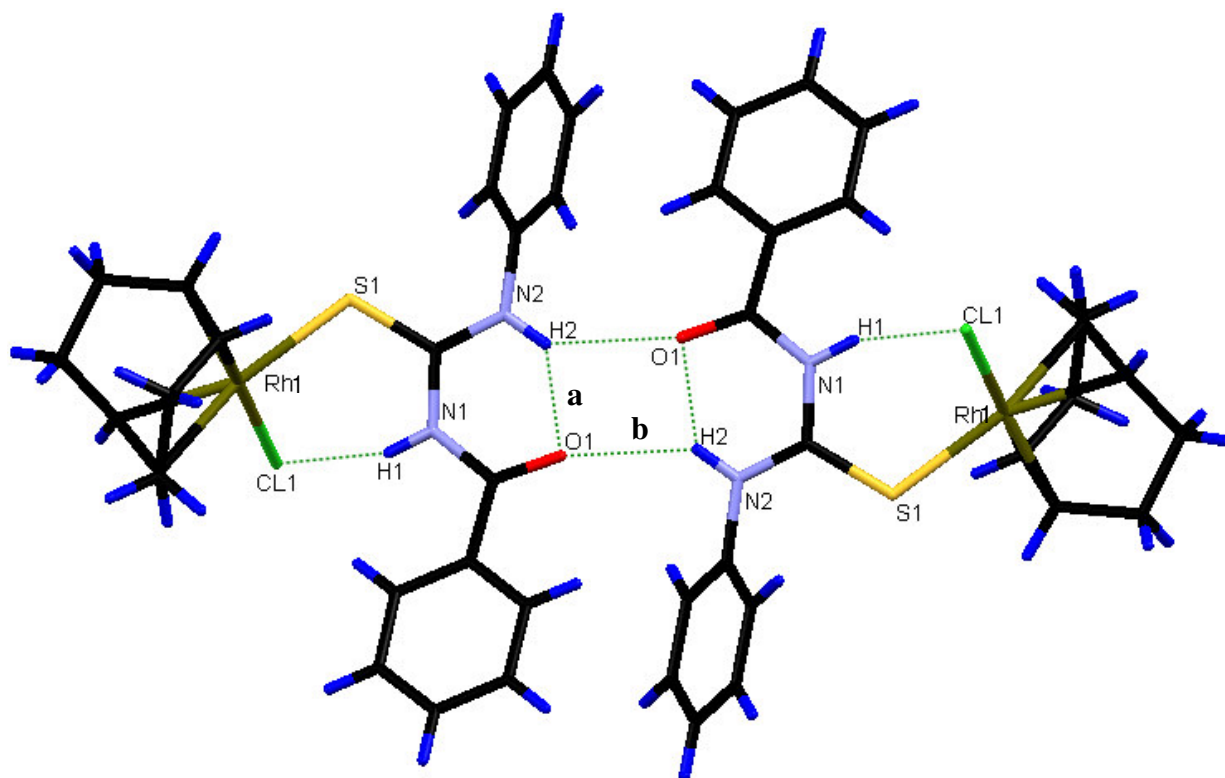


**Figure 6.12** An illustration of hydrogen bonding found in the crystal packing of the compound [Rh(COD)(Cl)(S-(N-PTH))]. Distances and angles: N2-H8...O1 (a) = 2.657(3) Å, 131.7 °; N2-H2...O1 (b) = 3.053(3) Å, 140.8 °; N1-H1...Cl1 = 3.253(3) Å, 147.7 °.

The molecules in the packing are orientated in such a way that the COD rings are in close approximation to each as shown in Figure 6.13. These orientations are stabilized by several Van der Waals interactions that exist between these rings of which some of these interactions are indicated in Figure 6.13. These short contacts are suspected to be the cause of the distortion found in the COD ring as six of its atoms are pulled in various directions.

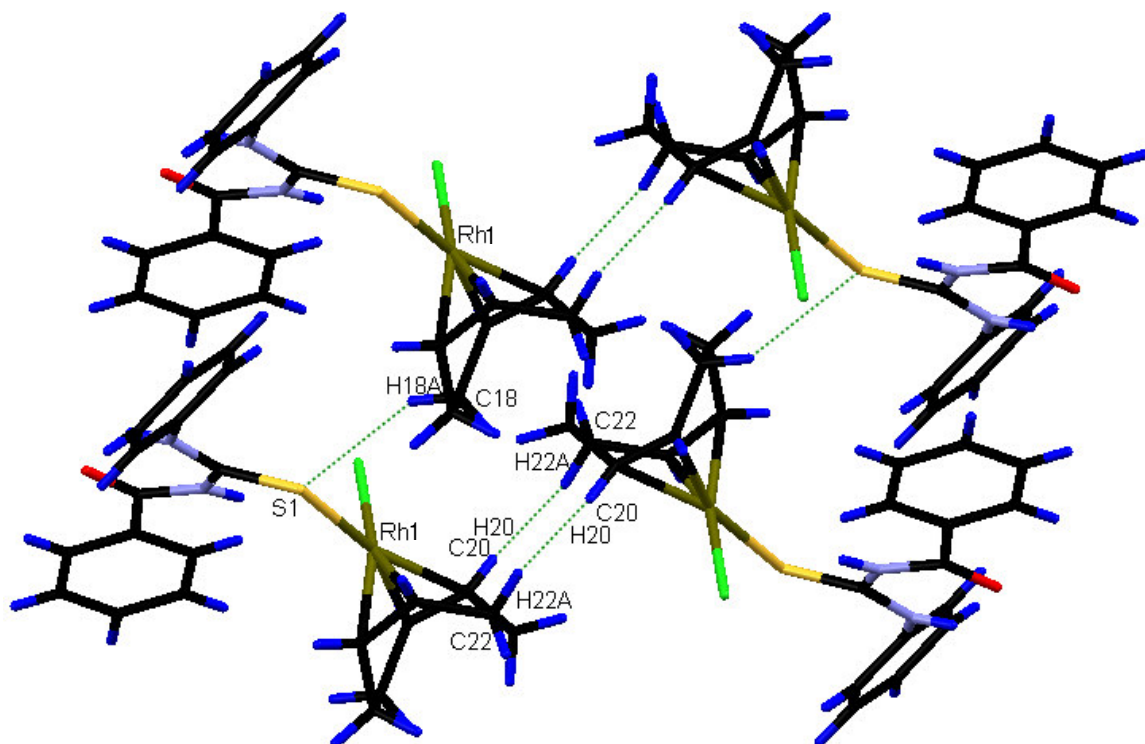


**Figure 6.13** An illustration of some short contacts that stabilizes the crystal packing of the compound  $[\text{Rh}(\text{COD})(\text{Cl})(\text{S}-(\text{N-PTH}))]$ . Distances and angles:  $\text{C18-H18A}\cdots\text{S1} = 2.711 \text{ \AA}$ ,  $140.1^\circ$ ;  $\text{H20}\cdots\text{H22A} = 2.324 \text{ \AA}$ .

This structure has recently been published in *Acta Crystallographica Section E*.<sup>12</sup>

<sup>12</sup> Kotze, P. D. R.; Roodt, A.; Venter, J. A.; Otto, S. (2010) *Acta Cryst.*, **E66**, m1028

### 6.6.5 Crystal structure of [Rh(COD)(Cl)(*S*-(*N*-tmPTH))]

(Synthesis described in Section 6.5.2; Supplementary data C4)

[Rh(COD)(Cl)(*S*-(*N*-tmPTH))] (*N*-tmPTH = *N*-benzoyl-*N'*-2,4,6-trimethylphenylthiourea) crystallized in the monoclinic space group having one independent molecule in the asymmetric unit. The structure is shown in Figure 6.14, where the atom labelling is indicated. Table 6.5 gives the general crystallographic data on the structure, while the most important bond distances and angles are provided in Table 6.11.

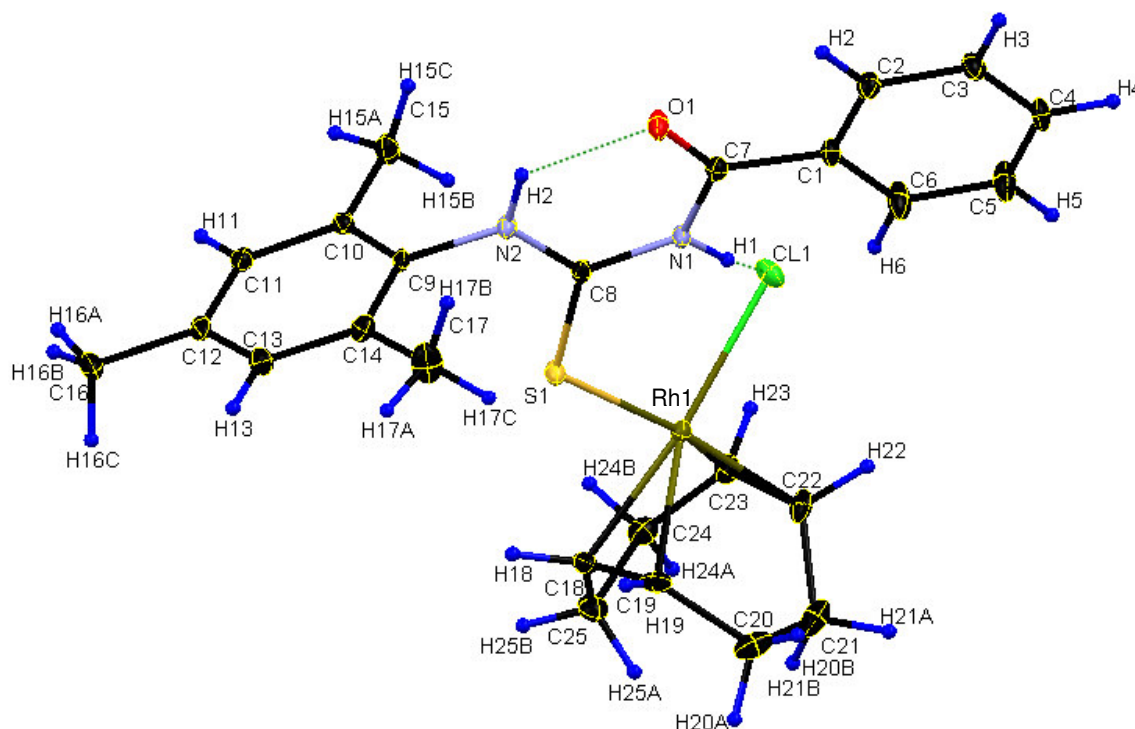


**Figure 6.14** A structural representation of the compound [Rh(COD)(Cl)(*S*-(*N*-tmPTH))] where the atom labelling is given (ellipsoid probability = 30 %).

**Table 6.11 List of selected bond distances and angles for the compound [Rh(COD)(Cl)(S-(*N*-tmPTH))].**

Atoms	Distance (Å)	Atoms	Angle (°)
Rh1-S1	2.351(1)	S1-Rh1-Cl1	95.99(3)
Rh1-Cl1	2.359(1)	Ct(C18,C19)-Rh1-Cl1	173.52
Rh1-C18	2.139(3)	Ct(C18,C19)-Rh1-S1	87.64
Rh1-C19	2.104(3)	Ct(C18,C19)-Rh1-Ct(C22,C23)	87.42
Rh1-C22	2.150(3)	Ct(C22,C23)-Rh1-Cl1	90.01
Rh1-C23	2.140(3)	Ct(C22,C23)-Rh1-S1	167.95
C8-S1	1.698(3)	C8-S1-Rh1	119.49(9)
C7-O1	1.224(3)	S1-C8...C7-O1	-164.38
C18-C19	1.397(4)		
C22-C23	1.389(4)		
Ct(C18,C19)-Rh1	2.003		
Ct(C22,C23)-Rh1	2.030		

Centroids for the carbon atoms C18 and C19 as well as C22 and C23 on the COD ring were calculated and linked to the rhodium atom Rh1 as shown in Figure 6.15, where the Ct(C18,C19)-Rh1 and Ct(C22,C23)-Rh1 distances were calculated to be 2.003 and 2.030 Å, respectively. It is observed in Figure 6.15 that the structure exhibit a square planar geometry about the rhodium centre similar to the complex described in Section 6.6.4. The chlorine atom Cl1 is *cis* with respect to the sulfur atom S1, where the Rh1-Cl1 and Rh1-S1 bonds have respective distances of 2.359(1) and 2.351(1) Å. The angles Ct(C18,C19)-Rh1-S1, Ct(C18,C19)-Rh1-Ct(C22,C23), Ct(C22,C23)-Rh1-Cl1 and S1-Rh1-Cl1 are also close to perpendicularity having respective values of 87.64, 87.42, 90.01 and 95.99(3) °. The angles Ct(C18,C19)-Rh1-Cl1 and Ct(C22,C23)-Rh1-S1 on the other hand are fairly bent away from linearity having respective values of 173.52 and 167.95 °, which lead to a significant distortion of the square planar conformation.



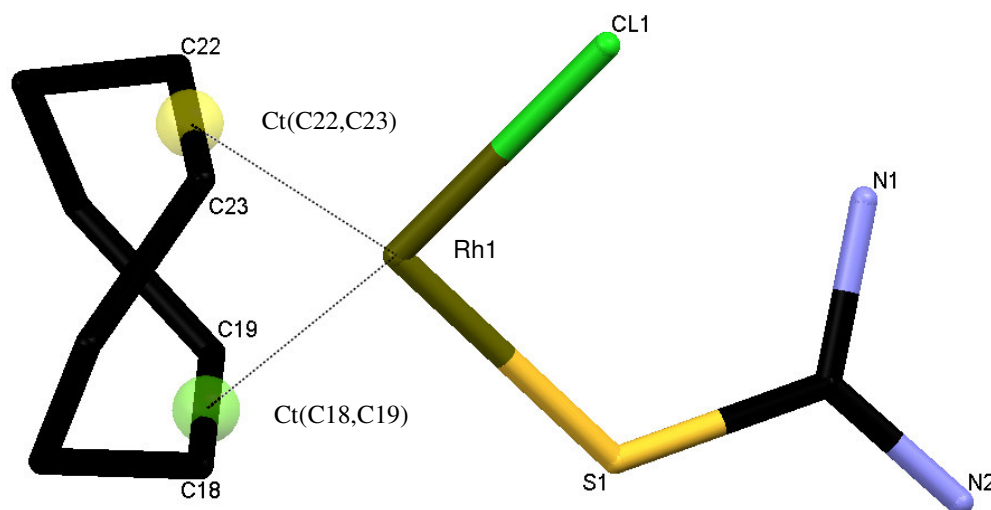


**Figure 6.15** The centroids Ct(C18,C19) and Ct(C22,C23) calculated to show the square planar conformation of the complex [Rh(COD)(Cl)(*S*-(*N*-tmPTH))]. Some fragments of the structure have been omitted for clarity.

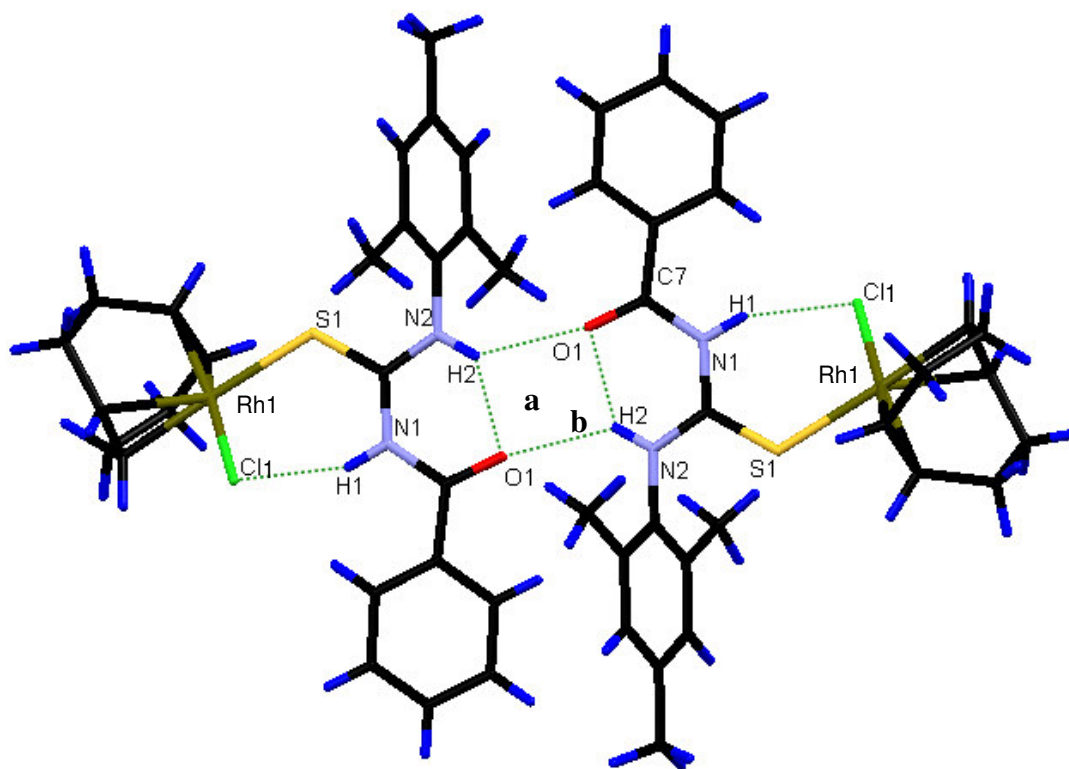


**Figure 6.16** Some hydrogen bond interactions found in the crystal packing of the compound [Rh(COD)(Cl)(*S*-(*N*-tmPTH))]. Distances and angles: N2-H2...O1 (a) = 2.668(3) Å, 130.2 °; N2-H2...O1 (b) = 3.161(3) Å, 139.5 °; N1-H1...Cl1 = 3.108(2) Å, 144.7 °.

Similar hydrogen bond interactions are found in the crystal packing of the compound  $[\text{Rh}(\text{COD})(\text{Cl})(S\text{-(}N\text{-tmPTH))}]$  as was observed for the structure of  $[\text{Rh}(\text{COD})(\text{Cl})(S\text{-(}N\text{-PTH))}]$  in Section 6.4.2, as illustrated in Figure 6.12. The preferred orientation of the ligand as was presented and discussed in Section 4.3 is also translated to the orientation found in the structure of  $[\text{Rh}(\text{COD})(\text{Cl})(S\text{-(}N\text{-tmPTH))}]$ , where the oxygen atom O1 is also *trans* with respect to the sulphur atom S1. Furthermore, intramolecular hydrogen bonding exist between this atom O1 and the nitrogen atom N2 (**a**) having an interaction distance of 2.668(3) Å and an angle N2-H2...O1 of 130.2 °. An intramolecular hydrogen bond interaction was also observed between the nitrogen atom N1 and the chlorine atom Cl1 having a distance of 3.108(2) Å and an angle N1-H1...Cl1 of 144.7 °. An intermolecular hydrogen bond interaction (**b**) also exist between the atoms N2 and O1 between molecules that are orientated around a centre of symmetry. This interaction has a distance of 3.161(3) Å and an angle of 139.5 ° and leads to the formation of dimers in the crystal packing.

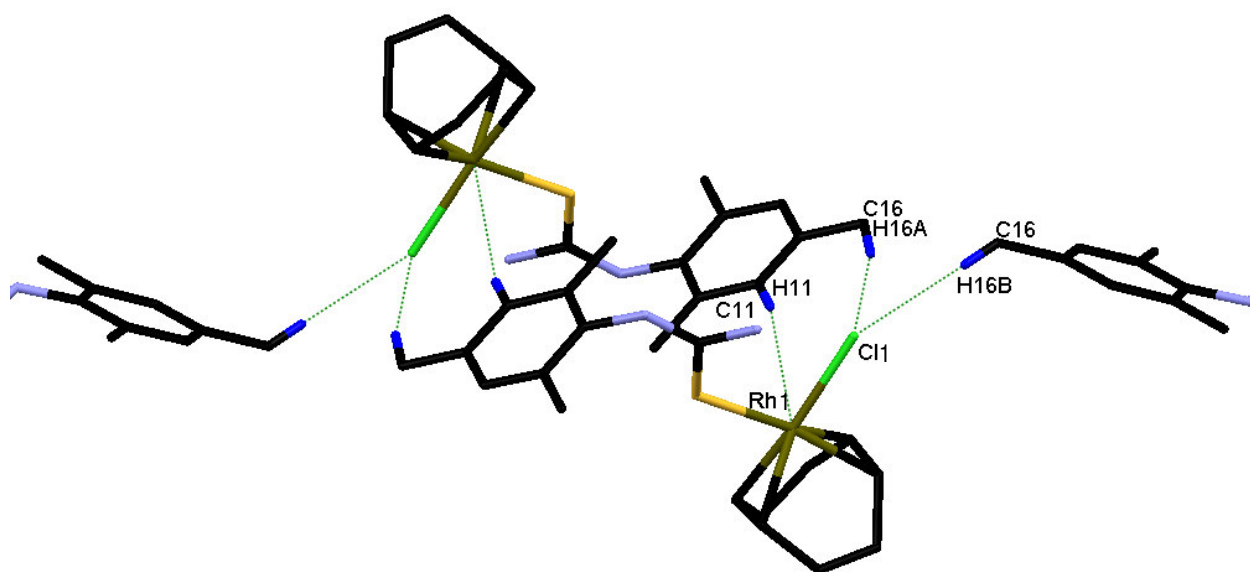


**Figure 6.17** A representation of some short contacts that stabilizes the crystal packing of the compound  $[\text{Rh}(\text{COD})(\text{Cl})(S\text{-(}N\text{-tmPTH))}]$ . Some fragments of the molecules as well as most of the hydrogens have been omitted for clarity. Distances and angles: C11-H11...Rh1 = 3.159 Å, 157.3 °; C16-H16A-Cl1 = 2.925 Å, 164.3 °; and C16-H16B-Cl1 = 2.768 Å, 137.0 °.

A large amount of soft contacts also exist in the crystal packing of  $[\text{Rh}(\text{COD})(\text{Cl})(S\text{-(}N\text{-tmPTH))}]$ , which primarily involve C...C contacts. However, a few exceptional short contacts are found, which involve Rh...C and Cl...C Van der Waals

interactions as shown in Figure 6.17. These interactions are given by C11-H11...Rh1 = 3.159 Å, 157.3 °; C16-H16A-C11 = 2.925 Å, 164.3 °; and C16-H16B-C11 = 2.768 Å, 137.0 °.

## 6.7 Results and discussion

### 6.7.1 [Rh(*S,O*-thioureato)(CO)<sub>2</sub>] complexes

Originally only thiourea ligands with formula PhC(O)NHC(S)**NHR** (thus where the terminal nitrogen is substituted by only one R-group) were utilized for the purpose of synthesizing the [Rh(*S,O*-thioureato)(CO)<sub>2</sub>] complexes from the route discussed in Section 6.3. A rapid IR analysis was performed on the different products that were obtained from these ligands, which indicated the presence of a dicarbonyl rhodium complex as identified by two distinct carbonyl stretching peaks. However, by comparing the different spectra of the different products it was observed that different rhodium species were present. Generally, two different main products were observed simultaneously at  $\pm 2070$  and  $2000\text{ cm}^{-1}$  as well as  $\pm 2040$  and  $1985\text{ cm}^{-1}$  as were indicated by the relative intensities of the peaks. Furthermore, these complexes were confirmed as unstable upon drying, as all of the products turned to dark red-brown oils in the process. An IR analysis on these oils revealed a different set of carbonyl peaks at  $\pm 2020$  and  $1965\text{ cm}^{-1}$ , indicating that the original products underwent a transformation or decomposition to other rhodium species most probably by molecular oxygen oxidation. Drying the samples under vacuum still resulted in the formation of oils. It seemed that the water molecules present held the solid product intact. Similar observations were made by Cauzzi *et al.*<sup>13</sup> when they attempted to synthesize a similar complex from [Rh( $\mu$ -Cl)(CO)<sub>2</sub>]<sub>2</sub>. Since the products were only stable as long as they were enclosed by solvent molecules, exact yields of the products were difficult to obtain. A summary of the different products obtained from the reaction of [Rh( $\mu$ -Cl)(CO)<sub>2</sub>]<sub>2</sub> with different thiourea ligands is given in Table 6.1. The well-known [Rh(*O,O*-acac)(CO)<sub>2</sub>] complex (acac = acetylacetonato) was also synthesized for the purpose as a reference compound, which is also given in Table 6.1.

---

<sup>13</sup> Cauzzi, D.; Lanfranchi, M.; Marzolini, G.; Predieri, G.; Tiripicchio, A.; Costa, M.; Zandoni, R. (1995) *J. Organomet. Chem.*, **488**, 115.

Based on the observations made in the literature as was discussed in Section 2.6 in Chapter 2, *S,O*-thiourea ligands can coordinate to metal centres in different ways. It was therefore possible that rhodium species with *S,O*-, *N,S*- or *S*- coordination can be obtained under the conditions. Although acac is somewhat different from the thiourea ligands, it is expected that the carbonyl stretching frequency values for  $[\text{Rh}(\text{O},\text{O}\text{-acac})(\text{CO})_2]$  should not differ that much from those for the  $[\text{Rh}(\text{S},\text{O}\text{-thioureato})(\text{CO})_2]$  complexes. It is therefore expected that the primary product as defined in Table 6.1 might probably be attributed to the  $[\text{Rh}(\text{S},\text{O}\text{-thioureato})(\text{CO})_2]$  complexes.

As indicated in Table 6.1, the secondary product has much lower  $\nu_{\text{CO}}$  values than the primary product, which suggested a higher electron-donation of the ligand to the rhodium centre. This could be the cause of either *N,S*- or *S*-coordination. With an *N,S*-coordination the close proximation of the nitrogen and sulphur atoms to the metal centre, which lead to the formation of a 4-membered ring, would lead to stronger  $\sigma$ -donation. This in turn will enhance the electron density of the metal centre compared to a 6-membered ring, where electron-delocalization occurs over a long distance. With an *S*-coordination the resulting complex is expected to have an electron-rich chlorido ligand in its coordination sphere in order to balance out the charge, since under the particular conditions no other suitable ligand exist for this purpose. The presence of both the S and Cl atoms on the metal centre would therefore have a higher  $\sigma$ -donation to the metal centre compare to a *S/O* combination. Later in this chapter these postulations will be shown to be feasible, since several structures were obtained in the present study that involves these type of coordination modes.

With the observations made above, several attempts were made to identify these complexes and also to direct the synthesis specifically towards the formation of the  $[\text{Rh}(\text{S},\text{O}\text{-thioureato})(\text{CO})_2]$  complexes. Crystallization techniques from several solvents ranging from acetone, ether, toluene, benzene, DCM, chloroform, etc. did not result in any crystal formation of the different products. Also NMR techniques could not provide suitable spectra for the different products. Firstly, several peaks were observed in the aromatic region of the  $^{13}\text{C}$  NMR spectrum between 120-140 ppm, which were attributed to the presence of different species in one sample. This was also indicated by several peaks observed at chemical shifts between 160-200 ppm, which is attributed to the CO groups present in the sample. Secondly,  $^1\text{H}$  NMR provided similar results and also indicated that the samples consisted of over 70 % of water. Therefore, having no structural data or proper NMR spectra, the products could not

be identified. It was therefore necessary to modify the synthetic route to enable more stable products.

A first modification included the use of sodium acetate during the reaction of  $[\text{Rh}(\mu\text{-Cl})(\text{CO})_2]_2$  with the different thiourea ligands. Using a basic medium in which the reaction can occur seemed logical at the time with the assumption that the secondary product involved a rhodium *S*-coordinated thiourea complex. Knowing that the oxygen atom of the thiourea ligand involved is held in its orientation *via* a hydrogen bond with one of the nitrogen atoms (see Chapter 4), the addition of the sodium acetate was expected to break the hydrogen bond by deprotonation and also enhance the deprotonation of the nitrogen atom between the two keto groups. Furthermore the addition of sodium would result in the formation of sodium chloride, which could enhance the removal of the chloride atoms by washing the precipitated product with water. The basic medium should thus enhance the possible coordination of the thiourea ligand *via* an *S,O*-fashion to the rhodium centre. Several attempts were made to synthesize the  $[\text{Rh}(\text{S},\text{O}\text{-thioureato})(\text{CO})_2]$  complexes *via* the route provided in Figure 6.1 using the modification of adding sodium acetate in the second step of the reaction scheme. At first it seemed successful in some cases where a single rhodium dicarbonyl complex was observed on the IR spectrum from peaks at  $\pm 2070$  and  $2000\text{ cm}^{-1}$ , which was expected to involve the  $[\text{Rh}(\text{S},\text{O}\text{-thioureato})(\text{CO})_2]$  complex. However, traces of other products were still observed in the IR spectra in many of the attempts and the final product was still found unstable upon drying.

Another modification involved the use of *S,O*-thiourea ligands with the formula  $\text{PhC}(\text{O})\text{NHC}(\text{S})\text{NR}_1\text{R}_2$  (thus where the terminal nitrogen is substituted by two R groups), where the hydrogen bond between the oxygen and terminal nitrogen is prevented, allowing free rotation of the carbonyl moiety. As was shown before in the literature<sup>14a,b,c,d</sup> this proved to be the determining factor that allowed these *S,O*-thiourea ligands to coordinate in a *S,O*-fashion to several metal centres. Following this discovery, three thiourea ligands of the form  $\text{PhC}(\text{O})\text{NHC}(\text{S})\text{NR}_1\text{R}_2$  were synthesized and characterized as was already presented in Chapter 3. These ligands were then also utilized for the synthesis of the corresponding  $[\text{Rh}(\text{S},\text{O}\text{-thioureato})(\text{CO})_2]$  complexes using the same methodology described in Figure 6.1.

<sup>14</sup> a) Koch, K. R.; du Toit, J.; Cairns, M. R.; Sacht, C (1994) *J. Chem. Soc., Dalton Trans.*, 785. b) Koch, K. R.; Hallale, O.; Bourne, S. A.; Miller, J.; Bacsá, J. (2001) *J. Mol. Struct.*, **561**, 185. c) Westra, A. N.; Esterhuysen, C.; Koch, K. R. (2004) *Acta Cryst.*, **C60**, m395. d) Westra, A. N.; Bourne, S. A.; Esterhuysen, C.; Koch, K. R. (2005) *Dalton Trans.*, 2162 and references within.

IR analysis on the consequent products showed satisfactory results, as only one rhodium dicarbonyl species was observed from the IR data for each case. The products with the corresponding  $\nu_{\text{CO}}$  values are reported in Table 6.2.

It is clear from Table 6.2 that the carbonyl stretching frequency values for the  $[\text{Rh}(\text{S},\text{O}\text{-thioureato})(\text{CO})_2]$  complexes with the ligands  $\text{PhC}(\text{O})\text{NHC}(\text{S})\text{NR}_1\text{R}_2$  correspond with those of the primary products of the other  $[\text{Rh}(\text{S},\text{O}\text{-thioureato})(\text{CO})_2]$  complexes containing the ligands  $\text{PhC}(\text{O})\text{NHC}(\text{S})\text{NHR}$  as was reported in Table 6.1. This provided additional confirmation that the primary products might indeed be the desired  $[\text{Rh}(\text{S},\text{O}\text{-thioureato})(\text{CO})_2]$  complexes. This was later proven to be the case following the successful characterization of the  $[\text{Rh}(\text{S},\text{O}\text{-thioureato})(\text{CO})(\text{PR}_1\text{R}_2\text{R}_3)]$  complexes of the ligand *N*-benzoyl-*N',N'*-diphenylthiourea, obtained from the first  $[\text{Rh}(\text{S},\text{O}\text{-thioureato})(\text{CO})_2]$  complex defined in Table 6.2 (where  $\text{R}_1, \text{R}_2 = \text{phenyl, phenyl}$ ), which will be discussed in more detail in Chapter 7. Unfortunately the  $[\text{Rh}(\text{S},\text{O}\text{-thioureato})(\text{CO})_2]$  complexes defined in Table 6.2 also transformed into dark brown oils upon drying and absolute characterization of these complexes could not be obtained.

Due to the instability of the complexes upon drying, and following the discovery that these complexes neither dissolve in methanol nor ethanol, it was decided to wash the precipitated products with methanol/ethanol after washing it with water first. The expectation was to remove the excess of water and also allow the products to dry quicker, since both alcohols evaporate much faster than water. IR spectroscopy clearly indicated that most of the water was removed, however, drying the products still resulted in the formation of oils. It was therefore decided to keep the few wet samples that only involved a single rhodium product just as it were for further study by oxidative addition of MeI, since a small amount of either alcohol was not expected to have significant influence on the reaction parameters. These studies will be presented in Chapter 8.

### 6.7.2 [Rh(*S,O*-thioureato)(CO)(PPh<sub>3</sub>)] complexes

It was clear that the rhodium dicarbonyl species containing thiourea ligands were only stable in solution and also difficult to analyze and identify. An alternative modification therefore involved the use of phosphine ligands to form more stable rhodium complexes of the type [Rh(*S,O*-thioureato)(CO)(PPh<sub>3</sub>)]. Apart from the greater stability many monocarbonylphosphine rhodium complexes have been shown in the literature to easily crystallize from various solvent systems. Thus several attempts were made to rather synthesize [Rh(*S,O*-thioureato)(CO)(PPh<sub>3</sub>)] complexes following the route discussed in Section 6.4. In the process of finding suitable conditions for the synthesis of these complexes structural data on a new type of rhodium thiourea complexes have been obtained where the corresponding thiourea ligands coordinated in different modes, which have to date not been reported.<sup>15</sup> The X-ray characterization of these complexes was presented in Sections 6.6.2 and 6.6.3, whereas their synthesis is discussed in Sections 6.7.3 and 6.7.4.

The products obtained from the first attempted synthetic route described in Section 6.4 were confirmed to be monocarbonyl rhodium species from the IR spectra of these compounds. A single carbonyl stretching peak was observed in the IR spectrum at around 1970-1975 cm<sup>-1</sup> for several of the expected [Rh(*S,O*-thioureato)(CO)(PPh<sub>3</sub>)] complexes as shown in Table 6.3. The [Rh(acac)(CO)(PPh<sub>3</sub>)] complex was also synthesized and analyzed as a reference compound, of which the  $\nu_{\text{CO}}$  value is also provided in Table 6.3. In some cases the Vaska-type complex [Rh(Cl)(CO)(PPh<sub>3</sub>)<sub>2</sub>] also precipitated as a by-product, due to the presence of chloride atoms in the reaction mixture. This was eliminated by washing the [Rh(*S,O*-thioureato)(CO)<sub>2</sub>] complex with large portions of water before performing the synthesis described in Figure 6.2.

By comparing the  $\nu_{\text{CO}}$  values of the [Rh(*S,O*-thioureato)(CO)(PPh<sub>3</sub>)] complexes with [Rh(acac)(CO)(PPh<sub>3</sub>)] it seemed probable at first that the specific products defined in Table 6.3 might be of the type [Rh(*S,O*-thioureato)(CO)(PPh<sub>3</sub>)]. However, analysis by NMR spectroscopy confirmed otherwise. The <sup>31</sup>P NMR spectrum revealed a singlet observed at  $\pm$  25-27 ppm (unreferenced) for each complex depending on the solvent used. This suggested two possible scenarios: i) This either indicated that the PPh<sub>3</sub> was not coordinated onto the Rh

---

<sup>15</sup> CSD version 5.31, updated May 2010. Allen, F. H. (2002). *Acta Cryst.*, **B58**, 380

centre and might have been catalytically oxidized, since no Rh-P coupling was observed or ii) the possible rhodium phosphine complex might be in a fast exchange equilibrium leading to broadening of the complex as well as free phosphine peaks on the NMR spectra, which is later shown to be possible in a phosphine exchange study presented in Chapter 9. Analysis of a clean pre-synthesized triphenylphosphine oxide *via*  $^{31}\text{P}$  NMR spectroscopy revealed an unreferenced chemical shift of  $\pm 27$  ppm. Referencing the phosphine oxide with a phosphoric acid standard provided a chemical shift of 29.9 ppm.

$^1\text{H}$  and  $^{13}\text{C}$  NMR spectra were also obtained for the products and triphenylphosphine oxide. A comparison of the chemical shifts observed on the  $^1\text{H}$  and  $^{13}\text{C}$  NMR spectra for the different compounds revealed that the major compound present in each sample was triphenylphosphine oxide, since the chemical shifts for the triphenylphosphine oxide were observed in each case. Under the particular reaction conditions it seemed that the triphenylphosphine was catalytically oxidized by the rhodium present in the sample. The type of rhodium species that were present could not be identified by NMR. Furthermore crystals of the particular complexes defined in Table 6.3 could also not be obtained in either of the solvents acetone, DCM, chloroform, toluene, benzene, DMF, DMSO, nitromethane, acetonitrile or ether and therefore no structural data could be obtained for these products.

The modifications on the synthetic procedure described in Figure 6.1 that were discussed in Section 6.6.1, were also utilized for the purpose of synthesizing the desired  $[\text{Rh}(S,O\text{-thioureato})(\text{CO})(\text{PPh}_3)]$  species. For many of the attempts that were made with these modifications some interesting results were obtained, which will be presented and discussed in Sections 6.7 and 6.8. Despite the failure of successfully synthesizing and characterizing the complexes defined in Table 6.3, final success was achieved upon utilizing the thiourea ligand *N*-benzoyl-*N',N'*-diphenylthiourea (*N*-dPTH), which provided the desired  $[\text{Rh}(S,O\text{-}(N\text{-dPTH})(\text{CO})(\text{PR}_1\text{R}_2\text{R}_3))]$  complexes with several tertiary phosphine ligands in ether. As was already mentioned the synthesis and characterization of these complexes will be presented and discussed in Chapter 7.



### 6.7.3 [Rh(*N,S*-thioureato)(CO)(PPh<sub>3</sub>)<sub>2</sub>] complexes

It was mentioned in Section 6.6.1 that one of the modifications that was applied to the synthetic route in Figure 6.1 involved the addition of sodium acetate during the reaction of [Rh( $\mu$ -Cl)(CO)<sub>2</sub>]<sub>2</sub> with some thiourea ligand. As part of the strategy to ensure the formation of one specific product, this modification was also applied for the synthesis of [Rh(*S,O*-thioureato)(CO)(PPh<sub>3</sub>)] complexes. After performing the synthesis described in Figure 6.1 with the necessary modification, the addition of PPh<sub>3</sub> to the resulting complexes in ether provided a surprising result where the consequent products showed to have carbonyl stretching frequency shifts at around 1920 cm<sup>-1</sup>. These products were found to be [Rh(*N,S*-thioureato)(CO)(PPh<sub>3</sub>)<sub>2</sub>] complexes as was elucidated by a X-ray analysis on one of these complexes. Since the [Rh(*S,O*-thioureato)(CO)<sub>2</sub>] complexes were directly used after their synthesis from the route in Figure 6.1, it was suspected that some of the sodium acetate dissolved along with the complexes in the ether solution. This could therefore have promoted a base-catalysed rearrangement of the thiourea ligand on the metal centre to enforce the *N,S*-coordination of the ligand to the metal centre in order to provide enough space for the incoming PPh<sub>3</sub> molecules to coordinate to the metal centre. This was easily confirmed by washing the [Rh(*S,O*-thioureato)(CO)<sub>2</sub>] complex with large portions of water before allowing it to react with PPh<sub>3</sub> in ether, which did not provide the corresponding [Rh(*N,S*-thioureato)(CO)(PPh<sub>3</sub>)<sub>2</sub>] complex.

This opened up a new venue of chemistry to be explored as these specific complexes have not been discovered before. Similar complexes have been reported before by Roodt *et al.*<sup>16</sup> with tropolonate ligands that form mono-charged 5-membered rings around the metal centre, which allowed the coordination of two YR<sub>1</sub>R<sub>2</sub>R<sub>3</sub> ligands (with Y being either As or P). In the particular case a surprising mono-charged 4-membered ring formed as will be shown later when discussing the structural data of the [Rh(*N,S*-thioureato)(CO)(PPh<sub>3</sub>)<sub>2</sub>] complex that was obtained. Table 6.4 gives the range of [Rh(*N,S*-thioureato)(CO)(PPh<sub>3</sub>)<sub>2</sub>] products that were obtained together with the corresponding  $\nu_{\text{CO}}$  values.

Although all four of these complexes defined in Table 6.4 crystallized upon evaporation of the solvent (ether), only one of these complexes provided suitable crystals for single-crystal

---

<sup>16</sup> Roodt, A.; Otto, S.; Steyl, G. (2003) *Coord. Chem. Rev.*, **245**, 121.

X-ray diffraction, namely  $[\text{Rh}(\text{N},\text{S}-(\text{N}-4\text{h}2\text{mPT}))(\text{CO})(\text{PPh}_3)_2]$  ( $\text{N}-4\text{h}2\text{mPT}$  = mono-deprotonated  $N$ -benzoyl- $N'$ -(4-hydroxy-2-methylphenyl)thioureato), which was discussed in Section 6.6.2.

#### 6.7.4 $[\text{Rh}(\text{N},\text{S}\text{-thioureato})(\text{S},\text{O}\text{-thioureato})(\text{PPh}_3)_2]$ complexes

Another compound that could be obtained upon the addition of  $\text{PPh}_3$  to the expected  $[\text{Rh}(\text{S},\text{O}\text{-thioureato})(\text{CO})_2]$  complexes included  $[\text{Rh}(\text{N},\text{S}\text{-thioureato})(\text{S},\text{O}\text{-thioureato})(\text{PPh}_3)_2]$  complexes. With the aim of finding protocols that could lead to the crystallization of  $[\text{Rh}(\text{S},\text{O}\text{-thioureato})(\text{CO})(\text{PPh}_3)]$  complexes, it was discovered that DMSO can also enhance the packing of molecules in a crystalline form *via* strong interactions between the molecules and the DMSO. Thus, a systematic variation of methods that were considered and attempted included a trial run with DMSO as well. The procedure was already described under the third attempt in Section 6.4.1. An IR analysis on the product revealed that no rhodium carbonyl species was present as concluded from the absence of any  $\nu_{\text{CO}}$  peaks in the IR spectrum. X-ray analysis was performed on the crystals in order to identify the resulting compound.

The surprising result was that the procedure described in Section 6.4.3 led to the formation of a bisthioureato complex,  $[\text{Rh}(\text{N},\text{S}-(\text{N}\text{-PT}))(\text{S},\text{O}-(\text{N}\text{-PT}))\text{PPh}_3)_2]$ , which is yet another peculiar compound that is first of its kind reported to date. A search on the CSD<sup>16</sup> revealed that no rhodium structure has been reported thus far where a simultaneous  $\text{N},\text{S}$ - and  $\text{S},\text{O}$ -coordination of any type of ligands have been observed. The structure was already discussed in Section 6.6.3.

#### 6.7.5 $[\text{Rh}(\text{COD})(\text{Cl})(\text{S}\text{-thioureato})]$ complexes

As was already discussed in Section 6.5, an alternative route that was attempted to synthesize  $[\text{Rh}(\text{S},\text{O}\text{-thioureato})(\text{CO})_2]$  involved the precursor  $[\text{Rh}(\text{COD})(\text{Cl})]_2$ . It was expected that the addition of an  $\text{S},\text{O}$ -functionalized thiourea ligand would result in the formation of complex **A** defined in Figure 6.3. However, structural data that was obtained from the X-ray analysis on the crystalline products that were obtained from the synthetic route defined in Figure 6.3 revealed that the ligands did not coordinated in the desired  $\text{S},\text{O}$ -fashion to produce the complex presented by **A**, but a  $\text{S}$ -coordination was favoured instead resulting in the formation

of the complex **B**. The formation of complex **B** above **A** can be ascribed to the formation of two hydrogen bond interactions that lead to the closure of two favourable 6-membered rings in the structure in comparison. For complex **A** to form the hydrogen bond interaction between the oxygen atom and the terminal nitrogen atom of the thiourea ligand firstly needs to be broken before allowing the formation of a single 6-membered ring *via* a *S,O*-coordination onto the metal centre.

It is therefore concluded from these results that a reaction route for complex **A** would result in a higher activation barrier compared to that of complex **B**, which favours the formation of the latter. Attempts were made to try and extract the chloro ligand from the metal centre and enhance the deprotonation of the thiourea ligand to allow a *S,O*-coordination. This was done by using either silver nitrate or sodium acetate salts, however, in both cases a complicated reaction mixture was obtained that could not be analysed in detail. Since the route in Figure 6.3 led to the use of extra processing methods during the synthesis of the  $[\text{Rh}(\text{S},\text{O}\text{-thioureato})(\text{CO})_2]$  complexes, it was discarded and attention was rather given to the original routes described before in Figure 6.1 and 6.2. The  $[\text{Rh}(\text{COD})(\text{Cl})(\text{S}\text{-thioureato})]$  structures that were obtained from the method described in Figure 6.3 were reported and discussed in Sections 6.6.4 and 6.6.5.

## 6.8 Conclusion

In this chapter the synthetic routes to complexes of the type  $[\text{Rh}(\text{S},\text{O}\text{-thioureato})(\text{CO})_2]$  and  $[\text{Rh}(\text{S},\text{O}\text{-thioureato})(\text{CO})(\text{PPh}_3)]$  were evaluated and discussed, where difficulties were presented on these complexes with regards to their instabilities, identifying the different species and directing the synthetic routes to one particular product. However, despite the difficulties, several unique rhodium species were discovered using certain modifications of the former synthetic routes, which revealed the ability of the *S,O*-functionalized thiourea ligands to coordinate in different ways including *S,O*-, *N,S*- and *S*-modes.

Firstly, It was shown by performing the synthesis described in Figures 6.1 and 6.2 in a basic medium by adding sodium acetate to the reaction mixture, several new Vaska-type rhodium complexes of the form  $[\text{Rh}(\text{N},\text{S}\text{-thioureato})(\text{CO})(\text{PPh}_3)_2]$  were obtained. These complexes exhibited very low  $\nu_{\text{CO}}$  values at around  $1920\text{ cm}^{-1}$ , which suggested that the rhodium centres were quite electron-rich. Structural data was obtained for one of these complexes, namely  $[\text{Rh}(\text{N},\text{S}\text{-(N-4h2mPT)})(\text{CO})(\text{PPh}_3)_2]$ , revealing a 5-coordinated rhodium centre having a significantly distorted trigonal bipyramidal conformation. The thiourea and CO ligands were positioned on the equatorial plane, whilst the  $\text{PPh}_3$  ligands coordinated *trans* to each other on the axial position. The thiourea ligand coordinated in a mono-charged fashion *via* its sulphur atom and the internal nitrogen atom with a very small bite angle of  $63.07(4)^\circ$ .

Another set of modifications on the synthetic route in Figure 6.2 resulted in the formation of the complex  $[\text{Rh}(\text{N},\text{S}\text{-(N-PT)})(\text{S},\text{O}\text{-(N-PT)})(\text{PPh}_3)_2]$ . These modifications involved dissolving the starting material  $[\text{Rh}(\text{S},\text{O}\text{-(N-PT)})(\text{CO})_2]$  in DMSO before adding  $\text{PPh}_3$ . After some time addition and evaporation of acetone to this mixture provided the crystals for the  $[\text{Rh}(\text{N},\text{S}\text{-(N-PT)})(\text{S},\text{O}\text{-(N-PT)})(\text{PPh}_3)_2]$  complex. This was the first rhodium complex having a simultaneous coordination of two of the same ligand in a *N,S*- and *S,O*-mode onto the same metal centre. This resulted in the formation of a Rh(III) octahedral complex, where the one thiourea ligand coordinated in its *enol* form *via* a divalent *N,S*-fashion, while the other ligand coordinated in a mono-charged *S,O*-mode. The *N,S*-coordination in this case involved the terminal nitrogen atom instead of the internal nitrogen atom, which also resulted in the formation of a very small bite angle of  $68.52(10)^\circ$ . The *S,O*-bite angle was almost  $90^\circ$  with a value of  $88.15(9)^\circ$ . The axial positions of the complex were occupied by two  $\text{PPh}_3$  ligands

located *trans* to each other. Further investigations on this complex is necessary in order to discover the mechanistic route behind the conversion of a Rh(I) dicarbonyl specie to the Rh(III) specie.

An alternative route in synthesizing  $[\text{Rh}(S,O\text{-thioureato})(\text{CO})_2]$  complexes, provided in Figure 6.3, was also discussed, which involved the precursor  $[\text{Rh}(\text{COD})(\text{Cl})]_2$ . Instead of the expected  $[\text{Rh}(\text{COD})(S,O\text{-thioureato})]$  complex, the synthetic route in Figure 6.3 led to the formation of a  $[\text{Rh}(\text{COD})(\text{Cl})(S\text{-thioureato})]$  complex, where the corresponding *S,O*-functionalized thiourea ligand coordinated only in a *S*-mode to the metal centre. Two structures of this type was reported in Section 6.4, which included  $[\text{Rh}(\text{COD})(\text{Cl})(S\text{-}(N\text{-PTH}))]$  and  $[\text{Rh}(\text{COD})(\text{Cl})(S\text{-}(N\text{-tmPTH}))]$ . Although these compounds crystallized in different space groups, namely triclinic  $P\bar{1}$  and monoclinic  $C2/c$ , respectively, great similarities exist between them. Both structures were square planar complexes where the thiourea ligands were revealed to exhibit the typical orientations of that of the free ligands. Furthermore the intramolecular hydrogen bond interaction between the oxygen atom and one of the nitrogen atoms in the free thiourea ligands is also found in the coordinated ligands. The complex structures are also further stabilized by hydrogen bond interactions between the the chloride atom and one of the nitrogen atoms of the coordinated thiourea ligand. The packing also involved the formation of dimers of molecules of the complexes, which in both cases are orientated around a centre of symmetry and stabilized by intermolecular hydrogen bonding

Finally, apart from the rhodium species that were presented and discussed in this chapter, successful synthesis and characterization of some  $[\text{Rh}(S,O\text{-thioureato})(\text{CO})(\text{PR}_1\text{R}_2\text{R}_3)]$  complexes were achieved with the ligand *N*-benzoyl-*N'*-diphenylthiourea and several tertiary phosphine ligands. The synthetic route as well as NMR, IR, X-ray and element analyses on these complexes are reported and described in Chapter 7.

# **CHAPTER 7**

## **THE SYNTHESIS AND CHARACTERIZATION OF**

### **[Rh(*S,O*-THIOUREATO)(CO)(PR<sub>1</sub>R<sub>2</sub>R<sub>3</sub>)] COMPLEXES**

#### **7.1 Introduction**

It was concluded from the previous chapter that *S,O*-functionalised thiourea ligands can coordinate in a range of different ways to a metal centre depending on the reaction conditions, the ligand as well as metal properties. As was mentioned before in Chapter 5 a main objective in this study was to find a reliable and consistent route to the synthesis of square planar [Rh(*S,O*-thioureato)(CO)(PPh<sub>3</sub>)] complexes. Despite the fact that some of the thiourea ligands under study provided several other rhodium species, a route was successfully developed to synthesise the desired complex for the ligand *N*-benzoyl-*N',N'*-diphenylthiourea (*N*-diPTH). This route seemed to be unique for this ligand specifically as [Rh(*S,O*-thioureato)(CO)(PPh<sub>3</sub>)] complexes still could not be obtained using this procedure for any other ligand in this study. It was therefore decided to investigate whether different [Rh(*S,O*-(*N*-diPT))(CO)(PR<sub>1</sub>R<sub>2</sub>R<sub>3</sub>)] complexes could be isolated using the same procedure and a range of phosphine ligands. This proved to be viable and as such the focus turned to synthesise these complexes. The synthetic route and the subsequent characterization of the resulting [Rh(*S,O*-(*N*-diPT))(CO)(PR<sub>1</sub>R<sub>2</sub>R<sub>3</sub>)] complexes are reported and discussed within this chapter.

#### **7.2 Reagents and equipment**

Unless otherwise stated all experiments were carried out in air, using analytical grade reagents. Rhodium(III)chloride hydrate (RhCl<sub>3</sub>.xH<sub>2</sub>O) as well as the phosphorus ligands PPh<sub>3</sub>, PPh<sub>2</sub>Cy, PPhCy<sub>2</sub> and PCy<sub>3</sub> were purchased from Sigma Aldrich. Dimethylformamide (DMF) and diethyl ether were obtained from Merck. These reagents were used as received. *N*-benzoyl-*N',N'*-diphenylthiourea (*N*-diPT) was synthesised and characterised as discussed in Chapter 3.

NMR spectroscopic data was acquired on either a Bruker Advance DPX 300 or Advance II 600 MHz spectrometer.  $^1\text{H}$  NMR data are listed in the order: chemical shift ( $\delta$ , reported in ppm and referenced to the residual solvent peak of  $\text{CD}_2\text{Cl}_2$  [ $\delta = 5.32$  ppm]), multiplicity, number of protons, assignment, coupling constant ( $J$ , in Hertz). Proton-decoupled  $^{13}\text{C}$  NMR data are listed in the order: chemical shift ( $\delta$ , reported in ppm and referenced to the residual solvent peak of  $\text{CD}_2\text{Cl}_2$  [ $\delta = 77.0$  ppm]), multiplicity, number of carbons, assignment, coupling constant ( $J$ , in Hertz) where appropriate. HMQC and HMBC experiments were performed to assist in the allocation of signals.  $^{31}\text{P}$  NMR data are listed in the order: chemical shift ( $\delta$ , reported in ppm and referenced to triphenylphosphine oxide [ $\delta = 29.9$  ppm]), multiplicity, number of phosphorus atoms, coupling constant ( $J$ , in Hertz) where appropriate.

FT-IR spectra were recorded on a Bruker Tensor 27 spectrophotometer in the range of 3000-600  $\text{cm}^{-1}$  in dry dichloromethane, using a NaCl solvent cell as well as *via* ATR.

### 7.3 Synthetic procedure for $[\text{Rh}(\text{S},\text{O}-(N\text{-diPT}))(\text{CO})(\text{PR}_1\text{R}_2\text{R}_3)]$ complexes

A range of  $[\text{Rh}(\text{S},\text{O}-(N\text{-diPT}))(\text{CO})(\text{PR}_1\text{R}_2\text{R}_3)]$  complexes were synthesised using the synthetic route given in Figure 7.1.

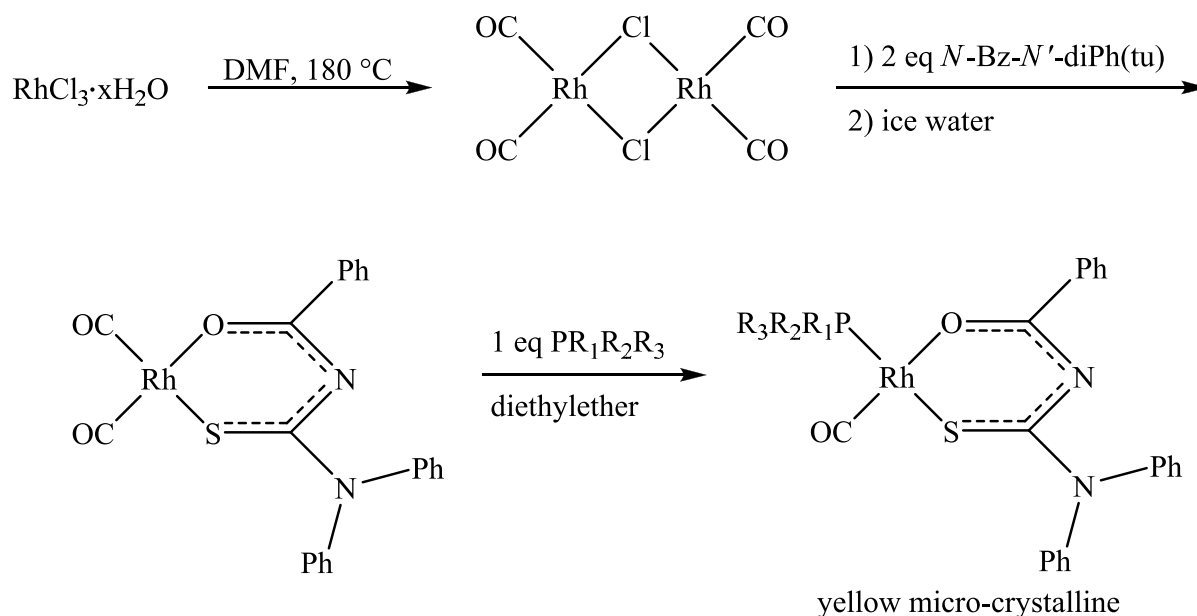
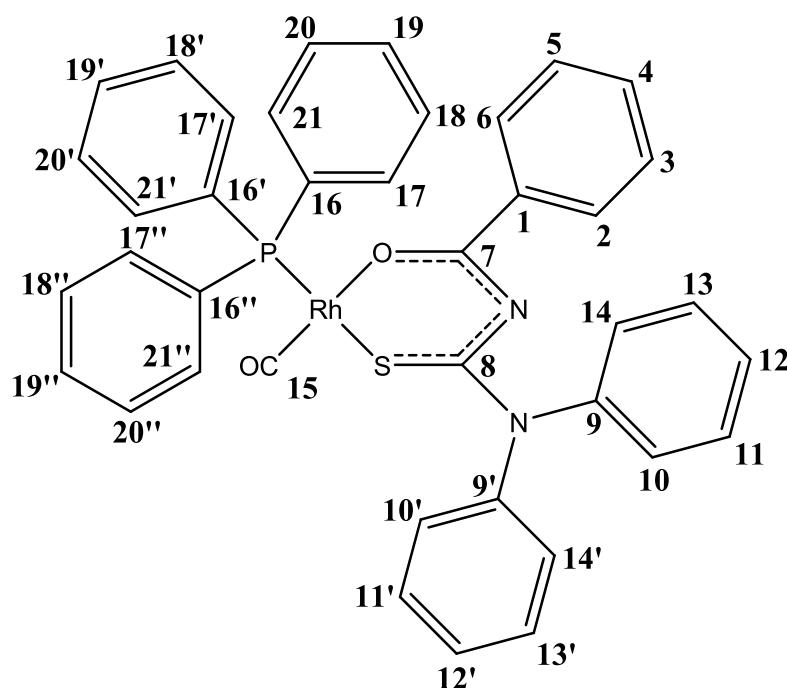


**Figure 7.1** Schematic representation of the procedure followed in the synthesis of the  $[\text{Rh}(\text{S},\text{O}-(N\text{-diPT}))(\text{CO})(\text{PR}_1\text{R}_2\text{R}_3)]$  complexes.

Each  $[\text{Rh}(\text{S},\text{O}-(N\text{-diPT}))(\text{CO})(\text{PR}_1\text{R}_2\text{R}_3)]$  complex that was synthesised is given and discussed in the next few sections (7.3.1-7.3.4).

### 7.3.1. Carbonyl(triphenylphosphine)(*S,O*-(*N*-benzoyl-*N'*,*N'*-diphenylthioureato)rhodium(I) $[\text{Rh}(\text{S},\text{O}-(N\text{-diPT}))(\text{CO})(\text{PPh}_3)]$



The complex carbonyltriphenylphosphine(*S,O*-(*N*-benzoyl-*N'*,*N'*-diphenylthiourea)rhodium(I)  $[\text{Rh}(\text{S},\text{O}-(N\text{-diPT}))(\text{CO})(\text{PPh}_3)]$  was synthesised by the procedure defined in Figure 7.1. First  $\text{RhCl}_3 \cdot x\text{H}_2\text{O}$  (100 mg, 0.478 mmol) was heated in DMF ( 5 mL) under reflux at 180 °C to produce the dimeric rhodium species tetra-carbonyl-di-chloro-dirhodium(I). *N*-diPTH (317.7 mg, 0.956 mmol) was added slowly to the cooled solution, which caused the yellow solution to change to a bright orange colour indicating the formation of the expected  $[\text{Rh}(\text{S},\text{O}-(N\text{-diPT}))(\text{CO})_2]$  complex. After about 10 minutes the complex was precipitated with the addition of ice water as a bright orange solid. A sample was analysed by IR spectroscopy, which revealed the presence of two carbonyl stretching frequency bands at 2071 and 2004  $\text{cm}^{-1}$ . After centrifugation the complex was dissolved in diethyl ether and carefully removed from the excess water. Triphenylphosphine (2 eq, 0.956 mmol) was added slowly to the ether solution until no more CO gas bubbles were observed. After a short time the desired complex  $[\text{Rh}(\text{S},\text{O}-(N\text{-diPT}))(\text{CO})(\text{PPh}_3)]$  precipitated from solution as a yellow micro-crystalline solid. The



product was filtered and washed with several portions of ether. The complex was re-dissolved in dichloromethane and re-crystallized as yellow needles by means of a two-layer diffusion technique using hexane. These crystals were suitable for X-ray analysis (Yield: 30 %).

$^1\text{H}$  NMR (600 MHz,  $\text{CD}_2\text{Cl}_2$ , 25 °C):  $\delta_{\text{H}}$  7.69-7.66 (m, 5H, H2, H6, H19, H19' and H19''), 7.47-7.38 (m, 16H, H3, H5, H10, H10', H11, H11', H13, H13', H14, H14', H17, H17', H17'', H21, H21' and H21''), 7.33-7.31 (m, 2H, H12 and H12'), 7.19 (tt, 1H, H4,  $J_{\text{H-H}} = 7.5$  Hz,  $J_{\text{H-H}} = 1.5$  Hz) 6.89-6.82 (m, 6H, H18, H18', H18'', H20, H20' and H20'').

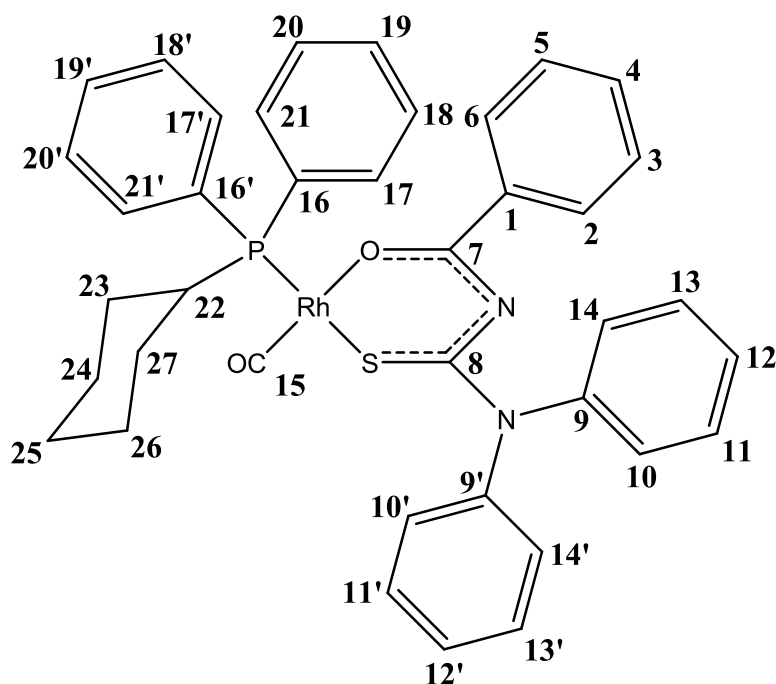
$^{13}\text{C}$  NMR (151 MHz,  $\text{CD}_2\text{Cl}_2$ , 25 °C):  $\delta_{\text{C}}$  191.1 (dd, 1C, C15,  $J_{\text{Rh-C}} = 74.1$  Hz,  $J_{\text{C-P}} = 21.1$  Hz), 178.9 (s, 1C, C8), 170.7 (s, 1C, C7), 145.8 (s, 2C, C9 and C9'), 137.5 (s, 1C, C1), 134.9 (d, 6C, C17, C17', C17'', C21, C21' and C21''),  $J_{\text{C-P}} = 12.1$  Hz), 133.4 (d, 3C, C16, C16' and C16'',  $J_{\text{C-P}} = 44.7$  Hz), 131.7 (s, 1C, C4), 130.9 (s, 3C, C19, C19' and C19''), 130.0 (s, 2C, C2 and C6), 129.8 (s, 4C, C10, C10', C14 and C14'), 129.0 (s, 4C, C11, C11', C13 and C13'), 129.0 (s, 6C, C18, C18', C18'', C20, C20' and C20''), 128.0 (s, 2C, C3 and C5), 127.7 (s, 2C, C12 and C12').

$^{31}\text{P}$  NMR (121 MHz,  $\text{CD}_2\text{Cl}_2$ , 25 °C):  $\delta_{\text{P}}$  38.2 (d,  $J_{\text{Rh-P}} = 152.3$  Hz).

IR  $\nu_{\text{max}}$  DCM/ $\text{cm}^{-1}$ : 1979 (CO),  $\nu_{\text{max}}$  ATR/ $\text{cm}^{-1}$ : 1963 (CO).

Element analysis (%): Found C, 63.6; H, 4.1; N, 3.95. Calculated for  $\text{RhC}_{39}\text{H}_{30}\text{N}_2\text{SO}_2\text{P}$ : C, 64.6; H, 4.2; N, 3.9.

### 7.3.2. Carbonyl(cyclohexyldiphenylphosphine)(*S,O*-(*N*-benzoyl-*N'*,*N'*-diphenylthioureato)rhodium(I) [Rh(*S,O*-(*N*-diPT))(*CO*)(PPh<sub>2</sub>Cy)]



The complex Carbonyl(cyclohexyldiphenylphosphine)(*S,O*-(*N*-benzoyl-*N'*,*N'*-diphenylthioureato)rhodium(I) [Rh(*S,O*-(*N*-diPT))(*CO*)(PPh<sub>2</sub>Cy)] was synthesised by the same methodology as described in 7.3.1 using the ligand cyclohexyldiphenylphosphine in this case. Yellow crystalline solid (Yield: 25 %).

<sup>1</sup>H NMR (600 MHz, CD<sub>2</sub>Cl<sub>2</sub>, 25 °C): δ<sub>H</sub> 7.83-7.81 (m, 4H, H2, H6, H19 and H19'), 7.45-7.44 (m, 8H, H10, H10', H11, H11', H13, H13', H14 and H14'), 7.43-7.38 (m, 6H, H3, H5, H17, H17', H21 and H21'), 7.33 (m, 2H, H12 and H12'), 7.25-7.22 (m, 1H, H4), 6.95-6.94 (m, 4H, H18, H18', H20 and H20'), 2.75-2.73 (m, 1H, H22), 2.11 and 1.80 (m, 4H, H23 and H27), 1.73 and 1.19 (m, 2H, H25), 1.45-1.41 (m, 4H, H24 and H26).

<sup>13</sup>C NMR (151 MHz, CD<sub>2</sub>Cl<sub>2</sub>, 25 °C): δ<sub>C</sub> 191.4 (dd, 1C, C15, *J*<sub>Rh-C</sub> = 73.8 Hz, *J*<sub>C-P</sub> = 21.3 Hz), 179.2 (s, 1C, C8), 170.6 (s, 1C, C7), 146.9 (s, 2C, C9 and C9'), 137.7 (s, 1C, C1), 134.2 (d, 4C, C17, C17', C21, C21', *J*<sub>C-P</sub> = 10.6 Hz), 132.6 (d, 2C, C16 and C16', *J*<sub>C-P</sub> = 39.9 Hz), 131.6 (s, 1C, C4), 130.5 (s, 2C, C19 and C19'), 130.0 (s, 2C, C2 and C6), 129.7 (s, 4C, C10, C10', C14 and C14'), 129.0 (s, 4C, C11, C11', C13 and C13'), 128.9 (s, 4C, C18, C18', C20

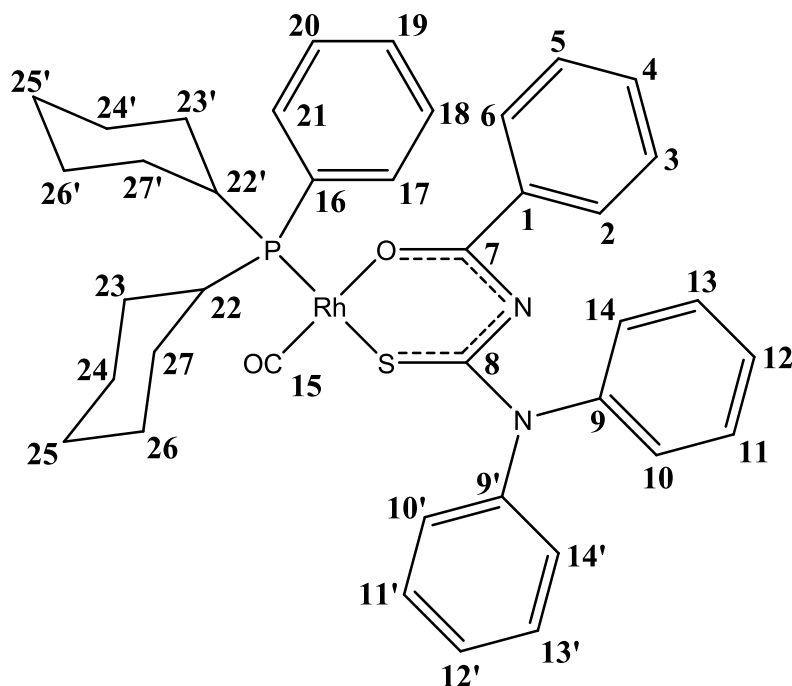
and C20'), 128.0 (s, 2C, C3 and C5), 127.7 (s, 2C, C12 and C12'), 35.9 (d, 1C, C22,  $J_{C-P}$  = 27.6 Hz), 29.4 (s, 2C, C24 and C26), 27.5 (d, 2C, C23 and C27,  $J_{C-P}$  = 12.7 Hz), 26.7 (s, 1C, C25).

$^{31}\text{P}$  NMR (121 MHz,  $\text{CD}_2\text{Cl}_2$ , 25 °C):  $\delta_{\text{P}}$  45.3 (d,  $J_{\text{Rh-P}}$  = 149.4 Hz).

IR  $\nu_{\text{max}}$  DCM/ $\text{cm}^{-1}$ : 1972 (CO),  $\nu_{\text{max}}$  ATR/ $\text{cm}^{-1}$ : 1966 (CO).

Element analysis (%): Found C, 64.1; H, 5.0; N, 4.1. Calculated for  $\text{RhC}_{39}\text{H}_{36}\text{N}_2\text{SO}_2\text{P}$ : C, 64.1; H, 5.0; N, 3.8.

### 7.3.3. Carbonyl(dicyclohexylphenylphosphine)(*S,O*-(*N*-benzoyl-*N',N'*-diphenylthioureato)rhodium(I) [ $\text{Rh}(\text{S},\text{O}-(\text{N-diPT}))(\text{CO})(\text{PPhCy}_2)$ ]



The complex Carbonyl(dicyclohexylphenylphosphine)(*S,O*-(*N*-benzoyl-*N',N'*-diphenylthioureato)rhodium(I) [ $\text{Rh}(\text{S},\text{O}-(\text{N-diPT}))(\text{CO})(\text{PPhCy}_2)$ ] was synthesised by the same methodology as described in 7.3.1 using the ligand dicyclohexylphenylphosphine in this case. Yellow crystalline solid (Yield: 32 %).

$^1\text{H}$  NMR (600 MHz,  $\text{CD}_2\text{Cl}_2$ , 25 °C):  $\delta_{\text{H}}$  7.80-7.77 (m, 3H, H2, H6, H19), 7.50-7.47 (m, 8H, H10, H10', H11, H11', H13, H13', H14 and H14'), 7.40-7.36 (m, 4H, H3, H5, H17 and H21), 7.35 (m, 2H, H12 and H12'), 7.24-7.22 (m, 1H, H4), 6.92-6.90 (m, 2H, H18 and H20), 2.69-2.67 (m, 2H, H22 and H22'), 2.15 and 1.84 (m, 8H, H23, H23', H27 and H27'), 1.70 and 1.21 (m, 4H, H25 and H25'), 1.47-1.43 (m, 8H, H24, H24', H26 and H26').

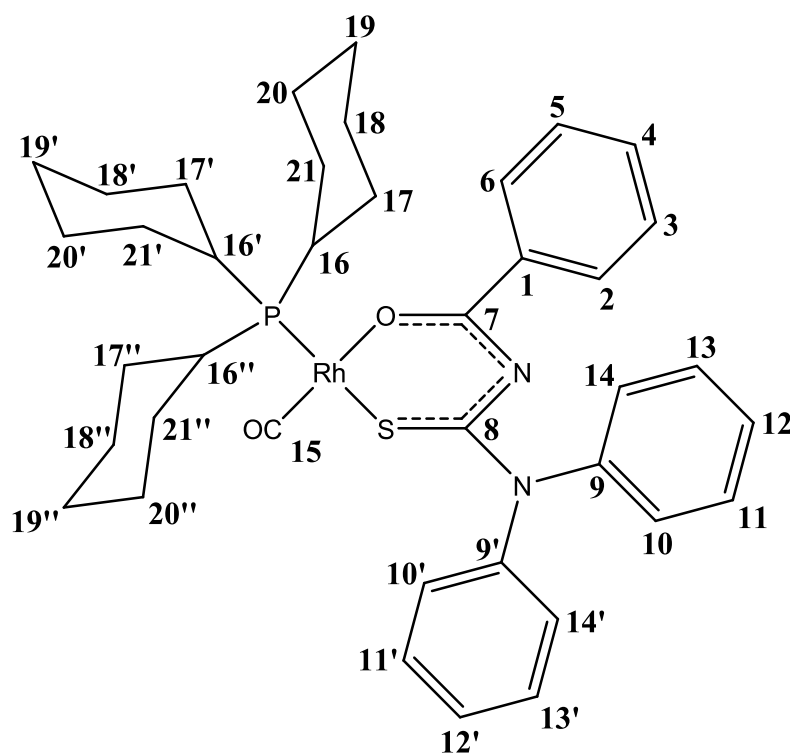
$^{13}\text{C}$  NMR (151 MHz,  $\text{CD}_2\text{Cl}_2$ , 25 °C):  $\delta_{\text{C}}$  191.4 (dd, 1C, C15,  $J_{\text{Rh-C}} = 73.8$  Hz,  $J_{\text{C-P}} = 21.3$  Hz), 179.2 (s, 1C, C8), 170.6 (s, 1C, C7), 146.9 (s, 2C, C9 and C9'), 137.7 (s, 1C, C1), 134.2 (d, 2C, C17, C21,  $J_{\text{C-P}} = 10.6$  Hz), 132.6 (d, 1C, C16,  $J_{\text{C-P}} = 39.9$  Hz), 131.6 (s, 1C, C4), 130.5 (s, 1C, C19), 130.0 (s, 2C, C2 and C6), 129.7 (s, 4C, C10, C10', C14 and C14'), 129.0 (s, 4C, C11, C11', C13 and C13'), 128.9 (s, 2C, C18, C20), 128.0 (s, 2C, C3 and C5), 127.7 (s, 2C, C12 and C12'), 35.9 (d, 2C, C22 and C22',  $J_{\text{C-P}} = 27.6$  Hz), 29.4 (s, 4C, C24, C24', C26 and C26'), 27.5 (d, 4C, C23, C23', C27 and C27',  $J_{\text{C-P}} = 12.7$  Hz), 26.7 (s, 2C, C25 and C25').

$^{31}\text{P}$  NMR (121 MHz,  $\text{CD}_2\text{Cl}_2$ , 25 °C):  $\delta_{\text{P}}$  49.5 (d,  $J_{\text{Rh-P}} = 149.0$  Hz).

IR  $\nu_{\text{max}}$  DCM/ $\text{cm}^{-1}$ : 1969 (CO),  $\nu_{\text{max}}$  ATR/ $\text{cm}^{-1}$ : 1961 (CO).

Element analysis (%): Found C, 62.7; H, 5.8; N, 4.0. Calculated for  $\text{RhC}_{39}\text{H}_{42}\text{N}_2\text{SO}_2\text{P}$ : C, 63.6; H, 5.8; N, 3.8.

**7.3.4. Carbonyl(tricyclohexylphosphine)(*S,O*-(*N*-benzoyl-*N',N'*-diphenylthioureato)rhodium(I) [Rh(*S,O*-(*N*-diPT))](CO)(PCy<sub>3</sub>)**



The complex Carbonyl(tricyclohexylphosphine)(*S,O*-(*N*-benzoyl-*N',N'*-diphenylthioureato)rhodium(I) [Rh(*S,O*-(*N*-diPT))](CO)(PCy<sub>3</sub>) was synthesised by the same methodology as described in 7.3.1 using the ligand tricyclohexylphosphine in this case. Yellow crystalline solid (Yield: 28 %).

<sup>1</sup>H NMR (600 MHz, CD<sub>2</sub>Cl<sub>2</sub>, 25 °C): δ<sub>H</sub> 7.68 (dd, 2H, H2 and H6, *J*<sub>H-H</sub> = 8.4 Hz, *J*<sub>H-H</sub> = 1.5 Hz), 7.44-7.43 (m, 8H, H10, H10', H11, H11', H13, H13', H14 and H14'), 7.37 (tt, 1H, H4, *J*<sub>H-H</sub> = 7.4 Hz, *J*<sub>H-H</sub> = 1.2 Hz), 7.33-7.31 (m, 2H, H12 and H12'), 7.21 (t, 2H, H3 and H5, *J*<sub>H-H</sub> = 7.8 Hz), 2.33-2.27 (m, 3H, H16, H16' and H16''), 2.05 and 1.80 (d, 12H, H17, H17', H17'', H21, H21' and H21'', *J* = 12 Hz), 1.65 and 1.25 (m, 18H, H18, H18', H18'', H19, H19', H19'', H20, H20' and H20'').

$^{13}\text{C}$  NMR (151 MHz,  $\text{CD}_2\text{Cl}_2$ , 25 °C):  $\delta_{\text{C}}$  191.9 (dd, 1C, C15,  $J_{\text{Rh-C}} = 75.2$  Hz,  $J_{\text{C-P}} = 20.7$  Hz), 179.8 (s, 1C, C8), 171.0 (s, 1C, C7), 146.0 (s, 2C, C9 and C9'), 138.7 (s, 1C, C1), 131.7 (s, 1C, C4), 130.1 (s, 2C, C2 and C6), 129.7 (s, 4C, C10, C10', C14 and C14'), 129.1 (s, 4C, C11, C11', C13 and C13'), 128.2 (s, 2C, C3 and C5), 127.6 (s, 2C, C12 and C12'), 34.2 (d, 3C, C16, C16' and C16'',  $J_{\text{C-P}} = 21.1$  Hz), 30.6 (s, 6C, C18, C18', C18'', C20, C20' and C20''), 28.3 (d, 6C, C17, C17', C17'', C21, C21' and C21'',  $J_{\text{C-P}} = 10.7$  Hz), 27.1 (s, 3C, C19, C19' and C19'').

$^{31}\text{P}$  NMR (121 MHz,  $\text{CD}_2\text{Cl}_2$ , 25 °C):  $\delta_{\text{P}}$  49.9 (d,  $J_{\text{Rh-P}} = 145.6$  Hz).

IR  $\nu_{\text{max}}$  DCM/ $\text{cm}^{-1}$ : 1963 (CO),  $\nu_{\text{max}}$  ATR/ $\text{cm}^{-1}$ : 1952 (CO).

Element analysis (%): Found C, 61.7; H, 6.55; N, 3.9. Calculated for  $\text{RhC}_{39}\text{H}_{48}\text{N}_2\text{SO}_2\text{P}$ : C, 63.1; H, 6.5; N, 3.8.

## 7.4 X-ray crystallographic study of $[\text{Rh}(\text{S},\text{O}-(\text{N-diPT}))(\text{CO})(\text{PR}_1\text{R}_2\text{R}_3)]$ complexes

### 7.4.1. Introduction

The structural data that could be obtained for some of the  $[\text{Rh}(\text{S},\text{O}-(\text{N-diPT}))(\text{CO})(\text{PR}_1\text{R}_2\text{R}_3)]$  complexes are provided in this section together with the respective crystal packing as well as molecular interactions. Attention is given on the effects of the different phosphine ligands as well as the non-symmetrical *S,O*-thiourea ligand on the general molecular orientation and geometry of the complexes. This can provide vital information regarding the role of these complexes as catalysts during the carbonylation and hydrogenation processes. Factors that determine the chemistry and catalytic properties of rhodium complexes include electro-steric influences of the ligands as well as *trans*-effect and *trans*-influence as was discussed in Chapters 1 and 2. Altering the electro-steric properties of phosphine ligands have been shown to alter the outcome of catalytic processes such as hydroformylation<sup>1a,b</sup> as well as carbonylation processes, of which many examples have been provided in Chapter 2. The *trans*-influence of different donor atoms in rhodium square-planar complexes have been illustrated by Roodt *et al.*<sup>2a,b</sup>. Note that although single crystals were obtained for the complex  $[\text{Rh}(\text{S},\text{O}-(\text{N-diPT}))(\text{CO})(\text{PPhCy}_2)]$  they were unsuitable for X-ray analysis. This was due to the fact that these crystals were too small and provided only weak and low angle reflections upon performing an initial unit cell determination. Several attempts to re-crystallize this complex did not provide larger crystalline solids and as such no structural data could be obtained for  $[\text{Rh}(\text{S},\text{O}-(\text{N-diPT}))(\text{CO})(\text{PPhCy}_2)]$

---

<sup>1</sup> a) Riihimäki, H.; Kangas, T.; Suomalainen, P.; Reinius, H.K.; Jääskeläinen, S.; Haukka, M.; Krause, A.O.I.; Pakkanen, T.A.; Pursiainen, J.T. (2003) *J. Mol. Catal. A: Chem.*, **200**, 81. b) Reinius, H.K.; Suomalainen, P.; Riihimäki, H.; Karvinen, E.; Pursiainen, J.; Krause, A.O.I. (2001) *J. Catal.*, **199**, 302.

<sup>2</sup> a) Steyn, G. J. J.; Roodt, A.; Poletaeva, I.; Varshavsky, Y.S. (1997) *J. Organomet. Chem.* 536. b) Roodt, A.; Steyn, G. J. J. (2000) *Recent Res. Devel. Inorg. Chem.*, **2**, 1.

The X-ray determined single crystal structures of the following molecules are reported:

1.  $[\text{Rh}(S,O\text{-}(N\text{-diPT})(\text{CO})(\text{PPh}_3))] =$   
Carbonyl(triphenylphosphine)(*S,O*-(*N*-benzoyl-*N'*,*N'*-diphenylthioureato))rhodium(I)
2.  $[\text{Rh}(S,O\text{-}(N\text{-diPT})(\text{CO})(\text{PPh}_2\text{Cy}))] =$   
Carbonyl(cyclohexyldiphenylphosphine)(*S,O*-(*N*-benzoyl-*N'*,*N'*-diphenylthioureato))  
rhodium(I)
3.  $[\text{Rh}(S,O\text{-}(N\text{-diPT})(\text{CO})(\text{PCy}_3))] =$   
Carbonyl(tricyclohexylphosphine)(*S,O*-(*N*-benzoyl-*N'*,*N'*-diphenylthioureato))rhodium(I)

## 7.4.2 Experimental

The above mentioned compounds were analysed by single crystal X-ray diffraction. The initial unit cell and data collections were performed on a Bruker X8 Apex II 4K Kappa CCD diffractometer using graphite monochromated Mo  $K\alpha$  radiation ( $\lambda = 0.70926 \text{ \AA}$ ) with  $\omega$ - and  $\phi$ -scans at 100(2) K as well as the Apex2 software package.<sup>3</sup> The optimum measurement method to collect more than a hemisphere of reciprocal space was predicted by COSMO.<sup>4</sup> Frame integration and data reductions were performed using the SAINT-Plus and XPREP<sup>5</sup> software packages, and a multi-scan absorption correction was performed on the data using SADABS.<sup>6</sup> The structures were solved by the direct methods package SIR97,<sup>7</sup> and refinement using the WinGX software package<sup>8</sup> incorporating SHELXL.<sup>9</sup> All non H-atoms were refined anisotropically. All H-atoms were positioned geometrically and refined using a riding model with fixed C-H distances of 0.95  $\text{\AA}$  (CH) [Uiso(H) = 1.2Ueq] for aromatic groups, 0.99  $\text{\AA}$  (CH) [Uiso(H) = 1.2Ueq] for methylene groups and 1.00  $\text{\AA}$  (CH) [Uiso(H) = 1.2Ueq] for methane groups. Molecular diagrams were drawn using the Mercury<sup>10</sup> package with a 50% thermal envelope probability for non-hydrogen atoms. General crystal data and refinement

<sup>3</sup> Bruker (2005). Apex2 (Version 1.0-27). Bruker AXS Inc., Madison, Wisconsin, USA.

<sup>4</sup> Bruker (2003). COSMO (Version 1.48). Bruker AXS Inc., Madison, Wisconsin, USA.

<sup>5</sup> Bruker (2004a). SAINT-Plus. Version 7.12 (including XPREP). Bruker AXS Inc., Madison, Wisconsin, USA.

<sup>6</sup> Bruker (2004b). SAINT-Plus. Version 7.12 (including XPREP). Bruker AXS Inc., Madison, Wisconsin, USA.

<sup>7</sup> Altomare, A., Burla, M. C., Camalli, M., Cascarano, G. L., Giacovazzo, C., Guagliardi, A., Moliterni, A. G. G., Polidori, G. & Spagna, R. (1999). *J. Appl. Cryst.*, **32**, 115.

<sup>8</sup> Farrugia, L. J. (1999). WinGX, *J. Appl. Cryst.*, **32**, 837.

<sup>9</sup> Sheldrick, G.M. (1997). SHELXL97. *Program for crystal structure refinement*. University of Göttingen, Germany.

<sup>10</sup> Macrae, C. F., Edgington, P. R., McCabe, P., Pidcock, E., Shields, G. P., Taylor, R., Towler, M. & van de Streek, J. (2006). *J. Appl. Cryst.* **39**, 453.



parameters are presented in Tables 4.1 and 4.2. A complete list of atomic coordinates, equivalent isotropic parameters, bond distances and angles, anisotropic displacement parameters and hydrogen coordinates for each individual dataset is given in Appendix D.

**Table 7.1 General crystal data for the following rhodium complexes,**  
**(i) [Rh(*S,O*-(*N*-diPT)(CO)(PPh<sub>3</sub>)], (ii) [Rh(*S,O*-(*N*-diPT)(CO)(PPh<sub>2</sub>Cy)] and**  
**(iii) [Rh(*S,O*-(*N*-diPT)(CO)(PCy<sub>3</sub>)].**

Identification code	(i)	(ii)	(iii)
Empirical formula	Rh1 C39 H30 O2 P1 S1 N2	Rh1 C39 H36 O2 P1 S1 N2	Rh1 C39 H48 O2 P1 S1 N2
Formula weight	724.6	730.6	742.7
Crystal system, space group	Monoclinic <i>P</i> <sub>2</sub> <sub>1</sub> / <i>c</i>	Monoclinic <i>P</i> <sub>2</sub> <sub>1</sub> / <i>c</i>	Monoclinic <i>P</i> <sub>2</sub> <sub>1</sub> / <i>c</i>
Unit cell dimensions			
<i>a</i> (Å)	9.4470(6)	9.7766(4)	9.6594(7)
<i>b</i> (Å)	18.4426(13)	23.2810(9)	24.5159(9)
<i>c</i> (Å)	37.7130(25)	14.8453(6)	14.9926(12)
<i>α</i> (°)	90.000	90.000	90.000
<i>β</i> (°)	95.344(3)	92.642(2)	93.144(2)
<i>γ</i> (°)	90.000	90.000	90.000
Volume (Å <sup>3</sup> )	6542(4)	3375(2)	3545(2)
<i>Z</i>	8	4	4
Density (calculated) (g/mL)	1.471	1.438	1.392
Absorption coefficient (mm <sup>-1</sup> )	0.673	0.653	0.622
<i>F</i> (000)	2960	1504	1552
Crystal size (mm <sup>3</sup> )	0.24 x 0.10 x 0.03	0.36 x 0.06 x 0.04	0.20 x 0.06 x 0.05
<i>Θ</i> range (°)	5.12 to 28.00	3.48 to 25.00	4.13 to 28.28
Completeness (%)	99.3	98.8	99.3
Index ranges	-12 ≤ <i>h</i> ≤ 12 -24 ≤ <i>k</i> ≤ 24 -49 ≤ <i>l</i> ≤ 49	-11 ≤ <i>h</i> ≤ 11 -27 ≤ <i>k</i> ≤ 27 -17 ≤ <i>l</i> ≤ 17	-12 ≤ <i>h</i> ≤ 7 -32 ≤ <i>k</i> ≤ 32 -19 ≤ <i>l</i> ≤ 19
Reflections collected	65459	32582	33110
Independent reflections	15707 [ <i>R</i> <sub>int</sub> = 0.0686]	5881 [ <i>R</i> <sub>int</sub> = 0.0632]	8726 [ <i>R</i> <sub>int</sub> = 0.0686]
Observed reflections	12043	4405	6330
Max/min transmission	0.9801 and 0.8552	0.9744 and 0.7990	0.9755 and 0.8070
Data/ restraints/ parameters	15707/0/829	5881/0/415	8726/0/415
Goodness-of-fit on <i>F</i> <sup>2</sup>	1.034	1.031	1.162
Final <i>R</i> indices [ <i>I</i> > 2σ( <i>I</i> )]	<i>R</i> 1 = 0.0437 w <i>R</i> 2 = 0.0778	<i>R</i> 1 = 0.0447 w <i>R</i> 2 = 0.0907	<i>R</i> 1 = 0.0584 w <i>R</i> 2 = 0.1264
<i>R</i> indices (all data)	<i>R</i> 1 = 0.0658 w <i>R</i> 2 = 0.0854	<i>R</i> 1 = 0.0703 w <i>R</i> 2 = 0.1008	<i>R</i> 1 = 0.0873 w <i>R</i> 2 = 0.1365
Largest diff. Peak/hole (e.Å <sup>-3</sup> )	0.506 and -0.701	0.788 and -0.621	2.161 and -0.902

### 7.4.3. Crystal structure of Carbonyl(triphenylphosphine)(*S,O*-(*N*-benzoyl-*N*',*N*'-diphenylthioureato))rhodium(I), [Rh(*S,O*-(*N*-diPT)(CO)(PPh<sub>3</sub>)]

#### 7.4.3.1 Results and discussion

(Synthesis described in Section 7.3.1, Supplementary data D1)

[Rh(*S,O*-(*N*-diPT)(CO)(PPh<sub>3</sub>)] crystallised having two independent molecules in the asymmetric unit and eight molecules in the unit cell of the monoclinic space group  $P2_1/c$ . Figure 7.2 represents the structure and subsequent atom labelling of the compound whilst the main bond distances as well as bond angles are presented in Table 7.2.

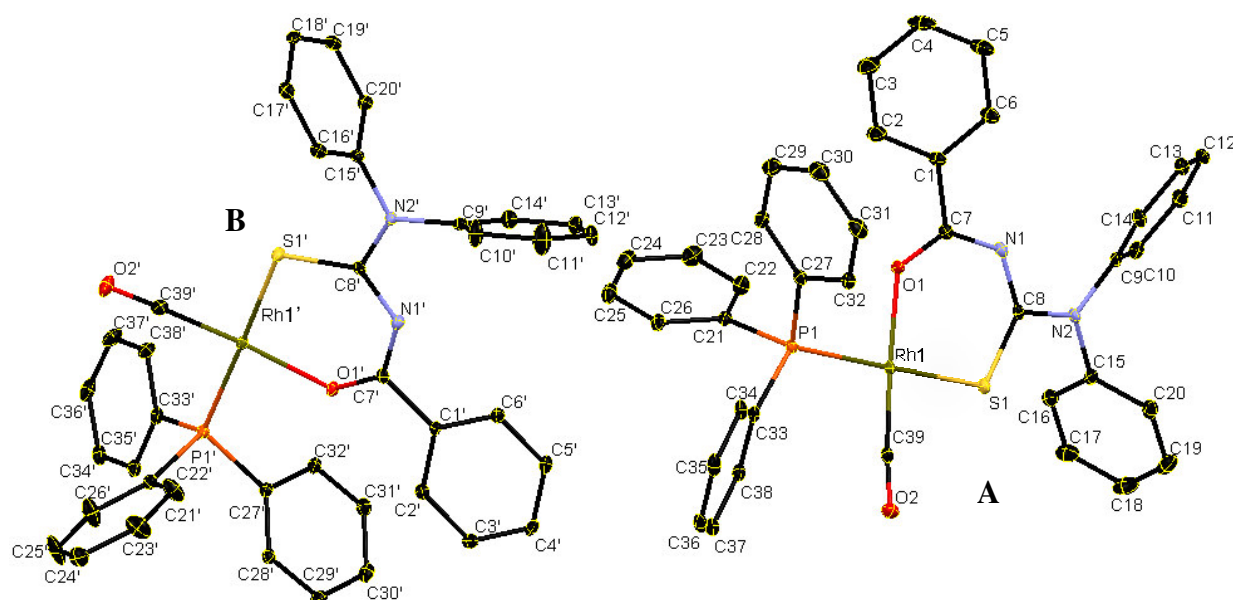


**Figure 7.2** A structural representation of [Rh(*S,O*-(*N*-diPT)(CO)(PPh<sub>3</sub>)] showing the independent molecules A and B, where the atom numbering scheme is provided (ellipsoid probability = 30%). Hydrogen atoms have been omitted for clarity.

**Table 7.2: Selected bond distances and angles for [Rh(S,O-(N-diPT)(CO)(PPh<sub>3</sub>)).**

Molecule A			
Atoms	Distance (Å)	Atoms	Angle (°)
Rh1-P1	2.291(1)	S1-Rh1-O1	91.1(1)
Rh1-S1	2.304(1)	P1-Rh1-C39	93.0(1)
Rh1-O1	2.039(2)	S1-Rh1-C39	88.9(1)
Rh1-C39	1.791(3)	O1-Rh1-P1	87.5(7)
C7-O1	1.277(4)	Rh1-P1-C21	113.9(1)
C8-S1	1.714(3)	Rh1-P1-C27	111.4(1)
C39-O2	1.154(4)	Rh1-P1-C33	118.0(1)
O1...S1 (bite distance)	3.105	Rh1-C39-O2	175.3(3)
Molecule B			
Atoms	Distance (Å)	Atoms	Angle (°)
Rh1'-P1'	2.278(1)	S1'-Rh1'-O1'	91.7(1)
Rh1'-S1'	2.312(1)	P1'-Rh1'-C39'	88.5(1)
Rh1'-O1'	2.037(2)	S1'-Rh1'-C39'	90.1(1)
Rh1'-C39'	1.804(3)	O1'-Rh1'-P1'	89.5(1)
C7'-O1'	1.267(3)	Rh1'-P1'-C21'	108.7(1)
C8'-S1'	1.711(3)	Rh1'-P1'-C27'	115.4(1)
C39'-O2'	1.153(4)	Rh1'-P1'-C33'	118.7(1)
O1'...S1' (bite distance)	3.126	Rh1'-C39'-O2'	177.6(3)

The first observation that can be made is that the reaction between the complex [Rh(N-diPT)(CO)<sub>2</sub>] and PPh<sub>3</sub> led to the substitution of only one CO ligand, which has been shown by several studies<sup>11a,b,c</sup> to be the expected outcome. Furthermore, the phosphine ligand substituted the CO ligand that was coordinated *trans* with respect to the sulphur atom around the metal centre. This observed *trans* influence was in accordance with the electronegativity of the donor atoms sulphur and oxygen, where it has been shown by these studies that sulphur has the higher donor ability and therefore has the largest *trans* influence. Other work<sup>12</sup> has shown that this substitution normally leads to a trigonal bipyramidal transition state where the CO ligand being displaced, the phosphine ligand and the donor atom with the largest *trans* influence (sulphur) occupies the equatorial positions. The other ligands, being the oxygen atom of the thiourea ligand and the other CO ligand, occupy the axial positions, which then lead to the expected *trans* P-Rh-S moiety. This outcome together with the <sup>31</sup>P NMR spectrum obtained for this complex, confirmed that only one isomer of this complex has therefore formed, which is important when utilising this complex for further studies, as discussed in Chapter 8 for the iodomethane oxidative addition reactions to these complexes.

<sup>11</sup> a) Graham, D. E.; Lamprecht, G. J.; Potgieter, I. M.; Roodt, A.; Leipoldt, J. G. (1991) *Transition Met. Chem.*, **16**, 193.

<sup>12</sup> Langford, C. H.; Gray, H. B. (1965) *Ligand Substitution Processes*, Benjamin, New York.

The bond lengths of Rh-P, Rh-O, Rh-S and Rh-C for molecule **A** were found to have values of 2.291(1), 2.039(2), 2.304(1) and 1.791(3) Å, respectively, while that for molecule **B** have respective values of 2.278(1), 2.312(1), 2.037(2) and 1.804(3) Å. In order to define the steric properties of the phosphine ligand the effective Tolman cone angle is calculated by using the observed Rh-P bond distances.<sup>13</sup> The values of the effective cone angle ( $\theta_E$ ) calculated for both molecule **A** and **B** are 142.8 and 147.9 °, respectively, which provides an average effective cone angle value of 145.4 °.

The thioureato ligand coordinated to the rhodium centre with bite distances O1...S1 and O1'...S1' of 3.105 and 3.126 Å and bite angles S1-Rh-O1 and S1'-Rh-O1' of 91.1(1) and 91.7(1) ° for molecules **A** and **B**, respectively. Being that this bite angle together with the angles of O-Rh-P, P-Rh-C and S-Rh-C are close to 90 ° (Table 7.2), the coordination moiety is found to be in a distorted square planar conformation. This is also suggested by the observation that the O, S, P and C atoms bonded to the rhodium centre are in plane across the coordination moiety. The sulphur and oxygen atoms of the thiourea ligand twisted slightly out of the plane across the thiourea bridge with dihedral angles O1-C7...C8-S1 and O1'-C7'...C8'-S1' of 8.27 and 9.15 °, respectively.

The C-O and C-S bond lengths for the respective molecules **A** and **B** are given by C7-O1 = 1.277(4) Å, C7'-O1' = 1.267(3) Å, C8-S1 = 1.714(3) Å and C8'-S1' = 1.711(3) Å. These bond lengths in comparison to the general C-O and C-S bond lengths that were observed for the free thiourea ligands in Chapter 3, suggested that both these C-O and C-S bonds still displayed a double-bond character with slightly longer lengths. This was an indication that delocalization of electron density took place upon coordination to the rhodium centre, where the oxygen and sulphur atoms shared the donation of electrons to the electron-poor centre. As such the thioureato ligand coordinated in a monoanionic fashion as expected, which is represented in Figure 7.3a. This is also observed on <sup>13</sup>C NMR where the chemical shifts of the C-S and C-O bonds shifted only slightly from 184.5 and 163.3 ppm to 178.9 and 170.7 ppm, respectively. This is a general feature for bidentate ligands of this kind where electron density is shared between donor atoms across the β-diketonato chain when coordinating to a metal centre (Figure 7.3b).<sup>14</sup>

<sup>13</sup> Tolman, C.A. (1977) *Chem Rev.*, **77**, 313.

<sup>14</sup> Nazzari, A.; Mueller-Westerhoff, U. T. (1980) *Transition Met. Chem.*, **5**, 1, 318.

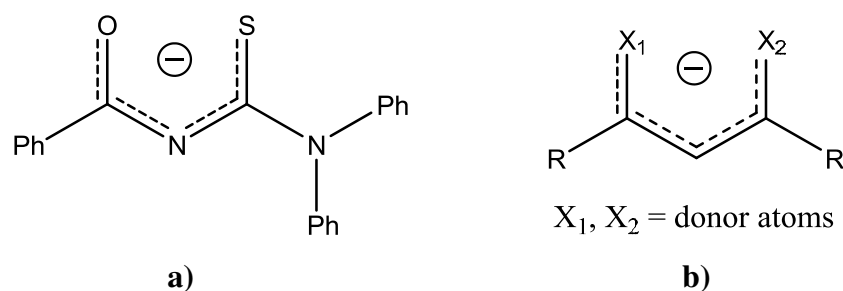


**Figure 7.3** A representation of a) electron-delocalization upon coordination of a thioureato ligand. b) shows the electron-delocalization for general  $\beta$ -diketonato ligands.

The carbonyl ligand in both molecules **A** and **B** are found to be close to linearity having angles Rh-C-O of 175.3(3) and 177.6(3) °, respectively, in each case. The respective bond lengths of the carbonyl ligands in molecules **A** and **B** were found to be 1.154(4) and 1.153(4) Å.

The crystal packing of [Rh(*S,O*-(*N*-diPT)(CO)(PPh<sub>3</sub>)] is primarily stabilized by Van der Waals interactions. Some of the few interactions that are found to be important in the packing include a phosphine ligand to ligand stacking interaction between symmetrical equivalent molecules of molecule **B**. This stacking involves C...C soft contacts that take place in a “head-to-head” fashion as shown by green dotted lines in Figure 7.4. The subsequent distance of the C36'-H36'...C29' interaction is equal to 2.844 Å and has an angle of 138.9 °.

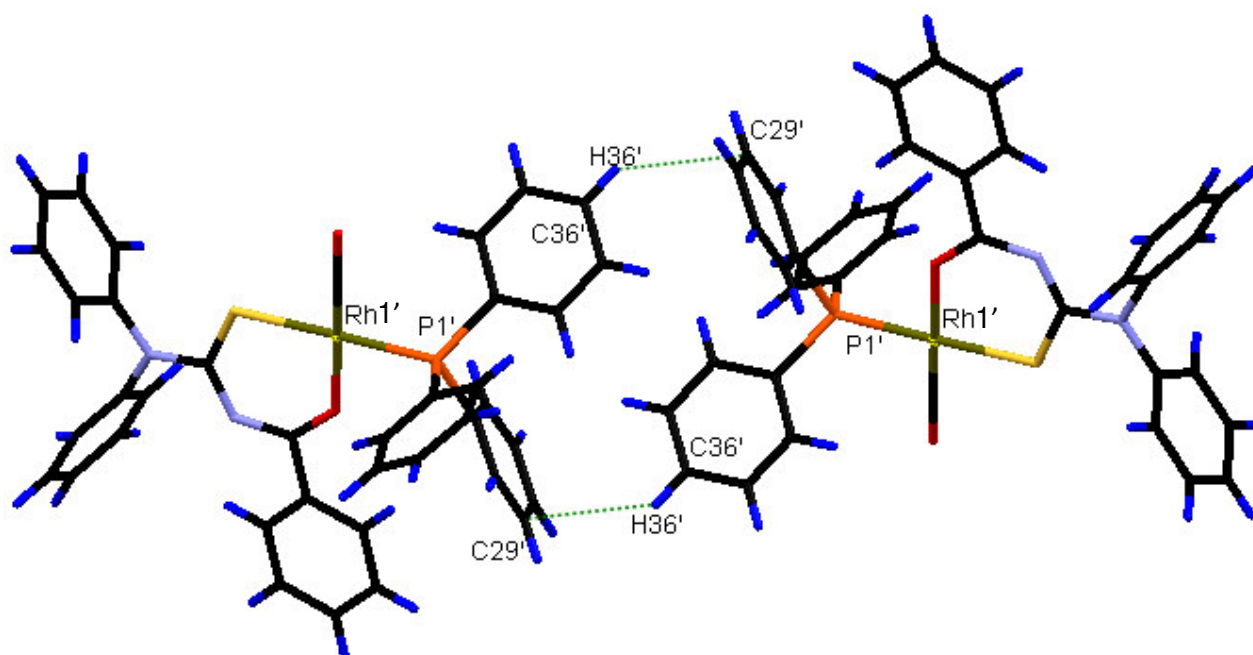


**Figure 7.4** An illustration of the phosphine ligand to ligand stacking interactions in the crystal packing of  $[\text{Rh}(\text{S},\text{O}-(\text{N}-\text{diPT})(\text{CO})(\text{PPh}_3)]$ . The interaction takes place in a “head-to-head” fashion between molecules of B of the asymmetric unit.  $\text{C}36'-\text{H}36'\cdots\text{C}29' = 2.844 \text{ \AA}$  and  $138.9^\circ$ .

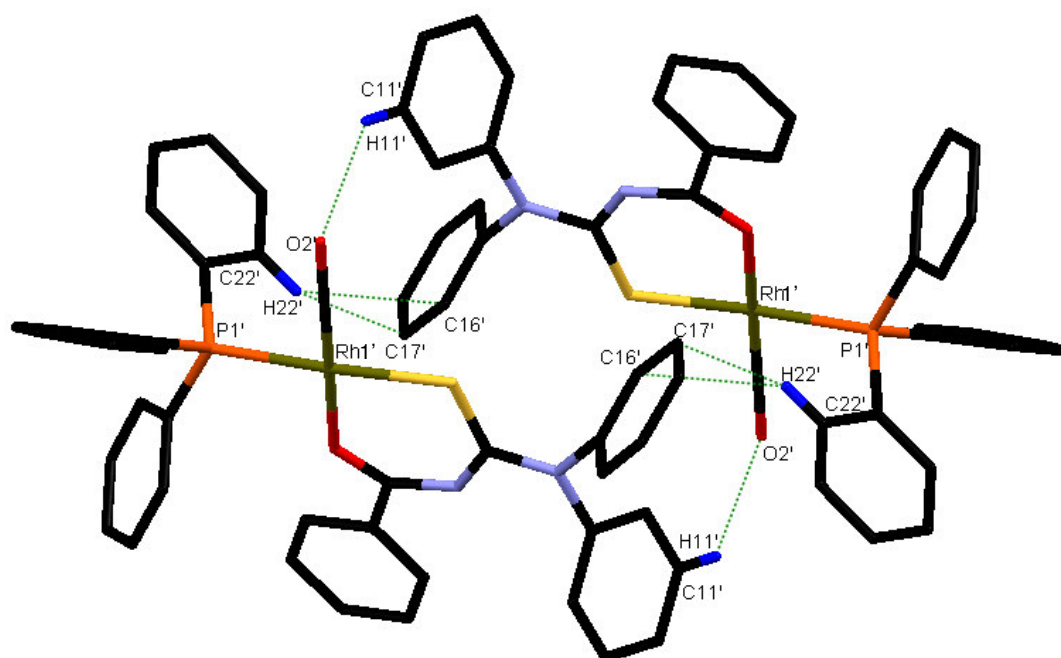


**Figure 7.5** Illustration of some soft contacts between molecules of molecule B in the crystal packing of  $[\text{Rh}(\text{S},\text{O}-(\text{N}-\text{diPT})(\text{CO})(\text{PPh}_3)]$ . Some of the hydrogen atoms have been omitted for clarity.

Other important Van der Waals interactions found between symmetrical equivalent molecules of the same molecule **B** is represented in Figure 7.5. This includes more C...C soft contacts as well as a C...O soft contact, which have respective interaction distances C22'-H22'...C16', C22'-H22'...C17' and C11'-H11'...O2' of 2.833, 2.818 and 2.692 Å. The subsequent angles of these interactions are given by C22'-H22'...C16' = 139.1 °, C22'-H22'...C17' = 138.5 ° and C11'-H11'...O2' = 136.9 °.

One important Van der Waals contact found between symmetrical equivalent molecules of molecule **A** includes a C...O soft contact. This contact results in a chain network between these molecules along the b axis as illustrated in Figure 7.6 and has a contact distance C30-H30...O2 of 2.512 Å as well as an angle of 152.9 °.

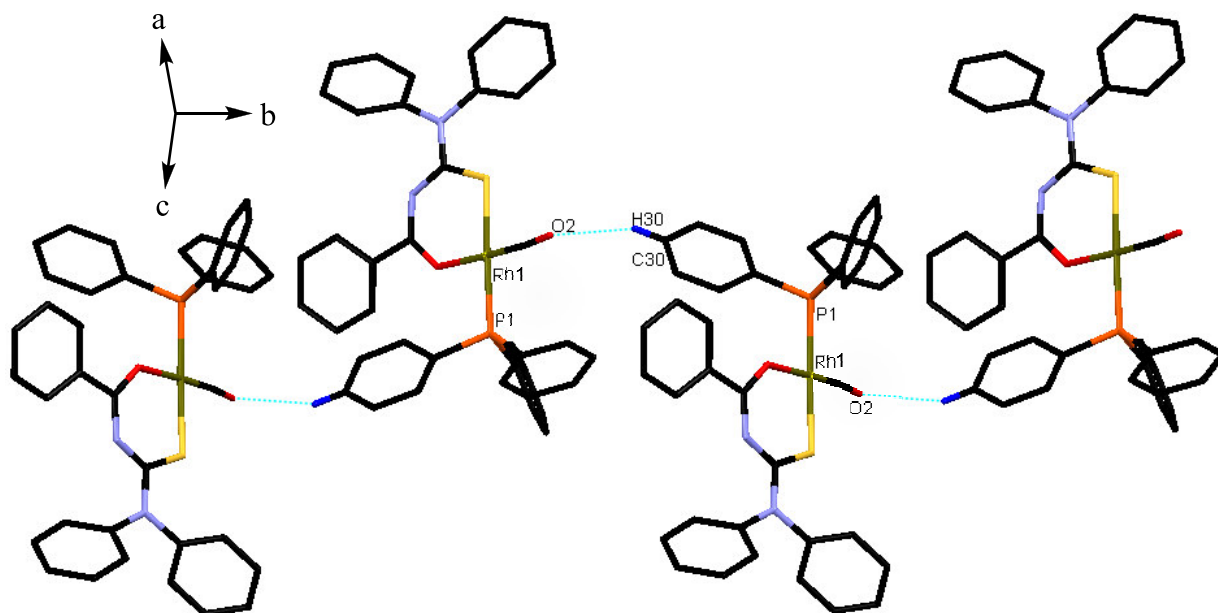


**Figure 7.6** Representation of a chain network found in the crystal packing along the b axis between molecules of **A** of  $[\text{Rh}(\text{S},\text{O}-(\text{N}-\text{diPT})(\text{CO})(\text{PPh}_3)]$  formed by a C...O soft contact. Some hydrogen atoms have been omitted for clarity.  $\text{C30-H30}\dots\text{O2} = 2.512 \text{ \AA}$  and  $152.9^\circ$ .

Several other Van der Waals interactions are also found between molecules of **A** and **B** due to very close approximations to each other, which primarily involves more C...C soft contacts.

**7.4.4. Crystal structure of carbonyl(cyclohexyldiphenylphosphine)(*S,O*-(*N*-benzoyl-*N'*,*N'*-diphenylthioureato))rhodium(I),  
[Rh(*S,O*-(*N*-diPT)(CO)(PPh<sub>2</sub>Cy)]**

**7.4.4.1 Results and discussion**

(Synthesis described in Section 7.3.2, Supplementary data D2)

[Rh(*S,O*-(*N*-diPT)(CO)(PPh<sub>2</sub>Cy)] crystallised in the monoclinic space group  $P2_1/c$  with 4 molecules in the unit cell. The structure and atom numbering scheme are provided in Figure 7.7, while the main bond distances and angles are given in Table 7.3.

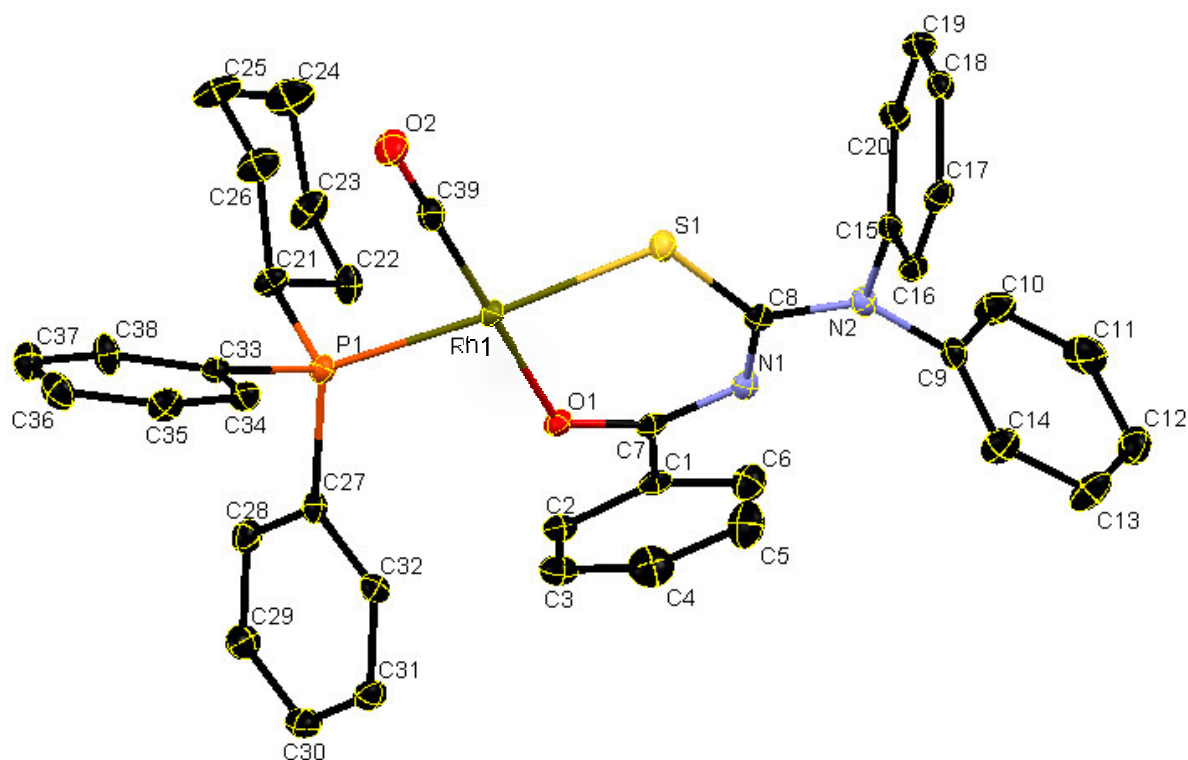


**Figure 7.7** A structural representation of the compound [Rh(*S,O*-(*N*-diPT)(CO)(PPh<sub>2</sub>Cy)], with atom numbering scheme as shown (ellipsoid probability = 30%). Hydrogen atoms have been omitted for clarity.



**Table 7.3: Selected bond distances and angles for [Rh(*S,O*-(*N*-diPT)(CO)(PPh<sub>2</sub>Cy)].**

Atoms	Distance (Å)	Atoms	Angle (°)
Rh1-P1	2.287(1)	S1-Rh1-O1	91.1(1)
Rh1-S1	2.312(1)	P1-Rh1-C39	89.0(1)
Rh1-O1	2.037(3)	S1-Rh1-C39	90.1(1)
Rh1-C39	1.798(5)	O1-Rh1-P1	89.5(1)
C7-O1	1.273(5)	Rh1-P1-C21	110.2(1)
C8-S1	1.725(4)	Rh1-P1-C27	115.0(1)
C39-O2	1.155(5)	Rh1-P1-C33	117.8(1)
O1...S1 <sub>(bite distance)</sub>	3.110	Rh1-C39-O2	177.8(4)

The phosphine ligand substituted the carbonyl that was *trans* to the sulphur atom coordinated the rhodium the same as with [Rh(*S,O*-(*N*-diPT)(CO)(PPh<sub>3</sub>)] in Section 7.4.3, adding more evidence to the stronger donor ability of sulphur compared to oxygen. Here the respective Rh1-P1, Rh1-S1, Rh1-O1 and Rh1-C39 bond distances were found to be 2.287(1), 2.312(1), 2.037(3) and 1.798(5) Å. Taking the Rh1-P1 distance into account the effective cone angle ( $\theta_E$ ) could be calculated, which was found to have a value of 154.0 °. This cone angle value is much higher than the average value obtained for PPh<sub>3</sub> in [Rh(*S,O*-(*N*-diPT)(CO)(PPh<sub>3</sub>)]], which can be explained by the smaller Rh1-P1-C21 angle of 110.2(1). The Rh-P-C angles which involves a phenyl group on the phosphorus atom is found to have values of about 115-118 °, with a few exceptions, as observed from both structures presented above. It would therefore seem that the cyclohexyl group in this case bended in slightly towards the rhodium centre, which together with its bulkier moiety led to the increase in the effective cone angle value.<sup>15</sup>

The bite angle S1-Rh1-O1 has a value of 91.1(1) °, while the other angles around the metal centre S1-Rh1-C39, O1-Rh1-P1 and P1-Rh1-C39 were all close to 90 ° (Table 7.3). These angles together with the atoms S1, O1, P1 and C39 being in the plane across the coordination moiety around the rhodium centre, revealed that the complex took on a distorted square planar conformation. In order to establish the 90 ° bite angle of the *S,O*-moiety to the metal centre, the sulphur and oxygen rotated slightly out of the plane across the thiourea bridge with a dihedral angle O1-C7...C8-S1 of -18.3 °. Furthermore, the bite distance O1...S1 of the thiourea ligand was found to be 3.110 Å. The bond distances C7-O1 and C8-S1 having values of 1.273(5) and 1.725(4) suggested that these bonds still kept their double bond character with electron-delocalization taking place across the thiourea bridge. This is once again

<sup>15</sup> Brink, A.; Roodt, A.; Steyl, G.; Visser, H. G. (2010) *Dalton Trans.*, **39**, 5572.

observed on the  $^{13}\text{C}$  NMR spectrum of this complex, where the C-S and C-O chemical shifts are found to be 179.2 and 170.6 ppm, respectively. This is once again close to the values of the free thiourea ligand for the C-S and C-O groups, being 184.5 and 163.3 ppm, respectively.

The carbonyl ligand coordination Rh1-C39-O2 was almost linear with an angle of  $177.8(4)^\circ$ . The respective bond lengths for Rh1-C39 and C39-O2 are 1.798(5) and 1.155(5) Å.

The crystal packing is stabilized by only a few Van der Waals interactions between adjacent molecules. One set of interactions include C...O contacts that exists between the carbonyl oxygen O2 and some of the carbons (C28 and C38) on the phosphine ligand as depicted in Figure 7.8. These interactions lead to the formation of a chain network of neighbouring molecules along c. The geometry of these interactions are given by C28-H28...O2 = 2.601 Å and  $120.2^\circ$  and C38-H38...O2 = 2.705 Å and  $126.9^\circ$ .

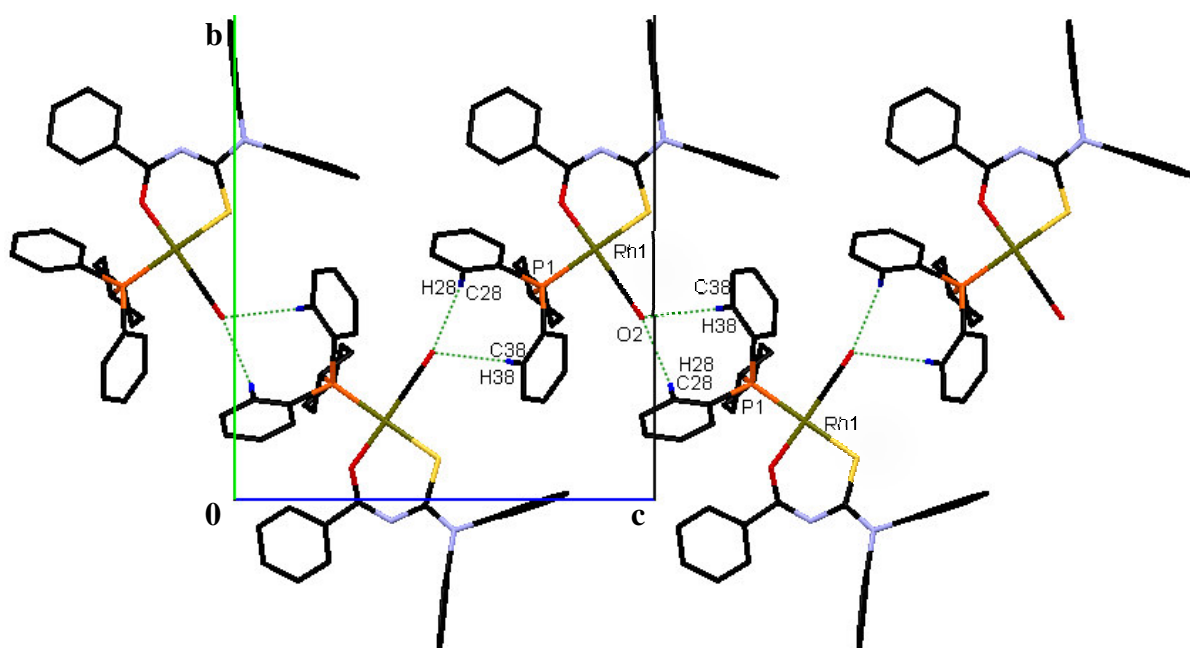


**Figure 7.8** An illustration of C...O soft contacts between adjacent molecules in the crystal packing of  $[\text{Rh}(\text{S},\text{O}-(\text{N}-\text{diPT})(\text{CO})(\text{PPh}_2\text{Cy})]$  along the c-axis. Some hydrogen atoms have been omitted for clarity. Distances and angles: C28-H28...O2 = 2.601 Å and  $120.2^\circ$ ; C38-H38...O2 = 2.705 Å and  $126.9^\circ$ .

Some of the other noteworthy short contacts involve phosphine ligand to phosphine ligand interactions between the cyclohexyl group of the one ligand and a phenyl group of the other

as shown in Figure 7.9. These interactions take place in a “head-to-tail” mode forming yet another chain network of adjacent molecules along the a-axis. The respective distances of the interactions C24-H24A...C34 and C35-H35...H25B are 2.893 and 2.360 Å, whereas the respective angles of these interactions are found to be 135.7 and 125.9 °.

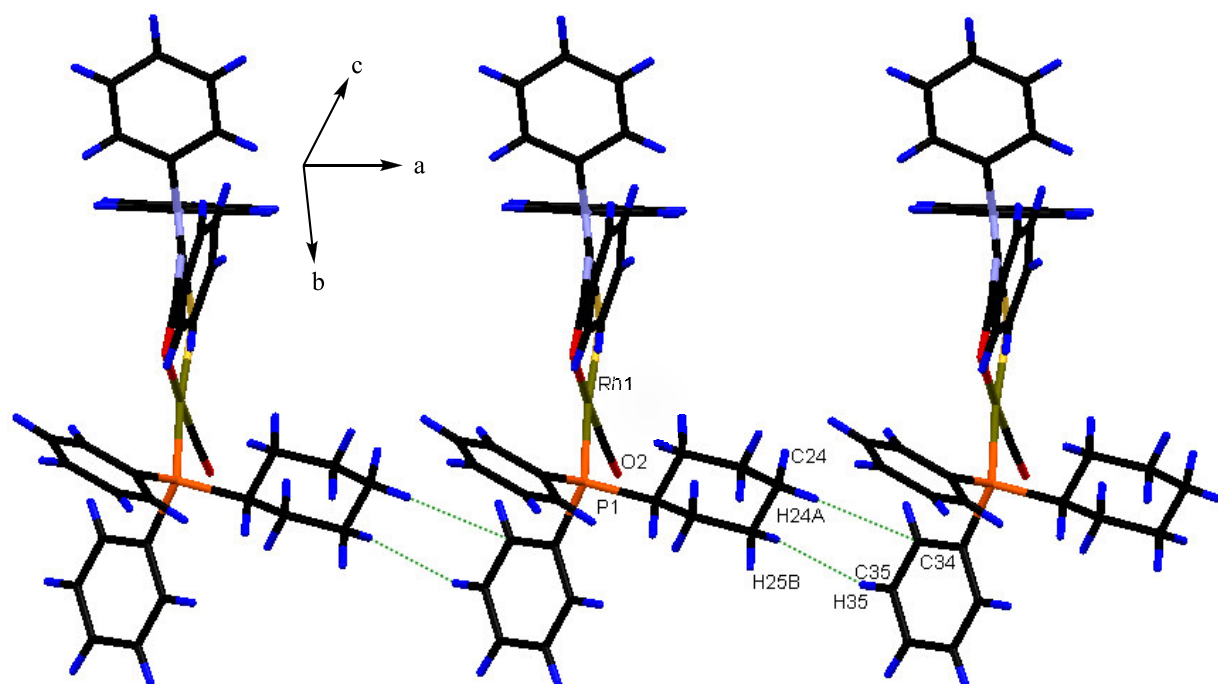


**Figure 7.9 Representation of phosphine ligand to ligand “head-to-tail” interactions found between neighbouring molecules in the crystal packing of [Rh(*S,O*-(*N*-diPT)(CO)(PPh<sub>2</sub>Cy)] along the a-axis. Distances and angles: C24-H24A...C34 = 2.893 Å, 135.7 °; C35-H35...H25B = 2.360 Å, 125.9 °.**

A few other interactions also exist between neighbouring molecules that are in close approximation to each other, which primarily involves C...C soft contacts.

**7.4.5. Crystal structure of carbonyl(tricyclohexylphosphine)(*S,O*-(*N*-benzoyl-*N,N'*-diphenylthioureato))rhodium(I),  
[Rh(*S,O*-(*N*-diPT)(CO)(PCy<sub>3</sub>)]**

**7.4.5.1 Results and discussion**

(Synthesis described in Section 7.3.4, Supplementary data D3)

The compound [Rh(*S,O*-(*N*-diPT)(CO)(PCy<sub>3</sub>)], crystallised in the monoclinic space group *P*2<sub>1</sub>/*c* (*Z* = 4). The structure and atom numbering scheme are presented in Figure 7.10, while the main bond distances and angles are given in Table 7.4.

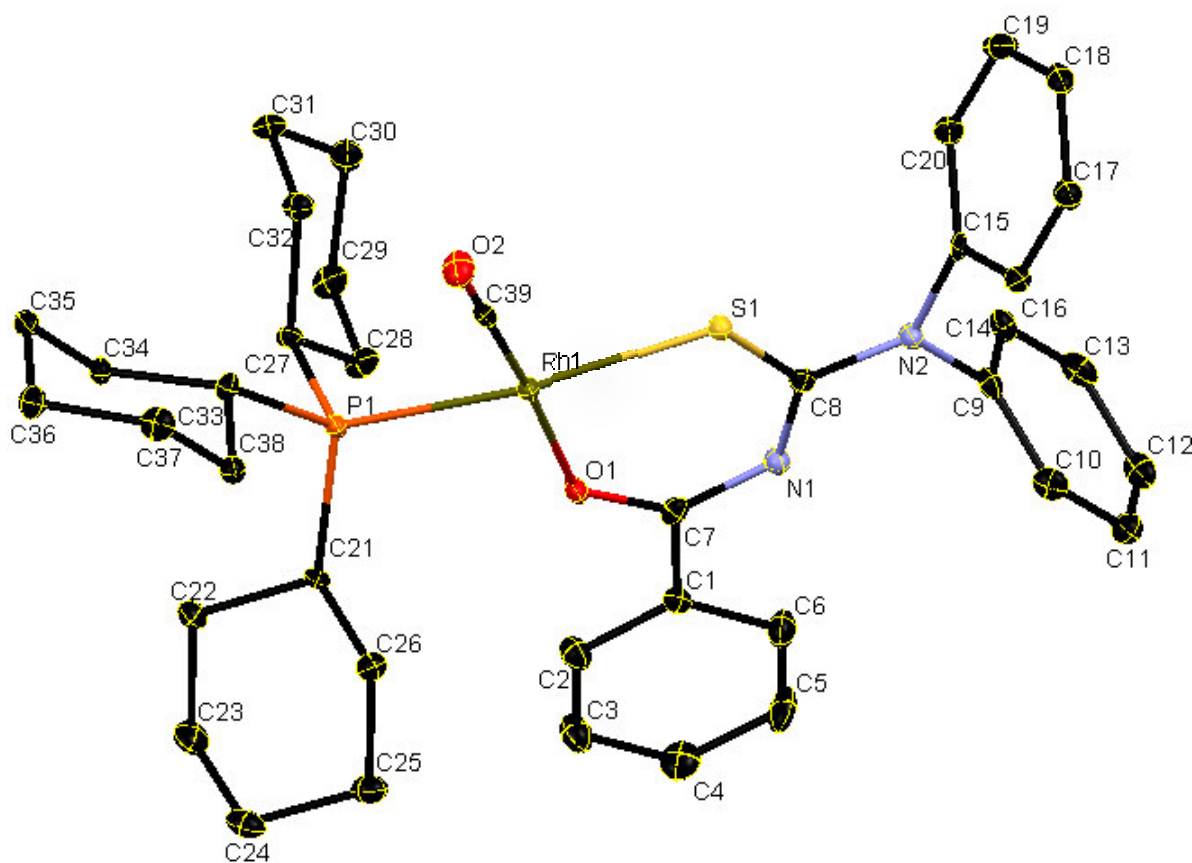


**Figure 7.10** Structural representation of [Rh(*S,O*-(*N*-diPT)(CO)(PCy<sub>3</sub>)], with the atom numbering scheme as shown (ellipsoid probability = 30%). Hydrogen atoms have been omitted for clarity.

**Table 7.4: Selected bond distances and angles for [Rh(*S,O*-(*N*-diPT)(CO)(PCy<sub>3</sub>)].**

Atoms	Distance (Å)	Atoms	Angle (°)
Rh1-P1	2.302(1)	S1-Rh1-O1	91.7(1)
Rh1-S1	2.329(1)	P1-Rh1-C39	90.2(2)
Rh1-O1	2.057(3)	S1-Rh1-C39	90.2(2)
Rh1-C39	1.788(5)	O1-Rh1-P1	88.7(1)
C7-O1	1.265(6)	Rh1-P1-C21	110.8(2)
C8-S1	1.705(5)	Rh1-P1-C27	110.1(2)
C39-O2	1.157(6)	Rh1-P1-C33	116.4(2)
O1...S1 (bite distance)	3.153	Rh1-C39-O2	178.0(5)

In this complex the phosphine ligand also substituted the carbonyl ligand that was *trans* with respect to the sulphur atom in the complex [Rh(*S,O*-(*N*-diPT)(CO)<sub>2</sub>] as was observed in the other structures in Sections 7.4.3 and 7.4.4. The resulting Rh1-P1 distance is observed to be 2.302(1) Å, from which the effective cone angle of the phosphine ligand was calculated to be 155.5 °. This cone angle revealed that the steric properties of this ligand is also much larger than that for PPh<sub>3</sub>, however, the value was fairly comparable to that for the PPh<sub>2</sub>Cy ligand. A closer look at the respective Rh-P-C angles (Table 7.4) for the different substituents on PCy<sub>3</sub> show that while two of these cyclohexyl rings are bent closely to the rhodium centre with angles of 110.8(2) and 110.1(2) °, respectively, the other cyclohexyl ring is found to be farther away from the rhodium centre with an angle of 116.4(2) °.

The thiourea ligand coordinated to the metal centre with a bite angle S1-Rh1-O1 of 91.7(1) ° having a bite distance O1...S1 of 3.153 Å. Although the angles around the metal centre S1-Rh1-O1, S1-Rh1-C39, P1-Rh1-C39 and O1-Rh1-P1 are all close to 90 ° (Table 7.4), a plane across the coordination moiety taking through S1, O1 and Rh1 (Figure 7.11) shows that the carbonyl ligand as well as the phosphorus atom are slightly twisted out of this plane. This might be the consequence of a bulkier phosphine ligand on the metal centre causing steric congestion around the rhodium centre. These observations altogether suggested that the complex took on a distorted square planar conformation. This can also be revealed by calculating the angles of O1-Rh1-C39 and S1-Rh1-P1 which are found to have values of 173.9(2) and 172.1(1) °, respectively. The oxygen and sulphur atoms are also slightly bended out of the plane across the thiourea bridge with a dihedral angle O1-C7...C8-S1 of 11.2 °.

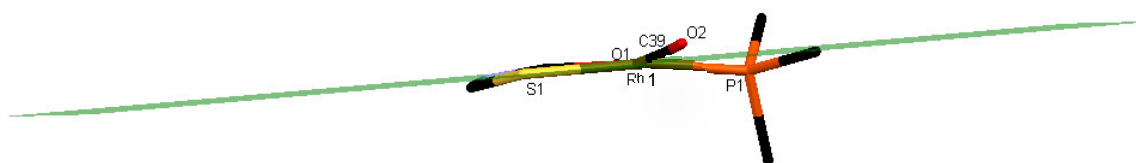


**Figure 7.11 A plane through the coordination moiety around the rhodium centre of  $[\text{Rh}(\text{S},\text{O}-(\text{N}-\text{diPT})(\text{CO})(\text{PCy}_3)]$ , illustrating a slightly distorted square planar conformation.**

The C7-O1 and C8-S1 distances of 1.265(6) and 1.705(5) Å again revealed that the thiourea ligand coordinated in a mono-anionic mode onto the metal centre with electron-delocalization taking place across the thiourea moiety. The carbonyl ligand was found to be close to linearity as indicated by an angle of 178.0(5) °, whereas the C39-O2 bond distance has a value of 1.157(6) Å.

Several Van der Waals interactions are observed between neighbouring molecules of  $[\text{Rh}(\text{S},\text{O}-(\text{N}-\text{diPT})(\text{CO})(\text{PCy}_3)]$  which help in stabilizing the crystal packing. One set of these interactions are presented in Figure 7.12, which are found between phosphine ligands of adjacent molecules as well as between a phosphine ligand and the carbonyl oxygen of a neighbouring molecule. These contacts create a close network between these molecules and the respective intermolecular distances and angles are given by: C22-H22A...O2 = 2.522 Å, 147.5 °; C23-H23A...H35B = 2.335 Å, 143.5 °; C18-H18...H24B = 2.355 Å, 123.1 °.

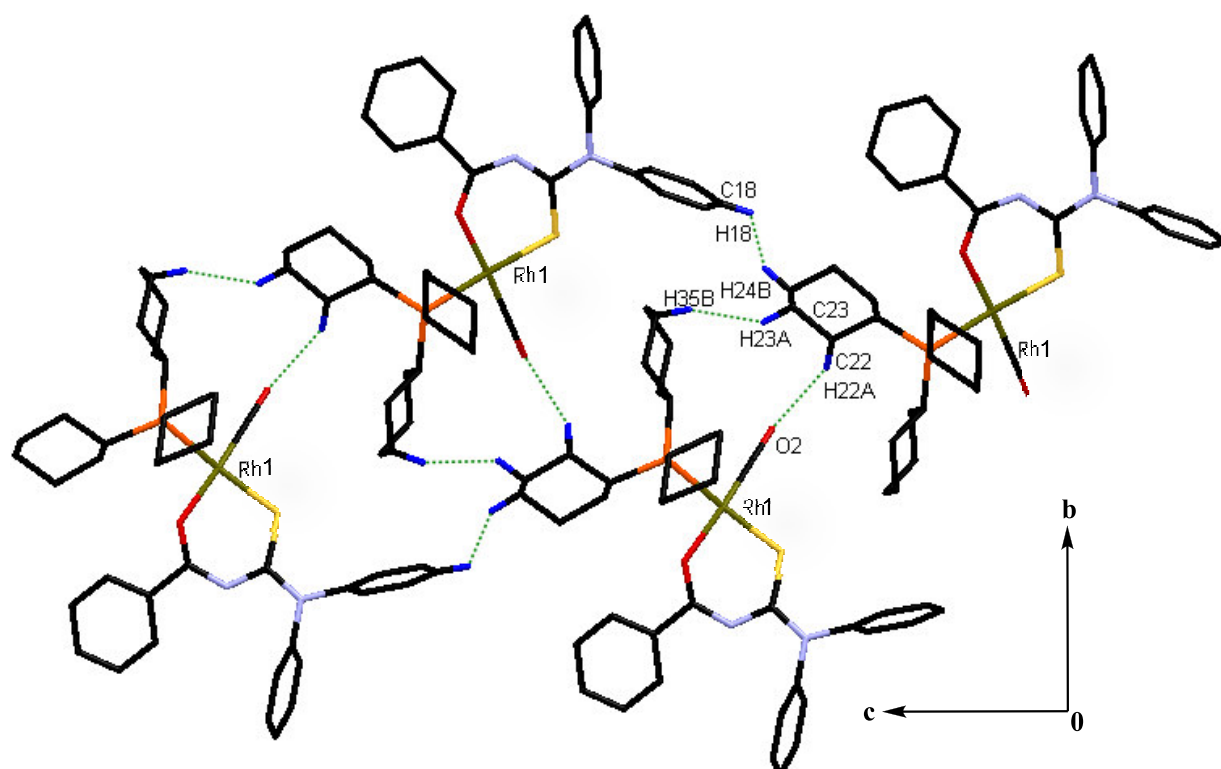


**Figure 7.12** An illustration of some soft contacts between molecules in the crystal packing of  $[\text{Rh}(\text{S},\text{O}-(\text{N-diPT})(\text{CO})(\text{PCy}_3)]$ . Distances and angles:  $\text{C22-H22A}\cdots\text{O2} = 2.522 \text{ \AA}$ ,  $147.5^\circ$ ;  $\text{C23-H23A}\cdots\text{H35B} = 2.335 \text{ \AA}$ ,  $143.5^\circ$ ;  $\text{C18-H18}\cdots\text{H24B} = 2.355 \text{ \AA}$ ,  $123.1^\circ$ .

Several  $\text{C}\cdots\text{C}$  and  $\text{C}\cdots\text{S}$  soft contacts are found between adjacent molecules as shown in Figure 7.13, that cause a close packing of these molecules to each other around the 2-fold screw-axis. The respective distances and angles of these interactions are listed in Table 7.5.

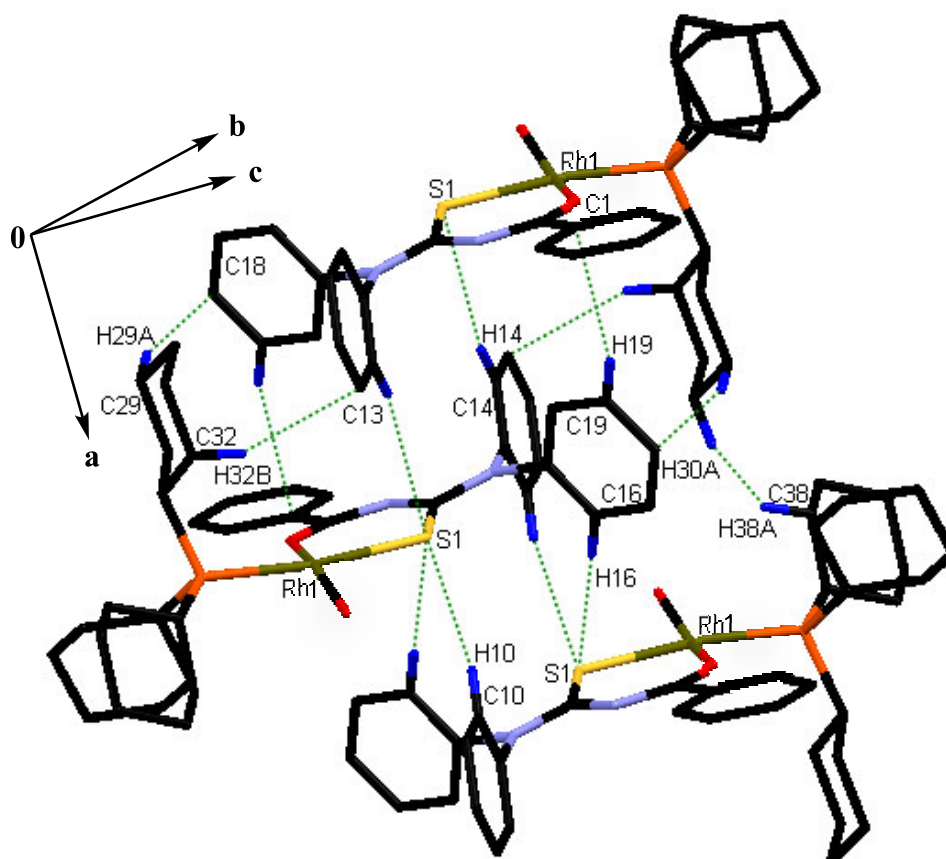


**Figure 7.13** An illustration of several soft contacts found between neighbouring molecules in the crystal packing of  $[\text{Rh}(\text{S},\text{O}-(\text{N-DiPT}))(\text{CO})(\text{PCy}_3)]$ . Some of the hydrogen atoms have been omitted for clarity. For distances and angles, see Table 7.5.

**Table 7.5** A list of distances and angles for some C...S and C...C soft contacts between adjacent molecules in the crystal packing of  $[\text{Rh}(\text{S},\text{O}-(\text{N-DiPT}))(\text{CO})(\text{PCy}_3)]$ .

Soft contact	Distance (Å)	Angle (°)
C10-H10...S1	2.968	167.7
C14-H14...S1	2.994	140.3
C16-H16...S1	2.851	179.4
C19-H19...C1	2.788	144.9
C29-H29A...C18	2.793	159.4
C32-H32B...C13	2.726	150.8
C38-H38A...H30A	2.273	137.9



## 7.4.6. Interpretation and correlation of structural properties of [Rh(*N*-diPT)(CO)(PR<sub>1</sub>R<sub>2</sub>R<sub>3</sub>)] complexes

### 7.4.6.1 Molecular geometry

Table 7.5 provides a summary of important geometrical parameters obtained from the crystallographic data as well as some selected analytical data.

**Table 7.6 Selected geometric parameters and analytical data for the complexes (i) [Rh(*S,O*-(*N*-diPT)(CO)(PPh<sub>3</sub>)], (ii) [Rh(*S,O*-(*N*-diPT)(CO)(PPh<sub>2</sub>Cy)] and (iii) [Rh(*S,O*-(*N*-diPT)(CO)(PCy<sub>3</sub>)].**

Selected parameters	(i)		(ii)	(iii)
	Molecule A	Molecule B		
<b>Rh1-P1 (Å)</b>	2.291(1)	2.278(1)	2.287(1)	2.302(1)
<b>Rh1-S1 (Å)</b>	2.304(1)	2.312(1)	2.312(1)	2.329(1)
<b>Rh1-O1 (Å)</b>	2.039(2)	2.037(2)	2.037(3)	2.057(3)
<b>Rh1-C39 (Å)</b>	1.791(3)	1.804(3)	1.798(5)	1.788(5)
<b>C39-O2 (Å)</b>	1.154(4)	1.153(4)	1.155(5)	1.157(6)
<b>Rh1-C39-O2 (°)</b>	175.3(3)	177.6(3)	177.8(4)	178.0(5)
<b>S1-Rh1-O1 (°)</b>	91.1(1)	91.7(1)	91.1(1)	91.7(1)
<b>Θ<sub>E</sub> (°) (phosphine)</b>	142.8	147.9	154.0	155.5
<b>ν<sub>CO</sub> (cm<sup>-1</sup>) (solid state)</b>	1963		1966	1952
<b>ν<sub>CO</sub> (cm<sup>-1</sup>) (DCM)</b>	1979		1972	1963
<b><sup>1</sup>J<sub>Rh-P</sub> (Hz) (DCM)</b>	152.3		149.4	145.6

By comparing the Rh-P, Rh-S, Rh-O and Rh-C bond lengths of [Rh(*S,O*-(*N*-diPT)(CO)(PPh<sub>3</sub>)] and [Rh(*S,O*-(*N*-diPT)(CO)(PPh<sub>2</sub>Cy)], it is noted that the values are very similar. The two independent molecules **A** and **B** of [Rh(*S,O*-(*N*-diPT)(CO)(PPh<sub>3</sub>)] revealed slight differences in the Rh-P as well as Rh-S bond lengths, where the respective values for the Rh-P bonds are 2.291(1) and 2.278(1) Å and that of the Rh-S bonds are 2.304(1) and 2.312(1) Å. However, the values of these bonds for [Rh(*S,O*-(*N*-diPT)(CO)(PPh<sub>2</sub>Cy)] compared well with those for molecule **B** of [Rh(*S,O*-(*N*-diPT)(CO)(PPh<sub>3</sub>)], where the Rh-P and Rh-S bond distances have values of 2.287(1) and 2.312(1) Å, respectively. The Rh-O bond lengths for molecules **A** and **B** of [Rh(*S,O*-(*N*-diPT)(CO)(PPh<sub>3</sub>)] as well as [Rh(*S,O*-(*N*-diPT)(CO)(PPh<sub>2</sub>Cy)] are similar having respective values of 2.039(2), 2.037(2) and 2.037(3) Å, respectively. The Rh-C bond length for [Rh(*S,O*-(*N*-diPT)(CO)(PPh<sub>2</sub>Cy)] compared well with that for molecule **B** of [Rh(*S,O*-(*N*-diPT)(CO)(PPh<sub>3</sub>)], having values of

1.798(5) and 1.804(3) Å, respectively. The Rh-C bond distance for molecule **A** of [Rh(*S,O*-(*N*-diPT)(CO)(PPh<sub>3</sub>))] was slightly different from the latter distances with a value of 1.791(3) Å. Thus the replacement of one phenyl ring with a cyclohexyl ring on the phosphine did not reveal to have much electronic influence on the geometric parameters of [Rh(*S,O*-(*N*-diPT)(CO)(PPh<sub>2</sub>Cy))]. Even though this was the case the first order coupling constants  $^1J_{Rh-P}$  on  $^{31}P$  NMR and the carbonyl stretching frequency  $\nu_{CO}$  on IR for these complexes revealed large differences in the electro-steric properties of the phosphine ligands.

Comparing the bond lengths of these two complexes mentioned before with [Rh(*S,O*-(*N*-diPT)(CO)(PCy<sub>3</sub>))], where the other two phenyl rings on the phosphine were replaced by cyclohexyl rings, more significant differences in the values were observed. More specifically, the Rh-P, Rh-S and Rh-O bond lengths increased with a value of about 0.01-0.02 Å from the values of the complexes mentioned above to values of 2.302(1), 2.329(1) and 2.057(3) Å, respectively. The slight increase in the Rh-P bond length suggested that PCy<sub>3</sub> is generally a better  $\sigma$ -donor and weaker  $\pi$ -acceptor than PPh<sub>3</sub> as would be expected from an electronic point of view. This was also reflected in the slight decrease in the Rh-C bond length of about 0.01 Å, where it is expected that a stronger  $\sigma$ -donating phosphine should allow more  $\pi$ -back donation to other ligands. However, it should be noted that these differences in the values are very small and do not necessarily truly reflect the electronic properties of the phosphine ligands.

The bond lengths of the carbonyl ligand on each complex were found to be comparable with values of 1.154(4), 1.153(4), 1.155(5) and 1.157(6) Å for molecule **A** of [Rh(*S,O*-(*N*-diPT)(CO)(PPh<sub>3</sub>))], molecule **B** of [Rh(*S,O*-(*N*-diPT)(CO)(PPh<sub>3</sub>))], [Rh(*S,O*-(*N*-diPT)(CO)(PPh<sub>2</sub>Cy))] and [Rh(*S,O*-(*N*-diPT)(CO)(PCy<sub>3</sub>))] , respectively. On the other hand the  $\nu_{CO}$  values for [Rh(*S,O*-(*N*-diPT)(CO)(PPh<sub>3</sub>))], [Rh(*S,O*-(*N*-diPT)(CO)(PPh<sub>2</sub>Cy))] and [Rh(*S,O*-(*N*-diPT)(CO)(PCy<sub>3</sub>))] in the solid state are 1963, 1966 and 1952, respectively. Thus even though large differences are found in the carbonyl frequency shifts ( $\nu_{CO}$ ) of these complexes, it is not reflected in the solid state geometry of these complexes. Surprisingly the  $\nu_{CO}$  values in the liquid phase were found to be much different from those obtained in the solid state, where the values for [Rh(*S,O*-(*N*-diPT)(CO)(PPh<sub>3</sub>))], [Rh(*S,O*-(*N*-diPT)(CO)(PPh<sub>2</sub>Cy))] and [Rh(*S,O*-(*N*-diPT)(CO)(PCy<sub>3</sub>))] shifted to 1979, 1972 and 1963, respectively. Note that the  $\nu_{CO}$  values in the liquid state followed the expected order of electron-donating properties of the phosphine ligands compared to those obtained in the solid state. This phenomenon is

not new as it has been shown by Kemp *et al.*<sup>16</sup> that packing effects in the solid state can have significant influences on the values of  $\nu_{\text{CO}}$  for rhodium complexes compared to the liquid state measurements. It has been shown that this is normally the effect of a bend in the Rh-carbonyl moiety, however, the Rh-C-O angles were found to be almost linear in all three  $[\text{Rh}(\text{S}, \text{O}-(N\text{-diPT})(\text{CO})(\text{PR}_1\text{R}_2\text{R}_3)]$  complexes reported here.

As was discussed before in Sections 7.4.3-7.4.5 the effective cone angles for each complex were calculated using the observed Rh-P distances. It is observed in Table 7.6 that these values followed the order of  $[\text{Rh}(\text{S}, \text{O}-(N\text{-diPT})(\text{CO})(\text{PCy}_3)] > [\text{Rh}(\text{S}, \text{O}-(N\text{-diPT})(\text{CO})(\text{PPh}_2\text{Cy})] > [\text{Rh}(\text{S}, \text{O}-(N\text{-diPT})(\text{CO})(\text{PPh}_3)]$ . This showed the expected order of steric increase from  $\text{PPh}_3$  to  $\text{PCy}_3$  with increasing values. It can be noted, however, that the values between  $[\text{Rh}(\text{S}, \text{O}-(N\text{-diPT})(\text{CO})(\text{PPh}_2\text{Cy})]$  and  $[\text{Rh}(\text{S}, \text{O}-(N\text{-diPT})(\text{CO})(\text{PCy}_3)]$  differed surprisingly only by a small amount. This can be explained by the fact that intermolecular interactions between molecules in the solid state can alter the orientations of the different phenyl and cyclohexyl rings. This has been illustrated by Ferguson *et al.*,<sup>17</sup> where it was revealed how the ligand orientations can differ from liquid to solid state. It can therefore be concluded that the values of the effective cone angle obtained in solid state do not necessarily reflect the true steric properties of the phosphine ligand in solution.

---

<sup>16</sup> Kemp, G.; Roodt, A.; Purcell, W. (1995) *Rhodium Express*, **12**, 21.

<sup>17</sup> Ferguson, G.; Roberts, P. J.; Alyea, E. C.; Khan, M. (1978) *Inorg. Chem.*, **17**, 2965.

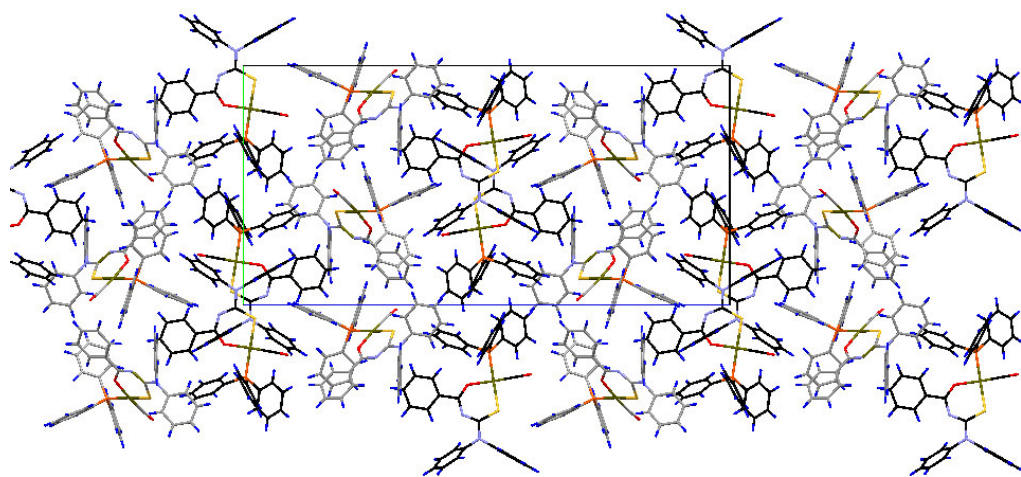
#### 7.4.6.2 Molecular packing

As was observed before in Sections 7.4.3-7.4.5 in all three structures that were solved and discussed, complexes of the type  $[\text{Rh}(S,O\text{-}(N\text{-diPT})(\text{CO})(\text{PR}_1\text{R}_2\text{R}_3))]$  were found to crystallize primarily in the monoclinic space group  $P2_1/c$ . Although there is not much data available on the CSD on  $[\text{Rh}(S,O\text{-thioureato})(\text{CO})(\text{PR}_1\text{R}_2\text{R}_3)]$  complexes, the two variations that have been reported by Roodt *et al.*<sup>18</sup> and Kemp *et al.*,<sup>19</sup> mentioned before in Chapter 2, which included carbonyl(triphenylphosphine)( $S,O\text{-}(N\text{-benzoyl-}N',N'\text{-dibenzylthioureato})\text{rhodium(I)}$ ) and carbonyl(triphenylarsine)( $S,O\text{-}(N\text{-benzoyl-}N',N'\text{-dibenzylthioureato})\text{rhodium(I)}$ ), revealed that this hold true for these complexes as well. The first complex crystallised in the monoclinic space group  $P2_1/n$  and the latter in  $P2_1/c$ . It might therefore be extended to say that this could be expected in general for any  $[\text{Rh}(S,O\text{-thioureato})(\text{CO})(\text{PR}_1\text{R}_2\text{R}_3)]$  complexes that might still be obtained.

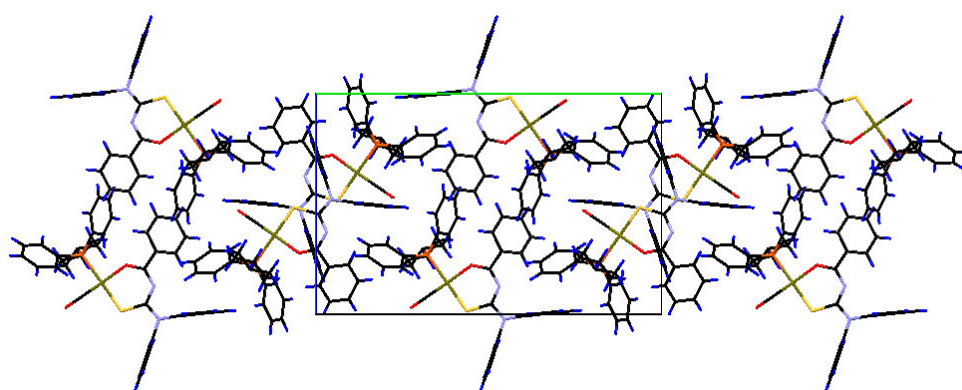
A summary of the general molecular packing across one layer in the unit cell is shown in Figure 7.14 for each of the complex structures that were reported in this chapter. Looking back in Table 7.1 it can be observed that the two structures of complexes  $[\text{Rh}(S,O\text{-}(N\text{-diPT})(\text{CO})(\text{PPh}_2\text{Cy}))]$  and  $[\text{Rh}(S,O\text{-}(N\text{-diPT})(\text{CO})(\text{PCy}_3))]$  were found to be isomorphous. This is based on the fact that the unit cell values are similar and a careful look in Figures 7.14b and 7.14c reveal that these structures are even packed in the same manner in the unit cell. The only difference as observed in Figures 7.14b and 7.14c, is that the general position (x, y, z) of a molecule of  $[\text{Rh}(S,O\text{-}(N\text{-diPT})(\text{CO})(\text{PPh}_2\text{Cy}))]$  changed to the position (x, y+0.5, 1-z) for a molecule of  $[\text{Rh}(S,O\text{-}(N\text{-diPT})(\text{CO})(\text{PCy}_3))]$ . It can be observed in both cases that the molecules orientated in the crystal packing in a wave-like fashion along the b-axis as indicated by red-dotted lines, which alters direction at each following layer along the c-axis.

<sup>18</sup> Roodt, A.; Leipoldt, J. G. (1994) *Rhodium Express*, **7-8**, 39.

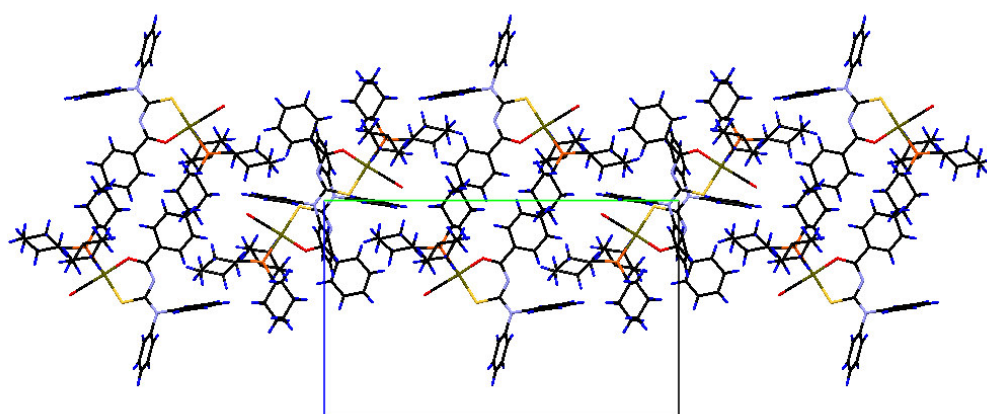
<sup>19</sup> Kemp, G.; Roodt, A.; Purcell, W. (1996) *Rhodium Express*, **16**, 17.



a)  $[\text{Rh}(\text{S},\text{O}-(\text{N-diPT})(\text{CO})(\text{PPh}_3)]$



b)  $[\text{Rh}(\text{S},\text{O}-(\text{N-diPT})(\text{CO})(\text{PPh}_2\text{Cy})]$



c)  $[\text{Rh}(\text{S},\text{O}-(\text{N-diPT})(\text{CO})(\text{PCy}_3)]$

**Figure 7.14** An illustration of the general molecular packing for each of the  $[\text{Rh}(\text{S},\text{O}-(\text{N-diPT})(\text{CO})(\text{PR}_1\text{R}_2\text{R}_3)]$  complexes that were reported in this chapter.

[Rh(*S,O*-(*N*-diPT)(CO)(PPh<sub>3</sub>)] has two independent molecules in the asymmetric unit (indicated by black and gray carbons, respectively in Figure 7.14a), which resulted in the lengthening of the *c*-axis of the unit cell with almost double the value compared to the other structures. The rest of the unit cell parameters are similar to the other two structures, which suggests that the isomorphism was broken by the addition of an independent molecule in the unit cell. However, considering that the general orientation and geometrical parameters of atoms in the different complex structures correlate well, it can be concluded that [Rh(*S,O*-(*N*-diPT)(CO)(PPh<sub>3</sub>)] is isostructural to complexes [Rh(*S,O*-(*N*-diPT)(CO)(PCy<sub>3</sub>)] and [Rh(*S,O*-(*N*-diPT)(CO)(PPh<sub>2</sub>Cy)]. A careful look in Figure 7.14 reveals that [Rh(*S,O*-(*N*-diPT)(CO)(PPh<sub>3</sub>)] also exhibit the wave-like pattern of molecules for both independent molecules in the crystal packing as observed for the other complexes.

It was already shown and discussed that no significant interactions were observed between molecules in the crystal packing of each of these structures and therefore these packings were majorly stabilized by basic Van der Waals interactions. Most of these contacts involved C...C and C...O soft contacts formed by the close approximation of neighbouring molecules.

## 7.5 Conclusion

The successful synthesis and characterization of four different [Rh(*S,O*-(*N*-diPT)(CO)(PR<sub>1</sub>R<sub>2</sub>R<sub>3</sub>)] complexes, where *N*-diPT is *N*-benzoyl-*N'*,*N'*-diphenylthiourea, are reported in Chapter 7. Despite the different coordination modes that the *S,O*-thiourea ligands display, as highlighted in Chapter 6, it was found that the synthetic route utilized in this chapter led to reproducible results for the synthesis of [Rh(*S,O*-(*N*-diPT)(CO)(PR<sub>1</sub>R<sub>2</sub>R<sub>3</sub>)]. NMR and IR spectroscopic techniques, together with elemental analysis could clearly identify and confirm the formation of these complexes. <sup>31</sup>P NMR spectroscopy showed that the electronic properties of the phosphine ligands on the complexes increased in the order of PPh<sub>3</sub> < PPh<sub>2</sub>Cy < PPhCy<sub>2</sub> < PCy<sub>3</sub> as suggested by the first-order coupling constants *J*<sub>Rh-P</sub>, which decreases in that order from 152.3 to 145.6 ppm. This is further confirmed by IR spectroscopy where the carbonyl stretching frequencies (ν<sub>CO</sub>) also decreases in the same order from 1979 to 1963 cm<sup>-1</sup> in the liquid state.

Further proof on the identity of these complexes was provided by the successful characterization of three of these complexes by single crystal X-ray diffraction. A summary of the major geometrical and spectroscopic differences between these three complexes are provided in Table 7.5, as a result of altering phosphine ligands. Very small differences were observed in the geometric parameters of these complexes, despite the large differences in the respective first order coupling constants ( $^1J_{Rh-P}$ ) and the carbonyl stretching frequencies ( $\nu_{CO}$ ).

The effective cone angles that were calculated using the Rh-P bond lengths, were found to follow the order  $[Rh(S,O-(N\text{-}diPT)(CO)(PCy_3)] > [Rh(S,O-(N\text{-}diPT)(CO)(PPh_2Cy)] > [Rh(S,O-(N\text{-}diPT)(CO)(PPh_3)]$ . This revealed the steric increase in the subsequent replacement of the phenyl rings on  $PPh_3$  with cyclohexyl rings. With the success of obtaining these  $[Rh(S,O-(N\text{-}diPT)(CO)(PR_1R_2R_3)]$  complexes and the related analytical data, the next step of the study which involves the kinetic study of oxidative addition of methyl iodide to these complexes was embarked upon. Here the electro-steric effects of the different phosphine ligands on the metal complexes are investigated by analysing the kinetic and thermodynamic parameters obtained from these oxidative addition reactions and comparing them to the geometric and analytical data obtained in Chapter 7.

# **CHAPTER 8**

## **KINETIC STUDY ON THE OXIDATIVE ADDITION OF IODOMETHANE TO $[\text{Rh}(\text{S},\text{O}\text{-THIOUREATO})(\text{CO})_2]$ and $[\text{Rh}(\text{S},\text{O}\text{-THIOUREATO})(\text{CO})(\text{PR}_1\text{R}_2\text{R}_3)]$ COMPLEXES**

### **8.1 Introduction**

Oxidative addition reactions on metal complexes were discussed in Chapter 2 in detail and it was clear from that section that it is one of the key features in many catalytic processes, including the carbonylation of methanol as well as cross-coupling reactions. It has been argued several times that this is the rate-determining step in the catalytic cycles of these processes depending on the nature of the reagent used, and therefore any influence on this step can determine the course of the whole catalytic cycle.<sup>1</sup> Due to the vital role that this reaction plays, a large amount of research has thus been focused on oxidative addition reactions in order to understand its kinetic properties and responses to external and internal influences.

Iodomethane oxidative addition on rhodium complexes, which is important in industrial processes such as the Monsanto and Cativa processes, has been studied intensively with a variety of mono- and bidentate ligands as was discussed in Chapter 2. In general, it was discovered that changing the type of ligand or altering the electro-steric properties of the ligand result in significant changes in the outcome of the catalytic process involved. One set of rhodium complexes on which little studies has been done include  $[\text{Rh}(\text{S},\text{O}\text{-thioureato})(\text{CO})_2]$  and  $[\text{Rh}(\text{S},\text{O}\text{-thioureato})(\text{CO})(\text{PR}_1\text{R}_2\text{R}_3)]$  complexes, which was a focus of this Ph.D. study. It was also clearly indicated in Chapters 6 and 7 that not much crystallographic data are available for these kinds of systems.

Several examples were already provided in Section 2.5 in Chapter 2 on oxidative addition reactions to Rh(I) complexes found in literature. These studies commenced after the

---

<sup>1</sup> van Leeuwen, P.W.N.M. (2004) *Homogeneous Catalysis, Understanding the art*, Kluwer Academic Publishers, Dordrecht.



discovery of the carbonylation processes mentioned above, which employed the use of metal carbonyl complexes. The CO ligand is essential to allow the formation of acyl adducts *via* CO migratory insertion into the metal alkyl bonds formed during the oxidative addition of alkyl iodides. In the Monsanto process the metal carbonyl species involved  $[\text{Rh}(\text{I})_2(\text{CO})_2]$  species, which was found to be relatively unstable and allow side reactions to occur, as was already discussed in Section 2.4.2 in Chapter 2. Several modifications of the catalyst shown in the examples provided in Section 2.5 in Chapter 2, revealed that rhodium carbonyl species containing phosphine ligands and/or bidentate ligands are generally found to be far more stable than the original catalyst. Furthermore, by tweaking the electro-steric properties of these ligands, the carbonylation process is directed towards different outcomes.

In the particular case where bidentate ligands containing a sulphur donor atom were utilized, it was shown that the oxidative addition of iodomethane to the corresponding complexes primarily led to the formation of Rh(III)-acyl complexes.<sup>2a,b,c</sup> Since the present Ph.D. study required the use of Rh(III)-acyl species for the mechanistic investigation of the reductive carbonylation of methanol, it was considered important to find possible ligands that would allow the formation of these species from the corresponding Rh(I) carbonyl complexes. Therefore, in conjunction with the conclusive evidence that sulphur-containing bidentate ligands lead to Rh(III)-acyl formation and the fact that little data is available on Rh complexes containing *S,O*-bidentate ligands, it was decided to synthesize and utilize Rh *S,O*-thiourea carbonyl species. The synthetic aspects and subsequent characterization of the thiourea ligands and corresponding Rh complexes were already presented and discussed in Chapters 3, 4, 6 and 7. In this chapter the oxidative addition of MeI to the synthesized  $[\text{Rh}(\text{S},\text{O}\text{-thioureato})(\text{CO})_2]$  and  $[\text{Rh}(\text{S},\text{O}\text{-thioureato})(\text{CO})(\text{PR}_1\text{R}_2\text{R}_3)]$  complexes are described for which the consequent kinetic and thermodynamic aspects are discussed.

The definition and effects of electro-steric properties of phosphine ligands were discussed in Chapter 1 and it was pointed out that large differences in these properties can lead to different outcomes in catalytic processes. As was discussed in Chapter 2, oxidative addition is one of the key reactions in many transition metal catalytic processes and has been shown through much research to be dependent on the metal as well as the ligands properties. In this study a

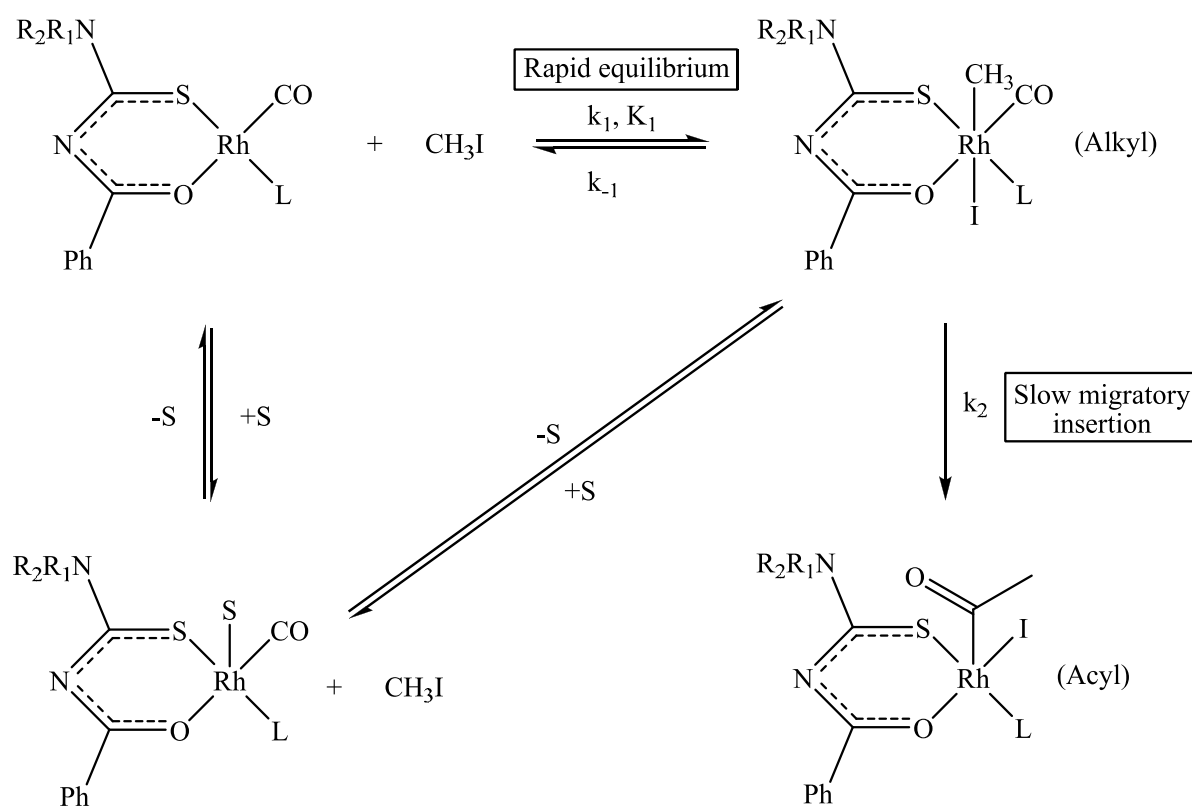
---

<sup>2</sup> a) Venter, J. A.; Leipoldt, J. G.; van Eldik, R. (1991) *Inorg. Chem.*, **30**, 2207. b) Steyn, G. J. J.; Roodt, A.; Leipoldt, J. G. (1993) *Rhodium Express*, **1**, 25. c) Gonsalvi, L; Adams, H.; Sunley, G. J.; Ditzel, E.; Haynes, A. (2002) *J. Am. Chem. Soc.*, **124**, 13597.

range of phosphines were chosen that followed a chronological order in the electro-steric properties of these ligands. These ligands were  $\text{PPh}_3$ ,  $\text{PPh}_2\text{Cy}$ ,  $\text{PPhCy}_2$ , and  $\text{PCy}_3$ , thus starting with triphenylphosphine and subsequently substituting a phenyl ring with a cyclohexyl ring up to tricyclohexylphosphine. The respective  $[\text{Rh}(N\text{-diPT})(\text{CO})(\text{PR}_1\text{R}_2\text{R}_3)]$  complexes of these ligands were then utilised to study the electro-steric influences of the phosphine ligands on the oxidative addition reaction.

## 8.2 Theoretical background

To assist and explain the results obtained from the oxidative addition reactions, some basic theoretical background will be discussed in this section. The proposed reaction route of iodomethane oxidative addition onto rhodium complexes is provided in Figure 8.1.<sup>3a,b</sup>



$\text{L} = \text{CO}$  or  $\text{PR}_1\text{R}_2\text{R}_3$ ,  $S = \text{solvent}$

**Figure 8.1** A representation of the reaction scheme for the iodomethane oxidative addition on rhodium  $S,O$ -thiourea complexes.

<sup>3</sup> a) Conradie, M. M.; Conradie, J. (2008) *Inorg. Chim. Acta*, **361**, 208. b) Roodt, A.; Steyn, G. J. J. (2000) *Recent Res. Devel. Inorg. Chem.*, **2**, 1.

Generally, the oxidative addition of iodomethane to rhodium complexes leads to the formation of two distinct species, namely, rhodium alkyl and rhodium acyl species as shown in Figure 8.1. First, as the iodomethane add to the rhodium complex the alkyl species forms, after which migratory insertion of the CO ligand into the metal-methyl group leads to the formation of the acyl species. In some cases a solvent pathway is also observed where a solvent molecule can easily co-ordinate onto the rhodium centre and be substituted upon the addition of an iodomethane molecule.

The general rate of the reaction as defined by the rate of formation of the rhodium(III) acyl species is given in Equation 8.1,

$$\frac{d[Rh(acyl)]}{dt} = k_2[Rh(alkyl)] \quad (8.1)$$

Since the total process involves a fast equilibrium (with  $k_1, k_{-1} \gg k_2$ ) in the first reaction shown in Figure 8.1, the pre-equilibrium approximation method is utilized in order to relate the total reaction rate to the starting materials.<sup>4a,b,c</sup> When the reaction reaches thermodynamic equilibrium, the forward reaction rate equals the backward reaction rate and is related by the equilibrium constant  $K_1$  in equation 8.2, where tu = *S,O*-thiourea ligand,

$$K_1 = \frac{[Rh(alkyl)]}{[Rh(tu)(CO)(L)][MeI]} = \frac{k_1}{k_{-1}} \quad (8.2)$$

Therefore, by rearranging the equation an expression for  $[Rh(alkyl)]$  is given by,

$$[Rh(alkyl)] = K_1[Rh(tu)(CO)(L)][MeI] \quad (8.3)$$

At some point of the reaction, where the Rh(III)-acyl species has not formed yet, the total rhodium concentration  $[Rh]_{tot}$  is given by,

$$[Rh]_{tot} = [Rh(tu)(CO)(L)] + [Rh(alkyl)] \quad (8.4)$$

---

<sup>4</sup> a) Upadhyay, S. K. (2006) *Chemical Kinetics and Reaction Dynamics*, Anamaya Publishers, New Delhi, Ch. 3. b) Rae, M.; Berberan-Santos, M. N. (2004) *J. Chem. Educ.*, **81**, 3, 436. c) Connors, K. A. (1990) *Chemical Kinetics, The Study of Reaction Rates in Solution*, VCH Publishers, New York, Ch. 3, 96.

Therefore, by rearranging the equation and substituting the resulting expression into equation 8.3, equation 8.5 is afforded,

$$\begin{aligned} K_1[MeI][Rh]_{tot} &= [Rh(alkyl)] + K_1[Rh(alkyl)][MeI] \\ &= [Rh(alkyl)](1 + K_1[MeI]) \end{aligned} \quad (8.5)$$

By rearranging the equation the expression for  $[Rh(alkyl)]$  is simplified to equation 8.6,

$$[Rh(alkyl)] = \frac{K_1[MeI][Rh]_{tot}}{1 + K_1[MeI]} \quad (8.6)$$

By substituting equation 8.6 into 8.1 the total reaction rate is given by equation 8.7,

$$\frac{d[Rh(acyl)]}{dt} = \frac{k_2 K_1 [MeI] [Rh]_{tot}}{1 + K_1 [MeI]} \quad (8.7)$$

From equation 8.7, it is observed that this reaction generally follows a second-order process where the rate is therefore dependent on both the overall rhodium complex and the iodomethane concentration. Although it is viable to analyse the kinetic parameters of a second-order reaction, it is often quite difficult and tedious. To overcome this situation the reaction rate is done under pseudo first-order conditions, therefore allowing the rate to be mainly dependent on only one of these concentrations. It is usual to keep the metal concentration constant and vary the reagent (MeI) concentration to a very large value compared to the metal concentration from which the dependence thereupon is determined. Thus if  $[MeI] \gg [Rh]_{tot}$ ,

$$\frac{d[Rh(acyl)]}{dt} = k_{obs}[Rh]_{tot} \quad (8.8)$$

where,

$$k_{obs} = \frac{k_2 K_1 [MeI]}{1 + K_1 [MeI]} \quad (8.9)$$

The Beer-Lambert law<sup>4a</sup> defines the relationship between the amount of energy a species absorb and its concentration as shown in equation 8.10,

$$A = \varepsilon \times l \times C \quad (8.10)$$

$A$  = absorbance,  $\varepsilon$  = molar extinction coefficient,  $C$  = concentration and  $l$  = light path length. Considering that the relationship between the concentration change of the species involved at times 0 and  $t$ , where  $\frac{[C]_t}{[C]_0} = \frac{A_\infty - A_t}{A_\infty - A_0}$ , the observed rate constant is given by equation 8.11,

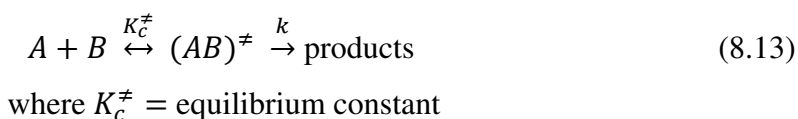
$$[C]_t = [C]_0 e^{k_{obs}t} \quad (8.11)$$

The Beer-Lambert law is modified using equation 8.11 to give equation 8.12,

$$A_t = A_\infty - (A_\infty - A_0)e^{k_{obs}t} \quad (8.12)$$

$A_t$  and  $A_\infty$  are the absorbance after time  $t$  and at the time of reaction completeness, respectively. A least-squares fit utilizing absorbance vs. time data for a first-order reaction, thus yields  $k_{obs}$  for the reaction. The data was analysed utilizing the computer software Scientist,<sup>5</sup> using equation 8.12 for  $k_{obs}$  determination.

In order to calculate the activation parameters of these reactions the Eyring equation is used, based on the Transition State Theory.<sup>4a</sup> The Transition State Theory states that an activated complex or transition state is in equilibrium with the reagents before the reaction occurs, and that the rate is given by the decomposition rate,  $k$ , of the activated complex to yield the products, as illustrated by equation 8.13,




---

<sup>5</sup> Scientist for Windows (32), Micromath Inc., Version 2.01, 1986-1995.

The exponential form of the Eyring equation is given by equation 8.14,

$$k = \frac{k_B T}{h} e^{-\Delta G^\ddagger / RT} \quad (8.14)$$

Here,  $k_B$  is the Boltzmann constant,  $h$  the Planck constant,  $\Delta G^\ddagger$  the Gibbs free energy of activation and absolute  $T$  the temperature at which the reaction takes place. This equation is rewritten in logarithmic form to yield equation 8.15,

$$\begin{aligned} \ln(k/T) &= \ln(k_B/h) + (-\Delta G^\ddagger / RT) \\ &= \ln(k_B/h) + (\Delta S^\ddagger / R) - (\Delta H^\ddagger / RT) \end{aligned} \quad (8.15)$$

Therefore if  $\ln(k/T)$  is plotted against  $1/T$ , the enthalpy of activation  $\Delta H^\ddagger$  is obtained from the slope of the plot whilst the entropy of activation  $\Delta S^\ddagger$  is obtained from the intercept of the plot. The Gibbs free energy of activation is calculated from these parameters using equation 8.16,

$$\Delta G^\ddagger = \Delta H^\ddagger - T\Delta S^\ddagger \quad (8.16)$$

The activation energy  $E_a$  for a reaction is calculated from the Arrhenius equation as given by equation 8.17,

$$k = Ae^{-E_a/RT} \quad (8.17)$$

The equation is rewritten in the logarithmic form to yield equation 8.18,

$$\ln k = \ln A - (E_a / RT) \quad (8.18)$$

Therefore if  $\ln k$  is plotted against  $1/T$ , the activation energy  $E_a$  is obtained from the slope of the plot.

A last concept that is also important is the reaction half-life, which is defined as the time that is required to convert 50% of the reactant during some reaction. The reaction half-life for first order reactions is calculated using equation 8.19,

$$t_{1/2} = \frac{\ln(2)}{k_{obs}} = \frac{0.6932}{k_{obs}} \quad (8.19)$$

### 8.3 Experimental

All kinetic experiments were carried out in air and all solvents were pre-dried over aluminiumoxide and distilled. The rhodium metal complexes were synthesised, characterized and purified as described in Chapter 7.

<sup>31</sup>P NMR spectra were recorded on a 300 MHz Bruker spectrometer. Only 32 scans were collected per spectrum since the oxidative addition reactions were relatively fast as will be shown later in this chapter. This was necessary in order to display the whole reaction profile for these reactions. <sup>31</sup>P chemical shifts are reported relative to triphenylphosphine oxide (29.9 ppm); positive shifts are downfield. The FT-IR spectra were recorded as liquid samples in dry organic solvents (toluene/dichloromethane) in a NaCl cell on a Bruker Tensor 27 spectrometer in the range of 2350-1600 cm<sup>-1</sup>, equipped with a temperature cell regulator accurate within 0.3 °C. UV/Vis absorbance spectra were collected on a Varian Cary 50 Conc spectrophotometer in a 1.000 ± 0.001 cm quartz cuvette, which was equipped with a temperature cell regulator accurate within 0.1 °C. Kinetic data was analyzed with the Scientist<sup>5</sup> software package.

UV/VIS spectrophotometry can also be used to study the kinetics of these reactions under pseudo first-order conditions, which provides the ability to analyse several reactions at the same time.<sup>3,6a,b</sup> It was therefore decided to do a few trial runs at different conditions in order to test whether this was a feasible method. In DCM the [Rh(*N*-diPT)(CO)(PR<sub>1</sub>R<sub>2</sub>R<sub>3</sub>)] complexes were found to have absorbance peaks at wavelengths of 250-265 nm. This already indicated a possible problem since iodomethane has an absorbance peak at 250 nm. Generally, there are two different background corrections available on the UV/VIS

---

<sup>6</sup> For a few examples see: a) Basson, S. S.; Leipoldt, J. G.; Roodt, A.; Venter, J. A.; van der Walt, T. J. (1986) *Inorg. Chim. Acta.*, **119**, 35. b) Roodt, A.; Otto, S.; Steyl, G. (2003) *Coord. Chem. Rev.*, **245**, 121.

spectrophotometer that are utilized: i) The zero function, which sets the matrix of the sample to an absorbance value of zero or ii) the baseline function, with which a spectrum of the sample matrix is taken and subtracted from the observed spectra. Due to the relative high concentration of iodomethane that had to be used in order to perform the oxidative addition reaction at pseudo first-order conditions, neither of the techniques was suitable. Firstly the iodomethane concentration was too large to set its absorbance value to zero and therefore was still present in the observed spectra. As a result the complex peak was obscured behind the iodomethane peak. The baseline function resulted in the subtraction of the complex absorbance value along with that of the iodomethane resulting in spectra that only displayed random noise. This was ascribed to the large concentration difference with a factor of at least 10 times between the metal complex and the iodomethane. Therefore no reaction could be observed on the spectra and as such UV/VIS spectrophotometry could not be utilised. It was therefore decided to analyse these oxidative addition reactions further *via* FT-IR spectroscopy.

## 8.4 Results and discussion

### 8.4.1 Oxidative addition of iodomethane to a range of $[\text{Rh}(\text{S},\text{O-thioureato})(\text{CO})_2]$ complexes

The importance of the use of  $[\text{Rh}(\text{S},\text{O-thioureato})(\text{CO})_2]$  complexes in this study was already discussed in Section 8.1. The synthesis of these complexes was shown and discussed in detail in Section 6.2 in Chapter 6. The difficulties that were encountered during the synthesis of these  $[\text{Rh}(\text{S},\text{O-thioureato})(\text{CO})_2]$  complexes were clearly stipulated. However, some of these complexes could be isolated in a fairly stable state, even though they could not be properly dried due to their instability upon the removal of solvent molecules as was discussed in Section 6.2 in Chapter 6. These complexes were characterized on IR spectroscopy, but their identity was only confirmed at a later stage by conclusive results that were discussed in Chapter 7. This included the structural identification of the  $[\text{Rh}(\text{N-diPT})(\text{CO})(\text{PR}_1\text{R}_2\text{R}_3)]$  complexes, which was obtained from  $[\text{Rh}(\text{N-diPT})(\text{CO})_2]$  as shown in Section 7.3. Furthermore,  $[\text{Rh}(\text{N-diPT})(\text{CO})_2]$  was synthesized by the same method as the other  $[\text{Rh}(\text{S},\text{O-thioureato})(\text{CO})_2]$  complexes reported in Section 6.2 in Chapter 6, which after IR



analysis provided similar  $\nu_{\text{CO}}$  values in comparison to those for the primary products reported in Table 6.1.

It was therefore accepted that the primary products defined in Table 6.1 were the  $[\text{Rh}(\text{S},\text{O}\text{-thioureato})(\text{CO})_2]$  complexes, even though no structural data could be obtained for any of these complexes. It has been shown before that Rh(III)-acyl complexes can also form crystals in solution of which a few examples<sup>7a,b,c</sup> were already discussed in Section 2.5 in Chapter 2. It was therefore decided to perform the iodomethane oxidative addition to the  $[\text{Rh}(\text{S},\text{O}\text{-thioureato})(\text{CO})_2]$  complexes and attempt to isolate the resulting complexes as crystals.

The oxidative addition of iodomethane to these complexes were monitored on IR spectroscopy in toluene in order to elucidate if Rh-acyl formation would occur and whether it was feasible to study the kinetics of these systems. Note that because these complexes were not sufficiently dry, the exact concentrations of these complexes could not be established accurately. However, since the rate of the iodomethane oxidative addition to these complexes is not dependent on the metal concentration under pseudo first-order conditions as was shown in Section 8.2, it was considered worthwhile to perform this reaction under these condition using sufficiently large iodomethane concentrations.

A representation of the time-resolved IR spectra that were obtained for the iodomethane oxidative addition to the  $[\text{Rh}(\text{N}\text{-tmPT})(\text{CO})_2]$  complex ( $\text{N}\text{-tmPT}$  =  $\text{N}\text{-benzoyl-}N'\text{-2,4,6-trimethylphenylthiourea}$ ) is given in Figure 8.2. Five different peaks were observed that formed and/or disappeared within the time range of the study. It is clear that quite complex kinetic behaviour is observed.

---

<sup>7</sup> a) Basson, S. S.; Leipoldt, J. G.; Roodt, A.; Venter, J. A. (1987) *Inorg. Chim. Acta*, **128**, 31. b) Gonsalvi, L; Adams, H.; Sunley, G. J.; Ditzel, E.; Haynes, A. (2002) *J. Am. Chem. Soc.*, **124**, 13597. c) Gonsalvi, L; Adams, H.; Sunley, G. J.; Ditzel, E.; Haynes, A. (1999) *J. Am. Chem. Soc.*, **121**, 11233.

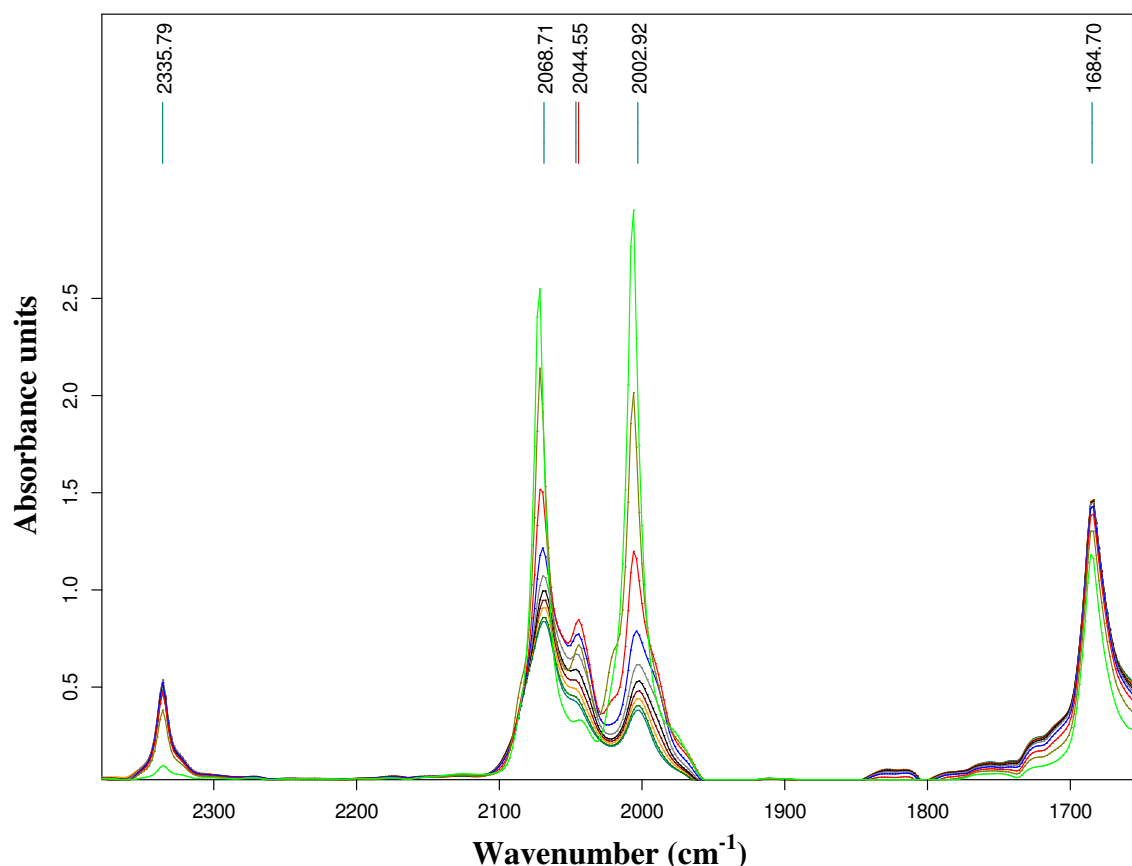


**Figure 8.2 IR spectra obtained for the iodomethane oxidative addition to  $[\text{Rh}(\text{N-}\text{tmPT})(\text{CO})_2]$  in toluene at 25 °C. Each spectrum was recorded at an interval of 430 min.  $[\text{Rh}] = 0.048 \text{ M}$ ,  $[\text{MeI}] = 0.4 \text{ M}$ , total time = 65 hrs.**

The change in the absorbance for each peak within a time period of 65 hrs is shown in Figure 8.3. First a peak at  $2336 \text{ cm}^{-1}$  was observed to form over time until it reached its maximum at about 1500 min and remained fairly constant from there. No true allocation could be made as to what species formed in this case, although it could be argued that this peak represents the carbonyl ligand in the  $[\text{Rh}(\text{N-}\text{tmPT})(\text{acyl})(\text{CO})(\text{I})]$  complex.

The peaks at 2069 and  $2003 \text{ cm}^{-1}$  represented the starting complex  $[\text{Rh}(\text{N-}\text{tmPT})(\text{CO})_2]$ , which disappeared over time as the reaction proceeded. However, it is observed in Figure 8.3 that the peak at  $2069 \text{ cm}^{-1}$  first increased for a while over a period of 150 min, before it started to decrease. This was possibly an indication that the expected peak representing the formation of the  $[\text{Rh}(\text{N-}\text{tmPT})(\text{COMe})(\text{CO})(\text{I})]$  was obscured behind the peak of the starting complex.

Another peak was observed at  $2045\text{ cm}^{-1}$ , which first increased to a maximum at about 825 min, after which it decreased during the rest of the time period. It was possible that this peak revealed the formation of the  $[\text{Rh}(\text{N-tmPT})(\text{ME})(\text{I})(\text{CO})_2]$  complex, since it is expected that this complex would form first after the addition of iodomethane and then convert to the  $[\text{Rh}(\text{N-tmPT})(\text{COMe})(\text{CO})(\text{I})]$  complex. Since  $[\text{Rh}(\text{N-tmPT})(\text{ME})(\text{I})(\text{CO})_2]$  is a dicarbonyl species, another peak was expected, which was probably obscured behind the  $[\text{Rh}(\text{N-tmPT})(\text{CO})_2]$  complex peaks.

Finally, a peak was observed from the beginning at  $1685\text{ cm}^{-1}$ , which in comparison to the  $\nu_{\text{CO}}$  value obtained for the free ligand in Chapter 3 most probably represented the carbonyl peak of the thiourea ligand in the complex  $[\text{Rh}(\text{N-tmPT})(\text{CO})_2]$ . It was worthy to note though that small increases in the absorbance value at this wavenumber was observed instead of decreases within the time period of the study.

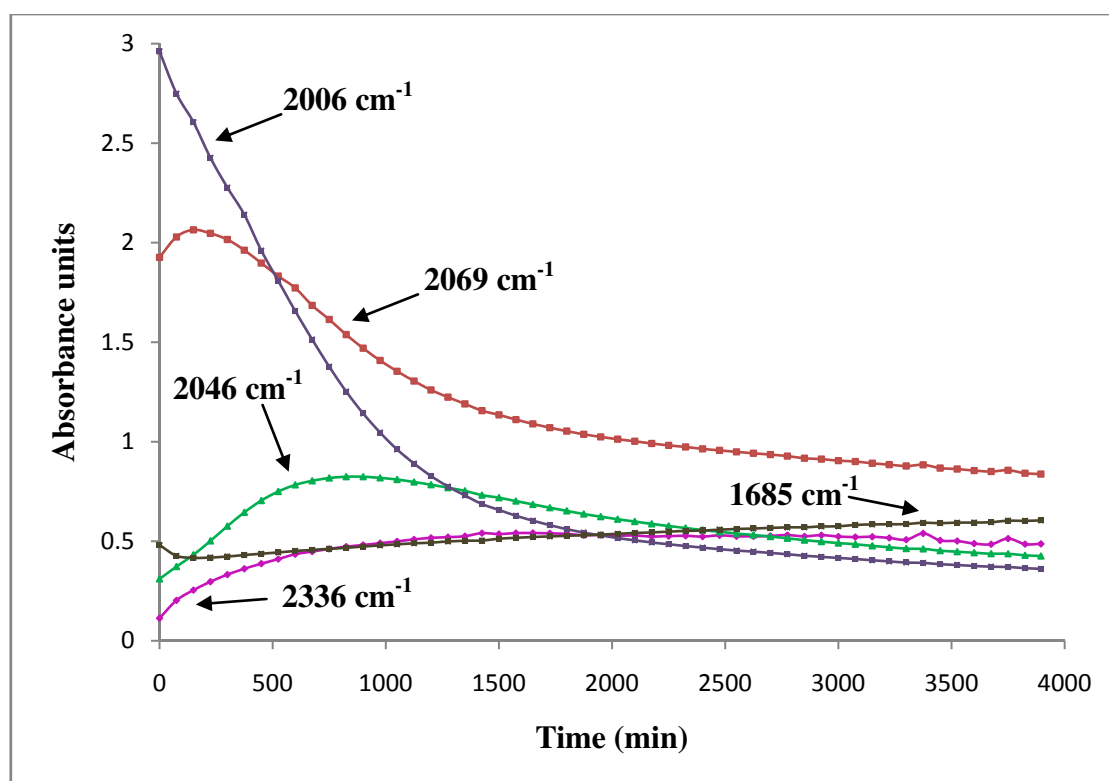


**Figure 8.3** A graphic illustration of the IR absorbance change vs. time for the iodomethane oxidative addition to  $[\text{Rh}(\text{N-tmPT})(\text{CO})_2]$  in toluene at  $25\text{ }^{\circ}\text{C}$ .  $[\text{Rh}] = 0.048\text{ M}$ ,  $[\text{MeI}] = 0.4\text{ M}$ , total time = 65 hrs, at 75 min intervals.

It is clear from this data that the oxidative addition of iodomethane to the  $[\text{Rh}(\text{N-Bz-N}'\text{-tmPh}(\text{tu})(\text{CO})_2)]$  complex is complicated and difficult to identify and allocate the species that forms during the reactions. A few more runs of the oxidative addition of iodomethane were done on two other complexes that could be isolated, namely  $[\text{Rh}(\text{N-NmT})(\text{CO})_2]$  and  $[\text{Rh}(\text{N-BFPT})(\text{CO})_2]$  (*N*-NmT and *N*-BFPT = *N*-benzoyl-*N'*-naphthalen-1-ylmethylthiourea and *N*-benzoyl-*N'*-2,6-dibromo-4-fluorophenylthiourea, respectively). The IR spectra obtained for the reactions for each of these complexes are provided in Figures 8.4 and 8.5, respectively.

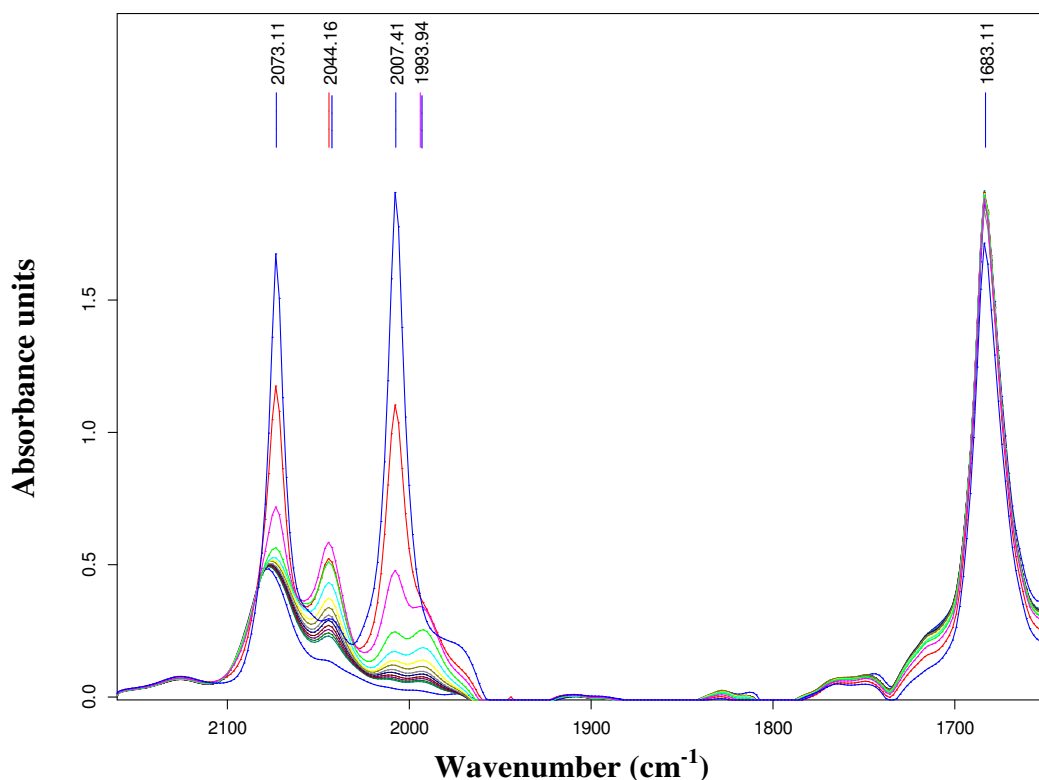


**Figure 8.4** IR spectra obtained for the iodomethane oxidative addition to  $[\text{Rh}(\text{N-NmPT})(\text{CO})_2]$  in toluene at 25 °C. Each spectrum was recorded at an interval of 225 min.  $[\text{Rh}] = 0.044 \text{ M}$ ,  $[\text{MeI}] = 1.6 \text{ M}$ , total time = 48 hrs.

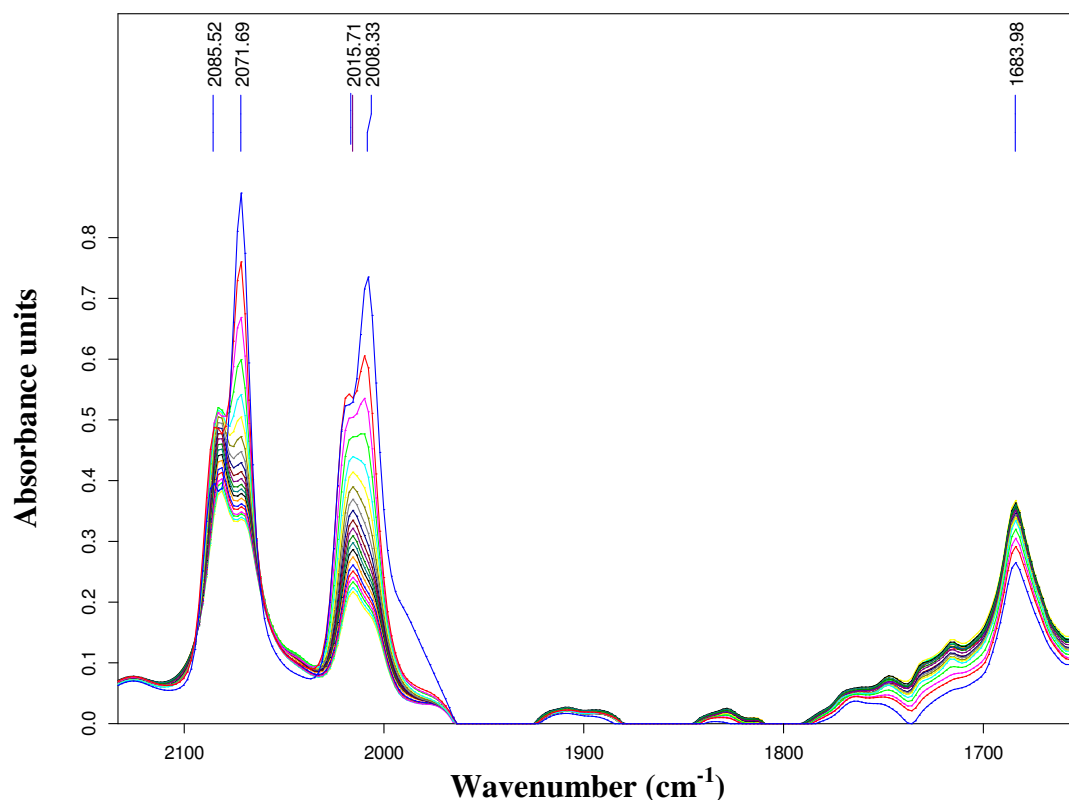


**Figure 8.5 IR spectra obtained for the iodomethane oxidative addition to  $[\text{Rh}(\text{N-BFPT})(\text{CO})_2]$  in toluene at 25 °C. Each spectrum was recorded at an interval of 140 min.  $[\text{Rh}] = 0.02 \text{ M}$ ,  $[\text{MeI}] = 1.6 \text{ M}$ , total time = 48 hrs.**

It is clear from the IR spectra shown in Figures 8.4 and 8.5 that a similar trend was observed for the oxidative addition of iodomethane to the complexes  $[\text{Rh}(\text{N-NmPT})(\text{CO})_2]$  and  $[\text{Rh}(\text{N-BFPT})(\text{CO})_2]$  as was found for complex  $[\text{Rh}(\text{N-tmPT})(\text{CO})_2]$ . It was therefore concluded from all these runs that the oxidative addition of iodomethane to  $[\text{Rh}(\text{S},\text{O-thioureato})(\text{CO})_2]$  complexes in general was found to be complicated and difficult to analyse. Furthermore, these reactions were very slow, and required between 48-60 hours for each reaction to reach completeness with a high iodomethane concentration of 1.6 M. Finally, no clear evidence could be obtained that the Rh(III)-acyl species were indeed forming in significant amounts, and attempts to crystallize these complexes proved to be difficult.

It was concluded from these results that it would be more realistic and feasible to activate these reactions significantly by introducing phosphine ligands to the Rh(I) complexes. It was thus decided to rather investigate the kinetic aspects on the iodomethane oxidative addition to

the range of  $[\text{Rh}(\text{N-diPT})(\text{CO})(\text{PR}_1\text{R}_2\text{R}_3)]$  complexes that were synthesized and characterized as shown in Chapter 7.

#### 8.4.2 Iodomethane oxidative addition to $[\text{Rh}(\text{N-diPT})(\text{CO})(\text{PR}_1\text{R}_2\text{R}_3)]$

With the success of isolating and characterizing the  $[\text{Rh}(\text{N-diPT})(\text{CO})(\text{PR}_1\text{R}_2\text{R}_3)]$  complexes from the ligand *N*-benzoyl-*N',N'*-diphenylthiourea (*N*-diPT), it was therefore decided to investigate the oxidative addition of iodomethane to this range of complexes. One advantage of these complexes that were discussed in Chapter 7, is the fact that only one isomer of these complexes are observed as was shown by NMR and IR spectroscopy. This makes mechanistic interpretation of the iodomethane oxidative addition to these complexes easier and direct correlation is made between the electro-steric properties of the phosphine ligands and the results of the reaction. Moreover, the process may also be monitored by  $^{31}\text{P}$  NMR spectroscopy. On the other hand it has been shown before that the oxidative addition of iodomethane can lead to *cis* and *trans* isomers depending on whether the iodomethane adds *cis* or *trans* to the rhodium centre.<sup>6a;8a,b</sup> It is therefore necessary to keep this in mind when interpreting the results of the iodomethane oxidative addition reactions.

In the next few sections (8.4.2.1-8.4.2.4) the oxidative addition of iodomethane to the  $[\text{Rh}(\text{N-diPT})(\text{CO})(\text{PR}_1\text{R}_2\text{R}_3)]$  complexes are stepwise reported in the order of  $\text{PR}_1\text{R}_2\text{R}_3 = \text{PPh}_3, \text{PCy}_3, \text{PPhCy}_2$  and  $\text{PPh}_2\text{Cy}$ . This is necessary in order to discuss the individual effects of the different phosphines on the outcome of the oxidative addition reactions. Each phosphine ligand varies significantly in their electro-steric properties, which is expected to greatly influence the outcome of the oxidative addition reactions. The two extremes  $\text{PPh}_3$  and  $\text{PCy}_3$  will firstly be discussed, since  $\text{PPh}_3$  is the most electron-poor ligand with the least steric congestion whereas  $\text{PCy}_3$  is the opposite. It was decided to discuss the results obtained for the  $[\text{Rh}(\text{N-diPT})(\text{CO})(\text{PPh}_2\text{Cy})]$  complex after discussing the results for the other complexes containing the other phosphine ligands, as this complex provided slightly different results.

---

<sup>8</sup> a) Venter, J. A.; Leipoldt, J. G.; van Eldik, R. (1991) *Inorg. Chem.*, **30**, 2207. b) Van Aswegen, K. G.; Leipoldt, J. G.; Potgieter, I. M.; Lamprecht, G. J.; Roodt, A.; van Zyl, G. J. (1991) *Transition Met. Chem.*, **16**, 369.

#### 8.4.2.1 Iodomethane oxidative addition to $[\text{Rh}(\text{N-diPT})(\text{CO})(\text{PPh}_3)]$

To first verify that oxidative addition of iodomethane would indeed occur to the  $[\text{Rh}(\text{S},\text{O-thioureato})(\text{CO})(\text{PR}_1\text{R}_2\text{R}_3)]$  complexes, a preliminary analysis was performed on FT-IR spectroscopy on the complex  $[\text{Rh}(\text{N-diPT})(\text{CO})(\text{PPh}_3)]$  at 25 °C. Figure 8.6 shows the IR spectra that were obtained for this reaction in DCM at intervals of six minutes. It is clearly observed that the disappearance of the peak at 1979  $\text{cm}^{-1}$  (the starting complex  $[\text{Rh}(\text{N-diPT})(\text{CO})(\text{PPh}_3)]$ ) led virtually to the direct appearance of a peak at 1715  $\text{cm}^{-1}$ , which indicated the formation of the Rh(III)-acyl complex  $[\text{Rh}(\text{N-diPT})(\text{COMe})(\text{I})(\text{PPh}_3)]$ . It was interesting to note that only a small peak at 2065  $\text{cm}^{-1}$  could be observed, which indicated the formation of the Rh(III)-alkyl complex  $[\text{Rh}(\text{N-diPT})(\text{Me})(\text{CO})(\text{I})(\text{PPh}_3)]$ . This implied that the rate of conversion to the Rh(III)-alkyl complex would be difficult to analyze and that the major reaction rate involved the almost ‘direct’ conversion of the starting complex to the Rh(III)-acyl complex.

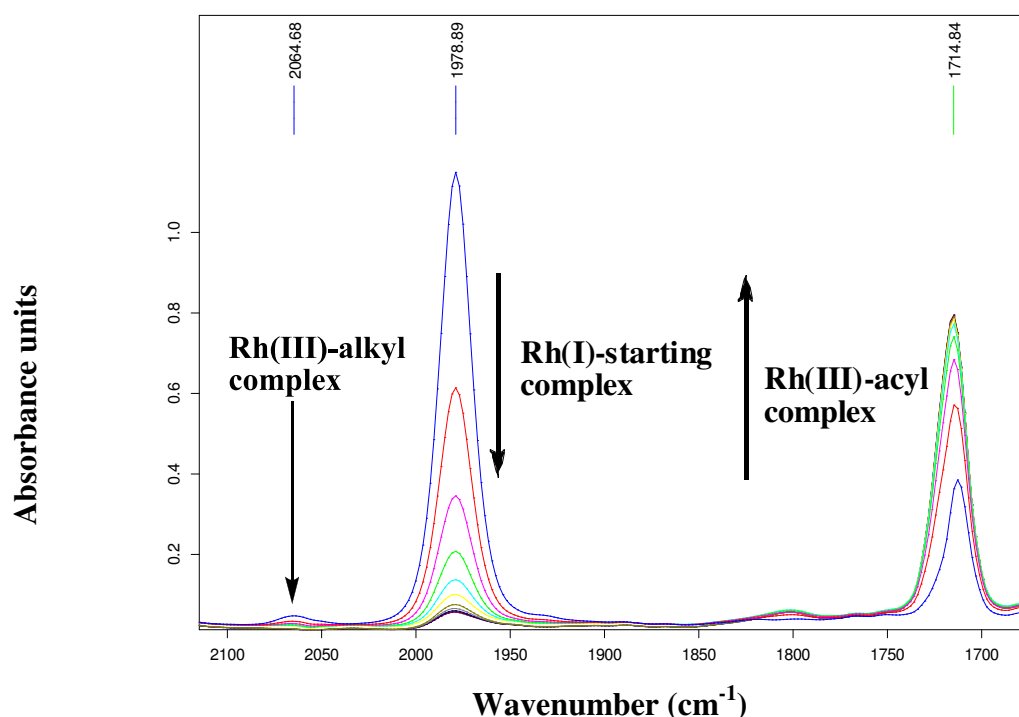


**Figure 8.6** IR spectra obtained for the iodomethane oxidative addition to  $[\text{Rh}(\text{N-diPT})(\text{CO})(\text{PPh}_3)]$  under pseudo first-order conditions in DCM at 25 °C. Each spectrum was recorded at an interval of 6 min.  $[\text{Rh}] = 0.0105 \text{ M}$ ,  $[\text{MeI}] = 0.4 \text{ M}$ ,  $T = 25 \text{ °C}$ , total time = 1 hr.

The change in the absorbance values for the different species over the time period at which the reaction was studied, is shown in Figure 8.7. The ‘direct’ conversion of the starting complex to the Rh(III)-acyl complex is evident by the comparison in the reaction rates of the two separate species. Note that the reaction rate was found to be relatively fast as both reactions reached completion after 60 min. The rate for the disappearance of the starting complex  $[\text{Rh}(\text{N-diPT})(\text{CO})(\text{PPh}_3)]$  ( $1.840(8) \times 10^{-3} \text{ s}^{-1}$ ) is basically equal to the rate of formation of the complex  $[\text{Rh}(\text{N-diPT})(\text{COMe})(\text{I})(\text{PPh}_3)]$  ( $2.01(2) \times 10^{-3} \text{ s}^{-1}$ ). This behaviour has been confirmed previously by several authors, where the oxidative addition of iodomethane to rhodium complexes having a bidentate ligand that has a sulphur donor atom, led primarily to the formation of Rh(III)-acyl complexes.<sup>9a,b,c</sup> Furthermore, it was shown that within a certain range of iodomethane concentrations, the rate of disappearance for the starting complex is virtually identical to the rate of formation of the Rh(III)-acyl complex with only a small detection of the Rh(III)-alkyl species observed.

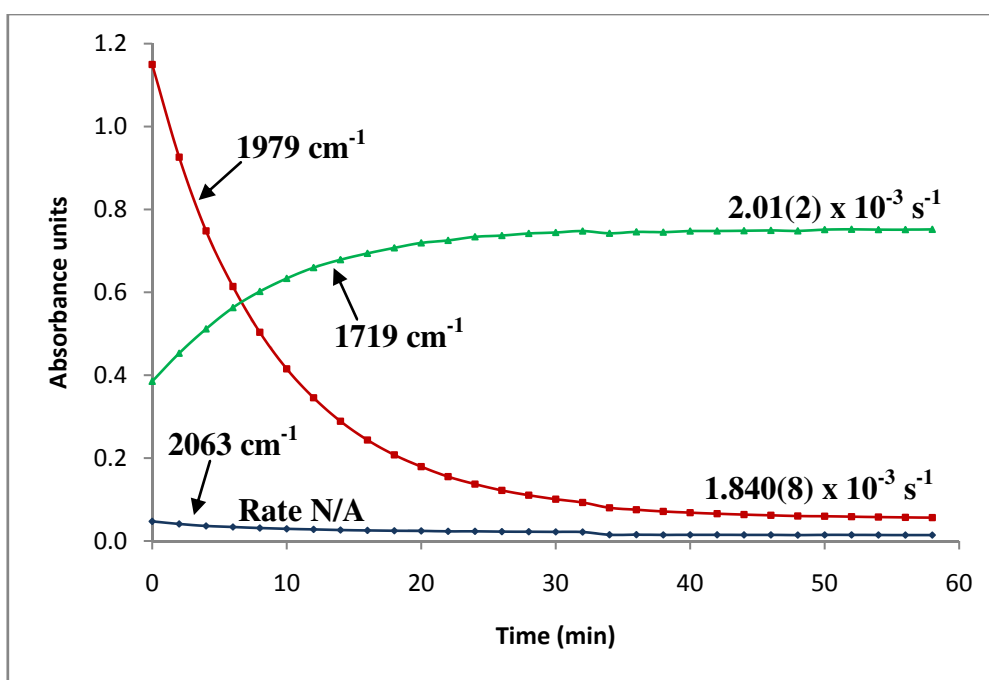


**Figure 8.7** Graph illustrating the IR absorbance change *vs.* Time for the iodomethane oxidative addition to  $[\text{Rh}(\text{N-diPT}(\text{CO})(\text{PPh}_3)]$  under pseudo first-order conditions in DCM at 25 °C. The species allocated to the different traces are given by Rh(I) complex =  $1979 \text{ cm}^{-1}$ , Rh(III)-alkyl =  $2063 \text{ cm}^{-1}$ , Rh(III)-acyl =  $1719 \text{ cm}^{-1}$ .  $[\text{Rh}] = 0.0105 \text{ M}$ ,  $[\text{MeI}] = 0.4 \text{ M}$ ,  $T = 25 \text{ °C}$ .

<sup>9</sup> a) Cheng, C.-H.; Spivack, B. D.; Eisenberg, R. (1977) *J. Am. Chem. Soc.*, **99**, 3003. b) Leipoldt, J. G.; Basson, S. S.; Botha, L. J. (1990) *Inorg. Chim. Acta*, **168**, 215. c) Steyn, G. J. J.; Roodt, A.; Leipoldt, J. G. (1992) *Inorg. Chem.*, **31**, 3477.



Steyn *et al.*<sup>9c</sup> explained this observation by means of the general rate expression for the pseudo first-order rate constant  $k_{obs}$  as was given in equation 8.9. If the equilibrium constant ( $K_I$ ) has a large value due to a fast formation of the Rh(III)-alkyl species (large  $k_I$ ), such that  $K_I[\text{MeI}] \gg 1$ , then the observed rate constant becomes equal to the rate constant  $k_2$ . On the other hand, first-order dependence of the observed rate constant on  $[\text{MeI}]$  will always be observed when  $K_I$  is so small that  $K_I[\text{MeI}] \ll 1$ , thus reducing the expression in 8.9 to equation 8.20,

$$k_{obs} = k_2 K_I [\text{MeI}] \quad (8.20)$$

Under these conditions the overall pseudo second-order rate constant is determined from a graph of  $k_{obs}$  vs.  $[\text{MeI}]$  and yields,

$$k_2' = k_2 K_I \quad (8.21)$$

Thus, regardless if either  $k_2$  or  $k_I$  has the larger value, if the value of  $k_I$  for the reverse reaction is much larger than that of  $k_2$ , then only small amounts of the Rh(III)-alkyl species will be observed during the oxidative addition reaction as has been described in Figure 8.6.

The observed change in the  $^{31}\text{P}$  NMR spectra for the iodomethane oxidative addition to the complex  $[\text{Rh}(N\text{-diPT})(\text{CO})(\text{PPh}_3)]$  is given in Figure 8.8. Due to the fast reaction rate that was observed on IR spectra, NMR spectra were obtained from only 32 scans to allow about  $\pm 2$  min intervals between successive scans. Moreover, in order to obtain suitable spectra a very high concentration of the starting complex was used whilst only a low concentration of iodomethane was employed in order to follow the progress of the reaction over a longer period. Thus, pseudo first-order conditions were not applicable here, but the spectra nevertheless describe the progress of the second-order process.

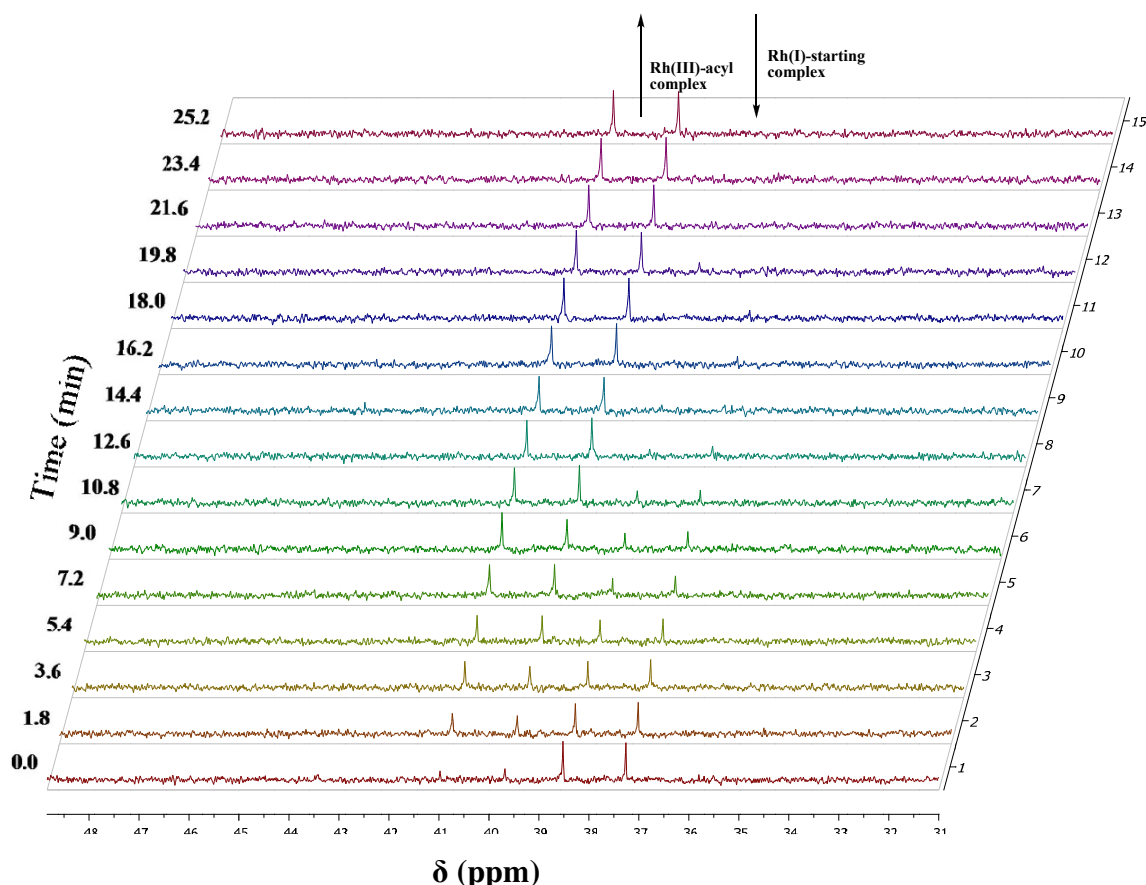


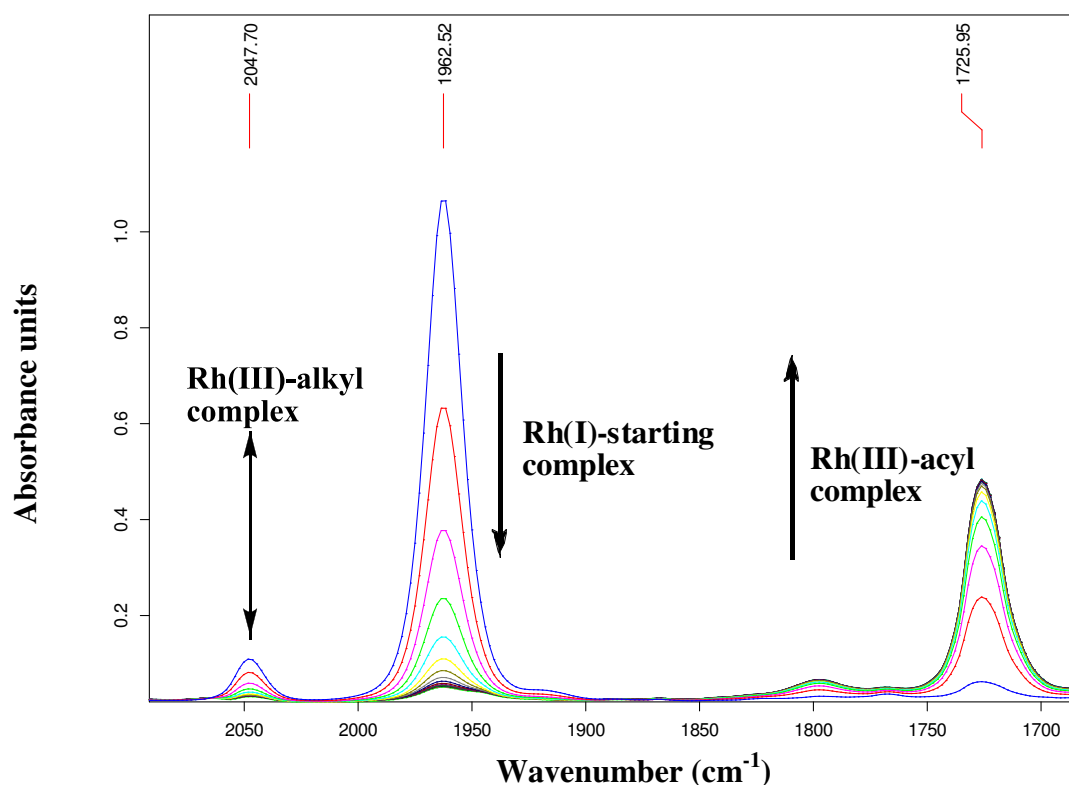
**Figure 8.8**  $^{31}\text{P}$  NMR spectra of the 2<sup>nd</sup> order iodomethane oxidative addition to  $[\text{Rh}(\text{N-diPT}(\text{CO})(\text{PPh}_3)]$ . Each spectrum was recorded at an interval of 1 min 48 sec.  $[\text{Rh}] = 0.05 \text{ M}$ ,  $[\text{MeI}] = 0.32 \text{ M}$ ,  $T = 25^\circ\text{C}$ , total time = 25.2 min.

As was mentioned before only one isomer of the starting complex  $[\text{Rh}(\text{N-diPT})(\text{CO})(\text{PPh}_3)]$  was observed. Furthermore the disappearance of the starting complex at 38.0 ppm ( $J_{\text{Rh-P}} = 152.3 \text{ Hz}$ ) led to the formation of a doublet at 40.5 ppm ( $J_{\text{Rh-P}} = 157.4 \text{ Hz}$ ), which is attributed to the formation of the Rh(III)-acyl complex. As was observed on the IR spectra, the amount of the Rh(III)-alkyl species that formed was so little that this complex was not observed on the NMR spectra. A direct conversion to the Rh(III)acyl complex was therefore concluded of which only one major isomer was present. It is also noticed from Figure 8.8 that the reaction has a  $t_{1/2}$  of about four minutes, which gives an observed rate value of  $\pm 2.9 \times 10^{-3} \text{ s}^{-1}$  as calculated from equation 8.19. This value correlate reasonably to that obtained from the IR studies.

The success of obtaining these viable and well-defined results for the oxidative addition of iodomethane to  $[\text{Rh}(\text{N-diPT})(\text{CO})(\text{PPh}_3)]$ , necessitated a more detailed analysis on the remaining complexes at 25 °C.

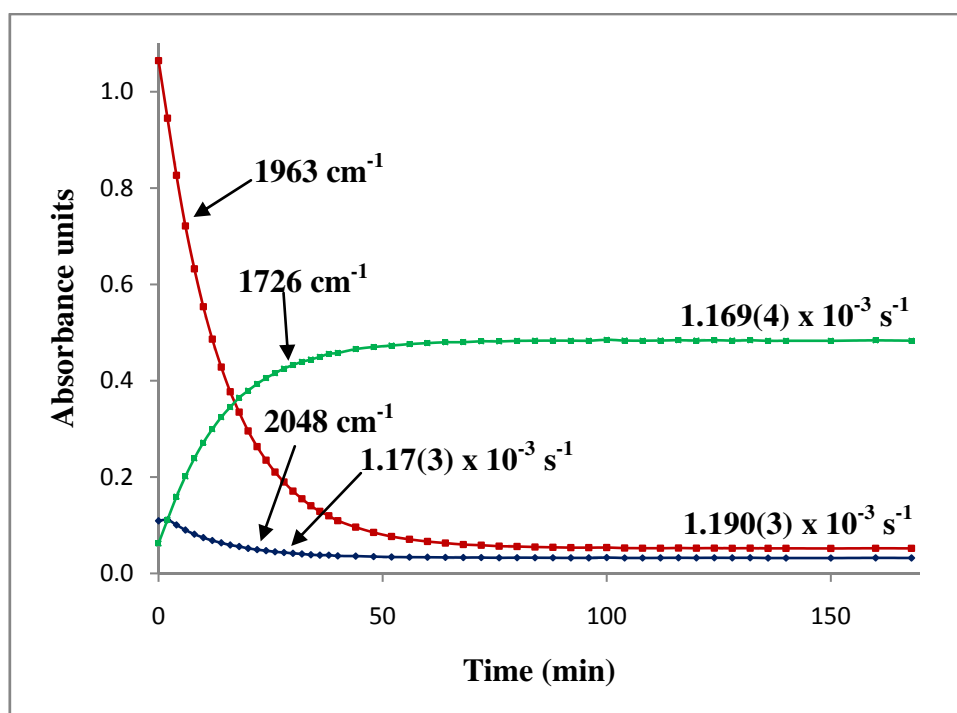
#### 8.4.2.2 Iodomethane oxidative addition to $[\text{Rh}(\text{N-diPT})(\text{CO})(\text{PCy}_3)]$

Figure 8.9 shows the IR spectra that were obtained at different time intervals of the reaction. As with the  $[\text{Rh}(\text{N-diPT})(\text{CO})(\text{PPh}_3)]$  complex, the starting complex  $[\text{Rh}(\text{N-diPT})(\text{CO})(\text{PCy}_3)]$  represented by the peak at  $1963\text{ cm}^{-1}$  decreased during the reaction, leading to the formation of both the Rh(III)alkyl species ( $2048\text{ cm}^{-1}$ ) and the Rh(III)acyl species ( $1726\text{ cm}^{-1}$ ). It was also observed that in this case the formation of the Rh(III)-alkyl species was more prominent than in the case of the iodomethane oxidative addition to  $[\text{Rh}(\text{N-diPT})(\text{CO})(\text{PPh}_3)]$ .



**Figure 8.9** IR spectra obtained for the iodomethane oxidative addition to  $[\text{Rh}(\text{N-diPT})(\text{CO})(\text{PCy}_3)]$  under pseudo first-order conditions in DCM at 25 °C. Each spectrum was recorded at an interval of 8 min.  $[\text{Rh}] = 0.010\text{ M}$ ,  $[\text{MeI}] = 0.4\text{ M}$ ,  $T = 25\text{ °C}$ , total time = 2.8 hrs.

Figure 8.10 shows the change in the absorbance values for the different species over the time period the reaction was studied. The first observation that is made here is that the relative formation of the Rh(III)-alkyl species is still significantly small enough that the rate of the formation of the Rh(III)-acyl species ( $1.169(4) \times 10^{-3} \text{ s}^{-1}$ ) was found to be equal to the rate of disappearance of the starting complex  $[\text{Rh}(\text{N-diPT})(\text{CO})(\text{PCy}_3)]$  ( $1.190(3) \times 10^{-3} \text{ s}^{-1}$ ) as was in the case of the complex  $[\text{Rh}(\text{N-diPT})(\text{CO})(\text{PPh}_3)]$ . Therefore the oxidative addition of iodomethane to  $[\text{Rh}(\text{N-diPT})(\text{CO})(\text{PCy}_3)]$  led primarily to the formation of the  $[\text{Rh}(\text{N-diPT})(\text{COMe})(\text{I})(\text{PCy}_3)]$  complex.



**Figure 8.10** A graph illustrating the IR absorbance change *vs.* time for the iodomethane oxidative addition to  $[\text{Rh}(\text{N-diPT})(\text{CO})(\text{PCy}_3)]$  under pseudo first-order conditions in DCM at 25 °C. The species allocated to the different traces are given by Rh(I) complex =  $1963 \text{ cm}^{-1}$ , Rh(III)-alkyl =  $2048 \text{ cm}^{-1}$ , Rh(III)-acyl =  $1726 \text{ cm}^{-1}$ .  $[\text{Rh}] = 0.010 \text{ M}$ ,  $[\text{MeI}] = 0.4 \text{ M}$ ,  $T = 25 \text{ }^{\circ}\text{C}$ , total time = 2.8 hrs.

However, even though only small changes in the intensity for the Rh(III)-alkyl species were observed on the IR spectrum, the data was sufficient enough to determine the rate of disappearance of the Rh(III)-alkyl species ( $1.17(3) \times 10^{-3} \text{ s}^{-1}$ ), which was found to be equal to that of the formation of the Rh(III)-acyl species. This established the fact that the Rh(III)-alkyl complex converts to the Rh(III)-acyl complex through migratory insertion. It

was also noted that these rates were found to be lower than those obtained for the previous complex  $[\text{Rh}(\text{N-diPT})(\text{CO})(\text{PPh}_3)]$ , which indicated that the change in the electro-steric properties of the phosphine ligand led to substantial influences on the oxidative addition reaction. This will be discussed in more detail later when all four complexes under study are compared together. Insufficient data was obtained to determine the rate of Rh(III)-alkyl formation, since the peak at  $2048\text{ cm}^{-1}$  already reached its maximum after the first scan on the IR spectrum. Thus, the Rh(III)-alkyl formation was completed within the first 2 min interval of the analysis. The IR spectrometer is limited in its ability to determine only moderate rates of reactions and therefore this reaction will need to be analyzed by techniques that can determine the rates of very fast reactions including stopped-flow methods. However, since the Rh(III)-alkyl species was formed within 2 min a limit of *ca.* 10 s for the half-life may be assumed, which in turn yields a  $k_{\text{obs}}$  value of  $> 0.06\text{ s}^{-1}$ . This value is more than an order-of-magnitude faster than the Rh(III)-acyl formation.

$^{31}\text{P}$  NMR spectra were also obtained for the oxidative addition of iodomethane to  $[\text{Rh}(\text{N-diPT})(\text{CO})(\text{PCy}_3)]$  as shown in Figure 8.11. As mentioned before, a high concentration of the Rh-complex and low concentration of the iodomethane were used to obtain suitable spectra for the analysis.

It is clear from Figure 8.11 that the starting complex is found as one isomer only, indicated by the presence of one doublet situated at 49.9 ppm ( $J_{\text{Rh-P}} = 145.6\text{ Hz}$ ). During the oxidative addition of iodomethane to  $[\text{Rh}(\text{N-diPT})(\text{CO})(\text{PCy}_3)]$ , formation of both the Rh(III)-alkyl and Rh(III)-acyl complexes were observed at 39.6 ( $J_{\text{Rh-P}} = 119.8\text{ Hz}$ ) and 43.5 ppm ( $J_{\text{Rh-P}} = 155.1$ ), respectively, as doublets. It is also noted that both these species were found in one major isomeric form, indicating that the iodomethane only added through one mode of either *cis* or *trans* addition. As was found by IR spectroscopy the peak for Rh(III)-alkyl species were significantly small compared to the starting complex and the Rh(III)-acyl peaks. This provided further proof that the iodomethane oxidative addition to  $[\text{Rh}(\text{N-diPT})(\text{CO})(\text{PCy}_3)]$  leads primarily to the formation of the acyl complex  $[\text{Rh}(\text{N-diPT})(\text{COMe})(\text{I})(\text{PCy}_3)]$  *via* a small amount of the Rh(III)-alkyl intermediate. The observed rate of formation of the Rh(III)-acyl species is therefore directly related to the rate of disappearance of the starting complex.

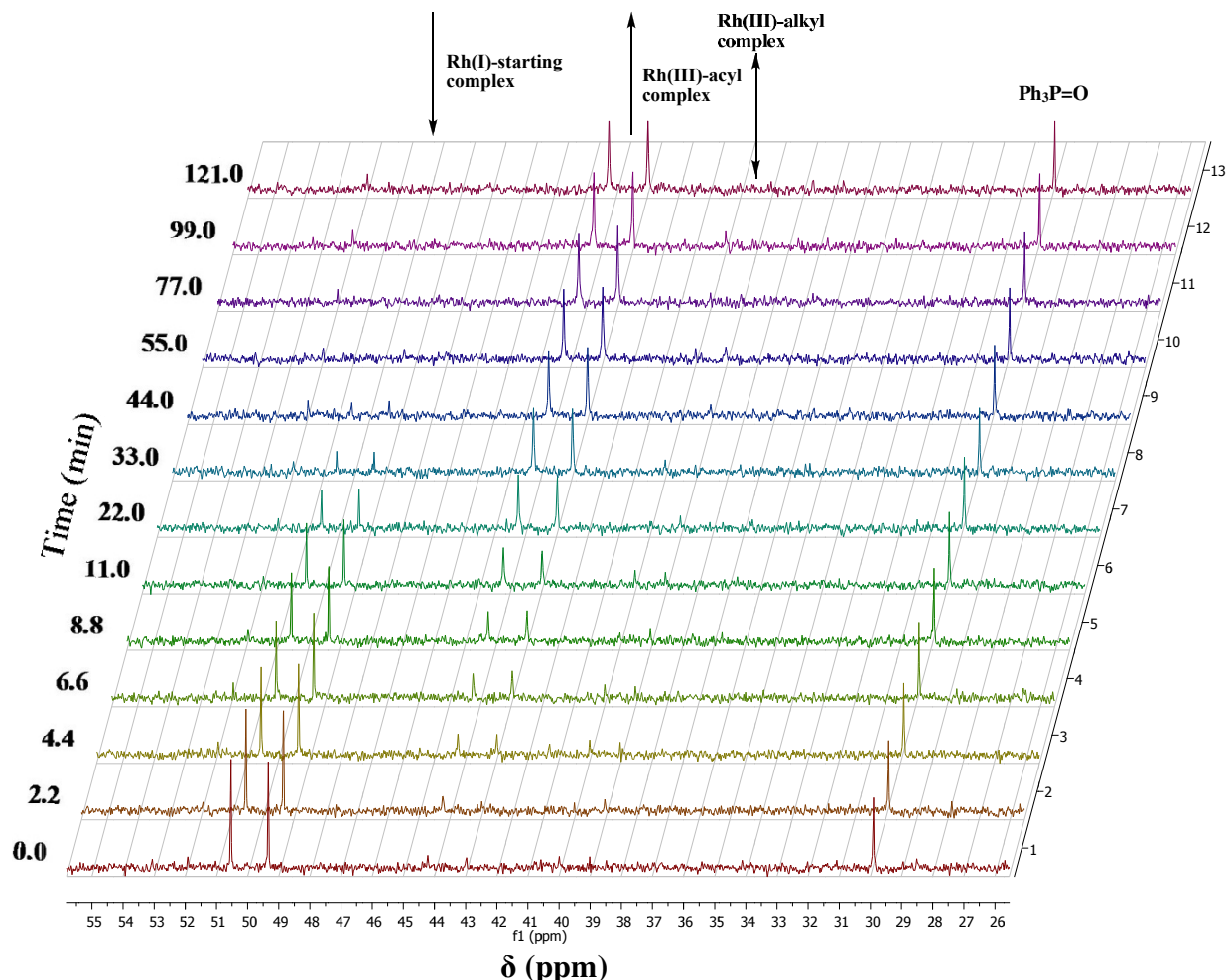


**Figure 8.11**  $^{31}\text{P}$  NMR spectra of the iodomethane oxidative addition to  $[\text{Rh}(\text{N-diPT}(\text{CO})(\text{PCy}_3)]$  under 2<sup>nd</sup> order conditions in DCM at 25 °C. The interval between each spectrum is indicated to the left of the spectra.  $[\text{Rh}] = 0.094 \text{ M}$ ,  $[\text{MeI}] = 0.4 \text{ M}$ ,  $T = 25 \text{ }^\circ\text{C}$ , total time = 2.09 hrs.

#### 8.4.2.3 Iodomethane oxidative addition to $[\text{Rh}(\text{N-diPT})(\text{CO})(\text{PPhCy}_2)]$

The next complex studied was  $[\text{Rh}(\text{N-diPT})(\text{CO})(\text{PPhCy}_2)]$ , where the oxidative addition of iodomethane to this complex was also performed on FT-IR spectroscopy at room temperature. The subsequent IR spectra that were obtained are presented in Figure 8.12 at intervals of 20 minutes. As mentioned to the previous complexes discussed in Sections 8.4.2.1 and 8.4.2.2 the amount of starting complex  $[\text{Rh}(\text{N-diPT})(\text{CO})(\text{PPhCy}_2)]$  observed at  $1969 \text{ cm}^{-1}$  decreased during the reaction, which led primarily to the formation of the Rh(III)-acyl species  $[\text{Rh}(\text{N-diPT})(\text{COMe})(\text{I})(\text{PPhCy}_2)]$  observed at  $1723 \text{ cm}^{-1}$ . The Rh(III)-alkyl complex was also detectable at  $2050 \text{ cm}^{-1}$ , but as in the case of the  $[\text{Rh}(\text{N-diPT})(\text{CO})(\text{PPh}_3)]$  complex this species was found in very small amounts.

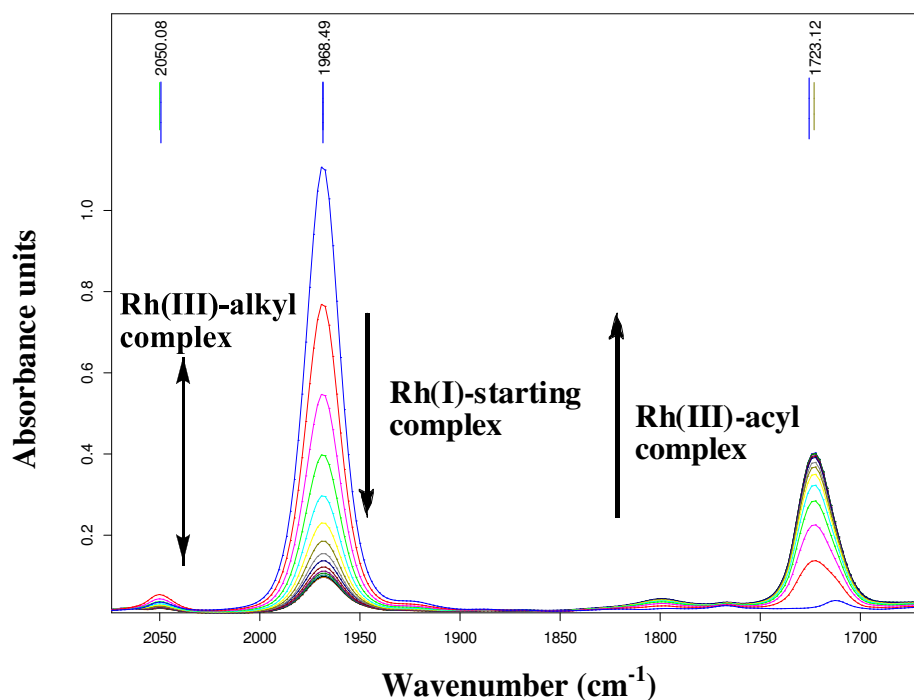


**Figure 8.12** IR spectra obtained for the iodomethane oxidative addition to  $[\text{Rh}(\text{N-diPT}(\text{CO})(\text{PPhCy}_2))]$  under pseudo first-order conditions in DCM at 25 °C. Each spectrum was recorded at an interval of 20 min.  $[\text{Rh}] = 0.0101 \text{ M}$ ,  $[\text{MeI}] = 0.4 \text{ M}$ ,  $T = 25 \text{ }^\circ\text{C}$ , total time = 12 hrs.

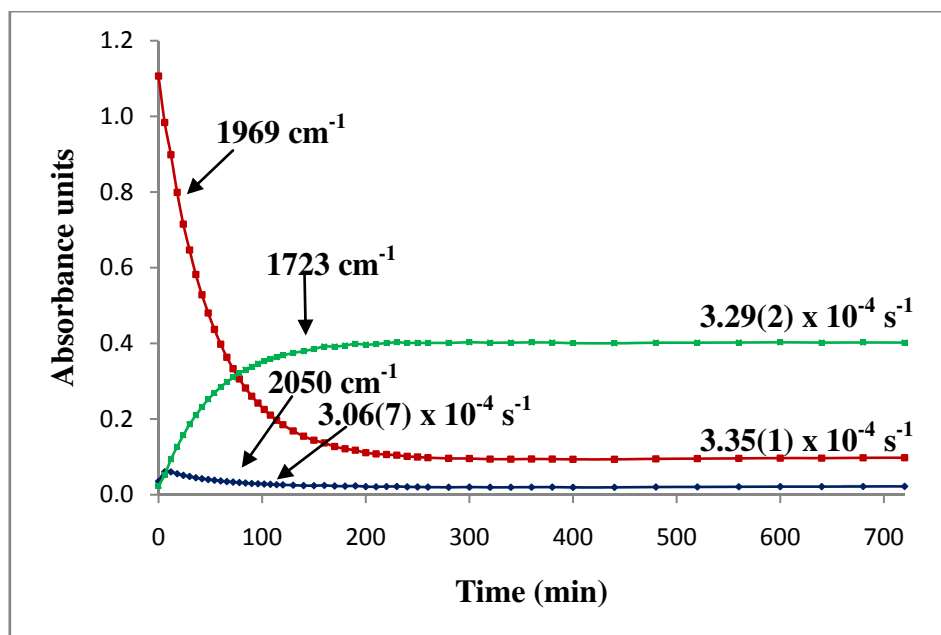


**Figure 8.13** A graph illustrating the IR absorbance change *vs.* time for the iodomethane oxidative addition to  $[\text{Rh}(\text{N-diPT}(\text{CO})(\text{PPhCy}_2))]$  under pseudo first-order conditions in DCM at 25 °C. The species allocated to the different traces are given by  $\text{Rh(I) complex} = 1969 \text{ cm}^{-1}$ ,  $\text{Rh(III)-alkyl} = 2050 \text{ cm}^{-1}$ ,  $\text{Rh(III)-acyl} = 1723 \text{ cm}^{-1}$ .  $[\text{Rh}] = 0.0101 \text{ M}$ ,  $[\text{MeI}] = 0.4 \text{ M}$ ,  $T = 25 \text{ }^\circ\text{C}$ , total time = 12 hrs.

The change in absorbance value for the different complexes is plotted against time in Figure 8.13. Since the amount of the Rh(III)-alkyl complex is small as found previously, the rate of disappearance of the starting complex was virtually identical to the rate of formation of the Rh(III)-acyl complex. It was also observed that the rates calculated for oxidative addition and migratory insertion reactions for the  $[\text{Rh}(\text{N-diPT})(\text{CO})(\text{PPhCy}_2)]$  complex were significantly lower than the previous complexes  $[\text{Rh}(\text{N-diPT})(\text{CO})(\text{PPh}_3)]$  and  $[\text{Rh}(\text{N-diPT})(\text{CO})(\text{PCy}_3)]$ , differing by factors of 6 and 4 times, respectively. This suggested that some unique irregularity was at play here, which is discussed later in this chapter.

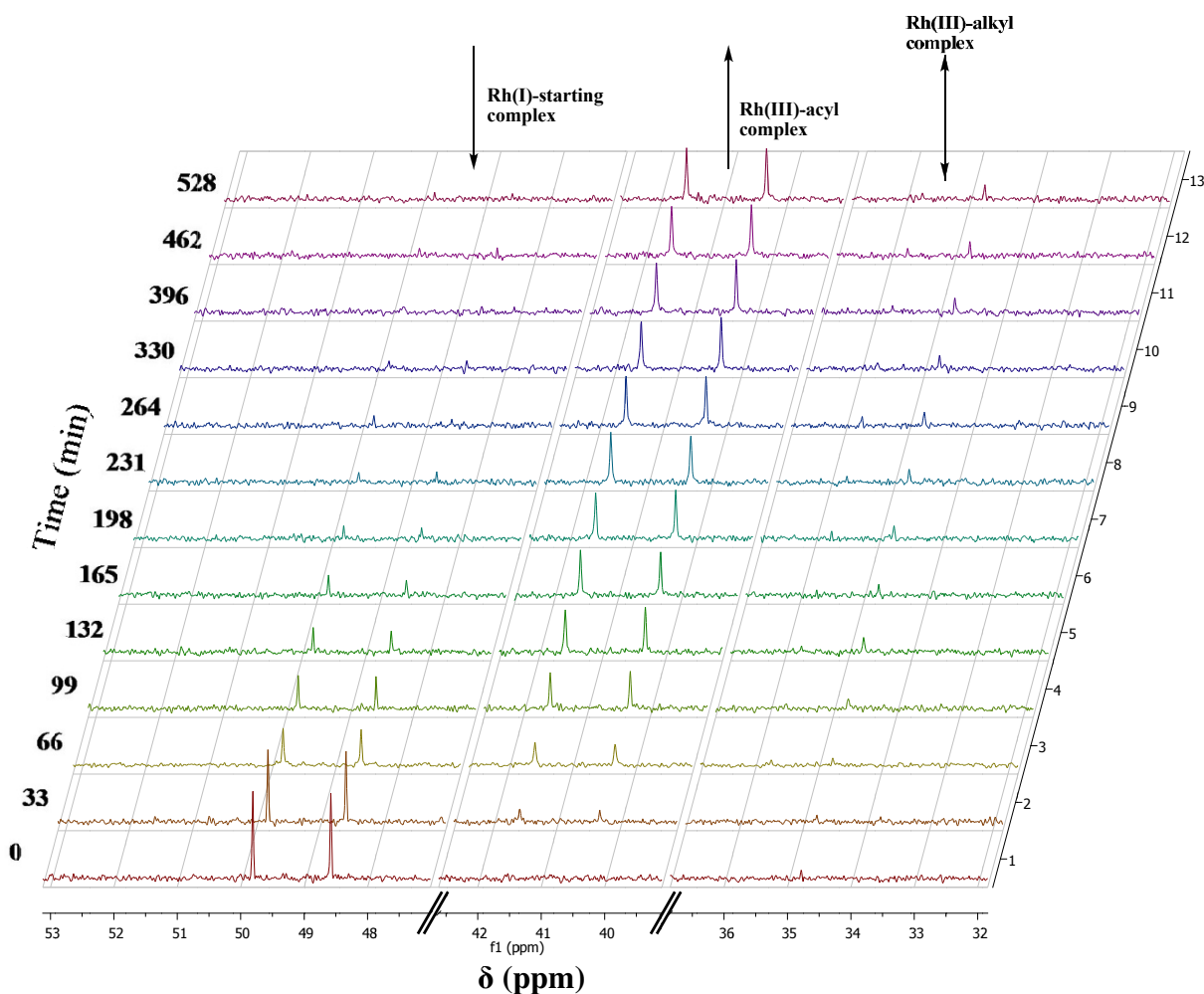


**Figure 8.14**  $^{31}\text{P}$  NMR spectra of the iodomethane oxidative addition to  $[\text{Rh}(\text{N-diPT})(\text{CO})(\text{PPhCy}_2)]$  under 2<sup>nd</sup> order conditions in DCM at 25 °C. The interval between each spectrum is indicated to the left of the spectra.  $[\text{Rh}] = 0.081 \text{ M}$ ,  $[\text{MeI}] = 0.4 \text{ M}$ ,  $T = 25 \text{ }^\circ\text{C}$ , total time = 8.8 hrs.

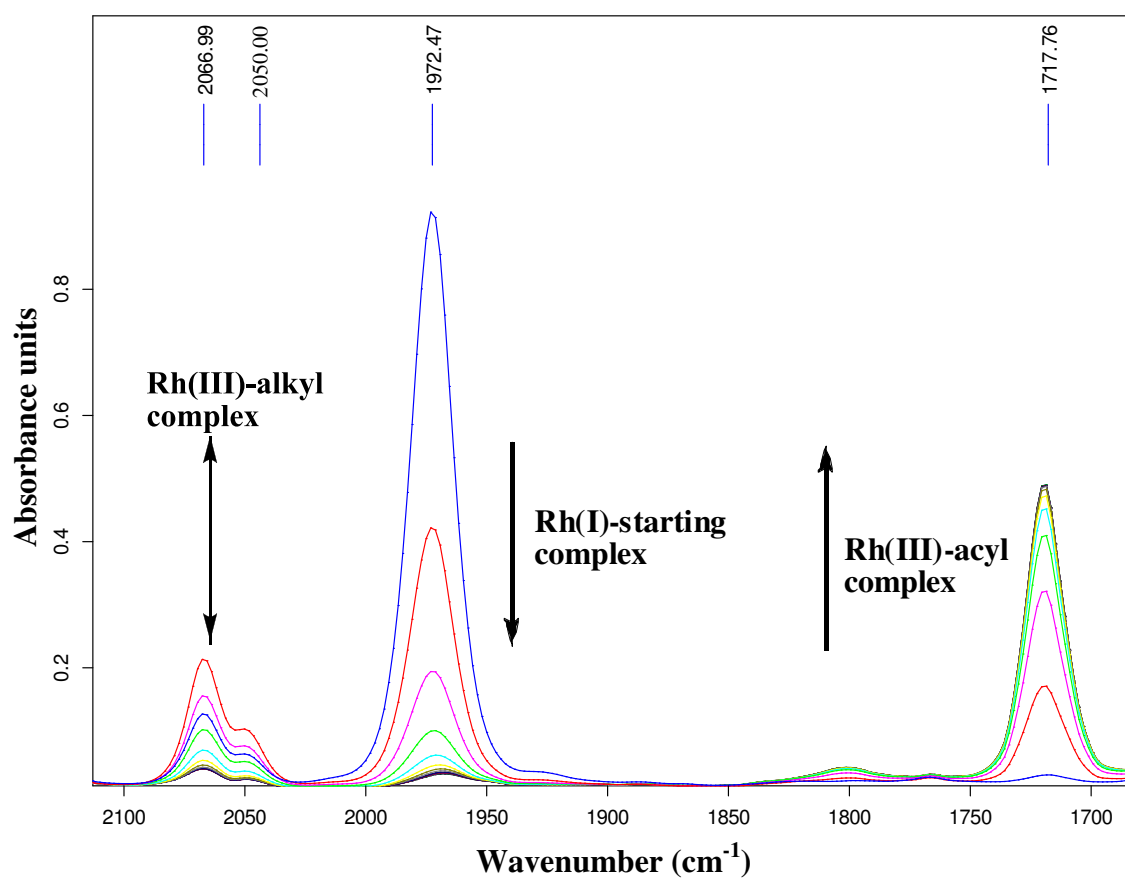


Figure 8.14 represents  $^{31}\text{P}$  NMR spectra that were obtained for the oxidative addition of iodomethane to  $[\text{Rh}(\text{N-diPT})(\text{CO})(\text{PPhCy}_2)]$ . The starting complex was observed at 49.3 ppm ( $J_{\text{Rh-P}} = 149.0$  Hz) as a doublet. Only one isomeric form of the complex was present. The oxidative addition reaction once again led to a decrease in the amounts of the starting complex, which subsequently led primarily to the formation of the Rh(III)-acyl complex at 41.0 ppm ( $J_{\text{Rh-P}} = 152.6$  Hz). Although the amounts are little the formation of Rh(III)-alkyl complex could also be detected at 33.1 ppm ( $J_{\text{Rh-P}} = 117.4$  Hz). It was also noted that only one isomer of the Rh(III)-alkyl and Rh(III)-acyl complexes were present on the  $^{31}\text{P}$  NMR spectra and therefore it could be concluded that the iodomethane added only *cis* or *trans* to the  $[\text{Rh}(\text{N-diPT})(\text{CO})(\text{PPhCy}_2)]$  complex.

#### 8.4.2.4 Iodomethane oxidative addition to $[\text{Rh}(\text{NdiPT})(\text{CO})(\text{PPh}_2\text{Cy})]$

The last complex for which the iodomethane oxidative addition reaction was studied is  $[\text{Rh}(\text{N-diPT})(\text{CO})(\text{PPh}_2\text{Cy})]$ , where the phosphine ligand had only one cyclohexyl group. The synthesis and characterization of this complex was reported in Chapter 7. The oxidative addition of iodomethane to this complex was also performed *via* FT-IR spectroscopy of which the resulting IR spectra are presented in Figure 8.15.

Oxidative addition on the complex  $[\text{Rh}(\text{N-diPT})(\text{CO})(\text{PPh}_2\text{Cy})]$  provided more unexpected results compared to the other complexes obtained in Sections 8.4.2.1-8.4.2.3. Firstly, the disappearance of the starting complex at  $1972\text{ cm}^{-1}$  lead to the formation of significant amounts of the alkyl intermediate  $[\text{Rh}(\text{N-diPT})(\text{Me})(\text{CO})(\text{I})(\text{PPh}_2\text{Cy})]$  as well as the acyl complex  $[\text{Rh}(\text{N-diPT})(\text{COMe})(\text{I})(\text{PPh}_2\text{Cy})]$ . Furthermore, it is clear that two separate peaks were observed for the formation of the Rh(III)-alkyl species, namely at  $2067$  and  $2050\text{ cm}^{-1}$ . This probably suggest that two isomers of the Rh(III)-alkyl complex have formed due to different addition of iodomethane in a *cis* and *trans* fashion. By comparing these values with those obtained for the previous complexes it is observed that there are discrepancies in these values. For the  $[\text{Rh}(\text{N-diPT})(\text{CO})(\text{PPh}_3)]$  complex the Rh(III)-alkyl complex was observed at  $2065\text{ cm}^{-1}$ , while the other two alkyl complexes  $[\text{Rh}(\text{N-diPT})(\text{Me})(\text{CO})(\text{I})(\text{PCy}_3)]$  and  $[\text{Rh}(\text{N-diPT})(\text{Me})(\text{CO})(\text{I})(\text{PPhCy}_2)]$  were observed at  $2048$  and  $2050\text{ cm}^{-1}$ , respectively. It therefore seems as if two alkyl species formed for the  $[\text{Rh}(\text{N-diPT})(\text{CO})(\text{PPh}_2\text{Cy})]$  complex. However, only one isomer of the Rh(III)-acyl complex was observed at  $1718\text{ cm}^{-1}$ .



**Figure 8.15** IR spectra obtained for the pseudo first-order iodomethane oxidative addition to  $[\text{Rh}(\text{N-diPT}(\text{CO})(\text{PPh}_2\text{Cy}))]$  in DCM at 25 °C. Each spectrum was recorded at an interval of 6 min.  $[\text{Rh}] = 0.0104 \text{ M}$ ,  $[\text{MeI}] = 0.4 \text{ M}$ ,  $T = 25 \text{ }^\circ\text{C}$ , total time = 1.3 hrs.

The change in absorbance units of each complex found during the reaction over a certain time period is presented in Figure 8.16. Generally, it is observed that the rate of the oxidative addition and migratory insertion reactions are higher than all the other complexes that were discussed before. Moreover, the rates of disappearance of the different isomers of the Rh(III)-alkyl species ( $2067$  and  $1050 \text{ cm}^{-1}$ ) were found to be similar and are also equal to the rate of formation of the Rh(III)-acyl complex ( $1719 \text{ cm}^{-1}$ ). This basically suggests that both Rh(III)-alkyl complexes are converted to the Rh(III)-acyl complex *via* migratory insertion and isomerisation. The rate of disappearance of the starting complex ( $1972 \text{ cm}^{-1}$ ) was found to be slightly higher than the rate of formation of the Rh(III)-acyl complex. However, due to the fast reaction rate too little data was obtained to calculate the rate of formation of the Rh(III)-alkyl species.

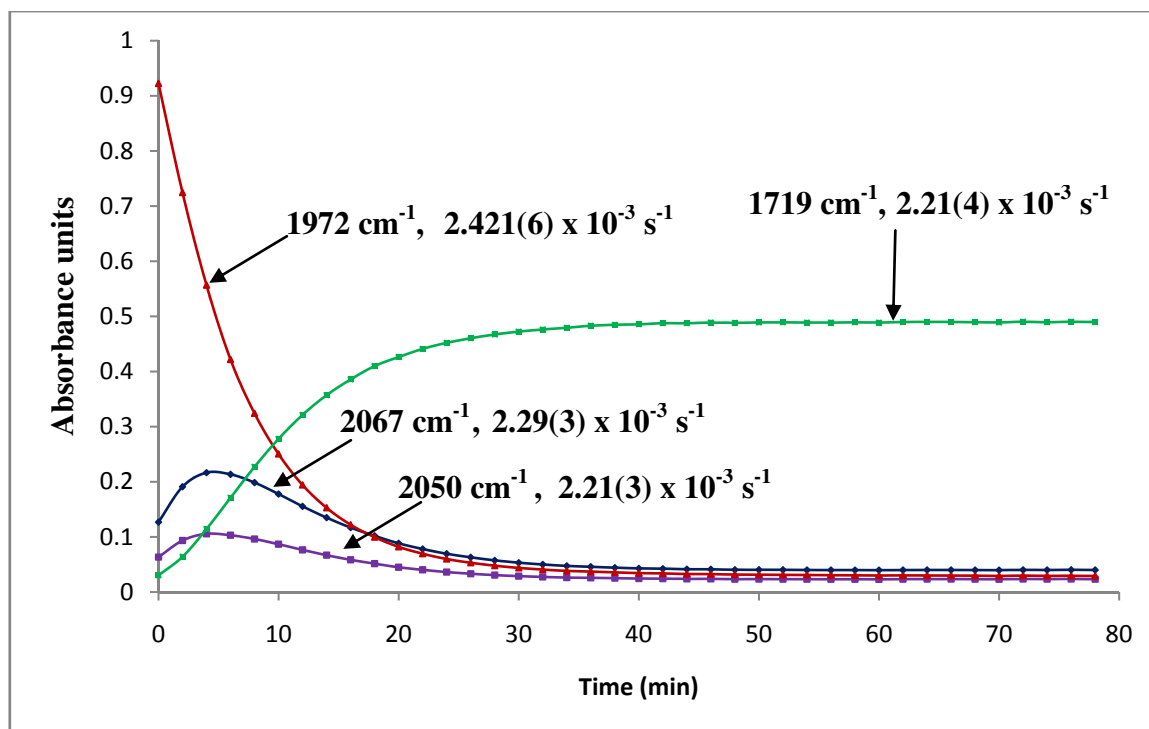


**Figure 8.16** A graph illustrating the IR absorbance change vs. time for several species found during the pseudo first-order iodomethane oxidative addition to  $[\text{Rh}(\text{N-diPT}(\text{CO})(\text{PPh}_2\text{Cy}))]$  in DCM at 25 °C. The species allocated to the different traces are given by Rh(I) complex = 1972  $\text{cm}^{-1}$ , Rh(III)-alkyl isomers = 2067 and 2050  $\text{cm}^{-1}$ , Rh(III)-acyl = 1719  $\text{cm}^{-1}$ .  $[\text{Rh}] = 0.0104 \text{ M}$ ,  $[\text{MeI}] = 0.4 \text{ M}$ ,  $T = 25 \text{ }^\circ\text{C}$ , total time = 1.3 hrs.

The oxidative addition of MeI to  $[\text{Rh}(\text{N-diPT}(\text{CO})(\text{PPh}_2\text{Cy}))]$  could also be followed on  $^{31}\text{P}$  NMR as shown in Figure 8.17. As mentioned for the other complexes before the reaction could only be performed under second-order conditions, due to the requirement of high complex concentrations. Only one isomer of the starting complex  $[\text{Rh}(\text{N-diPT}(\text{CO})(\text{PPh}_2\text{Cy}))]$  was observed by  $^{31}\text{P}$  NMR spectroscopy at 45.3 ppm (d,  $J_{\text{Rh-P}} = 149.4 \text{ Hz}$ ), as expected. The iodomethane oxidative addition to this complex only yielded the formation of the Rh(III)-acyl species under the second-order conditions as observed by  $^{31}\text{P}$  NMR spectroscopy at 41.8 ppm (d,  $J_{\text{Rh-P}} = 152.2 \text{ Hz}$ ). No indication of the formation of Rh(III)-alkyl species was observed by  $^{31}\text{P}$  NMR. It is not exactly clear why the outcome differs for the oxidative addition reaction studied by IR and  $^{31}\text{P}$  NMR spectroscopy.

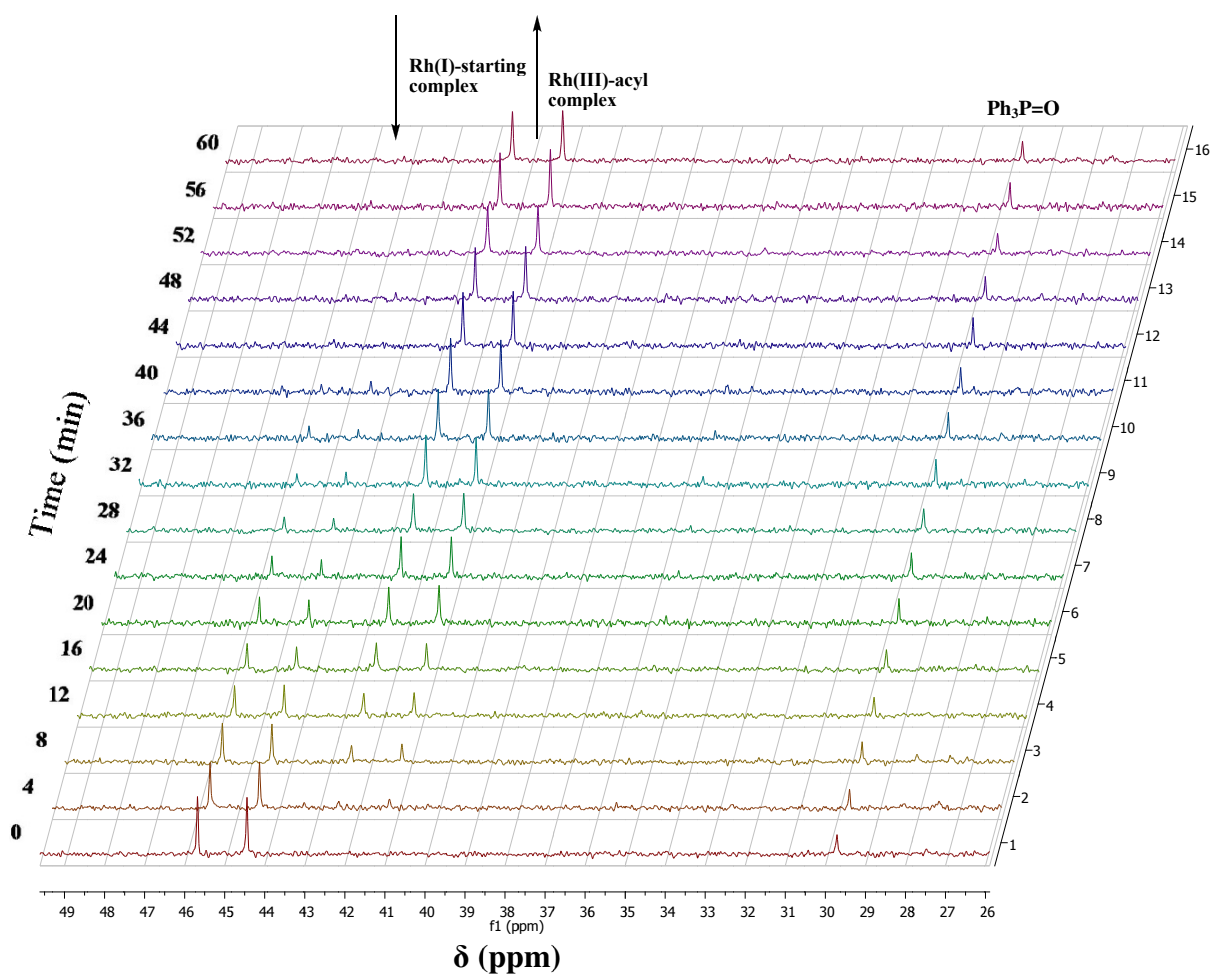


**Figure 8.17**  $^{31}\text{P}$  NMR spectra of the 2<sup>nd</sup> order iodomethane oxidative addition to  $[\text{Rh}(\text{N-diPT}(\text{CO})(\text{PPh}_2\text{Cy}))]$  in DCM at 25 °C. The interval between each spectrum is 4 min.  $[\text{Rh}] = 0.094 \text{ M}$ ,  $[\text{MeI}] = 0.4 \text{ M}$ ,  $T = 25 \text{ }^\circ\text{C}$ , total time = 1 hr.

A summary of all the preliminary data obtained from the IR and  $^{31}\text{P}$  NMR spectroscopic experiments is given in Table 8.1.

**Table 8.1 Analytical data obtained for the iodomethane oxidative addition to [Rh(*N*-diPT)(CO)(PR<sub>1</sub>R<sub>2</sub>R<sub>3</sub>)] complexes in DCM at 25 °C.**

Complex		$k_{obs}$ (s <sup>-1</sup> ) <sup>a</sup>	$\nu_{(CO)}$ (cm <sup>-1</sup> )	$\delta$ <sup>31</sup> P NMR (ppm)	$J_{Rh-P}$ (Hz)
[Rh( <i>N</i> -diPT)(CO)(PPh <sub>3</sub> )]	Rh(I)	0.001840(8)	1979	38.0	152.3
	Rh(III)-alkyl	-	2063	-	-
	Rh(III)-acyl	0.00201(3)	1719	40.5	157.4
[Rh( <i>N</i> -diPT)(CO)(PPh <sub>2</sub> Cy)]	Rh(I)	0.002421(6)	1972	45.3	149.4
	Rh(III)-alkyl <sup>1</sup>	0.00229(3)	2067	-	-
	Rh(III)-alkyl <sup>2</sup>	0.00221(3)	2050	-	-
	Rh(III)-acyl	0.00221(4)	1719	41.8	152.2
[Rh( <i>N</i> -diPT)(CO)(PPhCy <sub>2</sub> )]	Rh(I)	0.000335(1)	1969	49.3	149.0
	Rh(III)-alkyl	-	2050	33.1	117.4
	Rh(III)-acyl	0.000329(2)	1723	41.0	152.6
[Rh( <i>N</i> -diPT)(CO)(PCy <sub>3</sub> )]	Rh(I)	0.001190(3)	1963	49.9	145.6
	Rh(III)-alkyl	0.00117(3)	2048	39.6	119.8
	Rh(III)-acyl	0.001186(3)	1726	43.5	155.1

<sup>a</sup> [MeI] = 0.4 M

#### 8.4.2.5 Electro-steric effects of phosphine ligands on the iodomethane oxidative addition to [Rh(*N*-diPT)(CO)(PR<sub>1</sub>R<sub>2</sub>R<sub>3</sub>)] complexes

Sections 8.4.2.1-8.4.2.4 clearly indicate that the iodomethane oxidative addition to [Rh(*N*-diPT)(CO)(PR<sub>1</sub>R<sub>2</sub>R<sub>3</sub>)] leads primarily to the formation of the expected Rh(III)-acyl species. Furthermore by varying the phosphine ligand (PR<sub>1</sub>R<sub>2</sub>R<sub>3</sub>) on the Rh(I) complex a significant change in the reaction profiles and rates were observed. As a result of these observations it was decided to perform a full analysis in order to determine the kinetic profiles of the oxidative addition of iodomethane to each of these complexes. In order to do this a range of iodomethane concentrations were chosen and as discussed before, the reactions were studied in DCM *via* IR spectroscopy at room temperature.

The resulting data was fitted on Scientist and the observed rate constants were plotted against iodomethane concentrations with respect to the disappearance of the starting complex [Rh(*N*-diPT)(CO)(PR<sub>1</sub>R<sub>2</sub>R<sub>3</sub>)], as shown in Figure 8.18. From these plots it was observed that no significant intercepts were obtained, which suggested that any possible solvent pathway or reductive elimination reactions that might have occur could be neglected. The data were treated as such assuming this negligible contribution to the overall observed rate constant. The pseudo second-order rate constants ( $k_2'$ ) that were obtained from the fitted data are provided in Table 8.2 together with some other essential analytical data.

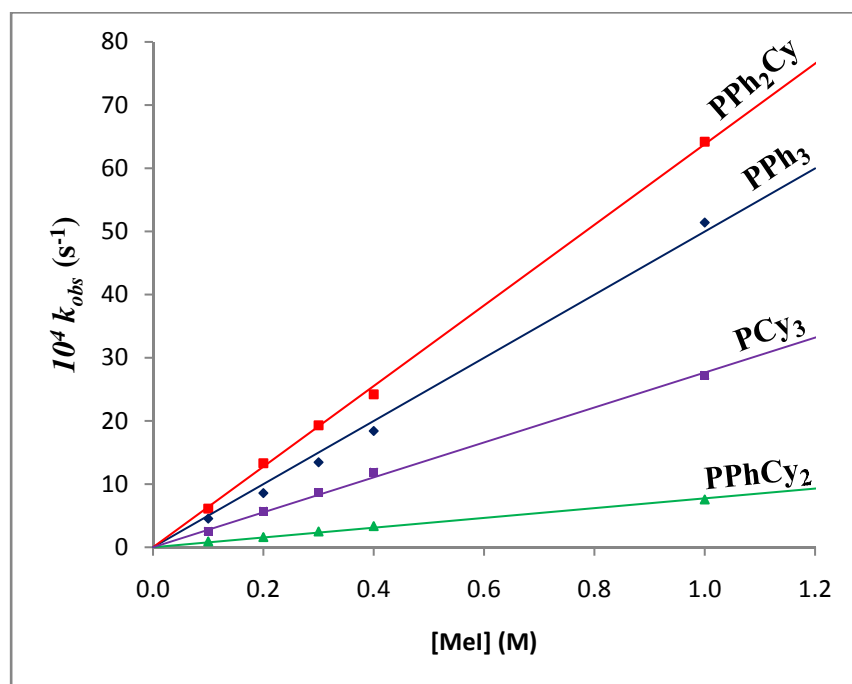


**Figure 8.18** Plots of the observed rate constants vs iodomethane concentrations for the iodomethane oxidative addition to  $[\text{Rh}(\text{N-diPT})(\text{CO})(\text{PR}_1\text{R}_2\text{R}_3)]$  with respect to the disappearance of the Rh(I) complex, where  $\text{PR}_1\text{R}_2\text{R}_3 = \text{PPh}_3$  (1979  $\text{cm}^{-1}$ ),  $\text{PPh}_2\text{Cy}$  (1972  $\text{cm}^{-1}$ ),  $\text{PPhCy}_2$  (1969  $\text{cm}^{-1}$ ), and  $\text{PCy}_3$  (1963  $\text{cm}^{-1}$ ).  $[\text{Rh}] = 0.010 \text{ M}$ .

**Table 8.2** Analytical data obtained for the iodomethane oxidative addition to  $[\text{Rh}(\text{N-diPT})(\text{CO})(\text{PR}_1\text{R}_2\text{R}_3)]$  complexes in DCM at 25 °C.

Complex	$k_2' (\text{M}^{-1} \cdot \text{s}^{-1})$	$t_{1/2} (\text{s})$	$\nu_{(\text{CO})} (\text{cm}^{-1})$	$J_{\text{Rh-P}} (\text{Hz})$	$\theta_{\text{E}} (^\circ)^{\text{a}}$	$\theta_{\text{E}} (^\circ)^{\text{b}}$
$[\text{Rh}(\text{N-diPT})(\text{CO})(\text{PPh}_3)]$	0.0055(2)	126.0	1979	152.3	144.6	149.3
$[\text{Rh}(\text{N-diPT})(\text{CO})(\text{PPh}_2\text{Cy})]$	0.0060(4)	115.5	1972	149.4	153.0	151.2
$[\text{Rh}(\text{N-diPT})(\text{CO})(\text{PPhCy}_2)]$	0.00082(3)	845.4	1969	149.0	-	163.5
$[\text{Rh}(\text{N-diPT})(\text{CO})(\text{PCy}_3)]$	0.0027(1)	256.7	1963	145.6	155.5	169.5

<sup>a</sup> Calculated from crystallographic data. <sup>b</sup> Reported for  $[\text{Rh}(\text{acac})(\text{CO})(\text{PR}_1\text{R}_2\text{R}_3)]$  complexes<sup>10</sup>

<sup>10</sup> Brink, A.; Roodt, A.; Steyl, G.; Visser, H. G. (2010) *Dalton Trans.*, **39**, 5572.

#### 8.4.2.6 Activation parameters of the iodomethane oxidative addition to $[\text{Rh}(\text{N-diPT})(\text{CO})(\text{PR}_1\text{R}_2\text{R}_3)]$ complexes

A temperature study was also performed on the iodomethane oxidative addition to  $[\text{Rh}(\text{N-diPT})(\text{CO})(\text{PR}_1\text{R}_2\text{R}_3)]$  in order to calculate the activation parameters of these reactions. One of the limitations regarding the fact that dichloromethane (DCM) was the only solvent in which these complexes dissolved easily in, is that this analysis could only be performed within a small temperature range. Firstly, because the boiling point of DCM is around 40 °C and therefore monitoring reactions from 30 °C and upwards becomes difficult as the solvent evaporates quite quickly from the IR cell. The other limitation is due to the fact that since only FT-IR spectroscopy could be used to study these reactions, low temperatures become problematic, because water easily starts condensing on the sodium chloride blocks of the IR cell. This firstly damages the cell and secondly also causes additional interferences on the IR spectra. Therefore, the lowest temperature at which the IR cell could be kept stable was 5 °C. With these limitations only three temperatures were therefore chosen to study these reactions, namely, 5, 15 and 25 °C.

The data obtained at 25 °C were already reported and discussed in the previous sections 8.4.2.1-8.4.2.5. Further oxidative addition reactions were performed at 5 and 15 °C using the same iodomethane concentrations as well as protocols that were discussed in these sections for each of the  $[\text{Rh}(\text{N-diPT})(\text{CO})(\text{PR}_1\text{R}_2\text{R}_3)]$  complexes. All the corresponding data were fitted on the Scientist software from which the observed rate constants at each iodomethane concentration and temperature were calculated. The observed rate constants were plotted against iodomethane concentration for each temperature, which are summarized in Figure 8.19.

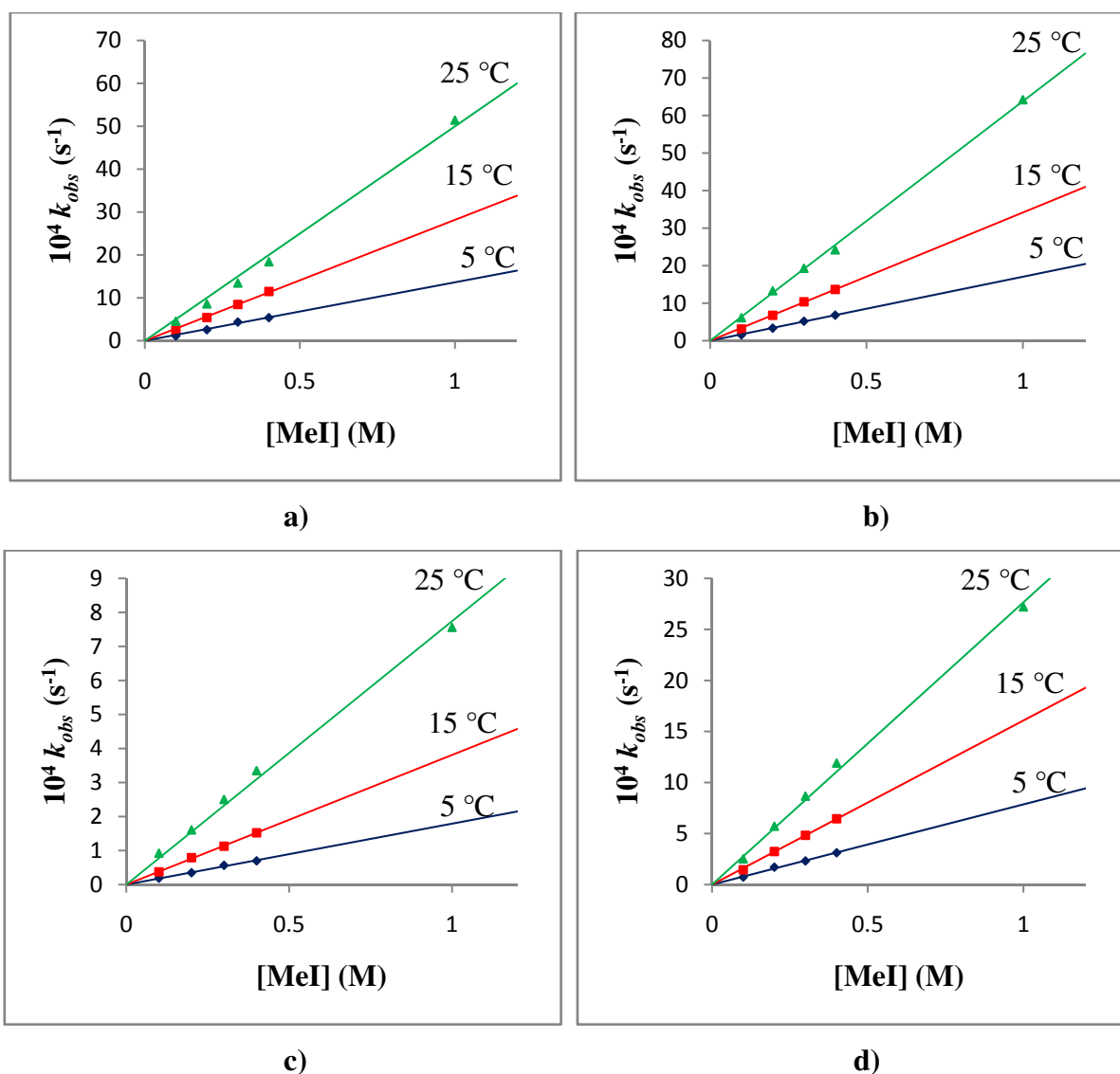


**Figure 8.19** Plots of the observed rate constants *vs* iodomethane concentrations for the iodomethane oxidative addition to  $[Rh(N-diPT)(CO)(PR_1R_2R_3)]$  at each temperature, where  $PR_1R_2R_3 =$  (a)  $PPh_3$ , (b)  $PPh_2Cy$ , (c)  $PPhCy_2$ , and (d)  $PCy_3$ .

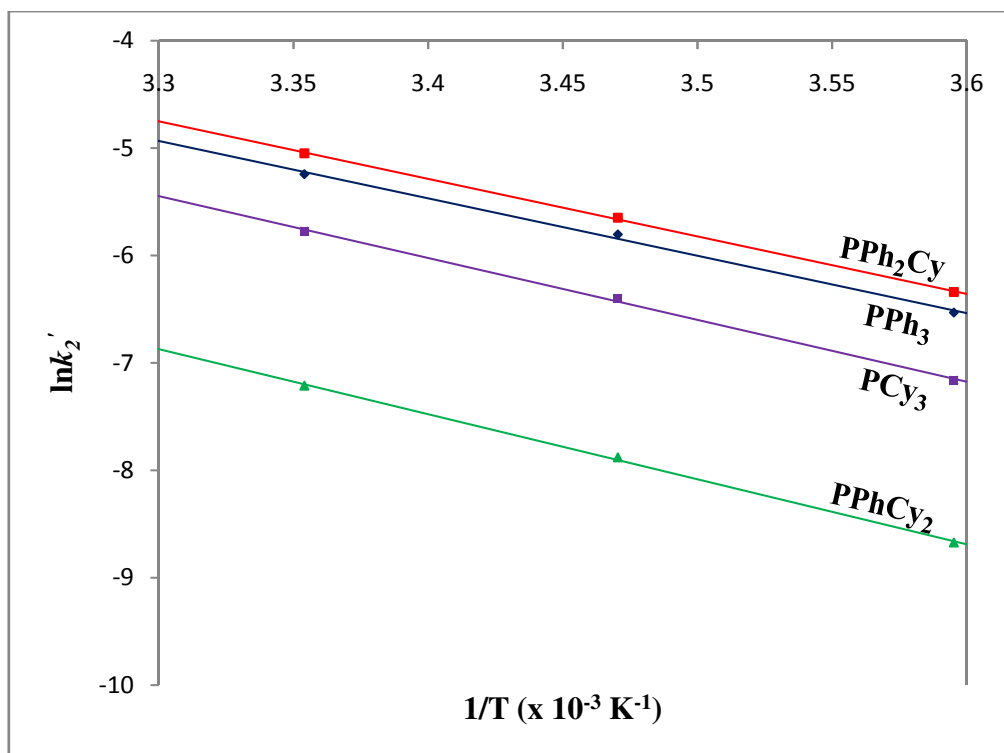
The experimental pseudo first-order rate constants for the oxidative addition reaction ( $k_2'$ ) were also calculated assuming a negligible contribution of the solvent pathway and reductive elimination reaction. The experimental pseudo first-order rate constants obtained for each complex were then plotted and fitted to the temperature using the relationship that was given in Equation 8.15. The activation parameters could then be calculated from equations 8.15 and 8.18, while the Gibbs free energy of activation for the oxidative addition reaction was obtained using equation 8.16.



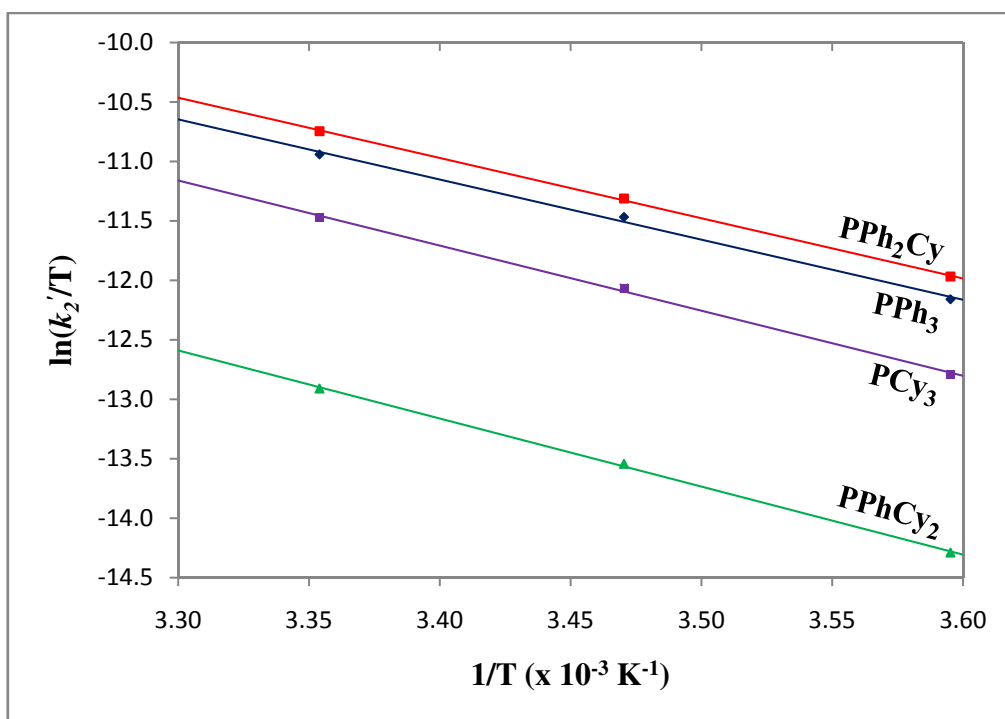
The fitted Arrhenius and Eyring plots for the iodomethane oxidative addition reaction are provided in Figures 8.20a and 8.20b, respectively. The activation parameters that were obtained from these plots are summarised in Table 8.3.

**Table 8.3 Thermodynamic parameters obtained from the Eyring plots for the iodomethane oxidative addition to [Rh(*N*-diPT)(CO)(PR<sub>1</sub>R<sub>2</sub>R<sub>3</sub>)] complexes in DCM.**

Complex	$E_a$ ( $k_2$ ) (kJ.mol <sup>-1</sup> )	$\Delta H^\ddagger$ ( $k_2$ ) (kJ.mol <sup>-1</sup> )	$\Delta S^\ddagger$ ( $k_2$ ) (J.K <sup>-1</sup> .mol <sup>-1</sup> )	$\Delta G^\ddagger$ ( $k_2$ ) (kJ.mol <sup>-1</sup> ) at 25 °C	% T $\Delta S^\ddagger$ ( $k_2$ ) at 25 °C
[Rh( <i>N</i> -diPT)(CO)(PPh <sub>3</sub> )]	43(2)	42(2)	-147(9)	85.8	51
[Rh( <i>N</i> -diPT)(CO)(PPh <sub>2</sub> Cy)]	44(1)	42(1)	-146(3)	85.5	51
[Rh( <i>N</i> -diPT)(CO)(PPhCy <sub>2</sub> )]	49(1)	48(1)	-144(4)	91.2	47
[Rh( <i>N</i> -diPT)(CO)(PCy <sub>3</sub> )]	46(2)	46(2)	-140(6)	87.7	48



a)



b)

**Figure 8.20** Arrhenius (a) and Eyring (b) plots obtained for the iodomethane oxidative addition to  $[\text{Rh}(\text{N-diPT})(\text{CO})(\text{PR}_1\text{R}_2\text{R}_3)]$  with respect to the disappearance of the  $\text{Rh}(\text{I})$  complex, where  $\text{PR}_1\text{R}_2\text{R}_3 = \text{PPh}_3, \text{PPh}_2\text{Cy}, \text{PPhCy}_2$ , and  $\text{PCy}_3$ .

It is clear from Table 8.3 that the oxidative addition reactions proceeded with large negative entropies of activation ( $\Delta S^\ddagger$ ), which is characteristic of associative activation. Although the activation parameters are very similar, a small decrease in the  $\Delta S^\ddagger$  values were observed for the complexes in the order of  $[\text{Rh}(\text{N-diPT})(\text{CO})(\text{PPh}_3)] > [\text{Rh}(\text{N-diPT})(\text{CO})(\text{PPh}_2\text{Cy})] > [\text{Rh}(\text{N-diPT})(\text{CO})(\text{PPhCy}_2)] > [\text{Rh}(\text{N-diPT})(\text{CO})(\text{PCy}_3)]$ . This suggests that an increase in the electron-donating properties of the phosphine ligand, led to a decrease in disorder by forming stronger bonds between the metal centre and the entering methyl and iodide ligands.

The  $\Delta H^\ddagger$  values, on the other hand, revealed a small increase for each complex in the order of  $[\text{Rh}(\text{N-diPT})(\text{CO})(\text{PPh}_3)] = [\text{Rh}(\text{N-diPT})(\text{CO})(\text{PPh}_2\text{Cy})] < [\text{Rh}(\text{N-diPT})(\text{CO})(\text{PCy}_3)] < [\text{Rh}(\text{N-diPT})(\text{CO})(\text{PPhCy}_2)]$ . This suggests that the energy requirement for these complexes increased in this order, which could lead to a slower reaction rate as the activation barrier is more difficult to overcome. This is confirmed by the direct correlation found between the  $\Delta H^\ddagger$  values and the pseudo first-order rate constant values for these complexes. It is also observed that the values of the Gibbs free energy ( $\Delta G^\ddagger$ ) for all of the complexes were similar ranging from 85.5-91.2 kJ/mol and are typical for this type of reactions.<sup>11</sup> The contributions of  $\Delta H^\ddagger$  and  $\Delta S^\ddagger$  to  $\Delta G^\ddagger$  at 25 °C are approximately the same. The  $E_a$  values are as expected virtually identical to the  $\Delta H^\ddagger$  values.

<sup>11</sup> a) Plutino, M. R.; Otto, S.; Roodt, A.; Elding, L. I. (1999) *Inorg. Chem.*, **38**, 1233. b) Otto, S.; Roodt, A. (2006) *J. Organomet. Chem.*, **691**, 4626. c) Otto, S.; Elding, L. I. (2002) *J. Chem. Soc., Dalton Trans.*, 2354.

## 8.5 Correlation of electro-steric effects of the [Rh(*N*-diPT)(CO)(PR<sub>1</sub>R<sub>2</sub>R<sub>3</sub>)] complexes

A summary of the most important kinetic and activation parameters are given in Table 8.4.

**Table 8.4 Important kinetic and activation parameters for the iodomethane oxidative addition to the following complexes: (i) [Rh(*N*-diPT)(CO)(PPh<sub>3</sub>)], (ii) [Rh(*N*-diPT)(CO)(PPh<sub>2</sub>Cy)], (iii) [Rh(*N*-diPT)(CO)(PPhCy<sub>2</sub>)], (iv) [Rh(*N*-diPT)(CO)(PCy<sub>3</sub>)].**

Complex	(i)	(ii)	(iii)	(iv)
$k_2'(\text{M}^{-1}.\text{s}^{-1})$ at 25 °C	0.0055(2)	0.0060(4)	0.00082(3)	0.0027(1)
$\nu_{\text{CO}} (\text{cm}^{-1})$	1979	1972	1969	1963
$J_{\text{Rh-P}} (\text{Hz})$	152.3	149.4	149.0	145.6
$\theta_{\text{E}} (^{\circ})^{\text{a}}$	144.6	153	-	155.5
$\theta_{\text{E}} (^{\circ})^{\text{b}}$	149.3	151.2	163.5	169.5
$\Delta H^{\ddagger} (k_2')$ (kJ.mol <sup>-1</sup> )	42(2)	42(1)	48(1)	46(2)
$\Delta S^{\ddagger} (k_2')$ (J.K <sup>-1</sup> .mol <sup>-1</sup> )	-147(9)	-146(3)	-144(4)	-140(6)
$\Delta G^{\ddagger} (k_2')$ (kJ.mol <sup>-1</sup> ) at 25 °C	85.8	85.5	91.2	87.7

<sup>a</sup> Calculated from crystallographic data. <sup>b</sup> Reported for [Rh(acac)(CO)(PR<sub>1</sub>R<sub>2</sub>R<sub>3</sub>)] complexes<sup>10</sup>

As was already mentioned in sections 8.2.4.1-8.2.4.4, an irregularity was observed in the observed rate constants from the oxidative addition reactions compared to the expected electro-steric properties of the phosphine ligands involved, which agrees with that reported by Brink *et al.*<sup>10</sup> and Janse van Rensburg.<sup>12</sup> Generally, by substituting a phenyl ring on a triphenylphosphine ligand with a bulkier cyclohexyl group, it is expected that the Tolmann cone angle of the ligand would increase. Therefore, the resulting phosphine is expected to exhibit more steric hindrance on the entering iodomethane during the oxidative addition reaction to the rhodium complexes. This in turn would lead to a decrease in the overall reaction rate if the steric properties dominate the electronic properties. This effect is expected to be more pronounced as additional phenyl rings are substituted by a cyclohexyl ring. Moreover, the substitution of a phenyl ring with a more electron-rich cyclohexyl group increases the electron density on the phosphorus atom, and as such its basicity. This in turn results in an increase in the electron density on the metal centre (which is clear from the corresponding  $\nu_{\text{CO}}$  values in Table 8.4), which is expected to undergo the oxidative addition

<sup>12</sup> Janse van Rensburg, J. M. (2008) *PhD Thesis*. University of Free State.

reaction at a faster rate. Additional substitution of phenyl rings with cyclohexyl rings should therefore increase the reaction rate subsequently, while at the same time increase the steric bulk of the tertiary phosphine.

It is clear from Table 8.4 and Figure 8.18 that the reaction rate increase for the oxidative addition reaction follows the order of  $[\text{Rh}(\text{N-diPT})(\text{CO})(\text{PPhCy}_2)] < [\text{Rh}(\text{N-diPT})(\text{CO})(\text{PCy}_3)] < [\text{Rh}(\text{N-diPT})(\text{CO})(\text{PPh}_3)] < [\text{Rh}(\text{N-diPT})(\text{CO})(\text{PPh}_2\text{Cy})]$ . By comparing this order of reaction rate constants to the respective  $J_{\text{Rh-P}}$  coupling constants of the different complexes, it is clear that no chronological trend exists between the electronic properties of the phosphine ligands and the rates of the different reactions. The coupling constants showed that the replacement of  $\text{PPh}_3$  with  $\text{PPh}_2\text{Cy}$  increased the electron density on the rhodium complex (as manifested in the increase in the  $J_{\text{Rh-P}}$  values), which led to a slight increase in the rate of the oxidative addition reaction. However, by replacing the  $\text{PPh}_2\text{Cy}$  with  $\text{PPhCy}_2$ , which led to a further increase in the electron density of the complex, a significant decrease was observed in the reaction rate.

In order to define the relationship between the steric properties of the phosphine ligands to the observed reaction rates, the effective cone angles for each ligand were calculated from the crystallographic data of the  $[\text{Rh}(\text{N-diPT})(\text{CO})(\text{PR}_1\text{R}_2\text{R}_3)]$  complexes that were obtained (Table 8.2). The  $\text{PPh}_3$  ligand in the complex  $[\text{Rh}(\text{N-diPT})(\text{CO})(\text{PPh}_3)]$  was found to have an effective cone angle of  $145.4^\circ$ , which was calculated as an average obtained between two independent molecules in the asymmetric unit of the  $[\text{Rh}(\text{N-diPT})(\text{CO})(\text{PPh}_3)]$  structure. By the replacement of one of the phenyl rings with a cyclohexyl ring the cone angle already showed an increase of  $7.6^\circ$ . These values compare well with those reported for the corresponding  $[\text{Rh}(\text{acac})(\text{CO})(\text{PR}_1\text{R}_2\text{R}_3)]$  complexes as shown in Table 8.4.<sup>10</sup> However, replacement of all the phenyl rings with cyclohexyl rings only showed a total increase in the effective cone angle of  $10.1^\circ$ . This value is also much smaller than that obtained for the  $[\text{Rh}(\text{acac})(\text{CO})(\text{PCy}_3)]$  complex, which was reported to be  $169.5^\circ$ . The smaller value for the  $[\text{Rh}(\text{N-diPT})(\text{CO})(\text{PCy}_3)]$  complex was ascribed to packing effects as was illustrated in Chapter 7.

By comparing the effective cone angle values with the rate of the oxidative addition reaction for each complex as mentioned above, no chronological trend could be found. The large decrease in the oxidative addition reaction rate for  $[\text{Rh}(\text{N-diPT})(\text{CO})(\text{PCy}_3)]$  compared to

$[\text{Rh}(\text{N-diPT})(\text{CO})(\text{PPh}_3)]$  was valid from a theoretical point of view, since  $\text{PCy}_3$  is bulkier than  $\text{PPh}_3$  causing more steric hindrance to the entering iodomethane. However, although the effective cone angle for the  $\text{PPh}_2\text{Cy}$  ligand in the complex  $[\text{Rh}(\text{N-diPT})(\text{CO})(\text{PPh}_2\text{Cy})]$  was found to be much larger than  $\text{PPh}_3$  in  $[\text{Rh}(\text{N-diPT})(\text{CO})(\text{PPh}_3)]$ , the oxidative addition reaction rate increased.

It was therefore clear that the effects of the steric and electronic properties of the phosphine ligands in the iodomethane oxidative addition to  $[\text{Rh}(\text{N-diPT})(\text{CO})(\text{PR}_1\text{R}_2\text{R}_3)]$  complexes could not be individually separated. Instead a combined effect of the respective properties should be taken in account. This order of reactivity towards iodomethane oxidative addition and the combinative effects of the steric and electronic properties of the phosphine ligands have been found to be similar for acetylacetonato and hydroxyquinolinato based rhodium complexes (see Figure 8.21).<sup>10,12</sup>

It was shown and discussed in sections 8.4.2.1-8.4.2.5 that the iodomethane oxidative addition to  $[\text{Rh}(\text{N-diPT})(\text{CO})(\text{PR}_1\text{R}_2\text{R}_3)]$  complexes, where  $\text{PR}_1\text{R}_2\text{R}_3 = \text{PPh}_3, \text{PPhCy}_2$  and  $\text{PCy}_3$ , primarily led to the formation of the Rh(III)-acyl species with only a small amount of Rh(III)-alkyl being present in the reaction mixture. It was therefore observed that the rate of disappearance of the Rh(I) complex was fairly equal to the rate of formation of the Rh(III)-acyl complex. This direct relationship is also observed in the activation parameters, as the values of  $\Delta S^\ddagger$  and  $\Delta H^\ddagger$  for the Rh(III)-acyl formation were found to be similar to those of the disappearance of the Rh(I) complex. It is therefore concluded that the formation of the Rh(III)-acyl complex was directly a consequence of the associative addition of iodomethane to the starting complex  $[\text{Rh}(\text{N-diPT})(\text{CO})(\text{PR}_1\text{R}_2\text{R}_3)]$ , as the formation and disappearance of the Rh(III)-alkyl intermediary was negligible in the overall reaction rate.

Finally, as was pointed out during the course of this chapter, the rapid equilibrium ( $K_I$ ) for the first step has been found to be quite small, implying a pronounced reductive elimination step. It is therefore concluded that the presence of an *S*-donor atom in the *L,L'*-bidentate ligand increases the reductive elimination step more than the oxidative addition. The nett overall effect of electro-steric properties of the  $\text{PR}_1\text{R}_2\text{R}_3$  ligand exacerbates this effect.

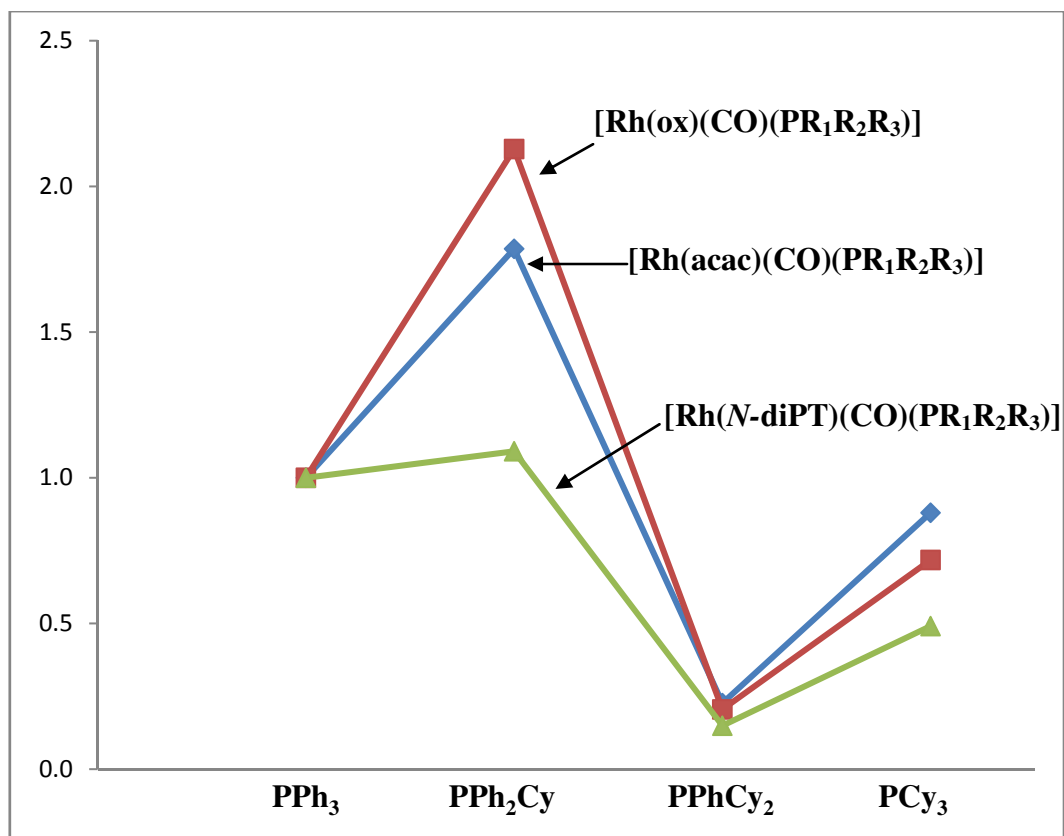


**Figure 8.21** Normalized reaction rates (relative to the PPh<sub>3</sub>) for *L,L'*-BID = hydroxyquinolinato, acetylacetonato and thioureato at T = 25 °C.<sup>10,12</sup>

## 8.6 Conclusion

The oxidative addition of iodomethane to [Rh(*S,O*-thioureato)(CO)<sub>2</sub>] and [Rh(*S,O*-thioureato)(CO)(PR<sub>1</sub>R<sub>2</sub>R<sub>3</sub>)] complexes were investigated and reported in this chapter. It was concluded that the oxidative addition to several [Rh(*S,O*-thioureato)(CO)<sub>2</sub>] complexes was quite complicated and very slow. The oxidative addition to a range of [Rh(*N*-diPT)(CO)(PR<sub>1</sub>R<sub>2</sub>R<sub>3</sub>)] complexes (*N*-diPT = *N*-benzoyl-*N',N'*-diphenylthioureato) on the other hand was well-defined and led primarily to the formation of the Rh(III)-acyl species, [Rh(*N*-diPT)(COMe)(I)(PR<sub>1</sub>R<sub>2</sub>R<sub>3</sub>)], *via* a small amount of the Rh(III)-alkyl intermediate, [Rh(*N*-diPT)(Me)(CO)(I)(PR<sub>1</sub>R<sub>2</sub>R<sub>3</sub>)]. The reaction rate for the different complexes increased in the order of [Rh(*N*-diPT)(CO)(PPhCy<sub>2</sub>)] < [Rh(*N*-diPT)(CO)(PCy<sub>3</sub>)] < [Rh(*N*-diPT)(CO)(PPh<sub>3</sub>)] < [Rh(*N*-diPT)(CO)(PPh<sub>2</sub>Cy)]. It was concluded that this order of reactivity was the result of a combined effect of the steric and electronic properties of the ligands. The activation parameters for the individual reactions were similar and typical of [Rh(BID)(CO)(PR<sub>1</sub>R<sub>2</sub>R<sub>3</sub>)] complexes.

It was therefore clear that the electro-steric properties of the different phosphine ligands play a vital role in the outcome of reactions such as the iodomethane oxidative addition.

To further investigate the role of the electro-steric properties of phosphine ligands in the catalytic reactivity of rhodium(I) complexes, it was decided to also analyze the kinetic and activation parameters of phosphine exchange reactions of the corresponding Vaska-type rhodium(I) complexes. This investigation is reported and discussed in Chapter 9.



# **CHAPTER 9**

## **KINETIC STUDY OF PHOSPHINE EXCHANGE REACTIONS**

### **OF VASKA-TYPE Rh COMPLEXES**

#### **9.1 Introduction**

Exchange reactions or substitution reactions play a fundamental role in many catalytic processes as well as synthetic routes. As with many of the other reactions involved in these processes, exchange reactions can have a large influence on the outcome of many of these processes and therefore a study of their thermodynamic and kinetic properties as well as mechanistic pathways is just as fundamentally important. In Chapter 2 some theoretical aspects on exchange/substitution reactions as well as examples were already discussed.

Several techniques are available to observe and analyze exchange processes of which the most studied include NMR techniques. As will be shown in more detail later in this chapter, a correlation exists between the kinetic parameters of an exchange reaction and the corresponding observed NMR spectra. Bain<sup>1</sup> stated that chemical exchange in magnetic resonance has a specific definition, which goes as follows: “It means that a chemical system is at macroscopic equilibrium, but at the microscopic level, an individual nucleus is exchanging its environment with another nucleus. The process causes no net change in the sample, but from the point of view of a particular nucleus, a chemical reaction has occurred.” This aspect is also sometimes referred to as dynamic NMR due to the fact that molecules exhibit constant motion.

Several studies have been performed on exchange processes and other reactions in equilibrium since the discovery of dynamic NMR. There is little literature available on phosphine exchange reactions of metal complexes, however, one author Fackler<sup>2</sup> already discussed the effect of phosphine exchange between the complex carbonylchlorobis(dimethylphenylphosphine)rhodium(I) and the free (CH<sub>3</sub>)<sub>2</sub>PhP ligand on

---

<sup>1</sup> Bain, A. D. (2008) *Chemical Exchange*. In *Modern Magnetic Resonance* edited by Webb, G. A., Springer, 421.

<sup>2</sup> Fackler, J. P., Jr. (1970) *Inorg. Chem.*, **9**, 11, 2625.

the proton magnetic resonance spectrum of the methyl group. Depending on the concentrations of the species relative to each other and the exchange rate, the methyl peak can appear either as a singlet, doublet or triplet. The author related his findings with those observed by Deeming *et al.*<sup>3</sup> Some other single-site exchange reactions that could be studied by NMR techniques were discussed in Chapter 2. The techniques are not restricted to single-site exchange though as it is feasible to study multi-site exchange reactions by NMR spectroscopy as well. An example includes work done by Allan *et al.*<sup>4</sup> where it is showed in detail how halogen exchange in mixtures of dimethyltin(IV)dihalides can be qualitatively analysed by proton magnetic resonance.

Apart from the system discussed before a proper study on phosphine exchange reactions of Vaska-type complexes have not yet been done before. In this study a range of Vaska-type rhodium complexes were synthesised and the exchange with their corresponding phosphines were investigated. This was feasible by using NMR techniques as will be discussed intensively in the following sections.

## 9.2 Synthesis of Vaska-type rhodium complexes $[\text{Rh}(\text{Cl})(\text{CO})(\text{PR}_1\text{R}_2\text{R}_3)_2]$

A series of well-known Vaska-type Rh-complexes  $[\text{Rh}(\text{Cl})(\text{CO})(\text{PR}_1\text{R}_2\text{R}_3)_2]$  were synthesised using the methodology as previously described by Singh *et al.*,<sup>5</sup> by utilising  $\text{PPh}_3$ ,  $\text{PPh}_2\text{Cy}$ ,  $\text{PPhCy}_2$  and  $\text{PCy}_3$  as the ligands. The general synthetic route is shown in Figure 9.1

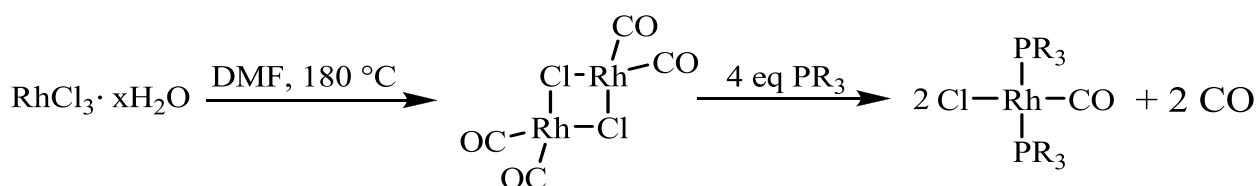


**Figure 9.1 Schematic representation of the procedure followed in the synthesis of the  $[\text{Rh}(\text{Cl})(\text{CO})(\text{PR}_1\text{R}_2\text{R}_3)_2]$  complexes.**

<sup>3</sup> Deeming, A. J.; Shaw, B. L. (1969) *J. Chem. Soc. A*, 597.

<sup>4</sup> Allan, E. A.; Hogben, M. G.; Reeves, L. W.; Shaw, K. N. (1972) *Pure Appl. Chem.*, **32**, 1-4, 9.

<sup>5</sup> Singh, M. M.; Szafran, Z.; Pike, R. M. (1990) *J. Chem. Educ.*, **67**, 7, A180.

### 9.2.1 Reagents and equipment

Unless otherwise stated all experiments were carried out in air, using analytical grade reagents. Rhodium(III)chloride hydrate ( $\text{RhCl}_3 \cdot x\text{H}_2\text{O}$ ) as well as the phosphorus ligands  $\text{PPh}_3$ ,  $\text{PPh}_2\text{Cy}$ ,  $\text{PPhCy}_2$  and  $\text{PCy}_3$  were purchased from Sigma Aldrich. Dimethylformamide (DMF), ethanol and diethyl ether were obtained from Merck. These reagents were used as received.

NMR spectroscopic data was acquired on a Bruker Advance DPX 300.  $^{31}\text{P}$  NMR data are listed in the order: chemical shift ( $\delta$ , reported in ppm and referenced to triphenylphosphine oxide [ $\delta = 29.9$  ppm]), multiplicity, number of phosphorus atoms, coupling constant ( $J$ , in Hz) where appropriate. FT-IR spectra were recorded on a Bruker Tensor 27 spectrophotometer in the range of  $3000\text{--}600\text{ cm}^{-1}$  in dry dichloromethane, using a NaCl solvent cell as well as *via* ATR.

### 9.2.2 $[\text{Rh}(\text{Cl})(\text{CO})(\text{PPh}_3)_2]$

$\text{RhCl}_3 \cdot x\text{H}_2\text{O}$  (100 mg, 0.48 mmol) was heated in DMF (5 ml) under reflux at  $180\text{ }^\circ\text{C}$  to produce the dimeric specie  $[(\text{Rh}(\mu\text{-Cl})(\text{CO})_2)]_2$ . Upon addition of triphenylphosphine (4 eq, 1.908 mmol) to the cooled solution the desired complex  $[\text{Rh}(\text{Cl})(\text{CO})(\text{PPh}_3)_2]$  precipitated as small bright yellow crystals from the solution. These crystals were washed with small portions of ethanol (2 ml) followed by ether (2 ml). (Yield = 178 mg, 61 %).

$^{31}\text{P}$  NMR (121 MHz,  $\text{CD}_2\text{Cl}_2$ ,  $25\text{ }^\circ\text{C}$ ):  $\delta_{\text{P}}$  30.5 (d,  $J_{\text{Rh-P}} = 128.9$  Hz).

IR  $\nu_{\text{max}}$  ATR/ $\text{cm}^{-1}$ : 1961 (CO).

### 9.2.3 [Rh(Cl)(CO)(PPh<sub>2</sub>Cy)<sub>2</sub>]

[Rh(Cl)(CO)(PPh<sub>2</sub>Cy)<sub>2</sub>] was synthesized by the same procedure as described in Section 9.2.2 using the ligand cyclohexyldiphenylphosphine (4 eq, 1.908 mmol) in this case. Yellow crystalline solid (Yield = 202 mg, 63 %).

<sup>31</sup>P NMR (121 MHz, CD<sub>2</sub>Cl<sub>2</sub>, 25 °C): δ<sub>P</sub> 37.8 (d,  $J_{Rh-P}$  = 123.2 Hz).

IR ν<sub>max</sub> ATR/cm<sup>-1</sup>: 1958 (CO).

### 9.2.4 [Rh(Cl)(CO)(PPhCy<sub>2</sub>)<sub>2</sub>]

[Rh(Cl)(CO)(PPhCy<sub>2</sub>)<sub>2</sub>] was synthesized by the same procedure as described in Section 9.2.2 using the ligand dicyclohexylphenylphosphine (4 eq, 1.908 mmol) in this case. Yellow crystalline solid (Yield = 197 mg, 65 %).

<sup>31</sup>P NMR (121 MHz, CD<sub>2</sub>Cl<sub>2</sub>, 25 °C): δ<sub>P</sub> 37.9 (d,  $J_{Rh-P}$  = 124.8 Hz).

IR ν<sub>max</sub> ATR/cm<sup>-1</sup>: 1963 (CO).

### 9.2.5 [Rh(Cl)(CO)(PCy<sub>3</sub>)<sub>2</sub>]

[Rh(Cl)(CO)(PCy<sub>3</sub>)<sub>2</sub>] was synthesized by the same procedure as described in Section 9.2.2 using the ligand tricyclohexylphosphine (4 eq, 1.908 mmol) in this case. Yellow crystalline solid (Yield = 268 mg, 90 %).

<sup>31</sup>P NMR (121 MHz, CD<sub>2</sub>Cl<sub>2</sub>, 25 °C): δ<sub>P</sub> 38.6 (d,  $J_{Rh-P}$  = 119.4 Hz).

IR ν<sub>max</sub> ATR/cm<sup>-1</sup>: 1941 (CO).

## 9.2.5 Conclusion

The  $[\text{Rh}(\text{Cl})(\text{CO})(\text{PR}_1\text{R}_2\text{R}_3)_2]$  complexes were characterised using IR as well as NMR spectroscopy. A summary of the necessary analytical data of these complexes is provided in Table 9.1.

**Table 9.1 Summary of the spectroscopic data for  $[\text{Rh}(\text{Cl})(\text{CO})(\text{PR}_1\text{R}_2\text{R}_3)_2]$  complexes.**

$[\text{Rh}(\text{Cl})(\text{CO})(\text{PR}_1\text{R}_2\text{R}_3)_2]$					
Complex nr	$\text{PR}_1\text{R}_2\text{R}_3$	% Yield	IR $\nu(\text{CO})$ ( $\text{cm}^{-1}$ )*	$^{31}\text{P}$ NMR $\delta$ (ppm)	$^1J_{\text{Rh-P}}$ (Hz)
<b>A</b>	$\text{PPh}_3$	61	1961**	30.5	128.9
<b>B</b>	$\text{PPh}_2\text{Cy}$	63	1958	37.8	123.2
<b>C</b>	$\text{PPhCy}_2$	65	1963	37.9	124.8
<b>D</b>	$\text{PCy}_3$	90	1941	38.6	119.4

\* Neat samples, ATR. \*\* One of two possible solid state variations. The other form of this complex usually has a carbonyl frequency shift at  $1979\text{ cm}^{-1}$ . This is usually caused by different packing effects.<sup>8,9</sup>

All the complexes were obtained in good yields as indicated in Table 9.1. It can also be observed that there is some chronological order in the values that were obtained, compared to the expected electronic structure of the phosphine present. This type of correlation has been shown and explained by various authors.<sup>6,7</sup> Yet complexes **B** and **C** are the exception where the values are in the opposite order as would have been expected of both the carbonyl stretching frequencies and the Rhodium-phosphorus coupling constant. Complex **A** has been reported before to have different carbonyl stretching frequencies due to different packing of the molecules in the solid state.<sup>8,9</sup> In this study, crystals were obtained having a carbonyl stretching frequency of  $1961\text{ cm}^{-1}$  of which the structure was solved by X-ray crystallography. The structure involved another polymorph of the expected  $[\text{Rh}(\text{Cl})(\text{CO})(\text{PPh}_3)_2]$  complex, which has already been reported before by previous authors<sup>8</sup> and is therefore not presented in this chapter.

<sup>6</sup> Roodt, A.; Otto, S.; Steyl, G. (2003) *Coord. Chem. Rev.*, **245**, 121.

<sup>7</sup> Tolman, C. A. (1970) *J. Am. Chem. Soc.*, **92**, 2953.

<sup>8</sup> Mills, A. M.; van der Vlugt, J. I.; Vogt, D.; Spek, A. L. (2002) *Private Commun.*

<sup>9</sup> Kemp, G.; Roodt, A.; Purcell, W. (1995) *Rhodium Express*, nr. 12, 21.

## 9.3 Line broadening study on the exchange reaction of $[\text{Rh}(\text{Cl})(\text{CO})(\text{PPh}_3)_2]$ with $\text{PPh}_3$

### 9.3.1 Theoretical background

#### 9.3.1.1 Origin of line broadening

Spectral lines are obtained when transitions occur between different sets of well-defined energy levels, and depending on the nature of these transitions the lines have different widths.<sup>10</sup> These various line widths that can be obtained are a result of two possible effects namely lifetime broadening and Doppler broadening. As described by the Heisenberg uncertainty principle it is impossible to define the exact energies of the levels in a transition, since no excited state has an infinite lifetime. Thus no excited state has an exactly defined energy. As the lifetime of an excited state decreases, the observed spectral lines will broaden, thus the name lifetime broadening. The energy spread  $\Delta E$  as given in Equation 9.1 is inversely proportional to the lifetime  $\Delta\tau$ ,

$$\Delta E \Delta\tau \geq h/2, (h = \text{Planck's constant}) \quad (9.1)$$

from which the corresponding broadening of the line is given by

$$\Delta\tilde{\nu} \approx 2.7 \times 10^{-12}/(\Delta\tau/\text{s}) \quad (9.2)$$

The second broadening effect involves the Doppler effect of light. In an active medium the molecules present travels in all directions, whilst the light is being amplified and emitted in only one direction. As described in the special relativity theory as an object approaches a static observer with a speed  $x$  and in the process emits radiation with a frequency of  $f$ , it appears to be emitting radiation at a frequency  $f' = 1/[1 - (x/c)] f$ . As the object moves away from the observer, its radiation appears to have a frequency  $f' = 1/[1 + (x/c)] f$ . This results in a range of Doppler shifts and the observed line is therefore broadened.

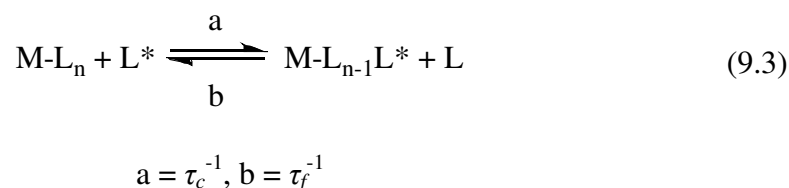
---

<sup>10</sup> Laidler, K. J.; Meiser, J. H.; Sanctuary, B. C. (2003) *Physical Chemistry 4<sup>th</sup> Ed.*, Houghton Mifflin Company, Boston, USA, 720-721.

In the case of NMR spectroscopy, should a single resonating nucleus jump frequently between two or more sites within a small time interval, a nonsinusoidal contribution to the FID will be obtained. This contribution involves a collection of components having various lengths and whose frequencies interchange between those for the different sites. As a result the total *xy* magnetisation will therefore decay by interference within a time that is closely related to the inverse of the weighted frequency difference of the components, which then results in the broadening of the observed line.<sup>11</sup>

### 9.3.1.2 Line broadening due to chemical exchange

Gutowsky *et al.*<sup>12</sup> developed the first quantitative theory for the analysis of a chemical exchange reaction using NMR spectroscopy. From there on many other authors optimised the mathematical basis around this theory in order to relate the observed outcome of the reaction to that of its thermodynamic properties.<sup>13,14,15</sup> In order to explain the relationship consider a general exchange reaction as given in Equation 9.3,



where the exchanging ligand is given by L and the free and co-ordinated sites are given by c and f, respectively.  $\tau_c$  and  $\tau_f$  are the mean lifetimes at each site while the nuclear sites  $\text{M-L}_n$  and  $\text{M-L}_{n-1}\text{L}^*$  are distinguished with chemical shifts of  $\nu_{\text{M-L}_n} = (\omega_{0\text{M-L}_n}/2\pi)$  and  $\nu_{\text{M-L}_{n-1}\text{L}^*} = (\omega_{0\text{M-L}_{n-1}\text{L}^*}/2\pi)$  ( $\omega$  = observed frequency). The exchange rate for the reaction is then given by Equation 9.4,

$$-d[\text{M-L}_n]/dt = n[\text{M-L}_n]/\tau_c \quad \text{and} \quad -d[\text{M-L}_{n-1}\text{L}^*]/dt = n[\text{M-L}_{n-1}\text{L}^*]/\tau_f \quad (9.4)$$

<sup>11</sup> Mason, J (1987) *Multinuclear NMR*, Plenum Press, New York, USA, 157.

<sup>12</sup> Gutowsky, H. S.; McCall, D. M.; Slichter, C. P. (1953) *J. Chem. Phys.*, **21**, 279.

<sup>13</sup> Pople, J. A.; Schneider, W. G.; Bernstein, H. J. (1959) *High-Resolution Nuclear Magnetic Resonance*, McGraw Hill, New York, USA.

<sup>14</sup> La Mar, G. N.; Horrocks, W. D.; Holm, R. H. (1973) *NMR of Paramagnetic Molecules*, Academic Press, New York, USA.

<sup>15</sup> Jackman, L. M.; Cotton, F. A. (1975) *Dynamic Nuclear Magnetic Resonance Spectroscopy*, Academic Press, New York, USA.

From this the exchange rate constant,  $k_{\text{ex}}$ , is given by Equation 9.5,

$$k_{\text{ex}} = 1/\tau_c = \text{rate}/(n[\text{M-L}_n]) = (k_B T/h) e^{-\Delta H^\ddagger/RT} e^{\Delta S^\ddagger/R} \quad (9.5)$$

The NMR signals that would be observed for the separate sites will vary in linewidth as the exchange rate varies. If spectra are obtained where the linewidths of the separate signals are relatively noticeable, the values of  $\tau_c$  and  $\tau_f$  can easily be obtained from these linewidths using the Equations 9.6a and 9.6b,

$$1/\tau_c = 1/T_{2c(\text{obs})} - 1/T_{2c} \quad (9.6a)$$

$$1/\tau_f = 1/T_{2f(\text{obs})} - 1/T_{2f} \quad (9.6b)$$

where  $1/T_{2c(\text{obs})}$  and  $1/T_{2f(\text{obs})}$  ( $T_2$  = transverse relaxation time) are equivalent to the observed linewidths and  $1/T_{2c}$  and  $1/T_{2f}$  are equivalent to the linewidths in the absence of exchange. In order to calculate the activation parameters,  $\Delta H^\ddagger$  and  $\Delta S^\ddagger$ , spectra have to be measured at various temperatures and the corresponding best-fit  $\tau_c$ -values calculated. From these values the first-order rate constant at each temperature can be determined using Equation 9.5, and plots of  $\ln k_{\text{ex}}$  vs.  $1/T$  will provide the thermodynamic values.

### 9.3.2 Experimental procedure

First, it was necessary to obtain preliminary information on the general behaviour of the  $[\text{Rh}(\text{Cl})(\text{CO})(\text{PPh}_3)_2]$  complex in solution at room temperature. Therefore a sample containing  $[\text{Rh}(\text{Cl})(\text{CO})(\text{PPh}_3)_2]$  (5 mg,  $7.2 \times 10^{-3}$  mmol) and  $\text{PPh}_3$  (3.8 mg,  $1.4 \times 10^{-2}$  mmol) was prepared within a NMR young tube. Deuterated THF (0.5 ml) was added to the sample under an inert atmosphere. After the solid components had dissolved the sample was degassed by means of a pump-freeze-flow method in which the sample was frozen in liquid nitrogen and gases within the tube were removed under vacuum. After allowing the sample to warm up to room temperature again, it was frozen again and the process was repeated several times. Degassing the sample was necessary in order to remove all possible oxygen and water to prevent it from reacting with either the complex or the phosphine. It has been shown that oxygen can oxidatively add to the Rh(I) centre to form an octahedral Rh(III) specie.<sup>16</sup> Water

<sup>16</sup> Selke, M.; Karney, W. L.; Khan, S. I.; Foote, C. S. (1995) *Inorg. Chem.*, **34**, 23, 5715.



and oxygen can easily oxidise phosphines to phosphine oxides especially in the presence of complexes that can act as catalysts during this conversion.<sup>17a,b,c</sup> All samples that were used during this study and referred to in this chapter were prepared in this manner.

Analysis of all the samples referred to in this chapter was performed by taking <sup>31</sup>P NMR spectra on a 500 MHz Varian spectrometer. The <sup>31</sup>P NMR spectrum of the first sample mentioned above revealed two broad peaks at 31.4 ppm and -2.0 ppm at room temperature, which correspond to the complex [Rh(Cl)(CO)(PPh<sub>3</sub>)<sub>2</sub>] and PPh<sub>3</sub>, respectively. The temperature on the spectrometer was then lowered to -80 °C after which another <sup>31</sup>P NMR spectrum was taken. The two peaks became more narrow where a doublet was observed at 30.0 ppm (<sup>1</sup>J<sub>Rh-P</sub> = 121.4 Hz) and a singlet at -6.3 ppm for the complex [Rh(Cl)(CO)(PPh<sub>3</sub>)<sub>2</sub>] and PPh<sub>3</sub>, respectively. The sample was scanned several times after some time period to observe if there were any changes in the composition, however, the reaction mixture was found to be in dynamic equilibrium as the composition remained unchanged.

It was clear from these results that this reaction system was suitable for line broadening studies. The strategy behind this study basically involved the preparation of several samples having different phosphine concentrations and taking <sup>31</sup>P NMR spectra at various temperatures. The phosphine concentration range that was implemented included 0.010 M (1 eq), 0.043 M (3 eq), 0.072 M (5 eq) and 0.114 M (8 eq) of PPh<sub>3</sub> and the concentration of [Rh(Cl)(CO)(PPh<sub>3</sub>)<sub>2</sub>] was kept at a constant value of 0.014 M. The temperature range at which the analysis was performed included 25, 15, 5, -5, -15 and -25 °C. The exact temperature at which each analysis was performed was measured using a pure methanol temperature standard. The <sup>31</sup>P NMR spectra were taken by performing a large amount of scans in order to ensure that the signal-to-noise ratio was fairly high. These spectra were then utilised to determine the observed rate constants by simulating them on software called gNMR from Ivorysoft.<sup>18</sup>

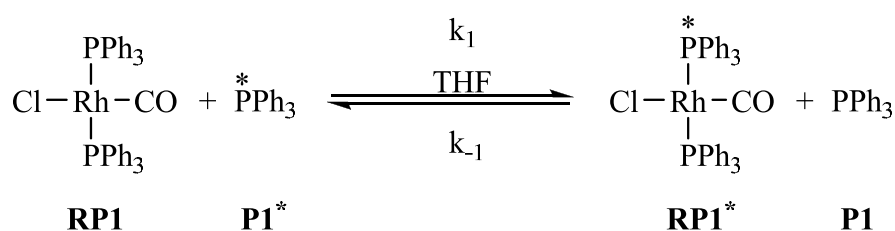
---

<sup>17</sup> a) Larpent, C.; Dabard, R.; Patin, H. (1987) *Inorg. Chem.*, **26**, 17, 2922. b) Sen, A.; Halpern, J. (1977) *J. Am. Chem. Soc.*, **99**, 25, 8337. c) Gao, R.; Ho, D. G.; Dong, T.; Khuu, D.; Franco, N.; Sezer, O.; Selke, M (2001) *Org. Lett.*, **3**, 23, 3719.

<sup>18</sup> Budzelaar, P. H. M. (2006) *gNMR*, v. 5.0.6.0, Ivorysoft, Cherwell Scientific Limited, Oxford, U.K.

### 9.3.3 Kinetic and thermodynamic analysis

The general phosphine exchange reaction that took place between  $[\text{Rh}(\text{Cl})(\text{CO})(\text{PPh}_3)_2]$  (**RP1**) and  $\text{PPh}_3$  (**P1**) is shown in Scheme 9.2. This was but a simple substitution where the free phosphine (**P1**) substituted one of the phosphines on the complex (**RP1**), which reproduced the same complex. This was confirmed by the spectra that were obtained, since only two peaks were observed in each case and no other possible products were observed. For clarification during the discussion in this session the rate for this reaction is provided in Equation 9.7.<sup>19</sup>

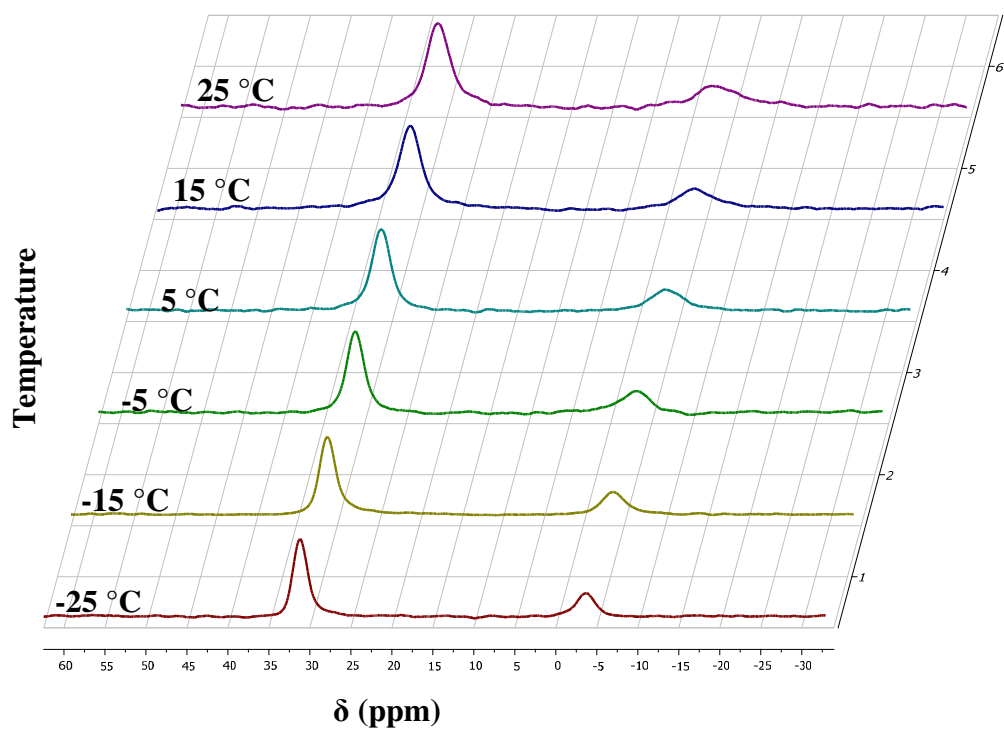


Scheme 9.2

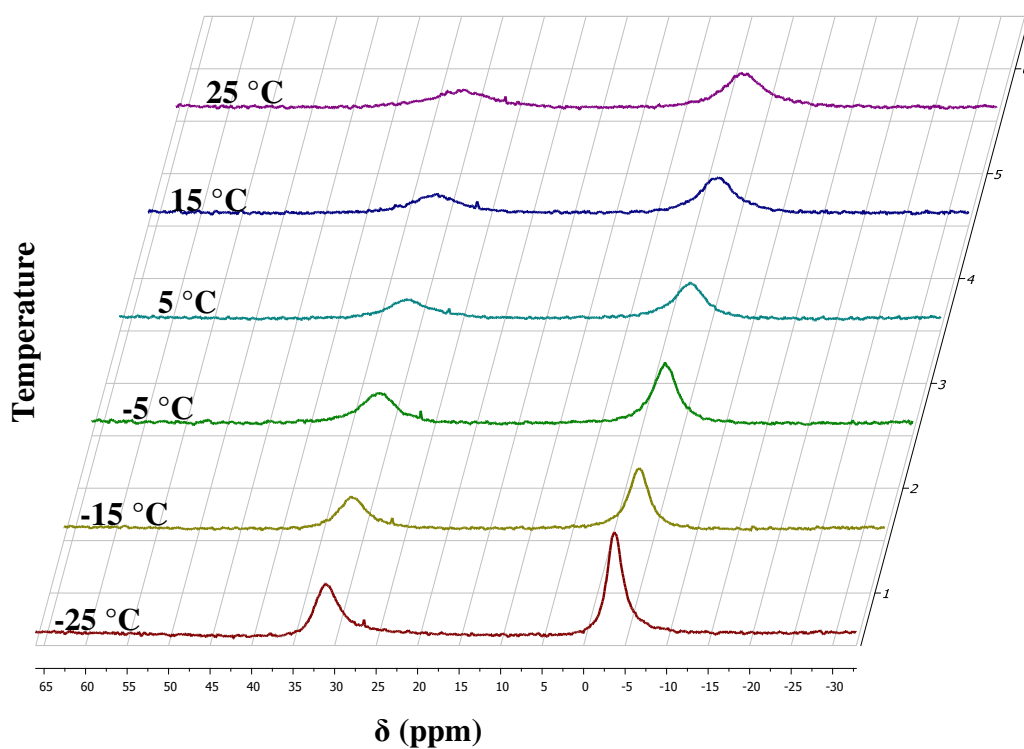
$$\begin{aligned}
 \frac{d[\text{RP1}^*]}{dt} &= k_{\text{exp}}[\text{RP1}][\text{P1}^*] \\
 \text{thus } \frac{d[\text{RP1}^*]}{dt} &= k_{\text{obs}}[\text{RP1}], \text{ where } k_{\text{obs}} = k_{\text{exp}}[\text{P1}^*] \quad (9.7)
 \end{aligned}$$

A representation is given in Figure 9.2 of typical spectra that were obtained during the study on the phosphine exchange reaction between  $[\text{Rh}(\text{Cl})(\text{CO})(\text{PPh}_3)_2]$  (**RP1**) and  $\text{PPh}_3$  (**P1**) over a range of temperatures. In all cases it was observed that as the temperature decreased from 25 °C to -25 °C the two broad peaks that were generally observed became more narrow and that in all cases. This is expected since, as given by the Arrhenius equation the rate of the reaction is directly related to temperature and, the linewidths of the NMR signals alters as the exchange rate varies. This is further illustrated in Figure 9.3 where plots of the observed rate constants vs temperature are given. It is clear that the data correlated well with an exponential fit, which once again is expected by the definition of the Arrhenius equation.

<sup>19</sup> Plutino, M. R.; Otto, S.; Roodt, A.; Elding, L. I. (1999) *Inorg. Chem.*, **38**, 1233.



(a)



(b)

**Figure 9.2:** A representation of the resulting spectra produced from the analysis of the phosphine exchange reaction between  $[\text{Rh}(\text{Cl})(\text{CO})(\text{PPh}_3)_2]$  and  $\text{PPh}_3$  across a temperature range for the samples containing (a) 1 eq of  $\text{PPh}_3$  and (b) 2 eq of  $\text{PPh}_3$ , respectively.  $[\text{Rh}] = 0.0142 \text{ M}$ .

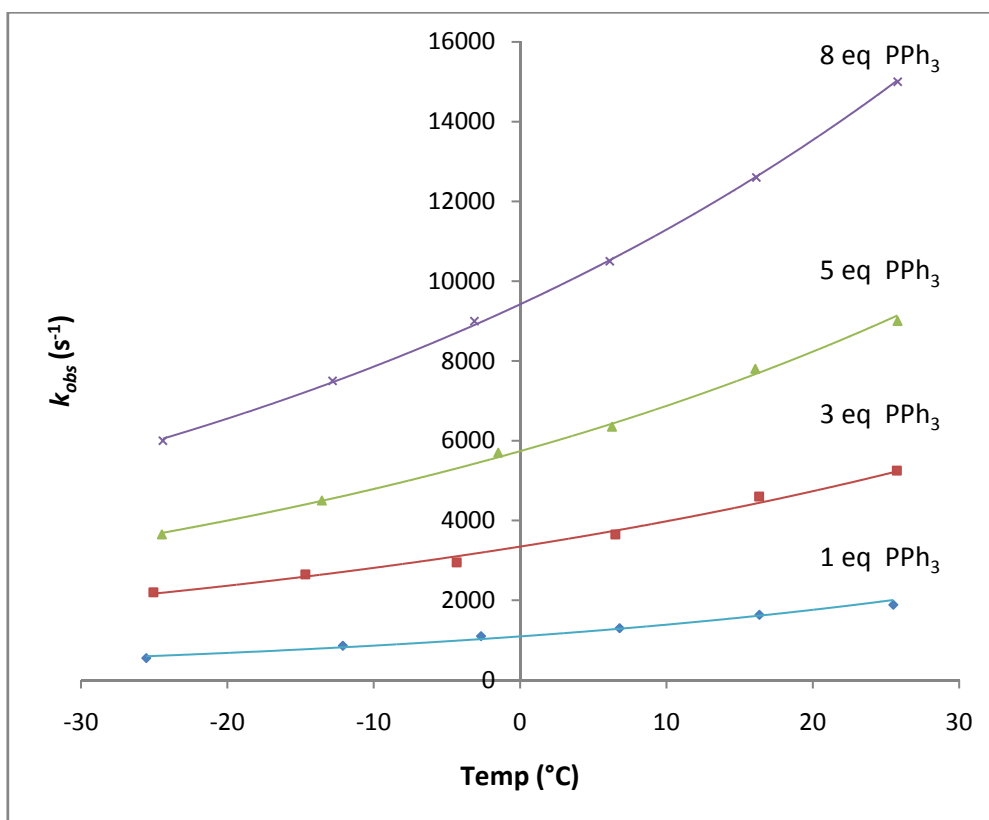


**Figure 9.3** Plots of the observed rate constants against temperature obtained from the analysis of the phosphine exchange reaction between  $[\text{Rh}(\text{Cl})(\text{CO})(\text{PPh}_3)_2]$  and  $\text{PPh}_3$  across a range of phosphine concentrations.  $[\text{Rh}] = 0.0142 \text{ M}$ .

An example for the spectra obtained from the analysis of the exchange reaction at different phosphine concentrations at  $-25^\circ\text{C}$  is provided in Figure 9.4. As the phosphine concentration increases broadening can be observed on the signal representing the rhodium complex ( $\pm 31 \text{ ppm}$ ), whilst the signal representing the free phosphine remains constant with respect to its linewidth. By considering that the concentration of the rhodium complex remained constant, this can be explained by the fact that the rate constant is directly proportional to the observed linewidths as was shown in Equation 9.6a. Thus, since the rhodium concentration remained constant, an increase in the total rate of the exchange reaction resulted in an increase in the rate constant value as can be elucidated from Equation 9.7, which in turn cause a direct increase in the linewidth of the signal representing the rhodium complex. Since the phosphine concentration increased in each case, it compensated for the increase in the rate, thus causing little changes in the linewidth of the signal representing the free phosphine.

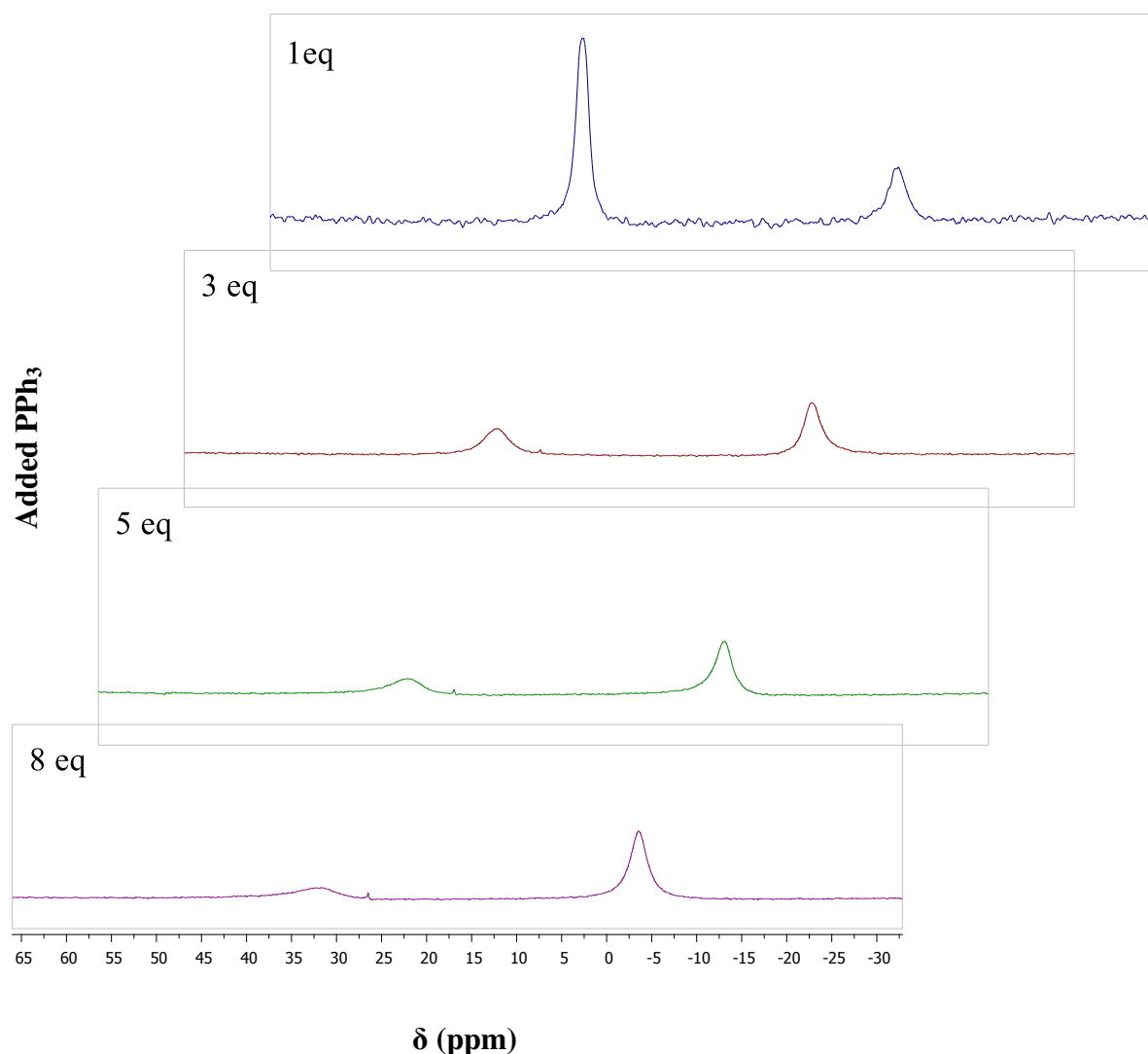


**Figure 9.4** A representation of the resulting spectra produced from the analysis of the phosphine exchange reaction between  $[\text{Rh}(\text{Cl})(\text{CO})(\text{PPh}_3)_2]$  and  $\text{PPh}_3$  across a range of phosphine concentrations at  $-25\text{ }^\circ\text{C}$ .  $[\text{Rh}] = 0.0142\text{ M}$ .

In Figure 9.5 the plots for the observed rate constants vs phosphine concentration are given. It is clear from these plots that there is a linear relationship between the observed rate constant and the phosphine concentration. The error in the intercepts was calculated to be less than 10%, which suggested that the presence of a possible solvent pathway was less important. It was therefore accepted that the kinetic parameters of the solvent pathway had a very small contribution to the exchange reaction rate and can be neglected. Thus from Equation 9.7 the experimental rate constant ( $k_{\text{exp}}$ ) could be obtained from the slopes of these plots at different temperatures. The observed rate constants obtained at various phosphine concentrations and temperatures together with the experimental rate constants are provided in Table 9.2.

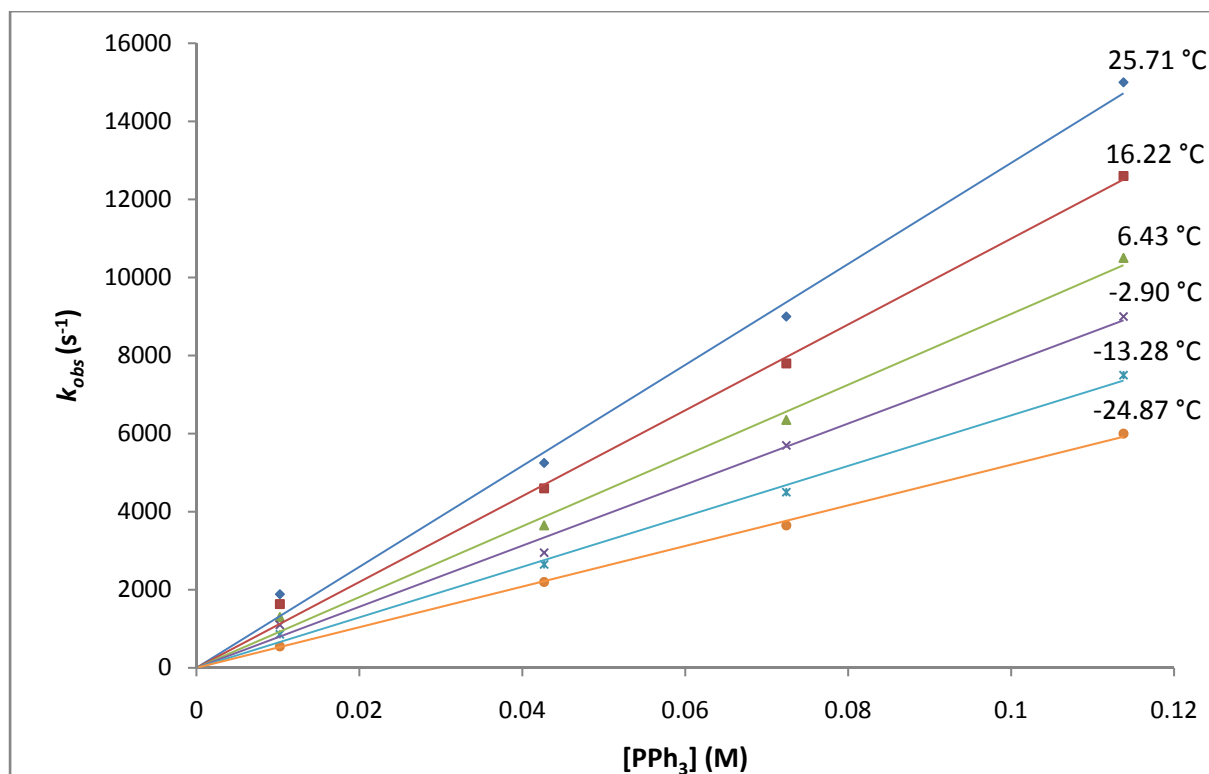


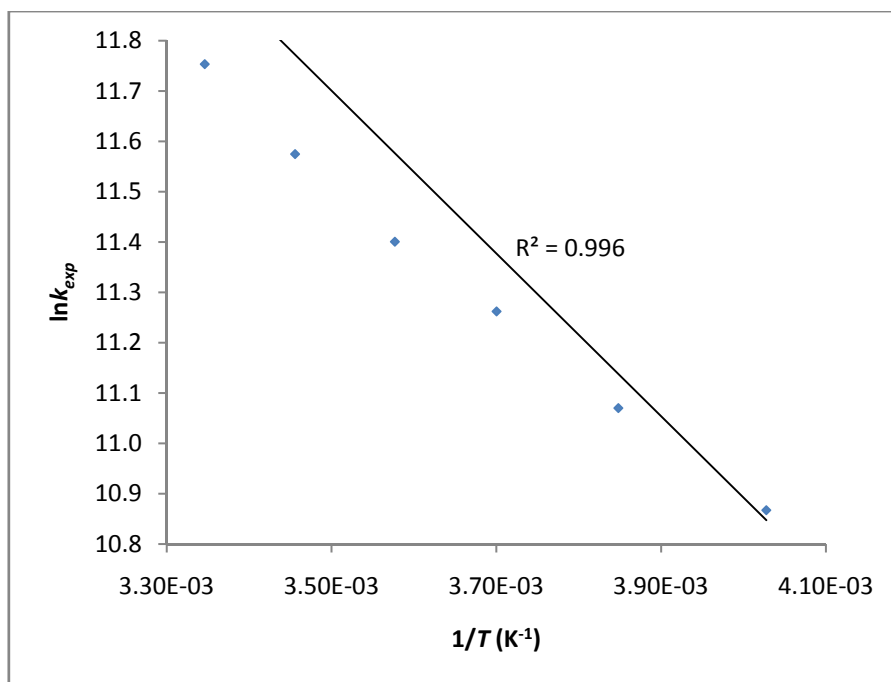
**Figure 9.5** Plots of the  $k_{obs}$  vs  $[PPh_3]$  obtained from the analysis of the phosphine exchange reaction between  $[Rh(Cl)(CO)(PPh_3)_2]$  and  $PPh_3$  across a temperature range.  
 $[Rh] = 0.0142\text{ M}$ .

**Table 9.2** Observed rate constants obtained at different temperatures ( $^{\circ}C$ ) of the phosphine exchange reaction between  $[Rh(Cl)(CO)(PPh_3)_2]$  and  $PPh_3$ .

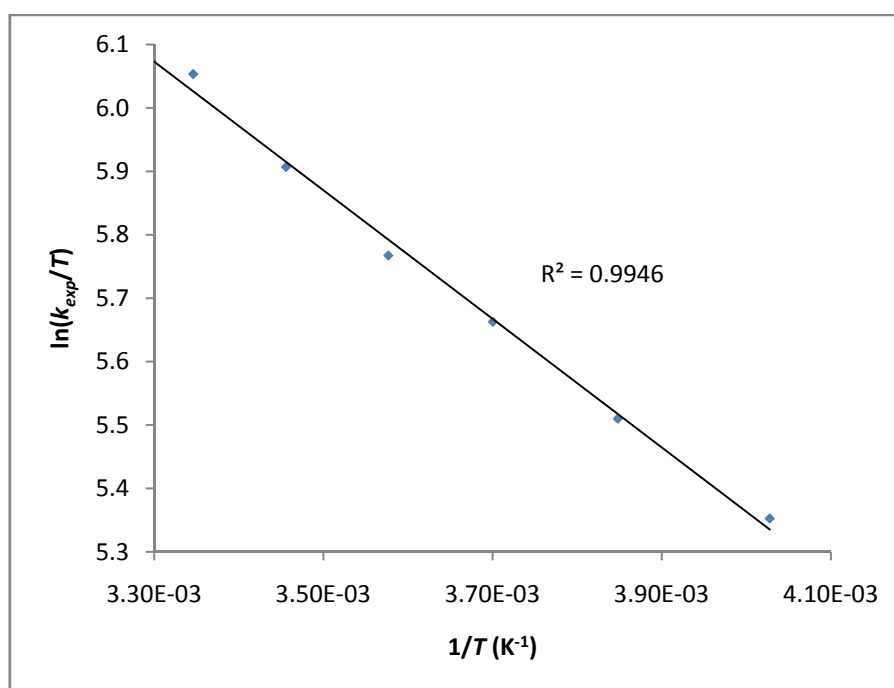
$[PPh_3]$ (M)	Average Temp ( $^{\circ}C$ )	$k_{obs} (s^{-1})^*$					
		25.71	16.22	6.43	-2.90	-13.28	-24.87
0.0102		1887	1635	1300	1100	860	550
0.0427		5250	4600	3650	2950	2650	2200
0.0724		9000	7800	6350	5700	4500	3650
0.1138		15000	12600	10500	9000	7500	6000
	$k_{exp} (M^{-1}.s^{-1})$	127174.3	106364.0	89381.6	77816.3	64224.0	52426.5

\* An error of less than 5% was assumed for each value

The data in Table 9.2 was utilised to construct the Arrhenius and Eyring plots provided in Figure 9.6, from which the thermodynamic values could be calculated. A good linear fit was obtained from the data.



(a)



(b)

**Figure 9.6** Arrhenius (a) and Eyring (b) plots for the exchange reaction between  $[\text{Rh}(\text{Cl})(\text{CO})(\text{PPh}_3)_2]$  and  $\text{PPh}_3$  where  $[\text{Rh}] = 0.0142 \text{ M}$ . (a) was used to calculate the activation energy ( $E_a = 10.7 \text{ kJ/mol}$ ), while (b) was used to calculate the enthalpy value ( $\Delta H^\ddagger = 8.43 \text{ kJ/mol}$ ) and entropy value ( $\Delta S^\ddagger = -119.25 \text{ J.K}^{-1}.\text{mol}^{-1}$ ).

The activation parameters for the exchange reaction between  $[\text{Rh}(\text{Cl})(\text{CO})(\text{PPh}_3)_2]$  and  $\text{PPh}_3$  were calculated from the plots given in Figure 9.6, of which a summary is given in Table 9.3

**Table 9.3 A summary of the activation parameters for the exchange reaction between  $[\text{Rh}(\text{Cl})(\text{CO})(\text{PPh}_3)_2]$  and  $\text{PPh}_3$ .**

$E_a$ (kJ/mol)	$\Delta H^\ddagger$ (kJ/mol)	$\Delta S^\ddagger$ (J.K <sup>-1</sup> .mol <sup>-1</sup> )
10.7	8.43	-119.25

By definition entropy is a measure of the disorder in a reaction system, therefore since a large negative value for the entropy would suggest a more ‘ordered’ system, it can be concluded that the exchange reaction between  $[\text{Rh}(\text{Cl})(\text{CO})(\text{PPh}_3)_2]$  and  $\text{PPh}_3$  follows an associative mechanism. This was also supported by the dependence of the rate of the reaction on the phosphine concentration as was observed before.<sup>20</sup> Another observation is that the contribution of  $T\Delta S^\ddagger$  to the Gibbs free energy of activation is quite large, whereas the enthalpy of activation is correspondingly small. The activation process is therefore primarily controlled by entropy, which leads to the formation of a stable transition state as the five co-ordinated complex is formed.

## 9.4. Magnetization transfer study on the exchange reaction of $[\text{Rh}(\text{Cl})(\text{CO})(\text{PPh}_2\text{Cy})_2]$ with $\text{PPh}_2\text{Cy}$

### 9.4.1 Theoretical background

Magnetization transfer is a “NMR method for determining kinetics of chemical exchange by perturbing the magnetization of nuclei in a particular site or sites and following the rate at which magnetic equilibrium is restored”.<sup>21</sup> Saturation and inversion are amongst others the most common perturbations from which the corresponding methods are referred to as “saturation transfer” and “selective inversion-recovery”. This analysis is performed for exchange reactions that are in equilibrium, for example exchange between *cis* and *trans* isomers.

<sup>20</sup> Huheey, J. E.; Keiter, E. A.; Keiter, R. L. (1993) *Inorganic Chemistry, Principles of Structure and Reactivity*, 4<sup>th</sup>

Ed., HarperCollins College Publishers, New York, USA, 540-541.

<sup>21</sup> Muller, P. (1994) *J. Pure Appl. Chem.*, **66**, 5, 1077.



In order to do magnetization transfer there are certain requirements that must be met. Firstly the nuclear sites under study must have separate resonances. If you consider a general exchange reaction as was given in Equation 9.3, this requirement will be satisfied when

$$\Delta\nu_{cf} \gg \frac{1}{\tau_c}, \frac{1}{\tau_f} \quad (9.8)$$

where  $\Delta\nu_{cf}$  is the difference in the chemical shifts between a pair of resonances for the different nuclear sites under study.<sup>22</sup> The other requirement is that the spin-lattice relaxation times ( $T_{1c}$  and  $T_{1f}$  in the absence of exchange) are not insignificant relative to the mean lifetime of the sites ( $\tau_{cf}$ ).<sup>23</sup>

There are several methods developed for magnetization transfer experiments with the purpose to obtain kinetic parameters, but since this study mainly involves inversion-transfer the method relevant to the study will be described. These methods were developed from equations that utilise equations designed by Bloch,<sup>24</sup> which have been modified for magnetization transfer by chemical exchange (only a few examples are listed).<sup>25,26,27,28</sup> These equations basically express the time dependence of the  $z$  component of the nuclear magnetization of the different sites with regard to their lifetimes, spin-lattice relaxation times and other parameters. Using Equation 9.3, these equations are expressed as follows,

$$\frac{dM_z^c}{dt} = -\left(\frac{M_z^c - M_e^c}{T_{1c}}\right) - \frac{M_z^c}{\tau_c} + \frac{M_z^f}{\tau_f} \quad (9.9a)$$

$$\frac{dM_z^f}{dt} = -\left(\frac{M_z^f - M_e^f}{T_{1f}}\right) + \frac{M_z^c}{\tau_c} - \frac{M_z^f}{\tau_f} \quad (9.9b)$$

where  $M_z^c$  and  $M_z^f$  are the nuclear magnetization and  $M_e^c$  and  $M_e^f$  the equilibrium magnetizations of the different sites.

<sup>22</sup> McLaughlin, A. C.; Leigh, J. S., Jr. (1973) *J. Magn. Reson.*, **9**, 296.

<sup>23</sup> Forsen, S.; Hoffman, R. A. (1963) *J. Chem. Phys.*, **39**, 2892.

<sup>24</sup> Bloch, F. (1946) *Phys. Rev.*, **70**, 460.

<sup>25</sup> McConnell, H. M. (1958) *J. Chem. Phys.*, **28**, 430.

<sup>26</sup> Alexander, S. (1962) *J. Chem. Phys.*, **37**, 967.

<sup>27</sup> Binsch, G. (1969) *J. Am. Chem. Soc.*, **91**, 1304.

<sup>28</sup> Robinson, G.; Chapman, B. E.; Kuchel, P. W. (1984) *Eur. J. Biochem.*, **143**, 643.

The exact solutions of these equations for magnetization transfer performed by an inversion of the resonance for the site f are given by

$$M^f(t) = c_f e^{(\lambda_1 t)} + c_2 e^{(\lambda_2 t)} + M_e^f \quad (9.10a)$$

$$M^c(t) = c_f \tau_c (\lambda_1 + 1/\tau_{1c}) e^{(\lambda_1 t)} + c_2 \tau_f (\lambda_2 + 1/\tau_{1f}) e^{(\lambda_2 t)} + M_e^c \quad (9.10b)$$

where  $M^c(t)$  and  $M^f(t)$  represent the time-dependent magnetizations,  $\tau_{1c}$  and  $\tau_{1f}$  represent the effective relaxation times of the different sites and t is the length of time in the pulse sequence during which inversion transfer takes place by chemical exchange.

The effective relaxation times are given by the following equations:

$$\frac{1}{\tau_{1f}} = \frac{1}{T_{1f}} + \frac{1}{\tau_f} \quad (9.11a)$$

$$\frac{1}{\tau_{1c}} = \frac{1}{T_{1c}} + \frac{1}{\tau_c} \quad (9.11b)$$

$\lambda_1$ ,  $\lambda_2$ ,  $c_1$  and  $c_2$  are quantities that are functions of the fundamental time constants, the equilibrium magnetizations and the magnetizations at  $t \approx 0$  ( $M_0^c$  and  $M_0^f$ ).

The method that is important in this study for the determination of kinetic values from inversion-transfer data involves fitting of data for a set of inversion-transfer times to Equation 9.10b.<sup>29</sup> From this fit, estimates of  $T_{1c}$ ,  $T_{1f}$ ,  $\tau_f$ ,  $M_0^c$  and  $M_0^f$  can be calculated. During the fitting process  $\tau_{1c}$  and  $\tau_{1f}$  are eliminated from Equation 9.10b using Equations 9.11a and 9.11b, and  $\tau_c$  is eliminated using the equation  $K_e = \tau_f/\tau_c$ , where  $K_e = M_e^f/M_e^c$ . Intensities that are measured when  $t > 5T_1$  are used for  $M_e^c$  and  $M_e^f$ . From here the thermodynamic values can be calculated as was shown in Equation 9.5.

---

<sup>29</sup> Alger, J. R.; Prestegard, J. H. (1977) *J. Magn. Reson.*, **27**, 137.

### 9.4.2 Experimental procedure

The next reaction system that was investigated was the phosphine exchange of  $[\text{Rh}(\text{Cl})(\text{CO})(\text{PPh}_2\text{Cy})_2]$  with  $\text{PPh}_2\text{Cy}$ . As in the case of the previous system, it was necessary to first get an idea of the composition of a sample containing both species at room temperature. A sample containing  $[\text{Rh}(\text{Cl})(\text{CO})(\text{PPh}_2\text{Cy})_2]$  (5mg,  $7.1 \times 10^{-3}$  mmol) and  $\text{PPh}_2\text{Cy}$  (3.8 mg,  $1.4 \times 10^{-2}$  mmol) was prepared within a NMR young tube. Deuterated benzene (0.5 ml) was added to the sample under an inert atmosphere, after which the sample was degassed by means of the pump-freeze-flow method as was described before. All the samples in this study were prepared in the same manner. A  $^{31}\text{P}$  NMR spectrum was then taken on the 500 MHz Varian spectrometer at 25 °C. The result was found to be different from that of the previous system, where two well-resolved narrow peaks were observed at 37.8 ppm (d,  $^1J_{\text{Rh-P}} = 123.2$  Hz) and -2.8 ppm, which corresponded to  $[\text{Rh}(\text{Cl})(\text{CO})(\text{PPh}_2\text{Cy})_2]$  and  $\text{PPh}_2\text{Cy}$ , respectively. Several scans were also undertaken over a period of time in order to check the stability of the composition. The result was that the system was in dynamic equilibrium as the composition did not change at all.

The preliminary results obtained above indicated that inversion magnetisation transfer was a suitable tool to study the exchange reaction. The method basically involved a pulse program on the NMR spectrometer where a selective  $180^\circ$  pulse and a non-selective  $90^\circ$  pulse were applied on the sample using suitable variable delay times between them as well as calculated coarse power and pulse width (Figure 9.7).

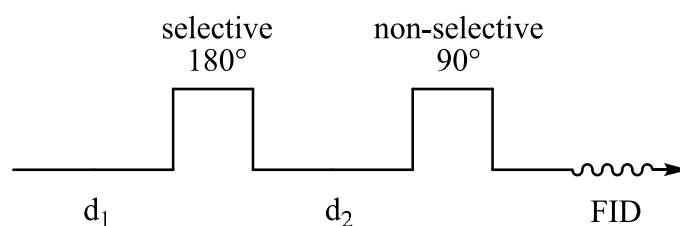


**Figure 9.7 Pulse sequence for an inversion magnetization transfer experiment.**

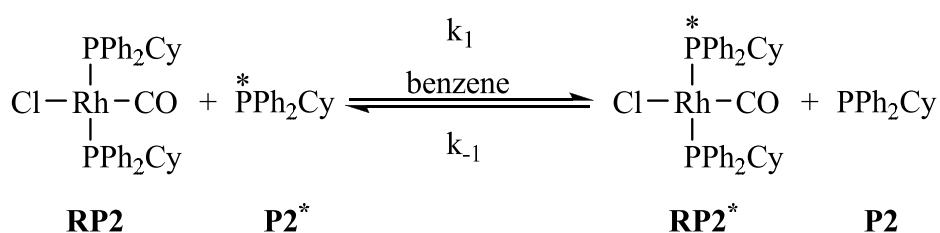
The result was the inversion of the peak representing the free phosphine on the  $^{31}\text{P}$  NMR spectrum, which underwent relaxation over a certain period and by following this relaxation, substitution was observed. In order to perform the study on this system a series of samples was prepared where the concentration of  $[\text{Rh}(\text{Cl})(\text{CO})(\text{PPh}_2\text{Cy})_2]$  was kept constant at about

0.013 M, and the concentration of PPh<sub>2</sub>Cy was varied with values of 0.013 (1 eq), 0.040 (3eq), 0.065 (5 eq) and 0.096 M (7 eq). Magnetisation transfer was performed on each sample at different temperatures including 15, 25, 35 and 45 °C by taking <sup>31</sup>P NMR spectra and applying the pulse program. The data obtained from these experiments were investigated using the CIFIT2 software designed by Bain *et al.*,<sup>30</sup> which then calculated the observed rate constants for each sample at different temperatures. The software utilizes equation 9.12 to fit the experimental data as a two-site exchange,

$$\frac{\partial}{\partial t} \begin{pmatrix} M_1(\infty) - M_1(t) \\ M_2(\infty) - M_2(t) \end{pmatrix} = -k \begin{pmatrix} K & -1 \\ -K & 1 \end{pmatrix} \begin{pmatrix} M_1(\infty) - M_1(t) \\ M_2(\infty) - M_2(t) \end{pmatrix} \quad (9.12)$$

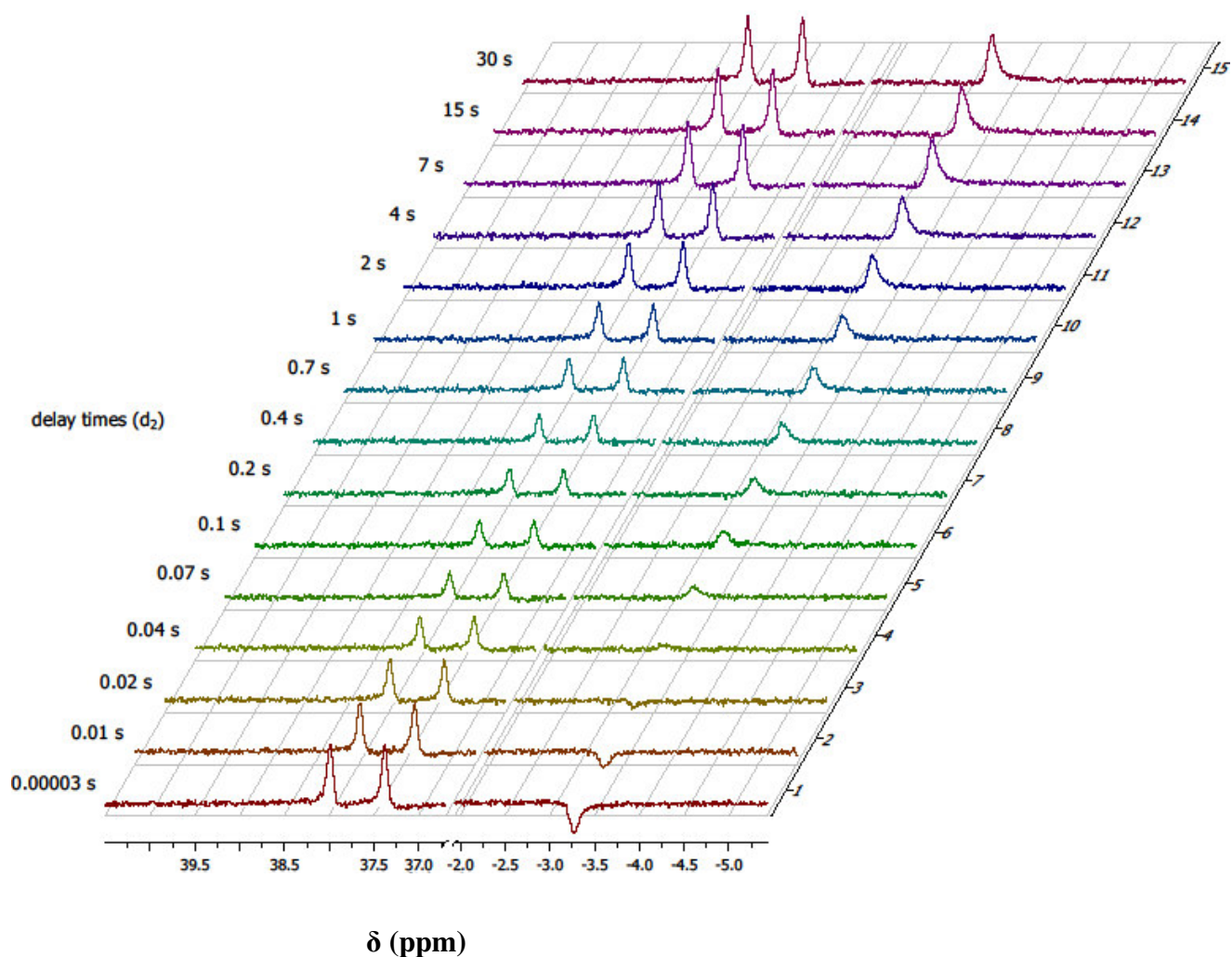
### 9.4.3 Kinetic and Thermodynamic analysis

Figure 9.8 shows a representation of the general profile obtained by an inversion magnetisation transfer experiment for one of the samples at room temperature. After applying the selective 180 ° pulse the inverted peak representing the free phosphine (**P2**) started to relax, which was observed at various delay times (d<sub>2</sub>) as indicated in the figure. This peak eventually relaxed back to its original position whereas the other peak which represented [Rh(Cl)(CO)(PPh<sub>2</sub>Cy)<sub>2</sub>] (**RP2**) also reduced over time and returned back to its original form. This suggested that phosphine exchange took place between the two species where PPh<sub>2</sub>Cy (**P2**) substituted one of the phosphine ligands on [Rh(Cl)(CO)(PPh<sub>2</sub>Cy)<sub>2</sub>] (**RP2**) to reproduce the same complex (Scheme 9.3). The rate expressions for the exchange reaction are similar to those described in Section 9.3.3.



Scheme 9.3

<sup>30</sup> Bain, A. D.; Cramer, J. A. (1996) *J. Magn. Reson.*, **118 A**, 21.



**Figure 9.8** A representation of the inversion magnetisation transfer profile for a sample containing  $\text{PPh}_2\text{Cy}$  (1 eq) and  $[\text{Rh}(\text{Cl})(\text{CO})(\text{PPh}_2\text{Cy})_2]$  at 15 °C.  $[\text{PPh}_2\text{Cy}] = 0.013 \text{ M}$ ,  $[\text{Rh}] = 0.013 \text{ M}$ . The different delay times were as indicated on the spectra.

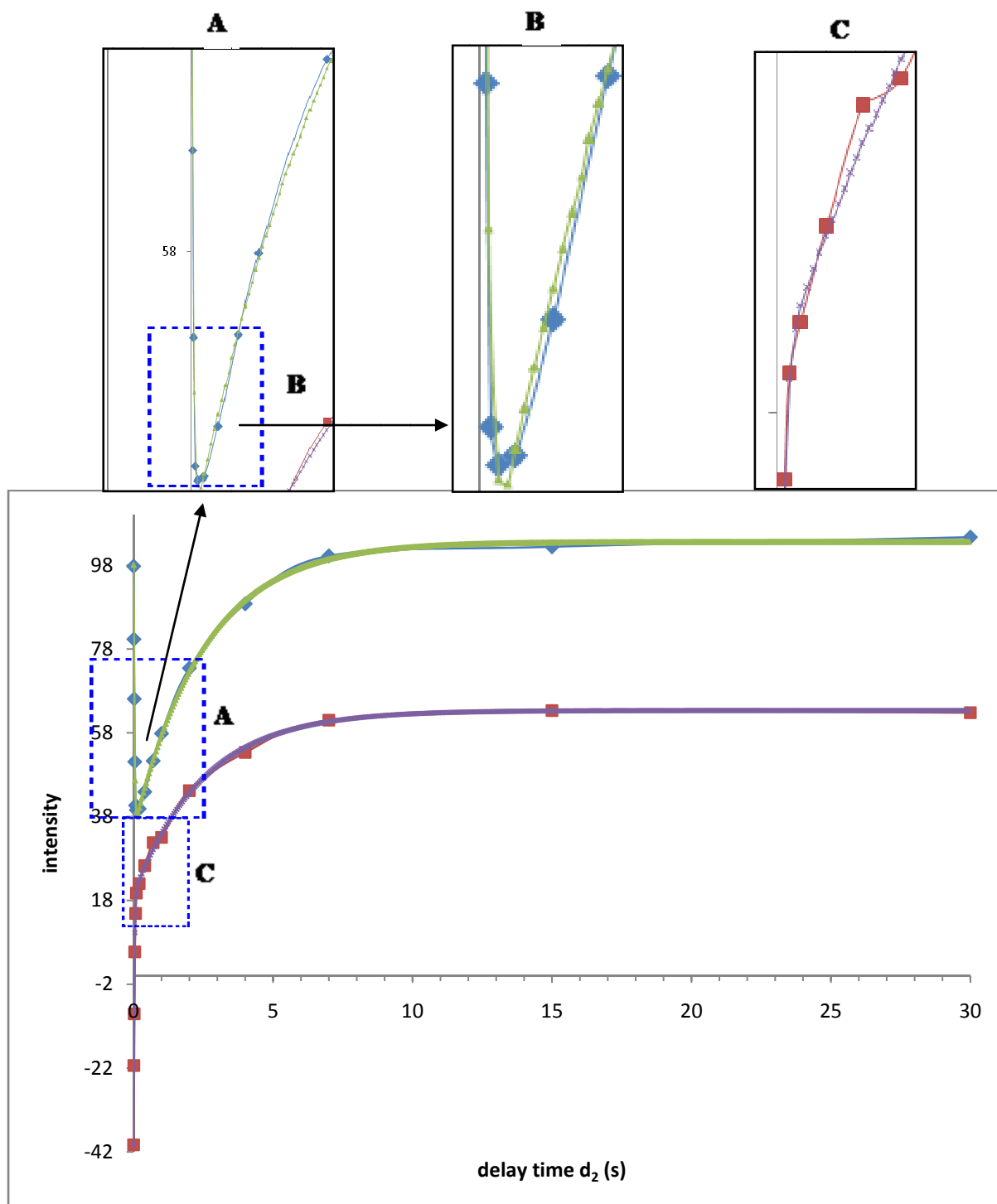


**Figure 9.9** A general plot obtained during an inversion magnetization transfer experiment for the exchange reaction  $\text{PPh}_2\text{Cy}$  (1 eq) and  $[\text{Rh}(\text{Cl})(\text{CO})(\text{PPh}_2\text{Cy})_2]$  at 15 °C.  $[\text{PPh}_2\text{Cy}] = 0.013 \text{ M}$ ,  $[\text{Rh}] = 0.013 \text{ M}$ . The experimental data (Rh complex (♦), free phosphine (■)) is provided along with the data fitted to equation 9.12 (Rh complex (▲), free phosphine (×)). Fragments of the plot are magnified in order to show the close relation between the experimental and fitted data.

Figure 9.9 (a) illustrates typical plots that were obtained from the magnetization transfer data. Using the CIFIT2 program, these data were fitted by varying values of the spin-lattice relaxation times and the magnetizations of the different species, as well as the rate constant of the exchange reaction. When the correct values were obtained a typical fit as illustrated in Figure 9.9 (b) was obtained, where the plot obtained from the fitted data corresponded to that of the experimental data. Using the collection of fitted data for each experiment at different phosphine concentrations and temperatures the different rate constants were calculated.

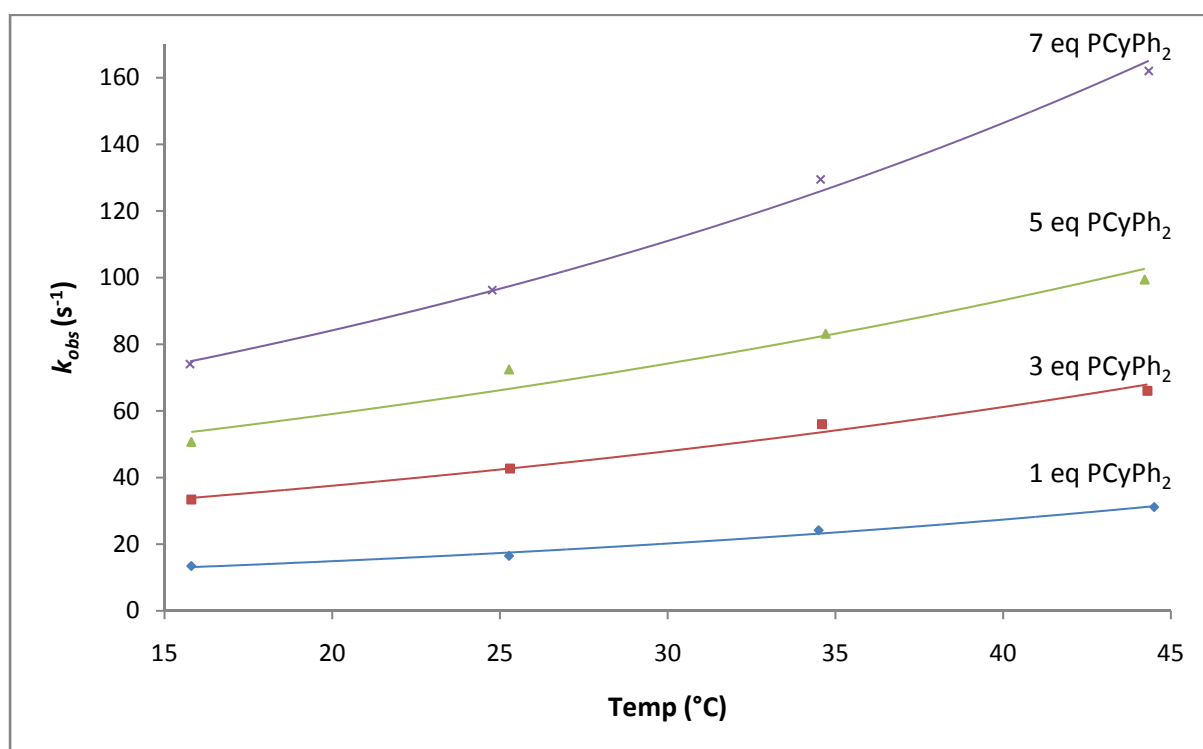


**Figure 9.10** Plots of the observed rate constants against temperature obtained from the analysis of the phosphine exchange reaction between  $[\text{Rh}(\text{Cl})(\text{CO})(\text{PPh}_2\text{Cy})_2]$  and  $\text{PPh}_2\text{Cy}$  across a range of phosphine concentrations.  $[\text{Rh}(\text{Cl})(\text{CO})(\text{PPh}_2\text{Cy})_2] = 0.013 \text{ M}$ .

The plots of rate constants versus temperature at different phosphine concentrations are provided in Figure 9.10. It was observed that the experimental data correlated well with an exponential fit as expected by the definition of the Arrhenius equation. The plots of rate constants versus phosphine concentration at different temperatures are provided in Figure 9.11. Generally, the data correlated well with a linear fit and the error in the intercepts was calculated to be less than 10%. Using the same argument as with the previous study, it was accepted that the possibility of a solvent pathway was negligible. Thus the experimental rate constants could be directly obtained from the slope of these plots as defined by Equation

9.12. The observed rate constants obtained at various phosphine concentrations and temperatures together with the experimental rate constants are provided in Table 9.4.

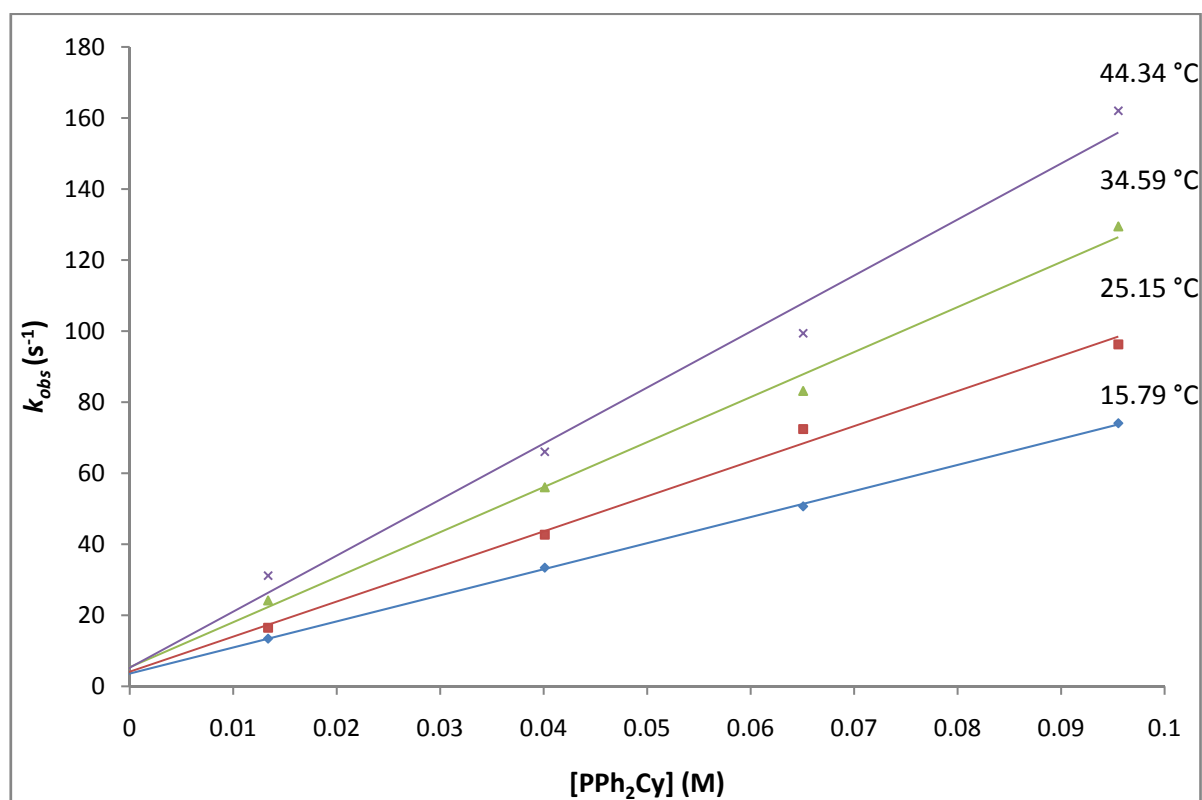


**Figure 9.11** Plots of the observed rate constants against phosphine concentration obtained from the analysis of the phosphine exchange reaction between  $[\text{Rh}(\text{Cl})(\text{CO})(\text{PPh}_2\text{Cy})_2]$  and  $\text{PPh}_2\text{Cy}$  across a temperature range.  $[\text{Rh}] = 0.013 \text{ M}$ .

**Table 9.4** Observed rate constants obtained at different temperatures (°C) of the phosphine exchange reaction between  $[\text{Rh}(\text{Cl})(\text{CO})(\text{PPh}_2\text{Cy})_2]$  and  $\text{PPh}_2\text{Cy}$ .

[PPh <sub>3</sub> ] (M)	Average Temp (°C)	$k_{obs} \text{ (s}^{-1}\text{)}^*$			
		15.79	25.15	34.59	44.34
0.013367		13.43	16.5	24.17	31.15
0.040102		33.4	42.7	56.03	66.02
0.065071		50.66	72.42	83.15	99.4
0.09553		74.06	96.25	129.46	162.02
	$k_{exp} \text{ (M}^{-1}\text{.s}^{-1}\text{)}$	734.16	987.68	1267.4	1576.7

\* An error of less than 5% was assumed for each value

In comparison it was observed that the rate constant values obtained for the exchange reaction between  $[\text{Rh}(\text{Cl})(\text{CO})(\text{PPh}_2\text{Cy})_2]$  and  $\text{PPh}_2\text{Cy}$  shown in Table 9.4 differed in magnitudes of 100 to those obtained for the exchange reaction between  $[\text{Rh}(\text{Cl})(\text{CO})(\text{PPh}_3)_2]$



and PPh<sub>3</sub> (Table 9.2). Therefore it was clear that a slight difference in the nature of the phosphine ligand could cause tremendous effects on the rates of these exchange reactions. From this it would seem that a more electron-rich phosphine ligand would result in slower exchange to take place, e.g. the rate of the exchange reaction between [Rh(Cl)(CO)(PR<sub>1</sub>R<sub>2</sub>R<sub>3</sub>)<sub>2</sub>] and PR<sub>1</sub>R<sub>2</sub>R<sub>3</sub> decreases as PR<sub>1</sub>R<sub>2</sub>R<sub>3</sub> increases in electron density. This can be explained in the fact that a more electron-rich phosphine undergoes better  $\sigma$ -donation onto the metal centre and in turn enhances the strength of the bond between the phosphorus atom and the metal centre. With the bonding of another one of these electron-rich phosphines *trans* to the first phosphine,  $\sigma$ -donation from this ligand enhances the  $\pi$ -back donation to the first phosphine and *vice versa*. Therefore since these Rh-P bonds are strong exchanging one of these phosphine ligands on the metal centre with an incoming phosphine becomes more difficult. Also there are differences in the steric properties of these ligands, since a cyclohexyl group is bulkier than a phenyl ring. Having a phosphine with bulkier groups coordinated onto the metal centre can cause more hindrance to the incoming phosphine, thus also decreasing the rate of the exchange reaction.

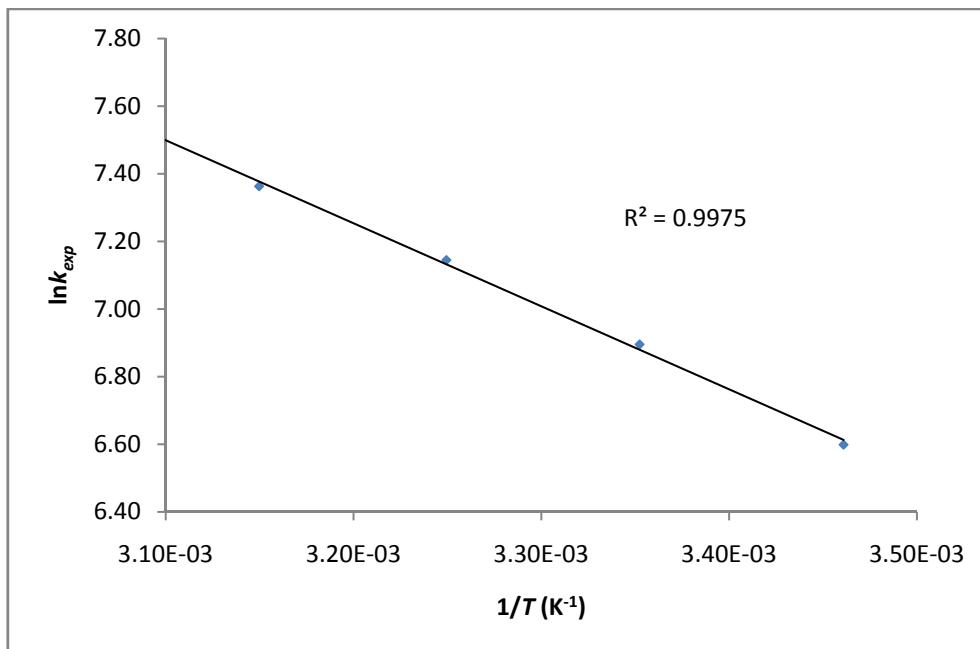
The calculated experimental rate constants were utilised to construct the Arrhenius and Eyring plots for this exchange reaction as given in Figure 9.12. Good linear fits for these plots were obtained as can be observed. The activation parameters for the exchange reaction were calculated, which is summarized in Table 9.5.

**Table 9.5 A summary of the activation parameters for the exchange reaction between [Rh(Cl)(CO)(PPh<sub>2</sub>Cy)<sub>2</sub>] and PPh<sub>2</sub>Cy.**

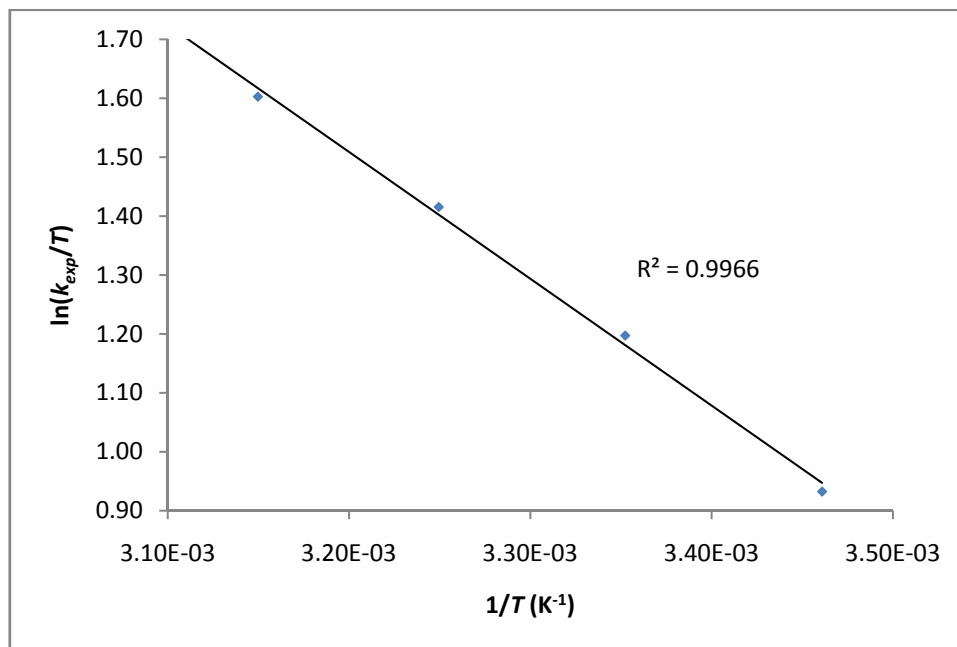
$E_a$ (kJ/mol)	$\Delta H^\ddagger$ (kJ/mol)	$\Delta S^\ddagger$ (J.K <sup>-1</sup> .mol <sup>-1</sup> )
20.4	17.90	-127.74

As with the previous system (Table 9.3) a large negative value for the entropy was also obtained for the exchange reaction between [Rh(Cl)(CO)(PPh<sub>2</sub>Cy)<sub>2</sub>] and PPh<sub>2</sub>Cy (Table 9.5), which suggested that this reaction also follows an associative mechanism. This was also supported by the dependence of the rate of the reaction on the phosphine concentration as was observed in Figure 9.11. As was discussed earlier, the rate of an exchange reaction between [Rh(Cl)(CO)(PR<sub>1</sub>R<sub>2</sub>R<sub>3</sub>)<sub>2</sub>] and PR<sub>1</sub>R<sub>2</sub>R<sub>3</sub> was found to be dependent on the nature of the phosphine ligand, which in turn also supported the associative mechanism for both systems under study.<sup>20</sup> As in the previous study the contribution of the  $T\Delta S^\ddagger$  to the Gibbs free

energy of activation is quite large, whereas the enthalpy of activation is correspondingly small. The activation process is therefore also primarily controlled by entropy, which leads to the formation of a stable transition state as the five co-ordinated complex is formed.



(a)



(b)

**Figure 9.12** Arrhenius (a) and Eyring (b) plots for the exchange reaction between  $[Rh(Cl)(CO)(PPh_2Cy)_2]$  and  $PPh_2Cy$  where  $[Rh] = 0.0142$  M. (a) was used to calculate the activation energy ( $E_a = 20.4$  kJ/mol), while (b) was used to calculate the enthalpy value ( $\Delta H^\ddagger = 17.90$  kJ/mol) and entropy value ( $\Delta S^\ddagger = -127.74$  J.K<sup>-1</sup>.mol<sup>-1</sup>).

Attempts were also made to try and study the exchange reaction between  $[\text{Rh}(\text{Cl})(\text{CO})(\text{PR}_1\text{R}_2\text{R}_3)_2]$  and  $\text{PR}_1\text{R}_2\text{R}_3$  utilising the phosphine ligands  $\text{PPhCy}_2$  and  $\text{PCy}_3$  as the  $\text{PR}_1\text{R}_2\text{R}_3$  derivatives. However, these reactions were found to be too slow to study it by inversion magnetization transfer experiments. Even at 70 °C and high phosphine concentrations the exchange could not be observed for either of these systems. Either different experimental conditions or techniques would be needed to study these systems, but due to time constraints this study could not be continued.

## 9.5. Conclusion

In this study the thermodynamic and kinetic parameters of phosphine exchange of Vaska-type rhodium complexes were investigated utilising NMR techniques. In NMR spectroscopy a relationship is found between the spin-lattice relaxation times, transverse relaxation times and magnetization values and the rate of exchange reactions. Depending on how fast the exchange will take place will determine the outcome of the NMR spectra obtained and in turn the type of NMR technique that can be utilised to study this rate. For relatively fast reactions the linewidth of NMR spectra tend to broaden to such a large extent that the mean lifetimes of the species in the samples can easily be calculated from these linewidths. The mean lifetimes obtained from the data is then inversely related to the rate of the exchange process. For slow reactions narrow well-defined chemical shifts are observed and in these cases the rate of an exchange reaction can easily be followed by measuring the magnetization obtained at several spin-relaxation times.

From this study it is evident that  $[\text{Rh}(\text{Cl})(\text{CO})(\text{PR}_1\text{R}_2\text{R}_3)_2]$  complexes are in equilibrium with its corresponding free phosphine. The rate observed for the exchange happening in this equilibrium was found to be dependent on the type of phosphine present in the system. It was clear from the results that a phosphine having electron-withdrawing groups such as triphenylphosphine undergoes fast exchange between the  $[\text{Rh}(\text{Cl})(\text{CO})(\text{PR}_1\text{R}_2\text{R}_3)_2]$  complex and the free phosphine. On NMR spectra fairly broad peaks for the separate species were observed. However, by replacing one of the electron-withdrawing substituents on the phosphine with a large electron-donating group such as cyclohexyl, the rate of exchange observed decreases by a factor of more than a hundred. It could be concluded that a phosphine with a strong basicity and larger steric hindrance lead to stronger Rh-P bond

formation and subsequently decrease the ability of an incoming phosphine to exchange with a coordinated phosphine.

The activation parameters of the phosphine exchange of these Vaska-type rhodium complexes were found to be similar though. It was found that these systems were largely controlled by entropy and due to the large negative entropy values obtained for these systems an associative mechanism for the exchange process was evident. This was also suggested by the direct dependence of the exchange reaction rate on phosphine concentrations.

# **CHAPTER 10**

## **EVALUATION OF THE Ph.D. STUDY**

### **10.1 Introduction**

The successes and failures of this Ph.D. study are discussed in the following sections, in terms of the aims described in Chapter 1, which is followed by some aspects which might be investigated in future.

### **10.2 *S,O*-functionalized thiourea bidentate ligands**

A principle aim in this study involved the investigation of the carbonylation/ hydrogenation of methanol. In order to do this a range of rhodium complexes were required that contained suitable ligands that would allow the formation of Rh(III)-acyl species from the iodomethane oxidative addition to these complexes. One set of ligands that was suitable for this purpose involved *S,O*-functionalized thiourea ligands, and several of these with different substituents on the terminal nitrogen of the thiourea moiety were easily synthesized and characterized (Chapter 3). In this way a range of thiourea ligands were obtained, which had systematically changing electro-steric properties, for the synthesis of various rhodium complexes. NMR and IR spectroscopy confirmed the identity of these compounds and also revealed that the thiourea ligands were in the *keto* conformation in solution.

A few of the thiourea ligands were also characterized by single crystal X-ray diffraction (Chapter 4). An important feature that was observed included a hydrogen bond found between the oxygen atom of the carbonyl group and one of the nitrogen atoms (N2) in the thiourea moiety. This interaction stabilizes the structural configurations of the compounds where the oxygen atom of the carbonyl group is *trans* with respect to the sulphur atom of the thiourea moiety. Some correlation existed between the electro-steric properties of the different substituents on the terminal nitrogen and the distance of the hydrogen bond interaction. The hydrogen atoms on the nitrogen atoms of the thiourea moiety also play a vital role in the crystal packing of compounds, which lead to the formation of either dimers or

polymeric chains of molecules in the solid state. Finally, it was also reported that the thiourea compounds exist mainly in the *keto* conformation in the solid state, which compares with the observations made in solution by NMR spectroscopy.

Although the thiourea ligands were expected to coordinate in an *S,O*-mode onto the rhodium centre it was clear from literature that these ligands have potentially four donor sites. Some examples were reported in Chapter 6 where some of the ligands coordinated in other modes as well including *S* and *N,S*. These results are summarized in Section 10.4.

### 10.3 Rhodium(I) diphosphine complexes

A set of rhodium complexes that were found to be suitable for the investigation of the homologation of methanol included rhodium diphosphine species. More specifically, the rhodium complexes of choice included the  $[\text{Rh}(\text{diphosphine})(\text{CO})_2]^+$  species. Attempts were made to synthesize  $[\text{Rh}(\text{diphosphine})(\text{CO})_2]^+$  complexes by using several precursors including  $[\text{Rh}(\text{COD})_2]^+$ ,  $[\text{Rh}(\text{acetone})_2(\text{coe})_2]^+$  and  $[\text{Rh}(\text{CO})_4]^+$  (Chapter 5). The corresponding procedures were not considered successful as none of the  $[\text{Rh}(\text{diphosphine})(\text{CO})_2]^+$  complexes were isolated. NMR and IR spectroscopy revealed that a mixture of products were obtained, which in most cases did not include any rhodium carbonyl complexes. However, the synthetic route that included the precursor  $[\text{Rh}(\text{CO})_4]^+$  led to the formation of cationic A-frame complexes instead. One of these complexes that was successfully characterized by single crystal X-ray diffraction was  $[\text{Rh}_2(\mu\text{-Cl})(\text{dppm})_2(\text{CO})_2]\text{BF}_4$ . This complex was a polymorph from an existing structure reported in literature, where the complex crystallised in the monoclinic space group  $P2_1/n$  ( $Z = 4$ ) compared to the reported triclinic space group  $P\bar{1}$  ( $Z = 2$ ). Since the  $[\text{Rh}(\text{diphosphine})(\text{CO})_2]^+$  complexes could not be obtained from several synthetic routes, it was decided to focus on the synthesis of  $[\text{Rh}(\text{S},\text{O}\text{-thioureato})(\text{CO})_2]$  and  $\text{Rh}(\text{S},\text{O}\text{-thioureato})(\text{CO})(\text{PR}_1\text{R}_2\text{R}_3)$  complexes instead.

## 10.4 Rhodium complexes of *S,O*-functionalized thiourea ligands

It was clear from literature that rhodium complexes, which contained bidentate ligands having at least one sulphur  $\sigma$ -donor atom proved to be successful in allowing the formation of Rh(III)-acyl species following the iodomethane oxidative addition to the corresponding complexes. It was expected that rhodium complexes with *S,O*-bidentate ligands would lead to similar results and therefore the choice of complexes for this study involved  $[\text{Rh}(\text{S},\text{O}\text{-thioureato})(\text{CO})_2]$  and  $[\text{Rh}(\text{S},\text{O}\text{-thioureato})(\text{CO})(\text{PR}_1\text{R}_2\text{R}_3)]$ .

Several attempts were made to synthesize  $[\text{Rh}(\text{S},\text{O}\text{-thioureato})(\text{CO})_2]$  complexes using two types of precursors, which included  $[\text{Rh}(\mu\text{-Cl})(\text{CO})_2]_2$  and  $[\text{Rh}(\text{COD})(\text{Cl})]_2$  (Chapter 6). The synthetic route involving  $[\text{Rh}(\mu\text{-Cl})(\text{CO})_2]_2$  primarily resulted in the formation of different dicarbonyl rhodium complexes as were confirmed by IR spectroscopy. NMR spectroscopy also indicated the presence of a mixture of products that formed from the corresponding synthetic procedure. Moreover, the products were only stable in solution, since the complexes transformed into dark oils upon drying. Several modifications were performed on the synthetic route in order to allow the formation of more stable complexes, however, these modification did not prove to be successful as similar results were obtained. Moreover, the resulting complexes were difficult to crystallize and therefore the identity of the products could not be ascertained.

The synthetic route involving  $[\text{Rh}(\text{COD})(\text{Cl})]_2$ , on the other hand, resulted in the formation of  $[\text{Rh}(\text{COD})(\text{Cl})(\text{S}\text{-thioureato})]$  complexes instead of the anticipated  $[\text{Rh}(\text{COD})(\text{S},\text{O}\text{-thioureato})]$  complexes. Structural data was obtained for two different  $[\text{Rh}(\text{COD})(\text{Cl})(\text{S}\text{-thioureato})]$  complexes, where *S*-thioureato = *N*-benzoyl-*N'*-phenylthioureato or *N*-benzoyl-*N'*-(2,4,6-trimethyl)phenylthioureato. It was reported that the preferred orientation of the free thiourea ligand, where the oxygen atom is held at a position *trans* to the sulphur atom by a hydrogen bond interaction, is translated to the orientation found in the structures of  $[\text{Rh}(\text{COD})(\text{Cl})(\text{S}\text{-thioureato})]$ . Moreover, the structural configuration was also stabilized by the presence of a hydrogen bond interaction between the chlorido ligand on the rhodium centre and the internal nitrogen (N1) of the thiourea moiety. Attempts were made to extract the chlorido ligand from the rhodium centre by using silver nitrate or sodium acetate, but were unsuccessful.

After obtaining these results from the synthesis of  $[\text{Rh}(\text{S},\text{O}\text{-thioureato})(\text{CO})_2]$ , it was decided to focus on  $[\text{Rh}(\text{S},\text{O}\text{-thioureato})(\text{CO})(\text{PR}_1\text{R}_2\text{R}_3)]$  complexes instead. It was expected that the addition of phosphine ligands would yield more stable rhodium thiourea complexes and enhance the crystallization ability of these complexes. Several attempts were made to synthesize  $[\text{Rh}(\text{S},\text{O}\text{-thioureato})(\text{CO})(\text{PR}_1\text{R}_2\text{R}_3)]$ , which resulted in the formation of different species depending on the reaction conditions (Chapter 6 and 7). One synthetic route that involved the precursor  $[\text{Rh}(\mu\text{-Cl})(\text{CO})_2]_2$  and triphenylphosphine led to the formation of monocarbonyl rhodium species as was confirmed by IR spectroscopy, having  $\nu_{\text{CO}}$  values of  $1970\text{-}1075\text{ cm}^{-1}$ . However, NMR spectroscopy revealed that the major product found in the corresponding samples was triphenylphosphine oxide. Thus, it was concluded that only small amounts of some monocarbonyl rhodium phosphine species were obtained, whereas most of the triphenylphosphine was assumed to be catalytically oxidized by the rhodium during the synthetic procedure that was followed.

By following the same synthetic route under more basic conditions (using sodium acetate) complexes of the type  $[\text{Rh}(\text{N},\text{S}\text{-thioureato})(\text{CO})(\text{PPh}_3)_2]$  were isolated. These complexes exhibited  $\nu_{\text{CO}}$  values of  $1918\text{-}1930\text{ cm}^{-1}$ , which suggested that the close proximity of the N and S atoms of the thiourea ligand led to stronger  $\sigma$ -donation to the rhodium centre. Structural data was obtained for one of the isolated complexes, namely,  $[\text{Rh}(\text{N},\text{S}\text{-}(N\text{-}4\text{h}2\text{mPT}))(\text{CO})(\text{PPh}_3)_2]$  ( $N\text{-}4\text{h}2\text{mPT}$  = mono-deprotonated  $N$ -benzoyl- $N'$ -(4-hydroxy-2-methylphenyl)thiourea). The thiourea ligand coordinated in an  $N,\text{S}$ -fashion with a small bite angle to the rhodium centre, which allowed enough space for two  $\text{PPh}_3$  molecules to coordinate *trans* to each other. This led to a distorted trigonal bipyramidal conformation, where the carbonyl ligand was *trans* to the  $N,\text{S}$ -moiety, analogous to typical square planar Vaska-type complexes.

Another modification to the synthetic route mentioned above, which involved the use of DMSO and acetone as the solvent, led to the formation of a Rh(III) complex with the ligand  $N$ -benzoyl- $N'$ -phenylthioureato, namely,  $[\text{Rh}(\text{N},\text{S}\text{-}(N\text{-PT}))(\text{S},\text{O}\text{-}(N\text{-PT}))(\text{PPh}_3)_2]$ . This is the first example of a rhodium complex involving the coordination of two of the same thiourea type bidentate ligand in a different mode. Structural data on this complex revealed that one of the ligands coordinated in a  $N,\text{S}$ -mode to the metal centre in its *enol* conformation instead of the expected *keto* conformation. The other ligand coordinated in a  $\text{S},\text{O}$ -mode in its *keto* conformation. Two  $\text{PPh}_3$  ligands coordinated *trans* to each other axially, which completed the



distorted octahedral conformation of the metal complex. The DMSO and acetone solvents played a vital role in the packing of the structure as several hydrogen bond and other Van der Waals interactions existed between the solvent molecules and the complex molecules.

Despite the difficulties that were encountered a range of  $[\text{Rh}(\text{S},\text{O}\text{-thioureato})(\text{CO})(\text{PR}_1\text{R}_2\text{R}_3)]$  complexes were successfully synthesized and characterized using the ligand *N*-benzoyl-*N',N'*-diphenylthiourea (*N*-diPT) and a range of phosphines having systematically changing electro-steric properties ( $\text{PPh}_3$ ,  $\text{PPh}_2\text{Cy}$ ,  $\text{PPhCy}_2$ ,  $\text{PCy}_3$ ) (Chapter 7). The identity of these complexes was confirmed by NMR and IR spectroscopy as well as elemental analysis.  $^{13}\text{C}$  NMR spectroscopy revealed a shift in the C-S and C-O peaks of the thiourea ligand from chemical shifts of 184.5 and 163.3 ppm to 178.9 and 170.7 ppm, respectively. This confirmed the *S,O*-coordination of the thiourea ligand to the rhodium centre, while  $^{31}\text{P}$  NMR confirmed that only one isomer of the complexes formed in solution, since only one doublet was observed in the spectrum. The  $\nu_{\text{CO}}$  values and first-order coupling constants  $J_{\text{Rh-P}}$  for the different complexes correlated well with the expected electro-steric properties of the corresponding phosphine ligands. Moreover, it was reported that the  $\nu_{\text{CO}}$  values in the solid state of these complexes differed from those obtained in solution. This phenomenon has been shown in literature to be the result of packing effects in the solid state.

Structural data was obtained for three of the  $[\text{Rh}(\text{N}\text{-diPT})(\text{CO})(\text{PR}_1\text{R}_2\text{R}_3)]$  complexes *via* single crystal X-ray diffraction. All of the complexes crystallized in the monoclinic space group  $P2_1/c$ , where the structures of  $[\text{Rh}(\text{N}\text{-diPT})(\text{CO})(\text{PPh}_2\text{Cy})]$  and  $[\text{Rh}(\text{N}\text{-diPT})(\text{CO})(\text{PCy}_3)]$  were isomorphous, whereas the  $[\text{Rh}(\text{N}\text{-diPT})(\text{CO})(\text{PPh}_3)]$  was isostructural to the other complexes. Moreover, it was observed that the phosphine ligand coordinated *trans* to the sulphur atom on the rhodium centre due to the higher *trans* influence of the sulphur atom compared to the oxygen atom. Small differences were observed in the geometrical parameters of these complexes even though the  $\nu_{\text{CO}}$  values and first-order coupling constants  $J_{\text{Rh-P}}$  had large differences. The effective cone angles of the different phosphine ligands were calculated using the Rh-P bond lengths, which revealed that the steric congestion increased in the subsequent replacement of the phenyl rings on  $\text{PPh}_3$  with cyclohexyl rings.

## 10.5 Iodomethane oxidative addition to rhodium(I) thioureato complexes

The reactivity of the  $[\text{Rh}(\text{N-diPT})(\text{CO})(\text{PR}_1\text{R}_2\text{R}_3)]$  complexes towards the iodomethane oxidative addition was investigated in order to establish whether the corresponding Rh(III)-acyl species,  $[\text{Rh}(\text{N-diPT})(\text{COMe})(\text{I})(\text{PR}_1\text{R}_2\text{R}_3)]$ , would form and to determine the kinetic and activation parameters thereof. All of the  $[\text{Rh}(\text{N-diPT})(\text{CO})(\text{PR}_1\text{R}_2\text{R}_3)]$  complexes, where  $\text{PR}_1\text{R}_2\text{R}_3 = \text{PPh}_3, \text{PPh}_2\text{Cy}, \text{PPhCy}_2$  and  $\text{PCy}_3$ , proved to be successful in this regard as a virtually 'direct' conversion of the Rh(I) complexes to the corresponding Rh(III)-acyl complexes was observed *via* small amounts of the Rh(III)-alkyl intermediate. The rate of the individual reactions decreased in the order of  $[\text{Rh}(\text{N-diPT})(\text{CO})(\text{PPh}_2\text{Cy})] > [\text{Rh}(\text{N-diPT})(\text{CO})(\text{PPh}_3)] > [\text{Rh}(\text{N-diPT})(\text{CO})(\text{PCy}_3)] > [\text{Rh}(\text{N-diPT})(\text{CO})(\text{PPhCy}_2)]$ . No direct correlation existed between this order of reactivity and either the steric or electronic properties of the phosphine ligands. It was therefore concluded that a combined effect of the separate properties had to be taken in account. The activation parameters for the individual oxidative addition reactions are similar, where the contributions of  $\Delta H^\ddagger$  and  $\Delta S^\ddagger$  to  $\Delta G^\ddagger$  at 25 °C are approximately the same. The reactions proceeded with large negative  $\Delta S^\ddagger$ , which is indicative of an associative activation.

## 10.6 Phosphine exchange of Vaska-type rhodium(I) complexes

It was clear that the electro-steric properties of phosphine ligands play a significant role in the reactivity of rhodium complexes towards substitution reactions such as the iodomethane oxidative addition. It was therefore decided to further investigate the electro-steric effects of different phosphine ligands by analyzing the kinetic and activation parameters of the phosphine exchange reactions of the corresponding Vaska-type rhodium(I) complexes. The kinetics were monitored by  $^{31}\text{P}$  NMR techniques that were suitable for studying reactions in equilibrium, namely, magnetization transfer and line broadening techniques.

Two reaction systems were analyzed for the exchange reaction between  $\text{PPh}_3$  and  $[\text{Rh}(\text{Cl})(\text{CO})(\text{PPh}_3)_2]$  as well as the exchange reaction between  $\text{PPh}_2\text{Cy}$  and  $[\text{Rh}(\text{Cl})(\text{CO})(\text{PPh}_2\text{Cy})_2]$ , respectively. The former reaction proved to undergo fast exchange, which resulted in the formation of broad peaks in the  $^{31}\text{P}$  NMR spectrum at room temperature. However, by replacing one of the phenyl group on the  $\text{PPh}_3$  with a cyclohexyl

group resulted in a large decrease in the exchange reaction rate. The exchange reaction between  $\text{PPh}_2\text{Cy}$  and  $[\text{Rh}(\text{Cl})(\text{CO})(\text{PPh}_2\text{Cy})_2]$  therefore provided well-resolved peaks in the  $^{31}\text{P}$  NMR spectrum at room temperature. Further substitution of the phenyl groups on the phosphine ligand with cyclohexyl groups ( $\text{PPhCy}_2$  and  $\text{PCy}_3$ ) led to extremely slow exchange processes, which could not be studied by magnetization transfer experiments due to limitations. This order of reactivity suggested that a phosphine with a stronger basicity and larger steric congestion lead to stronger Rh-P bond formation, which subsequently leads to a significant decrease in the ability of an entering phosphine to exchange with a coordinated phosphine.

These reactions also proceeded with large negative  $\Delta S^\ddagger$ , which suggested that the exchange process followed an associative mechanism forming a stable transition state of a 5-coordinated rhodium complex. Moreover, the contribution of  $\Delta S^\ddagger$  to  $\Delta G^\ddagger$  was much larger than  $\Delta H^\ddagger$  and it was therefore concluded that the exchange reactions were primarily controlled by entropy.

## 10.7 Future work

Although Rh(III)-acyl species were successfully obtained from the iodomethane oxidative addition to the  $[\text{Rh}(N\text{-diPT})(\text{CO})(\text{PR}_1\text{R}_2\text{R}_3)]$  complexes as confirmed by the kinetics and spectroscopy, the further investigation on the reductive elimination/hydrogenation of the acyl group/acyl iodide could not be performed due to time constraints. Thus, it is necessary to investigate the activation parameters and mechanistic pathways of this process using the isolated  $[\text{Rh}(N\text{-diPT})(\text{COMe})(\text{I})(\text{PR}_1\text{R}_2\text{R}_3)]$  complexes in order to conclude the initial aim of this study in more detail.

Furthermore, with the success of obtaining a synthetic route to the formation of  $[\text{Rh}(N\text{-diPT})(\text{CO})(\text{PR}_1\text{R}_2\text{R}_3)]$  complexes, the range of complexes that can be synthesized from this route with several other commercially available phosphines as well as arsines and stibines is quite significant. This can expand the range of complexes with systematically changing electro-steric properties that can be utilize to perform further investigations on the effects of these properties on catalytic reactions such as the iodomethane oxidative addition, reductive elimination as well as phosphine exchange processes.

Moreover, since not much work has been done rhodium complexes with *S,O*-functionalized thiourea ligands and taking the diverse coordination modes of these ligands in account, further investigations are required to understand the mechanistic pathways of the coordination of thiourea ligands to rhodium centres. This could allow the design of suitable synthetic routes to different types of complexes that can be obtained from these thiourea ligands, which in turn expands the endless variety of rhodium complexes that can still be synthesized and investigated.

Finally, future experiments should be designed to further investigate and explore the applications of these thiourea type ligands and the different bonding modes encountered in this Ph.D. investigation.

## APPENDIX A

### CRYSTAL DATA OF THIOUREA MOLECULAR COMPOUNDS

#### A1. Crystal data of *N*-benzoyl-*N*'-(2,4,6-trimethylphenyl)thiourea (*N*-tmPTH)

Table A1.1. Atomic coordinates and equivalent isotropic displacement parameters ( $\text{\AA}^2$ ) for *N*-tmPTH.  $U_{(\text{eq})}$  is defined as one third of the trace of the orthogonalized  $U^{\text{ij}}$  tensor.

Atom	x/a	y/b	z/c	$U_{(\text{eq})}$
C(1)	0.9046(2)	-0.0235(3)	0.2542(2)	0.01853
C(1')	0.8141(2)	0.3210(3)	0.4196(2)	0.01868
C(2)	0.8820(2)	0.0363(3)	0.3233(2)	0.02142
C(2')	0.8203(3)	0.2627(3)	0.5131(2)	0.02266
C(3)	0.8186(3)	-0.0127(3)	0.4012(2)	0.02616
C(3')	0.7056(3)	0.2465(3)	0.5572(2)	0.0305
C(4)	0.7812(3)	-0.1230(3)	0.4105(2)	0.02495
C(4')	0.5862(3)	0.2912(3)	0.5082(2)	0.03326
C(5)	0.8046(3)	-0.1845(3)	0.3422(2)	0.02351
C(5')	0.5799(3)	0.3491(3)	0.4154(2)	0.02776
C(6)	0.8640(2)	-0.1326(3)	0.2636(2)	0.02166
C(6')	0.6942(2)	0.3618(3)	0.3705(2)	0.02202
C(7)	0.9712(2)	0.0247(3)	0.1685(2)	0.01873
C(7')	0.9350(2)	0.3363(3)	0.3684(2)	0.01889
C(8)	1.1260(2)	0.1512(3)	0.1033(2)	0.01762
C(8')	1.1276(2)	0.4064(3)	0.3748(2)	0.01803
C(9)	1.2210(2)	0.1522(3)	-0.0449(2)	0.01751
C(9')	1.3048(2)	0.3762(3)	0.2608(2)	0.01854
C(10)	1.1969(3)	0.2905(3)	-0.0990(2)	0.02049
C(10')	1.3060(3)	0.5053(3)	0.2061(2)	0.02225
C(11)	1.2899(3)	0.3085(3)	-0.1659(2)	0.02319
C(11')	1.4261(3)	0.5025(3)	0.1612(2)	0.02388
C(12)	1.4030(3)	0.1951(3)	-0.1792(2)	0.02366
C(12')	1.5401(3)	0.3772(3)	0.1680(2)	0.0233
C(13)	1.4216(3)	0.0588(3)	-0.1246(2)	0.0236
C(13')	1.5347(3)	0.2510(3)	0.2240(2)	0.02199
C(14)	1.3323(3)	0.0342(3)	-0.0575(2)	0.0192
C(14')	1.4187(3)	0.2480(3)	0.2717(2)	0.0191

C(15)	1.0784(3)	0.4183(3)	-0.0860(2)	0.02916
C(15')	1.1845(3)	0.6440(3)	0.1951(2)	0.03089
C(16)	1.5043(3)	0.2182(3)	-0.2503(2)	0.03379
C(16')	1.6665(3)	0.3789(3)	0.1151(2)	0.03097
C(17)	1.3547(3)	-0.1141(3)	0.0007(2)	0.0271
C(17')	1.4168(3)	0.1103(3)	0.3348(2)	0.0262
N(1)	1.0390(2)	0.1080(2)	0.1683(1)	0.02018
N(1')	1.00667(19)	0.38799(22)	0.40515(13)	0.01881
N(2)	1.12864(19)	0.12658(23)	0.02526(13)	0.01999
N(2')	1.17982(19)	0.36986(23)	0.30198(13)	0.01984
O(1)	0.96911(17)	-0.01259(19)	0.10248(11)	0.02415
O(1')	0.96617(16)	0.30636(20)	0.29794(11)	0.0247
S(1)	1.21734(6)	0.22595(8)	0.13047(4)	0.0222
S(1')	1.19534(6)	0.47002(8)	0.43288(4)	0.02278

**Table A1.2. Hydrogen coordinates and isotropic displacement parameters ( $\text{\AA}^2$ ) for *N*-tmPTH.**

Atom	x/a	y/b	z/c	$U_{\text{(eq)}}$
H(1)	1.02614	0.13865	0.21544	0.02421
H(1')	0.9725	0.41252	0.45363	0.02258
H(2)	0.90991	0.11097	0.31746	0.02571
H(2')	0.9019	0.23426	0.54663	0.02719
H(2'')	1.13434	0.33892	0.27636	0.0238
H(2A)	1.07104	0.09292	0.01603	0.02398
H(3)	0.80115	0.02994	0.44784	0.03139
H(3')	0.70945	0.20482	0.62096	0.03659
H(4)	0.73907	-0.15734	0.46404	0.02994
H(4')	0.50771	0.28189	0.53878	0.03991
H(5)	0.78003	-0.26173	0.3493	0.02821
H(5')	0.49714	0.38015	0.38241	0.03331
H(6)	0.87699	-0.17223	0.21576	0.02599
H(6')	0.69118	0.39834	0.30645	0.02643
H(11)	1.27518	0.40171	-0.20377	0.02783
H(11')	1.42992	0.58962	0.12458	0.02865
H(13)	1.49808	-0.01984	-0.13376	0.02832
H(13')	1.61245	0.16442	0.22992	0.02639
H(15A)	1.10033	0.63126	0.19051	0.04633
H(15A')	0.99916	0.39418	-0.06632	0.04375
H(15B)	1.19292	0.71535	0.13999	0.04633
H(15B')	1.0548	0.49599	-0.14326	0.04375

H(15C)	1.18107	0.67577	0.24746	0.04633
H(15C)	1.10385	0.44797	-0.04003	0.04375
H(16A)	1.57699	0.12634	-0.24981	0.05068
H(16B)	1.54448	0.27689	-0.23749	0.05068
H(16C)	1.45727	0.26636	-0.30988	0.05068
H(16D)	1.47551	0.32005	-0.28164	0.05068
H(16E)	1.50801	0.1695	-0.29396	0.05068
H(16F)	1.59522	0.18004	-0.22157	0.05068
H(16G)	1.7365	0.28181	0.1279	0.04646
H(16H)	1.70237	0.43701	0.13291	0.04646
H(16I)	1.64236	0.41917	0.05027	0.04646
H(16J)	1.65099	0.47686	0.07949	0.04646
H(16K)	1.68512	0.32165	0.07448	0.04646
H(16L)	1.74513	0.33949	0.15712	0.04646
H(17A)	1.44158	-0.18155	-0.01394	0.04065
H(17B)	1.27937	-0.13659	-0.01051	0.04065
H(17C)	1.35758	-0.12091	0.06452	0.04065
H(17D)	1.50191	0.03125	0.32971	0.0393
H(17E)	1.33845	0.09694	0.3185	0.0393
H(17F)	1.40903	0.11332	0.39707	0.0393

**Table A1.3. Anisotropic displacement parameters ( $\text{\AA}^2$ ) for *N*-tmPTH. The anisotropic displacement factor exponent takes the form:  $-2\pi^2[h^2a^{*2}U^{11} + \dots + 2hka^*b^*U^{23}]$ .**

Atom	$U^{11}$	$U^{22}$	$U^{33}$	$U^{12}$	$U^{13}$	$U^{23}$
C(1)	0.015(1)	0.020(2)	0.020(1)	-0.006(1)	-0.001(1)	-0.006(1)
C(1')	0.018(1)	0.020(2)	0.023(1)	-0.010(1)	0.006(1)	-0.012(1)
C(2)	0.019(1)	0.022(2)	0.026(2)	-0.009(1)	0.004(1)	-0.010(1)
C(2')	0.021(1)	0.030(2)	0.024(2)	-0.012(1)	0.004(1)	-0.014(1)
C(3')	0.035(2)	0.047(2)	0.022(2)	-0.028(2)	0.012(1)	-0.014(1)
C(3)	0.025(2)	0.033(2)	0.023(2)	-0.012(1)	0.006(1)	-0.014(1)
C(4')	0.026(2)	0.056(2)	0.036(2)	-0.027(2)	0.014(1)	-0.027(2)
C(4)	0.020(2)	0.028(2)	0.020(1)	-0.008(1)	0.003(1)	-0.003(1)
C(5')	0.021(2)	0.037(2)	0.035(2)	-0.015(1)	0.002(1)	-0.019(2)
C(5)	0.022(2)	0.020(2)	0.026(2)	-0.008(1)	0.002(1)	-0.006(1)
C(6')	0.019(1)	0.029(2)	0.023(1)	-0.011(1)	0.003(1)	-0.013(1)
C(6)	0.017(1)	0.024(2)	0.023(2)	-0.006(1)	0.001(1)	-0.009(1)
C(7)	0.016(1)	0.016(2)	0.024(2)	-0.005(1)	0.002(1)	-0.008(1)
C(7')	0.018(1)	0.019(2)	0.021(1)	-0.007(1)	0.001(1)	-0.008(1)
C(8')	0.014(1)	0.016(2)	0.019(1)	-0.005(1)	0.001(1)	-0.002(1)
C(8)	0.015(1)	0.019(2)	0.018(1)	-0.005(1)	0.002(1)	-0.006(1)

C(9)	0.014(1)	0.023(2)	0.018(1)	-0.009(1)	0.006(1)	-0.010(1)
C(9')	0.012(1)	0.031(2)	0.019(1)	-0.012(1)	0.005(1)	-0.013(1)
C(10)	0.020(1)	0.023(2)	0.020(1)	-0.008(1)	0.001(1)	-0.010(1)
C(10')	0.019(1)	0.025(2)	0.023(2)	-0.009(1)	0.003(1)	-0.008(1)
C(11')	0.029(2)	0.024(2)	0.023(2)	-0.017(1)	0.005(1)	-0.006(1)
C(11)	0.027(2)	0.023(2)	0.021(1)	-0.013(1)	0.003(1)	-0.007(1)
C(12)	0.024(2)	0.030(2)	0.024(2)	-0.014(1)	0.005(1)	-0.014(1)
C(12')	0.018(1)	0.037(2)	0.022(2)	-0.012(1)	0.004(1)	-0.018(1)
C(13)	0.018(1)	0.027(2)	0.026(2)	-0.005(1)	0.006(1)	-0.017(1)
C(13')	0.016(1)	0.025(2)	0.026(2)	-0.006(1)	0.000(1)	-0.013(1)
C(14')	0.018(1)	0.025(2)	0.019(1)	-0.008(1)	0.000(1)	-0.012(1)
C(14)	0.017(1)	0.022(2)	0.021(1)	-0.008(1)	-0.001(1)	-0.009(1)
C(15')	0.023(2)	0.028(2)	0.040(2)	-0.009(1)	0.007(1)	-0.011(1)
C(15)	0.030(2)	0.027(2)	0.027(2)	-0.008(1)	0.002(1)	-0.008(1)
C(16)	0.035(2)	0.046(2)	0.028(2)	-0.023(2)	0.014(1)	-0.016(2)
C(16')	0.023(2)	0.045(2)	0.033(2)	-0.018(2)	0.011(1)	-0.020(2)
C(17)	0.027(2)	0.028(2)	0.028(2)	-0.013(1)	0.001(1)	-0.009(1)
C(17')	0.022(2)	0.023(2)	0.030(2)	-0.008(1)	0.002(1)	-0.006(1)
N(1')	0.016(1)	0.027(1)	0.020(1)	-0.012(1)	0.006(1)	-0.012(1)
N(1)	0.022(1)	0.031(1)	0.017(1)	-0.015(1)	0.008(1)	-0.016(1)
N(2)	0.018(1)	0.028(1)	0.021(1)	-0.013(1)	0.004(1)	-0.012(1)
N(2')	0.016(1)	0.029(1)	0.021(1)	-0.012(1)	0.004(1)	-0.012(1)
O(1)	0.027(1)	0.030(1)	0.023(1)	-0.014(1)	0.004(1)	-0.014(1)
O(1')	0.022(1)	0.039(1)	0.023(1)	-0.018(1)	0.008(1)	-0.016(1)
S(1)	0.0192(4)	0.0312(5)	0.0235(4)	-0.0135(3)	0.0051(3)	-0.0146(3)
S(1')	0.0190(4)	0.0328(5)	0.0250(4)	-0.0145(3)	0.0063(3)	-0.0159(3)

**Table A1.4. Complete listing of bond lengths (Å) for *N*-tmPTH.**

Bond	Distance	Bond	Distance
C(1) - C(2)	1.387(4)	C(1) - C(6)	1.385(4)
C(1) - C(7)	1.496(4)	C(1') - C(2')	1.390(4)
C(1') - C(6')	1.396(4)	C(1') - C(7')	1.491(4)
C(2) - H(2)	0.950(3)	C(2) - C(3)	1.392(4)
C(2') - H(2')	0.950(3)	C(2') - C(3')	1.393(4)
C(3') - H(3')	0.950(3)	C(3') - C(4')	1.382(4)
C(3) - H(3)	0.950(3)	C(3) - C(4)	1.376(4)
C(4') - H(4')	0.950(3)	C(4') - C(5')	1.379(4)
C(4) - H(4)	0.950(3)	C(4) - C(5)	1.386(4)
C(5') - H(5')	0.950(3)	C(5') - C(6')	1.383(4)
C(5) - H(5)	0.950(3)	C(5) - C(6)	1.386(4)
C(6') - H(6')	0.950(3)	C(6) - H(6)	0.950(3)
C(7) - N(1)	1.374(4)	C(7) - O(1)	1.231(3)



C(7') - N(1')	1.375(3)	C(7') - O(1')	1.226(4)
C(8') - N(1')	1.403(4)	C(8') - N(2')	1.323(4)
C(8') - S(1')	1.670(3)	C(8) - N(1)	1.407(4)
C(8) - N(2)	1.328(3)	C(8) - S(1)	1.662(3)
C(9) - C(10)	1.395(4)	C(9) - C(14)	1.402(4)
C(9) - N(2)	1.437(4)	C(9') - C(10')	1.392(4)
C(9') - C(14')	1.397(4)	C(9') - N(2')	1.443(4)
C(10) - C(11)	1.392(4)	C(10) - C(15)	1.504(4)
C(10') - C(11')	1.394(4)	C(10') - C(15')	1.504(4)
C(11') - H(11')	0.950(3)	C(11') - C(12')	1.387(4)
C(11) - H(11)	0.950(3)	C(11) - C(12)	1.384(4)
C(12) - C(13)	1.392(5)	C(12) - C(16)	1.508(4)
C(12') - C(13')	1.390(5)	C(12') - C(16')	1.516(4)
C(13) - H(13)	0.950(3)	C(13) - C(14)	1.381(4)
C(13') - H(13')	0.950(3)	C(13') - C(14')	1.389(4)
C(14') - C(17')	1.510(4)	C(14) - C(17)	1.505(4)
C(15') - H(15A)	0.980(3)	C(15') - H(15B)	0.980(3)
C(15') - H(15C)	0.980(3)	C(15) - H(15A)	0.980(3)
C(15) - H(15B)	0.980(3)	C(15) - H(15C)	0.980(3)
C(16) - H(16A)	0.980(4)	C(16) - H(16B)	0.980(3)
C(16) - H(16C)	0.980(3)	C(16) - H(16D)	0.980(4)
C(16) - H(16E)	0.980(3)	C(16) - H(16F)	0.980(3)
C(16') - H(16G)	0.980(3)	C(16') - H(16H)	0.980(3)
C(16') - H(16I)	0.980(3)	C(16') - H(16J)	0.980(4)
C(16') - H(16K)	0.980(3)	C(16') - H(16L)	0.980(3)
C(17) - H(17A)	0.980(3)	C(17) - H(17B)	0.980(3)
C(17) - H(17C)	0.980(3)	C(17') - H(17D)	0.980(3)
C(17') - H(17E)	0.980(3)	C(17') - H(17F)	0.980(3)
N(1') - H(1')	0.880(2)	N(1) - H(1)	0.880(2)
N(2) - H(2A)	0.880(2)	N(2') - H(2')	0.880(2)

**Table A1.5. Complete listing of bond angles (°) for *N*-tmPTH.**

Angle	value	Angle	value
C(1')-C(2')-C(3')	119.3(3)	C(1)-C(2)-C(3)	120.2(3)
C(1)-C(2)-H(2)	119.9(3)	C(1')-C(2')-H(2')	120.3(3)
C(1')-C(6')-C(5')	119.9(3)	C(1)-C(6)-C(5)	120.4(3)
C(1)-C(6)-H(6)	119.8(3)	C(1')-C(6')-H(6')	120.1(3)
C(1)-C(7)-N(1)	116.7(3)	C(1')-C(7')-N(1')	115.4(3)
C(1')-C(7')-O(1')	121.7(3)	C(1)-C(7)-O(1)	121.4(3)
C(2)-C(1)-C(6)	119.5(3)	C(2)-C(1)-C(7)	123.0(3)
C(2')-C(1')-C(7')	121.7(3)	C(2')-C(1')-C(6')	120.1(3)
C(2)-C(3)-C(4)	119.8(3)	C(2')-C(3')-C(4')	120.0(3)
C(2')-C(3')-H(3')	120.0(3)	C(2)-C(3)-H(3)	120.1(3)

C(3)-C(4)-C(5)	120.4(3)	C(3')-C(4')-C(5')	120.7(3)
C(3')-C(4')-H(4')	119.7(3)	C(3)-C(4)-H(4)	119.8(3)
C(4)-C(5)-C(6)	119.6(3)	C(4')-C(5')-C(6')	119.9(3)
C(4')-C(5')-H(5')	120.1(3)	C(4)-C(5)-H(5)	120.2(3)
C(5')-C(6')-H(6')	120.1(3)	C(5)-C(6)-H(6)	119.8(3)
C(6)-C(1)-C(7)	117.6(3)	C(6')-C(1')-C(7')	118.1(3)
C(7')-N(1')-C(8')	128.0(3)	C(7)-N(1)-C(8)	129.0(3)
C(7)-N(1)-H(1)	115.5(3)	C(7')-N(1')-H(1')	116.0(2)
C(8')-N(1')-H(1')	116.0(2)	C(8)-N(1)-H(1)	115.5(3)
C(8)-N(2)-C(9)	123.2(2)	C(8')-N(2')-C(9')	125.8(2)
C(8')-N(2')-H(2')	117.1(2)	C(8)-N(2)-H(2A)	118.4(3)
C(9)-N(2)-H(2A)	118.4(3)	C(9')-N(2')-H(2')	117.1(3)
C(9)-C(10)-C(11)	117.5(3)	C(9')-C(10')-C(11')	117.4(3)
C(9')-C(10')-C(15')	122.4(3)	C(9)-C(10)-C(15)	122.8(3)
C(9')-C(14')-C(13')	118.1(3)	C(9)-C(14)-C(13)	117.8(3)
C(9)-C(14)-C(17)	121.1(3)	C(9')-C(14')-C(17')	121.0(3)
C(10)-C(11)-C(12)	122.3(3)	C(10')-C(11')-C(12')	122.4(3)
C(10')-C(11')-H(11')	118.8(3)	C(10)-C(11)-H(11)	118.9(3)
C(10)-C(15)-H(15A)	109.5(3)	C(10)-C(15)-H(15B)	109.5(3)
C(10')-C(15')-H(15A)	109.5(3)	C(10')-C(15')-H(15B)	109.5(3)
C(10)-C(15)-H(15C)	109.5(3)	C(10')-C(9')-C(14')	122.1(3)
C(10')-C(15')-H(15C)	109.5(3)	C(10)-C(9)-N(2)	120.2(3)
C(10)-C(9)-C(14)	122.1(3)	C(10')-C(9')-N(2')	120.1(3)
C(11)-C(10)-C(15)	119.8(3)	C(11')-C(12')-C(13')	118.2(3)
C(11)-C(12)-C(13)	118.2(3)	C(11)-C(12)-C(16)	121.1(3)
C(11')-C(12')-C(16')	120.5(3)	C(12)-C(13)-C(14)	122.1(3)
C(12')-C(13')-C(14')	121.7(3)	C(12')-C(13')-H(13')	119.1(3)
C(12)-C(13)-H(13)	118.9(3)	C(12)-C(16)-H(16B)	109.5(3)
C(12)-C(16)-H(16A)	109.5(3)	C(12)-C(16)-H(16D)	109.5(3)
C(12)-C(16)-H(16C)	109.5(3)	C(12)-C(16)-H(16F)	109.5(3)
C(12)-C(16)-H(16E)	109.5(3)	C(12')-C(16')-H(16G)	109.5(3)
C(12')-C(16')-H(16H)	109.5(3)	C(12')-C(16')-H(16I)	109.5(3)
C(12')-C(16')-H(16J)	109.5(3)	C(12')-C(16')-H(16K)	109.5(3)
C(12')-C(16')-H(16L)	109.5(3)	C(13')-C(12')-C(16')	121.3(3)
C(13)-C(12)-C(16)	120.7(3)	C(13)-C(14)-C(17)	121.1(3)
C(13')-C(14')-C(17')	120.8(3)	C(14)-C(17)-H(17B)	109.5(3)
C(14)-C(17)-H(17A)	109.5(3)	C(14')-C(17')-H(17E)	109.5(3)
C(14)-C(17)-H(17C)	109.5(3)	C(14')-C(9')-N(2')	117.5(3)
C(14')-C(17')-H(17D)	109.5(3)	C(14')-C(17')-H(17F)	109.5(3)
C(14)-C(9)-N(2)	117.8(3)	H(2')-C(2')-C(3')	120.3(3)
H(2)-C(2)-C(3)	119.9(3)	H(3)-C(3)-C(4)	120.1(3)

H(3')-C(3')-C(4')	120.0(3)	H(4)-C(4)-C(5)	119.8(3)
H(4')-C(4')-C(5')	119.6(3)	H(5)-C(5)-C(6)	120.2(3)
H(5')-C(5')-C(6')	120.1(3)	H(11)-C(11)-C(12)	118.9(3)
H(11')-C(11')-C(12')	118.8(3)	H(13')-C(13')-C(14')	119.1(3)
H(13)-C(13)-C(14)	118.9(3)	H(15A)-C(15)-H(15B)	109.5(3)
H(15A)-C(15)-H(15C)	109.5(3)	H(15A)-C(15')-H(15B)	109.5(3)
H(15A)-C(15')-H(15C)	109.5(3)	H(15B)-C(15)-H(15C)	109.5(3)
H(16A)-C(16)-H(16B)	109.5(3)	H(15B)-C(15')-H(15C)	109.5(3)
H(16A)-C(16)-H(16D)	141.1(3)	H(16A)-C(16)-H(16C)	109.5(3)
H(16A)-C(16)-H(16F)	56.3(2)	H(16A)-C(16)-H(16E)	56.3(2)
H(16B)-C(16)-H(16D)	56.2(2)	H(16B)-C(16)-H(16C)	109.5(3)
H(16B)-C(16)-H(16F)	56.2(2)	H(16B)-C(16)-H(16E)	141.1(3)
H(16C)-C(16)-H(16E)	56.3(2)	H(16C)-C(16)-H(16D)	56.3(2)
H(16D)-C(16)-H(16E)	109.5(3)	H(16C)-C(16)-H(16F)	141.1(3)
H(16E)-C(16)-H(16F)	109.5(3)	H(16D)-C(16)-H(16F)	109.5(3)
H(16G)-C(16')-H(16I)	109.5(3)	H(16G)-C(16')-H(16H)	109.5(3)
H(16G)-C(16')-H(16K)	56.2(2)	H(16G)-C(16')-H(16J)	141.1(3)
H(16H)-C(16')-H(16I)	109.5(3)	H(16G)-C(16')-H(16L)	56.3(2)
H(16H)-C(16')-H(16K)	141.1(3)	H(16H)-C(16')-H(16J)	56.2(2)
H(16I)-C(16')-H(16J)	56.3(2)	H(16H)-C(16')-H(16L)	56.3(2)
H(16I)-C(16')-H(16L)	141.1(3)	H(16I)-C(16')-H(16K)	56.2(2)
H(16J)-C(16')-H(16L)	109.5(3)	H(16J)-C(16')-H(16K)	109.5(3)
H(17A)-C(17)-H(17C)	109.5(3)	H(16K)-C(16')-H(16L)	109.5(3)
H(17D)-C(17')-H(17F)	109.5(3)	H(17A)-C(17)-H(17B)	109.5(3)
H(17D)-C(17')-H(17E)	109.5(3)	H(17B)-C(17)-H(17C)	109.5(3)
H(17E)-C(17')-H(17F)	109.5(3)	N(1)-C(7)-O(1)	121.8(3)
N(1')-C(8')-S(1')	118.4(2)	N(1')-C(7')-O(1')	122.9(3)
N(1')-C(8')-N(2')	116.5(3)	N(1)-C(8)-N(2)	116.3(3)
N(1)-C(8)-S(1)	118.0(2)	N(2)-C(8)-S(1)	125.7(2)
N(2')-C(8')-S(1')	125.1(2)		

## A2. Crystal data of *N*-benzoyl-*N*'-(2,6-dibromo-4-fluorophenyl)thiourea (*N*-BFPTH)

**Table A2.1. Atomic coordinates and equivalent isotropic displacement parameters ( $\text{\AA}^2$ ) for *N*-BFPTH.  $U_{\text{(eq)}}$  is defined as one third of the trace of the orthogonalized  $U^{ij}$  tensor.**

Atom	x/a	y/b	z/c	$U_{\text{(eq)}}$
Br(1)	0.32648(3)	-0.01382(2)	0.33224(3)	0.02053
Br(2)	-0.19774(3)	0.31131(2)	0.45563(2)	0.01824
C(1)	0.6018(3)	0.3888(2)	0.8689(2)	0.0112
C(2)	0.7042(3)	0.3181(2)	0.9641(2)	0.01466
C(3)	0.8349(3)	0.3875(3)	1.0829(2)	0.01817
C(4)	0.8617(3)	0.5275(3)	1.1084(2)	0.01851
C(5)	0.7583(3)	0.5982(2)	1.0154(2)	0.01601
C(6)	0.6287(3)	0.5293(2)	0.8952(2)	0.01261
C(7)	0.4579(3)	0.3098(2)	0.7467(2)	0.01038
C(8)	0.2808(3)	0.3145(2)	0.5042(2)	0.01025
C(9)	0.0434(3)	0.1355(2)	0.3776(2)	0.01215
C(10)	-0.1327(3)	0.1681(2)	0.3413(2)	0.01286
C(11)	-0.2606(3)	0.1017(2)	0.2182(2)	0.0153
C(12)	-0.2058(3)	0.0034(2)	0.1329(2)	0.0154
C(13)	-0.0340(3)	-0.0340(2)	0.1638(2)	0.01583
C(14)	0.0895(3)	0.0335(2)	0.2876(2)	0.01372
F(1)	-0.32640(19)	-0.06053(14)	0.01141(15)	0.02205
N(1)	0.4129(2)	0.3668(2)	0.6289(2)	0.01064
N(2)	0.1751(2)	0.2042(2)	0.5023(2)	0.01185
O(1)	0.3832(2)	0.2007(2)	0.7512(2)	0.01465
S(1)	0.25866(7)	0.38846(5)	0.36628(5)	0.01331

**Table A2.2. Hydrogen coordinates and isotropic displacement parameters ( $\text{\AA}^2$ ) for *N*-BFPTH.**

Atom	x/a	y/b	z/c	$U_{\text{(eq)}}$
H(1)	0.47474	0.44439	0.63367	0.01276
H(2)	0.18731	0.17341	0.5801	0.01422
H(2A)	0.68404	0.2222	0.94729	0.01759
H(3)	0.90602	0.3394	1.1468	0.0218
H(4)	0.9514	0.57525	1.19001	0.02221
H(5)	0.77631	0.69422	1.03421	0.01921
H(6)	0.55865	0.57782	0.83105	0.01513
H(11)	-0.38126	0.12334	0.19391	0.01836
H(13)	-0.00142	-0.1033	0.10271	0.019

**Table A2.3. Anisotropic displacement parameters ( $\text{\AA}^2$ ) for *N*-BFPTH. The anisotropic displacement factor exponent takes the form:  $-2\pi^2[h^2a^{*2}U^{11} + \dots + 2hka^*b^*U^{23}]$ .**

Atom	$U^{11}$	$U^{22}$	$U^{33}$	$U^{12}$	$U^{13}$	$U^{23}$
C(1)	0.0105(9)	0.0145(10)	0.0075(9)	-0.0006(8)	0.0022(8)	0.0008(7)
C(2)	0.014(1)	0.016(1)	0.012(1)	0.001(1)	0.001(1)	0.003(1)
C(3)	0.013(1)	0.027(1)	0.012(1)	0.001(1)	-0.001(1)	0.006(1)
C(4)	0.013(1)	0.026(1)	0.011(1)	-0.005(1)	0.001(1)	0.000(1)
C(5)	0.017(1)	0.015(1)	0.014(1)	-0.005(1)	0.006(1)	-0.003(1)
C(6)	0.013(1)	0.015(1)	0.011(1)	0.000(1)	0.004(1)	0.003(1)
C(7)	0.0104(9)	0.0116(9)	0.0089(9)	0.0027(7)	0.0024(8)	0.0015(7)
C(8)	0.0087(9)	0.0115(9)	0.0093(9)	0.0015(7)	0.0016(7)	0.0001(7)
C(9)	0.012(1)	0.011(1)	0.011(1)	-0.003(1)	0.000(1)	0.002(1)
C(10)	0.013(1)	0.012(1)	0.014(1)	0.000(1)	0.003(1)	0.003(1)
C(11)	0.010(1)	0.016(1)	0.018(1)	-0.002(1)	-0.001(1)	0.005(1)
C(12)	0.015(1)	0.014(1)	0.011(1)	-0.006(1)	-0.004(1)	0.002(1)
C(13)	0.017(1)	0.013(1)	0.014(1)	-0.002(1)	0.002(1)	0.000(1)
C(14)	0.010(1)	0.013(1)	0.016(1)	0.000(1)	0.001(1)	0.004(1)
O(1)	0.0164(8)	0.0123(7)	0.0125(7)	-0.0019(6)	0.0004(6)	0.0030(6)
F(1)	0.0187(7)	0.0224(7)	0.0144(7)	-0.0034(6)	-0.0081(5)	-0.0012(5)
S(1)	0.0126(3)	0.0153(3)	0.0091(2)	-0.0030(2)	-0.0016(2)	0.0044(2)
BR(1)	0.0127(1)	0.0203(1)	0.0238(1)	0.0049(1)	0.0003(1)	-0.0014(1)
BR(2)	0.0148(1)	0.0192(1)	0.0191(1)	0.0038(1)	0.0044(1)	-0.0003(1)
N(1)	0.0107(8)	0.0100(8)	0.0087(8)	-0.0024(6)	-0.0002(7)	0.0020(6)
N(2)	0.0114(8)	0.0126(8)	0.0086(8)	-0.0017(7)	-0.0010(7)	0.0022(7)

**Table A2.4. Complete listing of bond lengths (Å) for *N*-BFPTH.**

<b>Bond</b>	<b>Distance</b>	<b>Bond</b>	<b>Distance</b>
C(1)-C(2)	1.397(4)	C(1)-C(6)	1.391(4)
C(1)-C(7)	1.483(3)	C(2)-H(2A)	0.950(3)
C(2)-C(3)	1.383(4)	C(3)-H(3)	0.950(3)
C(3)-C(4)	1.386(4)	C(4)-H(4)	0.950(3)
C(4)-C(5)	1.386(4)	C(5)-H(5)	0.950(3)
C(5)-C(6)	1.386(4)	C(6)-H(6)	0.950(3)
C(7)-O(1)	1.227(3)	C(7)-N(1)	1.382(3)
C(8)-S(1)	1.668(3)	C(8)-N(1)	1.382(3)
C(8)-N(2)	1.336(3)	C(9)-C(10)	1.391(4)
C(9)-C(14)	1.392(4)	C(9)-N(2)	1.420(3)
C(10)-C(11)	1.390(4)	C(10)-BR(2)	1.885(3)
C(11)-H(11)	0.950(3)	C(11)-C(12)	1.374(4)
C(12)-C(13)	1.376(4)	C(12)-F(1)	1.349(3)
C(13)-H(13)	0.950(3)	C(13)-C(14)	1.384(4)
C(14)-BR(1)	1.882(3)	N(1)-H(1)	0.880(2)
N(2)-H(2)	0.880(2)		

**Table A2.5. Complete listing of bond angles (°) for *N*-BFPTH.**

<b>Angle</b>	<b>value</b>	<b>Angle</b>	<b>value</b>
C(1)-C(2)-C(3)	120.0(3)	C(1)-C(2)-H(2A)	120.0(3)
C(1)-C(6)-H(6)	120.2(3)	C(1)-C(6)-C(5)	119.6(2)
C(1)-C(7)-O(1)	121.6(2)	C(1)-C(7)-N(1)	116.1(2)
C(2)-C(1)-C(6)	120.0(2)	C(2)-C(1)-C(7)	117.8(2)
C(2)-C(3)-H(3)	120.1(3)	C(2)-C(3)-C(4)	119.8(3)
C(3)-C(4)-C(5)	120.3(3)	C(3)-C(4)-H(4)	119.8(3)
C(4)-C(5)-H(5)	119.9(3)	C(4)-C(5)-C(6)	120.2(3)
C(5)-C(6)-H(6)	120.2(3)	C(6)-C(1)-C(7)	122.1(2)
C(7)-N(1)-C(8)	126.8(2)	C(7)-N(1)-H(1)	116.6(2)
C(8)-N(1)-H(1)	116.6(2)	C(8)-N(2)-C(9)	121.5(2)
C(8)-N(2)-H(2)	119.3(2)	C(9)-C(10)-C(11)	121.3(2)
C(9)-C(10)-BR(2)	119.7(2)	C(9)-C(14)-C(13)	121.9(3)
C(9)-C(14)-BR(1)	119.8(2)	C(9)-N(2)-H(2)	119.3(2)
C(10)-C(11)-H(11)	121.3(3)	C(10)-C(11)-C(12)	117.5(3)
C(10)-C(9)-C(14)	118.3(2)	C(10)-C(9)-N(2)	121.5(2)
C(11)-C(12)-F(1)	118.6(3)	C(11)-C(10)-BR(2)	118.9(2)
C(11)-C(12)-C(13)	123.8(3)	C(12)-C(13)-H(13)	121.4(3)
C(12)-C(13)-C(14)	117.1(3)	C(13)-C(12)-F(1)	117.6(2)
C(13)-C(14)-BR(1)	118.3(2)	C(14)-C(9)-N(2)	120.2(2)
H(2A)-C(2)-C(3)	120.0(3)	H(3)-C(3)-C(4)	120.1(3)
H(4)-C(4)-C(5)	119.8(3)	H(5)-C(5)-C(6)	119.9(3)
H(11)-C(11)-C(12)	121.3(3)	H(13)-C(13)-C(14)	121.4(3)
N(1)-C(8)-N(2)	116.3(2)	O(1)-C(7)-N(1)	122.3(2)
S(1)-C(8)-N(2)	123.3(2)	S(1)-C(8)-N(1)	120.4(2)

### A3. Crystal data of *N*-benzoyl-*N*'-(2,3,4,5,6-pentafluorophenyl)thiourea (*N*-FPTH)

**Table A3.1. Atomic coordinates and equivalent isotropic displacement parameters ( $\text{\AA}^2$ ) for *N*-FPTH.  $U_{\text{(eq)}}$  is defined as one third of the trace of the orthogonalized  $U^{\text{ij}}$  tensor.**

Atom	x/a	y/b	z/c	$U_{\text{(eq)}}$
C(1)	0.12089(5)	-0.07749(15)	0.09938(15)	0.01657
C(2)	0.09969(5)	-0.00467(17)	0.18361(16)	0.02009
C(3)	0.05444(6)	-0.04069(18)	0.18431(17)	0.02517
C(4)	0.02997(5)	-0.14925(19)	0.10207(17)	0.02608
C(5)	0.05112(6)	-0.22283(19)	0.01877(18)	0.02802
C(6)	0.09626(6)	-0.18669(17)	0.01684(17)	0.02332
C(7)	0.16877(5)	-0.04263(15)	0.08859(14)	0.01474
C(8)	0.24673(5)	0.05847(15)	0.22378(14)	0.01448
C(9)	0.31533(5)	0.03720(15)	0.14599(14)	0.01516
C(10)	0.33045(5)	0.15177(15)	0.08732(15)	0.01708
C(11)	0.37769(5)	0.16957(15)	0.09679(15)	0.01851
C(12)	0.41053(5)	0.07138(16)	0.16613(16)	0.01982
C(13)	0.39657(5)	-0.04196(16)	0.22829(16)	0.02074
C(14)	0.34906(5)	-0.05879(15)	0.21720(15)	0.01793
F(1)	0.29908(3)	0.24725(10)	0.01871(10)	0.02588
F(2)	0.39168(3)	0.28007(10)	0.03770(10)	0.02588
F(3)	0.45603(3)	0.08579(11)	0.17186(11)	0.02979
F(4)	0.42872(3)	-0.13685(11)	0.29711(11)	0.03263
F(5)	0.33599(3)	-0.17081(10)	0.27606(10)	0.02612
N(1)	0.19979(4)	0.02035(13)	0.20340(12)	0.01543
N(2)	0.26643(4)	0.01399(13)	0.12923(12)	0.01578
O(1)	0.17968(4)	-0.06932(11)	-0.01566(10)	0.01769
S(1)	0.27547(1)	0.15386(4)	0.36092(4)	0.01784



**Table A3.2. Hydrogen coordinates and isotropic displacement parameters ( $\text{\AA}^2$ ) for *N*-FPTH.**

Atom	x/a	y/b	z/c	$U_{\text{eq}}$
H(1)	0.18842	0.03856	0.27206	0.01852
H(2)	0.24883	-0.03043	0.05535	0.01893
H(2A)	0.11623	0.06966	0.24056	0.02411
H(3)	0.04004	0.00947	0.24167	0.0302
H(4)	-0.00111	-0.17315	0.10274	0.0313
H(5)	0.03465	-0.29802	-0.03697	0.03363
H(6)	0.11049	-0.23664	-0.04106	0.02799

**Table A3.3. Anisotropic displacement parameters ( $\text{\AA}^2$ ) for *N*-FPTH. The anisotropic displacement factor exponent takes the form:  $-2\pi^2[h^2a^{*2}U^{11} + \dots + 2hka^*b^*U^{23}]$ .**

Atom	$U^{11}$	$U^{22}$	$U^{33}$	$U^{12}$	$U^{13}$	$U^{23}$
C(1)	0.0146(7)	0.0181(7)	0.0167(7)	0.0004(6)	0.0044(5)	0.0040(5)
C(2)	0.0145(7)	0.0249(8)	0.0206(7)	-0.0005(6)	0.0051(6)	-0.0002(6)
C(3)	0.0178(7)	0.0348(9)	0.0254(8)	-0.0003(7)	0.0104(6)	0.0007(7)
C(4)	0.0145(7)	0.0341(9)	0.0300(8)	-0.0038(7)	0.0073(6)	0.0059(7)
C(5)	0.0208(8)	0.0293(9)	0.0326(9)	-0.0086(7)	0.0061(7)	-0.0042(7)
C(6)	0.0198(8)	0.0256(8)	0.0256(8)	-0.0036(6)	0.0084(6)	-0.0051(6)
C(7)	0.0134(7)	0.0146(6)	0.0161(7)	0.0015(5)	0.0043(5)	0.0038(5)
C(8)	0.0127(6)	0.0153(6)	0.0153(7)	-0.0003(5)	0.0040(5)	0.0031(5)
C(9)	0.0116(6)	0.0189(7)	0.0150(6)	-0.0008(5)	0.0042(5)	-0.0021(5)
C(10)	0.0146(7)	0.0189(7)	0.0173(7)	0.0026(6)	0.0043(5)	0.0010(6)
C(11)	0.0178(7)	0.0196(7)	0.0190(7)	-0.0040(6)	0.0070(6)	0.0003(6)
C(12)	0.0104(7)	0.0252(8)	0.0236(8)	-0.0021(6)	0.0048(6)	-0.0042(6)
C(13)	0.0143(7)	0.0218(7)	0.0233(8)	0.0039(6)	0.0015(6)	0.0004(6)
C(14)	0.0170(7)	0.0179(7)	0.0188(7)	-0.0015(6)	0.0054(6)	0.0005(5)
F(1)	0.0177(5)	0.0242(5)	0.0351(5)	0.0046(4)	0.0070(4)	0.0125(4)
F(2)	0.0221(5)	0.0267(5)	0.0300(5)	-0.0072(4)	0.0096(4)	0.0060(4)
F(3)	0.0110(4)	0.0373(6)	0.0404(6)	-0.0024(4)	0.0070(4)	-0.0001(5)
F(4)	0.0168(5)	0.0310(5)	0.0446(6)	0.0072(4)	0.0012(4)	0.0105(5)
F(5)	0.0218(5)	0.0230(5)	0.0317(5)	-0.0013(4)	0.0055(4)	0.0105(4)
N(1)	0.0137(6)	0.0191(6)	0.0149(6)	-0.0009(5)	0.0065(5)	-0.0003(5)
N(2)	0.0119(6)	0.0197(6)	0.0157(6)	-0.0021(5)	0.0042(5)	-0.0020(5)
O(1)	0.0150(5)	0.0228(5)	0.0156(5)	0.0000(4)	0.0053(4)	0.0002(4)
S(1)	0.0162(2)	0.0212(2)	0.0167(2)	-0.0039(1)	0.0058(1)	-0.0031(1)

**Table A3.4. Complete listing of bond lengths (Å) for *N*-FPTH.**

<b>Bond</b>	<b>Distance</b>	<b>Bond</b>	<b>Distance</b>
C(1)-C(2)	1.392(3)	C(8)-N(1)	1.389(2)
C(1)-C(6)	1.394(3)	C(8)-N(2)	1.337(2)
C(1)-C(7)	1.493(2)	C(9)-C(10)	1.382(3)
C(2)-C(3)	1.385(3)	C(9)-N(2)	1.422(2)
C(2)-H(2A)	0.950(2)	C(10)-F(1)	1.334(2)
C(3)-H(3)	0.950(2)	C(11)-C(10)	1.383(2)
C(4)-C(3)	1.386(3)	C(11)-C(12)	1.377(3)
C(4)-C(5)	1.388(3)	C(11)-F(2)	1.339(2)
C(4)-H(4)	0.950(2)	C(12)-C(13)	1.377(3)
C(5)-H(5)	0.950(2)	C(12)-F(3)	1.338(2)
C(6)-C(5)	1.386(3)	C(13)-F(4)	1.343(2)
C(6)-H(6)	0.950(2)	C(14)-C(13)	1.386(2)
C(7)-N(1)	1.381(2)	C(14)-C(9)	1.384(3)
C(7)-O(1)	1.225(2)	C(14)-F(5)	1.337(2)
C(8)-S(1)	1.663(2)	N(1)-H(1)	0.880(2)

**Table A3.5. Complete listing of bond angles (°) for *N*-FPTH.**

C(1)-C(2)-C(3)	119.9(2)	C(10)-C(11)-F(2)	120.7(2)
C(1)-C(2)-H(2A)	120.0(2)	C(10)-C(9)-N(2)	121.6(2)
C(1)-C(6)-C(5)	120.4(2)	C(11)-C(10)-C(9)	121.4(2)
C(1)-C(6)-H(6)	119.8(2)	C(11)-C(10)-F(1)	118.7(2)
C(1)-C(7)-N(1)	115.8(2)	C(11)-C(12)-C(13)	120.2(2)
C(1)-C(7)-O(1)	121.7(2)	C(11)-C(12)-F(3)	119.7(2)
C(2)-C(1)-C(6)	119.4(2)	C(12)-C(11)-C(10)	119.5(2)
C(2)-C(3)-C(4)	120.6(2)	C(12)-C(11)-F(2)	119.8(2)
C(2)-C(3)-H(3)	119.7(2)	C(12)-C(13)-F(4)	120.1(2)
C(3)-C(4)-C(5)	119.6(2)	C(13)-C(12)-F(3)	120.0(2)
C(4)-C(3)-H(3)	119.7(2)	C(13)-C(14)-C(9)	121.2(2)
C(4)-C(5)-C(6)	120.0(2)	C(13)-C(14)-F(5)	118.8(2)
C(4)-C(5)-H(5)	120.0(2)	C(14)-C(13)-C(12)	119.6(2)
C(6)-C(5)-H(5)	120.0(2)	C(14)-C(13)-F(4)	120.3(2)
C(7)-C(1)-C(2)	123.5(2)	C(14)-C(9)-C(10)	118.0(2)
C(7)-C(1)-C(6)	117.1(2)	C(14)-C(9)-N(2)	120.3(2)
C(7)-N(1)-H(1)	116.0(2)	H(2A)-C(2)-C(3)	120.0(2)
C(8)-N(1)-C(7)	128.0(2)	H(4)-C(4)-C(3)	120.2(2)
C(8)-N(1)-H(1)	116.0(2)	H(4)-C(4)-C(5)	120.2(2)
C(8)-N(2)-C(9)	121.1(2)	H(6)-C(6)-C(5)	119.8(2)
C(8)-N(2)-H(2)	119.4(2)	N(1)-C(7)-O(1)	122.5(2)
C(9)-C(10)-F(1)	119.9(2)	N(1)-C(8)-N(2)	116.6(2)
C(9)-C(14)-F(5)	120.0(2)	N(1)-C(8)-S(1)	119.9(2)
C(9)-N(2)-H(2)	119.4(2)	N(2)-C(8)-S(1)	123.5(2)

#### A4. Crystal data of *N*-benzoyl-*N*'-phenethylthiourea (*N*-PeTH)

**Table A4.1.** Atomic coordinates and equivalent isotropic displacement parameters ( $\text{\AA}^2$ ) for *N*-PeTH.  $U_{\text{(eq)}}$  is defined as one third of the trace of the orthogonalized  $U^{ij}$  tensor.

Atom	x/a	y/b	z/c	$U_{\text{(eq)}}$
C(1)	0.28577(11)	0.10054(21)	0.07331(7)	0.01519
C(2)	0.24922(11)	0.31265(23)	0.05457(7)	0.01868
C(3)	0.13571(12)	0.36754(24)	0.05214(7)	0.02102
C(4)	0.05882(11)	0.21282(24)	0.06907(7)	0.021
C(5)	0.09475(12)	0.00198(25)	0.08780(7)	0.02159
C(6)	0.20760(11)	-0.05473(23)	0.08938(7)	0.01873
C(7)	0.40622(11)	0.02621(22)	0.07873(7)	0.01565
C(8)	0.60323(11)	0.17230(22)	0.08816(7)	0.0158
C(9)	0.76617(11)	-0.07229(22)	0.11394(7)	0.01634
C(10)	0.78858(11)	-0.11455(25)	0.19168(7)	0.02124
C(11)	0.91126(11)	-0.16370(23)	0.21714(7)	0.01825
C(12)	0.95722(12)	-0.36795(23)	0.20462(8)	0.02078
C(13)	1.07107(12)	-0.41240(24)	0.22664(8)	0.02314
C(14)	1.13983(12)	-0.25301(26)	0.26182(7)	0.02196
C(15)	1.09474(12)	-0.05114(25)	0.27522(7)	0.02206
C(16)	0.98137(12)	-0.00569(24)	0.25281(7)	0.01941
N(1)	0.48549(9)	0.19052(19)	0.07716(6)	0.0172
N(2)	0.64595(9)	-0.02889(19)	0.09264(6)	0.01628
O(1)	0.43227(8)	-0.16806(16)	0.08506(5)	0.02121
S(1)	0.67858(3)	0.40498(6)	0.09424(2)	0.02241

**Table A4.2. Hydrogen coordinates and isotropic displacement parameters ( $\text{\AA}^2$ ) for *N*-PeTH.**

Atom	x/a	y/b	z/c	$U_{\text{eq}}$
H(1)	0.45842	0.3235	0.06808	0.02065
H(2)	0.60005	-0.14097	0.08238	0.01953
H(2A)	0.30183	0.41949	0.04349	0.02242
H(3)	0.11069	0.51156	0.03884	0.02522
H(4)	-0.01854	0.25148	0.06781	0.0252
H(5)	0.04211	-0.10374	0.09957	0.02591
H(6)	0.23179	-0.20014	0.10147	0.02247
H(9A)	0.81124	0.05544	0.10228	0.0196
H(9B)	0.78945	-0.20204	0.0888	0.0196
H(10A)	0.76525	0.01621	0.21632	0.02549
H(10B)	0.74176	-0.24019	0.20294	0.02549
H(12)	0.91039	-0.47795	0.18083	0.02494
H(13)	1.10166	-0.55182	0.21759	0.02776
H(14)	1.21762	-0.28265	0.27662	0.02636
H(15)	1.14148	0.05729	0.29991	0.02647
H(16)	0.95138	0.13426	0.26187	0.02329

**Table A4.3. Anisotropic displacement parameters ( $\text{\AA}^2$ ) for *N*-PeTH. The anisotropic displacement factor exponent takes the form:  $-2\pi^2[h^2a^{*2}U^{11} + \dots + 2hka^*b^*U^{23}]$ .**

Atom	$U^{11}$	$U^{22}$	$U^{33}$	$U^{12}$	$U^{13}$	$U^{23}$
C(1)	0.0147(6)	0.0173(7)	0.0135(6)	-0.0022(5)	0.0017(5)	-0.0015(5)
C(2)	0.0157(6)	0.0197(7)	0.0201(7)	-0.0030(5)	0.0004(5)	0.0023(5)
C(3)	0.0187(7)	0.0178(7)	0.0255(7)	0.0012(5)	-0.0006(6)	0.0012(5)
C(4)	0.0147(6)	0.0242(8)	0.0241(7)	0.0001(5)	0.0025(5)	-0.0022(6)
C(5)	0.0172(7)	0.0228(7)	0.0256(7)	-0.0036(5)	0.0059(6)	0.0020(6)
C(6)	0.0182(6)	0.0164(7)	0.0216(7)	-0.0023(5)	0.0029(5)	0.0017(5)
C(7)	0.0148(6)	0.0166(6)	0.0155(6)	-0.0026(5)	0.0021(5)	0.0001(5)
C(8)	0.0141(6)	0.0178(7)	0.0155(6)	-0.0026(5)	0.0023(5)	-0.0001(5)
C(9)	0.0120(6)	0.0159(6)	0.0213(7)	-0.0006(5)	0.0028(5)	0.0007(5)
C(10)	0.0150(6)	0.0292(8)	0.0197(7)	0.0018(5)	0.0032(5)	-0.0009(6)
C(11)	0.0169(6)	0.0229(7)	0.0154(6)	0.0003(5)	0.0041(5)	0.0017(5)
C(12)	0.0194(7)	0.0195(7)	0.0232(7)	-0.0020(5)	0.0024(6)	0.0001(5)
C(13)	0.0229(7)	0.0206(7)	0.0264(8)	0.0044(6)	0.0053(6)	0.0039(6)
C(14)	0.0154(6)	0.0309(8)	0.0196(7)	0.0019(6)	0.0026(5)	0.0066(6)
C(15)	0.0202(7)	0.0277(8)	0.0179(7)	-0.0055(6)	0.0013(5)	0.0004(6)
C(16)	0.0203(7)	0.0195(7)	0.0187(7)	0.0007(5)	0.0039(5)	-0.0004(5)
N(1)	0.0132(5)	0.0139(6)	0.0247(6)	-0.0010(4)	0.0035(4)	0.0017(4)

N(2)	0.0129(5)	0.0138(5)	0.0221(6)	-.0032(4)	0.0024(4)	-.0003(4)
O(1)	0.0156(5)	0.0164(5)	0.0314(6)	-.0012(4)	0.0024(4)	0.0025(4)
S(1)	0.0163(2)	0.0136(2)	0.0378(2)	-.0038(1)	0.0053(2)	-.0005(1)

**Table A4.4. Complete listing of bond lengths (Å) for *N*-PeTH.**

<b>Bond</b>	<b>Distance</b>	<b>Bond</b>	<b>Distance</b>
C(1)-C(6)	1.395(2)	C(11)-C(16)	1.394(2)
C(1)-C(7)	1.497(2)	C(12)-C(13)	1.393(3)
C(2)-C(1)	1.394(2)	C(12)-H(12)	0.950(2)
C(2)-C(3)	1.390(2)	C(13)-H(13)	0.950(2)
C(2)-H(2A)	0.950(2)	C(14)-C(13)	1.388(3)
C(3)-H(3)	0.950(2)	C(14)-C(15)	1.381(3)
C(4)-C(3)	1.387(2)	C(14)-H(14)	0.950(2)
C(4)-C(5)	1.385(3)	C(15)-H(15)	0.950(2)
C(4)-H(4)	0.950(2)	C(16)-C(15)	1.390(3)
C(5)-H(5)	0.950(2)	C(16)-H(16)	0.950(2)
C(6)-C(5)	1.387(2)	N(1)-C(7)	1.380(2)
C(6)-H(6)	0.950(2)	N(1)-C(8)	1.396(2)
C(9)-C(10)	1.525(2)	N(1)-H(1)	0.880(2)
C(9)-H(9A)	0.990(2)	N(2)-C(8)	1.324(2)
C(9)-H(9B)	0.990(2)	N(2)-C(9)	1.461(2)
C(10)-H(10A)	0.990(2)	N(2)-H(2)	0.880(2)
C(10)-H(10B)	0.990(2)	O(1)-C(7)	1.224(2)
C(11)-C(10)	1.508(2)	S(1)-C(8)	1.673(2)
C(11)-C(12)	1.394(2)		

**Table A4.5. Complete listing of bond angles (°) for *N*-PeTH.**

Angle	Value	Angle	Value
C(1)-C(2)-C(3)	119.9(2)	C(16)-C(11)-C(10)	120.9(2)
C(1)-C(6)-C(5)	120.4(2)	C(16)-C(11)-C(12)	118.6(2)
C(1)-C(6)-H(6)	119.8(2)	C(16)-C(15)-C(14)	120.4(2)
C(2)-C(1)-C(6)	119.4(2)	C(16)-C(15)-H(15)	119.8(2)
C(2)-C(1)-C(7)	124.0(2)	H(1)-N(1)-C(7)	115.9(2)
C(2)-C(3)-H(3)	119.9(2)	H(10A)-C(10)-H(10B)	107.8(2)
C(3)-C(4)-C(5)	120.1(2)	H(12)-C(12)-C(13)	119.7(2)
C(4)-C(3)-C(2)	120.3(2)	H(14)-C(14)-C(13)	120.1(2)
C(4)-C(3)-H(3)	119.9(2)	H(16)-C(16)-C(15)	119.7(2)
C(4)-C(5)-C(6)	120.0(2)	H(2)-N(2)-C(8)	118.7(2)
C(4)-C(5)-H(5)	120.0(2)	H(2A)-C(2)-C(1)	120.0(2)
C(6)-C(1)-C(7)	116.5(2)	H(4)-C(4)-C(3)	120.0(2)
C(6)-C(5)-H(5)	120.0(2)	H(6)-C(6)-C(5)	119.8(2)
C(8)-N(1)-C(7)	128.2(2)	H(9A)-C(9)-C(10)	109.7(2)
C(8)-N(2)-C(9)	122.7(2)	N(1)-C(7)-C(1)	115.8(2)
C(9)-C(10)-H(10A)	109.0(2)	N(2)-C(9)-C(10)	109.9(2)
C(9)-C(10)-H(10B)	109.0(2)	N(2)-C(9)-H(9A)	109.7(2)
C(11)-C(10)-C(9)	112.7(2)	O(1)-C(7)-N(1)	122.5(2)
C(11)-C(10)-H(10A)	109.0(2)	S(1)-C(8)-N(1)	117.6(1)
C(11)-C(10)-H(10B)	109.0(2)	H(1)-N(1)-C(8)	115.9(2)
C(11)-C(12)-C(13)	120.7(2)	H(14)-C(14)-C(15)	120.1(2)
C(11)-C(12)-H(12)	119.7(2)	H(2)-N(2)-C(9)	118.7(2)
C(11)-C(16)-C(15)	120.6(2)	H(2A)-C(2)-C(3)	120.0(2)
C(11)-C(16)-H(16)	119.7(2)	H(4)-C(4)-C(5)	120.0(2)
C(12)-C(11)-C(10)	120.5(2)	H(9A)-C(9)-H(9B)	108.2(2)
C(12)-C(13)-H(13)	120.0(2)	H(9B)-C(9)-C(10)	109.7(2)
C(14)-C(13)-C(12)	120.0(2)	N(2)-C(8)-N(1)	117.0(2)
C(14)-C(13)-H(13)	120.0(2)	N(2)-C(9)-H(9B)	109.7(2)
C(14)-C(15)-H(15)	119.8(2)	O(1)-C(7)-C(1)	121.8(2)
C(15)-C(14)-C(13)	119.7(2)	S(1)-C(8)-N(2)	125.4(2)

## A5. Crystal data of *N*-benzoyl-*N'*-(naphthalene-1-ylmethyl)thiourea (*N*-NmTH)

**Table A5.1. Atomic coordinates and equivalent isotropic displacement parameters ( $\text{\AA}^2$ ) for *N*-NmTH.  $U_{\text{(eq)}}$  is defined as one third of the trace of the orthogonalized  $U^{\text{ij}}$  tensor.**

Atom	x/a	y/b	z/c	$U_{\text{(eq)}}$
C(1)	0.49422(11)	0.80716(16)	0.86545(14)	0.01674
C(2)	0.56291(11)	0.80936(17)	0.97107(15)	0.01825
C(3)	0.59489(11)	0.91929(18)	1.02335(15)	0.02131
C(4)	0.55838(12)	1.02785(17)	0.97026(16)	0.0222
C(5)	0.49024(12)	1.02604(17)	0.86515(16)	0.02296
C(6)	0.45820(12)	0.91637(17)	0.81264(15)	0.02139
C(7)	0.45695(11)	0.69323(16)	0.80312(14)	0.01694
C(8)	0.45621(10)	0.46898(16)	0.82391(14)	0.01525
C(9)	0.37777(11)	0.33403(16)	0.67032(14)	0.01655
C(10)	0.31357(10)	0.28229(16)	0.66820(13)	0.01567
C(11)	0.28332(11)	0.34570(17)	0.70616(14)	0.01947
C(12)	0.22445(11)	0.29550(18)	0.70534(15)	0.02286
C(13)	0.19550(11)	0.18196(18)	0.66526(14)	0.02145
C(14)	0.22417(10)	0.11333(17)	0.62381(13)	0.01777
C(15)	0.19355(11)	-0.00366(17)	0.57928(14)	0.02042
C(16)	0.22050(11)	-0.06884(17)	0.53791(14)	0.02142
C(17)	0.27918(11)	-0.01952(17)	0.53842(14)	0.02091
C(18)	0.31001(11)	0.09334(17)	0.58078(13)	0.0177
C(19)	0.28384(10)	0.16321(16)	0.62476(13)	0.01595
N(1)	0.47850(9)	0.58804(13)	0.86135(11)	0.0163
N(2)	0.40612(9)	0.45312(14)	0.71983(12)	0.01728
O(1)	0.40971(8)	0.69305(12)	0.70578(10)	0.02285
S(1)	0.49433(3)	0.35620(4)	0.91282(3)	0.01936



**Table A5.2. Hydrogen coordinates and isotropic displacement parameters ( $\text{\AA}^2$ ) for *N*-NmTH.**

Atom	x/a	y/b	z/c	$U_{\text{(eq)}}$
H(1)	0.51017	0.59702	0.93056	0.01956
H(2)	0.38925	0.51756	0.6788	0.02074
H(2A)	0.58791	0.73529	1.00736	0.02189
H(3)	0.6417	0.92051	1.09537	0.02558
H(4)	0.58019	1.10321	1.00609	0.02664
H(5)	0.46541	1.10023	0.82898	0.02755
H(6)	0.41157	0.91555	0.74048	0.02567
H(9A)	0.42266	0.2767	0.70879	0.01986
H(9B)	0.35754	0.33995	0.59667	0.01986
H(11)	0.30235	0.42521	0.73365	0.02336
H(12)	0.20486	0.34107	0.73288	0.02743
H(13)	0.15597	0.14885	0.66516	0.02574
H(15)	0.15365	-0.03718	0.57823	0.0245
H(16)	0.19968	-0.14727	0.50887	0.02569
H(17)	0.2976	-0.06477	0.50919	0.02509
H(18)	0.34965	0.12513	0.58056	0.02124

**Table A5.3. Anisotropic displacement parameters ( $\text{\AA}^2$ ) for *N*-NmTH. The anisotropic displacement factor exponent takes the form:  $-2\pi^2[h^2a^{*2}U^{11} + \dots + 2hka^*b^*U^{23}]$ .**

Atom	$U^{11}$	$U^{22}$	$U^{33}$	$U^{12}$	$U^{13}$	$U^{23}$
C(1)	0.0209(9)	0.0149(9)	0.0193(9)	-0.0013(7)	0.0152(8)	-0.0006(7)
C(2)	0.0189(9)	0.0162(9)	0.0222(9)	-0.0003(7)	0.0144(8)	0.0004(7)
C(3)	0.0196(9)	0.0244(10)	0.0218(9)	-0.0045(8)	0.0142(8)	-0.0049(8)
C(4)	0.029(1)	0.017(1)	0.029(1)	-0.007(1)	0.023(1)	-0.007(1)
C(5)	0.032(1)	0.015(1)	0.027(1)	0.003(1)	0.021(1)	0.004(1)
C(6)	0.025(1)	0.019(1)	0.019(1)	0.000(1)	0.014(1)	0.002(1)
C(7)	0.0176(9)	0.0157(9)	0.0188(9)	-0.0011(7)	0.0122(8)	0.0008(7)
C(8)	0.0165(9)	0.0144(9)	0.0182(9)	-0.0007(7)	0.0127(8)	-0.0003(7)
C(9)	0.0174(9)	0.0159(9)	0.0143(8)	-0.0026(7)	0.0092(8)	-0.0029(7)
C(10)	0.0162(9)	0.0159(9)	0.0122(8)	-0.0017(7)	0.0079(7)	0.0007(7)
C(11)	0.0212(9)	0.0175(9)	0.0164(9)	-0.0016(7)	0.0106(8)	-0.0030(7)
C(12)	0.0199(9)	0.0298(11)	0.0200(9)	-0.0014(8)	0.0133(8)	-0.0053(8)
C(13)	0.0176(9)	0.0282(11)	0.0172(9)	-0.0045(8)	0.0106(8)	-0.0024(8)
C(14)	0.0158(9)	0.0204(9)	0.0128(8)	-0.0011(7)	0.0072(7)	0.0016(7)
C(15)	0.0198(9)	0.0202(10)	0.0176(9)	-0.0035(7)	0.0104(8)	0.0015(7)
C(16)	0.024(1)	0.016(1)	0.017(1)	-0.002(1)	0.010(1)	0.000(1)
C(17)	0.023(1)	0.019(1)	0.019(1)	0.003(1)	0.012(1)	-0.001(1)

C(18)	0.0176(9)	0.0192(9)	0.0147(8)	0.0009(7)	0.0097(8)	0.0019(7)
C(19)	0.0153(9)	0.0178(9)	0.0121(8)	0.0010(7)	0.0076(7)	0.0023(7)
N(1)	0.0191(8)	0.0133(7)	0.0124(7)	-0.0016(6)	0.0083(6)	-0.0004(6)
N(2)	0.0208(8)	0.0132(7)	0.0149(7)	-0.0022(6)	0.0102(7)	0.0007(6)
O(1)	0.0277(7)	0.0181(7)	0.0163(6)	-0.0021(6)	0.0112(6)	0.0012(5)
S(1)	0.0250(3)	0.0139(2)	0.0154(2)	0.0006(2)	0.0112(2)	0.0011(2)

**Table A5.4. Complete listing of bond lengths (Å) for *N*-BFPTH.**

<b>Bond</b>	<b>Distance</b>	<b>Bond</b>	<b>Distance</b>
C(1)-C(6)	1.395(3)	C(14)-C(13)	1.416(3)
C(1)-C(7)	1.489(3)	C(14)-C(15)	1.420(3)
C(2)-C(1)	1.393(3)	C(15)-C(16)	1.366(3)
C(2)-C(3)	1.386(3)	C(15)-H(15)	0.950(2)
C(2)-H(2A)	0.950(2)	C(16)-H(16)	0.950(2)
C(3)-C(4)	1.392(3)	C(17)-C(16)	1.407(3)
C(3)-H(3)	0.950(2)	C(17)-C(18)	1.372(3)
C(4)-H(4)	0.950(2)	C(17)-H(17)	0.950(2)
C(5)-C(4)	1.385(3)	C(18)-H(18)	0.950(2)
C(5)-C(6)	1.385(3)	C(19)-C(10)	1.434(3)
C(5)-H(5)	0.950(2)	C(19)-C(14)	1.426(3)
C(6)-H(6)	0.950(2)	C(19)-C(18)	1.414(3)
C(9)-H(9A)	0.990(2)	N(1)-C(7)	1.378(3)
C(9)-H(9B)	0.990(2)	N(1)-C(8)	1.396(3)
C(10)-C(11)	1.369(3)	N(1)-H(1)	0.880(2)
C(10)-C(9)	1.515(3)	N(2)-C(8)	1.326(3)
C(11)-C(12)	1.412(3)	N(2)-C(9)	1.455(3)
C(11)-H(11)	0.950(2)	N(2)-H(2)	0.880(2)
C(12)-H(12)	0.950(2)	O(1)-C(7)	1.229(3)
C(13)-C(12)	1.365(3)	S(1)-C(8)	1.676(2)
C(13)-H(13)	0.950(2)		

**Table A5.5. Complete listing of bond angles (°) for *N*-NmTH.**

Angle	Value	Angle	Value
C(1)-C(6)-H(6)	119.9(2)	C(17)-C(16)-H(16)	120.1(2)
C(2)-C(1)-C(6)	119.5(2)	C(17)-C(18)-H(18)	119.4(2)
C(2)-C(1)-C(7)	123.5(2)	C(18)-C(17)-C(16)	120.6(2)
C(2)-C(3)-C(4)	120.0(2)	C(19)-C(10)-C(11)	119.4(2)
C(2)-C(3)-H(3)	120.0(2)	C(19)-C(10)-C(9)	118.6(2)
C(3)-C(2)-C(1)	120.2(2)	C(19)-C(14)-C(13)	119.6(2)
C(3)-C(4)-C(5)	120.0(2)	C(19)-C(14)-C(15)	119.1(2)
C(3)-C(4)-H(4)	120.0(2)	C(19)-C(18)-C(17)	121.2(2)
C(5)-C(4)-H(4)	120.0(2)	C(19)-C(18)-H(18)	119.4(2)
C(5)-C(6)-C(1)	120.2(2)	H(1)-N(1)-C(7)	116.1(2)
C(5)-C(6)-H(6)	119.9(2)	H(1)-N(1)-C(8)	116.0(2)
C(6)-C(5)-C(4)	120.2(2)	H(11)-C(11)-C(12)	119.3(2)
C(7)-C(1)-C(6)	117.0(2)	H(13)-C(13)-C(12)	119.9(2)
C(7)-N(1)-C(8)	127.9(2)	H(15)-C(15)-C(16)	119.5(2)
C(9)-C(10)-C(11)	122.1(2)	H(17)-C(17)-C(16)	119.7(2)
C(9)-N(2)-C(8)	123.0(2)	H(17)-C(17)-C(18)	119.7(2)
C(10)-C(11)-C(12)	121.4(2)	H(2)-N(2)-C(8)	118.5(2)
C(10)-C(11)-H(11)	119.3(2)	H(2)-N(2)-C(9)	118.5(2)
C(10)-C(19)-C(18)	122.9(2)	H(2A)-C(2)-C(1)	119.9(2)
C(10)-C(9)-H(9A)	108.7(2)	H(2A)-C(2)-C(3)	119.9(2)
C(10)-C(9)-H(9B)	108.7(2)	H(3)-C(3)-C(4)	120.0(2)
C(11)-C(12)-H(12)	119.8(2)	H(5)-C(5)-C(4)	119.9(2)
C(13)-C(12)-C(11)	120.5(2)	H(5)-C(5)-C(6)	119.9(2)
C(13)-C(12)-H(12)	119.8(2)	H(9A)-C(9)-H(9B)	107.6(2)
C(14)-C(13)-C(12)	120.2(2)	N(1)-C(7)-C(1)	115.8(2)
C(14)-C(13)-H(13)	119.9(2)	N(1)-C(8)-N(2)	117.4(2)
C(14)-C(15)-C(16)	121.1(2)	N(2)-C(9)-C(10)	114.3(2)
C(14)-C(15)-H(15)	119.5(2)	N(2)-C(9)-H(9A)	108.7(2)
C(14)-C(19)-C(10)	118.9(2)	N(2)-C(9)-H(9B)	108.7(2)
C(14)-C(19)-C(18)	118.2(2)	O(1)-C(7)-C(1)	122.1(2)
C(15)-C(14)-C(13)	121.2(2)	O(1)-C(7)-N(1)	122.1(2)
C(15)-C(16)-C(17)	119.8(2)	S(1)-C(8)-N(1)	118.1(2)
C(15)-C(16)-H(16)	120.1(2)	S(1)-C(8)-N(2)	124.5(2)

## A6. Crystal data of *N*-benzoyl-*N'*-cyclohexylthiourea (*N*-CyTH)

**Table A6.1. Atomic coordinates and equivalent isotropic displacement parameters ( $\text{\AA}^2$ ) for *N*-CyTH.  $U_{\text{(eq)}}$  is defined as one third of the trace of the orthogonalized  $U^{\text{ij}}$  tensor.**

Atom	x/a	y/b	z/c	$U_{\text{(eq)}}$
C(1)	-0.2085(4)	1.0574(1)	0.7815(1)	0.02553
C(1')	0.1050(3)	0.4778(1)	0.7114(1)	0.02107
C(2)	-0.1856(4)	1.1092(1)	0.7018(1)	0.02996
C(2')	0.1080(4)	0.4288(1)	0.7918(1)	0.02549
C(3)	-0.3733(4)	1.1763(1)	0.6737(1)	0.03136
C(3')	-0.0430(4)	0.3590(1)	0.8246(1)	0.02944
C(4)	-0.5859(4)	1.1920(1)	0.7247(1)	0.02973
C(4')	-0.2008(4)	0.3386(1)	0.7783(1)	0.0298
C(5)	-0.6098(4)	1.1403(1)	0.8040(1)	0.02856
C(5')	-0.2074(3)	0.3878(1)	0.6989(1)	0.02705
C(6)	-0.4217(4)	1.0730(1)	0.8326(1)	0.0259
C(6')	-0.0538(3)	0.4571(1)	0.6653(1)	0.02295
C(7)	-0.0042(4)	0.9837(1)	0.8064(1)	0.02707
C(7')	0.2687(3)	0.5529(1)	0.6804(1)	0.0227
C(8)	0.1799(3)	0.8851(1)	0.9260(1)	0.01929
C(8')	0.5439(3)	0.6270(1)	0.5612(1)	0.02435
C(9)	0.4403(3)	0.7408(1)	0.9156(1)	0.01786
C(9')	0.7949(4)	0.7454(2)	0.5772(1)	0.03539
C(10)	0.4396(3)	0.6809(1)	0.8579(1)	0.02031
C(10')	0.8494(5)	0.7713(2)	0.6514(2)	0.04182
C(11)	0.5546(3)	0.5823(1)	0.8924(1)	0.02275
C(11')	1.0322(8)	0.8272(3)	0.6419(2)	0.03196
C(11A)	0.6491(13)	0.8532(3)	0.6660(3)	0.04942
C(12)	0.8141(3)	0.5821(1)	0.9135(1)	0.02424
C(12')	0.9661(8)	0.9168(3)	0.5805(3)	0.03312
C(12A)	0.5968(11)	0.9332(3)	0.5978(3)	0.04819
C(13)	0.8151(3)	0.6460(1)	0.9681(1)	0.02291
C(13')	0.9168(8)	0.8944(3)	0.5035(2)	0.03064
C(13A)	0.5359(9)	0.8986(3)	0.5290(3)	0.03907
C(14)	0.7034(3)	0.7445(1)	0.9316(1)	0.02123
C(14')	0.7284(5)	0.8312(2)	0.5126(2)	0.0474
N(1)	0.0301(3)	0.9604(1)	0.8863(1)	0.02109
N(1')	0.3707(3)	0.5662(1)	0.6012(1)	0.02108
N(2)	0.3120(3)	0.8320(1)	0.8822(1)	0.01938
N(2')	0.5942(3)	0.6848(1)	0.6014(1)	0.03333

O(1)	0.1227(3)	0.9456(1)	0.7580(1)	0.04216
O(1')	0.3107(3)	0.5992(1)	0.7239(1)	0.03291
S(1)	0.17851(9)	0.86514(3)	1.02542(2)	0.02465
S(1')	0.68349(9)	0.61982(3)	0.47052(3)	0.0262

**Table A6.2. Hydrogen coordinates and isotropic displacement parameters ( $\text{\AA}^2$ ) for *N*-CyTH.**

Atom	x/a	y/b	z/c	$U_{\text{(eq)}}$
H(1)	-0.05137	0.9972	0.91512	0.02531
H(1')	0.32126	0.53303	0.57335	0.02529
H(2)	0.32347	0.8528	0.82973	0.02326
H(2')	0.49891	0.68679	0.64635	0.04
H(2A)	-0.04102	1.0983	0.66681	0.03596
H(2A')	0.21356	0.44355	0.82373	0.03059
H(3)	-0.35668	1.21177	0.61962	0.03763
H(3')	-0.03879	0.32495	0.87883	0.03533
H(4)	-0.71477	1.23787	0.70531	0.03567
H(4')	-0.30481	0.29077	0.80118	0.03576
H(5)	-0.75509	1.15111	0.83873	0.03427
H(5')	-0.31682	0.37402	0.66763	0.03245
H(6)	-0.43843	1.03775	0.88675	0.03107
H(6')	-0.05698	0.49043	0.61077	0.02755
H(9)	0.34384	0.71216	0.96754	0.02143
H(9')	0.94654	0.71022	0.55603	0.04247
H(10A)	0.53451	0.70797	0.80595	0.02437
H(10B)	0.2676	0.67958	0.84835	0.02437
H(10C)	0.694(4)	0.809(2)	0.670(2)	0.03143
H(10D)	0.878(4)	0.713(1)	0.693(1)	0.03143
H(11A)	0.44866	0.55283	0.94112	0.02731
H(11B)	0.5632	0.54561	0.85277	0.02731
H(11C)	1.19289	0.7964	0.6233	0.03835
H(11D)	1.0463	0.84014	0.69357	0.03835
H(11E)	0.49155	0.82657	0.68858	0.0593
H(11F)	0.70079	0.87714	0.7078	0.0593
H(12A)	0.92623	0.60258	0.86366	0.02909
H(12B)	0.87714	0.51831	0.9407	0.02909
H(12C)	1.1037	0.9559	0.56817	0.03974
H(12D)	0.8169	0.9513	0.60227	0.03974
H(12E)	0.74272	0.96828	0.57978	0.05783
H(12F)	0.45546	0.97504	0.61457	0.05783

H(13A)	0.7195	0.62108	1.02051	0.0275
H(13B)	0.98728	0.64735	0.97754	0.0275
H(13C)	0.86653	0.95332	0.46518	0.03676
H(13D)	1.0744	0.86724	0.47928	0.03676
H(13E)	0.3769	0.87138	0.54427	0.04688
H(13F)	0.52047	0.95078	0.48084	0.04688
H(14A)	0.70079	0.78363	0.96898	0.02548
H(14B)	0.80436	0.77167	0.88093	0.02548
H(14C)	0.7261(5)	0.8146(3)	0.4603(7)	0.05687
H(14D)	0.559(2)	0.862(0)	0.528(0)	0.05687

**Table A6.3. Anisotropic displacement parameters ( $\text{\AA}^2$ ) for *N*-CyTH. The anisotropic displacement factor exponent takes the form:  $-2\pi^2[h^2a^{*2}U^{11} + \dots + 2hka^*b^*U^{23}]$ .**

Atom	$U^{11}$	$U^{22}$	$U^{33}$	$U^{12}$	$U^{13}$	$U^{23}$
C(1)	0.035(1)	0.024(1)	0.019(1)	0.006(1)	-0.008(1)	-0.008(1)
C(1')	0.0224(8)	0.0214(8)	0.0190(8)	0.0022(7)	-0.0016(6)	-0.0072(7)
C(2)	0.040(1)	0.029(1)	0.019(1)	0.008(1)	-0.006(1)	-0.008(1)
C(2')	0.031(1)	0.027(1)	0.019(1)	0.002(1)	-0.004(1)	-0.009(1)
C(3)	0.046(1)	0.027(1)	0.021(1)	0.005(1)	-0.012(1)	-0.006(1)
C(3')	0.040(1)	0.026(1)	0.019(1)	0.002(1)	0.000(1)	-0.004(1)
C(4)	0.033(1)	0.024(1)	0.033(1)	0.006(1)	-0.015(1)	-0.009(1)
C(4')	0.031(1)	0.026(1)	0.030(1)	-0.003(1)	0.004(1)	-0.006(1)
C(5')	0.0228(9)	0.0285(10)	0.0302(10)	-0.0002(7)	-0.0048(7)	-0.0085(8)
C(5)	0.028(1)	0.028(1)	0.031(1)	0.001(1)	-0.007(1)	-0.010(1)
C(6)	0.031(1)	0.025(1)	0.022(1)	0.000(1)	-0.006(1)	-0.006(1)
C(6')	0.0221(8)	0.0246(9)	0.0207(8)	0.0018(7)	-0.0041(7)	-0.0047(7)
C(7')	0.0244(9)	0.0241(9)	0.0207(8)	0.0006(7)	-0.0037(7)	-0.0087(7)
C(7)	0.036(1)	0.026(1)	0.017(1)	0.007(1)	-0.004(1)	-0.006(1)
C(8)	0.0214(8)	0.0183(8)	0.0174(8)	-0.0020(6)	-0.0010(6)	-0.0039(6)
C(8')	0.0282(9)	0.0172(8)	0.0267(9)	0.0000(7)	-0.0005(7)	-0.0068(7)
C(9')	0.041(1)	0.032(1)	0.038(1)	-0.004(1)	-0.007(1)	-0.015(1)
C(9)	0.0198(8)	0.0163(8)	0.0169(8)	0.0001(6)	-0.0025(6)	-0.0041(6)
C(10)	0.0222(8)	0.0201(8)	0.0204(8)	-0.0010(7)	-0.0053(6)	-0.0072(7)
C(10')	0.047(1)	0.045(1)	0.043(1)	0.005(1)	-0.017(1)	-0.027(1)
C(11)	0.0272(9)	0.0178(8)	0.0254(9)	-0.0009(7)	-0.0072(7)	-0.0075(7)
C(11')	0.034(2)	0.037(2)	0.028(2)	-0.013(2)	0.002(2)	-0.011(2)
C(11A)	0.087(4)	0.026(2)	0.037(2)	0.007(2)	-0.008(2)	-0.017(2)
C(12)	0.0249(9)	0.0221(9)	0.0268(9)	0.0035(7)	-0.0059(7)	-0.0097(7)
C(12')	0.038(2)	0.029(2)	0.035(2)	-0.014(2)	0.004(2)	-0.014(2)
C(12A)	0.065(3)	0.037(3)	0.043(3)	-0.007(2)	-0.003(2)	-0.013(2)

C(13)	0.0203(8)	0.0258(9)	0.0248(9)	0.0007(7)	-0.0072(7)	-0.0093(7)
C(13')	0.036(2)	0.024(2)	0.028(2)	-0.007(2)	0.004(2)	-0.003(2)
C(13A)	0.041(2)	0.044(3)	0.038(2)	0.006(2)	-0.008(2)	-0.023(2)
C(14)	0.0202(8)	0.0217(9)	0.0241(8)	-0.0030(7)	-0.0030(7)	-0.0092(7)
C(14')	0.051(1)	0.038(1)	0.057(2)	-0.001(1)	-0.020(1)	-0.014(1)
N(1)	0.0273(8)	0.0195(7)	0.0144(7)	0.0047(6)	-0.0017(6)	-0.0051(6)
N(1')	0.0264(8)	0.0196(7)	0.0189(7)	-0.0036(6)	-0.0034(6)	-0.0067(6)
N(2')	0.0372(9)	0.0310(9)	0.0358(9)	-0.0079(7)	0.0066(7)	-0.0190(8)
N(2)	0.0233(7)	0.0186(7)	0.0145(6)	0.0015(6)	-0.0012(5)	-0.0037(5)
O(1)	0.061(1)	0.040(1)	0.017(1)	0.026(1)	-0.005(1)	-0.009(1)
O(1')	0.0372(8)	0.0395(8)	0.0290(7)	-0.0090(6)	0.0010(6)	-0.0206(6)
S(1)	0.0367(3)	0.0207(2)	0.0146(2)	0.0053(2)	-0.0038(2)	-0.0049(2)
S(1')	0.0376(3)	0.0180(2)	0.0209(2)	-0.0057(2)	0.0023(2)	-0.0031(2)

**Table A6.4. Complete listing of bond lengths (Å) for N-CyTH.**

Bond	Distance	Bond	Distance
C(1)-C(2)	1.396(3)	C(10')-C(11')	1.369(5)
C(1')-C(2')	1.400(3)	C(10)-H(10A)	0.990(2)
C(1)-C(6)	1.395(3)	C(10)-H(10B)	0.990(2)
C(1')-C(6')	1.393(3)	C(10')-H(10C)	1.01(3)
C(1)-C(7)	1.490(3)	C(10')-H(10D)	0.98(2)
C(1')-C(7')	1.485(3)	C(11)-C(12)	1.528(3)
C(2)-C(3)	1.385(4)	C(11')-C(12')	1.518(7)
C(2')-C(3')	1.383(3)	C(11)-H(11A)	0.990(2)
C(2)-H(2A)	0.950(3)	C(11)-H(11B)	0.990(2)
C(2')-H(2A')	0.950(2)	C(11')-H(11C)	0.990(5)
C(3)-C(4)	1.391(4)	C(11')-H(11D)	0.990(4)
C(3')-C(4')	1.388(3)	C(11A)-C(12A)	1.479(8)
C(3)-H(3)	0.950(3)	C(11A)-H(10C)	0.67(3)
C(3')-H(3')	0.950(2)	C(11A)-H(11E)	0.990(7)
C(4)-C(5)	1.390(3)	C(11A)-H(11F)	0.990(6)
C(4')-C(5')	1.389(3)	C(12)-C(13)	1.531(3)
C(4)-H(4)	0.950(3)	C(12)-H(12A)	0.990(2)
C(4')-H(4')	0.950(3)	C(12)-H(12B)	0.990(2)
C(5)-C(6)	1.391(3)	C(12')-H(12C)	0.990(5)
C(5')-C(6')	1.388(3)	C(12')-H(12D)	0.990(5)
C(5)-H(5)	0.950(3)	C(12A)-C(13A)	1.530(7)
C(5')-H(5')	0.950(2)	C(12A)-H(12E)	0.990(6)
C(6)-H(6)	0.950(2)	C(12A)-H(12F)	0.990(6)
C(6')-H(6')	0.950(2)	C(13)-C(14)	1.530(3)
C(7)-N(1)	1.379(3)	C(13')-C(14')	1.471(5)

C(7')-N(1')	1.384(3)	C(13)-H(13A)	0.990(2)
C(7)-O(1)	1.225(3)	C(13)-H(13B)	0.990(2)
C(7')-O(1')	1.228(3)	C(13')-H(13C)	0.990(5)
C(8)-N(1)	1.390(3)	C(13')-H(13D)	0.990(5)
C(8')-N(1')	1.394(3)	C(13A)-C(14')	1.413(6)
C(8)-N(2)	1.324(3)	C(13A)-H(13E)	0.990(5)
C(8')-N(2')	1.339(3)	C(13A)-H(13F)	0.990(5)
C(8)-S(1)	1.679(2)	C(13A)-H(14D)	0.557(8)
C(8')-S(1')	1.677(2)	C(14)-H(14A)	0.990(2)
C(9)-C(10)	1.526(3)	C(14)-H(14B)	0.990(2)
C(9')-C(10')	1.534(4)	C(14')-H(14C)	1.014(12)
C(9)-C(14)	1.527(3)	C(14')-H(14D)	1.014(11)
C(9')-C(14')	1.512(4)	N(1')-H(1')	0.880(2)
C(9)-H(9)	1.000(2)	N(2)-H(2)	0.880(2)
C(9')-H(9')	1.000(3)	N(1)-H(1)	0.880(2)
C(9)-N(2)	1.465(3)	N(2')-H(2')	0.880(2)
C(10)-C(11)	1.530(3)		

**Table A6.5. Complete listing of bond angles (°) for *N*-CyTH.**

Angle	Value	Angle	Value
C(1)-C(2)-C(3)	120.1(2)	C(12)-C(13)-H(13A)	109.3(2)
C(1')-C(2')-C(3')	119.9(2)	C(12)-C(13)-H(13B)	109.3(2)
C(1)-C(2)-H(2A)	120.0(2)	C(12')-H(12D)-H(12E)	115.8(3)
C(1')-C(2')-H(2A')	120.0(2)	C(12A)-C(11A)-H(10C)	134.6(23)
C(1)-C(6)-C(5)	119.8(2)	C(12A)-C(13A)-C(14')	108.4(4)
C(1')-C(6')-C(5')	120.0(2)	C(12A)-C(13A)-H(13E)	110.0(5)
C(1)-C(6)-H(6)	120.1(2)	C(12A)-C(13A)-H(13F)	110.0(5)
C(1')-C(6')-H(6')	120.0(2)	C(12A)-C(13A)-H(14D)	121.2(10)
C(1)-C(7)-N(1)	116.4(2)	C(13')-C(14')-C(13A)	91.8(3)
C(1')-C(7')-N(1')	116.3(2)	C(13)-C(14)-H(14A)	110.0(2)
C(1)-C(7)-O(1)	121.1(2)	C(13)-C(14)-H(14B)	110.0(2)
C(1')-C(7')-O(1')	120.9(2)	C(13')-C(14')-H(14C)	110.2(5)
C(2)-C(1)-C(6)	119.8(2)	C(13')-C(14')-H(14D)	110.2(6)
C(2')-C(1')-C(6')	119.8(2)	C(13A)-C(14')-H(14C)	114.4(4)
C(2)-C(1)-C(7)	117.0(2)	C(13A)-C(14')-H(14D)	18.7(5)
C(2')-C(1')-C(7')	117.1(2)	C(13A)-H(14D)-C(14')	125.7(16)
C(2)-C(3)-C(4)	120.1(2)	C(14')-C(13A)-H(14D)	35.7(12)
C(2')-C(3')-C(4')	120.1(2)	C(14)-C(9)-N(2)	113.4(2)
C(2)-C(3)-H(3)	120.0(3)	H(10A)-C(10)-C(11)	109.5(2)
C(2')-C(3')-H(3')	119.9(2)	H(10A)-C(10)-H(10B)	108.1(2)
C(3)-C(4)-C(5)	120.0(2)	H(10B)-C(10)-C(11)	109.5(2)



C(3')-C(4')-C(5')	120.3(2)	H(10C)-C(10')-H(10D)	109.5(20)
C(3)-C(4)-H(4)	120.0(2)	H(11A)-C(11)-C(12)	109.4(2)
C(3')-C(4')-H(4')	119.8(2)	H(11A)-C(11)-H(11B)	108.0(2)
C(4)-C(5)-C(6)	120.2(2)	H(11B)-C(11)-C(12)	109.4(2)
C(4')-C(5')-C(6')	119.9(2)	H(11C)-C(11')-C(12')	110.1(4)
C(4)-C(5)-H(5)	119.9(2)	H(11C)-C(11')-H(11D)	108.4(4)
C(4')-C(5')-H(5')	120.0(2)	H(11D)-C(11')-C(12')	110.1(4)
C(5)-C(6)-H(6)	120.1(2)	H(11E)-C(11A)-C(12A)	107.5(6)
C(5')-C(6')-H(6')	120.0(2)	H(11E)-C(11A)-H(10C)	83.4(19)
C(6)-C(1)-C(7)	123.1(2)	H(11E)-C(11A)-H(11F)	107.0(5)
C(6')-C(1')-C(7')	123.1(2)	H(11F)-C(11A)-C(12A)	107.5(5)
C(7)-N(1)-C(8)	126.9(2)	H(11F)-C(11A)-H(10C)	110.9(22)
C(7')-N(1')-C(8')	126.4(2)	H(12A)-C(12)-C(13)	109.3(2)
C(7)-N(1)-H(1)	116.6(2)	H(12A)-C(12)-H(12B)	108.0(2)
C(7')-N(1')-H(1')	116.8(2)	H(12B)-C(12)-C(13)	109.3(2)
C(8)-N(1)-H(1)	116.6(2)	H(12C)-C(12')-H(12D)	108.3(4)
C(8')-N(1')-H(1')	116.8(2)	H(12D)-H(12E)-C(12A)	107.5(4)
C(8)-N(2)-C(9)	124.1(2)	H(12E)-C(12A)-C(13A)	109.8(5)
C(8)-N(2)-H(2)	118.0(2)	H(12E)-C(12A)-H(12F)	108.2(5)
C(8')-N(2')-H(2')	117.1(2)	H(12F)-C(12A)-C(13A)	109.8(5)
C(9)-C(10)-C(11)	110.5(2)	H(13A)-C(13)-C(14)	109.3(2)
C(9')-C(10')-C(11')	117.9(3)	H(13A)-C(13)-H(13B)	107.9(2)
C(9)-C(10)-H(10A)	109.6(2)	H(13B)-C(13)-C(14)	109.3(2)
C(9)-C(10)-H(10B)	109.6(2)	H(13C)-C(13')-C(14')	108.1(4)
C(9')-C(10')-H(10C)	106.2(14)	H(13C)-C(13')-H(13D)	107.3(4)
C(9')-C(10')-H(10D)	107.0(12)	H(13D)-C(13')-C(14')	108.1(4)
C(9)-C(14)-C(13)	108.6(2)	H(13E)-C(13A)-C(14')	110.0(5)
C(9')-C(14')-C(13')	107.4(3)	H(13E)-C(13A)-H(13F)	108.4(5)
C(9')-C(14')-C(13A)	120.6(3)	H(13E)-C(13A)-H(14D)	74.4(13)
C(9)-C(14)-H(14A)	110.0(2)	H(13F)-C(13A)-C(14')	110.0(4)
C(9)-C(14)-H(14B)	110.0(2)	H(13F)-C(13A)-H(14D)	124.3(9)
C(9')-C(14')-H(14C)	110.2(5)	H(14A)-C(14)-H(14B)	108.4(2)
C(9')-C(14')-H(14D)	110.2(4)	H(14C)-C(14')-H(14D)	108.5(5)
C(9)-N(2)-H(2)	118.0(2)	H(2A)-C(2)-C(3)	119.9(2)
C(10)-C(11)-C(12)	111.1(2)	H(2A')-C(2')-C(3')	120.1(2)
C(10')-C(11')-C(12')	108.1(4)	H(3)-C(3)-C(4)	120.0(3)
C(10)-C(11)-H(11A)	109.4(2)	H(3')-C(3')-C(4')	119.9(2)
C(10)-C(11)-H(11B)	109.4(2)	H(4)-C(4)-C(5)	120.0(2)
C(10')-C(11')-H(11C)	110.1(4)	H(4')-C(4')-C(5')	119.9(2)
C(10')-C(11')-H(11D)	110.1(4)	H(5)-C(5)-C(6)	119.9(2)
C(10)-C(9)-C(14)	110.9(2)	H(5')-C(5')-C(6')	120.0(2)

C(10')-C(9')-C(14')	110.6(2)	H(9)-C(9)-C(10)	108.1(2)
C(10)-C(9)-N(2)	108.0(2)	H(9')-C(9')-C(10')	108.7(3)
C(10')-H(10C)-C(11A)	139.2(31)	H(9)-C(9)-C(14)	108.1(2)
C(11')-C(10')-H(10C)	104.0(14)	H(9')-C(9')-C(14')	108.6(2)
C(11')-C(10')-H(10D)	111.9(14)	H(9)-C(9)-N(2)	108.1(2)
C(11)-C(12)-C(13)	111.5(2)	N(1)-C(7)-O(1)	122.6(2)
C(11)-C(12)-H(12A)	109.3(2)	N(1')-C(7')-O(1')	122.8(2)
C(11)-C(12)-H(12B)	109.3(2)	N(1)-C(8)-N(2)	116.9(2)
C(11')-C(12')-H(12C)	109.8(4)	N(1')-C(8')-N(2')	115.8(2)
C(11')-C(12')-H(12D)	109.8(4)	N(1)-C(8)-S(1)	119.0(2)
C(11A)-C(12A)-C(13A)	109.3(5)	N(1')-C(8')-S(1')	119.2(2)
C(11A)-C(12A)-H(12E)	109.8(6)	N(2)-C(8)-S(1)	124.1(2)
C(11A)-C(12A)-H(12F)	109.8(5)	N(2')-C(8')-S(1')	124.9(2)
C(12)-C(13)-C(14)	111.7(2)		

## A7. Crystal data of *N*-benzoyl-*N'*-isopentylthiourea (*N*-ipTH)

**Table A7.1. Atomic coordinates and equivalent isotropic displacement parameters ( $\text{\AA}^2$ ) for *N*-ipTH.  $U_{\text{(eq)}}$  is defined as one third of the trace of the orthogonalized  $U^{\text{ij}}$  tensor.**

Atom	x/a	y/b	z/c	$U_{\text{(eq)}}$
C(1)	0.8171(2)	0.3614(2)	0.5121(1)	0.01717
C(1')	0.3960(2)	-0.3481(2)	0.1194(1)	0.0163
C(2)	0.9609(2)	0.3443(2)	0.5284(2)	0.01928
C(2')	0.2712(2)	-0.4453(2)	0.1046(1)	0.01867
C(3)	1.0737(2)	0.4300(2)	0.6163(2)	0.02116
C(3')	0.1901(2)	-0.5317(2)	0.0047(2)	0.02308
C(4)	1.0430(2)	0.5321(2)	0.6877(2)	0.02244
C(4')	0.2339(2)	-0.5216(2)	-0.0798(2)	0.02505
C(5)	0.9001(2)	0.5478(2)	0.6725(2)	0.02021
C(5')	0.3579(2)	-0.4250(2)	-0.0651(2)	0.02352
C(6)	0.7862(2)	0.4624(2)	0.5842(1)	0.01845
C(6')	0.4382(2)	-0.3374(2)	0.0339(2)	0.02039
C(7)	0.6994(2)	0.2664(2)	0.4168(1)	0.01699
C(7')	0.4827(2)	-0.2510(2)	0.2245(1)	0.01774
C(8)	0.4806(2)	0.2601(2)	0.2755(1)	0.01672
C(8')	0.58995(19)	-0.23682(18)	0.40835(14)	0.01606
C(9)	0.3080(2)	0.0479(2)	0.1563(1)	0.01822
C(9')	0.6958(2)	-0.0202(2)	0.5487(1)	0.01834
C(10)	0.3355(2)	0.0071(2)	0.0515(1)	0.01958
C(10')	0.8642(2)	0.0129(2)	0.5780(1)	0.01807
C(11)	0.1939(2)	-0.0576(2)	-0.0414(1)	0.02128
C(11')	0.9418(2)	0.0812(2)	0.6948(1)	0.01885
C(12)	0.2323(2)	-0.1011(2)	-0.1427(2)	0.02782
C(12')	0.8878(2)	0.2038(2)	0.7409(2)	0.02151
C(13)	0.0963(2)	-0.1759(2)	-0.0306(2)	0.02569
C(13')	1.1095(2)	0.1178(2)	0.7163(2)	0.02449
N(1)	0.60578(16)	0.32409(15)	0.36233(11)	0.01674
N(1')	0.51726(17)	-0.30481(15)	0.30216(11)	0.01754
N(2)	0.44134(17)	0.12826(14)	0.24220(11)	0.01772
N(2')	0.62413(17)	-0.10488(15)	0.44021(12)	0.01786
O(1)	0.68891(15)	0.14603(13)	0.38801(10)	0.02442
O(1')	0.52174(15)	-0.13126(12)	0.24005(10)	0.02191
S(1)	0.38963(5)	0.35346(5)	0.21886(4)	0.02016
S(1')	0.62818(5)	-0.32650(5)	0.48625(4)	0.01979

**Table A7.2. Hydrogen coordinates and isotropic displacement parameters ( $\text{\AA}^2$ ) for *N*-ipTH.**

Atom	x/a	y/b	z/c	$U_{\text{(eq)}}$
H(1)	0.62772	0.41182	0.38511	0.02008
H(1')	0.49038	-0.39229	0.28252	0.02105
H(2)	0.49866	0.08665	0.27352	0.02126
H(2')	0.60239	-0.06633	0.39337	0.02144
H(2A)	0.98153	0.27416	0.47938	0.02314
H(2A')	0.24179	-0.45242	0.16258	0.0224
H(3)	1.17186	0.4189	0.62759	0.0254
H(3')	0.10462	-0.59769	-0.00579	0.0277
H(4)	1.12053	0.59158	0.74743	0.02692
H(4')	0.17868	-0.58123	-0.14805	0.03006
H(5)	0.8795	0.61701	0.72224	0.02425
H(5')	0.38787	-0.41893	-0.1232	0.02822
H(6)	0.68796	0.47318	0.57362	0.02215
H(6')	0.52198	-0.26995	0.04375	0.02447
H(9A)	0.23153	0.09951	0.15352	0.02186
H(9B)	0.26901	-0.03324	0.16987	0.02186
H(9C)	0.66445	-0.06586	0.59409	0.02201
H(9D)	0.66289	0.06376	0.56139	0.02201
H(10A)	0.39948	-0.05632	0.05069	0.02349
H(10B)	0.38992	0.08701	0.04346	0.02349
H(10C)	0.89621	0.07184	0.54132	0.02169
H(10D)	0.89572	-0.07049	0.55371	0.02169
H(11)	0.13585	0.01097	-0.04432	0.02554
H(11')	0.91899	0.01589	0.72974	0.02262
H(12A)	0.1408	-0.14184	-0.20159	0.04173
H(12B)	0.29236	-0.16614	-0.14071	0.04173
H(12C)	0.28819	-0.02322	-0.15104	0.04173
H(12D)	0.94013	0.24392	0.81586	0.03227
H(12E)	0.7811	0.17724	0.72958	0.03227
H(12F)	0.90749	0.26881	0.70702	0.03227
H(13A)	0.00724	-0.21419	-0.09159	0.03854
H(13B)	0.06754	-0.1453	0.03251	0.03854
H(13C)	0.15164	-0.24383	-0.02603	0.03854
H(13D)	1.15864	0.16202	0.79133	0.03673
H(13E)	1.13432	0.17826	0.67971	0.03673
H(13F)	1.14297	0.03675	0.69159	0.03673

**Table A7.3. Anisotropic displacement parameters ( $\text{\AA}^2$ ) for *N*-ipTH. The anisotropic displacement factor exponent takes the form:  $-2\pi^2[h^2a^{*2}U^{11} + \dots + 2hka^*b^*U^{23}]$ .**

Atom	$U^{11}$	$U^{22}$	$U^{33}$	$U^{12}$	$U^{13}$	$U^{23}$
C(1')	0.0172(9)	0.0133(9)	0.0162(9)	0.0048(7)	0.0014(7)	0.0046(7)
C(1)	0.022(1)	0.013(1)	0.018(1)	0.002(1)	0.006(1)	0.009(1)
C(2)	0.023(1)	0.016(1)	0.022(1)	0.006(1)	0.009(1)	0.009(1)
C(2')	0.023(1)	0.016(1)	0.018(1)	0.006(1)	0.005(1)	0.008(1)
C(3)	0.017(1)	0.023(1)	0.027(1)	0.005(1)	0.006(1)	0.014(1)
C(3')	0.021(1)	0.018(1)	0.026(1)	0.001(1)	0.002(1)	0.008(1)
C(4)	0.021(1)	0.021(1)	0.021(1)	-0.001(1)	0.000(1)	0.010(1)
C(4')	0.030(1)	0.019(1)	0.019(1)	0.005(1)	0.000(1)	0.004(1)
C(5')	0.030(1)	0.024(1)	0.019(1)	0.011(1)	0.009(1)	0.010(1)
C(5)	0.025(1)	0.017(1)	0.017(1)	0.005(1)	0.005(1)	0.006(1)
C(6)	0.018(1)	0.017(1)	0.021(1)	0.004(1)	0.005(1)	0.009(1)
C(6')	0.019(1)	0.017(1)	0.026(1)	0.004(1)	0.007(1)	0.011(1)
C(7')	0.0153(9)	0.0176(9)	0.0214(10)	0.0045(7)	0.0058(8)	0.0081(8)
C(7)	0.021(1)	0.016(1)	0.015(1)	0.005(1)	0.007(1)	0.006(1)
C(8')	0.0129(9)	0.0166(9)	0.0181(9)	0.0028(7)	0.0046(7)	0.0058(8)
C(8)	0.0190(9)	0.0181(9)	0.0137(9)	0.0023(7)	0.0078(7)	0.0052(7)
C(9')	0.020(1)	0.016(1)	0.016(1)	0.003(1)	0.005(1)	0.002(1)
C(9)	0.018(1)	0.015(1)	0.019(1)	0.002(1)	0.004(1)	0.005(1)
C(10')	0.018(1)	0.017(1)	0.017(1)	0.003(1)	0.005(1)	0.004(1)
C(10)	0.022(1)	0.016(1)	0.018(1)	0.002(1)	0.005(1)	0.005(1)
C(11)	0.024(1)	0.018(1)	0.019(1)	0.006(1)	0.003(1)	0.005(1)
C(11')	0.019(1)	0.019(1)	0.018(1)	0.002(1)	0.005(1)	0.007(1)
C(12)	0.033(1)	0.027(1)	0.018(1)	0.003(1)	0.003(1)	0.005(1)
C(12')	0.022(1)	0.020(1)	0.017(1)	-0.001(1)	0.005(1)	0.002(1)
C(13')	0.020(1)	0.025(1)	0.023(1)	0.003(1)	0.002(1)	0.006(1)
C(13)	0.021(1)	0.023(1)	0.024(1)	0.000(1)	0.002(1)	0.003(1)
N(1)	0.0199(8)	0.0124(7)	0.0158(8)	0.0014(6)	0.0045(6)	0.0041(6)
N(1')	0.0197(8)	0.0129(8)	0.0167(8)	0.0020(6)	0.0019(6)	0.0044(6)
N(2')	0.0206(8)	0.0133(8)	0.0173(8)	0.0029(6)	0.0022(6)	0.0057(6)
N(2)	0.0226(9)	0.0129(8)	0.0154(8)	0.0028(6)	0.0030(7)	0.0049(6)
O(1)	0.0302(8)	0.0139(7)	0.0236(7)	0.0052(6)	0.0003(6)	0.0055(6)
O(1')	0.0259(7)	0.0141(7)	0.0223(7)	0.0020(5)	0.0020(6)	0.0074(6)
S(1)	0.0220(3)	0.0154(2)	0.0204(3)	0.0041(2)	0.0019(2)	0.0067(2)
S(1')	0.0229(3)	0.0178(2)	0.0179(2)	0.0031(2)	0.0043(2)	0.0077(2)

**Table A7.4. Complete listing of bond lengths (Å) for *N*-ipTH.**

<b>Bond</b>	<b>Distance</b>	<b>Bond</b>	<b>Distance</b>
C(1)-C(2)	1.396(3)	C(9')-C(10')	1.524(3)
C(1')-C(2')	1.394(3)	C(9)-H(9A)	0.990(2)
C(1)-C(6)	1.386(3)	C(9)-H(9B)	0.990(2)
C(1')-C(6')	1.395(3)	C(9')-H(9C)	0.990(2)
C(1)-C(7)	1.490(3)	C(9')-H(9D)	0.990(2)
C(1')-C(7')	1.484(3)	C(9)-N(2)	1.461(3)
C(2)-C(3)	1.387(3)	C(9')-N(2')	1.457(3)
C(2')-C(3')	1.389(3)	C(10)-C(11)	1.531(3)
C(2)-H(2A)	0.950(2)	C(10')-C(11')	1.525(3)
C(2')-H(2A')	0.950(2)	C(10)-H(10A)	0.990(2)
C(3)-C(4)	1.388(3)	C(10)-H(10B)	0.990(2)
C(3')-C(4')	1.388(3)	C(10')-H(10C)	0.990(2)
C(3)-H(3)	0.950(2)	C(10')-H(10D)	0.990(2)
C(3')-H(3')	0.950(2)	C(11)-C(12)	1.527(3)
C(4)-C(5)	1.382(3)	C(11')-C(12')	1.528(3)
C(4')-C(5')	1.385(3)	C(11)-C(13)	1.533(3)
C(4)-H(4)	0.950(2)	C(11')-C(13')	1.528(3)
C(4')-H(4')	0.950(2)	C(11)-H(11)	1.000(3)
C(5)-C(6)	1.393(3)	C(11')-H(11')	1.000(2)
C(5')-C(6')	1.383(3)	C(12)-H(12A)	0.980(3)
C(5)-H(5)	0.950(2)	C(12)-H(12B)	0.980(3)
C(5')-H(5')	0.950(3)	C(12)-H(12C)	0.980(3)
C(6)-H(6)	0.950(2)	C(12')-H(12D)	0.980(2)
C(6')-H(6')	0.950(2)	C(12')-H(12E)	0.980(2)
C(7)-N(1)	1.379(3)	C(12')-H(12F)	0.980(2)
C(7')-N(1')	1.379(3)	C(13)-H(13A)	0.980(2)
C(7)-O(1)	1.226(3)	C(13)-H(13B)	0.980(3)
C(7')-O(1')	1.229(3)	C(13)-H(13C)	0.980(3)
C(8)-N(1)	1.394(3)	C(13')-H(13D)	0.980(3)
C(8')-N(1')	1.398(3)	C(13')-H(13E)	0.980(3)
C(8)-N(2)	1.323(3)	C(13')-H(13F)	0.980(3)
C(8')-N(2')	1.324(3)	N(1)-H(1)	0.880(2)
C(8)-S(1)	1.680(2)	N(1')-H(1')	0.880(2)
C(8')-S(1')	1.679(2)	N(2)-H(2)	0.880(2)
C(9)-C(10)	1.518(3)	N(2')-H(2')	0.880(2)

**Table A7.5. Complete listing of bond angles (°) for *N*-ipTH.**

Angle	Value	Angle	Value
C(1)-C(2)-C(3)	119.8(2)	C(11)-C(12)-H(12C)	109.5(2)
C(1')-C(2')-C(3')	119.8(2)	C(11')-C(12')-H(12D)	109.5(2)
C(1)-C(2)-H(2A)	120.1(2)	C(11')-C(12')-H(12E)	109.5(2)
C(1')-C(2')-H(2A')	120.1(2)	C(11')-C(12')-H(12F)	109.5(2)
C(1)-C(6)-C(5)	119.6(2)	C(11)-C(13)-H(13A)	109.5(2)
C(1')-C(6')-C(5')	119.9(2)	C(11)-C(13)-H(13B)	109.5(2)
C(1)-C(6)-H(6)	120.2(2)	C(11)-C(13)-H(13C)	109.5(2)
C(1')-C(6')-H(6')	120.0(2)	C(11')-C(13')-H(13D)	109.5(2)
C(1)-C(7)-N(1)	115.2(2)	C(11')-C(13')-H(13E)	109.5(2)
C(1')-C(7')-N(1')	115.5(2)	C(11')-C(13')-H(13F)	109.5(2)
C(1)-C(7)-O(1)	122.2(2)	C(12)-C(11)-C(13)	110.5(2)
C(1')-C(7')-O(1')	121.6(2)	C(12')-C(11')-C(13')	110.8(2)
C(2)-C(1)-C(6)	120.2(2)	H(10A)-C(10)-C(11)	108.8(2)
C(2')-C(1')-C(6')	119.9(2)	H(10A)-C(10)-H(10B)	107.7(2)
C(2)-C(1)-C(7)	117.9(2)	H(10B)-C(10)-C(11)	108.8(2)
C(2')-C(1')-C(7')	121.4(2)	H(10C)-C(10')-C(11')	108.9(2)
C(2)-C(3)-C(4)	119.9(2)	H(10C)-C(10')-H(10D)	107.7(2)
C(2')-C(3')-C(4')	120.0(2)	H(10D)-C(10')-C(11')	108.9(2)
C(2)-C(3)-H(3)	120.1(2)	H(11)-C(11)-C(12)	107.9(2)
C(2')-C(3')-H(3')	120.0(2)	H(11')-C(11')-C(12')	107.9(2)
C(3)-C(4)-C(5)	120.3(2)	H(11)-C(11)-C(13)	107.9(2)
C(3')-C(4')-C(5')	120.3(2)	H(11')-C(11')-C(13')	107.9(2)
C(3)-C(4)-H(4)	119.8(2)	H(12A)-C(12)-H(12B)	109.5(2)
C(3')-C(4')-H(4')	119.9(2)	H(12A)-C(12)-H(12C)	109.5(2)
C(4)-C(5)-C(6)	120.2(2)	H(12B)-C(12)-H(12C)	109.5(3)
C(4')-C(5')-C(6')	120.1(2)	H(12D)-C(12')-H(12E)	109.5(2)
C(4)-C(5)-H(5)	119.9(2)	H(12D)-C(12')-H(12F)	109.5(2)
C(4')-C(5')-H(5')	119.9(2)	H(12E)-C(12')-H(12F)	109.5(2)
C(5)-C(6)-H(6)	120.2(2)	H(13A)-C(13)-H(13B)	109.5(2)
C(5')-C(6')-H(6')	120.0(2)	H(13A)-C(13)-H(13C)	109.5(2)
C(6)-C(1)-C(7)	121.9(2)	H(13B)-C(13)-H(13C)	109.5(2)
C(6')-C(1')-C(7')	118.7(2)	H(13D)-C(13')-H(13E)	109.5(2)
C(7)-N(1)-C(8)	127.8(2)	H(13D)-C(13')-H(13F)	109.5(2)
C(7')-N(1')-C(8')	127.7(2)	H(13E)-C(13')-H(13F)	109.5(2)
C(7)-N(1)-H(1)	116.1(2)	H(2A)-C(2)-C(3)	120.1(2)
C(7')-N(1')-H(1')	116.2(2)	H(2A')-C(2')-C(3')	120.1(2)
C(8)-N(1)-H(1)	116.1(2)	H(3)-C(3)-C(4)	120.1(2)
C(8')-N(1')-H(1')	116.2(2)	H(3')-C(3')-C(4')	120.0(2)
C(8)-N(2)-C(9)	123.6(2)	H(4)-C(4)-C(5)	119.8(2)

C(8')-N(2')-C(9')	123.5(2)	H(4')-C(4')-C(5')	119.9(2)
C(8)-N(2)-H(2)	118.2(2)	H(5)-C(5)-C(6)	119.9(2)
C(8')-N(2')-H(2')	118.3(2)	H(5')-C(5')-C(6')	119.9(2)
C(9)-C(10)-C(11)	113.9(2)	H(9A)-C(9)-C(10)	109.0(2)
C(9')-C(10')-C(11')	113.5(2)	H(9A)-C(9)-H(9B)	107.8(2)
C(9)-C(10)-H(10A)	108.8(2)	H(9A)-C(9)-N(2)	109.0(2)
C(9)-C(10)-H(10B)	108.8(2)	H(9B)-C(9)-C(10)	109.0(2)
C(9')-C(10')-H(10C)	108.9(2)	H(9B)-C(9)-N(2)	109.0(2)
C(9')-C(10')-H(10D)	108.9(2)	H(9C)-C(9')-C(10')	109.1(2)
C(9)-N(2)-H(2)	118.2(2)	H(9C)-C(9')-H(9D)	107.8(2)
C(9')-N(2')-H(2')	118.3(2)	H(9C)-C(9')-N(2')	109.1(2)
C(10)-C(11)-C(12)	110.3(2)	H(9D)-C(9')-C(10')	109.1(2)
C(10')-C(11')-C(12')	112.3(2)	H(9D)-C(9')-N(2')	109.1(2)
C(10)-C(11)-C(13)	112.2(2)	N(1)-C(7)-O(1)	122.6(2)
C(10')-C(11')-C(13')	109.9(2)	N(1')-C(7')-O(1')	122.8(2)
C(10)-C(11)-H(11)	107.9(2)	N(1)-C(8)-N(2)	117.4(2)
C(10')-C(11')-H(11')	107.9(2)	N(1')-C(8')-N(2')	117.0(2)
C(10)-C(9)-N(2)	112.9(2)	N(1)-C(8)-S(1)	118.7(2)
C(10')-C(9')-N(2')	112.5(2)	N(1')-C(8')-S(1')	118.4(2)
C(11)-C(12)-H(12A)	109.5(2)	N(2)-C(8)-S(1)	123.9(2)
C(11)-C(12)-H(12B)	109.5(2)	N(2')-C(8')-S(1')	124.6(2)



## APPENDIX B

### CRYSTAL DATA OF RHODIUM(I) BIPHOSPHINE CARBONYL COMPLEXES

#### **B1. Crystal data of di-carbonyl-chlorido-di-(bis(diphenylphosphine)methane)- di-rhodium(I) tetrafluoroborate, $[\text{Rh}_2(\mu\text{-Cl})(\text{dppm})_2(\text{CO})_2]^+\text{BF}_4^-$**

**Table B1.1. Atomic coordinates and equivalent isotropic displacement parameters ( $\text{\AA}^2$ ) for  $[\text{Rh}_2(\mu\text{-Cl})(\text{dppm})_2(\text{CO})_2]^+\text{BF}_4^-$ .  $U_{(\text{eq})}$  is defined as one third of the trace of the orthogonalized  $U^{ij}$  tensor.**

Atom	x/a	y/b	z/c	$U_{(\text{eq})}$
C(1)	0.1616(5)	0.2647(2)	0.8153(3)	0.01524
C(2)	0.1819(6)	0.2410(2)	0.8746(3)	0.01745
C(3)	0.0764(5)	0.2421(2)	0.9183(3)	0.01914
C(4)	-0.0493(6)	0.2673(2)	0.9030(3)	0.02432
C(5)	-0.0695(6)	0.2919(2)	0.8440(3)	0.02587
C(6)	0.0347(5)	0.2903(2)	0.8008(3)	0.01991
C(7)	0.3899(5)	0.3257(2)	0.7549(3)	0.01733
C(8)	0.5341(6)	0.3285(3)	0.7533(3)	0.02254
C(9)	0.6027(6)	0.3790(3)	0.7457(3)	0.02656
C(10)	0.5251(7)	0.4267(3)	0.7384(3)	0.03457
C(11)	0.3828(7)	0.4256(3)	0.7410(3)	0.03955
C(12)	0.3131(6)	0.3752(2)	0.7489(3)	0.02995
C(13)	0.1492(5)	0.2126(2)	0.5603(3)	0.01756
C(14)	0.1719(6)	0.1721(2)	0.5149(3)	0.02184
C(15)	0.0675(6)	0.1595(2)	0.4696(3)	0.03043
C(16)	-0.0586(6)	0.1882(2)	0.4703(3)	0.02934
C(17)	-0.0811(6)	0.2279(3)	0.5155(3)	0.02658
C(18)	0.0212(5)	0.2403(2)	0.5605(3)	0.02103
C(19)	0.3759(5)	0.2889(2)	0.5798(3)	0.01583
C(20)	0.5123(6)	0.3026(2)	0.5982(3)	0.01992
C(21)	0.5784(6)	0.3489(3)	0.5719(3)	0.02661
C(22)	0.5074(6)	0.3804(2)	0.5268(3)	0.02461
C(23)	0.3724(6)	0.3671(2)	0.5080(3)	0.02487
C(24)	0.3071(6)	0.3214(2)	0.5347(3)	0.02106

C(25)	0.4556(5)	0.0644(2)	0.8736(2)	0.0135
C(26)	0.4578(6)	0.0975(3)	0.9285(3)	0.02654
C(27)	0.3964(7)	0.0790(3)	0.9816(3)	0.03517
C(28)	0.3293(6)	0.0278(3)	0.9821(3)	0.03087
C(29)	0.3253(6)	-0.0055(3)	0.9296(3)	0.02781
C(30)	0.3904(6)	0.0128(3)	0.8753(3)	0.02422
C(31)	0.7228(5)	0.0903(2)	0.8217(3)	0.0168
C(32)	0.8097(5)	0.1332(2)	0.8025(3)	0.01678
C(33)	0.9527(6)	0.1309(2)	0.8158(3)	0.02148
C(34)	1.0093(6)	0.0851(3)	0.8475(3)	0.02507
C(35)	0.9229(6)	0.0422(2)	0.8659(3)	0.02125
C(36)	0.7808(5)	0.0443(2)	0.8529(3)	0.0189
C(37)	0.4392(5)	0.0105(2)	0.6162(2)	0.01383
C(38)	0.3792(5)	0.0258(2)	0.5586(3)	0.02007
C(39)	0.3032(6)	-0.0117(3)	0.5215(3)	0.02526
C(40)	0.2874(6)	-0.0656(3)	0.5418(3)	0.02685
C(41)	0.3480(7)	-0.0822(3)	0.5980(3)	0.03801
C(42)	0.4235(6)	-0.0449(2)	0.6362(3)	0.02688
C(43)	0.7140(5)	0.0549(2)	0.6493(2)	0.01572
C(44)	0.7997(5)	0.1019(2)	0.6429(3)	0.02124
C(45)	0.9383(6)	0.0958(3)	0.6305(3)	0.02945
C(46)	0.9977(6)	0.0435(3)	0.6246(3)	0.03118
C(47)	0.9138(6)	-0.0032(3)	0.6321(3)	0.0301
C(48)	0.7741(6)	0.0019(3)	0.6443(3)	0.02245
C(49)	0.5057(5)	0.0394(2)	0.7433(2)	0.01477
C(50)	0.1983(5)	0.2570(2)	0.6831(3)	0.01642
C(51)	0.5482(6)	0.2136(2)	0.8344(3)	0.01842
C(52)	0.5399(6)	0.1661(2)	0.5781(3)	0.01744
Cl(1)	0.25601(13)	0.12717(6)	0.71834(6)	0.01707
O(1)	0.6196(4)	0.2346(2)	0.8718(2)	0.02962
O(2)	0.6115(4)	0.1763(2)	0.5369(2)	0.02883
P(1)	0.30049(14)	0.25848(6)	0.75836(7)	0.0141
P(2)	0.29143(14)	0.22884(6)	0.61592(7)	0.01332
P(3)	0.53540(14)	0.09301(6)	0.80406(6)	0.01271
P(4)	0.52841(14)	0.06406(6)	0.66317(6)	0.01315
Rh(1)	0.42953(4)	0.17781(2)	0.77964(2)	0.0141
Rh(2)	0.42291(4)	0.15001(2)	0.64072(2)	0.01341
B(1)	0.4349(7)	0.1169(3)	0.1626(3)	0.02337
F(1)	0.3720(3)	0.1693(1)	0.1672(2)	0.02775
F(2)	0.3468(3)	0.0806(1)	0.1288(2)	0.02343
F(3)	0.4616(3)	0.0947(1)	0.2223(2)	0.02967

F(4)	0.5611(3)	0.1229(1)	0.1319(2)	0.03396
------	-----------	-----------	-----------	---------

**Table B1.2. Hydrogen coordinates and isotropic displacement parameters ( $\text{\AA}^2$ ) for  $[\text{Rh}_2(\mu\text{-Cl})(\text{dppm})_2(\text{CO})_2]^+\text{BF}_4^-$ .**

Atom	x/a	y/b	z/c	$U_{\text{eq}}$
H(2)	0.26715	0.22414	0.88524	0.02094
H(3)	0.09088	0.22577	0.95766	0.02297
H(4)	-0.12048	0.26801	0.93189	0.02918
H(5)	-0.15398	0.30946	0.83382	0.03105
H(6)	0.01983	0.30654	0.76139	0.02389
H(8)	0.58622	0.29573	0.75748	0.02705
H(9)	0.69989	0.38048	0.74551	0.03187
H(10)	0.57018	0.46062	0.73148	0.04149
H(11)	0.33218	0.45882	0.73748	0.04746
H(12)	0.21602	0.37439	0.75024	0.03594
H(14)	0.25702	0.15319	0.51457	0.02621
H(15)	0.08249	0.13211	0.43936	0.03652
H(16)	-0.12811	0.18051	0.43996	0.0352
H(17)	-0.16632	0.24666	0.51579	0.0319
H(18)	0.00446	0.26724	0.59099	0.02524
H(20)	0.55989	0.28092	0.62817	0.02391
H(21)	0.66928	0.35831	0.58455	0.03194
H(22)	0.55137	0.41102	0.509	0.02953
H(23)	0.32546	0.38862	0.47759	0.02985
H(24)	0.21584	0.31236	0.52212	0.02527
H(26)	0.50156	0.13233	0.92845	0.03185
H(27)	0.39964	0.10099	1.01776	0.0422
H(28)	0.28642	0.01582	1.01834	0.03705
H(29)	0.27978	-0.03991	0.93014	0.03337
H(30)	0.38983	-0.01	0.83991	0.02906
H(32)	0.77205	0.16367	0.78059	0.02015
H(33)	1.01034	0.16004	0.80335	0.02578
H(34)	1.10505	0.08336	0.85635	0.03008
H(35)	0.96082	0.01147	0.88724	0.0255
H(36)	0.7237	0.01491	0.86506	0.02268
H(38)	0.39033	0.06236	0.54443	0.02408
H(39)	0.26332	-0.00032	0.48323	0.03032
H(40)	0.23559	-0.09105	0.51757	0.03222
H(41)	0.33852	-0.11923	0.61087	0.04561
H(42)	0.46278	-0.05669	0.6745	0.03226

H(44)	0.762	0.13757	0.647	0.02548
H(45)	0.99354	0.12752	0.62604	0.03534
H(46)	1.09197	0.03968	0.61586	0.03741
H(47)	0.95285	-0.03878	0.62882	0.03612
H(48)	0.71959	-0.02995	0.64916	0.02694
H(49A)	0.56976	0.00858	0.75141	0.01773
H(49B)	0.41133	0.02506	0.74665	0.01773
H(50A)	0.11484	0.23464	0.68881	0.0197
H(50B)	0.16832	0.29485	0.67305	0.0197

**Table B1.3. Anisotropic displacement parameters ( $\text{\AA}^2$ ) for  $[\text{Rh}_2(\mu\text{-Cl})(\text{dppm})_2(\text{CO})_2]^+\text{BF}_4^-$ .**

The anisotropic displacement factor exponent takes the form:  $-2\pi^2[\text{h}^2\text{a}^{*2}\text{U}^{11} + \dots + 2\text{hka}^*\text{b}^*\text{U}^{23}]$ .

Atom	$\text{U}^{11}$	$\text{U}^{22}$	$\text{U}^{33}$	$\text{U}^{12}$	$\text{U}^{13}$	$\text{U}^{23}$
C(1)	0.018(3)	0.011(3)	0.017(3)	-0.002(2)	0.001(2)	-0.002(2)
C(2)	0.021(3)	0.010(3)	0.021(3)	-0.001(2)	-0.003(2)	-0.002(2)
C(3)	0.024(3)	0.022(3)	0.011(3)	-0.008(3)	0.001(2)	0.002(3)
C(4)	0.021(3)	0.028(4)	0.024(4)	-0.001(3)	0.007(3)	-0.005(3)
C(5)	0.021(3)	0.022(4)	0.035(4)	0.008(3)	0.002(3)	0.000(3)
C(6)	0.023(3)	0.013(3)	0.023(3)	0.002(3)	-0.001(2)	0.002(3)
C(7)	0.021(3)	0.020(3)	0.011(3)	-0.006(3)	0.000(2)	-0.002(2)
C(8)	0.022(3)	0.026(4)	0.020(3)	-0.002(3)	0.003(2)	0.002(3)
C(9)	0.025(3)	0.027(4)	0.027(4)	-0.011(3)	0.001(3)	0.000(3)
C(10)	0.042(4)	0.028(4)	0.034(4)	-0.019(3)	-0.005(3)	0.009(3)
C(11)	0.043(4)	0.013(4)	0.061(5)	-0.003(3)	-0.014(4)	0.007(3)
C(12)	0.027(4)	0.015(3)	0.047(5)	-0.002(3)	-0.009(3)	-0.003(3)
C(13)	0.023(3)	0.016(3)	0.014(3)	-0.003(3)	0.003(2)	0.004(2)
C(14)	0.026(3)	0.020(3)	0.019(3)	-0.002(3)	-0.004(2)	0.003(3)
C(15)	0.044(4)	0.015(3)	0.032(4)	-0.002(3)	-0.011(3)	-0.003(3)
C(16)	0.033(4)	0.019(4)	0.036(4)	-0.010(3)	-0.014(3)	0.009(3)
C(17)	0.021(3)	0.026(4)	0.031(4)	-0.004(3)	-0.011(3)	0.010(3)
C(18)	0.023(3)	0.017(3)	0.023(4)	-0.004(3)	-0.001(2)	0.001(3)
C(19)	0.020(3)	0.009(3)	0.018(3)	0.005(2)	0.006(2)	-0.001(2)
C(20)	0.023(3)	0.023(3)	0.014(3)	0.001(3)	0.001(2)	-0.002(3)
C(21)	0.025(3)	0.029(4)	0.026(4)	-0.013(3)	0.002(3)	-0.008(3)
C(22)	0.031(4)	0.015(3)	0.028(4)	-0.010(3)	0.007(3)	-0.002(3)
C(23)	0.030(4)	0.017(3)	0.028(4)	0.004(3)	0.005(3)	0.008(3)
C(24)	0.018(3)	0.021(3)	0.024(3)	-0.003(3)	0.004(2)	0.004(3)
C(25)	0.012(3)	0.015(3)	0.014(3)	0.002(2)	0.003(2)	0.005(2)
C(26)	0.045(4)	0.019(3)	0.016(3)	-0.002(3)	-0.003(3)	0.001(3)

C(27)	0.045(4)	0.039(4)	0.021(4)	0.011(3)	0.007(3)	0.002(3)
C(28)	0.028(4)	0.040(4)	0.025(4)	0.013(3)	0.013(3)	0.017(3)
C(29)	0.022(3)	0.033(4)	0.029(4)	0.002(3)	0.002(3)	0.015(3)
C(30)	0.023(3)	0.025(4)	0.024(4)	0.002(3)	0.003(3)	0.007(3)
C(31)	0.017(3)	0.015(3)	0.018(3)	0.002(2)	0.001(2)	-0.003(3)
C(32)	0.021(3)	0.009(3)	0.021(3)	-0.001(2)	0.003(2)	0.000(2)
C(33)	0.022(3)	0.017(3)	0.026(4)	-0.005(3)	0.007(3)	-0.005(3)
C(34)	0.016(3)	0.032(4)	0.026(4)	0.005(3)	-0.002(2)	-0.011(3)
C(35)	0.025(3)	0.017(3)	0.021(3)	0.009(3)	-0.003(2)	-0.006(3)
C(36)	0.017(3)	0.014(3)	0.026(3)	0.001(2)	0.006(2)	-0.006(3)
C(37)	0.009(3)	0.014(3)	0.018(3)	0.001(2)	0.000(2)	-0.001(2)
C(38)	0.023(3)	0.018(3)	0.020(3)	0.002(3)	-0.002(2)	-0.005(3)
C(39)	0.027(3)	0.029(4)	0.019(3)	-0.001(3)	-0.006(3)	-0.005(3)
C(40)	0.027(3)	0.027(4)	0.026(4)	-0.004(3)	-0.002(3)	-0.008(3)
C(41)	0.054(5)	0.026(4)	0.033(4)	-0.017(3)	-0.013(3)	0.005(3)
C(42)	0.039(4)	0.021(3)	0.020(4)	-0.008(3)	-0.012(3)	0.000(3)
C(43)	0.015(3)	0.018(3)	0.014(3)	0.003(2)	0.001(2)	0.002(2)
C(44)	0.015(3)	0.024(3)	0.025(4)	-0.004(3)	-0.005(2)	0.007(3)
C(45)	0.022(3)	0.038(4)	0.029(4)	-0.007(3)	-0.001(3)	0.009(3)
C(46)	0.016(3)	0.057(5)	0.021(4)	0.006(3)	0.001(3)	0.003(3)
C(47)	0.032(4)	0.029(4)	0.029(4)	0.018(3)	-0.004(3)	-0.004(3)
C(48)	0.021(3)	0.026(4)	0.020(3)	0.000(3)	-0.005(2)	-0.005(3)
C(49)	0.013(3)	0.012(3)	0.019(3)	-0.003(2)	0.001(2)	0.004(2)
C(50)	0.012(3)	0.014(3)	0.023(3)	0.000(2)	-0.001(2)	0.002(3)
C(51)	0.018(3)	0.012(3)	0.025(4)	0.005(2)	-0.001(2)	0.000(3)
C(52)	0.019(3)	0.005(3)	0.028(4)	0.003(2)	-0.003(3)	0.006(2)
O(1)	0.023(2)	0.031(3)	0.035(3)	0.005(2)	-0.007(2)	-0.016(2)
O(2)	0.031(2)	0.024(2)	0.032(3)	0.006(2)	0.013(2)	0.009(2)
Cl(1)	0.0168(7)	0.0170(7)	0.0174(8)	-0.0011(6)	0.0002(5)	0.0010(6)
P(1)	0.0145(8)	0.0128(8)	0.0150(8)	0.0006(6)	0.0006(6)	0.0003(6)
P(2)	0.0144(7)	0.0098(8)	0.0157(8)	0.0001(6)	-0.0008(6)	0.0013(6)
P(3)	0.0142(7)	0.0107(8)	0.0133(8)	0.0005(6)	0.0000(6)	0.0000(6)
P(4)	0.0143(7)	0.0130(8)	0.0122(8)	0.0000(6)	0.0002(6)	0.0000(6)
Rh(1)	0.0144(2)	0.0117(2)	0.0161(3)	0.0011(2)	-0.0013(2)	-0.0011(2)
Rh(2)	0.0142(2)	0.0120(2)	0.0141(2)	0.0004(2)	0.0015(2)	0.0014(2)
B(1)	0.027(4)	0.017(4)	0.026(4)	0.001(3)	-0.002(3)	-0.006(3)
F(1)	0.033(2)	0.017(2)	0.033(2)	-0.003(2)	-0.006(2)	0.001(2)
F(2)	0.024(2)	0.018(2)	0.028(2)	-0.004(1)	-0.004(1)	-0.002(2)
F(3)	0.042(2)	0.018(2)	0.029(2)	-0.002(2)	-0.005(2)	0.003(2)
F(4)	0.031(2)	0.028(2)	0.043(2)	-0.009(2)	0.006(2)	0.001(2)

**Table B1.4. Complete listing of bond lengths (Å) for [Rh<sub>2</sub>(μ-Cl)(dppm)<sub>2</sub>(CO)<sub>2</sub>]<sup>+</sup>BF<sub>4</sub><sup>-</sup>.**

<b>Bond</b>	<b>Distance</b>	<b>Bond</b>	<b>Distance</b>
C(1)-C(2)	1.391(8)	C(1)-C(6)	1.385(8)
C(1)-P(1)	1.830(6)	C(2)-H(2)	0.930(6)
C(2)-C(3)	1.391(8)	C(3)-H(3)	0.930(6)
C(3)-C(4)	1.375(8)	C(4)-H(4)	0.930(6)
C(4)-C(5)	1.393(9)	C(5)-H(5)	0.930(6)
C(5)-C(6)	1.377(8)	C(6)-H(6)	0.930(6)
C(7)-C(8)	1.382(8)	C(7)-C(12)	1.394(8)
C(7)-P(1)	1.820(6)	C(8)-H(8)	0.930(6)
C(8)-C(9)	1.385(9)	C(9)-H(9)	0.930(6)
C(9)-C(10)	1.364(9)	C(10)-H(10)	0.930(7)
C(10)-C(11)	1.364(10)	C(11)-H(11)	0.930(7)
C(11)-C(12)	1.389(9)	C(12)-H(12)	0.930(7)
C(13)-C(14)	1.387(8)	C(13)-C(18)	1.392(8)
C(13)-P(2)	1.819(6)	C(14)-H(14)	0.930(6)
C(14)-C(15)	1.400(9)	C(15)-H(15)	0.930(6)
C(15)-C(16)	1.388(9)	C(16)-H(16)	0.930(7)
C(16)-C(17)	1.371(9)	C(17)-H(17)	0.930(6)
C(17)-C(18)	1.381(8)	C(18)-H(18)	0.930(6)
C(19)-C(20)	1.390(8)	C(19)-C(24)	1.385(8)
C(19)-P(2)	1.825(6)	C(20)-H(20)	0.930(6)
C(20)-C(21)	1.396(9)	C(21)-H(21)	0.930(6)
C(21)-C(22)	1.381(9)	C(22)-H(22)	0.930(6)
C(22)-C(23)	1.377(8)	C(23)-H(23)	0.930(6)
C(23)-C(24)	1.388(8)	C(24)-H(24)	0.930(6)
C(25)-C(26)	1.410(8)	C(25)-C(30)	1.379(8)
C(25)-P(3)	1.818(6)	C(26)-H(26)	0.930(6)
C(26)-C(27)	1.362(9)	C(27)-H(27)	0.930(7)
C(27)-C(28)	1.380(10)	C(28)-H(28)	0.930(7)
C(28)-C(29)	1.369(9)	C(29)-H(29)	0.930(7)
C(29)-C(30)	1.398(9)	C(30)-H(30)	0.930(6)
C(31)-C(32)	1.388(8)	C(31)-C(36)	1.390(8)
C(31)-P(3)	1.821(6)	C(32)-H(32)	0.930(6)
C(32)-C(33)	1.389(8)	C(33)-H(33)	0.930(6)
C(33)-C(34)	1.386(9)	C(34)-H(34)	0.930(6)
C(34)-C(35)	1.381(9)	C(35)-H(35)	0.930(6)
C(35)-C(36)	1.379(8)	C(36)-H(36)	0.930(6)
C(37)-C(38)	1.387(8)	C(37)-C(42)	1.399(8)
C(37)-P(4)	1.819(6)	C(38)-H(38)	0.930(6)
C(38)-C(39)	1.384(8)	C(39)-H(39)	0.930(6)

C(39)-C(40)	1.367(9)	C(40)-H(40)	0.930(6)
C(40)-C(41)	1.371(9)	C(41)-H(41)	0.930(7)
C(41)-C(42)	1.392(9)	C(42)-H(42)	0.930(6)
C(43)-C(44)	1.398(8)	C(43)-C(48)	1.392(8)
C(43)-P(4)	1.821(6)	C(44)-H(44)	0.930(6)
C(44)-C(45)	1.366(8)	C(45)-H(45)	0.930(7)
C(45)-C(46)	1.378(10)	C(46)-H(46)	0.930(6)
C(46)-C(47)	1.385(10)	C(47)-H(47)	0.930(7)
C(47)-C(48)	1.373(8)	C(48)-H(48)	0.930(6)
C(49)-H(49A)	0.970(5)	C(49)-H(49B)	0.970(5)
C(49)-P(3)	1.834(6)	C(49)-P(4)	1.821(6)
C(50)-H(50A)	0.970(5)	C(50)-H(50B)	0.970(6)
C(50)-P(1)	1.852(6)	C(50)-P(2)	1.833(6)
C(51)-O(1)	1.149(7)	C(51)-Rh(1)	1.815(6)
C(52)-O(2)	1.154(8)	C(52)-Rh(2)	1.805(6)
P(1)-Rh(1)	2.324(2)	P(2)-Rh(2)	2.315(2)
P(3)-Rh(1)	2.315(2)	P(4)-Rh(2)	2.329(2)
B(1)-F(1)	1.392(8)	B(1)-F(2)	1.395(8)
B(1)-F(3)	1.393(8)	B(1)-F(4)	1.395(8)

**Table B1.5. Complete listing of bond angles (°) for  $[\text{Rh}_2(\mu\text{-Cl})(\text{dppm})_2(\text{CO})_2]^+\text{BF}_4^-$ .**

Angle	Value	Angle	Value
C(1)-C(2)-C(3)	120.8(5)	C(25)-P(3)-C(31)	104.6(3)
C(1)-C(2)-H(2)	119.6(6)	C(25)-P(3)-C(49)	104.6(3)
C(1)-C(6)-C(5)	120.6(6)	C(25)-P(3)-Rh(1)	108.7(2)
C(1)-C(6)-H(6)	119.7(6)	C(26)-C(25)-C(30)	118.3(5)
C(1)-P(1)-C(50)	101.5(3)	C(26)-C(25)-P(3)	117.8(5)
C(1)-P(1)-C(7)	107.8(3)	C(26)-C(27)-C(28)	120.3(6)
C(1)-P(1)-Rh(1)	109.2(2)	C(26)-C(27)-H(27)	119.9(7)
C(2)-C(1)-C(6)	118.8(5)	C(27)-C(28)-C(29)	120.7(6)
C(2)-C(1)-P(1)	118.9(4)	C(27)-C(28)-H(28)	119.6(7)
C(2)-C(3)-C(4)	119.8(6)	C(28)-C(29)-C(30)	119.2(6)
C(2)-C(3)-H(3)	120.1(6)	C(28)-C(29)-H(29)	120.4(6)
C(3)-C(4)-C(5)	119.6(6)	C(29)-C(30)-H(30)	119.6(6)
C(3)-C(4)-H(4)	120.2(6)	C(30)-C(25)-P(3)	123.8(5)
C(4)-C(5)-C(6)	120.4(6)	C(31)-C(32)-C(33)	120.4(5)
C(4)-C(5)-H(5)	119.8(6)	C(31)-C(32)-H(32)	119.8(6)
C(5)-C(6)-H(6)	119.7(6)	C(31)-C(36)-C(35)	120.1(5)
C(6)-C(1)-P(1)	122.3(5)	C(31)-C(36)-H(36)	119.9(6)
C(7)-C(12)-C(11)	119.5(6)	C(31)-P(3)-C(49)	104.6(3)
C(7)-C(12)-H(12)	120.2(6)	C(31)-P(3)-Rh(1)	119.9(2)

C(7)-C(8)-C(9)	121.4(6)	C(32)-C(31)-C(36)	119.3(5)
C(7)-C(8)-H(8)	119.3(6)	C(32)-C(31)-P(3)	120.5(4)
C(7)-P(1)-C(50)	102.7(3)	C(32)-C(33)-C(34)	119.9(6)
C(7)-P(1)-Rh(1)	119.4(2)	C(32)-C(33)-H(33)	120.0(6)
C(8)-C(7)-C(12)	118.7(6)	C(33)-C(34)-C(35)	119.7(6)
C(8)-C(7)-P(1)	120.9(5)	C(33)-C(34)-H(34)	120.2(6)
C(8)-C(9)-C(10)	118.8(6)	C(34)-C(35)-C(36)	120.7(6)
C(8)-C(9)-H(9)	120.6(6)	C(34)-C(35)-H(35)	119.7(6)
C(9)-C(10)-C(11)	121.3(6)	C(35)-C(36)-H(36)	119.9(6)
C(9)-C(10)-H(10)	119.4(7)	C(36)-C(31)-P(3)	120.2(4)
C(10)-C(11)-C(12)	120.3(6)	C(37)-C(38)-C(39)	122.0(6)
C(10)-C(11)-H(11)	119.9(7)	C(37)-C(38)-H(38)	119.0(6)
C(11)-C(12)-H(12)	120.2(6)	C(37)-C(42)-C(41)	119.0(6)
C(12)-C(7)-P(1)	120.2(5)	C(37)-C(42)-H(42)	120.5(6)
C(13)-C(14)-C(15)	120.4(6)	C(37)-P(4)-C(43)	105.6(3)
C(13)-C(14)-H(14)	119.8(6)	C(37)-P(4)-C(49)	102.7(3)
C(13)-C(18)-C(17)	120.0(6)	C(37)-P(4)-Rh(2)	108.2(2)
C(13)-C(18)-H(18)	120.0(6)	C(38)-C(37)-C(42)	118.2(5)
C(13)-P(2)-C(19)	103.0(3)	C(38)-C(37)-P(4)	118.4(5)
C(13)-P(2)-C(50)	102.4(3)	C(38)-C(39)-C(40)	119.3(6)
C(13)-P(2)-Rh(2)	111.4(2)	C(38)-C(39)-H(39)	120.3(6)
C(14)-C(13)-C(18)	119.3(5)	C(39)-C(40)-C(41)	119.9(6)
C(14)-C(13)-P(2)	118.2(5)	C(39)-C(40)-H(40)	120.0(6)
C(14)-C(15)-C(16)	119.3(6)	C(40)-C(41)-C(42)	121.5(6)
C(14)-C(15)-H(15)	120.4(6)	C(40)-C(41)-H(41)	119.2(7)
C(15)-C(16)-C(17)	120.2(6)	C(41)-C(42)-H(42)	120.5(6)
C(15)-C(16)-H(16)	119.9(6)	C(42)-C(37)-P(4)	123.4(5)
C(16)-C(17)-C(18)	120.9(6)	C(43)-C(44)-C(45)	120.5(6)
C(16)-C(17)-H(17)	119.6(6)	C(43)-C(44)-H(44)	119.8(6)
C(17)-C(18)-H(18)	120.0(6)	C(43)-C(48)-C(47)	120.1(6)
C(18)-C(13)-P(2)	122.5(5)	C(43)-C(48)-H(48)	119.9(6)
C(19)-C(20)-C(21)	120.4(6)	C(43)-P(4)-C(49)	104.8(3)
C(19)-C(20)-H(20)	119.8(6)	C(43)-P(4)-Rh(2)	119.4(2)
C(19)-C(24)-C(23)	120.9(6)	C(44)-C(43)-C(48)	118.4(5)
C(19)-C(24)-H(24)	119.5(6)	C(44)-C(43)-P(4)	119.7(5)
C(19)-P(2)-C(50)	105.8(3)	C(44)-C(45)-C(46)	121.3(6)
C(19)-P(2)-Rh(2)	119.3(2)	C(44)-C(45)-H(45)	119.4(7)
C(20)-C(19)-C(24)	119.1(5)	C(45)-C(46)-C(47)	118.4(6)
C(20)-C(19)-P(2)	119.4(5)	C(45)-C(46)-H(46)	120.8(7)
C(20)-C(21)-C(22)	119.3(6)	C(46)-C(47)-C(48)	121.3(6)
C(20)-C(21)-H(21)	120.4(6)	C(46)-C(47)-H(47)	119.4(6)



C(21)-C(22)-C(23)	121.0(6)	C(47)-C(48)-H(48)	119.9(6)
C(21)-C(22)-H(22)	119.5(6)	C(48)-C(43)-P(4)	121.9(5)
C(22)-C(23)-C(24)	119.3(6)	C(49)-P(3)-Rh(1)	113.2(2)
C(22)-C(23)-H(23)	120.3(6)	C(49)-P(4)-Rh(2)	114.4(2)
C(23)-C(24)-H(24)	119.5(6)	C(50)-P(1)-Rh(1)	114.6(2)
C(24)-C(19)-P(2)	121.6(4)	C(50)-P(2)-Rh(2)	113.1(2)
C(25)-C(26)-C(27)	120.6(6)	C(51)-Rh(1)-P(1)	93.1(2)
C(25)-C(26)-H(26)	119.7(6)	C(51)-Rh(1)-P(3)	90.4(2)
C(25)-C(30)-C(29)	120.9(6)	C(52)-Rh(2)-P(2)	90.2(2)
C(25)-C(30)-H(30)	119.6(6)	C(52)-Rh(2)-P(4)	93.7(2)
H(11)-C(11)-C(12)	119.9(7)	H(10)-C(10)-C(11)	119.4(7)
H(15)-C(15)-C(16)	120.4(7)	H(14)-C(14)-C(15)	119.8(6)
H(17)-C(17)-C(18)	119.6(6)	H(16)-C(16)-C(17)	119.9(6)
H(21)-C(21)-C(22)	120.3(6)	H(2)-C(2)-C(3)	119.6(6)
H(23)-C(23)-C(24)	120.3(6)	H(20)-C(20)-C(21)	119.8(6)
H(27)-C(27)-C(28)	119.9(7)	H(22)-C(22)-C(23)	119.5(6)
H(29)-C(29)-C(30)	120.4(6)	H(26)-C(26)-C(27)	119.7(6)
H(3)-C(3)-C(4)	120.1(6)	H(28)-C(28)-C(29)	119.6(7)
H(33)-C(33)-C(34)	120.1(6)	H(32)-C(32)-C(33)	119.8(6)
H(35)-C(35)-C(36)	119.7(6)	H(34)-C(34)-C(35)	120.2(6)
H(39)-C(39)-C(40)	120.4(6)	H(38)-C(38)-C(39)	119.0(6)
H(41)-C(41)-C(42)	119.2(7)	H(4)-C(4)-C(5)	120.2(6)
H(45)-C(45)-C(46)	119.4(6)	H(40)-C(40)-C(41)	120.0(7)
H(47)-C(47)-C(48)	119.4(7)	H(44)-C(44)-C(45)	119.7(6)
H(49A)-C(49)-H(49B)	107.6(5)	H(46)-C(46)-C(47)	120.8(7)
H(49A)-C(49)-P(4)	108.6(4)	H(49A)-C(49)-P(3)	108.6(4)
H(49B)-C(49)-P(4)	108.6(4)	H(49B)-C(49)-P(3)	108.6(4)
H(5)-C(5)-C(6)	119.8(6)	H(50A)-C(50)-P(1)	108.5(4)
H(50A)-C(50)-H(50B)	107.5(5)	H(50B)-C(50)-P(1)	108.5(4)
H(50A)-C(50)-P(2)	108.5(4)	H(8)-C(8)-C(9)	119.3(6)
H(50B)-C(50)-P(2)	108.5(4)	H(9)-C(9)-C(10)	120.6(7)
F(1)-B(1)-F(2)	109.8(5)	F(1)-B(1)-F(3)	110.3(6)
F(1)-B(1)-F(4)	108.9(5)	F(2)-B(1)-F(3)	108.9(5)
F(2)-B(1)-F(4)	109.8(6)	F(3)-B(1)-F(4)	109.1(5)
O(1)-C(51)-Rh(1)	176.0(5)	O(2)-C(52)-Rh(2)	178.1(5)
P(1)-C(50)-P(2)	115.2(3)	P(3)-C(49)-P(4)	114.5(3)
P(1)-Rh(1)-P(3)	173.7(1)	P(2)-Rh(2)-P(4)	172.5(1)

## APPENDIX C

### CRYSTAL DATA OF RHODIUM COMPLEXES CONTAINING S,O-FUNCTIONALIZED THIOUREA LIGANDS

**C1. Crystal data of Carbonylbis(triphenylphosphine)(*N,S*-(*N*-benzoyl-*N'*-(4-hydroxy-2-methylphenyl)thiourea))rhodium(I)**

**[Rh(*N,S*-(*N*-4h2mPT))(CO)(PPh<sub>3</sub>)<sub>2</sub>]**

**Table C1.1. Atomic coordinates and equivalent isotropic displacement parameters (Å<sup>2</sup>) for [Rh(*N,S*-(*N*-4h2mPT))(CO)(PPh<sub>3</sub>)<sub>2</sub>].  $U_{(eq)}$  is defined as one third of the trace of the orthogonalized  $U^{ij}$  tensor.**

Atom	x/a	y/b	z/c	$U_{(eq)}$
C(1)	0.1930(2)	0.1439(2)	0.6449(1)	0.01634
C(2)	0.0590(2)	0.2069(2)	0.6205(1)	0.0225
C(3)	-0.0259(2)	0.1417(2)	0.6289(1)	0.02934
C(4)	0.0242(2)	0.0123(2)	0.6602(1)	0.03213
C(5)	0.1577(2)	-0.0510(2)	0.6831(1)	0.02645
C(6)	0.2420(2)	0.0144(2)	0.6762(1)	0.02006
C(7)	0.28403(19)	0.21529(17)	0.63437(9)	0.01588
C(8)	0.46703(19)	0.23741(16)	0.68028(9)	0.01468
C(9)	0.58359(19)	0.36849(17)	0.60269(9)	0.01605
C(10)	0.6142(2)	0.4252(2)	0.6492(1)	0.01818
C(11)	0.7048(2)	0.4851(2)	0.6287(1)	0.01963
C(12)	0.7635(2)	0.4903(2)	0.5610(1)	0.01856
C(13)	0.7338(2)	0.4329(2)	0.5148(1)	0.0189
C(14)	0.6442(2)	0.3706(2)	0.5347(1)	0.01741
C(15)	0.6156(2)	0.3071(2)	0.4836(1)	0.02089
C(16)	0.15496(19)	0.40684(16)	0.76160(9)	0.01461
C(17)	0.0392(2)	0.4513(2)	0.7217(1)	0.01854
C(18)	0.0083(2)	0.5624(2)	0.6704(1)	0.02204
C(19)	0.0922(2)	0.6291(2)	0.6584(1)	0.02141
C(20)	0.2085(2)	0.5846(2)	0.6970(1)	0.02025
C(21)	0.2401(2)	0.4742(2)	0.7486(1)	0.01753
C(22)	0.24571(19)	0.31563(17)	0.89979(9)	0.01467
C(23)	0.3710(2)	0.2459(2)	0.9332(1)	0.01832

C(24)	0.4041(2)	0.2913(2)	0.9847(1)	0.02483
C(25)	0.3124(2)	0.4060(2)	1.0032(1)	0.02668
C(26)	0.1880(2)	0.4757(2)	0.9704(1)	0.02515
C(27)	0.1545(2)	0.4322(2)	0.9185(1)	0.01973
C(28)	0.04753(19)	0.23515(16)	0.85763(9)	0.01438
C(29)	0.0024(2)	0.1803(2)	0.8152(1)	0.0186
C(30)	-0.1156(2)	0.1556(2)	0.8349(1)	0.02249
C(31)	-0.1874(2)	0.1814(2)	0.8977(1)	0.02235
C(32)	-0.1423(2)	0.2331(2)	0.9406(1)	0.0227
C(33)	-0.0257(2)	0.2606(2)	0.9206(1)	0.01796
C(34)	0.63338(19)	-0.10513(17)	0.68364(9)	0.01521
C(35)	0.5976(2)	-0.1703(2)	0.6441(1)	0.02025
C(36)	0.6363(2)	-0.1633(2)	0.5734(1)	0.02707
C(37)	0.7132(2)	-0.0937(2)	0.5415(1)	0.02856
C(38)	0.7501(2)	-0.0296(2)	0.5805(1)	0.02309
C(39)	0.7092(2)	-0.0339(2)	0.6510(1)	0.0179
C(40)	0.73145(19)	-0.13795(16)	0.82019(9)	0.01442
C(41)	0.7151(2)	-0.1006(2)	0.8842(1)	0.01691
C(42)	0.8297(2)	-0.1237(2)	0.9201(1)	0.02008
C(43)	0.9628(2)	-0.1837(2)	0.8916(1)	0.02253
C(44)	0.9803(2)	-0.2225(2)	0.8285(1)	0.02245
C(45)	0.8661(2)	-0.2003(2)	0.7928(1)	0.01818
C(46)	0.5571(2)	-0.2591(2)	0.8018(1)	0.01523
C(47)	0.4267(2)	-0.2618(2)	0.8191(1)	0.02109
C(48)	0.4140(2)	-0.3788(2)	0.8365(1)	0.02662
C(49)	0.5299(2)	-0.4927(2)	0.8361(1)	0.02452
C(50)	0.6598(2)	-0.4907(2)	0.8178(1)	0.0216
C(51)	0.6736(2)	-0.3750(2)	0.8013(1)	0.01863
C(52)	0.3390(2)	-0.0079(2)	0.8790(1)	0.02038
N(1)	0.37337(16)	0.18330(14)	0.68549(8)	0.01394
N(2)	0.48573(17)	0.31189(14)	0.62052(8)	0.01634
O(1)	0.27194(15)	0.29886(14)	0.57987(7)	0.02428
O(2)	0.85348(15)	0.54963(14)	0.54251(7)	0.02491
O(3)	0.30554(16)	-0.05888(14)	0.93160(8)	0.03257
P(1)	0.20719(5)	0.25966(4)	0.82935(2)	0.01183
P(2)	0.57572(5)	-0.10610(4)	0.77608(2)	0.01222
S(1)	0.55264(5)	0.19845(4)	0.75508(2)	0.01676
Rh(1)	0.38792(1)	0.07898(1)	0.79938(1)	0.01217

**Table C1.2. Hydrogen coordinates and isotropic displacement parameters ( $\text{\AA}^2$ ) for  
[Rh(*N,S*-(*N*-4h2mPT))(CO)(PPh<sub>3</sub>)<sub>2</sub>].**

Atom	x/a	y/b	z/c	U <sub>(eq)</sub>
H(2)	0.42922	0.32831	0.58735	0.01961
H(2A)	0.02577	0.29476	0.59802	0.02699
H(3)	-0.11827	0.18516	0.61332	0.03521
H(4)	-0.03398	-0.03256	0.66573	0.03855
H(5)	0.19198	-0.1398	0.70371	0.03173
H(6)	0.33357	-0.02912	0.6929	0.02408
H(10)	0.57275	0.4229	0.69531	0.02182
H(11)	0.72667	0.52253	0.6608	0.02355
H(13)	0.77526	0.43593	0.46876	0.02268
H(15A)	0.52385	0.36136	0.46451	0.03134
H(15B)	0.61752	0.22329	0.50789	0.03134
H(15C)	0.68703	0.2953	0.44542	0.03134
H(17)	-0.01885	0.40586	0.72943	0.02225
H(18)	-0.07112	0.59269	0.64333	0.02645
H(19)	0.06973	0.70542	0.6237	0.0257
H(20)	0.26714	0.62953	0.68828	0.02429
H(21)	0.32004	0.44422	0.77518	0.02104
H(23)	0.43442	0.16683	0.92078	0.02198
H(24)	0.48994	0.24332	1.0071	0.02979
H(25)	0.33497	0.43671	1.03836	0.03202
H(26)	0.12468	0.55427	0.98343	0.03018
H(27)	0.06935	0.48172	0.89567	0.02368
H(29)	0.05285	0.15978	0.77277	0.02231
H(2B)	0.84507	0.58608	0.50017	0.03736
H(30)	-0.14721	0.12091	0.80514	0.02699
H(31)	-0.26755	0.16362	0.91132	0.02682
H(32)	-0.19096	0.2499	0.98391	0.02724
H(33)	0.00396	0.29713	0.95015	0.02155
H(35)	0.54638	-0.21975	0.66568	0.0243
H(36)	0.60973	-0.20672	0.54663	0.03248
H(37)	0.74036	-0.08991	0.49323	0.03427
H(38)	0.80379	0.01758	0.55902	0.02771
H(39)	0.7332	0.01218	0.67706	0.02148
H(41)	0.62414	-0.05867	0.90357	0.0203
H(42)	0.81721	-0.09865	0.96396	0.02409
H(43)	1.04163	-0.19794	0.91539	0.02703
H(44)	1.07146	-0.26476	0.80941	0.02694
H(45)	0.87922	-0.22765	0.74955	0.02182

H(47)	0.34622	-0.18389	0.81902	0.02531
H(48)	0.32491	-0.38016	0.8488	0.03194
H(49)	0.5206	-0.57214	0.84837	0.02943
H(50)	0.73947	-0.56882	0.81662	0.02592
H(51)	0.76316	-0.37451	0.78953	0.02235

**Table C1.3. Anisotropic displacement parameters ( $\text{\AA}^2$ ) for  $[\text{Rh}(\text{N},\text{S}-(\text{N}-4\text{h}2\text{mPT}))(\text{CO})(\text{PPh}_3)_2]$ . The anisotropic displacement factor exponent takes the form:  $-2\pi^2[\text{h}^2\text{a}^*\text{U}^{11} + \dots + 2\text{hka}^*\text{b}^*\text{U}^{23}]$ .**

Atom	$\text{U}^{11}$	$\text{U}^{22}$	$\text{U}^{33}$	$\text{U}^{12}$	$\text{U}^{13}$	$\text{U}^{23}$
C(1)	0.018(1)	0.018(1)	0.013(1)	-0.008(1)	0.001(1)	-0.004(1)
C(2)	0.021(1)	0.021(1)	0.022(1)	-0.007(1)	-0.003(1)	0.001(1)
C(3)	0.020(1)	0.031(1)	0.036(1)	-0.011(1)	-0.010(1)	0.001(1)
C(4)	0.029(1)	0.032(1)	0.042(1)	-0.020(1)	-0.008(1)	-0.002(1)
C(5)	0.026(1)	0.019(1)	0.036(1)	-0.011(1)	-0.007(1)	-0.002(1)
C(6)	0.019(1)	0.018(1)	0.024(1)	-0.006(1)	-0.003(1)	-0.005(1)
C(7)	0.015(1)	0.016(1)	0.015(1)	-0.005(1)	0.002(1)	-0.005(1)
C(8)	0.015(1)	0.012(1)	0.015(1)	-0.003(1)	0.002(1)	-0.005(1)
C(9)	0.015(1)	0.015(1)	0.017(1)	-0.006(1)	-0.003(1)	0.001(1)
C(10)	0.020(1)	0.019(1)	0.014(1)	-0.008(1)	0.000(1)	-0.001(1)
C(11)	0.023(1)	0.021(1)	0.018(1)	-0.011(1)	-0.005(1)	-0.003(1)
C(12)	0.017(1)	0.018(1)	0.020(1)	-0.008(1)	-0.004(1)	0.003(1)
C(13)	0.020(1)	0.019(1)	0.014(1)	-0.008(1)	0.000(1)	0.001(1)
C(14)	0.019(1)	0.014(1)	0.016(1)	-0.005(1)	-0.004(1)	0.000(1)
C(15)	0.027(1)	0.022(1)	0.015(1)	-0.012(1)	0.000(1)	-0.003(1)
C(16)	0.017(1)	0.010(1)	0.013(1)	-0.002(1)	0.001(1)	-0.003(1)
C(17)	0.019(1)	0.018(1)	0.018(1)	-0.006(1)	0.000(1)	-0.005(1)
C(18)	0.022(1)	0.022(1)	0.016(1)	-0.002(1)	-0.005(1)	-0.004(1)
C(19)	0.027(1)	0.014(1)	0.015(1)	-0.003(1)	0.003(1)	-0.001(1)
C(20)	0.023(1)	0.016(1)	0.021(1)	-0.008(1)	0.005(1)	-0.004(1)
C(21)	0.017(1)	0.015(1)	0.018(1)	-0.004(1)	0.000(1)	-0.005(1)
C(22)	0.017(1)	0.016(1)	0.012(1)	-0.009(1)	0.002(1)	-0.003(1)
C(23)	0.019(1)	0.019(1)	0.017(1)	-0.008(1)	0.000(1)	-0.003(1)
C(24)	0.029(1)	0.032(1)	0.018(1)	-0.018(1)	-0.006(1)	0.001(1)
C(25)	0.042(1)	0.033(1)	0.016(1)	-0.025(1)	0.001(1)	-0.007(1)
C(26)	0.035(1)	0.024(1)	0.021(1)	-0.015(1)	0.005(1)	-0.011(1)
C(27)	0.021(1)	0.018(1)	0.020(1)	-0.007(1)	0.002(1)	-0.006(1)
C(28)	0.0115(9)	0.0103(8)	0.0177(9)	-0.0019(7)	-0.0013(7)	-0.0005(7)
C(29)	0.018(1)	0.018(1)	0.019(1)	-0.006(1)	0.002(1)	-0.007(1)
C(30)	0.020(1)	0.021(1)	0.030(1)	-0.009(1)	-0.002(1)	-0.008(1)

C(31)	0.017(1)	0.021(1)	0.029(1)	-0.010(1)	0.002(1)	-0.002(1)
C(32)	0.021(1)	0.027(1)	0.019(1)	-0.010(1)	0.004(1)	-0.005(1)
C(33)	0.017(1)	0.019(1)	0.017(1)	-0.006(1)	-0.001(1)	-0.003(1)
C(34)	0.0115(9)	0.0137(8)	0.0152(9)	-0.0002(7)	-0.0007(7)	-0.0029(7)
C(35)	0.021(1)	0.019(1)	0.021(1)	-0.007(1)	-0.001(1)	-0.005(1)
C(36)	0.033(1)	0.030(1)	0.021(1)	-0.012(1)	-0.003(1)	-0.010(1)
C(37)	0.034(1)	0.033(1)	0.014(1)	-0.010(1)	0.001(1)	-0.006(1)
C(38)	0.023(1)	0.024(1)	0.019(1)	-0.008(1)	0.002(1)	-0.002(1)
C(39)	0.018(1)	0.016(1)	0.017(1)	-0.004(1)	-0.001(1)	-0.004(1)
C(40)	0.016(1)	0.012(1)	0.015(1)	-0.006(1)	-0.001(1)	0.000(1)
C(41)	0.017(1)	0.014(1)	0.017(1)	-0.004(1)	0.000(1)	-0.002(1)
C(42)	0.025(1)	0.019(1)	0.015(1)	-0.008(1)	-0.003(1)	-0.002(1)
C(43)	0.021(1)	0.024(1)	0.022(1)	-0.008(1)	-0.009(1)	0.001(1)
C(44)	0.015(1)	0.023(1)	0.025(1)	-0.004(1)	0.000(1)	-0.003(1)
C(45)	0.017(1)	0.019(1)	0.018(1)	-0.006(1)	0.000(1)	-0.005(1)
C(46)	0.020(1)	0.012(1)	0.014(1)	-0.007(1)	-0.001(1)	-0.002(1)
C(47)	0.020(1)	0.017(1)	0.025(1)	-0.007(1)	-0.003(1)	-0.002(1)
C(48)	0.026(1)	0.025(1)	0.033(1)	-0.016(1)	-0.002(1)	-0.002(1)
C(49)	0.035(1)	0.018(1)	0.024(1)	-0.015(1)	-0.007(1)	0.002(1)
C(50)	0.029(1)	0.014(1)	0.019(1)	-0.005(1)	-0.004(1)	-0.002(1)
C(51)	0.021(1)	0.017(1)	0.017(1)	-0.007(1)	0.001(1)	-0.003(1)
C(52)	0.018(1)	0.013(1)	0.022(1)	0.000(1)	0.002(1)	-0.002(1)
N(1)	0.0138(8)	0.0127(7)	0.0141(7)	-0.0043(6)	0.0008(6)	-0.0034(6)
N(2)	0.0184(9)	0.0187(8)	0.0127(7)	-0.0094(7)	-0.0012(6)	-0.0007(6)
O(1)	0.0296(8)	0.0291(8)	0.0174(7)	-0.0182(7)	-0.0068(6)	0.0051(6)
O(2)	0.0278(8)	0.0337(8)	0.0192(7)	-0.0215(7)	-0.0033(6)	0.0026(6)
O(3)	0.0327(9)	0.0238(8)	0.0249(8)	-0.0039(7)	0.0089(7)	0.0045(6)
P(1)	0.0118(2)	0.0107(2)	0.0118(2)	-0.0036(2)	0.0003(2)	-0.0025(2)
P(2)	0.0124(2)	0.0109(2)	0.0125(2)	-0.0041(2)	0.0004(2)	-0.0025(2)
S(1)	0.0195(3)	0.0166(2)	0.0139(2)	-0.0076(2)	-0.0022(2)	-0.0010(2)
Rh(1)	0.0126(1)	0.0105(1)	0.0120(1)	-0.0039(1)	0.0007(1)	-0.0016(1)

**Table C1.4. Complete listing of bond lengths (Å) for [Rh(*N,S*-(*N*-4h2mPT))](CO)(PPh<sub>3</sub>)<sub>2</sub>].**

<b>Bond</b>	<b>Distance</b>	<b>Bond</b>	<b>Distance</b>
C(1)-C(2)	1.390(3)	C(1)-C(6)	1.392(3)
C(1)-C(7)	1.494(3)	C(2)-H(2A)	0.950(2)
C(2)-C(3)	1.383(3)	C(3)-H(3)	0.950(3)
C(3)-C(4)	1.390(4)	C(4)-H(4)	0.950(3)
C(4)-C(5)	1.375(4)	C(5)-H(5)	0.950(3)
C(5)-C(6)	1.383(3)	C(6)-H(6)	0.950(2)
C(7)-N(1)	1.356(3)	C(7)-O(1)	1.251(3)
C(8)-N(1)	1.372(3)	C(8)-N(2)	1.336(3)
C(8)-S(1)	1.704(2)	C(9)-C(10)	1.392(3)
C(9)-C(14)	1.400(3)	C(9)-N(2)	1.422(3)
C(10)-H(10)	0.950(2)	C(10)-C(11)	1.384(3)
C(11)-H(11)	0.950(2)	C(11)-C(12)	1.389(3)
C(12)-C(13)	1.386(3)	C(12)-O(2)	1.372(3)
C(13)-H(13)	0.950(2)	C(13)-C(14)	1.395(3)
C(14)-C(15)	1.511(3)	C(15)-H(15A)	0.980(3)
C(15)-H(15B)	0.980(2)	C(15)-H(15C)	0.980(3)
C(16)-C(17)	1.390(3)	C(16)-C(21)	1.399(3)
C(16)-P(1)	1.838(2)	C(17)-H(17)	0.950(2)
C(17)-C(18)	1.392(3)	C(18)-H(18)	0.950(2)
C(18)-C(19)	1.382(3)	C(19)-H(19)	0.950(2)
C(19)-C(20)	1.380(3)	C(20)-H(20)	0.950(2)
C(20)-C(21)	1.389(3)	C(21)-H(21)	0.950(2)
C(22)-C(23)	1.393(3)	C(22)-C(27)	1.398(3)
C(22)-P(1)	1.824(2)	C(23)-H(23)	0.950(2)
C(23)-C(24)	1.394(3)	C(24)-H(24)	0.950(3)
C(24)-C(25)	1.380(4)	C(25)-H(25)	0.950(2)
C(25)-C(26)	1.380(4)	C(26)-H(26)	0.950(3)
C(26)-C(27)	1.388(3)	C(27)-H(27)	0.950(2)
C(28)-C(29)	1.401(3)	C(28)-C(33)	1.391(3)
C(28)-P(1)	1.830(2)	C(29)-H(29)	0.950(2)
C(29)-C(30)	1.388(3)	C(30)-H(30)	0.950(2)
C(30)-C(31)	1.384(4)	C(31)-H(31)	0.950(3)
C(31)-C(32)	1.379(3)	C(32)-H(32)	0.950(2)
C(32)-C(33)	1.392(3)	C(33)-H(33)	0.950(2)
C(34)-C(35)	1.392(3)	C(34)-C(39)	1.393(3)
C(34)-P(2)	1.834(2)	C(35)-H(35)	0.950(2)
C(35)-C(36)	1.388(3)	C(36)-H(36)	0.950(2)
C(36)-C(37)	1.384(4)	C(37)-H(37)	0.950(3)
C(37)-C(38)	1.382(3)	C(38)-H(38)	0.950(3)

C(38)-C(39)	1.388(3)	C(39)-H(39)	0.950(2)
C(40)-C(41)	1.392(3)	C(40)-C(45)	1.397(3)
C(40)-P(2)	1.831(2)	C(41)-H(41)	0.950(2)
C(41)-C(42)	1.386(3)	C(42)-H(42)	0.950(2)
C(42)-C(43)	1.388(3)	C(43)-H(43)	0.950(2)
C(43)-C(44)	1.381(3)	C(44)-H(44)	0.950(3)
C(44)-C(45)	1.384(3)	C(45)-H(45)	0.950(2)
C(46)-C(47)	1.393(3)	C(46)-C(51)	1.398(3)
C(46)-P(2)	1.834(2)	C(47)-H(47)	0.950(2)
C(47)-C(48)	1.394(3)	C(48)-H(48)	0.950(3)
C(48)-C(49)	1.380(4)	C(49)-H(49)	0.950(2)
C(49)-C(50)	1.386(4)	C(50)-H(50)	0.950(2)
C(50)-C(51)	1.385(3)	C(51)-H(51)	0.950(3)
C(52)-O(3)	1.158(3)	C(52)-Rh(1)	1.800(2)
N(2)-H(2)	0.880(2)	O(2)-H(2B)	0.840(2)
P(1)-Rh(1)	2.310(1)	P(2)-Rh(1)	2.331(1)
Rh(1)-S(1)	2.623(1)	Rh(1)-N(1)	2.278(2)

**Table C1.5. Complete listing of bond angles (°) for [Rh(*N,S*-(*N*-4h2mPT))](CO)(PPh<sub>3</sub>)<sub>2</sub>].**

Angle	Value	Angle	Value
C(1)-C(2)-C(3)	119.9(2)	C(1)-C(2)-H(2A)	120.0(2)
C(1)-C(6)-H(6)	120.0(2)	C(1)-C(6)-C(5)	120.1(2)
C(1)-C(7)-N(1)	116.5(2)	C(1)-C(7)-O(1)	118.0(2)
C(2)-C(1)-C(6)	119.7(2)	C(2)-C(1)-C(7)	119.2(2)
C(2)-C(3)-H(3)	120.1(3)	C(2)-C(3)-C(4)	119.9(2)
C(3)-C(4)-C(5)	120.3(3)	C(3)-C(4)-H(4)	119.8(3)
C(4)-C(5)-H(5)	120.0(3)	C(4)-C(5)-C(6)	120.1(2)
C(6)-C(1)-C(7)	121.0(2)	C(5)-C(6)-H(6)	120.0(2)
C(8)-N(2)-C(9)	129.5(2)	C(7)-N(1)-C(8)	122.0(2)
C(9)-C(10)-C(11)	120.3(2)	C(8)-N(2)-H(2)	115.3(2)
C(9)-C(14)-C(15)	121.7(2)	C(9)-C(10)-H(10)	119.9(2)
C(9)-N(2)-H(2)	115.3(2)	C(9)-C(14)-C(13)	118.2(2)
C(10)-C(11)-H(11)	120.1(2)	C(10)-C(11)-C(12)	119.8(2)
C(10)-C(9)-C(14)	120.6(2)	C(10)-C(9)-N(2)	122.0(2)
C(11)-C(12)-O(2)	118.2(2)	C(11)-C(12)-C(13)	119.9(2)
C(12)-C(13)-H(13)	119.4(2)	C(12)-C(13)-C(14)	121.2(2)
C(14)-C(15)-H(15A)	109.5(2)	C(12)-O(2)-H(2B)	109.5(2)
C(14)-C(15)-H(15C)	109.5(2)	C(13)-C(12)-O(2)	121.8(2)
C(14)-C(9)-N(2)	117.4(2)	C(13)-C(14)-C(15)	120.1(2)
C(16)-C(17)-C(18)	119.9(2)	C(14)-C(15)-H(15B)	109.5(2)
C(16)-C(21)-H(21)	119.8(2)	C(16)-C(17)-H(17)	120.0(2)



C(16)-P(1)-C(22)	100.7(1)	C(16)-C(21)-C(20)	120.5(2)
C(16)-P(1)-RH(1)	116.9(1)	C(16)-P(1)-C(28)	105.3(1)
C(17)-C(16)-C(21)	119.0(2)	C(17)-C(16)-P(1)	123.5(2)
C(17)-C(18)-H(18)	119.7(2)	C(17)-C(18)-C(19)	120.6(2)
C(18)-C(19)-C(20)	119.9(2)	C(18)-C(19)-H(19)	120.1(2)
C(19)-C(20)-H(20)	120.0(2)	C(19)-C(20)-C(21)	120.1(2)
C(21)-C(16)-P(1)	117.4(2)	C(20)-C(21)-H(21)	119.8(2)
C(22)-C(23)-C(24)	120.4(2)	C(22)-C(23)-H(23)	119.8(2)
C(22)-C(27)-H(27)	119.9(2)	C(22)-C(27)-C(26)	120.2(2)
C(22)-P(1)-RH(1)	113.7(1)	C(22)-P(1)-C(28)	106.3(1)
C(23)-C(22)-C(27)	118.8(2)	C(23)-C(22)-P(1)	120.1(2)
C(23)-C(24)-H(24)	119.9(2)	C(23)-C(24)-C(25)	120.2(2)
C(24)-C(25)-C(26)	119.8(2)	C(24)-C(25)-H(25)	120.1(3)
C(25)-C(26)-H(26)	119.7(3)	C(25)-C(26)-C(27)	120.5(2)
C(27)-C(22)-P(1)	121.0(2)	C(26)-C(27)-H(27)	119.9(2)
C(28)-C(29)-C(30)	120.4(2)	C(28)-C(29)-H(29)	119.8(2)
C(28)-C(33)-H(33)	119.8(2)	C(28)-C(33)-C(32)	120.5(2)
C(29)-C(28)-C(33)	118.7(2)	C(28)-P(1)-RH(1)	112.7(1)
C(29)-C(30)-H(30)	119.9(2)	C(29)-C(28)-P(1)	117.7(2)
C(30)-C(31)-C(32)	119.8(2)	C(29)-C(30)-C(31)	120.2(2)
C(31)-C(32)-H(32)	119.8(2)	C(30)-C(31)-H(31)	120.1(2)
C(33)-C(28)-P(1)	123.6(2)	C(31)-C(32)-C(33)	120.4(2)
C(34)-C(35)-C(36)	120.4(2)	C(32)-C(33)-H(33)	119.8(2)
C(34)-C(39)-H(39)	119.8(2)	C(34)-C(35)-H(35)	119.8(2)
C(34)-P(2)-C(40)	104.4(1)	C(34)-C(39)-C(38)	120.5(2)
C(34)-P(2)-RH(1)	115.7(1)	C(34)-P(2)-C(46)	101.5(1)
C(35)-C(34)-C(39)	118.8(2)	C(35)-C(34)-P(2)	121.2(2)
C(35)-C(36)-H(36)	119.8(3)	C(35)-C(36)-C(37)	120.4(2)
C(36)-C(37)-C(38)	119.5(2)	C(36)-C(37)-H(37)	120.2(3)
C(37)-C(38)-H(38)	119.8(2)	C(37)-C(38)-C(39)	120.3(2)
C(39)-C(34)-P(2)	120.0(2)	C(38)-C(39)-H(39)	119.7(2)
C(40)-C(41)-C(42)	120.9(2)	C(40)-C(41)-H(41)	119.5(2)
C(40)-C(45)-H(45)	119.8(2)	C(40)-C(45)-C(44)	120.3(2)
C(40)-P(2)-RH(1)	112.1(1)	C(40)-P(2)-C(46)	103.2(1)
C(41)-C(40)-C(45)	118.7(2)	C(41)-C(40)-P(2)	118.7(2)
C(41)-C(42)-H(42)	120.1(2)	C(41)-C(42)-C(43)	119.7(2)
C(42)-C(43)-C(44)	119.9(2)	C(42)-C(43)-H(43)	120.1(2)
C(43)-C(44)-H(44)	119.7(2)	C(43)-C(44)-C(45)	120.5(2)
C(45)-C(40)-P(2)	122.6(2)	C(44)-C(45)-H(45)	119.8(2)
C(46)-C(47)-C(48)	120.1(2)	C(46)-C(47)-H(47)	119.9(2)
C(46)-C(51)-H(51)	119.7(2)	C(46)-C(51)-C(50)	120.7(2)

C(47)-C(46)-C(51)	118.8(2)	C(46)-P(2)-Rh(1)	118.2(1)
C(47)-C(48)-H(48)	119.7(3)	C(47)-C(46)-P(2)	120.9(2)
C(48)-C(49)-C(50)	119.7(2)	C(47)-C(48)-C(49)	120.5(2)
C(49)-C(50)-H(50)	119.9(2)	C(48)-C(49)-H(49)	120.1(3)
C(51)-C(46)-P(2)	120.3(2)	C(49)-C(50)-C(51)	120.1(2)
C(52)-Rh(1)-P(1)	85.9(1)	C(50)-C(51)-H(51)	119.7(2)
H(11)-C(11)-C(12)	120.1(2)	C(52)-Rh(1)-P(2)	92.0(1)
H(13)-C(13)-C(14)	119.4(2)	H(10)-C(10)-C(11)	119.9(2)
H(15A)-C(15)-H(15C)	109.5(2)	H(15A)-C(15)-H(15B)	109.5(2)
H(18)-C(18)-C(19)	119.7(2)	H(15B)-C(15)-H(15C)	109.5(2)
H(20)-C(20)-C(21)	120.0(2)	H(17)-C(17)-C(18)	120.0(2)
H(24)-C(24)-C(25)	119.9(2)	H(19)-C(19)-C(20)	120.1(2)
H(26)-C(26)-C(27)	119.7(3)	H(23)-C(23)-C(24)	119.8(2)
H(3)-C(3)-C(4)	120.1(3)	H(25)-C(25)-C(26)	120.1(3)
H(30)-C(30)-C(31)	119.9(2)	H(29)-C(29)-C(30)	119.8(2)
H(32)-C(32)-C(33)	119.8(2)	H(2A)-C(2)-C(3)	120.0(2)
H(36)-C(36)-C(37)	119.8(3)	H(31)-C(31)-C(32)	120.1(2)
H(38)-C(38)-C(39)	119.8(2)	H(35)-C(35)-C(36)	119.8(2)
H(42)-C(42)-C(43)	120.1(2)	H(37)-C(37)-C(38)	120.2(3)
H(44)-C(44)-C(45)	119.8(2)	H(4)-C(4)-C(5)	119.8(3)
H(48)-C(48)-C(49)	119.7(3)	H(41)-C(41)-C(42)	119.5(2)
H(5)-C(5)-C(6)	120.0(3)	H(43)-C(43)-C(44)	120.1(2)
H(50)-C(50)-C(51)	119.9(2)	H(47)-C(47)-C(48)	119.9(2)
N(1)-C(7)-O(1)	125.5(2)	H(49)-C(49)-C(50)	120.1(2)
N(1)-C(8)-S(1)	113.6(2)	N(1)-C(8)-N(2)	120.7(2)
O(3)-C(52)-Rh(1)	176.9(2)	N(1)-Rh(1)-C(52)	156.75(9)
P(1)-Rh(1)-P(2)	176.4(1)	N(2)-C(8)-S(1)	125.7(2)
P(2)-Rh(1)-N(1)	93.94(4)	P(1)-Rh(1)-N(1)	89.16(4)
S(1)-Rh(1)-C(52)	139.83(7)	S(1)-Rh(1)-N(1)	63.07(5)
S(1)-Rh(1)-P(2)	86.61(2)	S(1)-Rh(1)-P(1)	93.16(2)

**C2. Crystal data of bis(triphenylphosphine)-*N,S*-(*N*-benzoyl-*N'*-phenylthiourea)-*S,O*-(*N*-benzoyl-*N'*-phenylthiourea)rhodium(I)**  
**[Rh(*N,S*-(*N*-PT))(*S,O*-(*N*-PT))(PPh<sub>3</sub>)<sub>2</sub>]**

**Table C2.1. Atomic coordinates and equivalent isotropic displacement parameters (Å<sup>2</sup>) for [Rh(*N,S*-(*N*-PT))(*S,O*-(*N*-PT))(PPh<sub>3</sub>)<sub>2</sub>].  $U_{\text{(eq)}}$  is defined as one third of the trace of the orthogonalized  $U^{\text{ij}}$  tensor.**

Atom	x/a	y/b	z/c	$U_{\text{(eq)}}$
C(1)	0.6146(5)	0.7042(4)	0.2257(2)	0.0206
C(2)	0.5100(5)	0.6678(4)	0.1711(2)	0.02506
C(3)	0.4778(5)	0.7476(5)	0.1483(3)	0.02893
C(4)	0.5492(5)	0.8638(5)	0.1802(3)	0.03033
C(5)	0.6535(6)	0.9003(5)	0.2339(3)	0.03906
C(6)	0.6872(5)	0.8216(5)	0.2573(3)	0.03157
C(7)	0.6421(4)	0.6154(4)	0.2535(2)	0.01731
C(8)	0.7623(5)	0.5983(4)	0.3509(2)	0.01923
C(9)	0.9518(5)	0.7768(4)	0.4262(2)	0.02057
C(10)	0.9824(5)	0.8529(4)	0.3842(3)	0.02396
C(11)	1.0704(5)	0.9690(4)	0.4109(3)	0.02804
C(12)	1.1313(5)	1.0113(5)	0.4776(3)	0.03069
C(13)	1.1022(5)	0.9355(4)	0.5193(3)	0.02835
C(14)	1.0125(5)	0.8179(4)	0.4941(2)	0.02562
C(15)	0.1584(4)	-0.1770(4)	0.1041(2)	0.0177
C(16)	0.1389(5)	-0.2866(4)	0.1127(2)	0.02112
C(17)	0.0337(5)	-0.3865(4)	0.0717(3)	0.02762
C(18)	-0.0542(5)	-0.3785(4)	0.0228(3)	0.03128
C(19)	-0.0361(5)	-0.2707(5)	0.0143(3)	0.0304
C(20)	0.0703(5)	-0.1702(4)	0.0540(2)	0.0247
C(21)	0.2707(4)	-0.0698(4)	0.1512(2)	0.01723
C(22)	0.3858(4)	0.1291(4)	0.1675(2)	0.01679
C(23)	0.3949(4)	0.2538(4)	0.0890(2)	0.01687
C(24)	0.3694(5)	0.1755(4)	0.0316(2)	0.02235
C(25)	0.3512(5)	0.2050(5)	-0.0290(2)	0.02724
C(26)	0.3546(5)	0.3088(5)	-0.0348(3)	0.02725
C(27)	0.3768(5)	0.3850(5)	0.0212(3)	0.02703
C(28)	0.3969(5)	0.3577(4)	0.0825(2)	0.02202
C(29)	0.8354(4)	0.5134(4)	0.2203(2)	0.01703
C(30)	0.8087(5)	0.5774(4)	0.1769(2)	0.01799

C(31)	0.8982(5)	0.6908(4)	0.1816(2)	0.02261
C(32)	1.0149(5)	0.7431(4)	0.2293(3)	0.02356
C(33)	1.0416(5)	0.6818(4)	0.2736(3)	0.02503
C(34)	0.9529(4)	0.5677(4)	0.2695(2)	0.01951
C(35)	0.8096(4)	0.3067(4)	0.2634(2)	0.01617
C(36)	0.7813(4)	0.2614(4)	0.3178(2)	0.01959
C(37)	0.8475(5)	0.2103(4)	0.3491(2)	0.02274
C(38)	0.9394(5)	0.2040(4)	0.3275(2)	0.0246
C(39)	0.9675(5)	0.2481(4)	0.2740(3)	0.0253
C(40)	0.9028(5)	0.2985(4)	0.2420(2)	0.02094
C(41)	0.6920(4)	0.2839(4)	0.1330(2)	0.01746
C(42)	0.6335(5)	0.1630(4)	0.1233(2)	0.02085
C(43)	0.6261(5)	0.0969(4)	0.0672(2)	0.02443
C(44)	0.6758(5)	0.1496(5)	0.0200(3)	0.02919
C(45)	0.7316(5)	0.2695(5)	0.0288(3)	0.02905
C(46)	0.7398(5)	0.3362(4)	0.0847(2)	0.02264
C(47)	0.3406(4)	0.4511(4)	0.2730(2)	0.01743
C(48)	0.4323(5)	0.5553(4)	0.3178(2)	0.02086
C(49)	0.4231(5)	0.6549(4)	0.3171(2)	0.02454
C(50)	0.3230(5)	0.6527(4)	0.2721(3)	0.02674
C(51)	0.2309(5)	0.5501(4)	0.2281(3)	0.02772
C(52)	0.2399(5)	0.4497(4)	0.2279(2)	0.02245
C(53)	0.3743(4)	0.3161(4)	0.3630(2)	0.01533
C(54)	0.4479(5)	0.2764(4)	0.3996(2)	0.01988
C(55)	0.4525(5)	0.2711(4)	0.4649(2)	0.02307
C(56)	0.3832(5)	0.3059(4)	0.4944(2)	0.02654
C(57)	0.3079(5)	0.3432(4)	0.4581(3)	0.02626
C(58)	0.3027(5)	0.3475(4)	0.3927(2)	0.02109
C(59)	0.2144(4)	0.1986(4)	0.2300(2)	0.01606
C(60)	0.1613(5)	0.1871(4)	0.1622(2)	0.02274
C(61)	0.0440(5)	0.0922(4)	0.1273(3)	0.02766
C(62)	-0.0201(5)	0.0074(4)	0.1582(3)	0.03025
C(63)	0.0329(5)	0.0161(4)	0.2244(3)	0.02562
C(64)	0.1488(4)	0.1106(4)	0.2597(2)	0.01915
C(65)	0.5507(6)	0.9975(7)	0.3907(5)	0.06586
C(66)	0.4255(5)	0.9315(6)	0.4047(3)	0.05125
C(67)	0.3287(6)	0.9576(5)	0.3707(4)	0.05276
C(68)	0.2021(6)	0.5574(5)	0.4004(3)	0.03694
C(69)	0.1982(5)	0.6645(5)	0.5093(3)	0.03453
N(1)	0.7364(4)	0.6592(3)	0.3105(2)	0.01899
N(2)	0.8651(4)	0.6556(3)	0.4048(2)	0.02011

N(3)	0.3019(4)	0.0284(3)	0.1271(2)	0.01875
N(4)	0.4227(3)	0.2339(3)	0.1531(2)	0.01416
O(1)	0.5755(3)	0.5124(3)	0.2199(2)	0.01713
O(2)	0.3246(3)	-0.0777(3)	0.2053(2)	0.02585
O(3)	0.4029(5)	0.8481(4)	0.4307(3)	0.06616
O(4)	0.0905(4)	0.4414(3)	0.4804(2)	0.03423
P(1)	0.71835(11)	0.36389(9)	0.21466(5)	0.01326
P(2)	0.36520(11)	0.32623(10)	0.27662(5)	0.01383
S(1)	0.67466(11)	0.45207(9)	0.35041(5)	0.01708
S(2)	0.47073(11)	0.15778(9)	0.25213(5)	0.0154
S(3)	0.09719(15)	0.53642(13)	0.44639(7)	0.03899
Rh(1)	0.54174(3)	0.34998(3)	0.24335(2)	0.01263

**Table C2.2. Hydrogen coordinates and isotropic displacement parameters ( $\text{\AA}^2$ ) for  $[\text{Rh}(\text{N},\text{S}-(\text{N-PT}))(\text{S},\text{O}-(\text{N-PT}))(\text{PPh}_3)_2]$ .**

Atom	x/a	y/b	z/c	$U_{\text{(eq)}}$
H(2)	0.46034	0.58804	0.14918	0.03007
H(3)	0.40662	0.72223	0.11071	0.03471
H(4)	0.52617	0.91809	0.16518	0.0364
H(5)	0.7034	0.98032	0.25524	0.04687
H(6)	0.75912	0.84769	0.29466	0.03788
H(10)	0.94329	0.82557	0.33791	0.02875
H(11)	1.08956	1.02134	0.38226	0.03365
H(12)	1.19238	1.09132	0.49474	0.03683
H(13)	1.14347	0.96356	0.56545	0.03402
H(14)	0.99287	0.76609	0.52295	0.03074
H(16)	0.19797	-0.29239	0.14677	0.02534
H(17)	0.02182	-0.46068	0.07698	0.03315
H(18)	-0.127	-0.44714	-0.0048	0.03754
H(19)	-0.09689	-0.26556	-0.01903	0.03648
H(20)	0.08327	-0.09642	0.04716	0.02964
H(24)	0.36466	0.1029	0.03443	0.02682
H(25)	0.33597	0.15266	-0.06749	0.03269
H(26)	0.34183	0.32769	-0.07675	0.03271
H(27)	0.37825	0.45611	0.01772	0.03243
H(28)	0.4124	0.41073	0.1206	0.02642
H(2A)	0.88035	0.61192	0.42996	0.02414
H(30)	0.72875	0.54254	0.14406	0.02159
H(31)	0.87969	0.73354	0.15185	0.02714
H(32)	1.07654	0.82086	0.23168	0.02827

H(33)	1.12108	0.71823	0.30684	0.03003
H(34)	0.97152	0.5262	0.30013	0.02341
H(36)	0.71783	0.26523	0.33332	0.02351
H(37)	0.82831	0.17926	0.3861	0.02729
H(38)	0.98352	0.16917	0.34958	0.02952
H(39)	1.03138	0.24404	0.25891	0.03037
H(40)	0.92223	0.32802	0.20466	0.02512
H(42)	0.59865	0.1259	0.15544	0.02501
H(43)	0.58654	0.01481	0.06119	0.02932
H(44)	0.6718	0.10426	-0.01829	0.03503
H(45)	0.76462	0.306	-0.00397	0.03486
H(46)	0.77833	0.41815	0.0902	0.02717
H(48)	0.50145	0.55802	0.34902	0.02503
H(49)	0.48622	0.72536	0.34777	0.02945
H(50)	0.3177	0.72142	0.27157	0.03209
H(51)	0.16096	0.54769	0.19783	0.03326
H(52)	0.1769	0.37979	0.19677	0.02693
H(54)	0.49546	0.2527	0.37978	0.02386
H(55)	0.50288	0.24377	0.48937	0.02768
H(56)	0.38769	0.304	0.53929	0.03185
H(57)	0.25956	0.36586	0.4778	0.03152
H(58)	0.24984	0.37222	0.36791	0.02531
H(60)	0.20611	0.24463	0.14028	0.02729
H(61)	0.00794	0.08586	0.08193	0.03319
H(62)	-0.10064	-0.05712	0.13427	0.0363
H(63)	-0.01088	-0.04339	0.24554	0.03075
H(64)	0.18418	0.11557	0.30497	0.02298
H(65A)	0.60988	0.97456	0.41388	0.09879
H(65B)	0.58578	1.08119	0.40593	0.09879
H(65C)	0.53728	0.97923	0.34309	0.09879
H(67A)	0.31722	0.94354	0.32317	0.07914
H(67B)	0.35581	1.03918	0.38739	0.07914
H(67C)	0.24865	0.90736	0.37879	0.07914
H(68A)	0.27807	0.56026	0.42779	0.05542
H(68B)	0.2257	0.63081	0.38618	0.05542
H(68C)	0.16126	0.49302	0.36164	0.05542
H(69A)	0.15473	0.66795	0.54149	0.05178
H(69B)	0.22042	0.7327	0.48977	0.05178
H(69C)	0.27526	0.66379	0.53142	0.05178

**Table C2.3. Anisotropic displacement parameters ( $\text{\AA}^2$ ) for  $[\text{Rh}(\text{N},\text{S}-(\text{N-PT}))(\text{S},\text{O}-(\text{N-PT}))(\text{PPh}_3)_2]$ . The anisotropic displacement factor exponent takes the form:  $-2\pi^2[\text{h}^2\text{a}^{*2}\text{U}^{11} + \dots + 2\text{hka}^*\text{b}^*\text{U}^{23}]$ .**

Atom	$\text{U}^{11}$	$\text{U}^{22}$	$\text{U}^{33}$	$\text{U}^{12}$	$\text{U}^{13}$	$\text{U}^{23}$
C(1)	0.021(3)	0.019(2)	0.027(3)	0.011(2)	0.013(2)	0.011(2)
C(2)	0.029(3)	0.021(3)	0.028(3)	0.014(2)	0.009(2)	0.008(2)
C(3)	0.028(3)	0.032(3)	0.034(3)	0.020(3)	0.010(2)	0.017(2)
C(4)	0.038(3)	0.024(3)	0.042(3)	0.021(3)	0.019(3)	0.020(2)
C(5)	0.040(4)	0.018(3)	0.056(4)	0.014(3)	0.009(3)	0.010(2)
C(6)	0.027(3)	0.023(3)	0.043(3)	0.014(2)	0.005(3)	0.009(2)
C(7)	0.012(2)	0.014(2)	0.027(3)	0.005(2)	0.009(2)	0.006(2)
C(8)	0.017(3)	0.019(2)	0.024(3)	0.009(2)	0.010(2)	0.004(2)
C(9)	0.015(3)	0.021(2)	0.027(3)	0.010(2)	0.008(2)	0.004(2)
C(10)	0.019(3)	0.026(3)	0.026(3)	0.010(2)	0.007(2)	0.006(2)
C(11)	0.027(3)	0.024(3)	0.035(3)	0.013(2)	0.013(2)	0.012(2)
C(12)	0.020(3)	0.022(3)	0.044(3)	0.007(2)	0.008(2)	0.004(2)
C(13)	0.020(3)	0.024(3)	0.032(3)	0.009(2)	-0.001(2)	0.002(2)
C(14)	0.022(3)	0.023(3)	0.029(3)	0.011(2)	0.001(2)	0.004(2)
C(15)	0.016(3)	0.014(2)	0.024(2)	0.006(2)	0.011(2)	0.005(2)
C(16)	0.019(3)	0.019(2)	0.028(3)	0.008(2)	0.013(2)	0.008(2)
C(17)	0.031(3)	0.017(3)	0.036(3)	0.010(2)	0.019(2)	0.006(2)
C(18)	0.026(3)	0.018(3)	0.033(3)	0.000(2)	0.006(2)	-0.003(2)
C(19)	0.024(3)	0.029(3)	0.027(3)	0.007(2)	0.002(2)	0.007(2)
C(20)	0.024(3)	0.020(3)	0.026(3)	0.009(2)	0.003(2)	0.008(2)
C(21)	0.015(2)	0.016(2)	0.026(3)	0.011(2)	0.009(2)	0.007(2)
C(22)	0.011(2)	0.020(2)	0.022(2)	0.009(2)	0.007(2)	0.006(2)
C(23)	0.009(2)	0.017(2)	0.023(2)	0.005(2)	0.004(2)	0.008(2)
C(24)	0.020(3)	0.023(3)	0.022(3)	0.010(2)	0.005(2)	0.007(2)
C(25)	0.024(3)	0.035(3)	0.022(3)	0.015(3)	0.005(2)	0.005(2)
C(26)	0.021(3)	0.033(3)	0.024(3)	0.010(2)	0.005(2)	0.014(2)
C(27)	0.020(3)	0.026(3)	0.034(3)	0.010(2)	0.006(2)	0.014(2)
C(28)	0.022(3)	0.018(2)	0.025(3)	0.008(2)	0.008(2)	0.009(2)
C(29)	0.016(3)	0.015(2)	0.024(2)	0.009(2)	0.011(2)	0.005(2)
C(30)	0.016(3)	0.020(2)	0.024(2)	0.011(2)	0.012(2)	0.007(2)
C(31)	0.029(3)	0.017(2)	0.030(3)	0.014(2)	0.018(2)	0.011(2)
C(32)	0.021(3)	0.011(2)	0.038(3)	0.004(2)	0.018(2)	0.006(2)
C(33)	0.017(3)	0.018(2)	0.036(3)	0.008(2)	0.005(2)	-0.001(2)
C(34)	0.015(3)	0.017(2)	0.027(3)	0.009(2)	0.006(2)	0.005(2)
C(35)	0.012(2)	0.012(2)	0.021(2)	0.004(2)	0.003(2)	0.005(2)
C(36)	0.013(2)	0.018(2)	0.023(2)	0.006(2)	0.004(2)	0.003(2)

C(37)	0.024(3)	0.022(3)	0.023(3)	0.012(2)	0.004(2)	0.009(2)
C(38)	0.019(3)	0.026(3)	0.032(3)	0.016(2)	0.003(2)	0.007(2)
C(39)	0.019(3)	0.021(3)	0.038(3)	0.011(2)	0.008(2)	0.006(2)
C(40)	0.016(3)	0.020(2)	0.028(3)	0.010(2)	0.008(2)	0.006(2)
C(41)	0.014(2)	0.017(2)	0.021(2)	0.008(2)	0.004(2)	0.001(2)
C(42)	0.016(3)	0.021(2)	0.025(3)	0.007(2)	0.009(2)	0.006(2)
C(43)	0.021(3)	0.018(2)	0.030(3)	0.007(2)	0.007(2)	0.001(2)
C(44)	0.025(3)	0.027(3)	0.027(3)	0.007(2)	0.010(2)	-0.003(2)
C(45)	0.028(3)	0.031(3)	0.026(3)	0.011(3)	0.014(2)	0.007(2)
C(46)	0.020(3)	0.017(2)	0.027(3)	0.005(2)	0.009(2)	0.005(2)
C(47)	0.016(3)	0.017(2)	0.026(3)	0.010(2)	0.011(2)	0.011(2)
C(48)	0.023(3)	0.024(3)	0.026(3)	0.016(2)	0.012(2)	0.013(2)
C(49)	0.028(3)	0.021(3)	0.030(3)	0.014(2)	0.014(2)	0.006(2)
C(50)	0.032(3)	0.024(3)	0.039(3)	0.021(3)	0.019(3)	0.016(2)
C(51)	0.029(3)	0.028(3)	0.038(3)	0.021(3)	0.013(2)	0.020(2)
C(52)	0.022(3)	0.022(3)	0.031(3)	0.014(2)	0.012(2)	0.012(2)
C(53)	0.012(2)	0.013(2)	0.016(2)	0.003(2)	0.004(2)	0.003(2)
C(54)	0.018(3)	0.014(2)	0.026(3)	0.006(2)	0.009(2)	0.006(2)
C(55)	0.020(3)	0.020(2)	0.023(3)	0.006(2)	0.003(2)	0.008(2)
C(56)	0.029(3)	0.023(3)	0.019(3)	0.007(2)	0.007(2)	0.005(2)
C(57)	0.025(3)	0.024(3)	0.033(3)	0.012(2)	0.015(2)	0.008(2)
C(58)	0.017(3)	0.023(3)	0.026(3)	0.010(2)	0.009(2)	0.009(2)
C(59)	0.011(2)	0.016(2)	0.026(2)	0.010(2)	0.007(2)	0.006(2)
C(60)	0.018(3)	0.027(3)	0.025(3)	0.012(2)	0.006(2)	0.006(2)
C(61)	0.021(3)	0.027(3)	0.029(3)	0.010(2)	0.001(2)	0.002(2)
C(62)	0.015(3)	0.019(3)	0.043(3)	0.005(2)	-0.002(2)	0.000(2)
C(63)	0.019(3)	0.016(2)	0.042(3)	0.007(2)	0.012(2)	0.011(2)
C(64)	0.018(3)	0.019(2)	0.026(3)	0.012(2)	0.007(2)	0.009(2)
C(65)	0.030(4)	0.057(5)	0.119(7)	0.023(4)	0.026(4)	0.039(4)
C(66)	0.015(3)	0.060(4)	0.078(5)	0.012(3)	0.010(3)	0.065(4)
C(67)	0.042(4)	0.027(3)	0.087(5)	0.015(3)	0.021(4)	0.009(3)
C(68)	0.048(4)	0.029(3)	0.036(3)	0.019(3)	0.016(3)	0.009(2)
C(69)	0.032(3)	0.041(3)	0.032(3)	0.019(3)	0.011(3)	0.007(2)
N(1)	0.016(2)	0.017(2)	0.025(2)	0.008(2)	0.008(2)	0.006(2)
N(2)	0.017(2)	0.017(2)	0.022(2)	0.007(2)	0.003(2)	0.005(2)
N(3)	0.018(2)	0.016(2)	0.021(2)	0.007(2)	0.007(2)	0.004(2)
N(4)	0.009(2)	0.012(2)	0.018(2)	0.003(2)	0.004(2)	0.002(1)
O(1)	0.017(2)	0.015(2)	0.022(2)	0.009(1)	0.007(1)	0.007(1)
O(2)	0.024(2)	0.016(2)	0.028(2)	0.006(2)	-0.001(2)	0.006(1)
O(3)	0.080(4)	0.056(3)	0.084(4)	0.043(3)	0.034(3)	0.040(3)
O(4)	0.037(2)	0.030(2)	0.037(2)	0.016(2)	0.011(2)	0.014(2)



P(1)	0.0103(6)	0.0118(6)	0.0172(6)	0.0052(5)	0.0041(5)	0.0037(4)
P(2)	0.0118(6)	0.0145(6)	0.0176(6)	0.0082(5)	0.0044(5)	0.0056(4)
S(1)	0.0147(6)	0.0136(6)	0.0198(6)	0.0055(5)	0.0029(5)	0.0039(4)
S(2)	0.0134(6)	0.0128(5)	0.0190(6)	0.0058(5)	0.0041(5)	0.0059(4)
S(3)	0.0375(9)	0.0378(8)	0.0411(8)	0.0188(7)	0.0111(7)	0.0082(6)
Rh(1)	0.0100(2)	0.0109(2)	0.0172(2)	0.0054(2)	0.0039(1)	0.0046(1)

**Table C2.4. Complete listing of bond lengths (Å) for [Rh(*N,S*-(*N*-PT))(*S,O*-(*N*-PT))(PPh<sub>3</sub>)<sub>2</sub>].**

Bond	Distance	Bond	Distance
C(1)-C(2)	1.389(7)	C(1)-C(6)	1.394(7)
C(1)-C(7)	1.511(7)	C(2)-H(2)	0.950(5)
C(2)-C(3)	1.390(8)	C(3)-H(3)	0.950(6)
C(3)-C(4)	1.384(8)	C(4)-H(4)	0.950(6)
C(4)-C(5)	1.375(9)	C(5)-H(5)	0.950(6)
C(5)-C(6)	1.392(9)	C(6)-H(6)	0.950(6)
C(7)-N(1)	1.341(6)	C(7)-O(1)	1.260(6)
C(8)-N(1)	1.324(7)	C(8)-N(2)	1.351(6)
C(8)-S(1)	1.733(5)	C(9)-C(10)	1.390(8)
C(9)-C(14)	1.398(7)	C(9)-N(2)	1.419(6)
C(10)-H(10)	0.950(5)	C(10)-C(11)	1.381(7)
C(11)-H(11)	0.950(6)	C(11)-C(12)	1.377(8)
C(12)-H(12)	0.950(6)	C(12)-C(13)	1.381(9)
C(13)-H(13)	0.950(6)	C(13)-C(14)	1.396(7)
C(14)-H(14)	0.950(6)	C(15)-C(16)	1.401(7)
C(15)-C(20)	1.395(7)	C(15)-C(21)	1.507(7)
C(16)-H(16)	0.950(5)	C(16)-C(17)	1.385(7)
C(17)-H(17)	0.950(6)	C(17)-C(18)	1.386(8)
C(18)-H(18)	0.950(6)	C(18)-C(19)	1.382(8)
C(19)-H(19)	0.950(6)	C(19)-C(20)	1.385(7)
C(20)-H(20)	0.950(6)	C(21)-N(3)	1.365(7)
C(21)-O(2)	1.239(6)	C(22)-N(3)	1.314(6)
C(22)-N(4)	1.342(6)	C(22)-S(2)	1.780(5)
C(23)-C(24)	1.408(7)	C(23)-C(28)	1.393(7)
C(23)-N(4)	1.414(6)	C(24)-H(24)	0.950(6)
C(24)-C(25)	1.386(8)	C(25)-H(25)	0.950(5)
C(25)-C(26)	1.383(8)	C(26)-H(26)	0.950(6)
C(26)-C(27)	1.383(7)	C(27)-H(27)	0.950(6)
C(27)-C(28)	1.387(8)	C(28)-H(28)	0.950(5)
C(29)-C(30)	1.402(7)	C(29)-C(34)	1.403(7)
C(29)-P(1)	1.816(5)	C(30)-H(30)	0.950(5)
C(30)-C(31)	1.377(7)	C(31)-H(31)	0.950(6)

C(31)-C(32)	1.383(7)	C(32)-H(32)	0.950(5)
C(32)-C(33)	1.385(8)	C(33)-H(33)	0.950(5)
C(33)-C(34)	1.384(7)	C(34)-H(34)	0.950(5)
C(35)-C(36)	1.396(7)	C(35)-C(40)	1.394(7)
C(35)-P(1)	1.840(5)	C(36)-H(36)	0.950(5)
C(36)-C(37)	1.399(7)	C(37)-H(37)	0.950(6)
C(37)-C(38)	1.368(8)	C(38)-H(38)	0.950(6)
C(38)-C(39)	1.374(8)	C(39)-H(39)	0.950(6)
C(39)-C(40)	1.383(8)	C(40)-H(40)	0.950(6)
C(41)-C(42)	1.397(7)	C(41)-C(46)	1.388(8)
C(41)-P(1)	1.837(5)	C(42)-H(42)	0.950(6)
C(42)-C(43)	1.381(7)	C(43)-H(43)	0.950(5)
C(43)-C(44)	1.379(8)	C(44)-H(44)	0.950(5)
C(44)-C(45)	1.388(8)	C(45)-H(45)	0.950(6)
C(45)-C(46)	1.379(7)	C(46)-H(46)	0.950(5)
C(47)-C(48)	1.397(7)	C(47)-C(52)	1.395(7)
C(47)-P(2)	1.833(5)	C(48)-H(48)	0.950(5)
C(48)-C(49)	1.387(8)	C(49)-H(49)	0.950(5)
C(49)-C(50)	1.383(8)	C(50)-H(50)	0.950(6)
C(50)-C(51)	1.379(7)	C(51)-H(51)	0.950(6)
C(51)-C(52)	1.394(8)	C(52)-H(52)	0.950(5)
C(53)-C(54)	1.394(7)	C(53)-C(58)	1.397(7)
C(53)-P(2)	1.842(5)	C(54)-H(54)	0.950(5)
C(54)-C(55)	1.392(7)	C(55)-H(55)	0.950(6)
C(55)-C(56)	1.394(8)	C(56)-H(56)	0.950(6)
C(56)-C(57)	1.384(8)	C(57)-H(57)	0.950(6)
C(57)-C(58)	1.390(8)	C(58)-H(58)	0.950(5)
C(59)-C(60)	1.412(7)	C(59)-C(64)	1.386(7)
C(59)-P(2)	1.821(5)	C(60)-H(60)	0.950(6)
C(60)-C(61)	1.387(7)	C(61)-H(61)	0.950(6)
C(61)-C(62)	1.372(8)	C(62)-H(62)	0.950(5)
C(62)-C(63)	1.389(8)	C(63)-H(63)	0.950(6)
C(63)-C(64)	1.378(7)	C(64)-H(64)	0.950(5)
C(65)-H(65A)	0.980(8)	C(65)-H(65B)	0.980(8)
C(65)-H(65C)	0.980(10)	C(65)-C(66)	1.519(10)
C(66)-C(67)	1.469(10)	C(66)-O(3)	1.228(10)
C(67)-H(67A)	0.980(8)	C(67)-H(67B)	0.980(7)
C(67)-H(67C)	0.980(7)	C(68)-H(68A)	0.980(7)
C(68)-H(68B)	0.980(6)	C(68)-H(68C)	0.980(6)
C(68)-S(3)	1.751(7)	C(69)-H(69A)	0.980(6)
C(69)-H(69B)	0.980(7)	C(69)-H(69C)	0.980(6)

C(69)-S(3)	1.772(6)	N(2)-H(2A)	0.880(5)
N(4)-Rh(1)	2.087(4)	O(4)-S(3)	1.492(5)
P(1)-Rh(1)	2.361(2)	P(2)-Rh(1)	2.369(2)
S(1)-Rh(1)	2.339(2)	S(2)-Rh(1)	2.330(2)
O(1)-Rh(1)	2.133(4)		

**Table C2.5. Complete listing of bond angles (°) for [Rh(*N,S*-(*N*-PT))(*S,O*-(*N*-PT))(PPh<sub>3</sub>)<sub>2</sub>].**

Angle	Value	Angle	Value
C(1)-C(2)-C(3)	120.3(5)	C(1)-C(2)-H(2)	119.9(5)
C(1)-C(6)-H(6)	120.2(6)	C(1)-C(6)-C(5)	119.6(6)
C(1)-C(7)-N(1)	114.3(4)	C(1)-C(7)-O(1)	116.2(5)
C(2)-C(1)-C(6)	119.4(5)	C(2)-C(1)-C(7)	119.7(5)
C(2)-C(3)-H(3)	119.9(6)	C(2)-C(3)-C(4)	120.2(5)
C(3)-C(4)-C(5)	119.6(6)	C(3)-C(4)-H(4)	120.2(6)
C(4)-C(5)-H(5)	119.5(6)	C(4)-C(5)-C(6)	121.0(6)
C(5)-C(6)-H(6)	120.2(6)	C(6)-C(1)-C(7)	120.7(5)
C(7)-N(1)-C(8)	125.8(5)	C(8)-N(2)-H(2A)	115.7(5)
C(8)-S(1)-Rh(1)	109.3(2)	C(8)-N(2)-C(9)	128.5(5)
C(9)-C(10)-H(10)	120.5(5)	C(9)-C(10)-C(11)	119.1(5)
C(9)-C(14)-C(13)	119.7(5)	C(9)-C(14)-H(14)	120.1(5)
C(10)-C(11)-H(11)	119.0(6)	C(9)-N(2)-H(2A)	115.7(5)
C(10)-C(9)-C(14)	119.7(5)	C(10)-C(11)-C(12)	122.1(5)
C(11)-C(12)-C(13)	118.9(5)	C(10)-C(9)-N(2)	124.4(5)
C(12)-C(13)-H(13)	119.8(6)	C(11)-C(12)-H(12)	120.5(6)
C(14)-C(9)-N(2)	115.8(5)	C(12)-C(13)-C(14)	120.5(5)
C(15)-C(16)-C(17)	120.2(5)	C(13)-C(14)-H(14)	120.1(5)
C(15)-C(20)-H(20)	119.9(5)	C(15)-C(16)-H(16)	119.9(5)
C(15)-C(21)-N(3)	113.2(4)	C(15)-C(20)-C(19)	120.2(5)
C(16)-C(15)-C(20)	119.1(5)	C(15)-C(21)-O(2)	119.7(5)
C(16)-C(17)-H(17)	120.0(6)	C(16)-C(15)-C(21)	119.0(5)
C(17)-C(18)-C(19)	120.1(5)	C(16)-C(17)-C(18)	120.1(5)
C(18)-C(19)-H(19)	119.8(6)	C(17)-C(18)-H(18)	120.0(6)
C(20)-C(15)-C(21)	121.7(5)	C(18)-C(19)-C(20)	120.3(5)
C(22)-N(4)-C(23)	125.2(4)	C(19)-C(20)-H(20)	119.9(5)
C(22)-S(2)-Rh(1)	82.3(2)	C(21)-N(3)-C(22)	118.2(4)
C(23)-C(24)-C(25)	119.6(5)	C(22)-N(4)-Rh(1)	103.8(3)
C(23)-C(28)-H(28)	119.4(5)	C(23)-C(24)-H(24)	120.2(5)
C(23)-N(4)-Rh(1)	130.7(3)	C(23)-C(28)-C(27)	121.2(5)
C(24)-C(23)-C(28)	118.4(5)	C(24)-C(23)-N(4)	123.2(5)
C(24)-C(25)-H(25)	119.3(6)	C(24)-C(25)-C(26)	121.4(5)
C(25)-C(26)-C(27)	119.3(5)	C(25)-C(26)-H(26)	120.4(6)

C(26)-C(27)-H(27)	119.9(6)	C(26)-C(27)-C(28)	120.1(5)
C(28)-C(23)-N(4)	118.4(5)	C(27)-C(28)-H(28)	119.4(5)
C(29)-C(30)-C(31)	120.1(5)	C(29)-C(30)-H(30)	120.0(5)
C(29)-C(34)-H(34)	120.0(5)	C(29)-C(34)-C(33)	120.1(5)
C(29)-P(1)-C(41)	105.4(3)	C(29)-P(1)-C(35)	103.9(3)
C(30)-C(29)-C(34)	118.9(5)	C(29)-P(1)-Rh(1)	112.1(2)
C(30)-C(31)-H(31)	119.6(5)	C(30)-C(29)-P(1)	120.6(4)
C(31)-C(32)-C(33)	119.9(5)	C(30)-C(31)-C(32)	120.7(5)
C(32)-C(33)-H(33)	119.9(5)	C(31)-C(32)-H(32)	120.1(5)
C(34)-C(29)-P(1)	120.5(4)	C(32)-C(33)-C(34)	120.3(5)
C(35)-C(36)-C(37)	119.2(5)	C(33)-C(34)-H(34)	120.0(5)
C(35)-C(40)-H(40)	119.4(5)	C(35)-C(36)-H(36)	120.4(5)
C(35)-P(1)-C(41)	97.0(3)	C(35)-C(40)-C(39)	121.3(5)
C(36)-C(35)-C(40)	118.5(5)	C(35)-P(1)-Rh(1)	117.8(2)
C(36)-C(37)-H(37)	119.4(5)	C(36)-C(35)-P(1)	122.3(4)
C(37)-C(38)-C(39)	119.8(5)	C(36)-C(37)-C(38)	121.3(5)
C(38)-C(39)-H(39)	120.1(6)	C(37)-C(38)-H(38)	120.1(5)
C(40)-C(35)-P(1)	119.0(4)	C(38)-C(39)-C(40)	119.9(5)
C(41)-C(42)-C(43)	120.5(5)	C(39)-C(40)-H(40)	119.4(5)
C(41)-C(46)-H(46)	119.9(5)	C(41)-C(42)-H(42)	119.7(5)
C(41)-P(1)-Rh(1)	118.5(2)	C(41)-C(46)-C(45)	120.2(5)
C(42)-C(41)-C(46)	118.8(5)	C(42)-C(41)-P(1)	116.5(4)
C(42)-C(43)-H(43)	119.8(5)	C(42)-C(43)-C(44)	120.3(5)
C(43)-C(44)-C(45)	119.3(5)	C(43)-C(44)-H(44)	120.3(6)
C(44)-C(45)-H(45)	119.6(6)	C(44)-C(45)-C(46)	120.8(5)
C(46)-C(41)-P(1)	124.1(4)	C(45)-C(46)-H(46)	119.9(5)
C(47)-C(48)-C(49)	120.5(5)	C(47)-C(48)-H(48)	119.7(5)
C(47)-C(52)-H(52)	119.7(5)	C(47)-C(52)-C(51)	120.6(5)
C(47)-P(2)-C(59)	106.0(3)	C(47)-P(2)-C(53)	101.1(3)
C(48)-C(47)-C(52)	118.4(5)	C(47)-P(2)-Rh(1)	112.7(2)
C(48)-C(49)-H(49)	119.7(6)	C(48)-C(47)-P(2)	116.8(4)
C(49)-C(50)-C(51)	119.5(5)	C(48)-C(49)-C(50)	120.6(5)
C(50)-C(51)-H(51)	119.8(6)	C(49)-C(50)-H(50)	120.2(6)
C(52)-C(47)-P(2)	124.8(4)	C(50)-C(51)-C(52)	120.4(5)
C(53)-C(54)-C(55)	120.7(5)	C(51)-C(52)-H(52)	119.7(5)
C(53)-C(58)-H(58)	119.6(5)	C(53)-C(54)-H(54)	119.6(5)
C(53)-P(2)-C(59)	103.3(3)	C(53)-C(58)-C(57)	120.8(5)
C(54)-C(53)-C(58)	118.5(5)	C(53)-P(2)-Rh(1)	116.5(2)
C(54)-C(55)-H(55)	120.0(5)	C(54)-C(53)-P(2)	122.8(4)
C(55)-C(56)-C(57)	119.7(5)	C(54)-C(55)-C(56)	120.0(5)
C(56)-C(57)-H(57)	119.9(5)	C(55)-C(56)-H(56)	120.2(6)

C(58)-C(53)-P(2)	118.6(4)	C(56)-C(57)-C(58)	120.2(5)
C(59)-C(60)-C(61)	120.3(5)	C(57)-C(58)-H(58)	119.6(5)
C(59)-C(64)-H(64)	119.5(5)	C(59)-C(60)-H(60)	119.9(5)
C(59)-P(2)-RHH1	115.7(2)	C(59)-C(64)-C(63)	120.9(5)
C(60)-C(59)-C(64)	118.3(5)	C(60)-C(59)-P(2)	120.3(4)
C(60)-C(61)-H(61)	119.9(6)	C(60)-C(61)-C(62)	120.3(5)
C(61)-C(62)-C(63)	120.0(5)	C(61)-C(62)-H(62)	120.0(6)
C(62)-C(63)-H(63)	119.9(6)	C(62)-C(63)-C(64)	120.2(5)
C(64)-C(59)-P(2)	121.4(4)	C(63)-C(64)-H(64)	119.5(5)
C(65)-C(66)-C(67)	113.8(7)	C(65)-C(66)-O(3)	120.6(6)
C(66)-C(67)-H(67B)	109.5(7)	C(66)-C(67)-H(67A)	109.5(7)
C(67)-C(66)-O(3)	124.0(7)	C(66)-C(67)-H(67C)	109.5(7)
C(68)-S(3)-O(4)	106.7(3)	C(68)-S(3)-C(69)	97.2(3)
H(2)-C(2)-C(3)	119.8(6)	C(69)-S(3)-O(4)	103.7(3)
H(3)-C(3)-C(4)	119.9(6)	H(4)-C(4)-C(5)	120.2(6)
H(11)-C(11)-C(12)	119.0(6)	H(5)-C(5)-C(6)	119.5(6)
H(13)-C(13)-C(14)	119.8(6)	H(10)-C(10)-C(11)	120.5(6)
H(17)-C(17)-C(18)	120.0(6)	H(12)-C(12)-C(13)	120.5(6)
H(19)-C(19)-C(20)	119.8(6)	H(16)-C(16)-C(17)	119.9(5)
H(25)-C(25)-C(26)	119.3(5)	H(18)-C(18)-C(19)	119.9(6)
H(27)-C(27)-C(28)	119.9(5)	H(24)-C(24)-C(25)	120.2(5)
H(31)-C(31)-C(32)	119.6(5)	H(26)-C(26)-C(27)	120.4(6)
H(33)-C(33)-C(34)	119.9(5)	H(30)-C(30)-C(31)	120.0(5)
H(37)-C(37)-C(38)	119.4(5)	H(32)-C(32)-C(33)	120.1(5)
H(39)-C(39)-C(40)	120.1(5)	H(36)-C(36)-C(37)	120.4(5)
H(43)-C(43)-C(44)	119.8(5)	H(38)-C(38)-C(39)	120.1(5)
H(45)-C(45)-C(46)	119.6(6)	H(42)-C(42)-C(43)	119.7(5)
H(49)-C(49)-C(50)	119.7(6)	H(44)-C(44)-C(45)	120.4(6)
H(51)-C(51)-C(52)	119.8(6)	H(48)-C(48)-C(49)	119.7(5)
H(55)-C(55)-C(56)	120.0(5)	H(50)-C(50)-C(51)	120.2(6)
H(57)-C(57)-C(58)	119.9(6)	H(54)-C(54)-C(55)	119.6(5)
H(61)-C(61)-C(62)	119.9(6)	H(56)-C(56)-C(57)	120.2(6)
H(63)-C(63)-C(64)	119.9(6)	H(60)-C(60)-C(61)	119.9(5)
H(65A)-C(65)-C(66)	109.5(8)	H(62)-C(62)-C(63)	120.0(6)
H(65A)-C(65)-H(65B)	109.5(8)	H(65A)-C(65)-H(65C)	109.5(8)
H(65B)-C(65)-C(66)	109.5(7)	H(65B)-C(65)-H(65C)	109.5(9)
H(67A)-C(67)-H(67B)	109.5(7)	H(65C)-C(65)-C(66)	109.5(7)
H(67B)-C(67)-H(67C)	109.5(7)	H(67A)-C(67)-H(67C)	109.5(7)
H(68A)-C(68)-H(68C)	109.5(6)	H(68A)-C(68)-H(68B)	109.5(6)
H(68B)-C(68)-H(68C)	109.5(6)	H(68A)-C(68)-S(3)	109.5(5)
H(68C)-C(68)-S(3)	109.5(5)	H(68B)-C(68)-S(3)	109.5(5)

H(69A)-C(69)-H(69C)	109.5(6)	H(69A)-C(69)-H(69B)	109.5(6)
H(69B)-C(69)-H(69C)	109.5(6)	H(69A)-C(69)-S(3)	109.5(5)
H(69C)-C(69)-S(3)	109.5(5)	H(69B)-C(69)-S(3)	109.5(5)
N(1)-C(7)-O(1)	129.5(5)	N(1)-C(8)-N(2)	118.4(5)
N(1)-C(8)-S(1)	129.5(4)	N(2)-C(8)-S(1)	111.9(4)
N(3)-C(21)-O(2)	127.1(5)	N(3)-C(22)-N(4)	126.1(5)
N(3)-C(22)-S(2)	128.7(4)	N(4)-C(22)-S(2)	105.2(4)
N(4)-Rh(1)-P(1)	89.7(2)	N(4)-Rh(1)-P(2)	90.9(2)
N(4)-Rh(1)-S(1)	170.1(2)	N(4)-Rh(1)-S(2)	68.5(2)
O(1)-Rh(1)-N(4)	101.66(13)	P(1)-Rh(1)-O(1)	92.18(12)
P(1)-Rh(1)-P(2)	175.9(1)	P(1)-Rh(1)-S(1)	88.8(1)
P(1)-Rh(1)-S(2)	92.1(1)	P(2)-Rh(1)-O(1)	91.69(12)
P(2)-Rh(1)-S(2)	84.3(1)	P(2)-Rh(1)-S(1)	89.9(1)
S(1)-Rh(1)-O(1)	88.15(9)	Rh(1)-O(1)-C(7)	132.3(3)
S(2)-Rh(1)-O(1)	169.26(10)	S(1)-Rh(1)-S(2)	101.8(1)

### C3. Crystal data of Chloridocyclooctadienyl(*S*-(*N*-benzoyl-*N'*-phenyl thioureato))rhodium(I), [Rh(COD)(Cl)(*S*-(*N*-PTH))]

Table C3.1. Atomic coordinates and equivalent isotropic displacement parameters ( $\text{\AA}^2$ ) for [Rh(COD)(Cl)(*S*-(*N*-PTH))].  $U_{\text{eq}}$  is defined as one third of the trace of the orthogonalized  $U^{ij}$  tensor.

Atom	x/a	y/b	z/c	$U_{\text{eq}}$
C(1)	0.4224(4)	0.2406(3)	0.4478(2)	0.01414
C(2)	0.5460(4)	0.1965(3)	0.5142(2)	0.02012
C(3)	0.7327(5)	0.2560(3)	0.5341(2)	0.02327
C(4)	0.7967(5)	0.3581(3)	0.4890(2)	0.02507
C(5)	0.6740(5)	0.4028(3)	0.4235(3)	0.02905
C(6)	0.4857(5)	0.3446(3)	0.4022(2)	0.02349
C(7)	0.2298(4)	0.1651(3)	0.4267(2)	0.01389
C(8)	-0.0240(4)	0.1125(3)	0.3035(2)	0.01336
C(9)	-0.2685(4)	-0.0678(3)	0.3069(2)	0.01347
C(10)	-0.4502(4)	-0.0205(3)	0.2777(2)	0.01485
C(11)	-0.6016(4)	-0.1101(3)	0.2445(2)	0.01732
C(12)	-0.5712(5)	-0.2455(3)	0.2407(2)	0.01951
C(13)	-0.3874(4)	-0.2921(3)	0.2693(2)	0.01829
C(14)	-0.2358(4)	-0.2028(3)	0.3022(2)	0.01712
C(15)	0.1023(4)	0.1668(3)	0.0137(2)	0.01502
C(16)	0.2794(4)	0.1337(3)	0.0590(2)	0.01527
C(17)	0.4898(4)	0.1720(3)	0.0324(2)	0.01958
C(18)	0.5617(4)	0.3056(3)	0.0829(2)	0.02245
C(19)	0.3923(4)	0.3992(3)	0.1073(2)	0.01673
C(20)	0.2382(4)	0.4284(3)	0.0496(2)	0.01466
C(21)	0.2254(4)	0.3724(3)	-0.0493(2)	0.01803
C(22)	0.0921(5)	0.2470(3)	-0.0644(2)	0.01825
Cl(1)	0.06345(11)	0.45959(7)	0.25606(5)	0.01837
N(1)	0.1287(3)	0.1887(2)	0.3482(2)	0.01467
N(2)	-0.1140(3)	0.0223(2)	0.3460(2)	0.01553
O(1)	0.1682(3)	0.0834(2)	0.4735(1)	0.01869
Rh(1)	0.13173(3)	0.28912(2)	0.13737(1)	0.01158
S(1)	-0.07827(10)	0.12944(7)	0.19410(5)	0.01483

**Table C3.2. Hydrogen coordinates and isotropic displacement parameters ( $\text{\AA}^2$ ) for  
[Rh(COD)(Cl)(*S*-(*N*-PTH))].**

Atom	x/a	y/b	z/c	U <sub>(eq)</sub>
H(1)	0.16491	0.25816	0.32488	0.01761
H(2A)	0.50368	0.12747	0.54499	0.02414
H(3)	0.81533	0.22657	0.5785	0.02793
H(4)	0.92237	0.39697	0.50258	0.03009
H(5)	0.71734	0.47219	0.39329	0.03486
H(6)	0.40327	0.37494	0.35813	0.02818
H(10)	-0.47066	0.07023	0.28017	0.01782
H(11)	-0.72382	-0.07905	0.22487	0.02079
H(12)	-0.67321	-0.30492	0.21908	0.0234
H(13)	-0.36622	-0.38279	0.26641	0.02194
H(14)	-0.11272	-0.23365	0.32096	0.02054
H(15)	-0.00469	0.0997	0.01216	0.01803
H(16)	0.27205	0.04822	0.08294	0.01833
H(17A)	0.48979	0.17728	-0.03189	0.02349
H(17B)	0.58281	0.10365	0.04539	0.02349
H(18A)	0.63438	0.28966	0.13751	0.02695
H(18B)	0.65389	0.34726	0.04552	0.02695
H(19)	0.42922	0.47242	0.15376	0.02008
H(2)	-0.07719	0.01734	0.40101	0.01863
H(20)	0.18555	0.51808	0.06255	0.01759
H(21A)	0.35898	0.35136	-0.07018	0.02164
H(21B)	0.1709	0.43877	-0.08435	0.02164
H(22A)	-0.04579	0.27238	-0.07434	0.0219
H(22B)	0.13337	0.19241	-0.11827	0.0219



**Table C3.3. Anisotropic displacement parameters ( $\text{\AA}^2$ ) for  $[\text{Rh}(\text{COD})(\text{Cl})(S\text{-(}N\text{-PTH))}]$ . The anisotropic displacement factor exponent takes the form:  $-2\pi^2[h^2a^{*2}U^{11} + \dots + 2hka^*b^*U^{23}]$ .**

Atom	$U^{11}$	$U^{22}$	$U^{33}$	$U^{12}$	$U^{13}$	$U^{23}$
C(1)	0.013(1)	0.015(1)	0.014(1)	-0.002(1)	0.001(1)	0.000(1)
C(2)	0.018(1)	0.027(2)	0.017(1)	-0.005(1)	0.001(1)	0.009(1)
C(3)	0.019(1)	0.028(2)	0.024(2)	-0.001(1)	-0.005(1)	0.008(1)
C(4)	0.017(1)	0.028(2)	0.029(2)	-0.007(1)	-0.002(1)	0.002(1)
C(5)	0.029(2)	0.025(2)	0.036(2)	-0.013(1)	-0.006(1)	0.013(1)
C(6)	0.023(1)	0.023(2)	0.025(2)	-0.007(1)	-0.007(1)	0.009(1)
C(7)	0.013(1)	0.015(1)	0.013(1)	-0.001(1)	0.001(1)	0.001(1)
C(8)	0.013(1)	0.014(1)	0.013(1)	0.000(1)	0.001(1)	0.000(1)
C(9)	0.015(1)	0.014(1)	0.011(1)	-0.004(1)	0.001(1)	0.001(1)
C(10)	0.018(1)	0.013(1)	0.014(1)	-0.001(1)	0.005(1)	0.003(1)
C(11)	0.014(1)	0.021(2)	0.017(1)	-0.002(1)	-0.003(1)	0.004(1)
C(12)	0.022(1)	0.018(1)	0.018(1)	-0.008(1)	-0.001(1)	0.001(1)
C(13)	0.024(1)	0.014(1)	0.017(1)	-0.002(1)	-0.004(1)	0.004(1)
C(14)	0.019(1)	0.019(1)	0.014(1)	-0.001(1)	-0.003(1)	0.003(1)
C(15)	0.018(1)	0.012(1)	0.014(1)	-0.004(1)	0.001(1)	-0.001(1)
C(16)	0.018(1)	0.009(1)	0.019(1)	0.000(1)	0.004(1)	0.000(1)
C(17)	0.014(1)	0.016(1)	0.028(2)	0.003(1)	0.004(1)	0.001(1)
C(18)	0.012(1)	0.018(1)	0.037(2)	-0.001(1)	0.002(1)	0.001(1)
C(19)	0.014(1)	0.012(1)	0.024(2)	-0.004(1)	0.004(1)	0.002(1)
C(20)	0.018(1)	0.009(1)	0.018(1)	-0.004(1)	0.003(1)	0.004(1)
C(21)	0.021(1)	0.015(1)	0.020(1)	-0.002(1)	0.004(1)	0.006(1)
C(22)	0.025(1)	0.017(1)	0.013(1)	-0.002(1)	0.001(1)	0.002(1)
N(1)	0.017(1)	0.014(1)	0.014(1)	-0.005(1)	-0.001(1)	0.005(1)
N(2)	0.017(1)	0.019(1)	0.011(1)	-0.006(1)	-0.003(1)	0.004(1)
O(1)	0.018(1)	0.023(1)	0.016(1)	-0.007(1)	-0.002(1)	0.007(1)
S(1)	0.0163(3)	0.0168(3)	0.0120(3)	-0.0051(3)	-0.0012(3)	0.0049(3)
Rh(1)	0.0121(1)	0.0101(1)	0.0127(1)	-0.0010(1)	0.0004(1)	0.0022(1)
Cl(1)	0.0245(3)	0.0138(3)	0.0166(3)	0.0010(3)	0.0037(3)	0.0002(3)

**Table C3.4. Complete listing of bond lengths (Å) for [Rh(COD)(Cl)(S-(N-PTH))].**

<b>Bond</b>	<b>Distance</b>	<b>Bond</b>	<b>Distance</b>
C(1)-C(2)	1.391(5)	C(1)-C(6)	1.393(5)
C(1)-C(7)	1.496(4)	C(2)-H(2A)	0.930(4)
C(2)-C(3)	1.388(5)	C(3)-H(3)	0.930(4)
C(3)-C(4)	1.374(5)	C(4)-H(4)	0.930(4)
C(4)-C(5)	1.381(5)	C(5)-H(5)	0.930(4)
C(5)-C(6)	1.395(5)	C(6)-H(6)	0.930(4)
C(7)-N(1)	1.384(4)	C(7)-O(1)	1.224(4)
C(8)-N(1)	1.381(4)	C(8)-N(2)	1.325(4)
C(8)-S(1)	1.696(3)	C(9)-C(10)	1.388(4)
C(9)-C(14)	1.386(5)	C(9)-N(2)	1.436(4)
C(10)-H(10)	0.930(3)	C(10)-C(11)	1.393(4)
C(11)-H(11)	0.930(3)	C(11)-C(12)	1.388(5)
C(12)-H(12)	0.930(4)	C(12)-C(13)	1.394(5)
C(13)-H(13)	0.930(3)	C(13)-C(14)	1.391(5)
C(14)-H(14)	0.930(3)	C(15)-H(15)	0.980(3)
C(15)-C(16)	1.410(4)	C(15)-C(22)	1.503(5)
C(15)-Rh(1)	2.105(3)	C(16)-H(16)	0.980(3)
C(16)-C(17)	1.528(4)	C(16)-Rh(1)	2.121(3)
C(17)-H(17A)	0.970(4)	C(17)-H(17B)	0.970(3)
C(17)-C(18)	1.537(5)	C(18)-H(18A)	0.970(4)
C(18)-H(18B)	0.970(4)	C(18)-C(19)	1.510(4)
C(19)-H(19)	0.980(3)	C(19)-C(20)	1.382(4)
C(19)-Rh(1)	2.144(3)	C(20)-H(20)	0.980(3)
C(20)-C(21)	1.520(5)	C(20)-Rh(1)	2.171(3)
C(21)-H(21B)	0.970(3)	C(21)-H(21A)	0.970(3)
C(22)-H(22A)	0.970(3)	C(21)-C(22)	1.537(5)
C(22)-H(22B)	0.970(3)	Cl(1)-Rh(1)	2.3849(8)
N(1)-H(1)	0.860(3)	N(2)-H(2)	0.860(3)
S(1)-Rh(1)	2.380(1)		

**Table C3.5. Complete listing of bond angles (°) for [Rh(COD)(Cl)(S-(N-PTH))].**

Angle	Value	Angle	Value
C(1)-C(2)-C(3)	119.6(3)	C(1)-C(2)-H(2A)	120.2(3)
C(1)-C(6)-H(6)	120.4(4)	C(1)-C(6)-C(5)	119.3(3)
C(1)-C(7)-N(1)	115.9(3)	C(1)-C(7)-O(1)	122.5(3)
C(2)-C(1)-C(6)	120.0(3)	C(2)-C(1)-C(7)	115.9(3)
C(2)-C(3)-H(3)	119.7(4)	C(2)-C(3)-C(4)	120.7(3)
C(3)-C(4)-C(5)	119.9(3)	C(3)-C(4)-H(4)	120.0(4)
C(4)-C(5)-C(6)	120.5(4)	C(4)-C(5)-H(5)	119.7(4)
C(5)-C(6)-H(6)	120.4(4)	C(6)-C(1)-C(7)	123.9(3)
C(7)-N(1)-C(8)	126.9(3)	C(7)-N(1)-H(1)	116.5(3)
C(8)-N(1)-H(1)	116.5(3)	C(8)-N(2)-H(2)	117.6(3)
C(8)-N(2)-C(9)	124.8(3)	C(8)-S(1)-Rh(1)	112.7(1)
C(9)-C(10)-C(11)	119.3(3)	C(9)-C(14)-H(14)	120.1(3)
C(9)-C(10)-H(10)	120.3(3)	C(9)-N(2)-H(2)	117.6(3)
C(9)-C(14)-C(13)	119.9(3)	C(10)-C(11)-C(12)	120.4(3)
C(10)-C(11)-H(11)	119.8(3)	C(10)-C(9)-N(2)	120.5(3)
C(10)-C(9)-C(14)	120.7(3)	C(11)-C(12)-H(12)	120.1(3)
C(11)-C(12)-C(13)	119.9(3)	C(12)-C(13)-C(14)	119.9(3)
C(12)-C(13)-H(13)	120.1(3)	C(13)-C(14)-H(14)	120.1(3)
C(14)-C(9)-N(2)	118.8(3)	C(15)-C(16)-C(17)	123.7(3)
C(15)-C(16)-H(16)	114.0(3)	C(15)-C(22)-C(21)	112.8(3)
C(15)-C(16)-Rh(1)	69.9(2)	C(15)-C(22)-H(22B)	109.0(3)
C(15)-C(22)-H(22A)	109.0(3)	C(15)-Rh(1)-C(19)	97.7(2)
C(15)-Rh(1)-C(16)	39.0(2)	C(16)-C(15)-Rh(1)	71.1(2)
C(15)-Rh(1)-S(1)	85.4(1)	C(16)-C(15)-C(22)	125.5(3)
C(16)-C(17)-C(18)	112.1(3)	C(16)-C(17)-H(17B)	109.2(3)
C(16)-C(17)-H(17A)	109.2(3)	C(16)-Rh(1)-C(19)	82.0(2)
C(16)-Rh(1)-S(1)	89.5(1)	C(17)-C(16)-Rh(1)	113.4(2)
C(17)-C(18)-C(19)	113.1(3)	C(17)-C(18)-H(18B)	109.0(3)
C(17)-C(18)-H(18A)	109.0(3)	C(18)-C(19)-C(20)	125.5(3)
C(18)-C(19)-H(19)	113.8(3)	C(19)-C(20)-C(21)	122.9(3)
C(18)-C(19)-Rh(1)	109.8(2)	C(19)-Rh(1)-S(1)	161.7(1)
C(19)-C(20)-H(20)	114.4(3)	C(20)-C(21)-C(22)	111.3(3)
C(20)-C(19)-Rh(1)	72.4(2)	C(20)-C(21)-H(21A)	109.4(3)
C(20)-C(21)-H(21B)	109.4(3)	C(21)-C(22)-H(22B)	109.0(3)
C(21)-C(22)-H(22A)	109.0(3)	C(22)-C(15)-Rh(1)	111.5(2)
H(2A)-C(2)-C(3)	120.2(4)	H(3)-C(3)-C(4)	119.7(4)
H(4)-C(4)-C(5)	120.0(4)	H(5)-C(5)-C(6)	119.7(4)
H(10)-C(10)-C(11)	120.3(3)	H(11)-C(11)-C(12)	119.8(3)
H(12)-C(12)-C(13)	120.1(3)	H(13)-C(13)-C(14)	120.1(3)

H(15)-C(15)-C(16)	113.7(3)	H(15)-C(15)-C(22)	113.7(3)
H(15)-C(15)-Rh(1)	113.7(3)	H(16)-C(16)-C(17)	114.0(3)
H(16)-C(16)-Rh(1)	114.0(3)	H(17A)-C(17)-H(17B)	107.9(3)
H(17A)-C(17)-C(18)	109.2(3)	H(17B)-C(17)-C(18)	109.2(3)
H(18A)-C(18)-C(19)	109.0(3)	H(18A)-C(18)-H(18B)	107.8(3)
H(19)-C(19)-Rh(1)	113.8(3)	H(18B)-C(18)-C(19)	109.0(3)
H(20)-C(20)-C(21)	114.4(3)	H(19)-C(19)-C(20)	113.8(3)
H(21A)-C(21)-H(21B)	108.0(3)	H(21A)-C(21)-C(22)	109.4(3)
H(21B)-C(21)-C(22)	109.4(3)	H(22A)-C(22)-H(22B)	107.8(3)
N(1)-C(7)-O(1)	121.6(3)	N(1)-C(8)-N(2)	118.5(3)
N(1)-C(8)-S(1)	119.1(3)	N(2)-C(8)-S(1)	122.2(3)

**C4. Crystal data of Chloridocyclooctadienyl(*S*-(*N*-benzoyl-*N'*-(2,4,6-trimethyl)phenylthioureato))rhodium(I), [Rh(COD)(Cl)(*S*-(*N*-tmPTH))]**

**Table C4.1. Atomic coordinates and equivalent isotropic displacement parameters ( $\text{\AA}^2$ ) for [Rh(COD)(Cl)(*S*-(*N*-tmPTH))].  $U_{\text{(eq)}}$  is defined as one third of the trace of the orthogonalized  $U^{\text{ij}}$  tensor.**

Atom	x/a	y/b	z/c	$U_{\text{(eq)}}$
C(1)	0.74094(11)	0.59704(32)	0.64940(10)	0.01747
C(2)	0.69353(12)	0.69739(33)	0.65647(11)	0.01983
C(3)	0.66832(12)	0.70737(34)	0.70598(11)	0.0227
C(4)	0.69058(12)	0.61678(35)	0.74842(11)	0.0226
C(5)	0.73720(13)	0.51633(42)	0.74189(11)	0.03391
C(6)	0.76285(13)	0.50626(39)	0.69242(11)	0.03137
C(7)	0.76531(11)	0.59385(32)	0.59485(10)	0.0178
C(8)	0.83911(11)	0.45618(31)	0.54186(10)	0.01492
C(9)	0.85236(11)	0.51003(31)	0.44818(9)	0.01534
C(10)	0.90890(11)	0.56955(31)	0.44066(10)	0.01619
C(11)	0.93379(12)	0.53286(32)	0.39203(10)	0.01799
C(12)	0.90404(12)	0.44222(32)	0.35285(10)	0.02002
C(13)	0.84749(13)	0.38755(35)	0.36218(10)	0.02287
C(14)	0.82044(12)	0.42011(34)	0.40991(10)	0.02062
C(15)	0.94189(12)	0.66760(35)	0.48259(11)	0.02457
C(16)	0.93157(14)	0.40505(36)	0.30066(11)	0.02718
C(17)	0.75895(13)	0.36303(42)	0.41921(12)	0.03477
C(18)	0.95531(12)	-0.00320(31)	0.56884(11)	0.02087
C(19)	0.89861(12)	-0.03930(32)	0.58516(11)	0.02235
C(20)	0.88545(14)	-0.15426(37)	0.62919(13)	0.03308
C(21)	0.92570(14)	-0.13186(39)	0.68072(13)	0.03263
C(22)	0.94584(12)	0.03732(36)	0.68842(11)	0.024
C(23)	0.99759(12)	0.10168(35)	0.67009(11)	0.0215
C(24)	1.04187(12)	0.01927(34)	0.63662(11)	0.02408
C(25)	1.01198(13)	-0.08142(36)	0.59221(11)	0.0267
Cl(1)	0.91316(3)	0.40132(9)	0.67441(3)	0.02435
N(1)	0.81246(9)	0.49167(25)	0.58887(8)	0.01568
N(2)	0.82598(9)	0.54189(26)	0.49839(8)	0.01627
O(1)	0.74476(8)	0.67491(23)	0.55750(7)	0.02325
Rh(1)	0.92371(1)	0.17990(2)	0.61865(1)	0.01467
S(1)	0.88635(3)	0.30124(8)	0.53863(3)	0.01783

**Table C4.2. Hydrogen coordinates and isotropic displacement parameters ( $\text{\AA}^2$ ) for  
[Rh(COD)(Cl)(S-(N-tmPTH))].**

Atom	x/a	y/b	z/c	U <sub>(eq)</sub>
H(1)	0.82699	0.44425	0.61825	0.01882
H(2)	0.80058	0.62014	0.50015	0.01953
H(2)	0.6781	0.75996	0.6272	0.02379
H(3)	0.63584	0.77649	0.71049	0.02725
H(4)	0.67359	0.6239	0.78235	0.02712
H(5)	0.75211	0.45323	0.77121	0.04069
H(6)	0.79538	0.43708	0.68822	0.03764
H(11)	0.97236	0.57146	0.38575	0.02159
H(13)	0.82659	0.32616	0.33528	0.02744
H(15A)	0.98067	0.69753	0.4699	0.03685
H(15B)	0.94778	0.60692	0.51598	0.03685
H(15C)	0.91882	0.76257	0.48935	0.03685
H(16A)	0.96946	0.46126	0.29927	0.04077
H(16B)	0.90453	0.43814	0.27038	0.04077
H(16C)	0.93864	0.29155	0.29837	0.04077
H(17A)	0.74359	0.30187	0.38799	0.05216
H(17B)	0.73284	0.45337	0.42431	0.05216
H(17C)	0.76021	0.29651	0.45143	0.05216
H(18)	0.95626	0.02572	0.52994	0.02505
H(19)	0.86652	-0.0326	0.5556	0.02682
H(20A)	0.89048	-0.26271	0.6157	0.03969
H(20B)	0.84341	-0.14189	0.63799	0.03969
H(21A)	0.90382	-0.16482	0.71214	0.03916
H(21B)	0.96111	-0.20038	0.6791	0.03916
H(22)	0.93373	0.08522	0.72278	0.02879
H(23)	1.01556	0.18594	0.69397	0.0258
H(24A)	1.06796	-0.04821	0.66037	0.0289
H(24B)	1.06725	0.09898	0.62025	0.0289
H(25A)	1.00224	-0.18584	0.60693	0.03204
H(25B)	1.03972	-0.09734	0.56333	0.03204

**Table C4.3. Anisotropic displacement parameters ( $\text{\AA}^2$ ) for  $[\text{Rh}(\text{COD})(\text{Cl})(\text{S}-(N\text{-tmPTH}))]$ .**

**The anisotropic displacement factor exponent takes the form:  $-2\pi^2[h^2a^{*2}U^{11} + \dots + 2hka^*b^*U^{23}]$ .**

Atom	$U^{11}$	$U^{22}$	$U^{33}$	$U^{12}$	$U^{13}$	$U^{23}$
C(1)	0.015(1)	0.023(2)	0.015(1)	0.001(1)	0.005(1)	0.000(1)
C(2)	0.019(1)	0.022(2)	0.019(1)	0.003(1)	0.003(1)	0.003(1)
C(3)	0.023(2)	0.024(2)	0.021(1)	0.007(1)	0.007(1)	-0.001(1)
C(4)	0.020(1)	0.034(2)	0.014(1)	0.001(1)	0.008(1)	-0.001(1)
C(5)	0.034(2)	0.051(2)	0.018(1)	0.016(2)	0.008(1)	0.009(1)
C(6)	0.028(2)	0.043(2)	0.024(2)	0.018(1)	0.012(1)	0.008(1)
C(7)	0.019(1)	0.017(1)	0.018(1)	0.000(1)	0.004(1)	0.001(1)
C(8)	0.015(1)	0.016(1)	0.014(1)	-0.003(1)	0.002(1)	0.001(1)
C(9)	0.021(1)	0.017(1)	0.009(1)	0.003(1)	0.005(1)	0.003(1)
C(10)	0.017(1)	0.016(1)	0.015(1)	0.002(1)	0.003(1)	0.001(1)
C(11)	0.018(1)	0.018(1)	0.018(1)	0.002(1)	0.005(1)	0.003(1)
C(12)	0.030(2)	0.018(1)	0.013(1)	0.008(1)	0.004(1)	0.005(1)
C(13)	0.031(2)	0.023(2)	0.014(1)	-0.002(1)	-0.004(1)	-0.001(1)
C(14)	0.022(1)	0.022(2)	0.018(1)	-0.001(1)	0.001(1)	0.004(1)
C(15)	0.024(2)	0.029(2)	0.021(1)	-0.006(1)	0.007(1)	-0.004(1)
C(16)	0.041(2)	0.024(2)	0.017(1)	0.006(1)	0.008(1)	-0.002(1)
C(17)	0.023(2)	0.052(2)	0.028(2)	-0.014(1)	0.000(1)	-0.006(2)
C(18)	0.030(2)	0.015(1)	0.017(1)	0.002(1)	0.000(1)	-0.003(1)
C(19)	0.026(2)	0.015(1)	0.026(1)	-0.002(1)	-0.003(1)	-0.005(1)
C(20)	0.029(2)	0.022(2)	0.047(2)	-0.005(1)	0.001(1)	0.008(1)
C(21)	0.028(2)	0.036(2)	0.034(2)	0.000(1)	0.004(1)	0.018(1)
C(22)	0.025(2)	0.032(2)	0.014(1)	0.003(1)	-0.001(1)	0.010(1)
C(23)	0.022(1)	0.025(2)	0.017(1)	0.000(1)	-0.004(1)	0.003(1)
C(24)	0.020(1)	0.024(2)	0.028(2)	0.002(1)	0.001(1)	0.004(1)
C(25)	0.030(2)	0.024(2)	0.027(2)	0.008(1)	0.003(1)	0.000(1)
N(1)	0.020(1)	0.017(1)	0.011(1)	0.004(1)	0.004(1)	0.003(1)
N(2)	0.016(1)	0.018(1)	0.015(1)	0.004(1)	0.005(1)	0.003(1)
O(1)	0.026(1)	0.028(1)	0.016(1)	0.011(1)	0.008(1)	0.006(1)
S(1)	0.0218(3)	0.0193(4)	0.0128(3)	0.0059(3)	0.0040(3)	0.0020(3)
Cl(1)	0.0257(4)	0.0283(4)	0.0186(3)	0.0059(3)	-0.0014(3)	-0.0077(3)
Rh(1)	0.0162(1)	0.0156(1)	0.0123(1)	0.0000(1)	0.0018(1)	0.0011(1)

**Table C4.4. Complete listing of bond lengths (Å) for [Rh(COD)(Cl)(S-(*N*-tmPTH))].**

<b>Bond</b>	<b>Distance</b>	<b>Bond</b>	<b>Distance</b>
C(1)-C(2)	1.386(4)	C(1)-C(6)	1.385(4)
C(1)-C(7)	1.495(4)	C(2)-H(2)	0.950(3)
C(2)-C(3)	1.391(4)	C(3)-H(3)	0.950(3)
C(3)-C(4)	1.376(4)	C(4)-H(4)	0.950(3)
C(4)-C(5)	1.370(5)	C(5)-H(5)	0.950(4)
C(5)-C(6)	1.394(4)	C(6)-H(6)	0.950(4)
C(7)-N(1)	1.386(4)	C(7)-O(1)	1.224(4)
C(8)-N(1)	1.381(4)	C(8)-N(2)	1.322(4)
C(8)-S(1)	1.698(3)	C(9)-C(10)	1.393(4)
C(9)-C(14)	1.387(4)	C(9)-N(2)	1.442(4)
C(10)-C(11)	1.400(4)	C(10)-C(15)	1.496(4)
C(11)-H(11)	0.950(3)	C(11)-C(12)	1.383(4)
C(12)-C(13)	1.388(4)	C(12)-C(16)	1.507(4)
C(13)-H(13)	0.950(3)	C(13)-C(14)	1.396(4)
C(14)-C(17)	1.498(5)	C(15)-H(15A)	0.980(3)
C(15)-H(15B)	0.980(3)	C(15)-H(15C)	0.980(3)
C(16)-H(16A)	0.980(4)	C(16)-H(16B)	0.980(3)
C(16)-H(16C)	0.980(4)	C(17)-H(17A)	0.980(4)
C(17)-H(17B)	0.980(4)	C(17)-H(17C)	0.980(4)
C(18)-H(18)	1.000(3)	C(18)-C(19)	1.397(4)
C(18)-C(25)	1.522(4)	C(18)-Rh(1)	2.139(3)
C(19)-H(19)	1.000(3)	C(19)-C(20)	1.511(5)
C(19)-Rh(1)	2.104(3)	C(20)-H(20A)	0.990(4)
C(20)-H(20B)	0.990(4)	C(20)-C(21)	1.535(5)
C(21)-H(21A)	0.990(4)	C(21)-H(21B)	0.990(4)
C(21)-C(22)	1.516(5)	C(22)-H(22)	1.000(3)
C(22)-C(23)	1.389(4)	C(22)-Rh(1)	2.150(3)
C(23)-H(23)	1.000(3)	C(23)-C(24)	1.510(4)
C(23)-Rh(1)	2.141(3)	C(24)-H(24A)	0.990(3)
C(24)-H(24B)	0.990(3)	C(24)-C(25)	1.521(4)
C(25)-H(25A)	0.990(4)	C(25)-H(25B)	0.990(3)
N(1)-H(1)	0.880(3)	N(2)-H(2)	0.880(3)
S(1)-Rh(1)	2.351(1)	Cl(1)-Rh(1)	2.359(1)



**Table C4.5. Complete listing of bond angles (°) for [Rh(COD)(Cl)(S-(*N*-tmPTH))].**

Angle	Value	Angle	Value
C(8)-N(1)-H(1)	116.4(3)	C(8)-N(2)-C(9)	121.5(3)
C(8)-N(2)-H(2)	119.3(3)	C(8)-S(1)-Rh(1)	119.5(1)
C(9)-C(10)-C(11)	116.9(3)	C(9)-C(14)-C(13)	117.3(3)
C(9)-C(10)-C(15)	121.8(3)	C(9)-N(2)-H(2)	119.3(3)
C(9)-C(14)-C(17)	121.1(3)	C(10)-C(11)-C(12)	122.1(3)
C(10)-C(11)-H(11)	118.9(3)	C(10)-C(15)-H(15B)	109.5(3)
C(10)-C(15)-H(15A)	109.5(3)	C(10)-C(9)-N(2)	118.5(3)
C(10)-C(15)-H(15C)	109.5(3)	C(10)-C(9)-C(14)	123.2(3)
C(11)-C(10)-C(15)	121.3(3)	C(11)-C(12)-C(13)	118.5(3)
C(11)-C(12)-C(16)	121.2(3)	C(12)-C(13)-C(14)	121.9(3)
C(12)-C(13)-H(13)	119.0(3)	C(12)-C(16)-H(16B)	109.5(3)
C(12)-C(16)-H(16A)	109.5(3)	C(12)-C(16)-H(16C)	109.5(3)
C(13)-C(12)-C(16)	120.3(3)	C(13)-C(14)-C(17)	121.5(3)
C(14)-C(17)-H(17A)	109.5(3)	C(14)-C(17)-H(17B)	109.5(3)
C(14)-C(17)-H(17C)	109.5(3)	C(14)-C(9)-N(2)	118.4(3)
C(18)-C(19)-C(20)	125.2(3)	C(18)-C(25)-H(25A)	109.5(3)
C(18)-C(19)-H(19)	113.9(3)	C(18)-Rh(1)-C(19)	38.4(2)
C(18)-C(19)-Rh(1)	72.1(2)	C(18)-Rh(1)-C(23)	81.2(2)
C(18)-C(25)-C(24)	110.7(3)	C(18)-Rh(1)-Cl(1)	166.1(1)
C(18)-C(25)-H(25B)	109.5(3)	C(18)-Rh(1)-S(1)	86.7(1)
C(18)-Rh(1)-C(22)	89.4(2)	C(19)-C(20)-H(20B)	108.9(3)
C(19)-C(18)-C(25)	123.5(3)	C(19)-Rh(1)-C(23)	98.1(2)
C(19)-C(18)-Rh(1)	69.4(2)	C(19)-Rh(1)-Cl(1)	154.8(1)
C(19)-C(20)-C(21)	113.2(3)	C(19)-Rh(1)-C(22)	82.2(2)
C(19)-C(20)-H(20A)	108.9(3)	C(19)-Rh(1)-S(1)	88.8(1)
C(20)-C(19)-Rh(1)	110.2(2)	C(20)-C(21)-H(21A)	109.1(3)
C(20)-C(21)-C(22)	112.3(3)	C(20)-C(21)-H(21B)	109.1(3)
C(21)-C(22)-C(23)	125.6(3)	C(21)-C(22)-Rh(1)	112.3(2)
C(21)-C(22)-H(22)	113.5(3)	C(22)-C(23)-C(24)	126.4(3)
C(22)-C(23)-H(23)	113.8(3)	C(22)-Rh(1)-C(23)	37.8(2)
C(22)-C(23)-Rh(1)	71.5(2)	C(22)-Rh(1)-Cl(1)	90.1(1)
C(22)-Rh(1)-S(1)	169.7(1)	C(23)-C(22)-Rh(1)	70.7(2)
C(23)-C(24)-C(25)	112.6(3)	C(23)-C(24)-H(24B)	109.1(3)
C(23)-C(24)-H(24A)	109.1(3)	C(23)-Rh(1)-Cl(1)	89.9(1)
C(23)-Rh(1)-S(1)	150.1(1)	C(24)-C(23)-Rh(1)	109.2(2)
C(24)-C(25)-H(25B)	109.5(3)	C(24)-C(25)-H(25A)	109.5(3)
C(25)-C(18)-Rh(1)	113.4(2)	H(2)-C(2)-C(3)	119.7(3)
H(3)-C(3)-C(4)	120.1(3)	H(4)-C(4)-C(5)	119.9(3)
H(5)-C(5)-C(6)	119.8(4)	H(11)-C(11)-C(12)	119.0(3)

H(13)-C(13)-C(14)	119.0(3)	H(15B)-C(15)-H(15C)	109.5(3)
H(15A)-C(15)-H(15B)	109.5(3)	H(15A)-C(15)-H(15C)	109.5(3)
H(16A)-C(16)-H(16B)	109.5(3)	H(16A)-C(16)-H(16C)	109.5(3)
H(16B)-C(16)-H(16C)	109.5(3)	H(17A)-C(17)-H(17B)	109.5(3)
H(17A)-C(17)-H(17C)	109.5(4)	H(17B)-C(17)-H(17C)	109.5(3)
H(18)-C(18)-C(19)	114.2(3)	H(18)-C(18)-C(25)	114.2(3)
H(18)-C(18)-Rh(1)	114.2(2)	H(19)-C(19)-C(20)	113.9(3)
H(19)-C(19)-Rh(1)	113.9(2)	H(20A)-C(20)-H(20B)	107.7(3)
H(20A)-C(20)-C(21)	108.9(3)	H(20B)-C(20)-C(21)	108.9(3)
H(21A)-C(21)-C(22)	109.2(3)	H(21A)-C(21)-H(21B)	107.9(4)
H(21B)-C(21)-C(22)	109.1(3)	H(22)-C(22)-Rh(1)	113.5(3)
H(22)-C(22)-C(23)	113.5(3)	H(23)-C(23)-Rh(1)	113.8(3)
H(23)-C(23)-C(24)	113.8(3)	H(24A)-C(24)-C(25)	109.1(3)
H(24B)-C(24)-C(25)	109.1(3)	H(24A)-C(24)-H(24B)	107.8(3)
H(25A)-C(25)-H(25B)	108.1(3)	N(1)-C(8)-N(2)	119.1(3)
N(1)-C(7)-O(1)	121.8(3)	N(1)-C(8)-S(1)	121.1(2)
N(2)-C(8)-S(1)	119.8(2)	S(1)-Rh(1)-Cl(1)	96.0(1)

## APPENDIX D

### CRYSTAL DATA OF [Rh(*S,O*-THIOUREATO)(CO)(PR<sub>1</sub>R<sub>2</sub>R<sub>3</sub>)] COMPLEXES

#### **D1. Crystal data of Carbonyl(triphenylphosphine)(*S,O*-(*N*-benzoyl-*N'*,*N'*-diphenylthioureato))rhodium(I), [Rh(*S,O*-(*N*-diPT)(CO)(PPh<sub>3</sub>)]**

**Table D1.1. Atomic coordinates and equivalent isotropic displacement parameters ( $\text{\AA}^2$ ) for [Rh(*S,O*-(*N*-diPT)(CO)(PPh<sub>3</sub>)].  $U_{\text{(eq)}}$  is defined as one third of the trace of the orthogonalized  $U^{\text{ij}}$  tensor.**

Atom	x/a	y/b	z/c	$U_{\text{(eq)}}$
C(1)	1.0023(3)	0.2815(2)	0.7821(1)	0.01808
C(1')	0.7772(3)	0.3794(2)	0.5971(1)	0.0117
C(2)	0.9467(4)	0.2814(2)	0.8149(1)	0.0283
C(2')	0.7961(3)	0.3092(2)	0.6105(1)	0.01427
C(3)	0.9841(4)	0.3354(2)	0.8396(1)	0.03763
C(3')	0.8143(3)	0.2975(2)	0.6470(1)	0.0164
C(4)	1.0749(4)	0.3905(2)	0.8313(1)	0.03591
C(4')	0.8123(3)	0.3558(2)	0.6701(1)	0.01767
C(5)	1.1296(4)	0.3911(2)	0.7988(1)	0.03348
C(5')	0.7915(3)	0.4255(2)	0.6570(1)	0.0184
C(6)	1.0946(3)	0.3364(2)	0.7742(1)	0.02282
C(6')	0.7749(3)	0.4372(2)	0.6206(1)	0.01621
C(7)	0.9604(3)	0.2243(2)	0.7555(1)	0.01453
C(7')	0.7602(3)	0.3914(2)	0.5578(1)	0.01326
C(8)	1.0225(3)	0.1727(2)	0.7013(1)	0.01342
C(8')	0.7579(3)	0.4866(2)	0.5155(1)	0.0124
C(9)	1.2319(3)	0.2327(2)	0.6794(1)	0.01434
C(9')	0.7471(3)	0.6026(2)	0.5464(1)	0.01546
C(10)	1.1942(3)	0.3052(2)	0.6804(1)	0.01897
C(10')	0.6255(3)	0.6051(2)	0.5636(1)	0.01942
C(11)	1.2973(4)	0.3580(2)	0.6797(1)	0.02093
C(11')	0.6219(4)	0.6455(2)	0.5943(1)	0.02375
C(12)	1.4389(4)	0.3390(2)	0.6773(1)	0.02213
C(12')	0.7407(4)	0.6838(2)	0.6078(1)	0.02702

C(13)	1.4760(3)	0.2670(2)	0.6759(1)	0.02197
C(13')	0.8630(4)	0.6818(2)	0.5903(1)	0.04002
C(14)	1.3729(3)	0.2135(2)	0.6770(1)	0.01894
C(14')	0.8665(4)	0.6411(2)	0.5594(1)	0.03043
C(15)	1.1466(3)	0.1182(2)	0.6534(1)	0.01695
C(15')	0.7445(3)	0.5990(2)	0.4808(1)	0.01373
C(16)	1.1935(3)	0.0521(2)	0.6664(1)	0.02165
C(16')	0.8679(3)	0.6150(2)	0.4654(1)	0.01623
C(17)	1.2235(4)	-0.0030(2)	0.6431(1)	0.02977
C(17')	0.8581(3)	0.6524(2)	0.4332(1)	0.01847
C(18)	1.2077(4)	0.0096(2)	0.6072(1)	0.0347
C(18')	0.7268(3)	0.6727(2)	0.4169(1)	0.01709
C(19)	1.1619(4)	0.0763(3)	0.5940(1)	0.03508
C(19')	0.6037(3)	0.6562(2)	0.4328(1)	0.01819
C(20)	1.1301(3)	0.1320(2)	0.6172(1)	0.02324
C(20')	0.6133(3)	0.6197(2)	0.4651(1)	0.01587
C(21)	0.6738(3)	0.0630(2)	0.8198(1)	0.01568
C(21')	0.9201(3)	0.1618(2)	0.4907(1)	0.0158
C(22)	0.8204(3)	0.0637(2)	0.8263(1)	0.0213
C(22')	1.0299(4)	0.2042(2)	0.5064(1)	0.03117
C(23)	0.8855(4)	0.0391(2)	0.8584(1)	0.02779
C(23')	1.1709(4)	0.1842(2)	0.5058(1)	0.03478
C(24)	0.8040(4)	0.0125(2)	0.8842(1)	0.02758
C(24')	1.2056(4)	0.1209(2)	0.4892(1)	0.02637
C(25)	0.6576(4)	0.0111(2)	0.8778(1)	0.02528
C(25')	1.0983(4)	0.0780(2)	0.4742(1)	0.04179
C(26)	0.5915(4)	0.0362(2)	0.8459(1)	0.01896
C(26')	0.9561(4)	0.0982(2)	0.4749(1)	0.03457
C(27)	0.5554(3)	0.1975(2)	0.7955(1)	0.01567
C(27')	0.7005(3)	0.1685(2)	0.5385(1)	0.01313
C(28)	0.5931(3)	0.2188(2)	0.8307(1)	0.01903
C(28')	0.7944(3)	0.1299(2)	0.5620(1)	0.01637
C(29)	0.5684(4)	0.2893(2)	0.8412(1)	0.02481
C(29')	0.7565(3)	0.1109(2)	0.5955(1)	0.01955
C(30)	0.5051(4)	0.3383(2)	0.8172(1)	0.02779
C(30')	0.6238(4)	0.1297(2)	0.6055(1)	0.0217
C(31)	0.4681(4)	0.3179(2)	0.7823(1)	0.02783
C(31')	0.5293(3)	0.1674(2)	0.5821(1)	0.01931
C(32)	0.4946(3)	0.2480(2)	0.7715(1)	0.02009
C(32')	0.5678(3)	0.1873(2)	0.5491(1)	0.01744
C(33)	0.4191(3)	0.0629(2)	0.7717(1)	0.01484

C(33')	0.6178(3)	0.1418(2)	0.4660(1)	0.01486
C(34)	0.2906(3)	0.0982(2)	0.7752(1)	0.01861
C(34')	0.5261(3)	0.1744(2)	0.4397(1)	0.01894
C(35)	0.1627(4)	0.0610(2)	0.7673(1)	0.02347
C(35')	0.4302(4)	0.1332(2)	0.4182(1)	0.02366
C(36)	0.1625(4)	-0.0101(2)	0.7562(1)	0.02393
C(36')	0.4260(4)	0.0591(2)	0.4227(1)	0.02388
C(37)	0.2897(4)	-0.0455(2)	0.7532(1)	0.02354
C(37')	0.5120(3)	0.0259(2)	0.4494(1)	0.02097
C(38)	0.4181(3)	-0.0092(2)	0.7610(1)	0.01867
C(38')	0.6081(3)	0.0672(2)	0.4714(1)	0.01866
C(39)	0.6186(3)	0.0538(2)	0.7060(1)	0.01549
C(39')	0.7604(3)	0.3022(2)	0.4390(1)	0.01691
N(1)	1.0371(3)	0.2209(1)	0.7278(1)	0.01528
N(1')	0.7669(3)	0.4605(1)	0.5487(1)	0.01376
N(2)	1.1274(3)	0.1764(1)	0.6783(1)	0.01456
N(2')	0.7524(3)	0.5601(1)	0.5144(1)	0.01294
O(1)	0.8587(2)	0.1836(1)	0.7634(1)	0.01831
O(1')	0.7405(2)	0.3349(1)	0.5389(1)	0.01449
O(2)	0.5458(2)	0.0199(1)	0.6861(1)	0.0233
O(2')	0.7758(3)	0.2910(1)	0.4095(1)	0.02552
P(1)	0.59216(8)	0.10710(4)	0.77974(2)	0.01281
P(1')	0.74181(8)	0.19724(4)	0.49446(2)	0.01222
Rh(1)	0.73515(2)	0.11083(1)	0.73393(1)	0.01188
Rh(1')	0.74415(3)	0.31936(1)	0.48549(1)	0.01177
S(1)	0.89200(8)	0.10977(4)	0.69068(2)	0.01473
S(1')	0.75849(9)	0.44274(4)	0.47549(2)	0.01581

**Table D1.2. Hydrogen coordinates and isotropic displacement parameters ( $\text{\AA}^2$ ) for  
[Rh(*S,O*-(*N*-diPT)(CO)(PPh<sub>3</sub>)].**

Atom	x/a	y/b	z/c	U <sub>(eq)</sub>
H(2)	0.88267	0.24427	0.82048	0.03396
H(2')	0.79639	0.26927	0.59463	0.01713
H(3)	0.94759	0.33459	0.86228	0.04515
H(3')	0.82818	0.24971	0.65608	0.01968
H(4)	1.09946	0.42792	0.84806	0.0431
H(4')	0.82521	0.34795	0.69512	0.0212
H(5)	1.19163	0.42907	0.79315	0.04018
H(5')	0.7886	0.46516	0.67298	0.02207
H(6)	1.13405	0.33667	0.75194	0.02739
H(6')	0.76179	0.48515	0.6117	0.01946
H(10)	1.09764	0.31858	0.68159	0.02277
H(10')	0.54364	0.57889	0.55439	0.02331
H(11)	1.27161	0.40764	0.68086	0.02511
H(11')	0.53763	0.64701	0.60622	0.0285
H(12)	1.50934	0.3756	0.67668	0.02656
H(12')	0.73842	0.71141	0.62897	0.03242
H(13)	1.57231	0.25389	0.67409	0.02637
H(13')	0.94473	0.70821	0.59943	0.04802
H(14)	1.39879	0.16378	0.67609	0.02273
H(14')	0.95024	0.63971	0.54727	0.03652
H(16)	1.20546	0.04405	0.69135	0.02598
H(16')	0.9578	0.60065	0.47659	0.01948
H(17)	1.25476	-0.04905	0.65204	0.03573
H(17')	0.94204	0.66411	0.4224	0.02216
H(18)	1.2284	-0.02784	0.59123	0.04164
H(18')	0.72072	0.69786	0.39485	0.02051
H(19)	1.15182	0.08433	0.56906	0.0421
H(19')	0.51344	0.66981	0.42153	0.02183
H(20)	1.09817	0.17789	0.60829	0.02789
H(20')	0.52975	0.60896	0.47628	0.01904
H(22)	0.8768	0.08112	0.80851	0.02556
H(22')	1.00772	0.24799	0.51794	0.0374
H(23)	0.98612	0.04045	0.86282	0.03335
H(23')	1.24389	0.21423	0.51684	0.04174
H(24)	0.84868	-0.00471	0.90617	0.03309
H(24')	1.30221	0.10743	0.48829	0.03164
H(25)	0.60191	-0.00733	0.89552	0.03034
H(25')	1.12081	0.03383	0.46307	0.05014

H(26)	0.49075	0.03527	0.84169	0.02276
H(26')	0.88334	0.06741	0.4644	0.04149
H(28)	0.63584	0.18496	0.84736	0.02283
H(28')	0.88492	0.1164	0.55512	0.01964
H(29)	0.59518	0.30379	0.86507	0.02977
H(29')	0.82154	0.08502	0.61158	0.02346
H(30)	0.48671	0.38628	0.82463	0.03335
H(30')	0.59786	0.11673	0.62838	0.02604
H(31)	0.42467	0.3519	0.76573	0.0334
H(31')	0.4378	0.17968	0.58881	0.02317
H(32)	0.471	0.23438	0.74736	0.02411
H(32')	0.50303	0.21405	0.53338	0.02093
H(34)	0.29005	0.14717	0.78293	0.02233
H(34')	0.52935	0.22539	0.4364	0.02273
H(35)	0.07502	0.08497	0.76961	0.02816
H(35')	0.36762	0.15592	0.40037	0.0284
H(36)	0.07501	-0.03475	0.75062	0.02872
H(36')	0.36308	0.03074	0.40725	0.02866
H(37)	0.28957	-0.09477	0.74573	0.02825
H(37')	0.50599	-0.02502	0.4528	0.02516
H(38)	0.5053	-0.03382	0.75898	0.02241
H(38')	0.66677	0.04449	0.48996	0.02239

**Table D1.3. Anisotropic displacement parameters ( $\text{\AA}^2$ ) for  $[\text{Rh}(S,O\text{-}(N\text{-diPT})(\text{CO})(\text{PPh}_3)]$ .**

**The anisotropic displacement factor exponent takes the form:  $-2\pi^2[h^2a^{*2}U^{11} + \dots + 2hka^*b^*U^{23}]$ .**

Atom	$U^{11}$	$U^{22}$	$U^{33}$	$U^{12}$	$U^{13}$	$U^{23}$
C(1)	0.016(2)	0.016(2)	0.022(2)	0.000(1)	0.002(1)	-0.004(1)
C(1')	0.011(1)	0.014(2)	0.010(1)	-0.001(1)	0.003(1)	-0.001(1)
C(2')	0.013(2)	0.014(2)	0.016(2)	-0.002(1)	0.003(1)	-0.001(1)
C(2)	0.030(2)	0.030(2)	0.027(2)	-0.008(2)	0.010(2)	-0.011(2)
C(3')	0.012(2)	0.019(2)	0.018(2)	0.000(1)	0.004(1)	0.005(1)
C(3)	0.044(3)	0.039(2)	0.031(2)	-0.007(2)	0.013(2)	-0.018(2)
C(4)	0.033(2)	0.026(2)	0.048(3)	-0.001(2)	0.001(2)	-0.023(2)
C(4')	0.016(2)	0.027(2)	0.010(2)	0.001(1)	0.003(1)	0.001(1)
C(5')	0.021(2)	0.020(2)	0.015(2)	-0.001(1)	0.004(1)	-0.004(1)
C(5)	0.027(2)	0.025(2)	0.049(3)	-0.009(2)	0.006(2)	-0.012(2)
C(6)	0.019(2)	0.019(2)	0.031(2)	-0.002(1)	0.007(1)	-0.006(1)
C(6')	0.018(2)	0.015(2)	0.016(2)	-0.001(1)	0.003(1)	-0.001(1)
C(7)	0.012(2)	0.014(2)	0.018(2)	0.001(1)	0.001(1)	0.002(1)

C(7')	0.009(1)	0.016(2)	0.015(2)	0.000(1)	0.003(1)	-0.001(1)
C(8)	0.013(2)	0.014(2)	0.014(2)	0.001(1)	0.001(1)	0.005(1)
C(8')	0.008(1)	0.015(1)	0.015(2)	0.001(1)	0.001(1)	-0.001(1)
C(9)	0.013(2)	0.018(2)	0.012(2)	-0.005(1)	0.002(1)	0.003(1)
C(9')	0.019(2)	0.014(2)	0.013(2)	0.001(1)	0.001(1)	0.003(1)
C(10')	0.015(2)	0.022(2)	0.022(2)	-0.003(1)	0.005(1)	-0.001(1)
C(10)	0.014(2)	0.021(2)	0.022(2)	-0.001(1)	0.005(1)	0.005(1)
C(11)	0.025(2)	0.019(2)	0.020(2)	-0.003(1)	0.005(1)	0.003(1)
C(11')	0.027(2)	0.026(2)	0.020(2)	0.004(1)	0.011(1)	0.001(1)
C(12')	0.036(2)	0.025(2)	0.021(2)	0.006(2)	0.009(2)	-0.009(1)
C(12)	0.020(2)	0.026(2)	0.020(2)	-0.012(1)	0.004(1)	0.000(1)
C(13')	0.031(2)	0.049(3)	0.041(2)	-0.015(2)	0.007(2)	-0.023(2)
C(13)	0.014(2)	0.031(2)	0.021(2)	-0.004(1)	0.003(1)	0.001(1)
C(14)	0.019(2)	0.022(2)	0.016(2)	0.001(1)	0.004(1)	0.002(1)
C(14')	0.022(2)	0.040(2)	0.031(2)	-0.009(2)	0.013(2)	-0.016(2)
C(15')	0.018(2)	0.008(1)	0.015(2)	-0.001(1)	0.001(1)	0.001(1)
C(15)	0.011(2)	0.026(2)	0.014(2)	-0.005(1)	0.006(1)	-0.002(1)
C(16')	0.014(2)	0.014(2)	0.021(2)	-0.002(1)	0.001(1)	0.001(1)
C(16)	0.017(2)	0.026(2)	0.022(2)	-0.003(1)	0.006(1)	-0.003(1)
C(17)	0.023(2)	0.028(2)	0.038(2)	-0.001(2)	0.005(2)	-0.010(2)
C(17')	0.016(2)	0.016(2)	0.024(2)	-0.001(1)	0.008(1)	0.002(1)
C(18)	0.023(2)	0.046(3)	0.036(2)	0.000(2)	0.007(2)	-0.020(2)
C(18')	0.025(2)	0.014(2)	0.013(2)	0.001(1)	0.004(1)	0.002(1)
C(19')	0.015(2)	0.017(2)	0.021(2)	0.002(1)	-0.001(1)	0.001(1)
C(19)	0.023(2)	0.064(3)	0.019(2)	-0.009(2)	0.005(1)	-0.008(2)
C(20')	0.014(2)	0.016(2)	0.018(2)	-0.001(1)	0.004(1)	0.003(1)
C(20)	0.016(2)	0.034(2)	0.020(2)	-0.005(1)	0.003(1)	0.004(1)
C(21)	0.022(2)	0.011(1)	0.014(2)	0.004(1)	0.004(1)	-0.001(1)
C(21')	0.018(2)	0.016(2)	0.014(2)	0.000(1)	0.004(1)	0.001(1)
C(22)	0.014(2)	0.027(2)	0.023(2)	0.004(1)	0.004(1)	0.001(1)
C(22')	0.021(2)	0.021(2)	0.052(3)	-0.001(1)	0.001(2)	-0.010(2)
C(23)	0.027(2)	0.027(2)	0.028(2)	0.008(2)	-0.002(2)	0.001(2)
C(23')	0.018(2)	0.029(2)	0.057(3)	-0.002(2)	0.002(2)	-0.002(2)
C(24)	0.047(2)	0.017(2)	0.018(2)	0.012(2)	0.000(2)	0.001(1)
C(24')	0.014(2)	0.035(2)	0.031(2)	0.003(1)	0.007(1)	0.003(2)
C(25')	0.027(2)	0.041(3)	0.059(3)	0.011(2)	0.010(2)	-0.024(2)
C(25)	0.039(2)	0.019(2)	0.020(2)	0.007(2)	0.010(2)	0.003(1)
C(26)	0.025(2)	0.016(2)	0.017(2)	0.002(1)	0.008(1)	-0.001(1)
C(26')	0.021(2)	0.032(2)	0.052(3)	-0.005(2)	0.008(2)	-0.021(2)
C(27)	0.015(2)	0.014(2)	0.019(2)	0.000(1)	0.005(1)	0.001(1)
C(27')	0.016(2)	0.011(1)	0.012(1)	-0.004(1)	0.003(1)	0.000(1)



C(28')	0.021(2)	0.013(2)	0.015(2)	-0.001(1)	0.003(1)	-0.001(1)
C(28)	0.023(2)	0.018(2)	0.016(2)	0.003(1)	0.004(1)	0.001(1)
C(29)	0.029(2)	0.023(2)	0.023(2)	0.002(1)	0.004(1)	-0.004(1)
C(29')	0.027(2)	0.016(2)	0.015(2)	-0.002(1)	-0.001(1)	0.003(1)
C(30)	0.031(2)	0.017(2)	0.036(2)	0.003(1)	0.006(2)	-0.003(2)
C(30')	0.033(2)	0.016(2)	0.017(2)	-0.008(1)	0.008(1)	-0.001(1)
C(31)	0.032(2)	0.015(2)	0.036(2)	0.003(1)	-0.001(2)	0.008(2)
C(31')	0.019(2)	0.019(2)	0.021(2)	-0.002(1)	0.006(1)	-0.002(1)
C(32)	0.025(2)	0.019(2)	0.016(2)	-0.001(1)	0.001(1)	0.003(1)
C(32')	0.020(2)	0.018(2)	0.014(2)	-0.001(1)	0.003(1)	-0.001(1)
C(33)	0.015(2)	0.018(2)	0.013(2)	-0.001(1)	0.004(1)	0.004(1)
C(33')	0.016(2)	0.016(2)	0.014(2)	-0.003(1)	0.004(1)	-0.003(1)
C(34)	0.018(2)	0.020(2)	0.019(2)	0.002(1)	0.005(1)	0.008(1)
C(34')	0.022(2)	0.018(2)	0.016(2)	-0.007(1)	0.002(1)	0.003(1)
C(35')	0.027(2)	0.027(2)	0.016(2)	-0.009(1)	-0.003(1)	0.002(1)
C(35)	0.017(2)	0.033(2)	0.021(2)	0.001(1)	0.005(1)	0.012(1)
C(36')	0.026(2)	0.029(2)	0.017(2)	-0.015(2)	0.004(1)	-0.006(1)
C(36)	0.017(2)	0.035(2)	0.019(2)	-0.012(1)	-0.003(1)	0.010(1)
C(37')	0.025(2)	0.018(2)	0.022(2)	-0.006(1)	0.011(1)	-0.005(1)
C(37)	0.029(2)	0.025(2)	0.018(2)	-0.008(1)	0.005(1)	0.002(1)
C(38')	0.023(2)	0.017(2)	0.016(2)	-0.002(1)	0.008(1)	-0.002(1)
C(38)	0.020(2)	0.021(2)	0.016(2)	0.000(1)	0.007(1)	0.002(1)
C(39)	0.016(2)	0.016(2)	0.015(2)	0.000(1)	0.006(1)	0.002(1)
C(39')	0.019(2)	0.013(2)	0.019(2)	-0.006(1)	0.001(1)	0.001(1)
N(1)	0.014(1)	0.014(1)	0.019(1)	-0.001(1)	0.004(1)	0.002(1)
N(1')	0.014(1)	0.014(1)	0.014(1)	-0.002(1)	0.003(1)	-0.001(1)
N(2')	0.017(1)	0.011(1)	0.011(1)	0.000(1)	0.003(1)	0.000(1)
N(2)	0.012(1)	0.015(1)	0.017(1)	-0.003(1)	0.006(1)	0.001(1)
O(1)	0.017(1)	0.024(1)	0.014(1)	-0.009(1)	0.006(1)	-0.003(1)
O(1')	0.019(1)	0.013(1)	0.012(1)	-0.003(1)	0.002(1)	-0.002(1)
O(2)	0.023(1)	0.025(1)	0.022(1)	-0.009(1)	0.002(1)	-0.004(1)
O(2')	0.035(1)	0.028(1)	0.014(1)	-0.008(1)	0.006(1)	-0.004(1)
P(1)	0.0134(4)	0.0127(4)	0.0130(4)	0.0001(3)	0.0044(3)	0.0013(3)
P(1')	0.0138(4)	0.0112(4)	0.0119(4)	-0.0013(3)	0.0025(3)	-0.0006(3)
S(1)	0.0142(4)	0.0175(4)	0.0132(4)	-0.0040(3)	0.0047(3)	-0.0010(3)
S(1')	0.0255(4)	0.0113(4)	0.0109(4)	-0.0014(3)	0.0029(3)	0.0001(3)
Rh(1)	0.0114(1)	0.0131(1)	0.0116(1)	-0.0015(1)	0.0034(1)	0.0004(1)
Rh(1')	0.0139(1)	0.0111(1)	0.0104(1)	-0.0019(1)	0.0019(1)	-0.0005(1)

**Table D1.4. Complete listing of bond lengths (Å) for [Rh(S,*O*-(*N*-diPT)(CO)(PPh<sub>3</sub>)].**

<b>Bond</b>	<b>Distance</b>	<b>Bond</b>	<b>Distance</b>
C(1)-C(2)	1.390(5)	C(1)-C(6)	1.387(5)
C(1)-C(7)	1.485(5)	C(1')-C(2')	1.395(5)
C(1')-C(6')	1.388(5)	C(1')-C(7')	1.494(4)
C(2')-H(2')	0.950(4)	C(2')-C(3')	1.387(5)
C(2)-H(2)	0.950(4)	C(2)-C(3)	1.387(6)
C(3')-H(3')	0.950(4)	C(3')-C(4')	1.387(5)
C(3)-H(3)	0.950(5)	C(3)-C(4)	1.385(6)
C(4)-H(4)	0.950(4)	C(4)-C(5)	1.373(6)
C(4')-H(4')	0.950(4)	C(4')-C(5')	1.384(5)
C(5')-H(5')	0.950(4)	C(5')-C(6')	1.383(5)
C(5)-H(5)	0.950(4)	C(5)-C(6)	1.389(6)
C(6)-H(6)	0.950(4)	C(6')-H(6')	0.950(4)
C(7)-N(1)	1.325(4)	C(7)-O(1)	1.277(4)
C(7')-N(1')	1.323(5)	C(7')-O(1')	1.267(4)
C(8)-N(1)	1.334(4)	C(8)-N(2)	1.378(4)
C(8)-S(1)	1.714(4)	C(8')-N(1')	1.337(4)
C(8')-N(2')	1.358(4)	C(8')-S(1')	1.711(4)
C(9)-C(10)	1.385(5)	C(9)-C(14)	1.390(5)
C(9)-N(2)	1.432(4)	C(9')-C(10')	1.371(5)
C(9')-C(14')	1.384(5)	C(9')-N(2')	1.443(4)
C(10')-H(10')	0.950(4)	C(10')-C(11')	1.380(5)
C(10)-H(10)	0.950(4)	C(10)-C(11)	1.378(5)
C(11)-H(11)	0.950(4)	C(11)-C(12)	1.393(5)
C(11')-H(11')	0.950(4)	C(11')-C(12')	1.382(6)
C(12')-H(12')	0.950(4)	C(12')-C(13')	1.383(6)
C(12)-H(12)	0.950(4)	C(12)-C(13)	1.375(5)
C(13')-H(13')	0.950(5)	C(13')-C(14')	1.389(6)
C(13)-H(13)	0.950(4)	C(13)-C(14)	1.391(5)
C(14)-H(14)	0.950(4)	C(14')-H(14')	0.950(4)
C(15')-C(16')	1.381(5)	C(15')-C(20')	1.377(5)
C(15')-N(2')	1.453(4)	C(15)-C(16)	1.371(5)
C(15)-C(20)	1.382(5)	C(15)-N(2)	1.450(5)
C(16')-H(16')	0.950(4)	C(16')-C(17')	1.392(5)
C(16)-H(16)	0.950(4)	C(16)-C(17)	1.390(6)
C(17)-H(17)	0.950(4)	C(17)-C(18)	1.367(6)
C(17')-H(17')	0.950(4)	C(17')-C(18')	1.384(5)
C(18)-H(18)	0.950(5)	C(18)-C(19)	1.380(7)
C(18')-H(18')	0.950(4)	C(18')-C(19')	1.390(5)
C(19')-H(19')	0.950(4)	C(19')-C(20')	1.388(5)

C(19)-H(19)	0.950(4)	C(19)-C(20)	1.398(6)
C(20')-H(20')	0.950(4)	C(20)-H(20)	0.950(4)
C(21)-C(22)	1.384(5)	C(21)-C(26)	1.400(5)
C(21)-P(1)	1.823(4)	C(21')-C(22')	1.387(5)
C(21')-C(26')	1.372(5)	C(21')-P(1')	1.825(4)
C(22)-H(22)	0.950(4)	C(22)-C(23)	1.384(5)
C(22')-H(22')	0.950(4)	C(22')-C(23')	1.384(6)
C(23)-H(23)	0.950(4)	C(23)-C(24)	1.384(6)
C(23')-H(23')	0.950(4)	C(23')-C(24')	1.377(6)
C(24)-H(24)	0.950(4)	C(24)-C(25)	1.382(6)
C(24')-H(24')	0.950(4)	C(24')-C(25')	1.367(6)
C(25')-H(25')	0.950(5)	C(25')-C(26')	1.396(6)
C(25)-H(25)	0.950(4)	C(25)-C(26)	1.384(5)
C(26)-H(26)	0.950(4)	C(26')-H(26')	0.950(4)
C(27)-C(28)	1.395(5)	C(27)-C(32)	1.386(5)
C(27)-P(1)	1.815(4)	C(27')-C(28')	1.391(5)
C(27')-C(32')	1.394(5)	C(27')-P(1')	1.820(4)
C(28')-H(28')	0.950(4)	C(28')-C(29')	1.390(5)
C(28)-H(28)	0.950(4)	C(28)-C(29)	1.385(5)
C(29)-H(29)	0.950(4)	C(29)-C(30)	1.376(6)
C(29')-H(29')	0.950(4)	C(29')-C(30')	1.386(5)
C(30)-H(30)	0.950(4)	C(30)-C(31)	1.383(6)
C(30')-H(30')	0.950(4)	C(30')-C(31')	1.383(5)
C(31)-H(31)	0.950(4)	C(31)-C(32)	1.382(5)
C(31')-H(31')	0.950(4)	C(31')-C(32')	1.378(5)
C(32)-H(32)	0.950(4)	C(32')-H(32')	0.950(4)
C(33)-C(34)	1.394(5)	C(33)-C(38)	1.389(5)
C(33)-P(1)	1.826(4)	C(33')-C(34')	1.391(5)
C(33')-C(38')	1.396(5)	C(33')-P(1')	1.826(4)
C(34)-H(34)	0.950(4)	C(34)-C(35)	1.398(5)
C(34')-H(34')	0.950(4)	C(34')-C(35')	1.385(5)
C(35')-H(35')	0.950(4)	C(35')-C(36')	1.377(5)
C(35)-H(35)	0.950(4)	C(35)-C(36)	1.375(6)
C(36')-H(36')	0.950(4)	C(36')-C(37')	1.377(5)
C(36)-H(36)	0.950(4)	C(36)-C(37)	1.382(5)
C(37')-H(37')	0.950(4)	C(37')-C(38')	1.397(5)
C(37)-H(37)	0.950(4)	C(37)-C(38)	1.393(5)
C(38')-H(38')	0.950(4)	C(38)-H(38)	0.950(4)
C(39)-O(2)	1.154(4)	C(39)-Rh(1)	1.791(4)
C(39')-O(2')	1.153(4)	C(39')-Rh(1')	1.804(4)
O(1)-Rh(1)	2.039(3)	O(1')-Rh(1')	2.037(2)

P(1)-Rh(1)	2.291(1)	P(1')-Rh(1')	2.278(1)
S(1)-Rh(1)	2.304(1)	S(1')-Rh(1')	2.313(1)

**Table D1.5. Complete listing of bond angles (°) for [Rh(*S,O*-(*N*-diPT)(CO)(PPh<sub>3</sub>)].**

Angle	Value	Angle	Value
C(1)-C(2)-C(3)	120.3(4)	C(1')-C(2')-C(3')	120.2(3)
C(1')-C(2')-H(2')	119.9(3)	C(1)-C(2)-H(2)	119.8(4)
C(1)-C(6)-C(5)	120.2(4)	C(1')-C(6')-C(5')	120.4(3)
C(1')-C(6')-H(6')	119.8(3)	C(1)-C(6)-H(6)	119.9(4)
C(1)-C(7)-N(1)	115.8(3)	C(1')-C(7')-N(1')	113.4(3)
C(1')-C(7')-O(1')	115.7(3)	C(1)-C(7)-O(1)	114.7(3)
C(2)-C(1)-C(6)	119.3(4)	C(2')-C(1')-C(6')	119.4(3)
C(2')-C(1')-C(7')	119.7(3)	C(2)-C(1)-C(7)	120.2(3)
C(2)-C(3)-C(4)	119.9(4)	C(2')-C(3')-C(4')	119.7(3)
C(2')-C(3')-H(3')	120.1(4)	C(2)-C(3)-H(3)	120.0(4)
C(3')-C(4')-C(5')	120.3(3)	C(3)-C(4)-C(5)	120.1(4)
C(3)-C(4)-H(4)	119.9(4)	C(3')-C(4')-H(4')	119.8(4)
C(4)-C(5)-C(6)	120.3(4)	C(4')-C(5')-C(6')	120.0(3)
C(4')-C(5')-H(5')	120.0(3)	C(4)-C(5)-H(5)	119.9(4)
C(5)-C(6)-H(6)	119.9(4)	C(5')-C(6')-H(6')	119.8(4)
C(6)-C(1)-C(7)	120.5(3)	C(6')-C(1')-C(7')	120.9(3)
C(7)-N(1)-C(8)	126.4(3)	C(7')-N(1')-C(8')	126.1(3)
C(7)-O(1)-Rh(1)	131.6(2)	C(7')-O(1')-Rh(1')	131.1(2)
C(8)-N(2)-C(15)	120.9(3)	C(8')-N(2')-C(15')	121.2(3)
C(8')-N(2')-C(9')	121.5(3)	C(8)-N(2)-C(9)	123.5(3)
C(8)-S(1)-Rh(1)	109.0(2)	C(8')-S(1')-Rh(1')	108.4(2)
C(9)-C(10)-C(11)	119.8(3)	C(9')-C(10')-C(11')	120.1(4)
C(9')-C(10')-H(10')	119.9(4)	C(9)-C(10)-H(10)	120.1(4)
C(9)-C(14)-C(13)	119.9(4)	C(9')-C(14')-C(13')	119.5(4)
C(9')-C(14')-H(14')	120.3(4)	C(9)-C(14)-H(14)	120.1(4)
C(9')-N(2')-C(15')	117.3(3)	C(9)-N(2)-C(15)	115.4(3)
C(10')-C(11')-C(12')	120.1(4)	C(10)-C(11)-C(12)	120.6(4)
C(10)-C(11)-H(11)	119.7(4)	C(10')-C(11')-H(11')	120.0(4)
C(10)-C(9)-C(14)	119.9(3)	C(10')-C(9')-C(14')	120.4(3)
C(10')-C(9')-N(2')	120.6(3)	C(10)-C(9)-N(2)	121.6(3)
C(11)-C(12)-C(13)	119.6(4)	C(11')-C(12')-C(13')	119.8(4)
C(11')-C(12')-H(12')	120.1(4)	C(11)-C(12)-H(12)	120.2(4)
C(12)-C(13)-C(14)	120.2(4)	C(12')-C(13')-C(14')	120.0(4)
C(12')-C(13')-H(13')	120.0(5)	C(12)-C(13)-H(13)	119.9(4)
C(13)-C(14)-H(14)	120.0(4)	C(13')-C(14')-H(14')	120.3(4)
C(14)-C(9)-N(2)	118.4(3)	C(14')-C(9')-N(2')	118.9(3)

C(15)-C(16)-C(17)	120.2(4)	C(15')-C(16')-C(17')	118.8(3)
C(15')-C(16')-H(16')	120.6(3)	C(15)-C(16)-H(16)	119.9(4)
C(15')-C(20')-C(19')	119.7(3)	C(15)-C(20)-C(19)	118.0(4)
C(15)-C(20)-H(20)	121.0(4)	C(15')-C(20')-H(20')	120.2(3)
C(16')-C(15')-C(20')	121.4(3)	C(16)-C(15)-C(20)	121.3(4)
C(16)-C(15)-N(2)	118.8(3)	C(16')-C(15')-N(2')	119.7(3)
C(16')-C(17')-C(18')	120.4(3)	C(16)-C(17)-C(18)	119.3(4)
C(16)-C(17)-H(17)	120.3(4)	C(16')-C(17')-H(17')	119.8(4)
C(17')-C(18')-C(19')	120.0(3)	C(17)-C(18)-C(19)	120.7(4)
C(17)-C(18)-H(18)	119.6(5)	C(17')-C(18')-H(18')	120.0(4)
C(18)-C(19)-C(20)	120.5(4)	C(18')-C(19')-C(20')	119.7(3)
C(18')-C(19')-H(19')	120.1(3)	C(18)-C(19)-H(19)	119.8(5)
C(19')-C(20')-H(20')	120.2(3)	C(19)-C(20)-H(20)	121.0(4)
C(20')-C(15')-N(2')	118.9(3)	C(20)-C(15)-N(2)	119.7(3)
C(21')-C(22')-C(23')	121.7(4)	C(21)-C(22)-C(23)	120.5(4)
C(21)-C(22)-H(22)	119.8(4)	C(21')-C(22')-H(22')	119.2(4)
C(21)-C(26)-C(25)	119.6(4)	C(21')-C(26')-C(25')	121.0(4)
C(21')-C(26')-H(26')	119.5(4)	C(21)-C(26)-H(26)	120.2(3)
C(21)-P(1)-C(27)	102.5(2)	C(21)-P(1)-C(33)	104.0(2)
C(21')-P(1')-C(27')	104.1(2)	C(21')-P(1')-C(33')	107.5(2)
C(21)-P(1)-Rh(1)	113.9(2)	C(22')-C(21')-C(26')	117.5(4)
C(21')-P(1')-Rh(1')	108.7(2)	C(22)-C(21)-P(1)	118.8(3)
C(22)-C(21)-C(26)	119.5(3)	C(22)-C(23)-C(24)	120.0(4)
C(22')-C(21')-P(1')	115.1(3)	C(22')-C(23')-H(23')	119.9(4)
C(22')-C(23')-C(24')	120.2(4)	C(23)-C(24)-C(25)	119.9(4)
C(22)-C(23)-H(23)	120.0(4)	C(23')-C(24')-H(24')	120.6(4)
C(23')-C(24')-C(25')	118.7(4)	C(24')-C(25')-C(26')	121.0(4)
C(23)-C(24)-H(24)	120.0(4)	C(24)-C(25)-H(25)	119.8(4)
C(24)-C(25)-C(26)	120.5(4)	C(25')-C(26')-H(26')	119.5(4)
C(24')-C(25')-H(25')	119.5(4)	C(26')-C(21')-P(1')	127.5(3)
C(25)-C(26)-H(26)	120.2(4)	C(27')-C(28')-C(29')	120.4(3)
C(26)-C(21)-P(1)	121.4(3)	C(27)-C(28)-H(28)	119.9(4)
C(27)-C(28)-C(29)	120.1(3)	C(27')-C(32')-C(31')	120.9(3)
C(27')-C(28')-H(28')	119.8(3)	C(27)-C(32)-H(32)	119.7(4)
C(27)-C(32)-C(31)	120.6(4)	C(27)-P(1)-C(33)	105.6(2)
C(27')-C(32')-H(32')	119.6(3)	C(27')-P(1')-C(33')	101.2(2)
C(27)-P(1)-Rh(1)	111.4(2)	C(28')-C(27')-C(32')	118.8(3)
C(27')-P(1')-Rh(1')	115.4(2)	C(28)-C(27)-P(1)	122.0(3)
C(28)-C(27)-C(32)	119.1(3)	C(28)-C(29)-C(30)	120.1(4)
C(28')-C(27')-P(1')	123.5(3)	C(28')-C(29')-H(29')	120.0(4)
C(28')-C(29')-C(30')	119.9(3)	C(29)-C(30)-C(31)	120.3(4)

C(28)-C(29)-H(29)	120.0(4)	C(29')-C(30')-H(30')	120.0(4)
C(29')-C(30')-C(31')	120.0(4)	C(30)-C(31)-C(32)	119.8(4)
C(29)-C(30)-H(30)	119.8(4)	C(30')-C(31')-H(31')	120.0(4)
C(30')-C(31')-C(32')	120.0(4)	C(31')-C(32')-H(32')	119.6(4)
C(30)-C(31)-H(31)	120.1(4)	C(32')-C(27')-P(1')	117.7(3)
C(31)-C(32)-H(32)	119.7(4)	C(33)-C(34)-C(35)	119.6(4)
C(32)-C(27)-P(1)	118.8(3)	C(33')-C(34')-H(34')	119.6(4)
C(33')-C(34')-C(35')	120.7(4)	C(33)-C(38)-C(37)	120.3(4)
C(33)-C(34)-H(34)	120.2(4)	C(33')-C(38')-H(38')	120.0(4)
C(33')-C(38')-C(37')	120.0(3)	C(33)-P(1)-Rh(1)	118.0(2)
C(33)-C(38)-H(38)	119.9(4)	C(33')-P(1')-Rh(1')	118.7(2)
C(34)-C(33)-C(38)	119.4(3)	C(34')-C(33')-C(38')	118.9(3)
C(34')-C(33')-P(1')	120.1(3)	C(34)-C(33)-P(1)	123.4(3)
C(34)-C(35)-C(36)	120.6(4)	C(34')-C(35')-C(36')	119.7(4)
C(34')-C(35')-H(35')	120.1(4)	C(34)-C(35)-H(35)	119.7(4)
C(35)-C(36)-C(37)	120.0(4)	C(35')-C(36')-C(37')	120.7(4)
C(35')-C(36')-H(36')	119.6(4)	C(35)-C(36)-H(36)	120.0(4)
C(36)-C(37)-C(38)	120.1(4)	C(36')-C(37')-C(38')	119.8(4)
C(36')-C(37')-H(37')	120.1(4)	C(36)-C(37)-H(37)	120.0(4)
C(37')-C(38')-H(38')	120.0(4)	C(37)-C(38)-H(38)	119.8(4)
C(38)-C(33)-P(1)	117.2(3)	C(38')-C(33')-P(1')	120.9(3)
C(39)-Rh(1)-O(1)	174.8(2)	C(39)-Rh(1)-P(1)	93.0(1)
C(39')-Rh(1')-O(1')	175.6(2)	C(39')-Rh(1')-P(1')	88.5(2)
C(39)-Rh(1)-S(1)	88.9(2)	C(39')-Rh(1')-S(1')	90.1(2)
H(2')-C(2')-C(3')	119.9(4)	H(2)-C(2)-C(3)	119.9(4)
H(3')-C(3')-C(4')	120.2(3)	H(3)-C(3)-C(4)	120.1(4)
H(4)-C(4)-C(5)	120.0(4)	H(4')-C(4')-C(5')	119.9(4)
H(5')-C(5')-C(6')	120.0(4)	H(5)-C(5)-C(6)	119.9(4)
H(10')-C(10')-C(11')	119.9(4)	H(10)-C(10)-C(11)	120.1(4)
H(11)-C(11)-C(12)	119.7(4)	H(11')-C(11')-C(12')	120.0(4)
H(12')-C(12')-C(13')	120.1(4)	H(12)-C(12)-C(13)	120.2(4)
H(13')-C(13')-C(14')	120.0(4)	H(13)-C(13)-C(14)	119.9(4)
H(16')-C(16')-C(17')	120.6(3)	H(16)-C(16)-C(17)	119.9(4)
H(17)-C(17)-C(18)	120.3(4)	H(17')-C(17')-C(18')	119.8(4)
H(18)-C(18)-C(19)	119.7(4)	H(18')-C(18')-C(19')	120.0(4)
H(19')-C(19')-C(20')	120.2(4)	H(19)-C(19)-C(20)	119.7(5)
H(22)-C(22)-C(23)	119.8(4)	H(22')-C(22')-C(23')	119.2(4)
H(23)-C(23)-C(24)	120.0(4)	H(23')-C(23')-C(24')	119.9(4)
H(24)-C(24)-C(25)	120.0(4)	H(24')-C(24')-C(25')	120.7(4)
H(25')-C(25')-C(26')	119.5(5)	H(25)-C(25)-C(26)	119.8(4)
H(28')-C(28')-C(29')	119.8(4)	H(28)-C(28)-C(29)	119.9(4)

H(29)-C(29)-C(30)	120.0(4)	H(29')-C(29')-C(30')	120.0(4)
H(30)-C(30)-C(31)	119.8(4)	H(30')-C(30')-C(31')	120.0(4)
H(31)-C(31)-C(32)	120.1(4)	H(31')-C(31')-C(32')	120.0(4)
H(34)-C(34)-C(35)	120.2(4)	H(34')-C(34')-C(35')	119.6(4)
H(35')-C(35')-C(36')	120.1(4)	H(35)-C(35)-C(36)	119.7(4)
H(36')-C(36')-C(37')	119.7(4)	H(36)-C(36)-C(37)	120.0(4)
H(37')-C(37')-C(38')	120.1(4)	H(37)-C(37)-C(38)	120.0(4)
N(1)-C(7)-O(1)	129.5(3)	N(1')-C(7')-O(1')	130.8(3)
N(1)-C(8)-N(2)	114.1(3)	N(1')-C(8')-N(2')	112.6(3)
N(1')-C(8')-S(1')	130.6(3)	N(1)-C(8)-S(1)	130.4(3)
N(2)-C(8)-S(1)	115.5(3)	N(2')-C(8')-S(1')	116.7(3)
O(1)-Rh(1)-S(1)	91.1(1)	O(1)-Rh(1)-P(1)	87.5(1)
O(1')-Rh(1')-S(1')	91.7(1)	O(1')-Rh(1')-P(1')	89.5(1)
O(2)-C(39)-Rh(1)	175.3(3)	O(2')-C(39')-Rh(1')	177.6(3)
P(1')-Rh(1')-S(1')	177.0(1)	P(1)-Rh(1)-S(1)	175.6(1)

**D2. Crystal data of carbonyl(cyclohexyldiphenylphosphine)(*S,O*-(*N*-benzoyl-*N'*,*N'*-diphenylthioureato))rhodium(I), [Rh(*S,O*-(*N*-diPT)(CO)(PPh<sub>2</sub>Cy)]**

**Table D2.1. Atomic coordinates and equivalent isotropic displacement parameters (Å<sup>2</sup>) for [Rh(*S,O*-(*N*-diPT)(CO)(PPh<sub>2</sub>Cy)].  $U_{(eq)}$  is defined as one third of the trace of the orthogonalized  $U^{ij}$  tensor.**

Atom	x/a	y/b	z/c	$U_{(eq)}$
C(1)	0.8018(4)	-0.0381(2)	0.2144(3)	0.02212
C(2)	0.8011(4)	-0.0117(2)	0.1298(3)	0.02443
C(3)	0.8509(4)	-0.0406(2)	0.0570(3)	0.03178
C(4)	0.9016(5)	-0.0956(2)	0.0677(3)	0.04191
C(5)	0.8985(5)	-0.1225(2)	0.1501(3)	0.04285
C(6)	0.8486(4)	-0.0941(2)	0.2241(3)	0.03337
C(7)	0.7646(3)	-0.0035(2)	0.2947(3)	0.01891
C(8)	0.7558(3)	-0.0083(2)	0.4539(3)	0.0197
C(9)	0.7302(4)	-0.1077(2)	0.5066(3)	0.02301
C(10)	0.8490(4)	-0.1391(2)	0.5025(3)	0.03674
C(11)	0.8413(5)	-0.1983(2)	0.4927(3)	0.04447
C(12)	0.7158(5)	-0.2256(2)	0.4880(3)	0.0373
C(13)	0.5982(5)	-0.1935(2)	0.4898(3)	0.03956
C(14)	0.6050(4)	-0.1348(2)	0.4986(3)	0.03531
C(15)	0.7301(4)	-0.0272(2)	0.6140(3)	0.02145
C(16)	0.6042(4)	-0.0217(2)	0.6525(3)	0.02347
C(17)	0.5981(4)	-0.0033(2)	0.7411(3)	0.02543
C(18)	0.7176(4)	0.0102(2)	0.7904(3)	0.0238
C(19)	0.8431(4)	0.0038(2)	0.7526(3)	0.02889
C(20)	0.8503(4)	-0.0150(2)	0.6646(3)	0.0257
C(21)	0.9313(4)	0.1897(2)	0.2040(3)	0.02344
C(22)	1.0052(4)	0.2237(2)	0.2779(3)	0.0397
C(23)	1.1535(4)	0.2349(2)	0.2547(4)	0.04404
C(24)	1.2271(5)	0.1798(2)	0.2353(4)	0.04719
C(25)	1.1539(4)	0.1441(2)	0.1663(3)	0.03557
C(26)	1.0059(4)	0.1337(2)	0.1875(3)	0.02849
C(27)	0.6717(4)	0.2467(2)	0.2365(3)	0.01988
C(28)	0.7136(4)	0.2935(2)	0.1867(3)	0.02985
C(29)	0.6436(5)	0.3454(2)	0.1883(3)	0.03261
C(30)	0.5251(4)	0.3498(2)	0.2365(3)	0.03284
C(31)	0.4843(4)	0.3042(2)	0.2869(3)	0.02951
C(32)	0.5546(4)	0.2523(2)	0.2866(3)	0.02595



C(33)	0.6716(4)	0.1450(2)	0.1303(3)	0.02257
C(34)	0.5491(4)	0.1155(2)	0.1383(3)	0.02222
C(35)	0.4826(4)	0.0916(2)	0.0623(3)	0.02922
C(36)	0.5341(4)	0.0984(2)	-0.0219(3)	0.03265
C(37)	0.6572(5)	0.1280(2)	-0.0306(3)	0.03388
C(38)	0.7226(4)	0.1520(2)	0.0449(3)	0.02803
C(39)	0.7720(4)	0.1829(2)	0.4264(3)	0.025
N(1)	0.7666(3)	-0.0318(1)	0.3723(2)	0.0202
N(2)	0.7371(3)	-0.0462(1)	0.5224(2)	0.02003
O(1)	0.7348(3)	0.0488(1)	0.2776(2)	0.02141
O(2)	0.7911(3)	0.2235(1)	0.4700(2)	0.03723
P(1)	0.75313(10)	0.17626(4)	0.23229(7)	0.0199
Rh(1)	0.74920(3)	0.11963(1)	0.35803(2)	0.01954
S(1)	0.76731(10)	0.06288(4)	0.48587(7)	0.02378

**Table D2.2. Hydrogen coordinates and isotropic displacement parameters ( $\text{\AA}^2$ ) for  $[\text{Rh}(\text{S},\text{O}-(\text{N}-\text{diPT})(\text{CO})(\text{PPh}_2\text{Cy})]$ .**

Atom	x/a	y/b	z/c	$U_{\text{(eq)}}$
H(2)	0.76628	0.02618	0.12239	0.02932
H(3)	0.85022	-0.02262	-0.00046	0.03813
H(4)	0.9388	-0.11488	0.0181	0.05029
H(5)	0.93073	-0.16089	0.15642	0.05143
H(6)	0.84651	-0.11287	0.28086	0.04004
H(10)	0.93551	-0.12044	0.50633	0.04409
H(11)	0.92287	-0.2202	0.48927	0.05337
H(12)	0.71095	-0.26629	0.48358	0.04477
H(13)	0.51152	-0.21197	0.4849	0.04747
H(14)	0.52312	-0.11283	0.4991	0.04237
H(16)	0.52231	-0.03059	0.61838	0.02816
H(17)	0.51212	0.00016	0.76798	0.03052
H(18)	0.71317	0.02384	0.85047	0.02856
H(19)	0.9247	0.01231	0.78721	0.03467
H(20)	0.93671	-0.01948	0.63868	0.03084
H(21)	0.93046	0.21291	0.14733	0.02813
H(22A)	1.00359	0.20219	0.3354	0.04764
H(22B)	0.95774	0.26079	0.28606	0.04764
H(23A)	1.15488	0.26029	0.20126	0.05285
H(23B)	1.20176	0.25488	0.30572	0.05285
H(24A)	1.31935	0.18905	0.21453	0.05663
H(24B)	1.23902	0.15742	0.29182	0.05663

H(25A)	1.20125	0.10672	0.16194	0.04269
H(25B)	1.1571	0.16342	0.10703	0.04269
H(26A)	1.00245	0.1091	0.24175	0.03418
H(26B)	0.95918	0.1131	0.13657	0.03418
H(28)	0.79127	0.28996	0.15095	0.03582
H(29)	0.67642	0.37775	0.15674	0.03914
H(30)	0.47294	0.38427	0.23443	0.03941
H(31)	0.40676	0.3081	0.32263	0.03541
H(32)	0.52317	0.2206	0.32028	0.03114
H(34)	0.51081	0.11167	0.19565	0.02667
H(35)	0.40072	0.07032	0.0686	0.03507
H(36)	0.48632	0.08317	-0.07367	0.03918
H(37)	0.69565	0.13159	-0.08793	0.04066
H(38)	0.80392	0.17367	0.03841	0.03364

**Table D2.3. Anisotropic displacement parameters ( $\text{\AA}^2$ ) for [Rh(*S,O*-(*N*-diPT)(CO)(PPh<sub>2</sub>Cy)]. The anisotropic displacement factor exponent takes the form:  $-2\pi^2[h^2a^{*2}U^{11} + \dots + 2hka^*b^*U^{23}]$ .**

Atom	$U^{11}$	$U^{22}$	$U^{33}$	$U^{12}$	$U^{13}$	$U^{23}$
C(1)	0.014(2)	0.026(2)	0.026(2)	-0.005(2)	0.002(2)	-0.003(2)
C(2)	0.021(2)	0.030(2)	0.023(3)	-0.004(2)	0.001(2)	-0.004(2)
C(3)	0.028(2)	0.041(3)	0.026(3)	-0.003(2)	0.000(2)	-0.003(2)
C(4)	0.046(3)	0.050(3)	0.031(3)	0.003(2)	0.013(2)	-0.013(3)
C(5)	0.052(3)	0.026(3)	0.051(3)	0.010(2)	0.011(2)	-0.004(2)
C(6)	0.036(3)	0.031(3)	0.034(3)	-0.002(2)	0.006(2)	-0.001(2)
C(7)	0.012(2)	0.024(2)	0.021(2)	-0.005(2)	0.004(2)	-0.003(2)
C(8)	0.010(2)	0.022(2)	0.026(3)	0.001(2)	0.002(2)	0.001(2)
C(9)	0.027(2)	0.023(2)	0.019(2)	0.000(2)	0.002(2)	0.003(2)
C(10)	0.023(2)	0.036(3)	0.051(3)	0.001(2)	-0.001(2)	-0.007(2)
C(11)	0.032(3)	0.040(3)	0.060(4)	0.017(2)	-0.009(2)	-0.005(3)
C(12)	0.047(3)	0.026(3)	0.038(3)	0.000(2)	0.002(2)	-0.001(2)
C(13)	0.028(3)	0.033(3)	0.059(3)	-0.008(2)	0.014(2)	-0.010(2)
C(14)	0.023(2)	0.031(3)	0.052(3)	0.001(2)	0.004(2)	-0.003(2)
C(15)	0.021(2)	0.022(2)	0.022(2)	-0.001(2)	0.001(2)	0.007(2)
C(16)	0.018(2)	0.024(2)	0.028(3)	-0.004(2)	0.000(2)	0.001(2)
C(17)	0.019(2)	0.023(2)	0.035(3)	-0.003(2)	0.004(2)	0.001(2)
C(18)	0.031(2)	0.023(2)	0.018(2)	-0.001(2)	0.000(2)	0.002(2)
C(19)	0.020(2)	0.035(3)	0.031(3)	-0.004(2)	-0.004(2)	0.002(2)
C(20)	0.017(2)	0.032(3)	0.028(3)	0.001(2)	0.002(2)	0.007(2)
C(21)	0.021(2)	0.026(2)	0.024(2)	-0.001(2)	0.005(2)	0.001(2)

C(22)	0.029(3)	0.041(3)	0.049(3)	-0.004(2)	0.003(2)	-0.012(2)
C(23)	0.026(3)	0.048(3)	0.058(3)	-0.013(2)	0.000(2)	-0.016(3)
C(24)	0.022(3)	0.056(3)	0.064(4)	0.002(2)	0.004(2)	-0.009(3)
C(25)	0.024(2)	0.031(3)	0.052(3)	0.000(2)	0.012(2)	-0.004(2)
C(26)	0.029(2)	0.026(2)	0.031(3)	0.004(2)	0.011(2)	0.005(2)
C(27)	0.020(2)	0.021(2)	0.018(2)	-0.001(2)	0.000(2)	-0.002(2)
C(28)	0.036(3)	0.029(3)	0.026(3)	0.007(2)	0.012(2)	0.008(2)
C(29)	0.043(3)	0.024(3)	0.031(3)	0.003(2)	0.005(2)	0.003(2)
C(30)	0.036(3)	0.028(3)	0.034(3)	0.013(2)	-0.001(2)	0.001(2)
C(31)	0.018(2)	0.030(3)	0.041(3)	0.002(2)	0.004(2)	-0.002(2)
C(32)	0.022(2)	0.027(2)	0.028(3)	-0.003(2)	0.000(2)	0.000(2)
C(33)	0.026(2)	0.017(2)	0.025(2)	0.002(2)	0.003(2)	0.001(2)
C(34)	0.022(2)	0.028(2)	0.017(2)	0.002(2)	0.002(2)	-0.001(2)
C(35)	0.024(2)	0.035(3)	0.029(3)	-0.008(2)	0.002(2)	0.001(2)
C(36)	0.036(3)	0.037(3)	0.025(3)	-0.005(2)	-0.004(2)	-0.004(2)
C(37)	0.040(3)	0.040(3)	0.022(3)	-0.008(2)	0.005(2)	0.001(2)
C(38)	0.031(2)	0.028(3)	0.025(3)	-0.004(2)	0.005(2)	0.001(2)
C(39)	0.027(2)	0.025(3)	0.023(2)	0.000(2)	0.004(2)	0.003(2)
N(1)	0.018(2)	0.021(2)	0.022(2)	-0.001(1)	0.005(1)	0.001(2)
N(2)	0.019(2)	0.023(2)	0.018(2)	0.000(1)	0.004(1)	0.003(2)
O(1)	0.024(1)	0.017(2)	0.023(2)	-0.002(1)	-0.001(1)	-0.004(1)
O(2)	0.054(2)	0.026(2)	0.031(2)	-0.005(1)	0.000(1)	-0.004(2)
P(1)	0.0206(5)	0.0191(6)	0.0202(6)	-0.0006(4)	0.0034(4)	0.0002(5)
S(1)	0.0302(6)	0.0216(6)	0.0197(6)	-0.0015(4)	0.0030(4)	0.0015(5)
Rh(1)	0.0199(2)	0.0193(2)	0.0196(2)	-0.0006(1)	0.0030(1)	0.0004(1)

**Table D2.4. Complete listing of bond lengths (Å) for [Rh(*S,O*-(*N*-diPT)(CO)(PPh<sub>2</sub>Cy)].**

Bond	Distance	Bond	Distance
C(1)-C(2)	1.397(6)	C(1)-C(6)	1.388(6)
C(1)-C(7)	1.496(6)	C(2)-H(2)	0.950(5)
C(2)-C(3)	1.381(6)	C(3)-H(3)	0.950(5)
C(3)-C(4)	1.379(7)	C(4)-H(4)	0.950(5)
C(4)-C(5)	1.376(8)	C(5)-H(5)	0.950(5)
C(5)-C(6)	1.391(7)	C(6)-H(6)	0.950(5)
C(7)-N(1)	1.327(5)	C(7)-O(1)	1.274(5)
C(8)-N(1)	1.337(6)	C(8)-N(2)	1.365(6)
C(8)-S(1)	1.725(4)	C(9)-C(10)	1.377(6)
C(9)-C(14)	1.377(6)	C(9)-N(2)	1.451(6)
C(10)-H(10)	0.950(5)	C(10)-C(11)	1.388(7)
C(11)-H(11)	0.950(5)	C(11)-C(12)	1.380(7)
C(12)-H(12)	0.950(5)	C(12)-C(13)	1.374(7)

C(13)-H(13)	0.950(5)	C(13)-C(14)	1.375(7)
C(14)-H(14)	0.950(5)	C(15)-C(16)	1.387(6)
C(15)-C(20)	1.395(6)	C(15)-N(2)	1.434(6)
C(16)-H(16)	0.950(4)	C(16)-C(17)	1.388(6)
C(17)-H(17)	0.950(4)	C(17)-C(18)	1.385(6)
C(18)-H(18)	0.950(4)	C(18)-C(19)	1.380(6)
C(19)-H(19)	0.950(5)	C(19)-C(20)	1.383(6)
C(20)-H(20)	0.950(4)	C(21)-H(21)	1.000(4)
C(21)-C(22)	1.510(7)	C(21)-C(26)	1.519(6)
C(21)-P(1)	1.837(4)	C(22)-H(22A)	0.990(5)
C(22)-H(22B)	0.990(5)	C(22)-C(23)	1.528(7)
C(23)-H(23A)	0.990(6)	C(23)-H(23B)	0.990(6)
C(23)-C(24)	1.505(7)	C(24)-H(24A)	0.990(5)
C(24)-H(24B)	0.990(6)	C(24)-C(25)	1.478(7)
C(25)-H(25A)	0.990(5)	C(25)-H(25B)	0.990(5)
C(25)-C(26)	1.514(6)	C(26)-H(26A)	0.990(5)
C(26)-H(26B)	0.990(5)	C(27)-C(28)	1.388(6)
C(27)-C(32)	1.399(6)	C(27)-P(1)	1.826(4)
C(28)-H(28)	0.950(5)	C(28)-C(29)	1.390(6)
C(29)-H(29)	0.950(5)	C(29)-C(30)	1.393(7)
C(30)-H(30)	0.950(5)	C(30)-C(31)	1.368(7)
C(31)-H(31)	0.950(5)	C(31)-C(32)	1.391(6)
C(32)-H(32)	0.950(5)	C(33)-C(34)	1.390(6)
C(33)-C(38)	1.393(6)	C(33)-P(1)	1.829(5)
C(34)-H(34)	0.950(4)	C(34)-C(35)	1.392(6)
C(35)-H(35)	0.950(5)	C(35)-C(36)	1.379(7)
C(36)-H(36)	0.950(5)	C(36)-C(37)	1.397(7)
C(37)-H(37)	0.950(5)	C(37)-C(38)	1.382(7)
C(38)-H(38)	0.950(5)	C(39)-O(2)	1.156(6)
C(39)-Rh(1)	1.797(5)	O(1)-Rh(1)	2.037(3)
P(1)-Rh(1)	2.287(2)	S(1)-Rh(1)	2.312(2)

**Table D2.5. Complete listing of bond angles (°) for [Rh(*S,O*-(*N*-diPT)(CO)(PPh<sub>2</sub>Cy)].**

Angle	Value	Angle	Value
C(1)-C(2)-C(3)	120.1(4)	C(1)-C(2)-H(2)	119.9(4)
C(1)-C(6)-H(6)	120.3(5)	C(1)-C(6)-C(5)	119.4(5)
C(1)-C(7)-N(1)	115.6(4)	C(1)-C(7)-O(1)	114.6(4)
C(2)-C(1)-C(6)	119.6(4)	C(2)-C(1)-C(7)	119.2(4)
C(2)-C(3)-H(3)	120.0(5)	C(2)-C(3)-C(4)	120.0(5)
C(3)-C(4)-C(5)	120.3(5)	C(3)-C(4)-H(4)	119.9(5)
C(4)-C(5)-H(5)	119.7(5)	C(4)-C(5)-C(6)	120.5(5)
C(6)-C(1)-C(7)	120.9(4)	C(5)-C(6)-H(6)	120.3(5)
C(8)-N(2)-C(9)	121.7(4)	C(7)-N(1)-C(8)	125.8(4)
C(8)-S(1)-RH(1)	108.7(2)	C(7)-O(1)-RH(1)	130.4(3)
C(9)-C(10)-C(11)	119.4(5)	C(8)-N(2)-C(15)	121.4(4)
C(9)-C(14)-H(14)	119.9(5)	C(9)-C(10)-H(10)	120.3(5)
C(9)-N(2)-C(15)	116.9(4)	C(9)-C(14)-C(13)	120.2(4)
C(10)-C(11)-H(11)	119.8(5)	C(10)-C(11)-C(12)	120.5(5)
C(10)-C(9)-C(14)	120.1(4)	C(10)-C(9)-N(2)	119.9(4)
C(11)-C(12)-C(13)	119.4(5)	C(11)-C(12)-H(12)	120.3(5)
C(12)-C(13)-H(13)	119.8(5)	C(12)-C(13)-C(14)	120.4(5)
C(13)-C(14)-H(14)	119.9(5)	C(14)-C(9)-N(2)	120.0(4)
C(15)-C(16)-C(17)	119.8(4)	C(15)-C(16)-H(16)	120.1(4)
C(15)-C(20)-H(20)	120.2(4)	C(15)-C(20)-C(19)	119.7(4)
C(16)-C(15)-C(20)	120.0(4)	C(16)-C(15)-N(2)	120.1(4)
C(16)-C(17)-H(17)	120.1(4)	C(16)-C(17)-C(18)	119.9(4)
C(17)-C(18)-C(19)	120.4(4)	C(17)-C(18)-H(18)	119.8(4)
C(18)-C(19)-H(19)	119.9(5)	C(18)-C(19)-C(20)	120.2(4)
C(20)-C(15)-N(2)	119.8(4)	C(19)-C(20)-H(20)	120.2(4)
C(21)-C(22)-C(23)	110.6(4)	C(21)-C(22)-H(22B)	109.5(4)
C(21)-C(22)-H(22A)	109.5(4)	C(21)-C(26)-H(26A)	109.3(4)
C(21)-C(26)-C(25)	111.5(4)	C(21)-P(1)-C(33)	105.1(2)
C(21)-C(26)-H(26B)	109.3(4)	C(21)-P(1)-C(27)	105.9(2)
C(21)-P(1)-RH(1)	109.7(2)	C(22)-C(21)-C(26)	110.5(4)
C(22)-C(23)-H(23B)	109.3(5)	C(22)-C(23)-C(24)	111.4(4)
C(22)-C(21)-P(1)	110.5(3)	C(22)-C(23)-H(23A)	109.3(4)
C(23)-C(24)-H(24B)	109.0(5)	C(23)-C(24)-C(25)	113.0(4)
C(23)-C(24)-H(24A)	109.0(5)	C(24)-C(25)-H(25B)	109.1(5)
C(24)-C(25)-C(26)	112.5(4)	C(24)-C(25)-H(25A)	109.1(4)
C(25)-C(26)-H(26B)	109.3(4)	C(25)-C(26)-H(26A)	109.3(4)
C(26)-C(21)-P(1)	111.0(3)	C(27)-C(28)-C(29)	121.0(4)
C(27)-C(32)-H(32)	120.1(4)	C(27)-C(28)-H(28)	119.5(4)

C(27)-P(1)-RH(1)	117.8(2)	C(27)-C(32)-C(31)	119.8(4)
C(27)-P(1)-C(33)	102.2(2)	C(28)-C(27)-C(32)	118.6(4)
C(28)-C(29)-H(29)	120.2(5)	C(28)-C(27)-P(1)	123.2(3)
C(28)-C(29)-C(30)	119.6(4)	C(29)-C(30)-C(31)	119.6(4)
C(29)-C(30)-H(30)	120.2(5)	C(30)-C(31)-H(31)	119.5(5)
C(30)-C(31)-C(32)	121.1(4)	C(31)-C(32)-H(32)	120.1(4)
C(32)-C(27)-P(1)	118.0(3)	C(33)-C(34)-C(35)	120.0(4)
C(33)-C(38)-H(38)	119.4(4)	C(33)-C(34)-H(34)	120.0(4)
C(33)-C(38)-C(37)	121.3(4)	C(33)-P(1)-RH(1)	115.0(2)
C(34)-C(33)-C(38)	118.8(4)	C(34)-C(35)-H(35)	119.6(4)
C(34)-C(33)-P(1)	118.0(3)	C(34)-C(35)-C(36)	120.8(4)
C(35)-C(36)-C(37)	119.5(4)	C(35)-C(36)-H(36)	120.3(5)
C(36)-C(37)-H(37)	120.3(5)	C(36)-C(37)-C(38)	119.5(4)
C(37)-C(38)-H(38)	119.4(5)	C(38)-C(33)-P(1)	123.1(3)
C(39)-RH(1)-P(1)	89.0(2)	C(39)-RH(1)-O(1)	176.5(2)
C(39)-RH(1)-S(1)	90.1(2)	H(2)-C(2)-C(3)	119.9(5)
H(3)-C(3)-C(4)	120.0(5)	H(4)-C(4)-C(5)	119.9(5)
H(5)-C(5)-C(6)	119.7(5)	H(10)-C(10)-C(11)	120.3(5)
H(11)-C(11)-C(12)	119.8(5)	H(12)-C(12)-C(13)	120.3(5)
H(13)-C(13)-C(14)	119.8(5)	H(16)-C(16)-C(17)	120.1(4)
H(17)-C(17)-C(18)	120.1(5)	H(18)-C(18)-C(19)	119.8(4)
H(19)-C(19)-C(20)	119.9(4)	H(21)-C(21)-C(22)	108.3(4)
H(21)-C(21)-P(1)	108.2(3)	H(21)-C(21)-C(26)	108.3(4)
H(22A)-C(22)-C(23)	109.5(4)	H(22A)-C(22)-H(22B)	108.1(5)
H(22B)-C(22)-C(23)	109.5(5)	H(23A)-C(23)-C(24)	109.3(5)
H(23B)-C(23)-C(24)	109.3(5)	H(23A)-C(23)-H(23B)	108.0(5)
H(24A)-C(24)-C(25)	109.0(5)	H(24B)-C(24)-C(25)	109.0(5)
H(24A)-C(24)-H(24B)	107.8(5)	H(25A)-C(25)-C(26)	109.1(4)
H(25B)-C(25)-C(26)	109.1(4)	H(25A)-C(25)-H(25B)	107.8(5)
H(26A)-C(26)-H(26B)	108.0(4)	H(28)-C(28)-C(29)	119.5(5)
H(29)-C(29)-C(30)	120.2(5)	H(30)-C(30)-C(31)	120.2(5)
H(31)-C(31)-C(32)	119.4(5)	H(34)-C(34)-C(35)	120.0(4)
H(35)-C(35)-C(36)	119.6(5)	H(36)-C(36)-C(37)	120.2(5)
H(37)-C(37)-C(38)	120.2(5)	N(1)-C(8)-S(1)	129.4(3)
N(1)-C(7)-O(1)	129.8(4)	N(1)-C(8)-N(2)	115.3(4)
N(2)-C(8)-S(1)	115.2(3)	O(1)-RH(1)-P(1)	89.5(1)
O(1)-RH(1)-S(1)	91.1(1)	O(2)-C(39)-RH(1)	177.8(4)
P(1)-RH(1)-S(1)	174.6(1)		

**D3. Crystal data of carbonyl(tricyclohexylphosphine)(*S,O*-(*N*-benzoyl-*N'*,*N'*-diphenylthioureato))rhodium(I), [Rh(*S,O*-(*N*-diPT)(CO)(PCy<sub>3</sub>)]**

**Table D3.1. Atomic coordinates and equivalent isotropic displacement parameters (Å<sup>2</sup>) for [Rh(*S,O*-(*N*-diPT)(CO)(PCy<sub>3</sub>)].  $U_{\text{eq}}$  is defined as one third of the trace of the orthogonalized  $U^{\text{ij}}$  tensor.**

Atom	x/a	y/b	z/c	$U_{\text{eq}}$
C(1)	0.8023(5)	-0.0374(2)	0.2849(3)	0.01872
C(2)	0.8219(5)	-0.0194(2)	0.3721(3)	0.02529
C(3)	0.8529(6)	-0.0558(2)	0.4414(3)	0.03104
C(4)	0.8643(6)	-0.1108(2)	0.4232(3)	0.03344
C(5)	0.8438(6)	-0.1293(2)	0.3368(4)	0.03664
C(6)	0.8133(6)	-0.0930(2)	0.2671(3)	0.02924
C(7)	0.7743(4)	0.0026(2)	0.2101(3)	0.01711
C(8)	0.7423(4)	0.0050(2)	0.0512(3)	0.01611
C(9)	0.7960(5)	-0.0855(2)	-0.0053(3)	0.01845
C(10)	0.9322(5)	-0.1021(2)	-0.0078(3)	0.02081
C(11)	0.9650(5)	-0.1567(2)	0.0052(3)	0.02605
C(12)	0.8617(5)	-0.1939(2)	0.0207(3)	0.02657
C(13)	0.7249(5)	-0.1771(2)	0.0227(3)	0.02573
C(14)	0.6918(5)	-0.1221(2)	0.0094(3)	0.02354
C(15)	0.7423(5)	-0.0109(2)	-0.1118(3)	0.01741
C(16)	0.8544(5)	0.0084(2)	-0.1558(3)	0.02243
C(17)	0.8345(5)	0.0225(2)	-0.2455(3)	0.02571
C(18)	0.7062(5)	0.0166(2)	-0.2892(3)	0.023
C(19)	0.5957(5)	-0.0026(2)	-0.2441(3)	0.02244
C(20)	0.6133(5)	-0.0166(2)	-0.1547(3)	0.02058
C(21)	0.7136(5)	0.1390(2)	0.3854(3)	0.01795
C(22)	0.7445(5)	0.1690(2)	0.4735(3)	0.0228
C(23)	0.7084(6)	0.1339(2)	0.5529(3)	0.03013
C(24)	0.5573(5)	0.1160(2)	0.5432(3)	0.02783
C(25)	0.5273(5)	0.0851(2)	0.4572(3)	0.02689
C(26)	0.5627(5)	0.1200(2)	0.3776(3)	0.02344
C(27)	0.9577(4)	0.1787(2)	0.2998(3)	0.01621
C(28)	1.0300(4)	0.1232(2)	0.3143(3)	0.02279
C(29)	1.1884(5)	0.1285(2)	0.3207(3)	0.02565
C(30)	1.2382(5)	0.1557(2)	0.2375(3)	0.02504
C(31)	1.1754(5)	0.2125(2)	0.2263(3)	0.02347
C(32)	1.0169(5)	0.2089(2)	0.2199(3)	0.02147

C(33)	0.7099(4)	0.2447(2)	0.2795(3)	0.01604
C(34)	0.7840(5)	0.2852(2)	0.3436(3)	0.01928
C(35)	0.7377(5)	0.3434(2)	0.3230(3)	0.0206
C(36)	0.5809(5)	0.3493(2)	0.3263(3)	0.02562
C(37)	0.5040(5)	0.3083(2)	0.2656(3)	0.02464
C(38)	0.5526(5)	0.2498(2)	0.2854(3)	0.01946
C(39)	0.6492(5)	0.1799(2)	0.1006(3)	0.01885
N(1)	0.7686(4)	-0.0201(2)	0.1300(2)	0.01774
N(2)	0.7617(4)	-0.0286(2)	-0.0192(2)	0.01726
O(1)	0.7666(3)	0.0522(1)	0.2326(2)	0.01899
O(2)	0.6042(4)	0.2174(1)	0.0627(2)	0.0294
P(1)	0.76834(12)	0.17274(4)	0.28341(7)	0.01503
Rh(1)	0.71302(4)	0.12055(1)	0.15890(2)	0.01501
S(1)	0.68853(11)	0.06988(4)	0.02763(7)	0.01704

**Table D3.2. Hydrogen coordinates and isotropic displacement parameters ( $\text{\AA}^2$ ) for  $[\text{Rh}(\text{S},\text{O}-(\text{N}-\text{diPT})(\text{CO})(\text{PCy}_3)]$ .**

Atom	x/a	y/b	z/c	$U_{\text{(eq)}}$
H(2)	0.8141	0.01838	0.38479	0.03035
H(3)	0.86616	-0.04285	0.50095	0.03725
H(4)	0.8862	-0.13586	0.47032	0.04013
H(5)	0.85061	-0.16724	0.32467	0.04396
H(6)	0.80003	-0.10611	0.20758	0.03508
H(10)	1.00294	-0.07629	-0.01836	0.02497
H(11)	1.0585	-0.16844	0.00348	0.03126
H(12)	0.88455	-0.23122	0.03002	0.03188
H(13)	0.65402	-0.2028	0.03295	0.03088
H(14)	0.5984	-0.11011	0.0106	0.02825
H(16)	0.94291	0.01197	-0.12553	0.02691
H(17)	0.90993	0.0363	-0.27673	0.03085
H(18)	0.69399	0.0257	-0.35073	0.0276
H(19)	0.50713	-0.00616	-0.2744	0.02693
H(20)	0.53744	-0.03002	-0.12343	0.02469
H(21)	0.76977	0.1047	0.39041	0.02154
H(22A)	0.84409	0.17872	0.47911	0.02735
H(22B)	0.69011	0.20324	0.47361	0.02735
H(23A)	0.76917	0.10143	0.55643	0.03615
H(23B)	0.72427	0.15504	0.60882	0.03615
H(24A)	0.53615	0.09253	0.59438	0.03339
H(24B)	0.49662	0.14853	0.54418	0.03339



H(25A)	0.42802	0.07493	0.45189	0.03227
H(25B)	0.58286	0.05113	0.4579	0.03227
H(26A)	0.50082	0.1522	0.37394	0.02813
H(26B)	0.54646	0.0986	0.32199	0.02813
H(27)	0.97823	0.20131	0.35445	0.01946
H(28A)	0.99913	0.10659	0.37006	0.02735
H(28B)	1.00197	0.0986	0.26422	0.02735
H(29A)	1.21777	0.15031	0.37391	0.03078
H(29B)	1.23077	0.09181	0.32733	0.03078
H(30A)	1.21129	0.13325	0.18445	0.03005
H(30B)	1.34056	0.15851	0.24201	0.03005
H(31A)	1.20809	0.22963	0.17152	0.02817
H(31B)	1.20585	0.23553	0.27793	0.02817
H(32A)	0.98698	0.18969	0.16399	0.02577
H(32B)	0.978	0.24623	0.2166	0.02577
H(33)	0.72929	0.25787	0.21824	0.01924
H(34A)	0.7634	0.27603	0.40581	0.02313
H(34B)	0.8854	0.2823	0.33832	0.02313
H(35A)	0.76621	0.35373	0.26292	0.02472
H(35B)	0.78388	0.3685	0.36699	0.02472
H(36A)	0.55406	0.34383	0.38849	0.03074
H(36B)	0.55351	0.38669	0.3079	0.03074
H(37A)	0.51966	0.31726	0.20253	0.02956
H(37B)	0.40329	0.31105	0.27394	0.02956
H(38A)	0.52681	0.23926	0.34605	0.02335
H(38B)	0.50549	0.22457	0.24208	0.02335

**Table D3.3. Anisotropic displacement parameters ( $\text{\AA}^2$ ) for  $[\text{Rh}(\text{S}, \text{O}-(N\text{-diPT})(\text{CO})(\text{PCy}_3)]$ .**

The anisotropic displacement factor exponent takes the form:  $-2\pi^2[\text{h}^2\text{a}^{*2}\text{U}^{11} + \dots + 2\text{hka}^*\text{b}^*\text{U}^{23}]$ .

Atom	$\text{U}^{11}$	$\text{U}^{22}$	$\text{U}^{33}$	$\text{U}^{12}$	$\text{U}^{13}$	$\text{U}^{23}$
C(1)	0.019(2)	0.019(2)	0.019(2)	0.001(2)	0.001(2)	0.001(2)
C(2)	0.034(3)	0.022(3)	0.020(2)	0.007(2)	0.002(2)	0.000(2)
C(3)	0.045(3)	0.026(3)	0.021(3)	0.006(2)	0.001(2)	0.001(2)
C(4)	0.044(3)	0.026(3)	0.029(3)	0.003(2)	-0.006(2)	0.009(2)
C(5)	0.056(4)	0.014(3)	0.038(3)	-0.001(2)	-0.010(3)	-0.001(2)
C(6)	0.041(3)	0.022(3)	0.024(3)	-0.003(2)	-0.004(2)	-0.001(2)
C(7)	0.014(2)	0.015(2)	0.022(2)	-0.001(2)	0.001(2)	0.001(2)
C(8)	0.016(2)	0.015(2)	0.017(2)	-0.001(2)	0.004(2)	-0.001(2)
C(9)	0.024(2)	0.017(2)	0.014(2)	0.006(2)	0.001(2)	-0.003(2)

C(10)	0.020(2)	0.025(2)	0.018(2)	0.003(2)	0.000(2)	-0.004(2)
C(11)	0.023(2)	0.033(3)	0.022(2)	0.011(2)	0.002(2)	0.001(2)
C(12)	0.037(3)	0.020(2)	0.023(2)	0.011(2)	0.002(2)	0.002(2)
C(13)	0.030(3)	0.020(2)	0.027(3)	0.000(2)	0.004(2)	0.001(2)
C(14)	0.020(2)	0.024(2)	0.027(2)	0.006(2)	0.003(2)	0.002(2)
C(15)	0.027(2)	0.009(2)	0.017(2)	0.000(2)	0.006(2)	-0.004(2)
C(16)	0.020(2)	0.025(3)	0.023(2)	-0.003(2)	0.004(2)	-0.002(2)
C(17)	0.028(3)	0.022(3)	0.028(3)	-0.002(2)	0.013(2)	0.004(2)
C(18)	0.037(3)	0.016(2)	0.016(2)	0.003(2)	0.005(2)	0.003(2)
C(19)	0.026(2)	0.021(2)	0.020(2)	0.002(2)	0.002(2)	-0.002(2)
C(20)	0.024(2)	0.017(2)	0.021(2)	-0.003(2)	0.006(2)	-0.002(2)
C(21)	0.024(2)	0.016(2)	0.014(2)	-0.002(2)	0.005(2)	0.001(2)
C(22)	0.029(3)	0.025(3)	0.014(2)	-0.001(2)	0.002(2)	0.000(2)
C(23)	0.040(3)	0.034(3)	0.016(2)	-0.002(2)	0.000(2)	0.004(2)
C(24)	0.031(3)	0.034(3)	0.020(2)	0.003(2)	0.008(2)	0.008(2)
C(25)	0.028(3)	0.026(3)	0.027(3)	-0.001(2)	0.009(2)	0.006(2)
C(26)	0.027(2)	0.023(2)	0.022(2)	-0.005(2)	0.005(2)	0.002(2)
C(27)	0.018(2)	0.015(2)	0.016(2)	0.001(2)	0.006(2)	-0.001(2)
C(28)	0.017(2)	0.017(2)	0.035(3)	0.003(2)	0.004(2)	0.004(2)
C(29)	0.020(2)	0.020(2)	0.037(3)	0.004(2)	0.003(2)	0.004(2)
C(30)	0.021(2)	0.027(3)	0.027(3)	-0.001(2)	0.003(2)	-0.003(2)
C(31)	0.022(2)	0.024(3)	0.025(2)	-0.005(2)	0.006(2)	0.002(2)
C(32)	0.022(2)	0.021(2)	0.022(2)	-0.001(2)	0.005(2)	0.003(2)
C(33)	0.019(2)	0.013(2)	0.016(2)	-0.001(2)	0.002(2)	0.000(2)
C(34)	0.026(2)	0.016(2)	0.016(2)	-0.002(2)	0.002(2)	-0.004(2)
C(35)	0.031(3)	0.014(2)	0.018(2)	-0.002(2)	0.005(2)	-0.001(2)
C(36)	0.033(3)	0.015(2)	0.029(3)	0.003(2)	0.005(2)	-0.003(2)
C(37)	0.024(2)	0.022(2)	0.027(3)	0.006(2)	0.000(2)	0.003(2)
C(38)	0.023(2)	0.016(2)	0.019(2)	-0.001(2)	0.003(2)	-0.001(2)
C(39)	0.026(2)	0.017(2)	0.013(2)	-0.005(2)	0.005(2)	-0.004(2)
N(1)	0.022(2)	0.015(2)	0.016(2)	0.001(1)	0.002(1)	0.000(1)
N(2)	0.022(2)	0.016(2)	0.014(2)	0.002(1)	0.002(1)	-0.001(1)
O(1)	0.029(2)	0.015(2)	0.014(2)	0.001(1)	0.003(1)	-0.002(1)
O(2)	0.044(2)	0.020(2)	0.024(2)	0.002(2)	-0.003(2)	0.003(1)
S(1)	0.0227(6)	0.0140(5)	0.0148(5)	0.0002(4)	0.0039(4)	-0.0011(4)
Rh(1)	0.0196(2)	0.0128(2)	0.0129(2)	-0.0009(1)	0.0032(1)	-0.0008(1)
P(1)	0.0199(6)	0.0128(5)	0.0127(5)	-0.0007(4)	0.0032(4)	-0.0012(4)

**Table D3.4. Complete listing of bond lengths (Å) for [Rh(*S,O*-(*N*-diPT)(CO)(PCy<sub>3</sub>)].**

<b>Bond</b>	<b>Distance</b>	<b>Bond</b>	<b>Distance</b>
C(1)-C(2)	1.383(7)	C(1)-C(6)	1.395(7)
C(1)-C(7)	1.503(7)	C(2)-H(2)	0.950(5)
C(2)-C(3)	1.388(7)	C(3)-H(3)	0.950(6)
C(3)-C(4)	1.383(8)	C(4)-H(4)	0.950(6)
C(4)-C(5)	1.377(8)	C(5)-H(5)	0.950(5)
C(5)-C(6)	1.392(8)	C(6)-H(6)	0.950(6)
C(7)-N(1)	1.323(6)	C(7)-O(1)	1.265(6)
C(8)-N(1)	1.344(6)	C(8)-N(2)	1.359(6)
C(8)-S(1)	1.704(5)	C(9)-C(10)	1.379(7)
C(9)-C(14)	1.375(7)	C(9)-N(2)	1.446(6)
C(10)-H(10)	0.950(5)	C(10)-C(11)	1.387(7)
C(11)-H(11)	0.950(5)	C(11)-C(12)	1.381(7)
C(12)-H(12)	0.950(5)	C(12)-C(13)	1.386(8)
C(13)-H(13)	0.950(5)	C(13)-C(14)	1.397(7)
C(14)-H(14)	0.950(5)	C(15)-C(16)	1.381(7)
C(15)-C(20)	1.378(7)	C(15)-N(2)	1.458(6)
C(16)-H(16)	0.950(5)	C(16)-C(17)	1.391(7)
C(17)-H(17)	0.950(5)	C(17)-C(18)	1.378(7)
C(18)-H(18)	0.950(5)	C(18)-C(19)	1.377(7)
C(19)-H(19)	0.950(5)	C(19)-C(20)	1.385(7)
C(20)-H(20)	0.950(5)	C(21)-H(21)	1.000(5)
C(21)-C(22)	1.527(7)	C(21)-C(26)	1.529(7)
C(21)-P(1)	1.842(5)	C(22)-H(22A)	0.990(5)
C(22)-H(22B)	0.990(5)	C(22)-C(23)	1.524(7)
C(23)-H(23A)	0.990(6)	C(23)-H(23B)	0.990(5)
C(23)-C(24)	1.523(8)	C(24)-H(24A)	0.990(5)
C(24)-H(24B)	0.990(6)	C(24)-C(25)	1.509(7)
C(25)-H(25A)	0.990(6)	C(25)-H(25B)	0.990(5)
C(25)-C(26)	1.523(7)	C(26)-H(26A)	0.990(5)
C(26)-H(26B)	0.990(5)	C(27)-H(27)	1.000(5)
C(27)-C(28)	1.539(7)	C(27)-P(1)	1.838(5)
C(28)-H(28A)	0.990(5)	C(28)-H(28B)	0.990(5)
C(28)-C(29)	1.534(7)	C(29)-H(29A)	0.990(5)
C(29)-H(29B)	0.990(5)	C(29)-C(30)	1.516(7)
C(30)-H(30A)	0.990(5)	C(30)-H(30B)	0.990(5)
C(30)-C(31)	1.524(7)	C(31)-H(31A)	0.990(5)
C(31)-H(31B)	0.990(5)	C(31)-C(32)	1.531(7)
C(32)-H(32A)	0.990(5)	C(32)-H(32B)	0.990(5)
C(33)-H(33)	1.000(5)	C(33)-C(34)	1.532(7)

C(33)-C(38)	1.532(7)	C(33)-P(1)	1.853(5)
C(34)-H(34A)	0.990(5)	C(34)-H(34B)	0.990(5)
C(34)-C(35)	1.521(7)	C(35)-H(35A)	0.990(5)
C(35)-H(35B)	0.990(5)	C(35)-C(36)	1.525(7)
C(36)-H(36A)	0.990(5)	C(36)-H(36B)	0.990(5)
C(36)-C(37)	1.521(7)	C(37)-H(37A)	0.990(5)
C(37)-H(37B)	0.990(5)	C(37)-C(38)	1.534(7)
C(38)-H(38A)	0.990(5)	C(38)-H(38B)	0.990(5)
C(39)-O(2)	1.154(6)	C(39)-Rh(1)	1.789(5)
S(1)-Rh(1)	2.328(2)	Rh(1)-P(1)	2.302(2)

**Table D3.5. Complete listing of bond angles (°) for [Rh(*S,O*-(*N*-diPT)(CO)(PCy<sub>3</sub>)].**

Angle	Value	Angle	Value
C(1)-C(2)-H(2)	119.5(5)	C(1)-C(2)-C(3)	121.0(5)
C(1)-C(6)-C(5)	119.7(5)	C(1)-C(6)-H(6)	120.1(5)
C(1)-C(7)-O(1)	116.1(4)	C(1)-C(7)-N(1)	113.6(4)
C(2)-C(1)-C(7)	120.5(5)	C(2)-C(1)-C(6)	119.0(5)
C(2)-C(3)-C(4)	119.7(5)	C(2)-C(3)-H(3)	120.1(5)
C(3)-C(4)-H(4)	120.1(6)	C(3)-C(4)-C(5)	119.8(5)
C(4)-C(5)-C(6)	120.7(5)	C(4)-C(5)-H(5)	119.7(6)
C(5)-C(6)-H(6)	120.1(5)	C(6)-C(1)-C(7)	120.5(5)
C(7)-N(1)-C(8)	127.0(4)	C(8)-N(2)-C(9)	120.9(4)
C(8)-N(2)-C(15)	122.9(4)	C(8)-S(1)-Rh(1)	107.9(2)
C(9)-C(10)-C(11)	119.4(5)	C(9)-C(14)-H(14)	120.4(5)
C(9)-C(10)-H(10)	120.3(5)	C(9)-N(2)-C(15)	116.2(4)
C(9)-C(14)-C(13)	119.2(5)	C(10)-C(11)-H(11)	120.0(5)
C(10)-C(11)-C(12)	120.0(5)	C(10)-C(9)-C(14)	121.3(5)
C(10)-C(9)-N(2)	119.4(4)	C(11)-C(12)-C(13)	120.3(5)
C(11)-C(12)-H(12)	119.8(5)	C(12)-C(13)-H(13)	120.2(5)
C(12)-C(13)-C(14)	119.7(5)	C(13)-C(14)-H(14)	120.4(5)
C(14)-C(9)-N(2)	119.2(4)	C(15)-C(16)-C(17)	118.4(5)
C(15)-C(16)-H(16)	120.8(5)	C(15)-C(20)-H(20)	120.5(5)
C(15)-C(20)-C(19)	119.1(5)	C(16)-C(15)-C(20)	121.6(5)
C(16)-C(15)-N(2)	119.6(4)	C(16)-C(17)-H(17)	119.8(5)
C(16)-C(17)-C(18)	120.5(5)	C(17)-C(18)-C(19)	120.2(5)
C(17)-C(18)-H(18)	119.9(5)	C(18)-C(19)-H(19)	119.9(5)
C(18)-C(19)-C(20)	120.2(5)	C(19)-C(20)-H(20)	120.5(5)
C(20)-C(15)-N(2)	118.7(4)	C(21)-C(22)-C(23)	111.2(4)
C(21)-C(22)-H(22B)	109.4(4)	C(21)-C(22)-H(22A)	109.4(4)
C(21)-C(26)-H(26A)	109.3(5)	C(21)-C(26)-C(25)	111.4(4)

C(21)-P(1)-C(27)	104.7(2)	C(21)-C(26)-H(26B)	109.4(4)
C(21)-P(1)-Rh(1)	111.0(2)	C(21)-P(1)-C(33)	110.7(2)
C(22)-C(21)-C(26)	110.7(4)	C(22)-C(21)-P(1)	116.7(4)
C(22)-C(23)-H(23B)	109.6(5)	C(22)-C(23)-C(24)	110.3(5)
C(22)-C(23)-H(23A)	109.6(5)	C(23)-C(24)-H(24B)	109.3(5)
C(23)-C(24)-H(24A)	109.4(5)	C(23)-C(24)-C(25)	111.4(4)
C(24)-C(25)-H(25B)	109.6(5)	C(24)-C(25)-C(26)	110.3(5)
C(24)-C(25)-H(25A)	109.6(5)	C(25)-C(26)-H(26A)	109.4(5)
C(25)-C(26)-H(26B)	109.4(5)	C(26)-C(21)-P(1)	112.9(3)
C(27)-C(28)-C(29)	112.2(4)	C(27)-C(28)-H(28B)	109.2(4)
C(27)-C(28)-H(28A)	109.2(4)	C(27)-P(1)-C(33)	103.1(2)
C(27)-P(1)-Rh(1)	109.7(2)	C(28)-C(27)-P(1)	112.9(3)
C(28)-C(29)-C(30)	110.3(4)	C(28)-C(29)-H(29B)	109.6(5)
C(28)-C(29)-H(29A)	109.6(5)	C(29)-C(30)-H(30B)	109.5(5)
C(29)-C(30)-C(31)	110.5(4)	C(29)-C(30)-H(30A)	109.5(5)
C(30)-C(31)-C(32)	110.2(4)	C(30)-C(31)-H(31B)	109.6(5)
C(30)-C(31)-H(31A)	109.6(5)	C(31)-C(32)-H(32B)	109.0(5)
C(31)-C(32)-H(32A)	109.0(5)	C(33)-C(34)-C(35)	111.0(4)
C(33)-C(34)-H(34B)	109.4(4)	C(33)-C(34)-H(34A)	109.4(4)
C(33)-C(38)-H(38A)	109.4(4)	C(33)-C(38)-C(37)	111.0(4)
C(33)-P(1)-Rh(1)	116.5(2)	C(33)-C(38)-H(38B)	109.4(4)
C(34)-C(33)-C(38)	110.0(4)	C(34)-C(35)-H(35B)	109.4(4)
C(34)-C(35)-C(36)	111.3(4)	C(34)-C(33)-P(1)	117.8(4)
C(34)-C(35)-H(35A)	109.4(4)	C(35)-C(36)-C(37)	111.8(4)
C(35)-C(36)-H(36B)	109.3(5)	C(35)-C(36)-H(36A)	109.3(5)
C(36)-C(37)-H(37B)	109.3(5)	C(36)-C(37)-C(38)	111.5(4)
C(36)-C(37)-H(37A)	109.3(5)	C(37)-C(38)-H(38A)	109.4(4)
C(37)-C(38)-H(38B)	109.4(4)	C(38)-C(33)-P(1)	112.1(3)
C(39)-Rh(1)-P(1)	90.1(2)	C(39)-Rh(1)-S(1)	90.3(2)
H(2)-C(2)-C(3)	119.5(5)	H(3)-C(3)-C(4)	120.1(6)
H(4)-C(4)-C(5)	120.1(6)	H(5)-C(5)-C(6)	119.7(6)
H(10)-C(10)-C(11)	120.3(5)	H(11)-C(11)-C(12)	120.0(5)
H(12)-C(12)-C(13)	119.8(5)	H(13)-C(13)-C(14)	120.2(5)
H(16)-C(16)-C(17)	120.8(5)	H(17)-C(17)-C(18)	119.8(5)
H(18)-C(18)-C(19)	119.9(5)	H(19)-C(19)-C(20)	119.9(5)
H(21)-C(21)-C(26)	105.1(4)	H(21)-C(21)-C(22)	105.1(4)
H(21)-C(21)-P(1)	105.1(4)	H(22A)-C(22)-H(22B)	108.0(5)
H(22B)-C(22)-C(23)	109.4(5)	H(22A)-C(22)-C(23)	109.4(5)
H(23A)-C(23)-H(23B)	108.1(5)	H(23A)-C(23)-C(24)	109.6(5)
H(23B)-C(23)-C(24)	109.6(5)	H(24A)-C(24)-C(25)	109.4(5)
H(24A)-C(24)-H(24B)	108.0(5)	H(25A)-C(25)-C(26)	109.6(5)

H(24B)-C(24)-C(25)	109.3(5)	H(25B)-C(25)-C(26)	109.6(5)
H(25A)-C(25)-H(25B)	108.1(5)	H(26A)-C(26)-H(26B)	108.0(5)
H(27)-C(27)-P(1)	107.8(4)	H(27)-C(27)-C(28)	107.8(4)
H(28A)-C(28)-C(29)	109.2(5)	H(28A)-C(28)-H(28B)	107.9(5)
H(28B)-C(28)-C(29)	109.2(4)	H(29A)-C(29)-C(30)	109.6(5)
H(29B)-C(29)-C(30)	109.6(5)	H(29A)-C(29)-H(29B)	108.1(5)
H(30A)-C(30)-C(31)	109.5(5)	H(30A)-C(30)-H(30B)	108.1(5)
H(30B)-C(30)-C(31)	109.5(5)	H(31A)-C(31)-C(32)	109.6(5)
H(31B)-C(31)-C(32)	109.6(5)	H(31A)-C(31)-H(31B)	108.1(5)
H(32A)-C(32)-H(32B)	107.8(5)	H(33)-C(33)-C(34)	105.3(4)
H(33)-C(33)-C(38)	105.3(4)	H(33)-C(33)-P(1)	105.3(4)
H(34A)-C(34)-H(34B)	108.0(5)	H(34A)-C(34)-C(35)	109.4(4)
H(34B)-C(34)-C(35)	109.4(4)	H(35A)-C(35)-C(36)	109.4(5)
H(35A)-C(35)-H(35B)	108.0(5)	H(35B)-C(35)-C(36)	109.4(4)
H(36A)-C(36)-H(36B)	107.9(5)	H(36A)-C(36)-C(37)	109.3(5)
H(36B)-C(36)-C(37)	109.3(5)	H(37A)-C(37)-C(38)	109.3(5)
H(37A)-C(37)-H(37B)	108.0(5)	H(37B)-C(37)-C(38)	109.3(5)
H(38A)-C(38)-H(38B)	108.0(5)	N(1)-C(7)-O(1)	130.3(5)
N(1)-C(8)-N(2)	112.1(4)	N(1)-C(8)-S(1)	130.6(4)
N(2)-C(8)-S(1)	117.3(4)	S(1)-Rh(1)-P(1)	172.1(1)
O(2)-C(39)-Rh(1)	177.9(5)		

## APPENDIX E

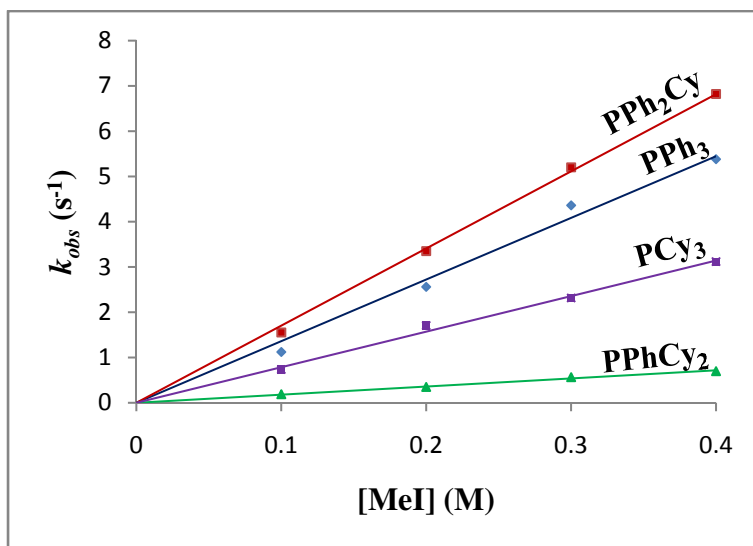
### SUPPLEMENTARY DATA FOR THE IODOMETHANE OXIDATIVE ADDITION TO [Rh(*N*-diPT)(CO)(PR<sub>1</sub>R<sub>2</sub>R<sub>3</sub>)]

**Table E.1 : Observed rate constants for the oxidative addition of iodomethane to (i) [Rh(*N*-diPT)(CO)(PPh<sub>3</sub>)], (ii) [Rh(*N*-diPT)(CO)(PPh<sub>2</sub>Cy)], (iii) [Rh(*N*-diPT)(CO)(PPhCy<sub>2</sub>)], (iv) [Rh(*N*-diPT)(CO)(PCy<sub>3</sub>)] at various temperatures and iodomethane concentrations.**

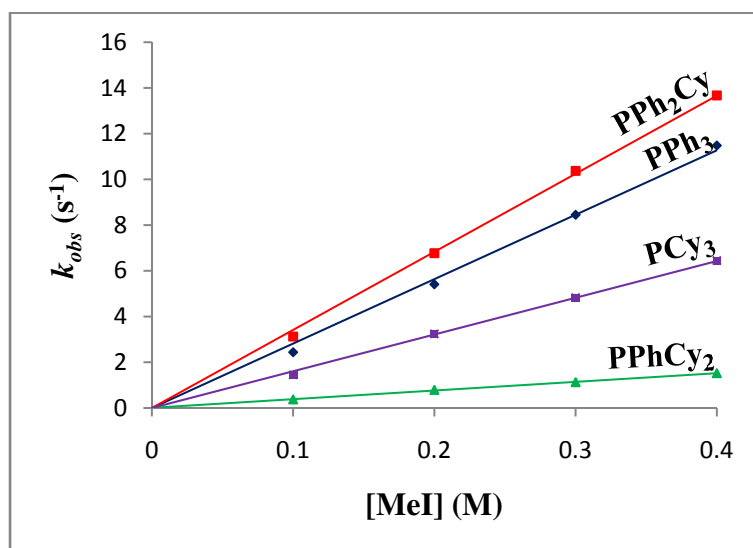
		$k_{obs} \text{ (x } 10^{-4} \text{ s}^{-1})$			
Temp (°C)	[MeI] (M)	(i)	(ii)	(iii)	(iv)
25	0.1	4.54(2)	6.12(3)	0.923(1)	2.52(2)
	0.2	8.58(2)	13.3(4)	1.606(6)	5.71(3)
	0.3	13.45(5)	19.3(1)	2.50(2)	8.66(2)
	0.4	18.4(3)	24.21(6)	3.347(7)	11.9(1)
	1	51.4(1)	64.2(3)	7.56(4)	27.2(2)
15	0.1	2.44(2)	3.126(8)	0.374(1)	1.447(5)
	0.2	5.41(4)	6.77(2)	0.791(2)	3.24(1)
	0.3	8.45(2)	10.37(5)	1.127(7)	4.83(2)
	0.4	11.48(7)	13.67(7)	1.523(8)	6.45(2)
5	0.1	1.121(8)	1.553(7)	0.188(3)	0.735(2)
	0.2	2.56(2)	3.35(2)	0.35(2)	1.707(4)
	0.3	4.36(1)	5.20(1)	0.566(2)	2.314(3)
	0.4	5.38(2)	6.82(2)	0.697(2)	3.119(5)

**Table E.2 : The rate constant  $k_2'$  values for the oxidative addition of iodomethane to (i) [Rh(*N*-diPT)(CO)(PPh<sub>3</sub>)], (ii) [Rh(*N*-diPT)(CO)(PPh<sub>2</sub>Cy)], (iii) [Rh(*N*-diPT)(CO)(PPhCy<sub>2</sub>)], (iv) [Rh(*N*-diPT)(CO)(PCy<sub>3</sub>)] at various temperatures.**

		$k_2' \text{ (x } 10^{-4} \text{ M}^{-1} \cdot \text{s}^{-1})$			
Temp (°C)		(i)	(ii)	(iii)	(iv)
25		55(2)	60(4)	8.2(3)	27(1)
15		30(2)	35(1)	3.8(1)	17(3)
5		15(2)	18(3)	1.7(2)	7.8(1)



a)



b)

**Figure E.1** Plots of observed rate constants *vs.* iodomethane concentration for the oxidative addition of iodomethane to [Rh(*N*-diPT)(CO)(PR<sub>1</sub>R<sub>2</sub>R<sub>3</sub>)] at a) 5 °C and b) 15 °C with respect to the disappearance of the Rh(I) complex, where PR<sub>1</sub>R<sub>2</sub>R<sub>3</sub> = PPh<sub>3</sub> (1979 cm<sup>-1</sup>), PPh<sub>2</sub>Cy (1972 cm<sup>-1</sup>), PPhCy<sub>2</sub> (1969 cm<sup>-1</sup>), and PCy<sub>3</sub> (1963 cm<sup>-1</sup>). [Rh] = 0.010 M.



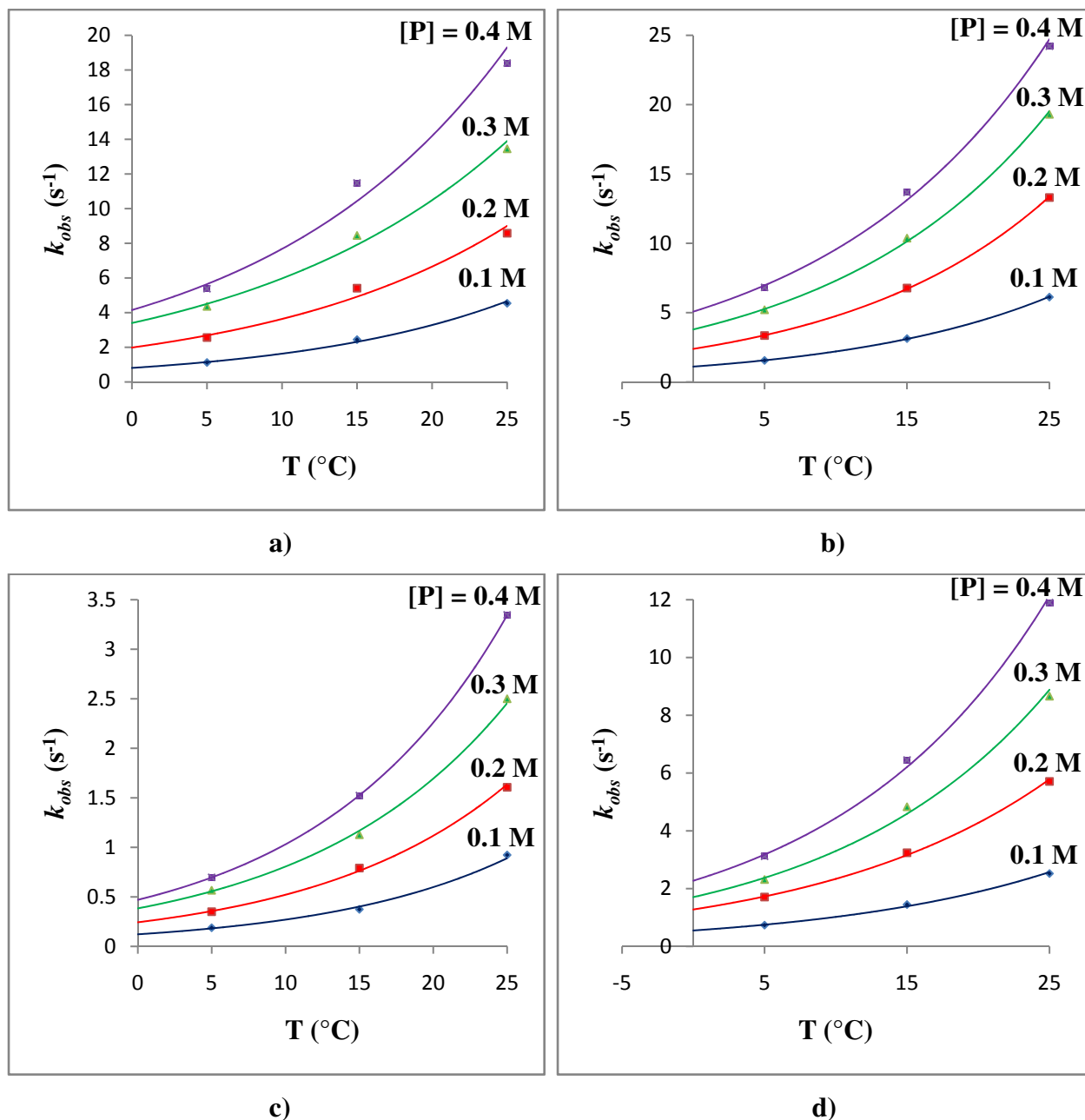


**Figure E.2** Plots of the observed rate constants *vs.* temperature for the oxidative addition of iodomethane to a)  $[\text{Rh}(\text{N-diPT})(\text{CO})(\text{PPh}_3)]$  b)  $[\text{Rh}(\text{N-diPT})(\text{CO})(\text{PPh}_2\text{Cy})]$  c)  $[\text{Rh}(\text{N-diPT})(\text{CO})(\text{PPhCy}_2)]$  d)  $[\text{Rh}(\text{N-diPT})(\text{CO})(\text{PCy}_3)]$  at different phosphine concentrations  $[P]$ .  $[\text{Rh}] = 0.010 \text{ M}$ .